Masamichi Kamihira
Yoshinori Katakura
Akira Ito
Editors

VOLUME 16

Animal Cell Technology: Basic & Applied Aspects

Proceedings of the 21st Annual and International Meeting of the Japanese Association for Animal Cell Technology (JAACT), Fukuoka, Japan, November 24-27, 2008

Springer

Animal Cell Technology:
Basic & Applied Aspects

Volume 16

For further volumes:
http://www.springer.com/series/7552

JAACT 2008 Organizing Committee

Meeting Chairman
Masamichi Kamihira (Kyushu University, Japan)

Meeting Vice Chairman
Yoshinori Katakura (Kyushu University, Japan)

Meeting Secretaries
Akira Ito (Kyushu University, Japan)
Hiroyuki Ijima (Kyushu University, Japan)
Hiroshi Mizumoto (Kyushu University, Japan)
Kiichiro Teruya (Kyushu University, Japan)
Yoshinori Kawabe (Kyushu University, Japan)

Organizing Boards:

P. M. Alves (Portugal)
K. Dairiki (Japan)
Y. Fuke (Japan)
S. Hashizume (Japan)
M. Hosobuchi (Japan)
K. Ikura (Japan)
M. Kamei (Japan)
T. Kuwata (Japan)
T. Matsumoto (Japan)
M. Nagao (Japan)
T. Omasa (Japan)
T. Shigehisa (Japan)
H. Shinmoto (Japan)
M. Tanokura (Japan)
H. Tsukamoto (Japan)
M. Yokota (Japan)
H. Anazawa (Japan)
D. Ejima (Japan)
Y. Fukui (Japan)
C. Hirashima (Japan)
H. Hoshi (Japan)
H. Isoda (Japan)
Y. Kamei (Japan)
M. Maeda-Yamamoto (Japan)
T. Matsushita (Japan)
H. Nakano (Japan)
M. Sato (Japan)
M. Shimizu (Japan)
M. Takagi (Japan)
M. Totsuka (Japan)
H. Tsumura (Japan)
S. Asahi (Japan)
A. Enomoto (Japan)
S. Hachimura (Japan)
T. Hisatsune (Japan)
S. Iijima (Japan)
T. Kadowaki (Japan)
S. Kida (Japan)
T. Matsuda (Japan)
Y. Miura (Japan)
K. Nishijima (Japan)
H. Satsu (Japan)
S. Shirahata (Japan)
Y. Taniyama (Japan)
M. Tsukahara (Japan)
K. Yagasaki (Japan)

Advisory Boards

D. W. Barnes (USA)
R. Sasaki (Japan)
J. Werenne (Belgium)
S. Kaminogawa (Japan)
G. H. Sato (USA)
K. Nagai (Japan)
T. Suzuki (Japan)

Masamichi Kamihira · Yoshinori Katakura · Akira Ito
Editors

Animal Cell Technology: Basic & Applied Aspects

Proceedings of the 21st Annual and International Meeting of the Japanese Association for Animal Cell Technology (JAACT), Fukuoka, Japan, November 24–27, 2008

Springer

Editors
Masamichi Kamihira
Kyushu University
Fac. Engineering
Dept. Chemical Engineering
744 Motooka
Nishi-ku
Fukuoka
819-0395 Japan

Yoshinori Katakura
Kyushu University
Fac. Agriculture
6-10-1 Hakozaki
Higashi-ku
Fukuoka
812-8581 Japan

Akira Ito
Kyushu University
Fac. Engineering
Dept. Chemical Engineering
744 Motooka
Nishi-ku
Fukuoka
819-0395 Japan

ISBN 978-90-481-3891-3 e-ISBN 978-90-481-3892-0
DOI 10.1007/978-90-481-3892-0
Springer Dordrecht Heidelberg London New York

Library of Congress Control Number: 2010921921

Preface

The 21st Annual and International Meeting of the Japanese Association for Animal Cell Technology (JAACT) "POWER OF CELLS" was held at the Fukuoka International Congress Center in Fukuoka, Japan from November 24–27, 2008. The meeting focused on recent advancements in the field of animal cell technology from both basic and applied aspects. We invited academic and industrial scientists from all over the world to make this meeting truly successful and scientifically fruitful. More than 340 participants from 14 countries joined the meeting and gave presentations (plenary & keynote lectures, 3; Murakami memorial lecture, 1; presentations by symposists, 37; technical seminars, 6; oral presentations, 30; poster presentations, 126). Fields and titles of 9 symposia were 1. "From Molecules and Genes to Therapies: Industrial ACT Perspectives", 2. "Stem Cells: Culture Technology to Clinical Application – Yasuo Kitagawa Memorial Symposium – ", 3. "Innovation for Tissue Engineering of Metabolic Organs", 4. "Cell Engineering – from Omics to Cell Culture Processes", 5. "Water and Life", 6. "Nutrigenomics: Lipid Metabolism and Cancer Prevention", 7. "Recent Progress in Cell Culture Process Development", 8. "Novel Production System for Biologics", 9. " Challenges on Down Stream Process Development for Biologics". All presentations (oral and poster) were brought together on the following topics.

1. Cell culture engineering
2. Production of biologicals
3. Functional cell lines
4. Glycoengineering
5. Immunologicals, monoclonal antibodies, and vaccines
6. Transplantation, artificial organs, and organ substitutes
7. Gene therapy
8. Transgenic animals
9. Safety and regulation
10. Cell regulatory factors and signal transduction
11. Functional substances in food and natural sources
12. Animal cells for in vitro assay

The editors hope this volume of Proceedings will greatly contribute to the development of animal cell technology for innovation of life science.

The editors express their sincere thanks to all the participants, symposium organizers, chairmen, speakers, members of the organizing committee, and the student staff of this meeting for their valuable contributions.

We also deeply thank to Commemorative Organization for The Japan World Exposition ’70, Fukuoka Convention & Visitors Bureau, ThermoFisher Scientific Japan, and Kao Foundation for Arts and Sciences for financial supports.

Japan

Masamichi Kamihira
Yoshinori Katakura
Akira Ito

Contents

Purification of Hepatoblasts from Fetal Mouse Livers by Using a Temperature-Reversible Gelation Polymer and Their Application in Regenerative Medicine 1
Koichiro Yori, Toru Koike and Nobuyoshi Shiojiri

Computer Aided Rational Design of Biochemical Systems 7
Hiroyuki Kurata

DNA Microarray in Nutrigenomics and Cancer Prevention Research: Elucidating Molecular Signatures of Cancer Preventive Phytochemicals 13
Thomas T.Y. Wang

DNA Microarray Technology Evaluation of Effect of Dietary Intake of Crude Rice Glycosphingolipids in Mice 19
Jun Shimizu

Integrated Pathway Analysis of Genome-Wide Expression Changes Associated with Serum-Free Suspension Adaptation of an Antibody-Producing Chinese Hamster Ovary (CHO) Cell Line . . 27
Yung-Shyeng Tsao, Ankit A. Merchant, Aaron Meyer, and Zhong Liu; Marsha Smith, Diane Levitan, and Eric Gustafson

Affordable Mab by Ensuring Low Cog 33
Bjorn Hammarberg and Bo Forsberg

Evaluation of Neurotoxicity of Environmental Chemicals Using Neural Stem Cells and Neuroblastoma Cells 41
Masami Ishido

Integration of Endothelial Cell-Covered Hepatocyte Spheroids for Construction of Vascularized Liver Tissue 45
Masakazu Inamori, Hiroshi Mizumoto, and Toshihisa Kajiwara

Characterization of Cell-Sized Vesicles Induced from Human Lymphoid Cell Lines 51
Makoto Yamanaka, Shigeki Nakamura, Aiko Inoue, Takashi Yasuda, Yuichi Inoue, and Hiroharu Kawahara

Dendrimer-Immobilized Culture Surface as a Tool to Promote Aggregate Formation of Anchorage-Dependent Cells 57
Mee-Hae Kim, Masahiro Kino-oka, Jun-ichi Miyazaki, and Masahito Taya

Advantage of Alagln as an Additive to Cell Culture Medium 65
Yasufumi Imamoto, Hisaya Tanaka, Ken Takahashi, Yoshinobu Konno, and Toshiyuki Suzawa

Supplementation of Phosphatidylcholine Protects the Hybridoma Cells from Apoptosis Induced by Serum Withdrawal 73
Beng Ti Tey, Kah Choon Yap, Hideki Yamaji, Abdul Manaf Ali, and Wen Siang Tan

Monoclonal Antibody Productivity of Hybridoma Cells Under Active Hypothermic Growth Condition 77
Beng Ti Tey, Sun Li Chong, Michelle Y.T. Ng, Duen Gang Mou, Saw Hoon Lim, and Abdul Manaf Ali

Efficient Selection of Cell Clones with Higher Productivity in the Production of Recombinant Human Monoclonal Antibodies 83
Ayako Ohshima, Yumiko Takamatsu, Koichi Yamamot, and Hiroyuki Saitoh

Continuous Cell Production from Three Dimensional Hematopoietic Microenvironment in Polyurethane Foam 89
Tadasu Jozaki, Kentarou Aoki, Hiroshi Mizumoto, and Toshihisa Kajiwara

A New Approach for Drug Discovery and Differentiation Study Using Cutting-Edge 3d Cell Culture System 95
Fujiko Ozawa, Yoshitaka Miyagawa, Masami Hiroyama, Nobutaka Kiyokawa, Akihiro Umezawa, Akito Tanoue, and Satoru Tanaka

Dimensional Cell Culture Dish for In Vivo-Like Cell Culture 103
Y. Furutani, T. Tamura, and M. Kodama

Characterization of the Erythropoietin (EPO) Protein Production in the Recombinant Human Cultured Cells, in which the Exogenous EPO Gene was Introduced into Hypoxanthine Phosphoribosyl Transferase (HPRT) Gene Locus 109
Toshiaki Banzai, Yukiko Koyama, and Shuji Sonezaki

Development of Protein High Expression System by Using Fructose Metabolism 115
Yuriko Tsukamoto, Shigeki Nakamura, Aiko Inoue, Norikazu Nishino, Yuichi Inoue, and Hiroharu Kawahara

Controlling Fucosylation Levels of Antibodies with Osmolality during Cell Culture 121
Yoshinobu Konno, Yuki Kobayashi, Ken Takahashi, Eiji Takahashi, Shinji Sakae, Masako Wakitani, Toshiyuki Suzawa, Keiichi Yano, Masamichi Koike, Kaori Wakamatu, and Shinji Hosoi

Comparison of Immunoresponses Between Cecal Patch Cells and Peyer's Patch Cells Stimulated by Bacterial Components 127
Takuma Konno, Akira Hosono, Yasuhiro Hiramatsu, Satoshi Hachimura, Kyoko Takahashi, and Shuichi Kaminogawa

Conjugate of β-Lactoglobulin with Carboxymethyl Dextran Increased the Antigen-Specific IgG1 Production, While It Decreased IgE Production Compared with Native β-Lactoglobulin . . . 133
Tadashi Yoshida, Yuko Shigihara, Manami Nakamura, and Makoto Hattori

Anti-Inflammatory Action of Epigallocatechin-3-Gallate at a Physiological Concentration through the 67-KDA Laminin Receptor in Lipopolysaccharide-Stimulated Raw264.7 Cells 139
Byun Eui Hong, Yoshinori Fujimura, Koji Yamada, and Hirofumi Tachibana

Enhancement of Antibody Production using Solution after Antibody Purification: Application of Spent Medium for Antibody Production 145
Akiko Ogawa, Sadaharu Fukui, and Satoshi Terada

Production of Human Monoclonal Antibodies Against FC Epsilon Receptor I Alpha by Combining In Vitro Immunization with Phage Display 151
Kosuke Tomimatsu, Shin-ei Matsumoto, Makiko Yamashita, Kiichiro Teruya, Yoshinori Katakura, Shigeru Kabayama, and Sanetaka Shirahata

Enhancement of Hepatocyte Function Through Heterotypic Cell-Cell Interactions Using E-Cadherin-Expressing NIH3T3 Cells . . . 159
Akira Ito, Takehiko Kiyohara, Yoshinori Kawabe, Hiroyuki Ijima, and Masamichi Kamihira

Magnetic Cell-Patterning for Tissue Engineering 165
Hirokazu Akiyama, Akira Ito, Yoshinori Kawabe, and Masamichi Kamihira

Magnetic Force-Based Tissue Engineering of Skeletal Muscle for Bio-Actuator 171
Yasunori Yamamoto, Masahiro Kato, Akira Ito, Yoshinori Kawabe, Kazunori Shimizu, Eiji Nagamori, and Masamichi Kamihira

Fabrication of Skeletal Muscle Tissue from C2C12 Myoblast Cell Towards the Use as Bio-Actuator 177
Hideaki Fujita, Kazunori Shimizu, and Eiji Nagamori

Retroviral Vectors Pseudotyped with Chimeric Vesicular Stomatitis Virus Glycoprotein for Antibody-Dependent Gene Transduction 185
Yujiro Kameyama, Yoshinori Kawabe, Akira Ito, and Masamichi Kamihira

Improvement of CPP-RBD for siRNA Delivery 191
Rina Kuwabara, Tamaki Endoh, Masahiko Sisido, and Takashi Ohtsuki

Production of Recombinant Human EPO and EPO/Fc Fusion Proteins by Chinese Hamster Ovary Cells 197
Carlos Alberto Penno, Yoshinori Kawabe, Akira Ito, and Masamichi Kamihira

Development of Oviduct-Specific Gene Expression System for Transgenic Avian Bioreactor 203
Yoshinori Kawabe, Kensaku Numata, Masashi Teramori, Akira Ito, and Masamichi Kamihira

Production of Therapeutic Proteins Composed of Seven Dominant Human T Cell Epitopes Derived from the Japanese Cedar Pollen Allergens 209
Yoshinori Kawabe, Yoshifumi Hayashida, Kensaku Numata, Akira Hishigae, Akira Ito, and Masamichi Kamihira

The Differentiation of C2C12 Cells to Myotube by Paraquat 215
Masaaki Okabe, Koichi Akiyama, Sogo Nishimoto, Takuya Sugahara, and Yoshimi Kakinuma

Molecular Cloning and Characterization of a Novel Canine Sulfotransferase 221
Katsuhisa Kurogi, Yoichi Sakakibara, Shin Yasuda, Ming-Cheh Liu, and Masahito Suiko

In Vitro Analysis of the Interaction Between Human Intestinal Epithelial Cells and Macrophage-Like Cells 231
Yoko Ishimoto, Hideo Satsu, Tetsunosuke Mochizuki, Mamoru Totsuka, and Makoto Shimizu

Role of Ubiquitination Promoted During Restimulation in the Induction of T Cell Anergy 237
Yohei Mizuguchi, Ai Yamamoto, Makoto Hattori, and Tadashi Yoshida

Expression Analysis of Senescence-Associated Genes: Their Possible Involvement in Diabetes 243
Miyako Udono, Kaori Mukae, Tsukasa Fujiki, Zhang Ping Bo, Hiroshi Fujii, Sanetaka Shirahata, and Yoshinori Katakura

Study of Butyrate Signal Transduction Pathways in Rat Hepatic Stem-Like Cells 247
Toshihiko Saheki, Yusuke Mukai, Ken'ichi Saito, Emi Tajima, Kentaro Katakura, Atsuyoshi Nishina, Mikiko Kishi, Takashi Izumi, Toshihiro Sugiyama, and Itaru Kojima

Growth Control of Mammalian Cells via a Human Artificial Chromosome Harboring a Chimeric Receptor 253
Masahiro Kawahara, Toshiaki Inoue, Xianying Ren, Takahiro Sogo, Hidetoshi Yamada, Motonobu Katoh, Hiroshi Ueda, Mitsuo Oshimura, and Teruyuki Nagamune

The Impact of Redox State on Regulation of the High-Affinity IgE Receptor Expression 259
Yoshinori Fujimura, Hayato Higo, Satomi Yano, Koji Yamada, and Hirofumi Tachibana

The Characteristic of Chimeric Receptors Based on Erythropoietin Receptor 265
Wenhai Liu, Masahiro Kawahara, Hiroshi Ueda, and Teruyuki Nagamune

Anti-Cancer and Structure-Activity Relationship of Natural Polyacetylenes 271
Soninkhishig Tsolmon, Yui Kurita, Si Won Hong, Parida Yamada, Hideyuki Shigemori, and Hiroko Isoda

Effect of Mongolian Medicinal Plant *Stellera Chamaejasme* on Chronic Leukemia Cells K562 277
Soninkhishig Tsolmon, Parida Yamada, and Hiroko Isoda

Capsaicin Induced the Upregulation of Transcriptional and Translational Expression of Glycolytic Enzymes Related to Energy Metabolism in Human Intestinal Epithelial Cells 281
Junkyu Han and Hiroko Isoda

Effect of Novel Compounds from *Thymelaea Hirsuta* on Melanogenesis 285
Myra O. Villareal, Yusaku Miyamae, Junkyu Han, Yamada Parida, Hideyuki Shigemori, and Hiroko Isoda

Electrolyzed Reduced Water Prolongs *Caenorhabditis elegans' Lifespan* 289
Hanxu Yan, Huaize Tian, Takeki Hamasaki, Masumi Abe, Noboru Nakamichi, Kiichiro Teruya, Yoshinori Katakura, Shinkatsu Morisawa, and Sanetaka Shirahata

Anti-Cancer Effects of Enzyme-Digested Fucoidan Extract from Seaweed Mozuku 295
Yoshiko Matsuda, Kiichiro Teruya, Sakiko Matsuda, Ayumi Nakano, Takuya Nishimoto, Masashi Ueno, Akitomo Niho, Makiko Yamashita, Hiroshi Eto, Yoshinori Katakura, and Sanetaka Shirahata

The Downregulation of Mast Cell Activation Through the Suppression of the High-Affinity IgE Receptor Expression by Green Tea Catechin Egcg 301
Hirofumi Tachibana, Yoshinori Fujimura, Yusuke Hasegawa, Satomi Yano, and Koji Yamada

Anti-Diabetes Effects of Hita Tenryou-Sui Water®, a Natural Reduced Water 307
Kazuhiro Osada, Yuping Li, Takeki Hamasaki, Masumi Abe, Noboru Nakamichi, Kiichiro Teruya, Yoshitoki Ishii, Ying Wang, Yoshinori Katakura, and Sanetaka Shirahata

Suppressive Effect of ERW on Lipid Peroxidation and Plasma Triglyceride Level 315
Masumi Abe, Shunpei Sato, Kazuko Toh, Takeki Hamasaki, Noboru Nakamichi, Kiichiro Teruya, Yoshinori Katakura, Shinkatsu Morisawa, and Sanetaka Shirahata

Growth Suppression of HL60 and L6 Cells by Atomic Hydrogen 323
Kensuke Nakanishi, Takeki Hamasaki, Takuro Nakamura, Masumi Abe, Kiichiro Teruya, Yoshinori Katakura, Shinkatsu Morisawa, and Sanetaka Shirahata

Insulin-Mimetic Activity of Inositol Derivatives Depends on Phosphorylation of PKCζ/λ in L6 Myotubes 327
Nhung Thuy Dang, Masanori Yamaguchi, Tadashi Yoshida, Ken-ichi Yoshida, and Hitoshi Ashida

Enhancement of Phagocytic Activity by a Crude Polysaccharide from Tea (*Camellia sinensis*) Extract 333
Manami Monobe, Kaori Ema, Keiko Azuma, and Mari Maeda-Yamamoto

Effects of Lupeol on Melanoma In Vitro and In Vivo: Fundamental and Clinical Trials 339
Keishi Hata, Kikumi Ogihara, Saori Takahashi, Takeshi Tsuka, Saburo Minami, and Yoshiharu Okamoto

The Effect of Secoisolariciresinol on 3t3-L1 Adipocytes and the Relationship Between Molecular Structure and the Activity 345
Shiori Tominaga, Takuya Sugahara, Sogo Nishimoto, Manami Yamawaki, Yuki Nakashima, Taro Kishida, Koichi Akiyama, Masafumi Maruyama, and Satoshi Yamauchi

Detection of Anti-Allergic Factors in Strawberry Extracts 353
Kazuhiro Mitsuda, Aiko Inoue, Norikazu Nishino, Yuichi Inoue, and Hiroharu Kawahara

Anti-Melanogenic Activity of Yacon Leaves in Mouse Melanoma Cells . 359
Tomoyuki Ishikawa, Toshio Hyakutake, Yasuaki Gondou, Mitsuhiro Sakai, Reiko Kinoshita, Jyunji Tottori, Hiroshi Kunitake, and Ken-Ichi Kusumoto

Cytokine Responses of Splenocytes of Female and Male Non-Obese Diabetic Mice Induced by Lactic Acid Bacteria 365
Atsushi Enomoto, Mohd Azraai Bin Jamal, Hiromi Mitsui, Hiromi Kimoto-Nira, Chise Suzuki, and Koko Mizumachi

Development of a High-Throughput Evaluation System for Antiviral Activities of Food Factors By Using Bioinformatics 371
Nozomu Eto, Kiyoko Nagahama, Shohei Miyamoto, Osayoshi Yamaguchi, Sayumi Miyauchi, Takako Iwata, Asuka Uchida, and Kunihito Yamamori

The Effects of Pesticides on Immune Cells 377
Sogo Nishimoto, Kota Kanda, Masaaki Okabe, Koichi Akiyama, Yoshimi Kakinuma, and Takuya Sugahara

Co-Cultured Hepatocyte-Spheroid Chip Constructed Using the Microfabrication Technique 383
Yusuke Sakai and Kohji Nakazawa

Micropatterned Hepatocyte Culture Using Microstencil Technique . . . 391
Yukako Shinmura, Ami Higuchi, Yusuke Sakai, and Kohji Nakazawa

Structural Features of Totally Designed Lipidic Materials for Small Interfering RNA Delivery System 397
Ken-Ichi Kusumoto

Thin-Film Assembly of Totally Designed Lipidic Materials as Gene Carrier in Mouse Embryonic Neural Stem Cells: Thin-Film Assembly of Lipidic Material as Potential Gene Carrier . . . 403
Ken-Ichi Kusumoto, Takahiro Nagata, and Itaru Hamachi

Transfection System Using a Cocktail of Totally Designed Lipidic Materials in Chinese Hamster Ovary Cells: Lipidic Cocktail as Potential Gene Carrier for CHO Cells 409
Ken-Ichi Kusumoto, Takahiro Nagata, Eiichi Kanazawal, Takanori Sakai, Yoshihiko Yoshikawa, Takahiro Ogata, Naomi Nakatani, Tomoyuki Ishikawa, Shintaro Koga, Akio Shirasu, Shinji Morishita, Takayuki Emura, and Itaru Hamachi

Size Dependent Heat Generation of Magnetic Nanoparticles Under AC Magnetic Field for Cancer Therapy 415
Jun Motoyama, Toshiyuki Hakata, Ryuji Kato, Noriyuki Yamashita, Tomio Morino, Takeshi Kobayashi, and Hiroyuki Honda

Functional Evaluation of Anticancer Drugs in Human Leukemia Cells Based on Metabolic Profiling Technique 423
Daisuke Miura, Yoshinori Fujimura, Hirofumi Tachibana, and Hiroyuki Wariishi

Extracts from the Root of *Platycodon grandiflorum* Modulate Induction of Inflammatory Changes in Coculture of Adipocytes and Macrophages 429
Ju-Hye Lee, Koji Yamada, and Hirofumi Tachibana

Position Specific Incorporation of Nonnatural Amino Acids into Proteins In Vivo 435
Satoshi Neki, Takashi Ohtsuki, and Masahiko Sisido

Novel Protease Inhibitor Inhibiting Proliferation of Influenza Virus: Purification and cDNA Cloning of a Novel Protease Inhibitor Secreted by MDCK Cells 441
Kiyoto Nishiyama, Keishin Sugawara, Kenji Soejima, Shin-ichi Abe, and Hiroshi Mizokami

Contributors

Masumi Abe Department of Genetic Resources Technology, Kyushu University, Fukuoka, Fukuoka 812-8581, Japan, masumie@agr.kyushu-u.ac.jp

Shin-ichi Abe Graduate School of Science and Technology, Kumamoto University, Kurokamimachi 2-39-1, Kumamoto 860-8555, Japan

Hirokazu Akiyama Department of Chemical Engineering, Faculty of Engineering, Kyushu University, 744 Motooka, Nishi-ku, Fukuoka 819-0395, Japan

Koichi Akiyama Integrated Center for Sciences, Ehime University, Matsuyama, Ehime 790-8566, Japan; Faculty of Agriculture, Ehime University, Matsuyama, Ehime 790-8566, Japan

Abdul Manaf Ali Department of Cell and Molecular Biology, Universiti Putra Malaysia, Selangor Darul Ehsan, Malaysia; Institute of Bioscience, Universiti Putra Malaysia, 43400 UPM Serdang, Selangor Darul Ehsan, Malaysia

Kentarou Aoki Department of Chemical Engineering, Kyushu University, Nishi-ku, Fukuoka, Japan

Hitoshi Ashida Graduate School of Agriculture Science, Kobe University, Nada-ku, Kobe, Hyogo 657-8501, Japan

Keiko Azuma National Institute of Vegetable and Tea Science, NARO, Shizuoka, Japan

Toshiaki Banzai Biotechnology Group, Research Institute, TOTO LTD., Kitakyushu-city, Fukuoka, 802-8601, Japan

Zhang Ping Bo Kyushu University, Higashi-ku, Fukuoka 812-8581, Japan

Sun Li Chong Biotechnology Program, Malaysia University of Science and Technology, Kelana Jaya, Selangor 47301, Malaysia

Nhung Thuy Dang Graduate School of Agriculture Science, Kobe University, Nada-ku, Kobe, Hyogo 657-8501, Japan

Kaori Ema National Institute of Vegetable and Tea Science, NARO, Shizuoka, Japan

Takayuki Emura ASTEC Corporation, Shime-machi, Fukuoka 811-2207, Japan

Tamaki Endoh Graduate School of Natural Science and Technology, Okayama University, Okayama, Japan

Atsushi Enomoto Department of Chemistry and Chemical Biology, Gunma University, Kiryu, Gunma 376-8515, Japan, enomoto@chem-bio.gunma-u.ac.jp

Nozomu Eto University of Miyazaki, Miyazaki 889-2192, Japan

Hiroshi Eto Daiichi Sangyo Co. Ltd., Japan

Bo Forsberg CMC Biologics A/S, Copenhagen, DK-2860, Denmark

Hiroshi Fujii Kyushu University, Higashi-ku, Fukuoka 812-8581, Japan

Tsukasa Fujiki Faculty of Agriculture, Kyushu University, Higashi-ku, Fukuoka 812-8581, Japan

Yoshinori Fujimura Innovation Center for Medical Redox Navigation, Kyushu University, Higashi-ku, Fukuoka 812-8582, Japan, fujimu@agr.kyushu-u.ac.jp

Yoshinori Fujimura Innovation Center for Medical Redox Navigation, Kyushu University, Fukuoka 812-8582, Japan, fujimu@agr.kyushu-u.ac.jp

Hideaki Fujita Toyota Central R&D Labs. Inc., Aichi 480-1192, Japan

Sadaharu Fukui Department of Chemistry and Biochemistry, Suzuka National College of Technology, Suzuka, Mie 510-0294, Japan

Y. Furutani Vessel Inc., Japan

Yasuaki Gondou Kurume City Office, Kurume, Fukuoka 830-8520, Japan

Eric Gustafson Functional Genomics, Discovery Technologies, Schering-Plough Research Institute, Kenilworth, NJ 07033, USA

Satoshi Hachimura Research Center for Food Safety, Graduate School of Agricultural and Life Sciences, The University of Tokyo, Tokyo 113-8657, Japan

Toshiyuki Hakata Toda Kogyo Corp., Hiroshima, 739-0652 Japan

Itaru Hamachi Department of Synthetic Chemistry and Biological Chemistry, Kyoto University, Katsura, Kyoto 615-8510, Japan

Takeki Hamasaki Department of Genetic Resources Technology, Kyushu University, Fukuoka, Fukuoka 812-8581, Japan

Bjorn Hammarberg ABD Life Sciences Ltd, Central, Hong Kong

Junkyu Han Graduate School of Life and Environmental Sciences, University of Tsukuba, Tsukuba, Ibaraki 305-8572, Japan

Byun Eui Hong Department of Bioscience and Biotechnology, Kyushu University, Higashi-ku, Fukuoka 812-8581, Japan

Si Won Hong Graduate School of Life and Environmental Sciences, University of Tsukuba, Tsukuba, Ibaraki 305-8572, Japan

Yusuke Hasegawa Kyushu University, Fukuoka 812-8581, Japan

Keishi Hata Institute for Food and Brewing, Akita Prefectural Agricultural, Forestry, and Fisheries Research Center, Araya-machi, Akita 010-1623, Japan, hata@arif.pref.akita.jp

Makoto Hattori Department of Applied Biological Science, Tokyo University of Agriculture and Technology, Fuchu, Tokyo 183-8509, Japan

Yoshifumi Hayashida Department of Chemical Engineering, Faculty of Engineering, Kyushu University, 744 Motooka, Nishi-ku, Fukuoka, 819-0395, Japan

Hayato Higo Kyushu University, Higashi-ku, Fukuoka 812-8581, Japan

Ami Higuchi Department of Life and Environment Engineering, University of Kitakyushu, Kitakyushu, Fukuoka 808-0135, Japan

Yasuhiro Hiramatsu Department of Food Science and Technology, College of Bioresource Sciences, Nihon University, Fujisawa-shi, Kanagawa 252-8510, Japan

Masami Hiroyama Department of Pharmacology, National Research Institute for Child Health and Development, Setagaya-ku, Tokyo, Japan

Akira Hishigae Department of Chemical Engineering, Faculty of Engineering, Kyushu University, 744 Motooka, Nishi-ku, Fukuoka, 819-0395, Japan

Hiroyuki Honda Graduate School of Engineering, Nagoya University, Nagoya, 464-8603 Japan

Shinji Hosoi Kyowa Hakko Kirin Co., LTD., Chiyoda-ku, Tokyo, 100-8185, Japan

Akira Hosono Department of Food Science and Technology, College of Bioresource Sciences, Nihon University, Fujisawa-shi, Kanagawa 252-8510, Japan, hosono@brs.nihon-u.ac.jp

Toshio Hyakutake Department of Biological Chemistry, Biotechnology and Food Research Institute, Fukuoka Industrial Technology Center, Kurume, Fukuoka 839-0861, Japan

Hiroyuki Ijima Department of Chemical Engineering, Kyushu University, Nishi-ku, Fukuoka 819-0395, Japan

Yasufumi Imamoto Bio Process Research and Development Laboratories, Production Division, Kyowa Hakko Kirin Co., Ltd., Takasaki-shi, Gunma 370-0013, Japan

Masakazu Inamori Department of Chemical Engineering, Kyushu University, Nishi-ku, Fukuoka, 819-0395, Japan

Aiko Inoue The Cell Engineering Center, Kitakyushu National College of Technology, Kitakyushu-shi, Fukuoka, 802-0985, Japan; The Cell Engineering Center, Kitakyushu National College of Technology, Kokuraminami-ku, Kitakyushu 802-0985, Japan

Toshiaki Inoue Department of Human Genome Science, Graduate School of Medical Science, Tottori University, Yonago, Tottori 683-8503, Japan

Yuichi Inoue The Cell Engineering Center, Kitakyushu National College of Technology, Kitakyushu-shi, Fukuoka, 802-0985, Japan; The Cell Engineering Center, Kitakyushu National College of Technology, Kokuraminami-ku, Kitakyushu 802-0985, Japan

Masami Ishido Environmental Risk Research Programme, National Institute for Environmental Studies, Tsukuba, Ibaraki 305-8506, Japan, ishidou@nies.go.jp

Yoshitoki Ishii Hita Tenryousui Co. Ltd., Hita 877-0074, Japan

Tomoyuki Ishikawa Department of Biological Chemistry, Biotechnology and Food Research Institute, Fukuoka Industrial Technology Center, Kurume, Fukuoka 839-0861, Japan

Yoko Ishimoto Department of Applied Biological Chemistry, Graduate School of Agricultural and Life Sciences, The University of Tokyo, Bunkyo-ku, Tokyo 113-8657, Japan

Hiroko Isoda Graduate School of Life and Environmental Sciences, University of Tsukuba, Tsukuba, Ibaraki 305-8572, Japan; Alliance for Research on North Africa, University of Tsukuba, Tsukuba, Ibaraki 305-8572, Japan

Akira Ito Department of Chemical Engineering, Faculty of Engineering, Kyushu University, 744 Motooka, Nishi-ku, Fukuoka 819–0395, Japan
akira@chem-eng.kyushu-u.ac.jp

Takako Iwata Miyazaki prefectural industrial support foundation, Miyazaki 880-0303, Japan

Takashi Izumi Department of Molecular Biochemistry, Gunma University, Graduate School of Medicine, Maebashi, Japan

Mohd Azraai Bin Jamal Department of Chemistry and Chemical Biology, Gunma University, Kiryu, Gunma 376-8515, Japan

Tadasu Jozaki Department of Chemical Engineering, Kyushu University, Nishi-ku, Fukuoka, Japan

Shigeru Kabayama Nihon Trim Co. Ltd., Oyodonaka, Kita-ku, Osaka 531-0076, Japan

Toshihisa Kajiwara Department of Chemical Engineering, Kyushu University, Nishi-ku, Fukuoka, 819-0395, Japan, kajiwara@chem-eng.kyushu-u.ac.jp

Yoshimi Kakinuma Integrated Center for Sciences (INCS), Ehime University, Tarumi, Matsuyama 790-8566, Japan; Faculty of Agriculture, Ehime University, Matsuyama, Ehime 790-8566, Japan

Yujiro Kameyama Department of Chemical Engineering, Faculty of Engineering, Kyushu University, 744 Motooka, Nishi-ku, Fukuoka 819-0395, Japan

Masamichi Kamihira Department of Chemical Engineering, Faculty of Engineering, Kyushu University, 744 Motooka, Nishi-ku, Fukuoka 819-0395, Japan; Graduate School of Systems Life Science, Kyushu University, Fukuoka 819-0395, Japan

Shuichi Kaminogawa Department of Food Science and Technology, College of Bioresource Sciences, Nihon University, Fujisawa-shi, Kanagawa 252-8510, Japan

Eiichi Kanazawa Department of Biological Chemistry, Biotechnology and Food Research Institute, Fukuoka Industrial Technology Center, Kurume, Fukuoka 839-0861, Japan

Kota Kanda Faculty of Agriculture, Ehime University, Matsuyama, Ehime 790-8566, Japan

Kentaro Katakura Department of Biological and Chemical Engineering, Gunma University, Kiryu, Japan

Yoshinori Katakura Faculty of Agriculture, Kyushu University, Higashi-ku, Fukuoka 812-8581, Japan, katakura@mac.com; Graduate School of System Life Science, Kyushu University, Fukuoka 812-0053, Japan, katakura@mac.com; Department of Genetic Resources Technology, Kyushu University, Fukuoka 812-8581, Japan, katakura@mac.com

Masahiro Kato Department of Chemical Engineering, Faculty of Engineering, Kyushu University, Fukuoka 819-0395, Japan

Ryuji Kato Graduate School of Engineering, Nagoya University, Nagoya, 464-8603 Japan

Motonobu Katoh Department of Human Genome Science, Graduate School of Medical Science, Tottori University, Yonago, Tottori 683-8503, Japan

Yoshinori Kawabe Department of Chemical Engineering, Faculty of Engineering, Kyushu University, 744 Motooka, Nishi-ku, Fukuoka 819-0395, Japan, kawabe@chem-eng.kyushu-u.ac.jp

Hiroharu Kawahara The Cell Engineering Center, Kitakyushu National College of Technology, Kitakyushu-shi, Fukuoka, 802-0985, Japan

Masahiro Kawahara Center for NanoBio Integration (CNBI), The University of Tokyo, Tokyo 113-8656, Japan; Department of Chemistry and Biotechnology, School of Engineering, The University of Tokyo, Bunkyo-ku, Tokyo 113-8656, Japan, kawahara@bio.t.u-tokyo.ac.jp

Mee-Hae Kim Division of Chemical Engineering, Graduate School of Engineering Science, Osaka University, Toyonaka, Osaka 565-0871, Japan

Hiromi Kimoto-Nira Functional Biomolecules Research Team, National Institute of Livestock and Grassland Science, Tsukuba, Ibaraki 305-0901, Japan

Masahiro Kino-oka Division of Chemical Engineering, Graduate School of Engineering Science, Osaka University, Toyonaka, Osaka 565-0871, Japan

Reiko Kinoshita Kurume Research Park, Kurume, Fukuoka 839-0864, Japan

Mikiko Kishi Department of Molecular Biochemistry, Gunma University, Graduate School of Medicine, Maebashi, Japan

Taro Kishida Ehime University, Matsuyama, Ehime 790-8566, Japan

Takehiko Kiyohara Graduate School of Systems Life Sciences, Kyushu University, Nishi-ku, Fukuoka 819-0395, Japan

Nobutaka Kiyokawa Department of Development Biology, National Research Institute for Child Health and Development, Setagaya-ku, Tokyo, Japan

Yuki Kobayashi Bioprocess Research and Development Laboratories, Kyowa Hakko Kirin Co., LTD., Takasaki-shi, Gunma 370-0013, Japan

Takeshi Kobayashi School of Bioscience and Biotechnology, Chubu University, Kasugai, 487-8501 Japan

M. Kodama Vessel Inc., Japan

Shintaro Koga Department of Biological Chemistry, Biotechnology and Food Research Institute, Fukuoka Industrial Technology Center, Kurume, Fukuoka 839-0861, Japan

Toru Koike Department of Biology, Shizuoka University, Suruga-ku, Shizuoka-City, Shizuoka 422-8529, Japan

Masamichi Koike BioWa, Inc., Princeton, NJ, 08540, USA

Itaru Kojima Department of Molecular Medicine, Institute for Molecular and Cellular Regulation, Gunma University, Maebashi, Japan

Yoshinobu Konno Bio Process Research and Development Laboratories, Production Division, Kyowa Hakko Kirin Co., Ltd., Takasaki-shi, Gunma 370-0013, Japan

Takuma Konno Department of Food Science and Technology, College of Bioresource Sciences, Nihon University, Fujisawa-shi, Kanagawa 252-8510, Japan

Yukiko Koyama Biotechnology Group, Research Institute, TOTO LTD., Kitakyushu-city, Fukuoka, 802-8601, Japan

Hiroshi Kunitake Kurume City Office, Kurume, Fukuoka 830-8520, Japan

Hiroyuki Kurata Department of Bioscience and Bioinformatics, Kyushu Institute of Technology, Iizuka, Fukuoka, 820-8502, Japan

Yui Kurita Graduate School of Life and Environmental Sciences, University of Tsukuba, Tsukuba, Ibaraki 305-8572, Japan

Katsuhisa Kurogi Department of Biochemistry and Applied Biosciences, University of Miyazaki, Miyazaki 889-2192 Japan, ng2801u@student.miyazaki-u.ac.jp

Ken-Ichi Kusumoto Department of Biological Chemistry, Biotechnology and Food Research Institute, Fukuoka Industrial Technology Center, Kurume, Fukuoka 839-0861, Japan

Rina Kuwabara Graduate School of Natural Science and Technology, Okayama University, Okayama, Japan

Ju-Hye Lee Kyushu University, Higashi-ku, Fukuoka, Japan

Diane Levitan Functional Genomics, Discovery Technologies, Schering-Plough Research Institute, Kenilworth, NJ 07033, USA

Yuping Li Department of Genetic Resources Technology, Kyushu University, Fukuoka 812-8581, Japan

Saw Hoon Lim Biotechnology Program, Malaysia University of Science and Technology, Kelana Jaya, Selangor 47301, Malaysia

Zhong Liu Protein Expression Technologies, GBSPD, Schering-Plough Research Institute, Union, NJ 07083, USA

Wenhai Liu Department of Chemistry and Biotechnology, The University of Tokyo, Tokyo 113-8656, Japan

Ming-Cheh Liu Department of Pharmacology, College of Pharmacy, The University of Toledo, Toledo, OH 43606 USA

Mari Maeda-Yamamoto National Institute of Vegetable and Tea Science, NARO, Shizuoka, Japan

Masafumi Maruyama Ehime University, Matsuyama, Ehime 790-8566, Japan

Yoshiko Matsuda Graduate School of Bioresource and Bioenvironmental Sciences, Kyushu University, Fukuoka, Japan, tomato@grt.kyushu-u.ac.jp

Sakiko Matsuda Graduate School of Bioresource and Bioenvironmental Sciences, Kyushu University, Fukuoka, Japan

Shin-ei Matsumoto Department of Genetic Resources Technology, Faculty of Agriculture, Kyushu University, Higashi-ku, Fukuoka 812-8581, Japan

Ankit A. Merchant Protein Expression Technologies, GBSPD, Schering-Plough Research Institute, Union, NJ 07083, USA

Aaron Meyer Bioengineering Department, University of California, Los Angeles, CA 90024, USA

Saburo Minami Department of Veterinary Clinical Medicine, School of Veterinary Medicine, Tottori University, Koyama-Minami, Tottori, Japan

Kazuhiro Mitsuda Graduate School of Life Science and Systems Engineering, Kyushu Institute of Technology, Wakamatsu-ku, Kitakyushu-shi, Fukuoka 808-0196, Japan, mitti_ mitimiti@yahoo.co.jp

Hiromi Mitsui Department of Chemistry and Chemical Biology, Gunma University, Kiryu, Gunma 376-8515, Japan

Daisuke Miura Innovation Center for Medical Redox Navigation, Kyushu University, Higashi-ku, Fukuoka 812-8582, Japan

Yoshitaka Miyagawa Department of Development Biology, National Research Institute for Child Health and Development, Setagaya-ku, Tokyo, Japan

Yusaku Miyamae Graduate School of Life and Environmental Sciences, University of Tsukuba, Tsukuba, Ibaraki 305-8572, Japan

Shohei Miyamoto University of Miyazaki, Miyazaki 889-2192, Japan

Sayumi Miyauchi University of Miyazaki, Miyazaki 889-2192, Japan

Jun-ichi Miyazaki Division of Stem Cell Regulation Research, Graduate School of Medicine, Osaka University, Suita, Osaka 565-0871, Japan

Hiroshi Mizokami The Chemo-Sero-Therapeutic Research Institute, Kikuchi Research Center, Kumamoto University, Kikuchi, Kumamoto 869-1298, Japan

Yohei Mizuguchi Department of Applied Biological Science, Tokyo University of Agriculture and Technology, Fuchu, Tokyo 183-8509, Japan, m_yohei_@hotmail.co.jp

Koko Mizumachi Functional Biomolecules Research Team, National Institute of Livestock and Grassland Science, Tsukuba, Ibaraki 305-0901, Japan

Hiroshi Mizumoto Department of Chemical Engineering, Kyushu University, Nishi-ku, Fukuoka 819-0395, Japan

Tetsunosuke Mochizuki Department of Applied Biological Chemistry, Graduate School of Agricultural and Life Sciences, The University of Tokyo, Bunkyo-ku, Tokyo 113-8657, Japan

Manami Monobe National Institute of Vegetable and Tea Science, NARO, Shizuoka, Japan, monobe@affrc.go.jp

Tomio Morino Nanotherapy Co., Ltd, Nagoya, 451-0044 Japan

Shinkatsu Morisawa Nihon Trim co. LTD, Osaka, Osaka 531-0076, Japan

Shinji Morishita ASTEC Corporation, Shime-machi, Fukuoka 811-2207, Japan

Jun Motoyama Graduate School of Engineering, Nagoya University, Nagoya, 464-8603 Japan

Duen Gang Mou Biotechnology Program, Malaysia University of Science and Technology, Kelana Jaya, Selangor 47301, Malaysia

Kaori Mukae Graduate School of System Life Sciences, Kyushu University, Higashi-ku, Fukuoka 812-8581, Japan

Yusuke Mukai Department of Biological and Chemical Engineering, Gunma University, Kiryu, Japan

Kiyoko Nagahama Miyazaki prefectural industrial support foundation, Miyazaki 880-0303, Japan

Eiji Nagamori Toyota Central R&D Labs. Inc., Aichi 480-1192, Japan, nagamori@mosk.tytlabs.co.jp

Teruyuki Nagamune Department of Chemistry and Biotechnology, School of Engineering, The University of Tokyo, Bunkyo-ku, Tokyo 113-8656, Japan; Department of Bioengineering, The University of Tokyo, Tokyo 113-8656, Japan

Takahiro Nagata Dojindo Laboratories, Mashiki-machi, Kumamoto 861-2202, Japan

Noboru Nakamichi Nihon Trim Co. Ltd., Osaka 531-0076, Japan; Functional Water Cell Analysis Center Co. Ltd., Fukuoka 812-0013, Japan

Shigeki Nakamura The Cell Engineering Center, Kitakyushu National College of Technology, Kitakyushu-shi, Fukuoka, 802-0985, Japan

Manami Nakamura Department of Applied Biological Science, Tokyo University of Agriculture and Technology, Fuchu, Tokyo 183-8509, Japan

Takuro Nakamura Department of Genetic Resources Technology, Kyushu University, Fukuoka, Fukuoka 812-8581, Japan

Shigeki Nakamura The Cell Engineering Center, Kitakyushu National College of Technology, Kitakyushu-shi, Fukuoka, 802-0985, Japan

Kensuke Nakanishi Department of Genetic Resources Technology, Kyushu University, Fukuoka, Fukuoka 812-8581, Japan

Ayumi Nakano Graduate School of Bioresource and Bioenvironmental Sciences, Kyushu University, Fukuoka, Japan

Yuki Nakashima Ehime University, Matsuyama, Ehime 790-8566, Japan

Naomi Nakatani Research and Development Laboratory, Nipro Corporation, Kusatsu-shi, Shiga 525-0055, Japan

Kohji Nakazawa Department of Life and Environment Engineering, The University of Kitakyushu, Kitakyushu, Fukuoka 808-0135, Japan, nakazawa@env.kitakyu-u.ac.jp

Satoshi Neki Department of Bioscience and Biotechnology, Okayama University, Okayama, Japan

Michelle Y.T. Ng Institute of Bioscience, Universiti Putra Malaysia, Selangor Darul Ehsan, Malaysia

Akitomo Niho Graduate School of Systems Life Sciences, Kyushu University, Fukuoka, Japan

Sogo Nishimoto Center for Marine Environmental Studies (CMES), Ehime University, Matsuyama, Ehime 790-8577, Japan, niss@agr.ehime-u.ac.jp

Takuya Nishimoto Graduate School of Bioresource and Bioenvironmental Sciences, Kyushu University, Fukuoka, Japan

Atsuyoshi Nishina Gunma Industrial Technology Center, Maebashi, Japan

Norikazu Nishino Graduate School of Life Science and Systems Engineering, Kyushu Institute of Technology, Kitakyushu-shi, Fukuoka, 808-0196, Japan

Kiyoto Nishiyama The Chemo-Sero-Therapeutic Research Institute, Kikuchi Research Center, Kikuchi, Kumamoto 869-1298, Japan

Kensaku Numata Department of Chemical Engineering, Faculty of Engineering, Kyushu University, 744 Motooka, Nishi-ku, Fukuoka 819-0395, Japan

Takahiro Ogata ASTEC Corporation, Shime-machi, Fukuoka 811-2207, Japan

Akiko Ogawa Department of Chemistry and Biochemistry, Suzuka National College of Technology, Suzuka, Mie 510-0294, Japan

Kikumi Ogihara Department of Pathology, Azabu University, Sagamihara, Kanagawa 229-8501, Japan

Ayako Ohshima Bio Process Research and Development Laboratories, Production Division, Kyowa Hakko Kirin Co., Ltd., Takasaki-shi, Gunma 370-0013, Japan

Takashi Ohtsuki Graduate School of Natural Science and Technology, Okayama University, Okayama, Japan; Department of Bioscience and Biotechnology, Okayama University, Okayama, Japan

Masaaki Okabe Center for Marine Environmental Studies (CMES), Ehime University, Matsuyama, Ehime 790-8577, Japan, okabema@agr.ehime-u.ac.jp

Yoshiharu Okamoto Department of Veterinary Clinical Medicine, School of Veterinary Medicine, Tottori University, Koyama-Minami, Tottori, Japan

Kazuhiro Osada Department of Genetic Resources Technology, Kyushu University, Fukuoka 812-8581, Japan

Mitsuo Oshimura Department of Human Genome Science, Graduate School of Medical Science, Tottori University, Yonago, Tottori 683-8503, Japan

Fujiko Ozawa SCIVAX Corporation, Kawasaki, Japan

Yamada Parida Alliance for Research on North Africa, University of Tsukuba, Tsukuba, Ibaraki 305-8572, Japan

Carlos Alberto Penno Graduate School of Systems Life Science, Kyushu University, Fukuoka 819–0395, Japan

Xianying Ren Department of Human Genome Science, Graduate School of Medical Science, Tottori University, Yonago, Tottori 683-8503, Japan

Toshihiko Saheki Department of Biological and Chemical Engineering, Gunma University, Kiryu, Japan, saheki@chem-bio.gunma-u.ac.jp

Ken'ichi Saito Department of Biological and Chemical Engineering, Gunma University, Kiryu, Japan

Hiroyuki Saitoh Bio Process Research and Development Laboratories, Production Division, Kyowa Hakko Kirin Co., Ltd., Takasaki-shi, Gunma 370-0013, Japan

Shinji Sakae Bioprocess Research and Development Laboratories, Kyowa Hakko Kirin Co., LTD., Takasaki-shi, Gunma 370-0013, Japan

Mitsuhiro Sakai Kurume City Office, Kurume, Fukuoka 830-8520, Japan

Yusuke Sakai Department of Life and Environment Engineering, The University of Kitakyushu, Fukuoka 808-0135, Japan

Takanori Sakai ASTEC Corporation, Shime-machi, Fukuoka 811-2207, Japan

Yoichi Sakakibara Department of Biochemistry and Applied Biosciences, University of Miyazaki, Miyazaki 889-2192, Japan

Shunpei Sato Department of Genetic Resources Technology, Kyushu University, Fukuoka, Fukuoka 812-8581, Japan

Hideo Satsu Department of Applied Biological Chemistry, Graduate School of Agricultural and Life Sciences, The University of Tokyo, Bunkyo-ku, Tokyo 113-8657, Japan

Hideyuki Shigemori Graduate School of Life and Environmental Sciences, University of Tsukuba, Tsukuba, Ibaraki 305-8572, Japan

Yuko Shigihara Department of Applied Biological Science, Tokyo University of Agriculture and Technology, Fuchu, Tokyo 183-8509, Japan

Jun Shimizu Department of Clinical Dietetics and Human Nutrition, Josai University, Sakado-shi, Saitama 350-0295, Japan

Kazunori Shimizu Toyota Central R&D Labs. Inc., Aichi 480-1192, Japan

Makoto Shimizu Department of Applied Biological Chemistry, Graduate School of Agricultural and Life Sciences, The University of Tokyo, Bunkyo-ku, Tokyo 113-8657, Japan, ams316@mail.ecc.u-tokyo.ac.jp

Yukako Shinmura Department of Life and Environment Engineering, University of Kitakyushu, Kitakyushu, Fukuoka 808-0135, Japan

Nobuyoshi Shiojiri Department of Biology, Shizuoka University, Suruga-ku, Shizuoka-City, Shizuoka 422-8529, Japan, sbnshio@ipc.shizuoka.ac.jp

Sanetaka Shirahata Faculty of Agriculture, Kyushu University, Higashi-ku, Fukuoka 812-8581, Japan, sirahata@grt.kyushu-u.ac.jp

Akio Shirasu Research and Development Laboratory, Nipro Corporation, Kusatsu-shi, Shiga 525-0055, Japan

Masahiko Sisido Graduate School of Natural Science and Technology, Okayama University, Okayama, Japan; Department of Bioscience and Biotechnology, Okayama University, Okayama, Japan

Marsha Smith Functional Genomics, Discovery Technologies, Schering-Plough Research Institute, Kenilworth, NJ 07033, USA

Kenji Soejima The Chemo-Sero-Therapeutic Research Institute, Kikuchi Research Center, Kumamoto University, Kikuchi, Kumamoto 869-1298, Japan

Takahiro Sogo Department of Chemistry and Biotechnology, School of Engineering, The University of Tokyo, Bunkyo-ku, Tokyo 113-8656, Japan

Shuji Sonezaki Biotechnology Group, Research Institute, TOTO LTD., Kitakyushu-city, Fukuoka, 802-8601, Japan, shuji.sonezaki@toto.co.jp

Takuya Sugahara Ehime University, Tarumi, Matsuyama 790-8566, Japan

Keishin Sugawara The Chemo-Sero-Therapeutic Research Institute, Kikuchi Research Center, Kumamoto University, Kikuchi, Kumamoto 869-1298, Japan

Toshihiro Sugiyama Department of Biochemistry, Akita University, School of Medicine, Akita, Japan

Masahito Suiko Department of Biochemistry and Applied Biosciences, University of Miyazaki, Miyazaki 889-2192, Japan

Toshiyuki Suzawa Bioprocess Research and Development Laboratories, Kyowa Hakko Kirin Co., LTD., Takasaki-shi, Gunma 370-0013, Japan

Chise Suzuki Functional Biomolecules Research Team, National Institute of Livestock and Grassland Science, Tsukuba, Ibaraki 305-0901, Japan

Hirofumi Tachibana Bio-Architecture Center, Kyushu University, Higashi-ku, Fukuoka 812-8581, Japan, tatibana@agr.kyushu-u.ac.jp

Emi Tajima Department of Biological and Chemical Engineering, Gunma University, Kiryu, Japan

Ken Takahashi Bioprocess Research and Development Laboratories, Kyowa Hakko Kirin Co., LTD., Takasaki-shi, Gunma 370-0013, Japan

Eiji Takahashi Bioprocess Research and Development Laboratories, Kyowa Hakko Kirin Co., LTD., Takasaki-shi, Gunma 370-0013, Japan

Kyoko Takahashi Department of Food Science and Technology, College of Bioresource Sciences, Nihon University, Fujisawa-shi, Kanagawa 252-8510, Japan

Saori Takahashi Institute for Food and Brewing, Akita Prefectural Agricultural, Forestry, and Fisheries Research Center, Araya-machi, Akita 010-1623, Japan

Yumiko Takamatsu Bio Process Research and Development Laboratories, Production Division, Kyowa Hakko Kirin Co., Ltd., Takasaki-shi, Gunma 370-0013, Japan

T. Tamura Vessel Inc., Japan

Wen Siang Tan Department of Microbiology, Universiti Putra Malaysia, Selangor Darul Ehsan, Malaysia

Hisaya Tanaka Bio Process Research and Development Laboratories, Production Division, Kyowa Hakko Kirin Co., Ltd., Takasaki-shi, Gunma 370-0013, Japan

Satoru Tanaka SCIVAX Corporation, Kawasaki, Japan

Akito Tanoue Department of Pharmacology, National Research Institute for Child Health and Development, Setagaya-ku, Tokyo, Japan

Masahito Taya Division of Chemical Engineering, Graduate School of Engineering Science, Osaka University, Toyonaka, Osaka 565-0871, Japan

Satoshi Terada Department of Applied Chemistry and Biotechnology, University of Fukui, Fukui 910-8507, Japan

Masashi Teramori Department of Chemical Engineering, Faculty of Engineering, Kyushu University, 744 Motooka, Nishi-ku, Fukuoka 819-0395, Japan

Kiichiro Teruya Graduate School of Systems Life Sciences, Kyushu University, Higashi-ku, Fukuoka 812-8581, Japan; Department of Genetic Resources Technology, Faculty of Agriculture, Kyushu University, Fukuoka, Fukuoka 812-8581, Japan; Graduate School of Bioresource and Bioenvironmental Sciences, Kyushu University, Fukuoka, Japan

Beng Ti Tey Institute of Bioscience, Universiti Putra Malaysia, Selangor Darul Ehsan, Malaysia; Department of Chemical and Environmental Engineering, Faculty of Engineering, Universiti Putra Malaysia, 43400 UPM Serdang, Selangor, Malaysia, btey@eng.upm.edu.my

Huaize Tian Department of Genetic Resources Technology, Kyushu University, Fukuoka 812-8581, Japan

Kazuko Toh Department of Genetic Resources Technology, Kyushu University, Fukuoka, Fukuoka 812-8581, Japan

Kosuke Tomimatsu Graduate School of Systems Life Sciences, Kyushu University, Higashi-ku, Fukuoka 812-8581, Japan

Shiori Tominaga Ehime University, Matsuyama, Ehime 790-8566, Japan, shiori-t@agr.ehime-u.ac.jp

Mamoru Totsuka Department of Applied Biological Chemistry, Graduate School of Agricultural and Life Sciences, The University of Tokyo, Bunkyo-ku, Tokyo 113-8657, Japan

Jyunji Tottori Kurume City Office, Kurume, Fukuoka 830-8520, Japan

Yung-Shyeng Tsao Protein Expression Technologies, BSPD, Merck Research Laboratories, Union, NJ 07083, USA, yung-shyeng.tsao@merck.com

Soninkhishig Tsolmon Graduate School of Life and Environmental Sciences, University of Tsukuba, Tsukuba, Ibaraki 305-8572, Japan

Takeshi Tsuka Department of Veterinary Clinical Medicine, School of Veterinary Medicine, Tottori University, Koyama-Minami, Tottori, Japan

Yuriko Tsukamoto Graduate School of Life Science and Systems Engineering, Kyushu Institute of Technology, Kitakyushu-shi, Fukuoka, 808-0196, Japan

Asuka Uchida Miyazaki prefectural industrial support foundation, Miyazaki 880-0303, Japan

Miyako Udono Graduate School of Bioresource and Bioenvironmental Sciences, Kyushu University, Higashi-ku, Fukuoka 812-8581, Japan

Hiroshi Ueda Department of Chemistry and Biotechnology, The University of Tokyo, Tokyo 113-8656, Japan

Masashi Ueno Graduate School of Bioresource and Bioenvironmental Sciences, Kyushu University, Fukuoka, Japan

Akihiro Umezawa Department of Reproductive Biology, National Research Institute for Child Health and Development, Setagaya-ku, Tokyo, Japan

Myra O. Villareal Graduate School of Life and Environmental Sciences, University of Tsukuba, Tsukuba, Ibaraki 305-8572, Japan

Kaori Wakamatu Graduate School of Engineering, Gunma University, Tenjin-cho, Kiryu-shi 376-8515, Japan

Masako Wakitani Bioprocess Research and Development Laboratories, Kyowa Hakko Kirin Co., LTD., Takasaki-shi, Gunma 370-0013, Japan

Thomas T.Y. Wang Diet, Genomics and Immunology Laboratory, Beltsville Human Nutrition Research Center, Agricultural Research Service, USDA, Beltsville, MD, USA

Ying Wang Department of Geriatrics and Cardiovascular Sciences, Central Hospital of Changchun, Changchun, Jilin 130051, China

Hiroyuki Wariishi Bio-Architecture Center, Kyushu University, Higashi-ku, Fukuoka 812-8581, Japan

Koji Yamada Department of Bioscience and Biotechnology, Kyushu University, Higashi-ku, Fukuoka 812-8581, Japan

Hidetoshi Yamada Department of Human Genome Science, Graduate School of Medical Science, Tottori University, Yonago, Tottori 683-8503, Japan

Parida Yamada Alliance for Research on North Africa, Universitiy of Tsukuba, Tsukuba, Ibaraki 305-8572, Japan

Koji Yamada Kyushu University, Higashi-ku, Fukuoka 812-8581, Japan

Masanori Yamaguchi Hokko Chemical Industry Co., Ltd, Atsugi, Kanagawa 243-0023, Japan

Osayoshi Yamaguchi University of Miyazaki, Miyazaki 889-2192, Japan

Hideki Yamaji Department of Chemical Science and Engineering, Graduate School of Engineering, Kobe University, Nada, Kobe 657-8501, Japan, btey@eng.upm.edu.my

Kunihito Yamamori University of Miyazaki, Miyazaki 889-2192, Japan

Koichi Yamamot Bio Process Research and Development Laboratories, Production Division, Kyowa Hakko Kirin Co., Ltd., Takasaki-shi, Gunma 370-0013, Japan

Yasunori Yamamoto Graduate School of Systems Life Sciences, Kyushu University, 744 Motooka, Nishi-ku, Fukuoka 819-0395, Japan, yyamamoto@chem-eng.kyushu-u.ac.jp

Ai Yamamoto Department of Applied Biological Science, Tokyo University of Agriculture and Technology, Fuchu, Tokyo 183-8509, Japan

Makoto Yamanaka Graduate School of Life Science and Systems Engineering, Kyushu Institute of Technology, Kitakyushu-shi, Fukuoka, 808-0196, Japan

Makiko Yamashita Department of Genetic Resources Technology, Faculty of Agriculture, Kyushu University, Higashi-ku, Fukuoka 812-8581, Japan; Graduate School of Systems Life Sciences, Kyushu University, Fukuoka, Japan

Noriyuki Yamashita Nanotherapy Co., Ltd, Nagoya, 451-0044 Japan

Satoshi Yamauchi Ehime University, Matsuyama, Ehime 790-8566, Japan

Manami Yamawaki Ehime University, Matsuyama, Ehime 790-8566, Japan

Hanxu Yan Graduate School of System Life Science, Kyushu University, Fukuoka 812-0053, Japan

Keiichi Yano Bioprocess Research and Development Laboratories, Kyowa Hakko Kirin Co., LTD., Takasaki-shi, Gunma 370-0013, Japan

Satomi Yano Kyushu University, Higashi-ku, Fukuoka 812-8581, Japan

Kah- Choon Yap Department of Chemical and Environmental Engineering, Universiti Putra Malaysia, Selangor Darul Ehsan, Malaysia

Takashi Yasuda Graduate School of Life Science and Systems Engineering, Kyushu Institute of Technology, Kitakyushu-shi, Fukuoka, 808-0196, Japan

Shin Yasuda Department of Bioscience, School of Agriculture, Tokai University, Aso, Kumamoto 869-1404 Japan

Koichiro Yori Department of Biology, Shizuoka University, Suruga-ku, Shizuooka-City, Shizuoka 422-8529, Japan

Tadashi Yoshida Fujicco Co., Ltd, Kobe, Hyogo 650-8558, Japan; Department of Applied Biological Science, Tokyo University of Agriculture and Technology, Fuchu, Tokyo 183-8509, Japan, tyoshi@cc.tuat.ac.jp

Ken-ichi Yoshida Graduate School of Agriculture Science, Kobe University, Nada-ku, Kobe, Hyogo 657-8501, Japan

Yoshihiko Yoshikawa Research and Development Laboratory, Nipro Corporation, Kusatsu-shi, Shiga 525-0055, Japan

Purification of Hepatoblasts from Fetal Mouse Livers by Using a Temperature-Reversible Gelation Polymer and Their Application in Regenerative Medicine

Purification of Hepatoblasts and Their Application in Regenerative Medicine

Koichiro Yori, Toru Koike and Nobuyoshi Shiojiri

1 Introduction

Hepatoblasts are liver progenitor cells generating both mature hepatocytes and biliary epithelial cells during fetal development, dependent on their positions placed in the liver (Fig. 1) [4]. They also have a remarkable growth potential during liver development [3]. The use of hepatoblasts and adult hapatocytes as cell sources in hybrid-type artificial liver models may allow to maintain their hepatic functions for longer periods, in which dying mature hepatocytes could be replaced by hepatocytes differentiated from hepatoblasts. Hepatoblasts can also be useful for cell transplantation therapy in regenerative medicine.

The thermo-reversible gelation polymer called Mebiol gel is a chemically synthesized biocompatible material. It is soluble below a lower critical solution temperature (LCST) and becomes solid above the LCST [8]. Within the gelation polymer, epithelial cells can grow whereas fibroblastic cells cannot survive because the latter cannot use the polymer as an anchorage. Because mammalian fetal livers contain various kinds of nonparenchymal cells such as hepatic stellate cells, endothelial cells and hemopoietic cells, the gelation polymer may be useful to separate hepatoblasts or hepatocytes from the nonparenchymal cells.

In the present study, we applied the gelation polymer to separate hepatoblasts or hepatocytes from nonparenchymal cells in cell suspensions of fetal mouse livers. As a result, the separation was successful and highly pure and viable hepatocyte preparations were obtained with a high recovery rate after culturing fetal mouse liver cells in the gelation polymer for 3 or 5 days. While hepatoblasts gave rise to

N. Shiojiri (✉)
Department of Biology, Shizuoka University, Suruga-ku, Shizuoka-City, Shizuoka 422-8529, Japan
e-mail: sbnshio@ipc.shizuoka.ac.jp

M. Kamihira et al. (eds.), *Animal Cell Technology: Basic & Applied Aspects*, Animal Cell Technology: Basic & Applied Aspects 16, DOI 10.1007/978-90-481-3892-0_1,

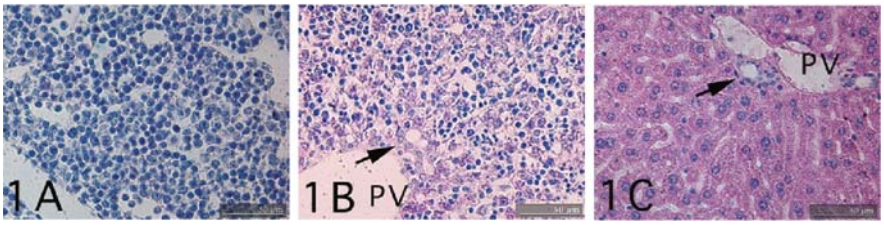

Fig. 1 Histogenesis of the mouse liver. (**A**) E12.5 liver. (**B**) E17.5 liver. (**C**) Adult liver. E12.5 liver is a hemopoietic organ, in which hemopoietic cells are abundant. Arrow indicates a bile duct or its precursor. H-E staining

hepatocytes within an authentic Mebiol gel, they differentiated into biliary epithelial cells forming cystic structures and expressing no hepatocyte marker in the presence of basal laminar components.

2 Materials and Methods

Cell culture and purification of hepatoblasts Briefly, E12.5 livers of C3H/HeSlc strain mice were diced and treated with dispase (1000 U/mL) (Godo Shusei) for 30 min at 37°C. The liver specimens were subsequently dispersed into single cells by pipetting, and filtrated through a nylon mesh filter. The filtrate was washed twice by centrifugation. The resulting cellular pellet was resuspended at a cell density of 7 10^6 cells/mL in thermo-reversible gelation polymer (Mebiol) containing DM-160 supplemented with 10% fetal calf serum. The gelation polymer containing fetal liver cells (10 μL) was placed and left for gelation on Teflon-coated glass slides (Ea Brown) at 37°C. Culture medium (60 μL) was then added on the gel. Basal laminar component gel (Matrigel; BD) was also mixed with the Mebiol gel. For reference, E12.5 liver cells were cultured on the glass slide without the gelation polymer. For isolation of cultured hepatoblasts/hepatocytes, the gelation polymer containing cultured cells was placed on ice to obtain its sol-condition. The resultant cell suspensions were filtrated by using a membrane filter (pore size 30 μm), and aggregates of fetal hepatoblasts/hepatocytes were trapped on the membrane filter. For immunohistochemistry, the cultured cells within the gelation polymer were fixed in a cold mixture of ethanol and acetic acid, and embedded in paraffin.

Immunohistochemistry. Hydrated sections were incubated for 1 h at room temperature with primary antibodies against alpha-fetoprotein (AFP), albumin, carbamoylphosphate synthase I (CPSI), HNF4α, cytokeratin, vimentin, desmin, PECAM-1, etc. After washing, sections were incubated with a Cy3 or fluorescein-labeled, species-specific donkey antibodies (Jackson ImmunoResearch Lab.) for 1 h at room temperature, washed again, and mounted.

RNA preparation and RT-PCR. Dissected livers were dissolved in TRIzol (Invitrogen) and total RNA was prepared according to the manufacturer's instructions. RT-PCR was performed as described [5]. Mouse β-actin mRNA was used as the internal control.

3 Results

3.1 Culture of E12.5 Liver Cells within Thermo-Reversible Gelation Polymer

When dispersed E12.5 liver cells were cultured in a Mebiol gel, hepatoblasts rapidly aggregated and formed spheroid structures on day 1 (Fig. 2). Nonparenchymal cells persisted to be dispersed in the gel. With culture, the hepatoblast spheroids enlarged and became compact and smoother on their surface (Fig. 2). When cultured liver cells on days 1 and 5 were immunohistochemically analyzed for their maturation, hepatoblasts gave rise to large hepatocytes, which expressed CPSI, albumin and AFP (Fig. 2). The contamination of nonparenchymal cells in the hepatoblast/hepatocyte aggregates was minimal on days 1 and 5; almost no positive immunoreactions of PECAM-1, desmin and vimentin were detected. Tissue sections stained for nuclei by DAPI showed that nuclei of hepatoblasts/hepatocytes were clearly positive, whereas those of nonparenchymal cells, which were recovered with hepatoblast/hepatocyte aggregates, were negative, suggesting that the latter may be dead.

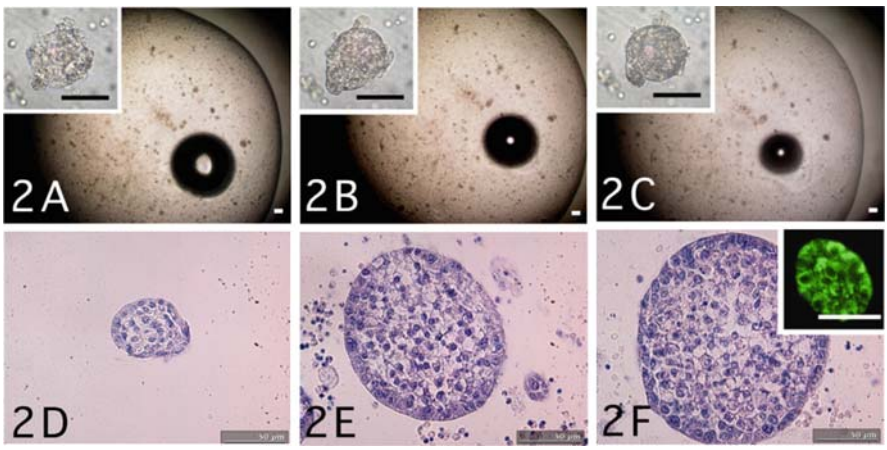

Fig. 2 Aggregate formation of E12.5 liver cells cultured in a Mebiol gel on days 1 (**A**, **D**), 3 (**B**, **E**) and 5 (**C**, **F**). (**A**-**C**) Phase-contrast micrographs. (Insets in **A**-**C**) Magnified view of hepatoblast/hepatocyte aggregates. (**D**-**F**) H-E staining. (Inset in **F**) Immunofluorescence of CPSI. Hepatoblasts form spherical aggregates and give rise to large hepatocytes expressing CPSI in a Mebiol gel on day 5. Bars in 2A-C indicate 100 μm. Bars in 2D-F indicate 50 μm

RT-PCR analysis of mRNAs for hepatocyte or nonparenchymal cell marker genes demonstrated that hepatocyte maturation proceeded well and nonparenchymal cells grew poorly or expressed very low levels of desmin, vimentin and PECAM-1 mRNAs in cultures of the fetal liver cells within the gelation polymer.

3.2 Separation of Cultured Fetal Hepatoblasts/Hepatocytes from Nonparenchymal Cells

After 3 or 5 days of culture within a gelation polymer, E12.5 liver cells in a Mebiol solution on ice were filtrated by using a membrane filter (pore size 30 μm) (Fig. 3), and trapped aggregates on the membrane filter were analyzed for gene expression for liver-specific markers and contamination of nonparenchymal cells. Immunohistochemical analysis demonstrated that the contamination of nonparenchymal cells was minimal and the purity of hepatocytes was almost 100%. RT-PCR analysis also demonstrated that very few nonparenchymal cells were contained in the trapped hepatocytes. Nonparenchymal cell fractions that passed through the membrane filter expressed vimentin and desmin very poorly, suggesting that they were dead.

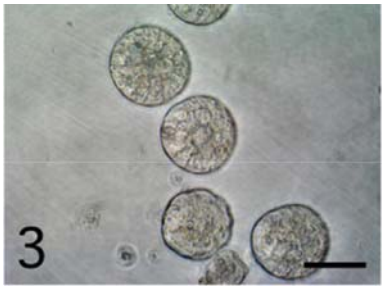

Fig. 3 Purified hepatoblast/hepatocyte aggregates through a membrane filter after culturing. E12.5 liver cells within a Mebiol gel for 5 days (Phase-contrast micrograph). Bar indicates 50 μm

3.3 Differentiation of Mature Hepatocytes from Hepatoblasts within Thermo-Reversible Gelation Polymer

The maturation state of differentiated hepatocytes cultured for 5 days within a Mebiol gel was further analyzed by using RT-PCR. Differentiated hepatocytes expressed CPSI, tyrosine aminotransferase, tryptophan oxygenase and glucose-6-phosphatase mRNAs as mature hepatocyte markers, the levels of which were much higher than those of E17.5 livers. Especially the expression of glucose-6-phosphase mRNA was close to that of adult livers. The level of their AFP mRNA expression also declined under that of E12.5 livers. These data showed that the differentiated hepatocytes were close to adult hepatocytes in maturation.

3.4 Induction of Biliary Cell Differentiation from Hepatoblasts with Basal Laminar Components

When E12.5 liver cells were cultured within a Mebiol gel containing 10–30% Matrigel, hepatoblasts formed cyst structures of various sizes with large lumina on day 1, and these structures persisted in culture through day 5 (Fig. 4). The growth of nonparenchymal cells was minimal, but some viable cells were present in these cultures. Immunohistochemical analyses showed that approximately 20% epithelial cells forming cystic structures did not express HNF4 (Fig. 4), although large hepatocytes also differentiated. RT-PCR analyses demonstrated that the expression of mature hepatocyte markers (CPSI and HNF4 mRNAs) was downregulated.

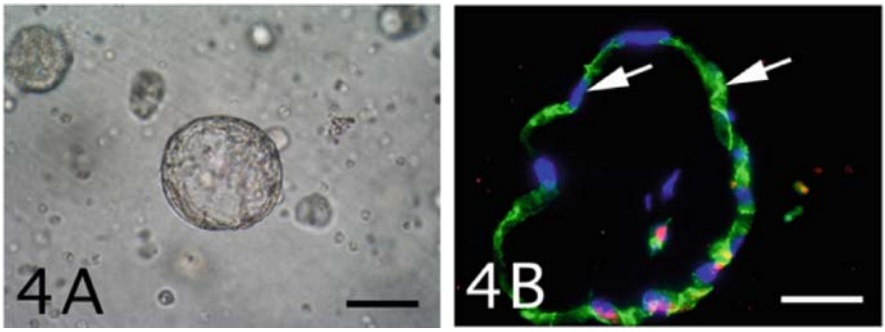

Fig. 4 Induction of biliary cell differentiation from hepatoblasts by basal laminar components. E12.5 liver cells were cultured in a Mebiol gel containing Matrigel (20%). (**A**) Phase-contrast micrograph of a cystic structure on day 5. (**B**) Double immunofluorescence of HNF4α (*red*) and cytokeratins (*green*). HNF4α-negative epithelial cells are observed in a cystic structure on day 5 (*arrows*). Blue, DAPI staining. PV, portal vein. Bars indicate 50 μm

4 Discussion

In the present study, we succeeded in isolation of hepatoblasts/hepatocytes in E12.5 liver cell suspensions with high recovery rate and purity by using a thermoreversible gelation polymer. Purified hepatocytes were highly viable and expressed liver-specific markers, although their growth was very limited in our standard culture condition without the conditioned medium or growth factors (data not shown). Our separation protocol is simpler and more efficient to purify fetal hepatoblasts/hepatocytes from fetal liver cell suspensions than other protocols using antibodies against E-cadherin or Dlk [2,7], although it takes 3 or 5 days to make their compact spheroids that can be trapped on the membrane filter used. However, the protocol does not include any antibody treatment and can also minimize protease treatment, which leads to a higher viability of hepatoblasts/hepatocytes.

It is noteworthy that hepatoblasts could give rise to mature hepatocytes without nonparenchymal cells within a Mebiol gel. We do not precisely know at present why nonparenchymal cells died in the gel. Nonparenchymal cells could adhere to hepatoblast aggregates for their survival, which did not occur in the gel. The three-dimensional structures (shapes) of mature hepatocytes have been demonstrated to be important in their gene expression, and cytoskeletal structures play an important role in this phenomenon [1]. Thus, the formation of spheroidal structures of hepatoblast/hepatocyte aggregates may work positively for their maturation. Nonparenchymal cells can also help hepatoblasts to make three-dimensional structures in vivo. As our preliminary data showed that the presence of the conditioned medium of E12.5 liver cells dramatically stimulated the growth of hepatoblasts (data not shown), soluble factors produced by nonparenchymal cells may play an important role in hepatoblast growth in vivo.

We also induced biliary cell differentiation in hepatoblasts by using basal laminar components, which agrees well with the data showing that fetal liver progenitor cell lines can construct cystic structures, responding to basal laminar components [6]. However, it still remains to be analyzed which molecules in basal laminar components are important, or whether other extracellular matrix components have a bile duct-inducing potency. These are questions to be resolved in the future.

In any event, our protocol for isolation of liver progenitor cells may be useful for their cell transplantation therapy, and our culture conditions controlling differentiation of hepatoblasts may be applicable to the development of a hybrid-type artificial liver model, in which adult hepatocytes and fetal hepatoblasts were incorporated.

References

1. Ikeda, T., Sawada, N., Satoh, M., and Mori, M. (1998) Induction of tyrosine aminotransferase of primary cultured rat hepatocytes depends on the organization of microtubules. *J. Cell Physiol*. **175**: 41–49.
2. Nitou, M., Sugiyama, Y., Ishikawa, K., and Shiojiri, N. (2002) Purification of fetal mouse hepatoblasts by magnetic beads coated with monoclonal anti-E-cadherin antibodies and their in vitro culture. *Exp. Cell Res*. **279**: 330–343.
3. Oertel, M., Menthena, A., Chen, Y., Teisner, B., Jensen, C., and Shafritz, D. (2008) Purification of fetal liver stem/progenitor cells containing all the repopulation potential for normal adult rat liver. *Gastroenterology* **134**: 823–832.
4. Shiojiri, N. (1997) Development and differentiation of bile ducts in the mammalian liver. *Microsc. Res. Tech*. **39**: 328–335.
5. Suzuki, A., Sekiya, S., Büscher, D., Izpisúa Belmonte, J.C., and Taniguchi, H. (2008) Tbx3 controls the fate of hepatic progenitor cells in liver development by suppressing p19ARF expression. *Development* **135**: 1589–1595.
6. Tanimizu, N., Miyajima, A., and Mostov, K.E. (2007) Liver progenitor cells develop cholangiocyte-type epithelial polarity in three-dimensional culture. *Mol. Cell Biol*. **18**: 1472–1479.
7. Tanimizu, N., Nishikawa, M., Saito, H., Tsujimura, T., and Miyajima, A. (2003) Isolation of hepatoblasts based on the expression of Dlk/Pref-1. *J. Cell Sci*. **116**: 1775–1786.
8. Yoshioka, H., Mikami, M., Mori, Y., and Tsuchida, E. (1994) A synthetic hydrogel with thermoreversible gelation. II. Effect of added salts. *J. Macromol. Sci*. **A31**: 121–125.

Computer Aided Rational Design of Biochemical Systems

Hiroyuki Kurata

1 Introduction

Goals of systems biotechnology are to construct a biochemical network map within a cell, to analyze the mechanism of how a molecular architecture generates particular cellular functions, and to rationally design a biochemical network for an engineering purpose [1]. To effectively perform such analysis and design, we have developed the comprehensive software suit, CADLIVE (Computer Aided Design of LIVing systEms), that consists of a network constructor [2], database, a pathway search module for virtual knockout mutants [3], an automatic layout module for drawing a large-scale network map [4], and a dynamic simulator with an optimizer [5]. The CADLIVE network constructor is a computational tool for drawing a large-scale map of biochemical networks and for registering their associated regulator-reaction equations (RREs). CADLIVE improves on Kohn's Molecular Interaction Map notation for dynamic simulation [6], which describes biochemical networks in a form that can be readily processed by both computers and humans. We have developed the dynamic simulator that provides a rule-based automatic way to convert biochemical network maps into mathematical models, which enables simulating their dynamics without going all the reactions down to the details of exact kinetic parameters. The simulator has a powerful optimizer that adjusts the dynamic model to experimental data.

In this paper, we introduce the CADLIVE system and apply it to the system analysis of complex regulation networks.

H. Kurata (✉)
Department of Bioscience and Bioinformatics, Kyushu Institute of Technology, Iizuka, Fukuoka 820-8502, Japan
e-mail: kurata@bio.kyutech.ac.jp

M. Kamihira et al. (eds.), *Animal Cell Technology: Basic & Applied Aspects*, Animal Cell Technology: Basic & Applied Aspects 16, DOI 10.1007/978-90-481-3892-0_2,

2 Methods

2.1 CADLIVE GUI Network Constructor

The CADLIVE network constructor is a software for drawing a large-scale map of biochemical networks and for registering their associated RREs in an extension of SBML [2, 3](Fig. 1). The RRE, Regulator (Modifier) (-0/->>/-II) Reactants -> Products, clearly shows the relationship between regulators and their regulated reactions and describes not only a mechanistic model but also a semantic model, i.e., a meaningful flow of signal transduction pathways. CADLIVE improves on Kohn's MIM notation for computer simulation [6], which describes signal transduction pathways and metabolic circuits in a form that can be readily processed by both computers and humans.

A major consideration in the CADLIVE's graphical notation is the capability to trace all known interactions of any given molecular species in the temporal order. Accordingly, each molecular species ideally appear only once in a diagram and all interactions involving those species should emanate from a single symbolic object.

Using the CADLIVE GUI network constructor, one is able to draw biochemical networks and to generate their associated regulator reaction equations (RREs).

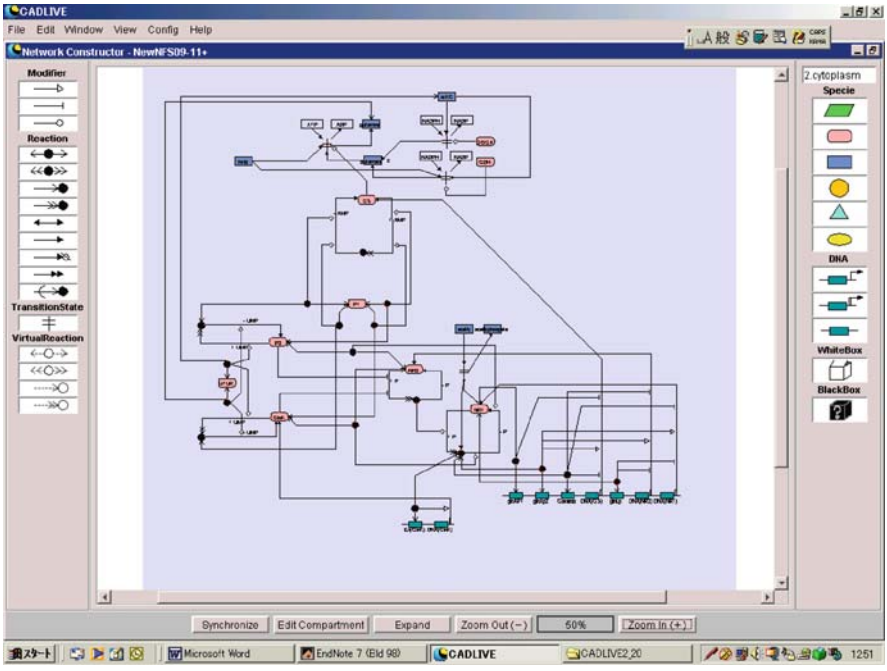

Fig. 1 CADLIVE GUI network constructor The ammonia assimilation network map

2.2 Automatic Layout System

Biochemical network maps are indispensable for an understanding of complex biochemical networks. Thus, CADLIVE implements an automatic layout program to draw a large-scale biochemical network map from RREs, which exhibits cluster structures clearly in relatively compact layout areas without any prior knowledge [4]. A network map is modeled as a system of interacting nodes on squared grids.

2.3 Pathway Search for a Virtual Knockout Mutants

We developed the pathway explorer, which is effective in exploring the flow of signals or mass in complex biochemical networks or in understanding molecular architectures, such as redundant pathways and feedback loops [3]. In addition, we developed the virtual knockout module that removes a target gene from a biochemical network, where the complexes and modified molecules derived from the target gene and the biochemical compounds catalyzed by the gene products are removed together. Combination of pathway search with virtual knockout function facilitates an understanding of the function of a target gene.

2.4 Dynamic Simulator with an Optimizer

A problem for dynamic simulation is that biochemical maps are not readily converted into a mathematical model, because the biochemical map is too complicated and heterogeneous and there are few kinetic parameters that have been measured in vivo. In order to overcome these problems, we presented the well-design rules that automatically convert a biochemical map into a mathematical model and developed the CADLIVE simulator that implements those rules to simulate and optimize the dynamics of biochemical models (Fig. 2) [5].

CADLIVE has a novel strategy, which divides a biochemical map into three layers and partitions the conversion process into two stages, with the well-designed conversion rules in an XML representation. Of course, the CADLIVE simulator supports biochemical maps generated by the GUI editor. In most biochemical networks, only a few kinetic parameters have been measured in vivo. To overcome this problem, the simulator implements the optimizer that tunes kinetic parameters by using a variety of genetic algorithms (GAs). In addition, Message Passing Interface (MPI) on Grid computing (Globus) is employed to achieve high-speed optimization.

2.5 Ammonia Assimilation System

The *E. coli* ammonia assimilation system consists of three layers: gene, protein, and metabolic layers (Fig. 1) [5]. In this system, glutamine and glutamate are synthesized by adding ammonia to 2-ketoglutarate by glutamine synthetase (GS),

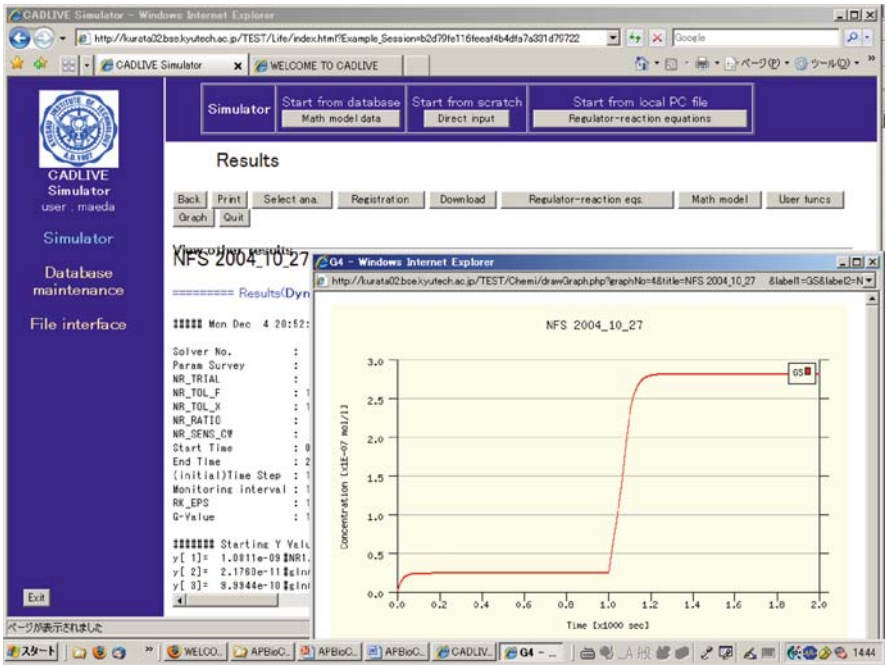

Fig. 2 CADLIVE dynamic simulator. A client-server model

glutamate synthase (GOGAT), and glutamate dehydrogenase (GDH). In the low concentration of ammonia, GS plays a major role in the ammonia assimilation. This system has multiple feedbacks that provide a robust property for the intracellular N/C ratio of the concentration of the nitrogen source (N) to that of the carbon source(C) against environmental stress. These feedbacks regulate the activity and synthesis of *glnA* (GS) and the transcription of nitrogen-regulated (*Ntr*) genes, *glnG* (NRI), *glnL* (NRII), *glnK* (GlnK) [7]. The PII protein plays a key role in regulation of such genes [8].

3 Results and Discussion

3.1 Mathematical Model Construction

We proposed the detailed mathematical model of the ammonia assimilation system at molecular interaction levels. We used the Two-Phase Partition (TPP) method to build mathematical model [5]. The TPP method divides the kinetics of molecular interactions into two phases, the molecular binding phase and the reaction phase. The mathematical model of this system consists of 53 algebraic equations (binding phase) and 19 differential equations (reaction phase). In order to build dynamic

models, it is required to adjust the kinetic parameters to experimental data. But the values of most kinetic parameters have not been measured because of experimental difficulties. Thus, we optimized parameters by using genetic algorithms.

3.2 Dynamic Simulation

We simulated the time course of the ammonia assimilation system, where the ammonia concentration decreased to one tenth on 1000 min. The ratio of the glutamine concentration to the 2-ketoglutarate concentration (N/C ratio) was maintained in a low ammonia concentration, indicating that the N/C ratio shows robustness against a changing ammonia concentration (Fig. 3).

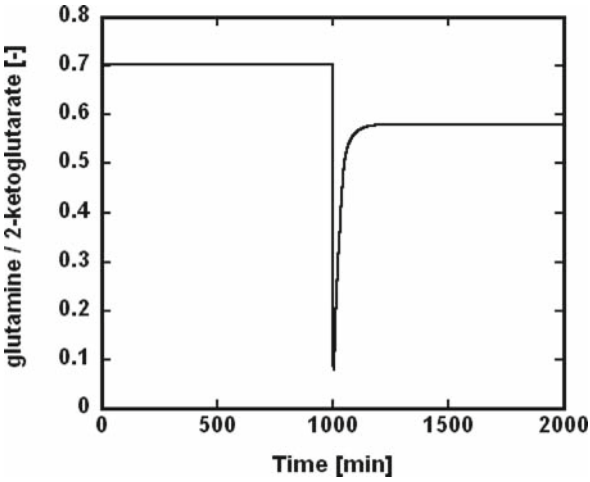

Fig. 3 Simulated time course of the N/C ratio.The ammonia concentration decreased to one tenth on 1000 min

We compared the simulated results of various knockout mutants with the experimental data, where the GS concentrations were simulated under ammonia-rich or ammonia-limiting medium. These simulations not only reproduced the typical dynamic features of wild type but also agreed with the experimental behaviors of many knockout mutants, Δ*glnG* (NRI), Δ*glnL* (NRII), Δ*glnD* (UTUR), Δ*glnB* (PII), and Δ*glnK* (GlnK). These results demonstrate the validity of the dynamic model [7].

3.3 System Analysis

Using the validated model predicted the physiological role of glnK. GlnK is the homolog of PII and the transcription regulation is different, but the physiological function remains to be elucidated [9]. The simulated result showed that GlnK was

involved in the hysteresis of the Ntr gene expressions with respect to the ammonia concentration. The hysteresis is caused by a positive feedback that consists of *glnAp2* (Enhancer) and *glnG*. On the other hand, the effect of the positive feedback is suppressed by *glnK*. The hysteresis appeared very clearly in the *glnK* knockout model, and did not appear in the *glnK* overexpression model. We predicted that the *glnK* gene is responsible for hysteresis or reversibility of *Ntr* gene expressions with respect to the ammonia concentration, demonstrating the molecular mechanism for the experimental observation of the runaway expression of the *Ntr* genes.

Acknowledgements This work was supported by KAKENHI (Grant-in-Aid for Scientific Research) on Priority Areas "Systems Genomics" from the Ministry of Education, Culture, Sports, Science and Technology of Japan and partially by KAKENHI (Grant-in-Aid for Scientific Research (B), 2006, 18300098).

References

1. Nishio, Y., Usuda, Y., Matsui, K., and Kurata, H. (2008) Computer-aided rational design of the phosphotransferase system for enhanced glucose uptake in *Escherichia coli*. Mol. Syst. Biol. **4**: 160.
2. Kurata, H., Matoba, N., and Shimizu, N. (2003) CADLIVE for constructing a large-scale biochemical network based on a simulation-directed notation and its application to yeast cell cycle. Nucleic Acids Res. **31**: 4071–4084.
3. Kurata, H., Inoue, K., Maeda, K., Masaki, K., Shimokawa, Y., et al. (2007) Extended CADLIVE: A novel graphical notation for design of biochemical network maps and computational pathway analysis. Nucleic Acids Res. **35**: e134.
4. Li, W. and Kurata, H. (2005) A grid layout algorithm for automatic drawing of biochemical networks. Bioinformatics **21**: 2036–2042.
5. Kurata, H., Masaki, K., Sumida, Y., and Iwasaki, R. (2005) CADLIVE dynamic simulator: Direct link of biochemical networks to dynamic models. Genome Res. **15**: 590–600.
6. Kohn, K.W. (1999) Molecular interaction map of the mammalian cell cycle control and DNA Repair systems. Mol. Biol. Cell **10**: 2703–2734.
7. Ninfa, A.J., Jiang P., Atkinson M.R., and Peliska J.A. (2000) Integration of antagonistic signals in the regulation of nitrogen assimilation in *Escherichia coli*. Curr. Top. Cell Regul. **36**: 31–75.
8. Ninfa, A.J. and Atkinson, M.R. (2000) PII signal transduction proteins. Trends Microbiol. **8**: 172–179.
9. Blauwkamp, T.A. and Ninfa, A.J. (2002) Physiological role of the GlnK signal transduction protein of *Escherichia coli*: Survival of nitrogen starvation. Mol. Microbiol. **46**: 203–214.

DNA Microarray in Nutrigenomics and Cancer Prevention Research: Elucidating Molecular Signatures of Cancer Preventive Phytochemicals

Thomas T.Y. Wang

1 Introduction

Population and experimental studies have implicated dietary components in the prevention of prostate cancer [1, 2]. In particular, consumption of a diet that is rich in fruits, vegetables, and legumes is associated with a decreased risk for prostate and other forms of cancer [1, 2]. Hence, there is much interest in pursuing the development of food-derived products or compounds as chemopreventive agents due to their expected safety and the fact that they are not perceived as medicine per se [2]. However, the molecular targets of phytochemicals, as well as the mechanisms that contribute to their beneficial effects on cancer, remain elusive. Further elucidation of the molecular targets, i.e. molecular signatures and mechanisms, would be important in understanding their cancer preventive properties. In our pursuit of these important and complex issues, we have taken two approaches to address these questions. One approach described in this report examined the effects of phytochemicals on specific pathways such as apoptosis [3]; the other used DNA microarray analysis as a global gene expression profiling tool [4]. Our work on resveratrol, a grape derived candidate cancer protective agent, is highlighted. Resveratrol [5] is a polyphenol (3, 4, 5 -trihydroxystilbene) categorized as a phytoalexin [6] found principally in the skin of grapes, peanuts, and other plant species [7]. Recent studies attributed a variety of health benefits to consumption of foods containing resveratrol, including protection against cancers, cardiovascular disease, and aging [8]. However, despite works [8–10] suggesting that resveratrol showed promise as a prostate cancer chemopreventive agent, the in vivo effects of resveratrol, as well as the mechanisms underlying those effects on prostate cancer, remain largely unknown.

In our example, microarray technology was used to identify genes modulated by resveratrol in the human prostate cancer LNCaP cell culture model. The information indicated modulation of androgen-dependent pathways as a possible mechanism of

T.T.Y. Wang (✉)
Diet, Genomics and Immunology Laboratory, Beltsville Human Nutrition Research Center, Agricultural Research Service, USDA, Beltsville, MD, USA
e-mail: tom.wang@ars.usda.gov

M. Kamihira et al. (eds.), *Animal Cell Technology: Basic & Applied Aspects*, Animal Cell Technology: Basic & Applied Aspects 16, DOI 10.1007/978-90-481-3892-0_3,

action. Microarray results were also use to compare other candidate cancer preventive compound such as genistein, a soy-derived phytochemicals. The molecular information was used to design an animal model to validate our in-vitro observation. These results demonstrated the utility of microarray and cell culture model technologies, and illustrated the feasibility of in-vivo/in-vitro complementary models to examine molecular mechanisms, identify molecular targets, and determine efficacy of diet-derived compounds.

2 Materials and Methods

2.1 Chemicals

Genistein, daidzein, Resveratrol, 17β-estradiol, dihydrotestosterone (DHT), and dimethylsulfoxide (DMSO) were purchased from Sigma Chemical Co. (St. Louis, MO). Equol was purchased from INDOFINE (Hillsborough, NJ). The synthetic androgen R1881 was from NEN Life Science Products (Boston, MA). Cell culture media and reagents were from Invitrogen (Carlsbad, CA).

2.2 Cells, Cell Culture and Cell Growth

LNCaP human prostate cancer cells were obtained from the American Type Culture Collection (Manassas, VA) and maintained in Media with 10% fetal bovine serum (FBS) (Invitrogen, Carlsbad, CA) [4]. Cells were incubated in ambient 5% CO_2 in air at 37°C. The LNCaP cells (5×10^4 cells/well) were plated in 24-well plates (Costar) for cell growth assays; and treatments were begun 24 h later. Cells were treated with 0, 1, 5, 10, or 25 μM resveratrol (DMSO as vehicle) for 0–96 h, and the medium containing resveratrol was replaced every 24 h. Cell growth was analyzed using the sulforhodamine B (SRB) assay [4]. For experiments using the synthetic androgen R1881 or 17 β-estradiol, cells were switched to Media with 10% charcoal/dextran-treated FBS (CDS, Hyclone, Logan, UT) 24 h after plating to minimize the effect of serum steroid hormones [4]. The cells were then incubated for an additional 24 h before the treatments were begun.

2.3 Analysis of the Effect of Resveratrol and Soy-Derived Phytochemicals on Global Gene Expression in LNCaP Cells

For microarray gene expression profiling experiments, LNCaP cells (2×10^7 cells/T-175 flask) were exposed to 0, 1, 5, or 25 μM phytochemicals for 48 h, total RNA was isolated, and microarray analysis performed using the Affymetrix (Affymetrix, Inc., Santa Clara, CA) platform [4]. The Affymetrix U133 chip was used for gene expression analysis. Responsive genes were identified using the MAS 5.0 suite

(Affymetrix) following criteria of a 1.5-fold increase and $p<0.01$ as a cut off [4]. Triplicate treatments were performed for each concentration, and gene expression in LNCaP cells was confirmed using real-time PCR [4].

2.4 Effects of Resveratrol on LNCaP Cancer Cell Xenografts in Athymic Nude Mice

To determine the prostate cancer protective effects of resveratrol in vivo, a nude mouse xenograft model [11] was used. Mice were randomly assigned to the following diet groups: (a) Control (AIN-93M) diet, (b) AIN-93 M supplemented with 50mg resveratrol/kg diet (RES50), or (c) AIN-93M supplemented with 100 mg resveratrol/kg diet (RES100). Pellet diets were prepared by Research Diets (New Brunswick, NJ). Twenty-two mice were used per treatment group. The cancer preventive efficacy of resveratrol was assessed by twice-weekly measurements of tumor volume using the equation: tumor volume (cm3) $= 0.523 \times$ [length (cm) $\times$ width^2 (cm^2)] [11]. Immunohistochemical (IHC) determination of steroid hormone-responsive pathway response, proliferation, apoptosis, and angiogenesis were performed as previously described [11]. Prostate specific antigen (PSA), a classic ARG responsive to both androgen and estrogen [12], was used to assess the effect of resveratrol on steroid hormone-dependent pathways proliferating cell nuclear antigen (PCNA) was used as a proliferation marker. Micro blood vessels were identified using Platelet/Endothelial Cell Adhesion Molecule 1 (PECAM-1) staining. The IHC Staining Protocol for Vascular Endothelial Growth Factor (VEGF) was used as previously reported [11].

2.5 Statistical Methods

For in vitro experiments, StatView (SAS Institute Inc., Cary, NC) software was used for statistical analysis. Multiple group data were analyzed using ANOVA followed by post-hoc analysis with Fisher's PLSD test. The unpaired Student's t-test was used to compare experiments with two groups. Values were considered significant at $p<0.05$. The mouse tumor data for each treatment group were analyzed using SAS® Proc MIXED (SAS Institute, Inc.) [11].

3 Results and Discussion

3.1 Effects of Resveratrol on LNCaP Cell Growth In Vitro

In vitro exposure of androgen-responsive LNCaP human prostate cancer cells to medium containing 10% FBS with various concentrations of resveratrol (0–25 μM),

relative to medium without resveratrol, resulted in concentration-dependent growth inhibition at concentrations as low as 5 μM. As both androgen and estrogen contribute to cell growth in LNCaP cells cultured in 10% FBS [12], we examined the interactive effects of resveratrol, androgen, and estrogen on growth to elucidate the underlying mechanism(s). LNCaP cells were cultured in 10% CDS with 1 nM synthetic androgen R1881 or 17 β-estradiol in the presence of 0, 1, 5, or 25 μM resveratrol for 96 h. Resveratrol inhibited cell growth induced by R1881 and or 17 β-estradiol in a concentration-dependent manner at concentrations as low as 1 μM for androgen and as low as 5 μM for 17 β-estradiol.

3.2 Comparison of Gene Expression Profiles of Resveratrol-Treated Cells

Microarray analysis of global gene expression profiles were performed on LNCaP cells treated with 0, 1, 5, and 25 μM resveratrol. The total number of genes altered in LNCaP cells ($p<0.01$, >1.5-fold) exposed to increasing concentrations of resveratrol as compare to controls was 121, 440 and 2042, respectively. The spatial separation of various treatments in the 3-D plot showed multi-dimensional scaling that suggested that resveratrol exerted concentration dependent effects on the LNCaP cells.

3.3 Microarray and RT-PCR Analysis of the Effects of Resveratrol on Specific Gene Expression in LNCaP Cells InVitro

Androgen-responsive genes (ARGs) appeared to be broadly affected by treatment with resveratrol. Expression of classic ARGs, such as KLK3 (commonly known as PSA, [13]), were down-regulated, while androgen-down-regulated genes such as BCHE [13], were up-regulated by resveratrol. Selected ARGs were subjected to RT-PCR confirmation. Consistent with the microarray results, expression of PSA and STK39 was up-regulated in response to resveratrol, while no changes were observed for B2M and SEPP1. Since expression of selected ARG mRNAs, as with cell growth, is subject to regulation by androgen and 17 β-estradiol [13], the effects of resveratrol on both androgen- and estrogen-mediated changes in ARGs were examined using RT-PCR. Treatment of LNCaP cells with resveratrol effectively inhibited the R1881-induced increase of several known ARGs: B2M, PSA, SEPP1, STK39 and IGF-1R [13]. Resveratrol also inhibited 17 β-estradiol induction of PSA, STK39 and IGF-1R. Expression of B2M and SEPP1 was not 17 β-estradiol inducible. Consistent with changes at the message level, the effect of resveratrol on the expression of the classic ARG, PSA, was also reflected at the protein expression level.

3.4 Effects of Resveratrol on an LNCaP Prostate Cancer Cell Xenograft Model

We validated our in vitro findings by using an in vivo LNCaP cell tumor xenograft model [11]. We found a significant delay in LNCaP tumor growth in nude mice consuming the RES50 or RES100 diet by week 3 and weeks 3–4, respectively, after injection of LNCaP cells. But there were no differences in tumor volume by the 7th week. By IHC analysis, expression of PSA was significantly less in tumors from mice fed resveratrol, and this effect was dose-dependent. The IHC analysis showed no differences between the treatments in overall levels of PCNA, a marker for proliferation. Interestingly, we observed significantly lower levels of apoptosis (as assessed by ApoTag) in tumors from the RES50- and RES100-fed mice compared to controls. Moreover, we also observed an increase in microvessel formation in RES100-fed mice as assessed by PECAM-1 staining, suggesting an increase in angiogenesis in this group. However, we did not observe qualitative differences in VEGF staining between the diet groups.

3.5 Specificity of Resveratrol on Gene Expression in LNCaP Cells

We also compared the effects of resveratrol to the soy derived cancer protective phytochemicals compounds genistein, daidzein, and equol. Microarray results identified ARG as a category of broadly modulated genes. Overall, the ARG and their androgen-dependent events appeared to be globally affected by the phytochemicals tested. However, there appeared to subtle difference as far as threshold and concentration–dependency of the compounds. In addition, a universal activation of p53-dependent events (indicated by up-regulation of CDKN1A (p21/WAF1/Cip1) a classic p53-responsive gene [14] involved in G0/G1 arrested by resveratrol as well as genistein) was observed at high concentrations (25 μM),

In summary, we showed the utility of microarray technology to identify genes related to specific signaling pathways (i.e. ARG) that are modulated in vitro by resveratrol compared to cells treated with other diet-derived compounds. In addition, we showed that complementary studies of in-vitro/in-vivo models are necessary to validate molecular changes observed in cell culture, but also to reveal the limitations of dietary treatments such as short term inhibition of tumor growth and potential deleterious effects related to increased angiogenesis.

This work was supported by U.S appropriated funds to USDA project number 1235-51530-052-00 (TTYW).

References

1. Greenwald, P., Clifford, C.K., and Milner, J.A. (2001) Diet and cancer prevention. *Eur. J. Cancer* **37**(8): 948–965.
2. Greenwald, P. (2001) Clinical trials of breast and prostate cancer prevention. *J. Nutr.* **131**(1): 176S–178S.

3. Po, L.S., Wang, T.T., Chen, Z.Y., and Leung, L.K. (2002) Genistein-induced apoptosis in MCF-7 cells involves changes in Bak and Bcl-x without evidence of anti-oestrogenic effects. *Br. J. Nutr*. **88**(5): 463–469.
4. Takahashi, Y., Lavigne, J.A., Hursting, S.D., Chandramouli, G.V., Perkins, S.N., Kim, Y.S., and Wang,T. T.(2006) Molecular signatures of soy-derived phytochemicals in androgen-responsive prostate cancer cells: A comparison study using DNA microarray. *Mol. Carcinog*. **45**: 943–956.
5. Stewart, J.R., Artime, M.C., and O'Brian, C.A. (2003) Resveratrol: a candidate nutritional substance for prostate cancer prevention. *J. Nutr*. **133:** 2440S–2443S.
6. Hain, R. Bieseler, B. Kindl, H. Schroder, G., and Stocker, R. (1990) Expression of a stilbene synthase gene in Nicotiana tabacum results in synthesis of the phytoalexin resveratrol. *Plant Mol. Biol*. **15**: 325–335.
7. Goldberg, D.M. Tsang, E. Karumanchiri, A. Diamandis, E. Soleas, G., and Ng, E. (1996) Method to assay the concentrations of phenolic constituents of biological interest in wines. *Anal. Chem*. **68**: 1688–1694.
8. Bhat, K.P.L. Kosmeder, J. W. 2nd, and Pezzuto, J.M. (2001) Biological effects of resveratrol. *Antioxid. Redox. Signal*. **3**: 1041–1064.
9. Baur, J.A. and Sinclair, D. A. (2006) Therapeutic potential of resveratrol: The in vivo evidence. *Nat. Rev. Drug Discov*. **5 :** 493–506.
10. Jang, M., Cai, L., Udeani, G.O., Slowing, K.V., Thomas, C.F., Beecher, C.W., Fong, H. H., Farnsworth, N.R., Kinghorn, A.D., Mehta, R.G., Moon, R.C., and Pezzuto, J. M. (1997) Cancer chemopreventive activity of resveratrol, a natural product derived from grapes. *Science* **275**: 218–220.
11. Wang, T.T., Hudson, T.S., Wang, T.C., Remsberg, C.M., Davies, N.M., Takahashi, Y., Kim, Y. S., Seifried, H., Vinyard, B.T., Perkins, S.N., and Hursting, S.D. (2008) Differential effects of resveratrol on androgen-responsive LNCaP human prostate cancer cells in vitro and in vivo. *Carcinogenesis* **29**(10): 2001–2010.
12. 12.Takahashi, Y., Perkins, S.N., Hursting, S.D., and Wang, T.T. (2007) 17beta-Estradiol differentially regulates androgen-responsive genes through estrogen receptor-beta- and extracellular-signal regulated kinase-dependent pathways in LNCaP human prostate cancer cells. *Mol. Carcinog*. **46 :** 117–129.
13. Nelson, P.S., Clegg, N., Arnold, H., et al. (2002) The program of androgen-responsive genes in neoplastic prostate epithelium. *Proc, Natl. Acad. Sci. USA*. **99:** 11890–11895.
14. El-Deiry, W.S., Tokino, T., and Velculescu, V.E. (1993) WAF1, a potential mediator of p53 tumor suppression. *Cell* **75:** 817–825.

DNA Microarray Technology Evaluation of Effect of Dietary Intake of Crude Rice Glycosphingolipids in Mice

Jun Shimizu

1 Introduction

Glycosphingolipids (GSLs) are complex carbohydrates consisting of sugars, long-chain fatty acids and sphingoid bases. Their basic skeletal structure, excluding the sugars is called a ceramides. Ceramides are the common of the various intercellular lipids in the skin, and they play an important role in barrier functions, for example, in retaining moisture and preventing the entry of foreign materials into the body. Additionally, ceramides are widely used in cosmetics and external applications [1, 2].

The raw materials for manufacturing GSLs have previously been mostly of animal origin. However, owing to the potential transmission of bovine spongiform encephalopathy through the use of such GSLs, GSLs are now manufactured from plant-derived materials has meant that plant-derived materials are now manufactured from plant-derived materials. Plant-derived GSLs have been used as dietary supplements for maintaining the skin integrity. However, the effects of dietary intake of plant-derived GSLs on the body have not yet been investigated.

In the present study, we examined the effects of dietary administration of crude rice-derived GSLs (RG), extracted from rice bran in mice. Thereafter, we carried out a DNA microarray analysis to examine the gene expression patterns in the liver and to ascertain the food function of RG.

2 Materials and Methods

2.1 GSLs

RG (Okayasu Co., Saitama, Japan) was obtained from a commercially available GSLs extracted from rice bran. Konjac GSL (KG; Okayasu Co.), a commercially

J. Shimizu (✉)
Department of Clinical Dietetics and Human Nutrition, Josai University,
Sakado-shi, Saitama 350-0295, Japan
e-mail: jshimizu@josai.ac.jp

M. Kamihira et al. (eds.), *Animal Cell Technology: Basic & Applied Aspects*, Animal Cell Technology: Basic & Applied Aspects 16, DOI 10.1007/978-90-481-3892-0_4,

available GSLs extracted from konjac comb, was used as the positive control. The GSLs content of both products was 50%.

2.2 Experimental Animals and Diets

Seven-week-old male specific pathogen-free C57BL/6 J mice were purchased from Tokyo Experimental Animals (Tokyo, Japan). The mice were maintained on an AIN-93G diet [3] containing 0.5% GSLs for 2 weeks. During the study period, the mice were provided *ad libitum* access to this diet and to deionized water. The mice were kept in a room maintained at a temperature of 23 ± 1°C, and with 50% a relative humidity, under a 12-h light cycle (light on at 07:00). The protocol for animal experimentation was approved by the Animal Care Committee of Josai University.

2.3 DNA Microarray Analysis

Total RNA of from the liver samples of mice that were fed on each diet was extracted using TRIzol reagent (Invitrogen, CA, USA) [4] and pooled. It was then used for DNA microarray analysis, which was performed on the CodeLink Expression Bioarray System (UniSet Mouse 20 K Bioarray, Amersham Biosciences, NJ, USA) according to the manufacturer's protocol.

2.4 Real-Time PCR Analysis

To validate the results of the microarray analysis for *CRAT* gene, we performed a real-time quantitative RT-PCR analysis on the Applied Biosystems 7500 Real-Time PCR Systems (Applied Biosystems, CA, USA) using the SYBR green PCR Master Mix (Applied Biosystems) using the Applied Biosystems 7500 Real-Time PCR Systems (Applied Biosystems). The PCR data obtained for each sample were normalized to the data obtained for glyceraldehyde-3-phosphate dehydrogenase (GADH), and the relative cDNA levels were calculated by the $2 - \Delta\Delta CT$ method [5].

2.5 Statistical Analysis

Data are expressed as the mean ± SEM. The control group was compared to with either the group that the RG group or the KG group using Student's t test with the level of significance set at $p < 0.05$.

3 Results

3.1 Changes in the Gene Expression Profile

Table 1 summarizes the gene expression profile in the liver of the mice: a total of 12,419 genes were detected. The genes were divided into several categories on the basis of their biological function, and the number of genes that were upregulated or downregulated expression was counted. The expression pattern of genes related to nutrient metabolism did not display any marked changes. The expression of the thyroid hormone receptor β – a nuclear receptor mainly responsible for increasing the basal metabolic rate – was upregulated in the RG group as compared to the control group, but by not more than 2-fold (data not shown).

Table 1 Numbers of gene whose expressions were up or down regulated compared with control group at least twofold or more in the liver of mouse fed experimental diets

	C (4,886)		RG (4,856)		KG (4,868)	
Genes (12,419) Expressed	Up	Down	Up	Down	Up	Down
Total	–	–	233	265	195	287
Apoptosis (153)	–	–	6	4	4	6
DNA repair (39)	–	–	1	2	1	4
DNA replication (34)	–	–	1	4	1	1
Transcription (618)	–	–	27	33	22	35
Cell cycle (149)	–	–	2	11	2	7
Cell adhesion (167)	–	–	8	10	4	16
Regulation cell cycle (59)	–	–	1	2	0	3
Regulation of transcription (584)	–	–	27	34	20	33
Carbohydrate metabolism (42)	–	–	0	1	2	0
Glucose metabolism (8)	–	–	0	1	1	1
Amino acid metabolism (42)	–	–	0	0	0	0
Fatty acid metabolism (20)	–	–	0	1	0	0
Immune response (41)	–	–	1	3	2	5
Lipid metabolism (47)	–	–	3	4	3	1
Protein biosynthesis (106)	–	–	4	1	5	5
Steroid biosynthesis (10)	–	–	1	0	1	0
Electron transport (111)	–	–	2	4	4	0

Abbreviations: C, control; RG, rice glycosphingolipid; KG, konjac glycosphingolipid.

3.2 Genes Involved in Energy Metabolism

Figure 1 shows the expression levels of genes related to energy metabolism, as determined by DNA microarray analysis. The percentages shown indicate the rate of change of expression in relation to the control group. In both the RG and KG groups, the expression of genes related to the glycolytic pathway genes tended to be upregulated, while the expression of genes related to the tricarboxylic acid (TCA)

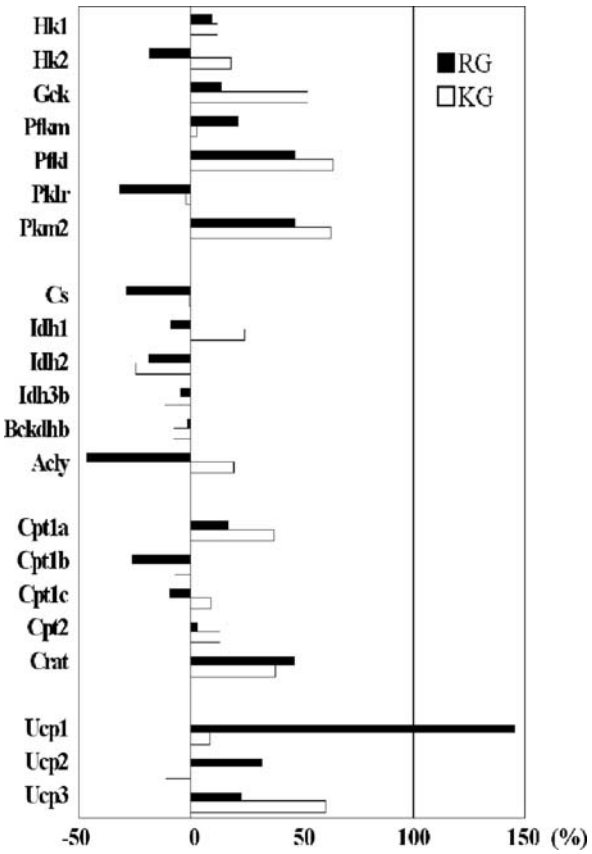

Fig. 1 Relative gene expression in the liver of mouse fed experimental diets. Percentage value shows the relative increase or decrease compared with control group
Abbreviation: RG, rice glycosphingolipid; KG, konjac glycosphingolipid; Hk1, hexokinase 1; Hk2, hexokinase 2; Gck, glucokinase; Pfkm, phosphofructokinase; Pfkl, phosphofructokinase, liver; Pklr, pyruvate kinase liver and red blood cell; Pkm2, pyruvate kinase, muscle; Cs, citrate synthase; Idh1, isocitrate dehydrogenase 1; Idh2, isocitrate dehydrogenase 2; Idh3b, isocitrate dehydrogenase 3 beta; Bckdhb, branched chain ketoacid dehydrogenase E1, beta polypeptide; Acly, ATP citrate lyase; Cpt1a, carnitine palmitoyltransferase 1a; Cpt1b, carnitine palmitoyltransferase 1b; Cpt 1c, carnitine palmitoyltransferase 1c, Cpt2, carnitine palmitoyltransferase 2; Crat, carnitine acetyltransferase; Ucp1, uncoupling protein 1; Ucp2, uncoupling protein 2; Ucp3, uncoupling protein 3.

cycle, such as citrate synthase (Cs), tended to be downregulated. With regard to lipid metabolism, the expression of the carnitine acetyltransferase (*CRAT*) gene was upregulated for in the RG group.

To confirm the expression of these genes and to quantify the gene expression in individual mice, a primer specific to the *CRAT* gene in the liver was prepared. The results of the PCR analysis revealed that the expression of *CRAT* was significantly upregulated in the RG group as compared to the control group (Fig. 2, $p = 0.014$).

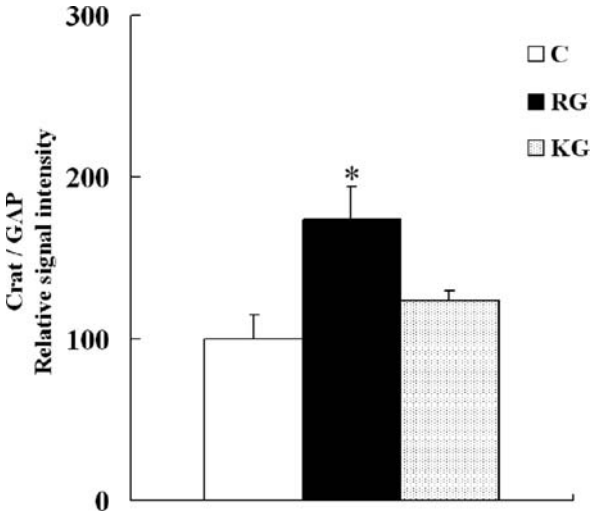

Fig. 2 mRNA levels of carnitine acetyltransferase (Crat) in the liver of mouse fed experimental diets. Values are means ± SE of 7 mice. *Significantly different from control group by Student's *t*-test at $p < 0.05$ Abbreviations: C, control; RG, rice glycosphingolipid; KG, konjac glycosphingolipid.

3.3 Genes Related to Drug Metabolism

The expression levels of genes related to drug metabolism are shown in Table 2. Of the 25 phase-I metabolizing enzymes, only CYP7a1 exhibited 2-fold upregulated expression in both the RG and KG groups.

Table 2 Numbers of drug related genes whose expressions were up or down regulated compared with the control group at least twofold or more in the liver of mouse fed experimental diets

	C		RG		KG	
Drug related genes (133)	Up	Down	Up	Down	Up	Down
Phase I metabolizing enzymes P 450 gene family (25)	–	–	0	0	1	0
Phase II metabolizing enzymes	–	–				
Acetyltransferases (7)	–	–	0	0	1	0
Epoxide hydrolases (3)	–	–	0	0	0	0
Glutathione S-transferases (16)	–	–	0	0	0	0
Metyltransferases (7)	–	–	0	0	0	0
Sulfotransferases (21)	–	–	0	0	0	3
UDP-glucosyltransferases (4)			0	1	0	1
Drug related transporters	–	–				
P-glycoprotein family (33)	–	–	1	2	2	1
Other (14)	–	–	1	0	0	1

Abbreviations: C, control; RG, rice glycosphingolipid; KG, konjac glycosphingolipid.

4 Discussion

Administration of GSLs tended to increase the expression of the genes involved in energy metabolism. In particularly, the mRNA expression of thyroid hormone receptor β (THRB) was upregulated in the RG group as compared to the control group. THRB plays a role in energy metabolism including basic metabolism. Subsequently, we subsequently focused on analyzed genes that are involved in lipid and carbohydrate metabolism. The results showed that mRNA expression of hexokinase 1 (Hk1) and phosphofrukcutokinase (Pfk) was higher in the KG and RG groups than in the control group. This suggested that the activity of the glycolytic pathway was elevated in the KG and RG groups. On the other hand, the mRNA expression of enzymes related to the TCA cycle, such as Cs, a rate-limiting enzyme, tended to be downregulated in the RG group. These findings suggest that the TCA cycle is not the only metabolic pathway that utilizes the acetyl coenzyme A (CoA) produced by the glycolytic pathway.

Analysis of the genes related to lipid metabolism revealed that the expression of *CRAT* gene was upregulated in the RG group as compared to the other 2 groups. The *CRAT* gene plays an important role in fatty acid metabolism. CRAT belongs to the family of carnitine acyltransferases. In the mitochondrial matrix, the acetyl group of acetyl CoA binds to carnitine in the mitochondrial matrix and catalyzes the synthesis of acetyl carnitine in a reversible reaction [6]. During fatty acid metabolism, some long-chain fatty acids are oxidized via β-oxidation in peroxisomes; the acetyl CoA produced in this reaction is then converted into acetylcarnitine by CRAT in the peroxisomes. Acetylcarnitine penetrate the peroxisomal and mitochondrial membranes, while acetyl CoA cannot. Acetylcarnitine present in peroxisomes then enters the mitochondria and is reconverted by CRAT into carnitine and acetyl CoA; thus, acetyl CoA is supplied to the TCA cycle [7]. We could not elucidate the precise mechanism underlying the increase in the *CRAT* gene expression due to GSLs consumption; however, it appears that GSLs enhances the metabolism of acetyl CoA, which is produced by lipid metabolism, particularly β-oxidation.

The effects of GSLs on the expression of genes related to drug metabolism were investigated. The expression of cytochrome 450 (Cyp), a phase-I metabolizing enzyme, was not markedly altered by dietary GSLs. This suggests that GSLs probably does not affect drug metabolism. Of the cytochromes involved in drug metabolism, only Cyp7a1 exhibited upregulated expression. Cyp7a1 is a rate-limiting enzyme involved in the conversion of cholesterols into bile acids in the liver; it plays an important role in cholesterol metabolism. The fact that the expression of the *Cyp7a1* was upregulated after the administration of GSLs indicates that GSLs appears to accelerate the conversion of cholesterols into bile acids.

These findings suggest that RG consumption enhances the metabolism of fatty acids and cholesterols without affecting the activity of enzymes involved in drug-metabolism. Further studies are required to elucidate the mechanisms underlying this function of RG and to identify the compounds involved.

References

1. Imokawa, G., Akasaki, S., Hattori, M., and Yoshizuka, N. (1986) Selective recovery of deranged water-holding properties by stratum corneum lipids. *J. Invest. Dermatol*. **87**: 758–761.
2. Goldstein, A.M. and Abramovits, W. (2003) Ceramides and the stratum corneum: structure, function, and new methods to promote repair. *Int. J. Dermatol*. **42**: 256–259.
3. Reeves, P.G., Nielsen, F.H., and Fahey, G.C. Jr. (1993) AIN-93 purified diets for laboratory rodents: final report of the American Institute of Nutrition ad hoc writing committee on the reformulation of the AIN-76A rodent diets. *J. Nutr*. **123**: 1939–1951.
4. Mano, H., Mori, R., Ozawa, T., Takeyama, K., Yoshizawa, Y., Kojima, R., Arao, Y., Masushige, S., and Kato, S. (1994) Positive and negative regulation of retinoid X receptor gene expression by thyroid hormone in the rat. Transcriptional and post-transcriptional controls by thyroid hormone. *J. Biol. Chem*. **269**: 1591–1594.
5. Monney, L., Sabatos, C.A., Gaglia, J.L., Ryu, A., Waldner, H., Chernova, T., Manning, S., Greenfield, E.A., Coyle, A.J., Sobel, R.A., Freeman, G.J., and Kuchroo, V.K. (2002) Th1-specific cell surface protein Tim-3 regulates macrophage activation and severity of an autoimmune disease. *Nature* **415**: 536–541.
6. McGarry, J.D. and Brown, N.F. (1997) Some Studies with Antisera to Growth Hormone. *Eur. J. Biochem*. **244**: 1–14.
7. Ramsay, R.R. and Zammit, V.A. (2004) Carnitine acyltransferases and their influence on CoA pools in health and disease. *Mol. Aspects Med*. **25**: 475–493.

Integrated Pathway Analysis of Genome-Wide Expression Changes Associated with Serum-Free Suspension Adaptation of an Antibody-Producing Chinese Hamster Ovary (CHO) Cell Line

Yung-Shyeng Tsao, Ankit A. Merchant, Aaron Meyer, and Zhong Liu;

Marsha Smith, Diane Levitan, and Eric Gustafson

1 Introduction

DNA microarray technologies have been used to understand cell line and cell culture process development, such as the study of super producers [1, 2] and temperature effect [3] on mouse-originated production cell lines. Although CHO cells have been commonly used in manufacturing biological products, limited hamster genetic data were available for the industry until the establishment of the CHO consortium [4]. We have used the CHO DNA microarray developed by the consortium to analyze the genome-wide expression profile changes of an antibody-producing CHO cell line during serum-free suspension-adaptation. The latter is necessary for manufacturing due to regulatory [5] and operational reasons. The profile changes were shown to be physiologically significant to the cell and consistent within metabolic pathways. Integrated pathway analysis has enhanced the power of DNA microarray technology in the understanding of the physiological changes in the production process and should have a profound impact on the development, understanding, and control of a cell culture process.

2 Materials and Methods

A gene-amplified CHO clone with the desirable antibody productivity has been isolated and grown in a serum-containing, nucleotide and nucleoside-deficient MEM-based medium in three T-75 flasks at 37°C. The cell line has been adapted to grow in suspension in three shake-flasks at 37°C in a proprietary serum-free protein free medium custom-made by Sigma. One sample was taken from each of the T-75 flasks (i.e., before adaptation) and each of the shake-flasks (i.e., after

Y.-S. Tsao (✉)
Protein Expression Technologies, BSPD, Merck Research Laboratories,
Union, NJ 07083, USA
e-mail: yung-shyeng.tsao@merck.com

M. Kamihira et al. (eds.), *Animal Cell Technology: Basic & Applied Aspects*, Animal Cell Technology: Basic & Applied Aspects 16, DOI 10.1007/978-90-481-3892-0_5,

adaptation) during the exponential growth phase. Total RNA was extracted from CHO cell pellets using TRIzol (Invitrogen) and the Qiagen RNeasy mini kit protocol. Total RNA (5 μg) from each sample was used to generate first-strand cDNA using a T7-Oligo (dT) primer. Following second-strand synthesis, in vitro transcription was performed with the BioArray, High Yield RNA Transcription Labeling Kit (Enzo Life Sciences, Inc) and 10 μg of fragmented cRNA were used for hybridization to custom Affymetrix microarray chips CHO1a520406F. Chips were washed using Affymetrix GeneChip Fluidics Station 450 and scanned using Affymetrix GeneChip Scanner 3000. CHP files were generated using Affymetrix MicroArray Suite version 5.0 (MAS5) software. Further analyses were performed using an S+ based package, ArrayAnalyzer (licensed from Insightful, Inc.). Data were filtered to exclude probe sets with the prefix AFFX (Affymetrix control probe sets), probe sets which were called "absent" in all experiments, and probe sets where less than 7 probe pairs registered data. All data were Log2 transformed. The data were then normalized to the median inter-quartile range for each probe set. Gene lists were generated by comparing the experimental group to the appropriate control using the following parameters: raw expression level over 100 for at least three of the twenty-one chips, multi-t-test with a *p*- value of <.05, a multiple testing correction using the Benjamini-Hochberg adjustment, and a fold change greater than 2, and a fold change greater than 1.5. Annotations and sequences of probes on the CHO1a520406F microarray chip were based on release version 02 (May 2007). The normalized gene expression levels prior to and after serum-free adaptation were compared. The genes with greater than or equal to 1.5 fold difference in expression were sorted out. Significant and meaningful changes in mRNA expression of proteins which participated in certain pathways or functions were carefully identified. Corresponding *p*-values for each identity and a combined *p*-value for each pathway/function were calculated according to Zaykins et al. [6], where the *p*-value cutoff was set to be < 0.001.

3 Results and Discussion

The following pathways were found either significantly up- or down-regulated. The gene expression fold change for each enzyme involved is shown in the corresponding figure(s). Since the *p*-values were generally lower than 0.01, we only show the combined *p*-value for each pathway to demonstrate the significance of the overall up- or down-regulation.

1. *Cells increase synthetic pathways to restore Extracellular Matrix (ECM) and counteract hypoxia-induced stresses* (Fig. 1). (1) According to the literature [7], *procollagen* can be modified by *lysyl hydroxylase* to produce collagen, which is bound to cells through *integrin*. While, *decorin* regulates the binding of *laminin* (through *nidogen*) and *fibronectin* to collagen and modulate the cell behavior during development. The combined p-value for ECM gene up-regulations is $2.7e^{-15}$. (2) Hypoxia can induce *cytochrome b5* to produce Reactive Oxygen Species (ROS) and thus induce the biosynthesis of *Hypoxia-Induced Factor* (HIF), which can

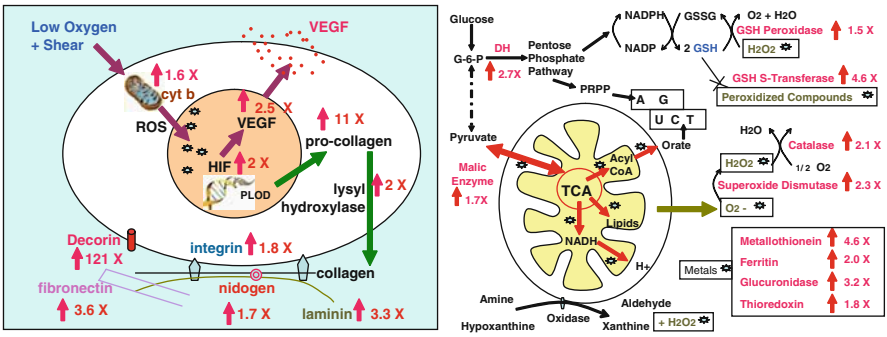

Fig. 1 Both Extracellular Matrix (ECM) proteins, Hypoxia-Induced (HIF) angiogenic pathway, and enzymes with Antioxidant Responsive Element (ARE) were up-regulated significantly

in turn induce the production of *Vascular Endothelial Growth Factor* (VEGF) to stimulate angiogenesis [8]. The combined p-value for HIF-induced angiogenic pathway gene up-regulation is $7.4e^{-9}$. (3) Hypoxia can also induce (a) enzymes with Antioxidant Responsive Element (ARE) [9, 10]**:** *glutathione peroxides*, *glutathione S-transferases*, *catalase* and *superoxide dismutase* to counteract the accumulation of H_2O_2, O_2-, and peroxidized compounds, (b) metalloproteins *metallothionein*, *ferritin*, *glucuronidase*, and *thioredoxin* to counteract metal-induced free radicals, (c) NADPH-producing enzymes *malic enzyme* and *glucose-6-phosphate dehydrogenase* to replenish glutathione for the processes. The combined p-value for ARE gene up-regulation is $7.4e^{-19}$.

2. *Cells reduce growth rate, while increase glycoprotein post-translational modification activities*. (Fig. 2) (1) Cell cycle-promoting proteins (*cyclinA*, *cyclinB*, *cdc2*, *cdk2*, *cdc20*, *MEKK*) [11] were down-regulated; while cell cycle-inhibiting proteins (*cdk2-associated protein*, *cyclineD-binding protein*), were up-regulated. The combined *p*-value for cell cycle down-regulation is $2.3\ e^{-17}$. This was consistent with the fact that cell growth rate had dropped 50% after serum-free suspension adaptation (data not shown). (2) glycoprotein-processing enzymes [11] were upregulated.

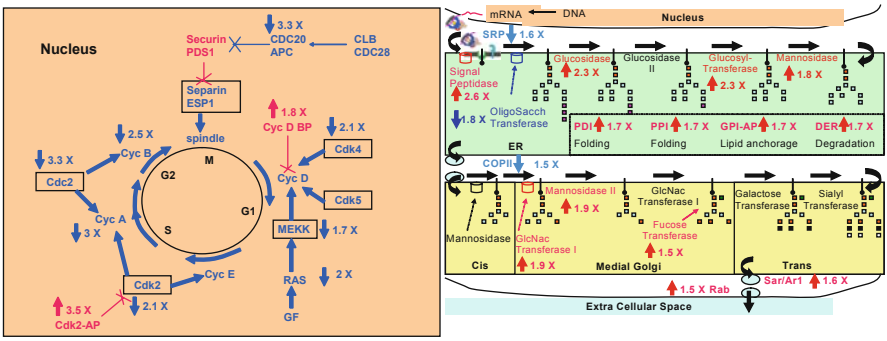

Fig. 2 Cell cycle were down-regulated, while glycoprotein post-translational modifications were up-regulated

(a) In ER, this includes *signal peptidase*, *glucosidase I*, *glucosyl transferase*, *mannosidase I*, *glycophosphotidylinositol-anchor protein*, *ubiquitin-dependent protease DER*, *disulfide isomerase*, *peptidyl prolyl isomerase*. The combined p-value for ER processing protein up-regulation is $3.5e^{-8}$. (b) In medial Golgi, this includes *glcnac transferase I*, *mannosidase II*, and *fucose transferase*. The combined p-value for Golgi processing protein up-regulation is $1.9e^{-8}$.

3. *Mitochondrial energy producing activities seemed to be down-regulated, while cytoplasmic fatty acid synthesis and transport were up-regulated*. (Fig. 3) (1) Energy producing activities and fatty acid catabolism in mitochondria seemed to be down-regulated; (2) While, fatty acids seemed to be transported through the *carnitine transporter* into the cytoplasm for elongation by *fatty acid synthetase*; (3) The energy was provided by the pentose phosphate pathway (PPP) through *G-6-P dehydrogenase* and *acetyl CoA synthetase*. (4) LDL docking proteins (*VLDLR*, *CD36*, *decorin*) and *fatty acid binding protein* were up-regulated. The combined *p*-value for fatty acid transport up-regulation is $9.8e^{-11}$.

4. *Both sterol synthesis and regulation are up-regulated*. (Fig. 4) (1) TCA provides substrates to synthesize *acetyl CoA* and *acetoacetyl CoA* in the cytoplasm. The latter was converted to *HMG-CoA* and subsequently *mevalonate*, *isopentenyl-PP*, *farnesyl-PP*, *lanosterol*, *7-dehydroxy cholesterol*, and *cholesterol*. The combined *p*-value for sterol synthesis up-regulation is $1.3\ e^{-16}$. (2) In addition, when cholesterol is low, *insig 1* released its partner complex *srebp* and *scap* to Golgi. The protease in Golgi then cut the complex and released a cytosolic part of srebp to the nucleus. This in turn activates all of the genes involved in sterol synthesis and control [12]. The combined *p*-value for sterol control up-regulation is $7e^{-4}$.

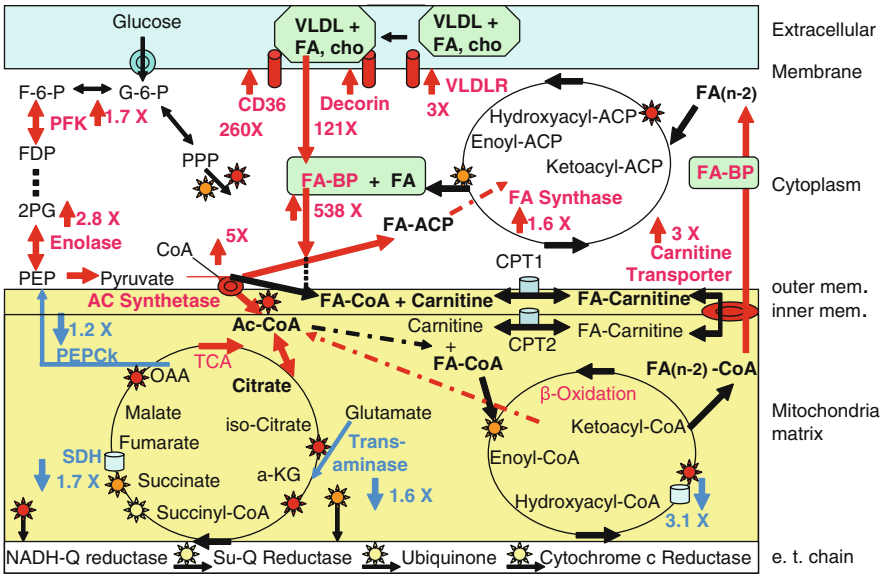

Fig. 3 Both TCA cycle and fatty acid β-oxidation were down-regulated, while both fatty acid synthesis and fatty acid transport were up-regulated

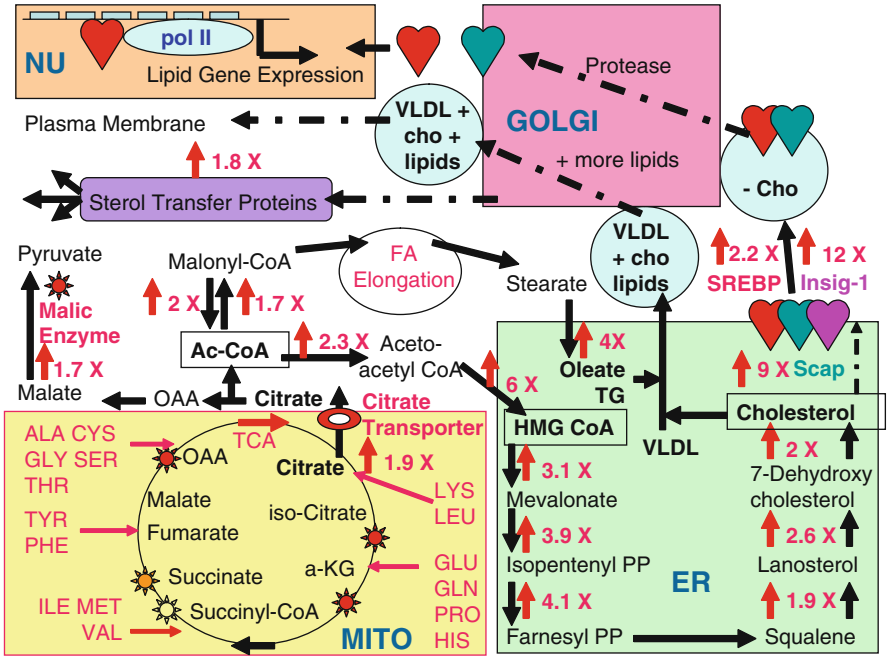

Fig. 4 Fatty acid synthesis is initiated in cytoplasm, while sterol synthesis is in ER and regulated through Golgi and the nucleus. All of the enzymes involved were up-regulated

4 Conclusion

Using DNA microarray technology, a genome-wide expression profile analysis was performed on an antibody-producing CHO cell line during serum-free suspension adaptation. The results suggest that suspension-adapted cells shifted their resources from cell growth to glycoprotein and lipid synthesis, as well as the processes to resolve hypoxia stress. Apoptosis, signal transduction pathways, and motor proteins were found to have no meaningful changes in gene expression during suspension adaptation. It is forseeable that genomic, proteomic and metabolomic technologies together will greatly advance our ability to understand and engineer cellular changes during process development.

References

1. Seth, G., Philip, R.J., Lau, A., Jium, K.Y., Yap, M., and Hu, W-S. (2007) Molecular portrait of high productivity in recombinant NS0 cells, Biotechnol. Bioeng. 97: 933–951.
2. Seth, G., Charaniya, S., Wlaschin, K.F., and Hu, W.-S. (2007) In pursuit of a super producer – alternative paths to high producing recombinant mammalian cells. Curr. Opin. Biotechnol. 18: 557–564.
3. Swiderek, H. and Al-Rubeai, M. (2007) Functional genome-wide analysis of antibody producing NS0 cell line cultivated at different temperatures. Biotechnol. Bioeng. 98: 616–630.

4. Dutton, G. (2007) Managing cell-line optimization process. Genet. Eng. News 27: 38–41.
5. Manual of standard operating procedures and policies: Processing of animal component information submitted in investigational and marketing applications/notifications. (2005) CBER, FDA, SOPP 8401.5, version #1, June 24.
6. Zaykins, D.V., Zhviotovsky, L.A., Westfall, P.H., and Weir, B.S. (2002) Truncated product method for combined p-values. Genet. Epidemiol. **22**: 170–185.
7. Iozzo, R.V. (1998) Matrix proteoglycans: from molecular design to cellular function. Annu. Rev. Biochem. **67**, 609–652.
8. Droge, W. (2002) Free radicals in the physiological control of cell function. Physiol. Rev. **82**; 47–95.
9. Waleh, N.S., Calaoagan, J., Murphy, B.J., Knapp, A.M., Sutherland, R.M., and Laderoute, K.R. (1998) The redox-sensitive human antioxidant responsive element induces gene expression under low oxygen conditions. Carcinogenesis **19**: 1333–1337.
10. Kalpakcioglu, B. and Senel, K. (2008) The interrelations of glutathione reductase, catalase, glutathione peroxidase, superoxide dismutase, and glucose-6-phosphate in the pathogenesis of rheumatoid arthritis. Clin. Rheumatol. **27**: 141–145.
11. Herscovics, A. (1999) Importance of glycosidases in mammalian glycoprotein biosynthesis, BBA **1473**: 96–107.
12. Rawson, R.B. (2003) The SREBP pathway – insights from insig and insects. Nat. Rev. Mol. Cell Biol. **4**: 631–640.

Affordable Mab by Ensuring Low Cog

Two-Step Chromatography Purification Processes

Bjorn Hammarberg and Bo Forsberg

1 Introduction

Mono-clonal antibodies (mAb) are an important class of drugs that is growing rapidly, with many more in the pipeline, posed to becoming the largest revenue generator in the pharma industry. However, the present price structure may not be sustainable as new molecules are coming to the market and current ones expand their indications. The high treatment cost often chronic conditions, Rheumatoid Arthritis, Psoriasis, and Cancer, with doses typically ranging from 50 mg to 2 g per injection, weekly to monthly basis, could in US reach USD 50.000 per patient and year. This put large strains on health care systems, as well as preventing many in developing world access. The manufacturing cost is just one part of the total cost of a biopharmaceutical drug, but by utilizing the combined industrial experience in large scale bio-processing to suggest a reliable manufacturing process it would be possible to reduce COG, thus be able to lower the treatment price.

Here we have taken well known unit operations, that can be readily process validated in a cGMP setting (EMEA or USFDA standards) and simulated mAb production costs based on real time data utilizing years of experience from the biopharma industry and bioprocessing taking into account both biological and engineering factors. The latter includes facility and equipment investments write-offs, utilization factors, etc. Realistic dynamic binding capacities, cycle-times, strip and CIP procedures for chromatography media with, proper virus validation showing the appropriate robustness are among the necessary ingredients to have an industrial process worth while to bring into a large scale commercial setting, with the aim of producing 1 metric ton or more.

B. Hammarberg (✉)
ABD Life Sciences Ltd, Central, Hong Kong
e-mail: bjorn.hammarberg@abd.com.hk

M. Kamihira et al. (eds.), *Animal Cell Technology: Basic & Applied Aspects*, Animal Cell Technology: Basic & Applied Aspects 16, DOI 10.1007/978-90-481-3892-0_6,

2 Method and Parameters

An Excel-based Cost of Goods (COG) simulation model was established in the 90ies by Mr Forsberg and has been developed over the years based on inputs from various small, pilot and large scale operations. This model have been expanded and further improved taking into account all costs associated with establishing and maintaining a large scale manufacturing facility fully operational.

The quality of parameters to be used in any simulation model is crucial of getting results correlating to a true operational scenario. Thus we have put extra emphasis in getting appropriate data, both by interviewing industry insiders and getting quotations from vendors in Scandinavia at the time of simulation with the exchange rate 1.50 USD/EUR, Feb/Mar 2008.

In Table 1 below the important parameters describing under which conditions the facility would operate and how long we estimate the technical and economical life time (Table 2).

Downstream processing (DSP) capturing mAb using Ion Exchange chromatography (IEX), is feasible whenever the mAb has a relatively high isoelectric point, as most cell proteins have lower iso-electric point, while the Protein A affinity chromatography is the "gold standard" for capture. See Table 3 below for details.

Establishing a green field site is costly, here we have used an estimate provided by the Finish engineering company Elomatic Oy and then expanded it into larger facilities based on gained experiences from similar projects. One size (facility) will not fit all; therefore three different sized facilities are considered 4.1.1–3. The facility is either placed in Europe or in a special "Free Economic Zone" in India where no

Table 1 Operational parameters

No	Unit	Value	Comments
1.1	Days	330	One month for maintenance and upgrades per year
1.2	Hours	24	Three work shifts to keep the facility operational around the clock
1.3	Days	7	Full week, including Saturday and Sunday
1.4	Years	20	Life time of the facility and some equipments
1.5	Years	10	Life time of most equipment having mechanical parts
1.6	kg/Year	500/1000	The amount of bulk produced in the facility
1.7	Batch/mo	1	The number of batches manufactured per month
1.8	EUR/h	15/50	Total man hour cost in India/EU
1.9	EUR/L	1	Buffer cost
1.10	EUR/L	0.5	WFI cost
1.11	EUR/L	7	Media cost

Table 2 Upstream processing (USP)

No	Unit	Value	Comments
2.1	g/L	1/2/5/10	Expression level in the cell culture. Protein free, chemical defined minimal growth media
2.2	Multiple	10x	Scale-up factor in upstream inoculums
2.3.1	L	10–100/20–200	Vessel size for disposable bags of wave type, working volume (wv)
2.3.2	L	1 k–10 k/2 k–20 k	Vessels in stainless steel
2.4.1			Disposable final vessel, let broth settle over night for easier harvesting using only depth filters, 2 in series
2.4.2	L	5 k	Harvest with PALL depth filters up to 5 k wv, 1st coarse porosity and 2nd fine (dual layer)
2.4.3	L	>5 k	Harvest with Alfa-Laval centrifuge + PALL depth filters for wv >5 k

Table 3 DSP, *also called "Multimodal chromatography" by GE healthcare

No	Unit	Value	Comments
3.1.1	Capture	IEX	"Work Beads 40S" from Bio-Works, 500x, stripping after 3x, then CIP, 500 cm/h
3.1.2		Protein A	Mab Select SuRe from GEHC, 100x, stripping and CIP as above, 500 cm/h
3.2	Inactivation	Low pH	
3.3	UF/Dia	0.22 μm	PALL TFF
3.4	Polishing	Mixed-mode *	Capto-Adhere from GEHC, 100x, CIP (no strip), 600 cm/h
3.5	Virus removal	Nano-filtration	Planova from Asahi Kasei, even though PALL offers a lower cost product, thus a potential upside.
3.6	UF		Sterile bulk, filled in freeze-thaw disposable bags

taxes are paid allowing equipment to be purchased without the heavy additions of duties and taxes. Therefore same equipment prices as in Europe have been used.

The facility cost includes all engineering CD/BD/DD and project management, construction, utilities, process equipment, automation, etc, installation, and full validation DQ/IQ/OQ/CV/PQ/PV, but not cost for land (Table 4).

Overhead is where the auxiliary costs are bundled. We have adopted a similar approach to a recent publication [1], and personal communication (Dr S. Fahrid, UCL). Others may separate certain items from each from other. Here "Maintenance", "Taxes", and "Insurances" are all factors of the total capital investment. While some of the non-production related labour costs are factors of "Operating Labour" (Table 5).

Table 4 Facility and Equipment

No	Unit	Value	Comment
4.1	EUR	40 M	The smallest facility, fewest production lines and only disposable USP equipment
4.2	EUR	60 M	For 2x 5 k cell culture lines, DSP and bulk fill.
4.3	EUR	75 M	For 3x 10 k bioreactors are needed, 1MEUR each
4.4	EUR	90 M	For 2x 20 k bioreactors are needed, 1.5 MEUR each
4.5	EUR	120 M	For 6x USP-lines

Table 5 Overhead

No	Unit	Value	Comment
5.1	%	10	Maintenance cost of sales price, GEHC typically charge (20%). The percentage of total investment cost.
5.2.	%	2	Local taxes (as above)
5.3.	%	1	Insurance (as above)
5.4	%	20	Supervisors, percentage of the total operating cost, just calculated for actual processing time to time for idle.
5.5	%	70	QA (as above), QC is factored into operating labour
5.6	%	100	General Management (as above), admin, security and top management
5.7	MW	2	Energy consumption for 4.2 facility
5.8	EUR/kWh	0.10	Based on Hong Kong prices

3 Results and Discussions

A series of calculation have been carried out for the four different expression levels outlined above, 1, 2, 5 and 10 g/L, either with the goal of producing 500 kg or 1 ton of mAb-bulk drug substance per year. The growth cycle is 20 days for the inoculums in 10x expansion steps, and 20 days final fed-batch cultivation time resulting in one batch per month.

By using protein free chemical defined minimal cell culture growth media, harvest can be simplified, with a possibility to just use depth filters in scales below 5 kL working volume, while larger scales still require centrifugation in combination with depth filters. In the case of just using disposable bioreactors of wave-type even for the final growth phase, the cells can be left to sediment over night as the bioreactor will be discarded anyway, thus making it easy to just harvest by depth filtration.

GE healthcare's Mab Select SuRe with improved NaOH resistance is a good choice for Protein A based capture of mAb from clarified process fluid, as this chromatography media can withstand harsher CIP and still be useable up to 100 times. Protein A resins have a high purchasing price and the amount used, number of cycles are important factors to keeping COG down, so instead of loading all of the clarified broth at once, we split the feed into up to 8 lots to limit the column size (maximum 1.2 m diameter) and the amount of media used (up to 30 cm bed height). The split fractions are pooled again after the virus removal step.

An alternative capture step is cation exchange chromatography (CIEX), but it is only possible when the pI of the mAb is relatively high so a sufficient difference to host cell proteins and DNA exist to prevent the latter to bind. Furthermore, CIEX has been shown to last up to 500 cycles as they can be readily CIP. We have chosen a newcomer on the market, Bio-Works and their Work Bead 40, which is a highly cross-linked agarose smaller size beads offering superior performance compared to similar priced competitors. We have used 20 g/L binding capacity of the protein A resin to be on the safe side and not the higher biding capacities others rely on [2], while we have used 50 g/L for the CIEX capture.

The development of mixed-mode or multimodal chromatography resins utilizing both IEX and HIC properties offers new opportunities in DSP as it essentially combines two chromatography steps in one. The Capto Adhere binding capacity, here 20 g/L and CIP allowing 100 cycles is on the safe side. With this step there is no need for an additional anion IEX chromatography either as column based or the membrane based. The overall process yield is 64% with the largest loss over the second chromatography step.

The expression level is the largest significant factor in reducing cost exemplified with Fig. 1 above. The bioreactor scale also significantly influences the price. By using 10 kL bioreactors keeping all other factors constant increases the COG to 30.2 €/g compared to 21 €/g for 20 kL, 10 g/L and 1,000 kg/year. By exchanging the capture step to CIEX will reduce COG with 2 €/g as the number of cycles are greatly expanded. The purchasing price has rather small impact.

The 1 kL disposable bioreactor would not really be cost effective for production for 500 kg per year unless 10 g/L expression level is ensured. With disposable bioreactors, a COG of 52 €/g is obtained, which is 80% higher than the 20 kL bioreactor case, with direct cost being the largest part, roughly 40 €/g, the investments cost is just minor. Interestingly 5 kL scale without centrifugation harvesting with just two depth filters in series gives a COG of 30 €/g for 500 kg/year which is far better than most processes running today.

India is rapidly becoming experts also in the biopharmaceutical field with the first biopharma drug in Asia outside Japan and Korea to get USFDA and EMEA

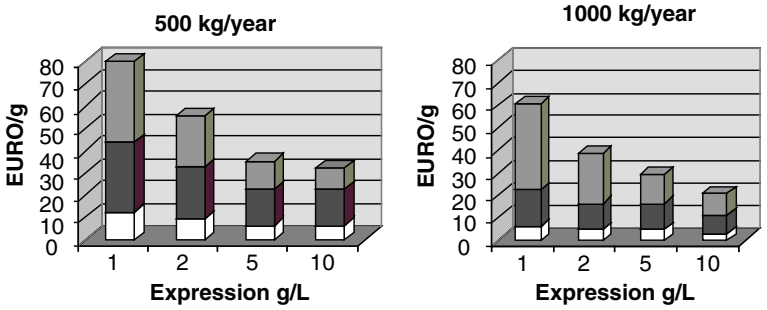

Fig. 1 20 kL bioreactor, 500 or 1,000 kg/year. Investment (*White*), Indirect Cost (*Dark grey*), Direct Cost (*Light grey*)

Table 6 Please provide a caption for this table

Area	Percentage of the selling price
R&D	20–30
Marketing & Sales	40–50
Manufacturing	5–15
Profit	15–20

approval. Thus we believe it is feasible to also run world class mAb production at the largest scale in India. Therefore, we calculated how much the variable cost could be reduced if production was shifted to India instead. For the 1 kL–5 kL case with 10 g/L, 500 kg per year a 42–46% reduction was obtained.

The excel model used does not allow for any dynamic simulation, thus we have assumed no batch failures or QC rejects, which may be over optimistic but anecdotal information suggest that the big-five operates to this level and it is possible.

The Manufacturing cost of the total price is often the smallest portion of the total pie. Based on discussions with biopharma people and information gathered at biotech conferences in 2008 a quite possible division is outlined in the Table 6 above. The lowest manufacturing cost is typical found at the big top 5 mAb manufacturers in the world, while COG in a developing country like mainland China is far higher, as titers and yields are lagging, scale is smaller and expensive imports hampering cost efficient production.

An additional cost would be to fill the formulated drug substance on a vial and make it ready for injection. A typical biopharmaceutical Fill and Finish cost is 10 € per vial [3].

Further lowering of COG is possible, for instance by shortening fed-batch time to 10 days allowing higher through-put of the facility, using resins with higher binding capacity, 50 g/L without getting too high viscosity, as well as resins with increased CIP resistance allowing significant larger amount of cycles before being discarded.

4 Conclusions

It is possible to produce mAb below 20 €/g if the expression level is high 10 g/L, 1 ton/year is manufactured, in 20 kL wv bioreactors, having CIEX capture and performed in India, 17 €/g, still with the seemingly more expensive protein A based capture step and done in Europe the COG can be as low as 21 €/g with Investment contributing with 3.2 € and overhead with 8.2 € the remaining 9.7 € from the 15 unit operations consisting of the efficient process used. This is in-line with other reports of 26–153 $/g [2].

The COG is greatly affected by the expression level and through put of the facility. Alternative chromatography resins, with longer life span (number of cycles)

and DBC will reduce variable costs. Effective operations in low salary geographic locations could further lower variable cost.

CHO-celled produced purified with conventional DSP can compete with transgenic hosts. Column chromatography is not a bottleneck.

Acknowledgements There authors are grateful to following persons suggestions, data and advice, Dr Suzanne S Farid, UCL (UK), Paul Liu, Pall Life Sciences (US), Mr Aulis Rajala, Elomatic Oy (Finland), Mr Thorsten Kimmel, Pharmadule (Sweden) and Jan Berglof, Bio-Works (Hong Kong).

References

1 Farid, S.S., Washbrook, J., Titchener-Hooker, N.J. (2007) Modelling biopharmaceutical manufacture: design and implementation of SimBiopharma. *Comput.Chem. Eng*. 31: 1141–1158.
2. Kelly, B. (2007) Very large scale monocloncal antibody purification: The case for conventional unit operations. *Biotechnol. Prog*. 23: 995–1008.
3. Werner, R.G. (2005) The development and production of biopharmaceuticals; Technological and Economical success factors. *Bioprocess Int*. 3(9): 6–15.

Evaluation of Neurotoxicity of Environmental Chemicals Using Neural Stem Cells and Neuroblastoma Cells

Masami Ishido

1 Introduction

The very large numbers of environmental chemicals that now exist have made assessing their neural risks challenging. Recently, environmental estrogens, known as endocrine disruptors or endocrine-disrupting chemicals, have been identified as a diverse group of synthetic and naturally occurring compounds that mimic the action of steroidal estrogens.

The nonlinear relationship between their effects and concentration has hampered their risk assessment. Furthermore, current risk assessment methods for environmental chemicals are based on adult physiology. However, recent reports have shown an increased incidence of neurodevelopmental disorders which may result from exposure to chemical in utero and during the early postnatal period. Actually, we have demonstrated that exposure of rat pups to some endocrine-disrupting chemicals, such as bisphenol A, octylphenol, nonylphenol, dibutylphthalate, diethylhexylphthalate, cyclohexylphthalate, tributyltin, and *p*-nitrotoluene caused hyperactivity in male Wistar rats, accompanied by changes in the expression of the mesencephalic dopamine transporter gene [1, 2].

In vivo animal studies provide useful data for hazard assessment, but the extensive resources and time were needed to complete single chemical evaluation. Therefore, the establishment of a simple test for developmental neurotoxicity is urgent. In this study, we have examined the effects of *p*-nitrotoluene on cultured neural stem cells isolated from the rat mesencephalon and on human neuroblastoma NB-1 cells.

M. Ishido (✉)
Environmental Risk Research Programme, National Institute for Environmental Studies, Tsukuba, Ibaraki 305-8506, Japan
e-mail: ishidou@nies.go.jp

M. Kamihira et al. (eds.), *Animal Cell Technology: Basic & Applied Aspects*, Animal Cell Technology: Basic & Applied Aspects 16, DOI 10.1007/978-90-481-3892-0_7,

2 Materials and Methods

2.1 Isolation of Rat Neural Stem Cells and Cell Culture

Pregnant Wistar rats at embryonic day 14 (E14) were obtained from Clea (Tokyo, Japan), and maintained in home cages at 22°C on a 12 h light-dark cycle, on MF diet (Oriental Yeast Corp., Tokyo, Japan) and distilled water ad libitum. On E15, they were killed by diethyl ether overdose. The embryos were removed and transferred to minimal essential medium (MEM; Sigma-Aldrich, Tokyo, Japan). Subsequently, the mesencephalons were dissected from the embryos and enzymatically digested with 50 U deoxyribonuclease I (Takara Corp., Kyoto, Japan) and 0.8 U papain (Sigma-Aldrich) at 32°C for 12 min. After stirring, the digestion mix was passed through a 70 μm cell strainer (BD Biosciences, MA, USA). The run-through, containing the neural stem cells, was centrifuged at 800 × *g* for 10 min, resuspended in Dulbecco's Modified Eagle's Medium/F12 medium (DMEM:F12, 1:1; Invitrogen, Tokyo, Japan), supplemented with B27(Invitrogen), 20 ng/ml basic fibroblast growth factor (bFGF; R&D Systems, Inc. MN, USA) and 10 ng/ml epidermal growth factor (EGF; Roche Applied Science, Tokyo, Japan), and cultured in uncoated dishes without serum. Fresh culture medium containing EGF and bFGF was added after 3–4 days in culture.

Human neuroblastoma NB-1 cells were cultured in 45% RPMI-1640 (Gibco BRL, Gaithersburg, MD) and 45% Eagles minimum essential medium (MEM; Sigma-Aldrich, St. Louis, MO), containing 10% fetal bovine serum (FBS), penicillin (100 U/ml), and streptomycin (100 μg /ml) in a humidified atmosphere of 95% air and 5% CO_2 at 37°C. Cells were sub-cultured once a week at a split ratio of 1:6. Cell viability was determined by means of the crystal violet staining method.

2.2 Determination of Length of Neuritis

Human neuroblastoma NB-1 cells (2×10^4) were grown in 45% RPMI-1640 and 45% MEM containing 10% FBS. The cells were then fixed with 11% glutaraldehyde. The fixed cells were stained with crystal violet. The images were photographed under microscope equipped with digital camera and analyzed by image analyzer soft (NeuroZoom). The neurite extension is expressed as the total length of neurites in micrometer per cell in randomly chosen microscope fields.

2.3 Immunostaining

For whole brain samples, 2-day-old rats were sacrificed by decapitation. Immunohistochemistry was carried out as described previously. In brief, fixed 30 μm coronal sections were blocked, incubated with primary anti-nestin

monoclonal antibody (1:100; Chemicon, CA, USA) and then with a fluorescein isothiocyanate (FITC)-conjugated secondary antibody (1:200; Sigma-Aldrich). Nuclei were counterstained with 4'6-diamino-2-phenylindole (DAPI; Invitrogen).

Cultured stem cells were fixed with 4% paraformaldehyde for 15 min at room temperature, permeabilized with 0.5% Triton X-100 and labeled as described previously, using primary antibodies against nestin (1:100; Chemicon), microtubule-associated proteins (MAPs; 1:100; Sigma-Aldrich), and glial fibrillary acidic protein (GFAP; 1:100; Sigma-Aldrich), or cy3-conjugated GFAP (1:100; Sigma-Aldrich). Secondary antibodies conjugated with Alexa 405 (1:200; Invitrogen), FITC (1:200; Sigma-Aldrich), TRITC (1:200; Sigma-Aldrich), or Alexa 488(1:200; Invitrogen) were properly used. Specimens were then observed with an inverted microscope (IX-70; Olympus, Tokyo, Japan) and images were captured using Viewfinder Lite version 1.0 camera software and a DP-50 digital (Olympus) or Leica TCS SP5 confocal microscope system equipped with an AF6000 inverted microscope (Leica Microsystems, Tokyo, Japan).

2.4 Enzyme-Linked Immunosorbent Assay for IL-6

For measurement of IL-6 proteins, NB-1 cells were plated in a 24 well and treated with *p*-nitrotoluene at 0.1–1 μM concentration for 48 h. Culture medium was then harvested. L-6 protein levels in the culture medium were measured by ELISA using Quantikine M (R&D System, Minneapolis, MN), according to the manufacturer's protocol.

3 Results and Discussion

In this study, we have examined the effects of *p*-nitrotoluene on cultured neural stem cells isolated from the rat mesencephalon. At embryonic day 15, these cells stained positive with antibodies against nestin, microtubule-associated proteins, and glial fibrillary acidic proteins. The treatment of cultured neurospheres with *p*-nitrotoluene (1 μM; 72 h) facilitated differentiation with two distinct morphologies outside the sphere, being neural and glial lineages. Neurospheres could therefore be used as a very simple primary assay for screening environmental chemicals for disruption of developmental programming.

Development of the nervous system involves the coordinated expression of specific cellular events including proliferation, differentiation, migration, neurite outgrowth, synaptogenesis, myelination, and programmed cell death. Chemical-mediated disruption of one or more of these processes can potentially impair the brain development. In this study, therefore we further investigated the neurotoxicity of *p*-nitrotoluene using cultured human neuroblastoma NB-1 cells. Addition of *p*-nitrotoluene to NB-1 cells promoted neurite outgrowth in dose dependent manner (0.1–1 μM). During the chemical-facilitated neurite outgrowth, IL-6 was secreted

into the culture medium. It was 1.6-fold by 1 μM *p*-nitrotoluene. Availability of extension of neurite is a useful marker to screen the chemicals.

In this way, we currently extend the culture system employed in this study to other environmental chemicals for evaluation of their neurotoxicity.

References

1. Ishido, M. (2009) Environmental contribution to attention deficit hyperactivity disorder. In S.M. Gordon and A.E. Mitchell (Eds). Attention Deficit Hyperactivity Disorder (ADHD), Nova Sci. Publisher, NY, 223–328.
2. Ishido, M., Masuo, Y., Suzuki, J.-S., Oka, S., Niki, E., and Morita, M. (2004) Dicyclohexylphthalate causes hyperactivity in the rat concomitantly with impairment of tyrosine hydroxylase immunoreactivity. *J. Neurochem*. **91**: 69–76.

Integration of Endothelial Cell-Covered Hepatocyte Spheroids for Construction of Vascularized Liver Tissue

Masakazu Inamori, Hiroshi Mizumoto, and Toshihisa Kajiwara

1 Introduction

Tissue vascularization by coculture with endothelial cells has been studied for the creation of viable, large tissues for therapeutic use [1]. To supply a sufficient mass of hepatocytes for cell transplantation, a high cell density tissue-like structure (organoid) is necessary because of the limited space for transplantation in the body. A spheroid is a spherical organoid assembled in vitro from monodispersed cells. Hepatocyte spheroids have a cell density close to that of native liver tissue and express liver specific functions at a high level. Using novel culture techniques to produce different shapes of hepatocyte organoids, we previously demonstrated that hepatocyte organoids should be approximately 100 μm in diameter to survive [2–4]. Based on this evidence, the arrangement of endothelial cells within the hepatocyte organoid at regular 100 μm intervals is a promising approach for the construction of a larger, vascularized liver tissue. The endothelial cell-covered hepatocyte spheroid is a candidate tissue unit to produce the alignment of endothelial cells at regular intervals in large hepatic tissues to allow for the in vitro construction of a vascularized tissue [5].

Different types of cells were cocultured with endothelial cells to form vascularized tissue in vitro [6, 7]. When endothelial cells were added to a non-endothelial spheroid, the behavior of the endothelial cells varied with the combination of cell types [8, 9]. In most cases, endothelial cells invaded the spheroid but did not cover the spheroid surface. We assume that extracellular matrix (ECM) molecules must be present on the surface of the spheroid for an endothelial cell coat to form. To keep endothelial cells on the surface of the spheroid, we attempted to coat the surface of the hepatocyte spheroids with type 1 collagen. Following successful construction of HUVEC-covered hepatocyte spheroids, we attempted the regular alignment of HUVECs within liver tissue by packing HUVEC-covered hepatocyte spheroids into hollow fibers used for plasma separation.

T. Kajiwara (✉)
Department of Chemical Engineering, Kyushu University, Nishi-ku, Fukuoka, 819-0395, Japan
e-mail: kajiwara@chem-eng.kyushu-u.ac.jp

M. Kamihira et al. (eds.), *Animal Cell Technology: Basic & Applied Aspects*, Animal Cell Technology: Basic & Applied Aspects 16, DOI 10.1007/978-90-481-3892-0_8,

2 Materials and Methods

2.1 HUVEC-Covered Hepatocyte Spheroid Culture

Human umbilical vein endothelial cells (HUVECs, Lonza Ltd, Basel, Switzerland) were purchased and subcultured in endothelial growth medium-2 (EGM-2) (Lonza). Primary rat hepatocytes were isolated from a male Wistar rat (7–8 weeks old) by the collagenase perfusion method. Viable cells (85–95%) were used for spheroid culture. Isolated hepatocytes were suspended in hepatocyte culture medium: DMEM with high glucose (Invitrogen, Carlsbad, CA) supplemented with 50 μg/L epidermal growth factor (EGF, BT-201) (Biomedical Technologies, Inc., Stoughton, MA), 10 mg/L insulin (Sigma-Aldrich, St. Louis, MO), 60 mg/L proline (Sigma-Aldrich), 7.5 mg/L hydrocortisone (Wako Pure Chemical Industries, Ltd., Osaka, Japan), 3.7 g/L $NaHCO_3$, 5.985 g/L HEPES, 50 μg/L linoleic acid, 0.1 μM copper ($CuSO_4 \cdot 5H_2O$), 3 nM selenium (H_2SeO_3), 50 pM zinc ($ZnSO_4 \cdot 7H_2O$), and antibiotics (58.5 mg/L penicillin, 100 mg/L streptomycin). They were then cultured in a 6 well plate (Nalge Nunc International KK, Tokyo, Japan) at a concentration of 1.5×10^6 viable hepatocytes/well in 1.5 ml hepatocyte culture medium. Cells were incubated on a rotary shaker at 80 rpm at 37 °C in a humidified 5% CO_2 atmosphere. The supernatant (1 ml per well) was replaced on day two, and hepatocyte spheroids were collected on day 4. Collected spheroids were filtered using a stainless wire mesh. Hepatocyte spheroids from 100 to 150 μm sieve fractions were used for further experiments.

A Collagen Gel Culturing Kit (Nitta Gelatin Inc., Osaka, Japan) was used to coat the surface of the hepatocyte spheroids. Hepatocyte spheroids were resuspended in 1 ml hepatocyte culture medium. Cellmatrix Type I-A was reconstituted by adding 10× culture medium and reconstitution buffer according to the manufacturer's instruction. Reconstituted collagen gel (1 ml) was added to the spheroid suspension (final concentration of collagen: 1.2 mg/ml). After adding the collagen gel, the spheroid suspension was incubated at 4°C for one hour and washed twice by adding 10 ml cold hepatocyte culture medium followed by centrifugation at 40×g for 60 s.

Agarose (4%) was coated onto a 100 mm cell culture dish (BD Falcon, Franklin Lakes, NJ) and substituted with EGM-2 before use. Collagen-coated hepatocyte spheroids (7,500–10,000 spheroids) and HUVECs (3×10^6 cells) were plated in 12 ml EGM-2 per dish. The supernatant (10 ml per dish) was replaced every 2 days. Hepatocyte spheroids without a collagen coat were also cocultured with HUVECs as a control.

2.2 Vascular Network Formation Using HUVEC-Covered Hepatocyte Spheroids

HUVEC-covered hepatocyte spheroids (collagen-coated hepatocyte spheroids cocultured for 4 days with HUVECs) were collected and inoculated into hollow fibers used for plasma separation (polyethylene treated with ethylene vinyl

alcohol, PE-EVAL, Asahi Kasei Medical Co., Ltd., Tokyo, Japan) (inner diameter: 330 μm, outer diameter: 430 μm) and packed by centrifugation (40×g for 180 s). Approximately 3 cm hollow fibers containing HUVEC-covered hepatocyte spheroids were cultured in a 60 mm Petri dish (BD Falcon) in EGM-2. Media were replaced every two days. For liver specific functions, HUVEC-covered hepatocyte spheroids were inoculated into two 3 cm hollow fibers and packed by centrifugation as described above and then cultured in 2 ml hepatocyte culture medium supplemented with EGM-2 SingleQuots (Lonza). Collagen-coated hepatocyte spheroids were also cultured in hollow fibers as a control. The albumin concentration of the culture supernatant from the identical culture dish was measured using an enzyme-linked immunosorbent assay. Error bars indicate the standard deviation of two individual culture dishes.

2.3 Immunofluorescent Microscopy

Samples were embedded in Tissue-Tek® O.C.T. Compound (Sakura Finetechnical Co., Ltd., Tokyo, Japan) and frozen in liquid nitrogen. Frozen sections were obtained using a cryostat (CM1100, Leica). Sections were fixed in acetone for 10 minutes at 4 °C followed by washing in PBS (5 minutes, three changes). Sections were incubated in blocking solution (PBS containing 10% skim milk and 6% glycine) for 20 minutes. Sections were washed in PBS and incubated in blocking solution containing primary antibodies (1:100) for one hour at room temperature. Rabbit polyclonal anti-human von Willebrand factor (vWF) (Dako, Glostrup, Denmark) was used for HUVECs and goat anti-mouse albumin (BETHYL Laboratories, Inc, Montgomery, TX) was used for primary rat hepatocytes. Then sections were washed in PBS and incubated in blocking solution containing secondary antibodies (1:100) for one hour at room temperature. Swine anti-rabbit IgG FITC-conjugated (Dako) and donkey anti-goat IgG rhodamine-conjugated (Millipore, Billerica, MA) antibodies were used as secondary antibodies. Images were captured with a fluorescent microscope (IX71, Olympus, Tokyo, Japan). In some experiments, rabbit anti-goat IgG rhodamine-conjugated antibody was used after reaction with swine anti-rabbit IgG FITC-conjugated antibody giving a yellow image for vWF.

3 Results

3.1 Hepatocyte Spheroid-HUVEC Coculture

Two days after plating on agarose coated dishes, some HUVECs formed HUVEC spheroids. Other HUVECs were attached to the surface of hepatocyte spheroids. Without collagen coating of the hepatocyte spheroids, some HUVECs invaded the hepatocyte spheroids. On day 4 of coculture, many collagen-coated hepatocyte spheroids were covered with a single layer of HUVECs (Fig. 1A), while HUVECs

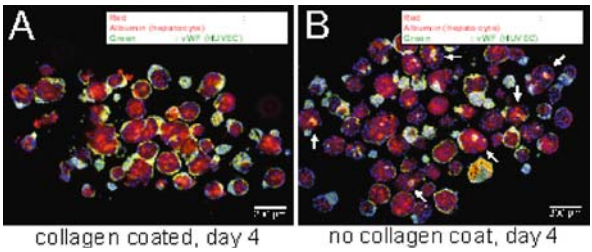

Fig. 1. Immunofluorescent microscopy of hepatocyte spheroid cocultured for 4 days with HUVECs stained for albumin (*drak grey*) and von Willebrand Factor (*white*). HUVEC invasion was observed (*white arrows*)

invaded some hepatocyte spheroids lacking a collagen coating, resulting in irregular distribution (Fig. 1B). The collagen coating of the hepatocyte spheroid prevented HUVEC invasion and facilitated HUVEC attachment to the spheroid surface.

3.2 Vascularized Liver Tissue Formation and Function

After packing HUVEC-covered hepatocyte spheroids into hollow fibers, HUVEC-covered hepatocyte spheroids adhered to each other, organizing into a large tissue during the culture time. HUVECs were distributed in regular intervals of approximately 100 μm. Some HUVECs invaded the hepatocyte spheroids forming a dense vascular network. On day 9, the HUVECs were observed to have a tubular morphology with a diameter of approximately 10–15 μm (Fig. 2A), close to that of a normal liver sinusoid [10].

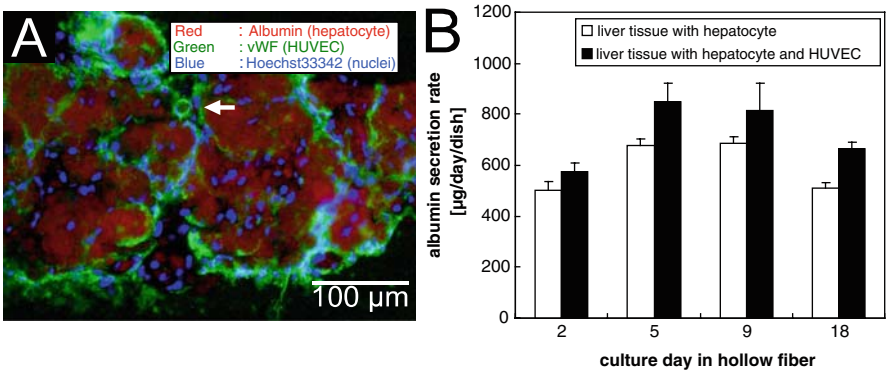

Fig. 2. (**A**) Immunofluorescent microscopy of HUVEC-covered hepatocyte spheroids 9 days cultured in hollow fibers stained for albumin (*drak grey*) and von Willebrand Factor (*white*). Tubular morphology of HUVECs were observed (*white arrows*). (**B**) Albumin secretion rate of liver tissue cultured in hollow fibers

The rate of albumin secretion of liver tissue comprised of hepatocytes and HUVECs was maintained at a higher level compared to that of liver tissue comprised of hepatocytes without HUVECs throughout the culture period (Fig. 2B).

4 Discussion

HUVEC-covered hepatocyte spheroids of 100–150 μm diameter ensure that HUVECs and hepatocytes coexist within a 100–150 μm proximity when they are packed into a hollow fiber to form a vascularized liver tissue. In this study, HUVECs invaded the hepatocyte spheroids, constructing a dense vascular network after packing in a hollow fiber. A similar phenomenon occurs during liver regeneration after partial hepatectomy. Hepatocytes proliferate to form a cluster after injury; then, stellate cells and sinusoidal endothelial cells invade the hepatocyte cluster [11, 12]. Regeneration of the liver will be one criterion for liver tissue construction. As for the effect of HUVEC coculture on the liver-specific functioning of hepatocytes when hepatocytes and HUVECs were aligned regularly, liver specific functions improved [13]. This result is in agreement with the improvement of liver-specific functioning by liver tissue comprised of hepatocytes and HUVECs (Fig. 2B). Coating collagen on the surface of cells or cell aggregates will serve other functions aside from heterologous cellular distribution control. One advantage is minimizing the inhibition of molecular transport by the ECM. Many types of ECM are barriers to molecular transport [14]. Compared to culture in a collagen gel, collagen coating of spheroids lead to less inhibition of exchange of nutrients and growth factors. Another report indicated that ECM coating of hepatocytes improved their adhesion to the liver during cell transplantation [15].

In conclusion, a spheroid covered by endothelial cells is a promising tissue unit for the construction of a vascularized tissue. Collagen coating of spheroids is also a candidate technique for the control of heterologous cellular distribution.

Acknowledgements This study was supported in part by a Grant-in-Aid for Scientific Research (B) 19360375 from the Japan Society for the Promotion of Science and supported by a grant from the Global-Centre of Excellence in Novel Carbon Resource Sciences, Kyushu University.

References

1. Kannan, R.Y., Salacinski, H.J., Sales, K., Butler, P., and Seifalian, A.M. (2005) The roles of tissue engineering and vascularisation in the development of micro-vascular networks: A review. *Biomaterials* **26**: 1857–1875.
2. Fukuda, J., Mizumoto, H., Nakazawa, K., Kajiwara, T., and Funatsu, K. (2004) Hepatocyte organoid culture in elliptic hollow fibers to develop a hybrid artificial liver. *Int. J. Artif. Organs* **27**: 1091–1099.
3. Mizumoto, H., Ishihara, K., Nakazawa, K., Ijima, H., Funatsu, K., and Kajiwara, T. (2008) A new culture technique for hepatocyte organoid formation and long-term maintenance of liver-specific functions. *Tissue Eng. Part C Methods* **14**: 167–175.

4. Ishihara, K., Mizumoto, H., Nakazawa, K., Kajiwara, T., and Funatsu, K. (2006) Formation of a sheet-shaped organoid using rat primary hepatocytes for long-term maintenance of liver-specific functions. *Int. J. Artif. Organs* **29**: 318–328.
5. Kelm, J.M., Djonov, V., Ittner, L.M., Fluri, D., Born, W., Hoerstrup, S.P., and Fussenegger, M. (2006) Design of custom-shaped vascularized tissues using microtissue spheroids as minimal building units. *Tissue Eng*. **12**: 2151–2160.
6. Rouwkema, J., de Boer, J., and Van Blitterswijk, C.A. (2006) Endothelial cells assemble into a 3-dimensional prevascular network in a bone tissue engineering construct. *Tissue Eng*. **12**: 2685–2693.
7. Stahl, A., Wenger, A., Weber, H., Stark, G.B., Augustin, H.G., and Finkenzeller, G. (2004) Bi-directional cell contact-dependent regulation of gene expression between endothelial cells and osteoblasts in a three-dimensional spheroidal coculture model. *Biochem. Biophys. Res. Commun*. **322**: 684–692.
8. Timmins, N.E., Dietmair, S., and Nielsen, L.K. (2004) Hanging-drop multicellular spheroids as a model of tumour angiogenesis. *Angiogenesis* **7**: 97–103.
9. Kunz-Schughart, L.A., Schroeder, J.A., Wondrak, M., van Rey, F., Lehle, K., Hofstaedter, F., and Wheatley, D.N. (2006) Potential of fibroblasts to regulate the formation of three-dimensional vessel-like structures from endothelial cells in vitro. *Am. J. Physiol. Cell Physiol*. **290**: C1385–1398.
10. Wack, K.E., Ross, M.A., Zegarra, V., Sysko, L.R., Watkins, S.C., and Stolz, D.B. (2001) Sinusoidal ultrastructure evaluated during the revascularization of regenerating rat liver. *Hepatology* **33**: 363–378.
11. Martinez-Hernandez, A. and Amenta, P.S. (1995) The extracellular matrix in hepatic regeneration. *FASEB J*. **9**: 1401–1410.
12. Sato, T., El-Assal, O.N., Ono, T., Yamanoi, A., Dhar, D.K., and Nagasue, N. (2001) Sinusoidal endothelial cell proliferation and expression of angiopoietin/Tie family in regenerating rat liver. *J. Hepatol*. **34**: 690–698.
13. Zinchenko, Y.S., Culberson, C.R., and Coger, R.N. (2006) Contribution of non-parenchymal cells to the performance of micropatterned hepatocytes. *Tissue Eng*. **12**: 2241–1251.
14. Ramanujan, S., Pluen, A., McKee, T.D., Brown, E.B., Boucher, Y., and Jain, R.K. (2002) Diffusion and convection in collagen gels: implications for transport in the tumor interstitium. *Biophys. J*. **83**: 1650–1660.
15. Kumaran, V., Joseph, B., Benten, D., and Gupta, S. (2005) Integrin and extracellular matrix interactions regulate engraftment of transplanted hepatocytes in the rat liver. *Gastroenterology* **129**: 1643–1653.

Characterization of Cell-Sized Vesicles Induced from Human Lymphoid Cell Lines

Makoto Yamanaka, Shigeki Nakamura, Aiko Inoue, Takashi Yasuda, Yuichi Inoue, and Hiroharu Kawahara

1 Introduction

Vesicles and liposome are widely used for the characterization of the membrane protein [4], the establishment of drug delivery system (DDS) [2], the modeling of artificial cells [3], the construction of the microreactor. In particular, membrane protein with the role of cell surface receptor in cell signaling is the key elements for drug candidate and research target. However, membrane-binding sites of those proteins have hydrophobicity and some membrane proteins change their structure and lose the activity by detachment from membrane. Therefore, it is difficult to produce membrane protein with the original structure and activity. We found the high concentration of sodium butyrate (NaB) induced mass production of cell-size vesicles in several human lymphoma cell lines, NaB serves as the histone deacetylase (HDAC) inhibitor and causes up-regulation of genes and proteins, inhibition of cell proliferation, and induction of apoptosis [5]. We examined the properties of the vesicles induced by NaB.

2 Material and Methods

2.1 Cell Line and Cell Culture

Three B lymphoma cell lines, Ramos (RA1), Nawalwa, and SK729-I, one T lymphoma cell line, Molt-4, two hybridoma cell lines, HB4C5, and AE6 were used in this study. SK729-I is a fusion partner cell line derived from Ramos (RA1). AE6 was generated by fusing peripheral blood lymphocytes from healthy adult with a fusion partner A4H12 derived from Molt-4 using an in vitro immunization method

M. Yamanaka (✉)
Graduate School of Life Science and Systems Engineering, Kyushu Institute of Technology, Kitakyushu-shi, Fukuoka 808-0196, Japan
e-mail: yamanaka-makoto@e-mail.jp

M. Kamihira et al. (eds.), *Animal Cell Technology: Basic & Applied Aspects*, Animal Cell Technology: Basic & Applied Aspects 16, DOI 10.1007/978-90-481-3892-0_9,

[1]. Cell were maintained in ERDF medium (Kyokuto Pharmaceutical Industrial Co., USA) contained 10% of FBS (Thermo Fisher Science Inc., Kanagawa, Japan), at 37°C in humidified 5% CO2/95% air.

2.2 Induction of Vesicles

Cells were cultured in the ERDF basal medium containing 10 μg/ml of insulin, 5.5 μg/ml of transferrin, 2 μg/ml of ethanolamine, 6.7 ng/ml of sodium selenite, 10 ng/ml of epidermal growth factor, and 5 mM of NaB (Sigma Chemical Co, USA) for one to two days.

2.3 Determination of Membrane Completeness and Mitochondrial Activity in the Vesicles

The completeness (or closing) of the vesicle membrane was determined by the trypan blue dye exclusion method. The mitochondrial activity was determinated by the MTT method.

2.4 Binding of the Cancer Specific Antibodies Expressing Vesicles with Cancer Cells

An IgM monoclonal antibody produced by AE6 cells reacted with human lung adenocarcinoma cell line A549 [1]. At first, AE6 cells were stained with the fluorescent dye DiI (Invitrogen, CA, USA) that can bind to cell membrane. After wash, the vesicles were induced from the DiI-stained AE6 cells by the treatment of NaB. Next, their vesicles were cultured with A549 cells for 2 hours. Finally, the binding of the vesicles to A549 cells was examined by fluorescence imaging.

In addition, reef coral fluorescent protein (RCFP) expression vector were introduced into the IgM-expressing vesicles by electroporation. Then, the vesicles containing RCFP vector were cultured with A549 cells. After 2 hours, the medium was exchanged to normal medium, and A549 cells were cultured more for 6 hours. Finally, the expression of the incorporated RCFP vector in A549 cells was determined by fluorescence imaging.

3 Results and Discussion

3.1 Induction of Vesicles

The vesicle induction of three B lymphoma cell lines, Ramos (RA1), Nawalwa, and SK729-I, one T lymphoma cell line, Molt-4, two hybridoma cell lines, HB4C5,

Table 1 Vesicle induction and its time from cells

Cell line	Vesicle induction	Induction time (day)
Ramos (RA1)	+	1
Namalwa	+	1
SK729-I	+	1
AE6	+	2
HB4C5	+	2
Molt-4	–	2

+ occurred, – not occured

and AE6 by the treatment of NaB was examined. IgM-producing cell line Ramos, Namalwa, SK729-I, AE6, and HB4C5 induced the vesicles, while non-Ig producer, Molt-4 cells did not induce them (Table 1). Among the cell lines tested, Ramos was the best induction at the rate of approximately 70% of total cell number. However, all cells were dead after NaB treatment. The induced vesicles were 4–6 μm of the same diameter as cell size in Ramos cells, and contained <5 μm in addition to cell size in AE6 cells (Fig. 1).

3.2 Membrane Completeness and Mitochondrial Activity

To evaluate the functional properties of the induced vesicles, their membrane completeness and mitochondrial activity were examined. Vesicles were not stained by the trypan blue dye exclusion method. Therefore, the vesicle's membrane has the completeness (Fig. 2), suggesting it can be available for a drug carrier.

In addition, the vesicles could not generate formazan from MTT, indicating that the mitochondrial activity of the vesicle was attenuated by the vesicle induction (Fig. 3).

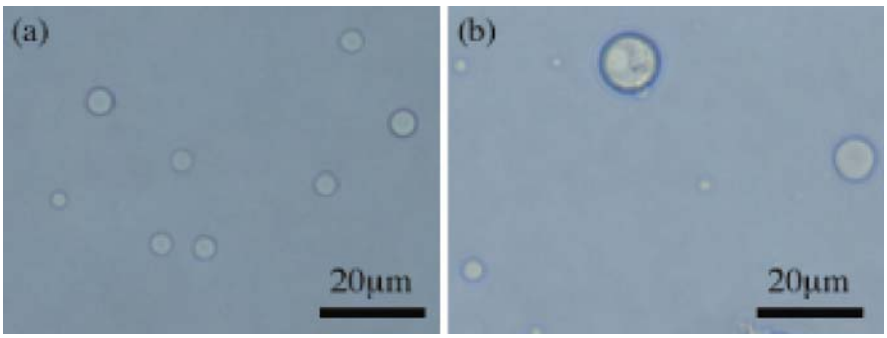

Fig. 1 Vesicles induced by cells. (**a**) Ramos, (**b**) AE6

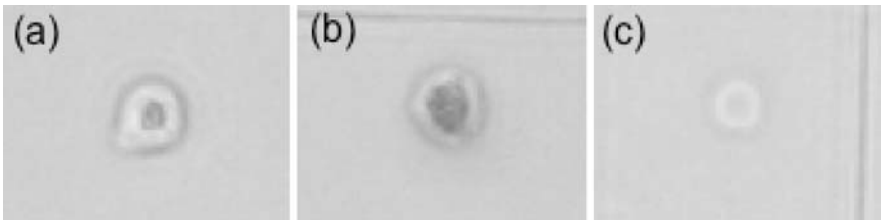

Fig. 2 Confirmation of membrane competeness by trypan blue dye exclusion. (**a**) viable cell, (**b**) dead cell, (**c**) vesicle

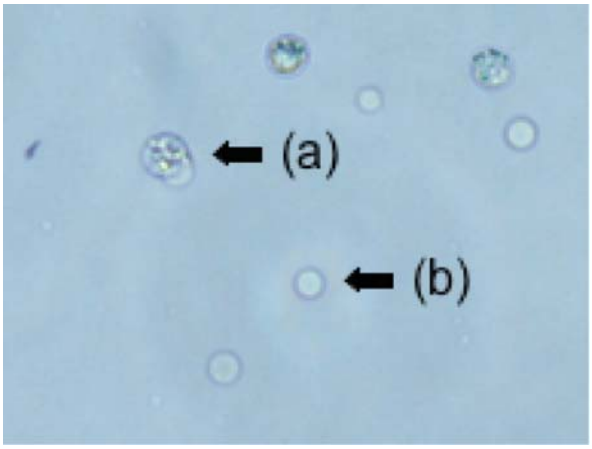

Fig. 3 Mitochondrial activity of cells and vesicles. (**a**) cell, (**b**) visicle

3.3 Binding of the Cancer Specific Antibodies in Vesicles with Cancer Cells

The induced vesicles had original cell membrane proteins and could express exogenous cell surface proteins on by transfection of their genes into the viable cells followed by cell treatment of NaB (data not shown). Thus, the binding of the cancer specific antibodies expressing vesicles with cancer cells was evaluated using the fluorescence staining method.

Microscopic observation showed that the DiI-stained vesicles of the lung cancer specific IgM producing AE6 cells were incorporated into the lung cancer A549 cells (Fig. 4). In addition, the movement of incorporated vesicles within the cells could be observed clearly.

However, the expression of RCFP in A549 cells by the binding of the vesicles containing the RCFP expression vector was not detected. Because transfection efficiency of gene into the vesicles by electroporation was low, it was not enough to detect RCFP expression in A549 cells.

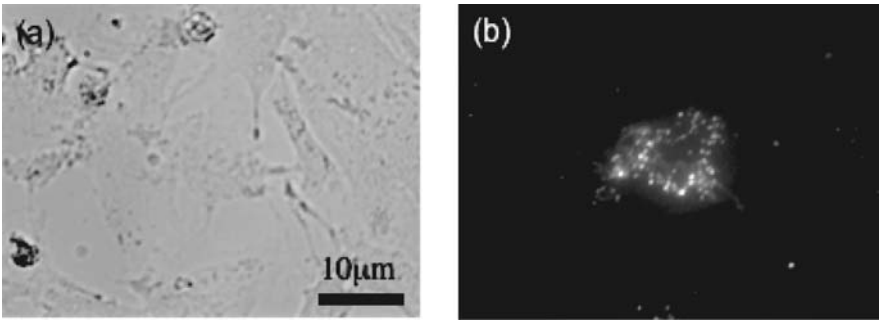

Fig. 4 Microscopic observation of DiI fluorescence-stained AE6 vesicle incorporated A549 cells. (**a**) bright field, (**b**) fluorescence imaging

4 Conclusions

We reported here several properties of cell-size vesicles induced from several lymphoma cell lines. However, the formation mechanism of the vesicles remains unclear. This study may be applicable to the development of the membrane protein production and active-targeting DDS using immunoglobulin producing cell lines.

References

1. Kawahara, H., Shirahata, S., Tachibana, H., and Murakami, H. (1992) In vitro immunization of human lymphocytes with human lung cancer cell line A549. *Hum. Antibod. Hybridomas* **3**: 8–13.
2. Suzuki, R., Oda, Y., Utoguchi, N., Kadowaki, N., and Maruyama, K. (2008) Development of novel antigen delivery system to dendritic cells using liposome technology in cancer immunotherapy. *Drug Delivery Sys*. 23(2): 123–129.
3. Noireaux, V., Libchaber, A., et al. (2004) A vesicle bioreactor as a step toward an artifical cell assembly. *Proc. Natl. Acad. Sci. USA* **101**:17669–17674.
4. Rigaud, J.L. and Levy D. (2003) Reconstitution of Membrane Proteins into Liposomes. *Method. Enzymol*. **372**: 65–86.
5. Vidali, G., Boffa, L.C., Bradbury, E.M., and Allfrey, V.G. (1978) Butyrate suppression of histone deacetylation leads to accumulation of multiacetylated forms of histones H3 and H4 and increased DNase I sensitivity of the associated DNA sequences. *Proc. Natl. Acad. Sci. USA* **75**(5): 2239–2243.

Dendrimer-Immobilized Culture Surface as a Tool to Promote Aggregate Formation of Anchorage-Dependent Cells

Mee-Hae Kim, Masahiro Kino-oka, Jun-ichi Miyazaki, and Masahito Taya

1 Introduction

In cultures of anchorage-dependent cells, the changes in cell morphology can cause variations in cell behaviors, and culture surface design is often employed to regulate the cell morphology. In our previous study [1], we designed the transporter-mediated anchoring by displaying D-glucose on a glass surface, and reported that the shape of rabbit chondrocytes and their adhesion were closely related to the density of D-glucose displayed on the surface. In the cultures with changed ratios of D- and L-glucose, it was found that 100% D-glucose-displayed surface provided a population of round-shaped cells with the promoted extracellular matrix (ECM) production. In the extended work with human mammary epithelial cells, the varied densities of D-glucose displayed were prepared by using starburst polyamidoamine dendrimer, which is a promising template for ligand display at terminals of dendric structure [1–4].

In the present study, the dendrimer template was employed for displaying D-glucose on a surface for culturing rabbit chondrocytes and mouse ES cells. Its unique structure is expected to yield physical features such as the dendrimer density on a surface and D-glucose quantity on dendrimer by changing the dendron core amount and generation number of dendrimer, respectively. Then we prepared various dendrimer-immobilized surfaces with D-glucose display and investigated the morphology, migration and aggregation of rabbit chondrocyte cells cultured on the prepared surfaces. In addition, the differentiation of the cells during monolayer growth was discussed in relation to ECM formation by the cells. Furthermore, we examined the morphological and functional responses of mouse ES cells cultured on the designed culture surfaces. The undifferentiated state of the cultured cells was confirmed by alkaline phosphatase (ALP) activity and gene expression analyses.

M.-H. Kim (✉)
Division of Chemical Engineering, Graduate School of Engineering Science,
Osaka University, Toyonaka, Osaka 565-0871, Japan
e-mail: mh-kim@cheng.es.osaka-u.ac.jp

M. Kamihira et al. (eds.), *Animal Cell Technology: Basic & Applied Aspects*, Animal Cell Technology: Basic & Applied Aspects 16, DOI 10.1007/978-90-481-3892-0_10,

2 Materials and Methods

2.1 Preparation of Glucose-Displayed Dendrimer Surfaces

The conventional polystyrene (PS) surface of a square 8-well plate (Nunc, Roskilde, Denmark) was used as a plain or starter material. Three types of dendrimer-immobilized surfaces with D-glucose display, that is, first-generation (G1) and fourth-generation (G4) surfaces as well as fourth-generation/low density (G4-LD) surface were designed by changing the generation number and density of synthesized dendrimers according to previous papers [1, 3, 5]. Briefly, the surface with fourth generation of dendrimer was designed as a structural template by stepwise addition of tris (2-aminoethyl) amine during the procedure for synthesis of dendrimer. Finally, D-glucose was displayed as terminal ligands on the template dendrimer.

2.2 Cell Isolation and Cultures

Rabbit chondrocyte cells. A biopsy of articular cartilage was harvested from hemeri, femora and tibias of Japanese white rabbits (about 1-month old), and chondrocytes were isolated by enzymatic digestion of the minced biopsy, as described elsewhere [1, 5]. The isolated cells were preserved in liquid nitrogen until examination. The primary culture was initiated by introducing the chondrocytes onto various surfaces in the well or flask immediately after thawing the cells. The culture was kept at 37°C under a 5% CO_2 atmosphere using Dulbecco's modified Eagle's medium (Sigma-Aldrich, St. Louis, MO, USA) with 10% fetal bovine serum, L-ascorbic acid and antibiotics. The seeding density was fixed at 1.0×10^4 viable cells per cm^2 of culture surface. At culture day 3, the spent medium was changed with fresh one.

Mouse ES cells. A feeder-free murine germline-competent ES cell line, EB3, was maintained on a surface of 0.1% gelatin coating in Glasgow minimum essential medium with 1000 U/ml leukemia inhibitory factor, as described previously [6, 7]. The seeding density of the cells was fixed at 5.0×10^3 cells/cm^2, unless otherwise stated. Passages 14–20 of undifferentiated ES cells were used in all the experiments, except for the blastocyst injection tests, which were performed using ES cells within 10 passages.

2.3 Staining of F-Actin and N-Cadherin

To visualize the organization of F-actin, cells were fixed in 4% paraformaldehyde for 15 min and permeabilized in 0.1% triton X-100 for 10 min at room temperature. Then the cells were incubated in a fluorescein phalloidin (Molecular Probes, Eugene, OR, USA). To investigate cell-cell contacts, the culture was conducted for 6 days in the single flask which provided two regions of G4 and G4-LD surfaces in

the same culture system. The cells were washed with PBS and premeabilized by the treatment with 0.5% Triton X-100 in PBS for 4 min. The premeabilized cells were incubated with a primary mouse antibody marking N-cadherin (Sigma-Aldrich) at 4°C overnight, after masking non-specific proteins. The cells were washed with Tris-buffered saline, followed by immunolabeling with Alexa Fluor 488 anti-mouse IgG (Molecular Probes) for 1 h. All samples were mounted and examined under a confocal laser scanning microscope.

2.4 RT-PCR Analysis

The RT-PCR analysis were performed according to conventional procedures, as described previously [6, 7]. Most of the primer sequences employed for the RT-PCR analysis was designed according to a PrimerBank database (http://pga.mgh.harvard.edu/primerbank/) [7].

3 Results and Discussion

3.1 Morphological Regulation and Aggregate Formation of Rabbit Chondrocytes on Dendrimer-Immobilized Surface with D-Glucose Display

To investigate the cell behaviors on various surfaces, rabbit chondrocyte cells were cultured on the modified surfaces with the varied generation numbers and densities of dendrimer used for D-glucose display. As shown in Fig. 1, the round-shaped cells

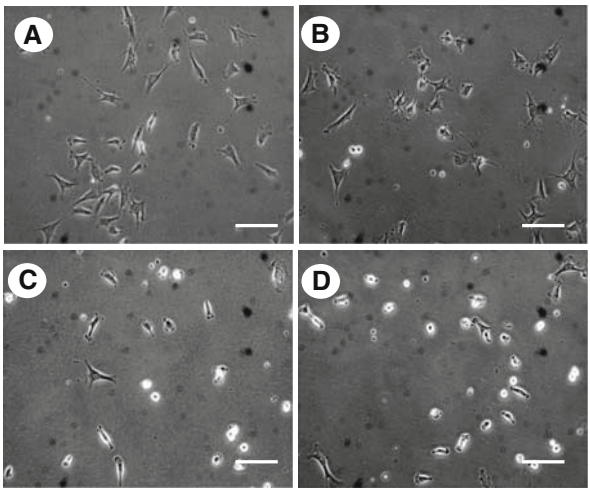

Fig. 1 Phase contrast images of chondrocytes cultured on PS (**A**), G1 (**B**), G4 (**C**) and G4-LD (**D**) surfaces. The images were taken in the cultures at day 3. (Scale bars = 100 μm)

were found to appear on G4 and G4-LD surfaces, while the cells on PS and G1 surfaces exhibited a stretch shape dominantly. To understand the cytoskeletal formation of the cells on various surfaces, the F-actin staining was conducted using the cells obtained at day 3. As seen in Fig. 2A-C, the stretch-shaped cells on PS, G1 and G4 surfaces were found to retain fully developed stress fibers with traversing F-actin. On G4-LD surface, however, the immature stress fibers were recognized not only in the round-shaped cells but also in the stretch-shaped cells (Fig. 2D). In

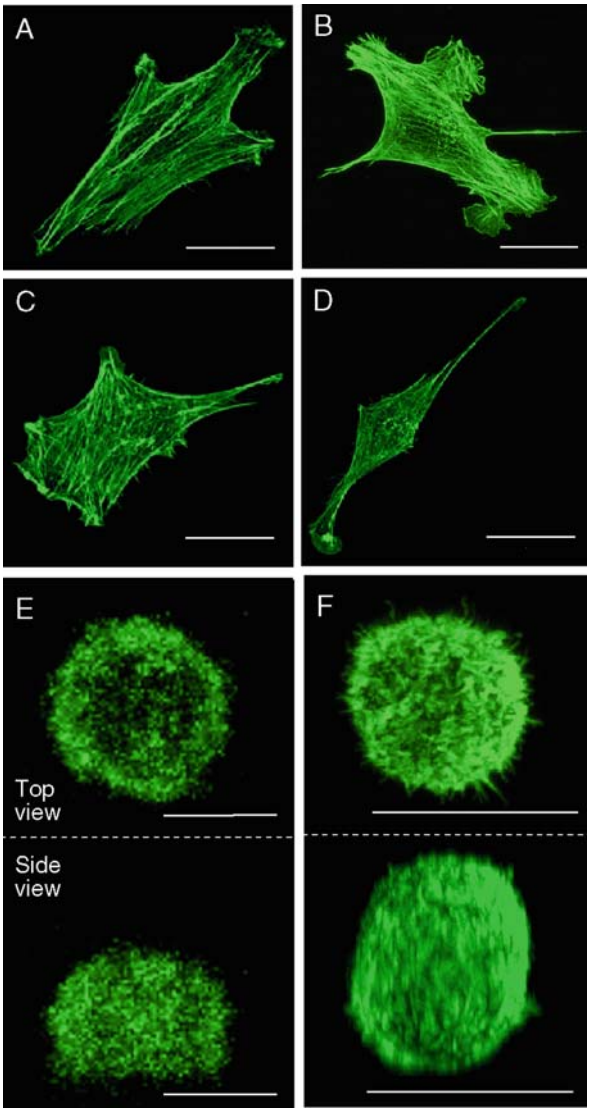

Fig. 2 Immunostaining of F-actin in stretch-shaped and round-shaped chondrocytes on PS (**A**), G1 (**B**), G4 (**C**, **E**) and G4-LD (**D**, **F**) surfaces. The images were taken in the cultures at days 3. (Scale bars = 20 μm)

addition, the stereoscopic examination revealed that the round-shaped cells on G4-LD surface exhibited a spherical shape having cortical actin organization. Based on the time-lapse observation, it was demonstrated that the cells on G4-LD surface exhibited active migration, associated with the periodic change of the cell morphologies in stretching and contracting manners (data not shown). Lasing the culture on G4-LD surface led to appreciable aggregation through cell division and cellular coalescence, while such aggregation did not occur on PS and G1 surfaces. Moreover, immunostaining of the cells provided an evidence that collagen type II formed exclusively around the round-shaped and aggregated cells on G4 and G4-LD surfaces. However, the formation of collagen type II was seldom recognized around the cells on PS and G1 surfaces (data not shown). It was thus suggested that cellular morphology can be a physiological measure to dominate the formation of collagen type II in association with cell aggregates.

To know the contribution of N-cadherin to cell-cell contacts, we conducted the N-cadherin staining of cells cultured in the single flask with two regions of G4 and G4-LD surfaces. As shown in Fig. 3, the cells dispersed in a confluent monolayer manner in the region of G4 surface with appreciably declining in N-cadherin formation, although the florescent intensity was still higher than those on PS and G1 surfaces (data not shown). On G4-LD surface, on the other hand, the N-cadherin formation was outstanding in almost all cells, including not only the round-shaped and aggregated cells but also stretched cells, and still significantly higher than that in the cells on G4 surface (Fig. 3C). Occasionally, the staining signal was intensified in the areas of cell-cell contacts among the aggregates. It was thus considered that this morphological change on the modified surface with the lowered dendrimer density was responsible for the promoted N-cadherin expression during aggregation, thereby facilitating the chondrogenic phenotypes with the abundant formation of collagen type II.

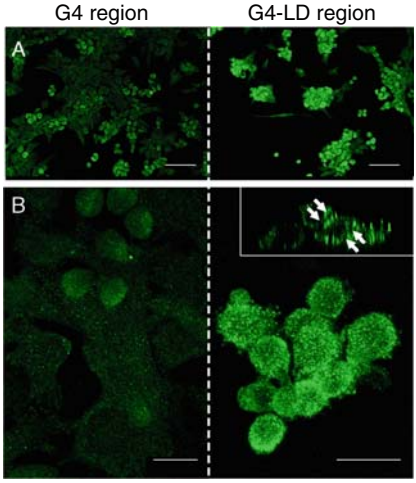

Fig. 3 Immunostaining of N-cadherin produced by chondrocytes cultured for 6 days on G4 (**A**) and G4-LD (**B**) surfaces. The panels B indicate the magnified images of cells, and the insertion in the right-hand panel is the cross-sectional image with the arrows pointing at the prominent expression of N-cadherin. (Scale bars = 100 (**A**) and 20 (**B**) μm)

3.2 Application of Designed Surface to Culturing Mouse ES Cells

The morphology of the ES single cells as well as the ES cell aggregates on the different culture surfaces were compared as indicated in Fig. 4. The single-cell observation on day 1 showed that most of the cells on the G4-LD surface were round, while those on the conventional gelatin-coated (GLN) surface exclusively showed a stretched morphology (Fig. 4A, B). Moreover, on day 4 the cells on the G4-LD surface formed loosely attached spherical aggregates, while those on the conventional surface formed flatter aggregates that were firmly attached to the surface (Fig. 4C, D).

The possibility of using G4-LD surface as a tool for enrichment of undifferentiated state of ES cells was investigated by culturing the cells for several passages. The undifferentiated cultured cells on the G4-LD and GLN surfaces were compared by both alkaline phosphatase (ALP) staining and RT-PCR analysis. The results showed that ALP activity of the spherical aggregate cells on the G4-LD surface increased with increasing the passage number (data not shown).

The result of RT-PCR analysis showed that undifferentiation cell markers (Rex-1 and Oct3/4) were detected at higher levels for spherical aggregate cells on G4-LD surface, compared to the cells grown on GLN surface (Fig. 5). Moreover, in the case of early differentiation markers, endodermal (GATA4), mesendodermal (Gsc) and meso-dermal (T, Wnt3) differentiation, the expressions were at lower levels for spherical aggregate cells on G4-LD surface, compared to those grown on GLN surface.

In conclusion, this study suggests that G4-LD surface can offer culture environment to promote cell-cell interactions, facilitating the cell aggregation, which can maintain the desired cell phenotypes during cultures.

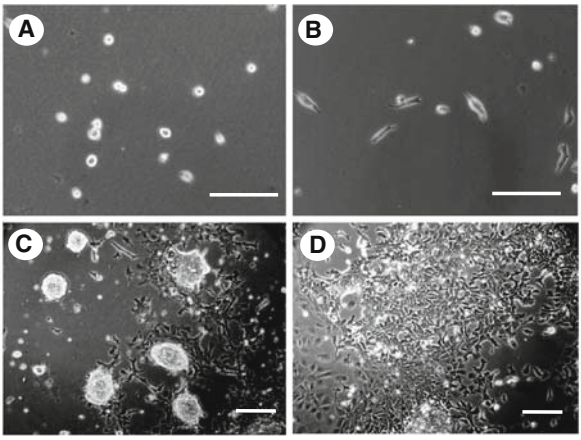

Fig. 4 Morphologies of ES cells cultured on G4-LD (**A**) and GLN (**B**) surfaces at day 1 (**A**, **B**) and 4 (**C**, **D**). (Scale bars = 100 μm)

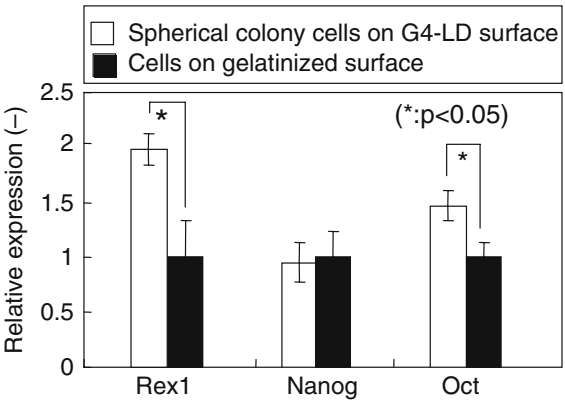

Fig. 5 RT-PCR analysis for 3 stem cell markers in ES cells cultured on G4-LD and GLN surfaces after being passaged 4 times. Values represent mean ± SD of 3 independent experiments

Acknowledgements The authors thank Japan Tissue Engineering Co., Ltd. for providing rabbit articular chondrocytes and Nissan Chemical Ind. for technical discussion. The present study was conducted as a part of the program "Center for integrated cell and tissue regulation" for the Center of Excellent (21st COE), Osaka University. This work received financial support in part by a Grant-in-Aid for Scientific Research (No. 17360398) from the Ministry of Education, Culture, Sports, Science and Technology. One of the authors (M.H.K.) expresses her thanks for financial support as Postdoctoral Fellow from the Japan Society for the Promotion of Science.

References

1. Kino-oka, M., Morinaga, Y., Kim, M.-H., Kawase, M., Yagi, K., and Taya, M. (2007) Morphological regulation of rabbit chondrocytes on glucose-displayed surface. *Biomaterials* **28**(9): 1680–1688.
2. Kim, M.-H., Kino-oka, M., Kawase, M., Yagi, K., and Taya, M. (2007) Response of human epithelial cells to culture surfaces with varied roughness prepared by immobilizing dendrimers with/without D-glucose display. *J. Biosci. Bioeng*. **103**(2): 192–199.
3. Kim, M.-H., Kino-oka, M., Kawase, M., Yagi, K., and Taya, M. (2007) Synergistic effect of D-glucose and epidermal growth factor display on dynamic behaviors of human epithelial cells. *J. Biosci. Bioeng*. **104**(5): 428–431.
4. Kim, M.-H., Kino-oka, M., Kawase, M., Yagi, K., and Taya, M. (2008) Glucose transporter mediation responsible for morphological changes of human epithelial cells on glucose-displayed surfaces. *J. Biosci. Bioeng*. **105**(4): 319–326.
5. Kim, M.-H., Kino-oka, M., Yoshiki, M., Sawada, Y., Kawase, M., Yagi, K., and Taya, M. (2009) Morphological regulation and aggregate formation of rabbit chondrocytes on dendrimer-immobilized surface with D-glucose display. *J. Biosci. Bioeng*. **107**(2): 196–205.
6. Niwa, H., Masui, S., Chambers, I., Smith, A.G., and Miyazaki, J. (2002) Phenotypic complementation establishes requirements for specific POU domain and generic transactivation function of Oct-3/4 in embryonic stem cells. *Mol. Cell Biol*. **22**(5): 1526–1536.
7. Mashayekhan, S., Kim, M.-H., Miyazaki, S., Tashiro, F., Kino-oka, M., Taya, M., and Miyazaki, J. (2008) Enrichment of undifferentiated mouse embryonic stem cells on a culture surface with a glucose-displaying dendrimer. *Biomaterials* **29**(31): 4236–4243.

Advantage of Alagln as an Additive to Cell Culture Medium

Application to Anti-CD20 Chimeric Antibody-Producing POTELLIGENT^{TM} CHO Cell Lines

Yasufumi Imamoto, Hisaya Tanaka, Ken Takahashi, Yoshinobu Konno, and Toshiyuki Suzawa

1 Introduction

Monoclonal antibodies (Mab) have been well-established therapeutics and are generally produced by cell culture. However, cost reduction by elevating production titer is a key challenge to be considered for the development of Mab production process. To achieve this, there are some choices and improvement of cell culture medium is one of the common methods.

In this study, we explored availability of dipeptides as substitutes for amino acid additives. Dipeptides were expensive ingredients and have not been suitable for the use of supplements in culture medium so far. Recently, a novel economical production method [1] has been invented, and provides an opportunity to take advantage of dipeptides as components of culture medium. We here investigated the effectiveness of two kinds of dipeptide, L-alanyl-L-glutamine (AlaGln) and L-alanyl-L-tyrosine (AlaTyr). As AlaGln is quite stable in water and produces less ammonia than Gln, it is expected to be a better nitrogen source. On the other hand, AlaTyr shows higher solubility in water than Tyr. Cell cultures were done to test the practicalities of these dipeptides feature.

2 Materials and Methods

2.1 Fed Batch Culture

Addition of dipeptide to culture medium was tested by cell culture using Erlenmeyer flask or 1 L Jar. Two kinds of Potelligent^{TM} Chinese hamster ovary cells (represented as A and B) expressing anti-CD20 chimeric antibody [2] were adopted to

Y. Imamoto (✉)
Bio Process Research and Development Laboratories, Production Division, Kyowa Hakko Kirin Co., Ltd., Takasaki-shi, Gunma 370-0013, Japan
e-mail: yasufumi.imamoto@kyowa-kirin.co.jp

M. Kamihira et al. (eds.), *Animal Cell Technology: Basic & Applied Aspects*, Animal Cell Technology: Basic & Applied Aspects 16, DOI 10.1007/978-90-481-3892-0_11,

evaluate the effectiveness. Dipeptides were added to basal culture medium and/or feed medium. Cell culture was started by inoculating the cells at 3.0×10^5 cells mL^{-1} in the serum-free medium. Fed-batch culture was carried out in 250 mL Erlenmeyer flask for 14 days without pH and DO controls. IMDM-based feed medium was added on days 4, 6, 9, and 11. Cell culture using 1 L-scale bioreactor was also performed under pH and DO controls. In this case, feed medium was added on days 3, 5, 7, 9, and 11. Additives (AlaGln, AlaTyr or ammonia) were added to culture medium prior to use.

2.2 Analysis

Mab titer was measured by Protein A HPLC. Viable cell was counted by a Cedex, using trypan blue exclusion. Early apoptotic ratio was measured by Guava EasyCyte. Gln concentration was determined by Nova 200, and AlaGln was derivatized with 9-fluorenylmethoxycarbonyl (Fmoc-Cl) and measured by HPLC.

3 Results and Discussions

3.1 Effect of Dipeptide Addition to Culture Medium

Effects of AlaGln and AlaTyr on cell culture were evaluated. In figures, combination of Gln (or Tyr) sources was indicated as Gln-AlaGln, for instance, where Gln was added in basal culture medium and AlaGln was supplemented in feed medium. The results for cell growth and Mab titer were shown in the following figures (Figs. 1, 2, 3, 4).

The results showed some advantages of dipeptides. Though the extent of efficacy was dependent on cell lines and culture methods (flask or jar), dipeptide addition improved production titer in almost all the cases.

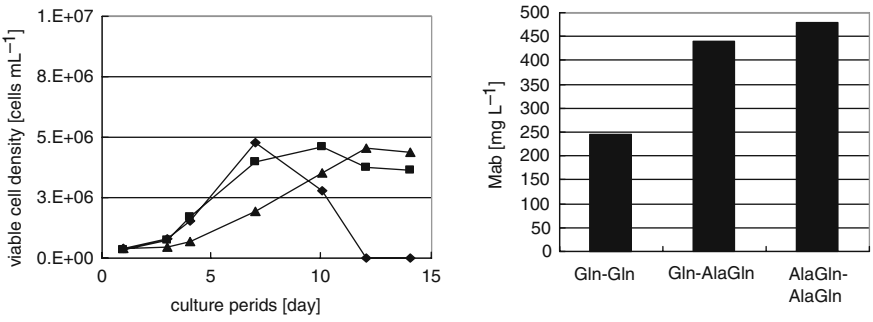

Fig. 1 Effect of AlaGln on cell growth and titer (Cell line A in Erlenmeyer flask) under Gln-Gln (♦), Gln-AlaGln (■), and AlaGln-AlaGln (▲) conditions, respectively

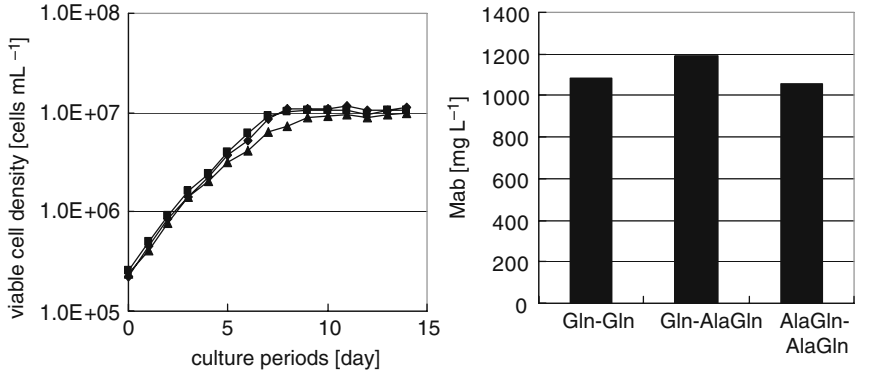

Fig. 2 Effect of AlaGln on cell growth and titer (Cell line A in 1 L Jar) under Gln-Gln (♦), Gln-AlaGln (■), and AlaGln-AlaGln (▲) conditions, respectively

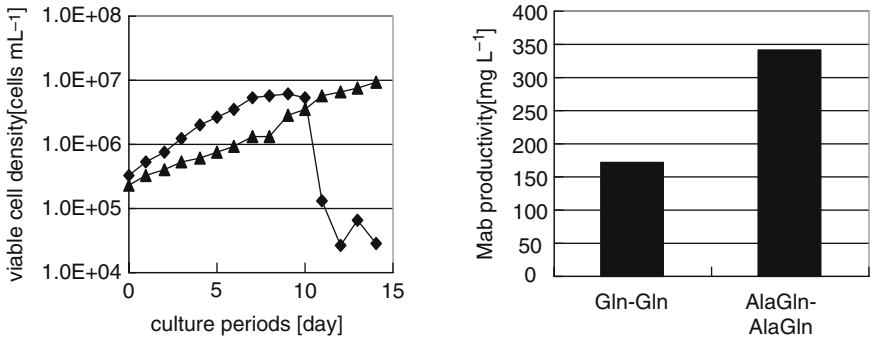

Fig. 3 Effect of AlaGln on cell growth and titer (Cell line B in 1 L Jar) under Gln-Gln (♦) and AlaGln-AlaGln (▲) conditions, respectively

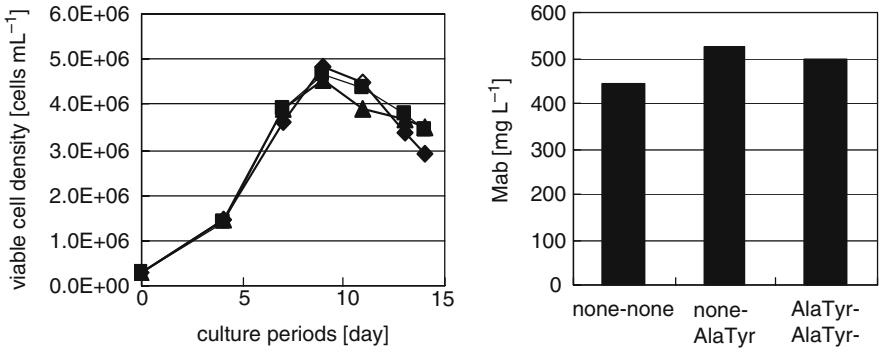

Fig. 4 Effect of AlaTyr on cell growth and titer (Cell line A in Erlenmeyer flask) under none-none (♦), none-AlaTyr (■), AlaTyr-AlaTyr (▲) conditions, respectively

To clarify the effect of AlaGln on cell culture, two parameters were measured; one was early apoptotic ratio as an index of cell physiology, and the other was time course change of Gln and AlaGln concentrations coupled with nitrogen source consumption. The results showed that AlaGln addition suppressed apoptotic ratio on the 8th day and the 10th day of cell culture (Fig. 5). Although the cells showed almost the same early apoptotic ratio on the 10th day for Gln-AlaGln and Gln-Gln conditions, apoptotic ratio was kept small for AlaGln-AlaGln condition.

As for time course change of Gln and AlaGln concentrations, Gln concentration was almost 0 mmol L^{-1} at the beginning of cell culture. On the other hand, AlaGln accumulated in the cell culture medium as AlaGln was supplemented with feed medium, because it was not consumed readily. As cell culture was developed, Gln concentration increased while AlaGln concentration decreased presumably due to decomposition of AlaGln which might be caused by peptidase released from dead cells (Fig. 6).

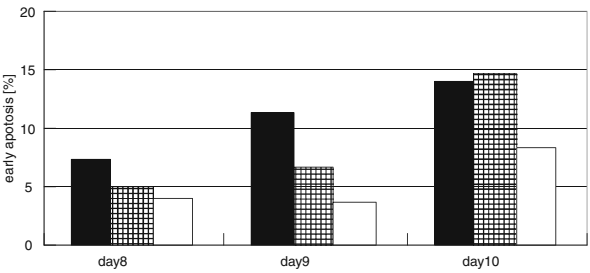

Fig. 5 Early apoptosis ratio during cell culture in 1 L Jar Gln-Gln (*black*), Gln-AlaGln (*mesh*), AlaGln-AlaGln (*white*)

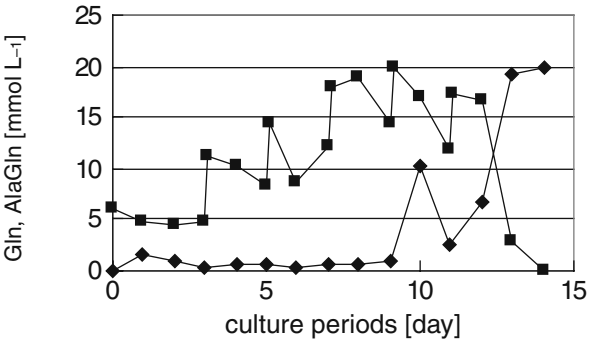

Fig. 6 Time course change of Gln (♦) and AlaGln (■) during cell culture supplemented with AlaGln in 1 L Jar

3.2 Controlling Ammonia Generation and Its Impact on Cell Culture

To compare stability of Gln and AlaGln quantitatively, time course change of ammonia in cell culture medium was measured (Fig. 7). The result showed that the stability of AlaGln was higher in the medium, and AlaGln produced less ammonia than Gln. Ammonia is well-known to inhibit cell growth and may have significant impact on Mab production titer.

Next, inhibition effect of ammonia on cell culture profile was tested using Erlenmeyer flask. Correlating with the increase of ammonia concentration, cell growth was confirmed to be decreased (Fig. 8).

The observation indicated above could be an advantage of AlaGln in medium preparation at manufacturing site of Mab, since cell culture medium on site is generally stored at ambient temperature until the use. During the storage, Gln in the medium degrades quickly to elevate ammonia accumulation, while AlaGln degrades moderately. To confirm this hypothesis, cell culture was performed in 1 L Jar under the mimetic condition of manufacture at scale (i.e., 24 mmol L^{-1} ammonia was added to culture medium). The results indicated that ammonia addition significantly suppressed cell growth and Mab production titer (Fig. 9). Based on these results, it was concluded that stored medium having an elevated ammonia level led to inhibit cell culture. To prevent ammonia generation during the storage of culture medium, AlaGln should be a better nitrogen source.

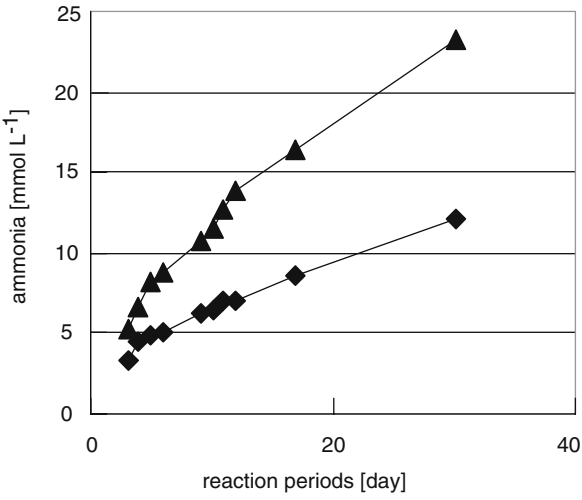

Fig. 7 Time course change of ammonia in basal medium containing Gln (▲) or AlaGln (♦)

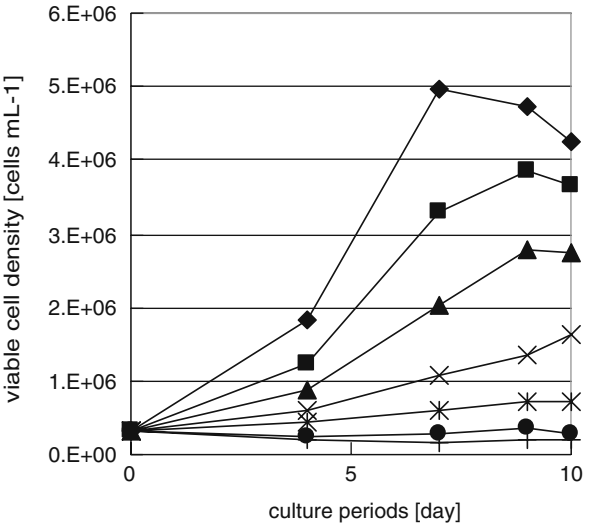

Fig. 8 Effect of ammonia (0 mmol L^{-1} (♦), 10 mmol L^{-1} (■), 20 mmol L^{-1} (▲), 30 mmol L^{-1} (×), 40 mmol L^{-1} (*), 50 mmol L^{-1} (●)) on cell culture of cell line A

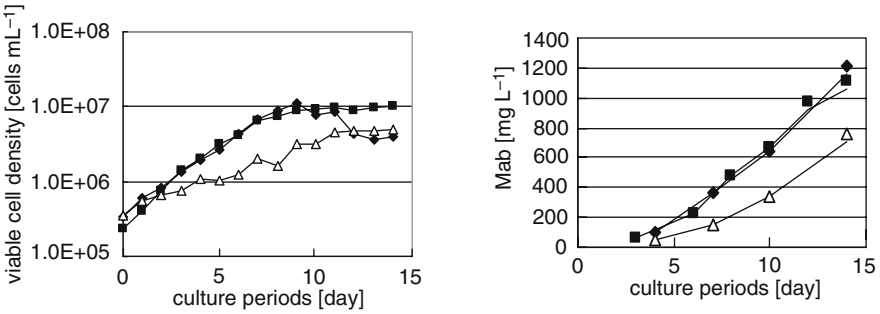

Fig. 9 Effect of ammonia on cell growth and titer of cell line A (1 L Jar) in Gln-Gln (♦), Gln-AlaGln (■), Gln-Gln plus ammonia (△) conditions

4 Conclusion

This article proposed advantages of using two kinds of dipeptide for cell culture, AlaGln and AlaTyr. Addition of these dipeptides increased Mab titer and improved cell growth, though degree of improvement was dependent on cell lines and culture method. Stability of AlaGln was higher than that of Gln, which generated ammonia significantly than AlaGln during the storage of cell culture medium. This may lead to the difference in culture performance, especially in manufacturing conditions. From these data, it was concluded that certain dipeptides could offer better performance in cell culture by replacing some amino acid additives.

References

1. Tabata, K. and Hashimoto, S. (2007) Fermentative production of L-alanyl-L-glutamine by a metabolically engineered Escherichia coli strain expressing L-amino acid alpha-ligase. *Appl. Environ. Microbiol*. **73**(20): 6378–6385.
2. Kanda, Y., Yamane-Ohnuki, N., Sakai, N., Yamano, K., Nakano, R., Inoue, M., Misaka, H., Iida, S., Wakitani, M., Konno, Y., Yano, K., Shitara, K., Hosoi, S., and Satoh, M. (2006) Comparison of cell lines for stable production of fucose-negative antibodies with enhanced ADCC. *Biotechnol. Bioeng*. **94**(4): 680–688.

Supplementation of Phosphatidylcholine Protects the Hybridoma Cells from Apoptosis Induced by Serum Withdrawal

Beng Ti Tey, Kah Choon Yap, Hideki Yamaji, Abdul Manaf Ali, and Wen Siang Tan

1 Introduction

Serum is an important mitogenic agent that promotes cell growth in mammalian cells. Since it is originated from other animals, it may contain infectious agents like viruses and prions, hence its uses during the manufacturing of monoclonal antibody are prohibited by regulatory agency. Studies that focused on serum replacement have led to the development of various serum and protein free medium formulations. However, the withdrawal of serum from the culture medium was reported to retard the cell growth and induce apoptosis [2, 5, 7, 8]. Furthermore, cells were more susceptible to apoptosis when they are cultivated in serum-free medium compared to those cultivated in medium supplemented with serum [4, 5]. Indeed, apoptosis is a major cell death mechanism in mammalian cell lines that used in biotherapeutic manufacturing (Reviewed in [6]).

In a recent report, Lee et al [3]. revealed that serum withdrawal can caused an elevation in cellular ROS levels, and induced apoptosis cell death in human U397 cells. ROS such as $O_2^{\bullet -}$ and H_2O_2 are important mediators of intracellular signaling pathway. In another study, Zweigner et al [10]. reported that the presence of H_2O_2 has strongly inhibited PtdCho synthesis and induced apoptosis in a human microglial cell line. It was proposed that the inhibition of PtdCho synthesis due to the lipid peroxidation or inhibition of choline phosphotransferase (CPT) by intracellular acidification by H_2O_2. Phosphatidylcholine (PtdCho) is an important phospholipid in eukaryotic cell membranes and it plays important role in signal transduction. It is synthesized via the cytidine diphosphocholine (CDP-choline) pathway. The inhibition of this pathway that led to the PtdCho deficiency is known to triggers apoptosis in many cell lines [1]. Hence, there may be a possible link between the serum withdrawal and PtdCho transduction pathway. In this study, the

B.T. Tey (✉)
Department of Chemical and Environmental Engineering, Faculty of Engineering, Universiti Putra Malaysia, 43400 UPM Serdang, Selangor, Malaysia
e-mail: btey@eng.upm.edu.my

M. Kamihira et al. (eds.), *Animal Cell Technology: Basic & Applied Aspects*, Animal Cell Technology: Basic & Applied Aspects 16, DOI 10.1007/978-90-481-3892-0_12,

effect of PtdCho supplementation on the apoptotic cell death induced by the serum withdrawal was investigated.

2 Materials and Methods

2.1 Cell Line

The hybridoma C_2E_7 cell line secreting the IgM antibody against the Mcf-7 breast cancer cells was used in this study.

2.2 Analysis of Cell Density and Viability

Cell density and viability were evaluated using a haemacytometer with trypan blue exclusion method.

2.3 Analysis of Apoptosis Level

Viable, early apoptotic, late apoptotic, necrotic and chromatin free (ghost) cells were identified by fluorescence microscopic analysis of plasma membrane integrity and nuclear morphology by double staining with propidium iodide (PI) and acridine orange (AO).

2.4 Batch Culture

Stock culture of the hybridoma C_2E_7 cells was first established. At mid-exponential phase of the culture, cells were harvested by centrifugation and resuspended at 2×10^5 cells/ml in a fresh medium containing 10% FBS or without any FBS (0%) and transferred into a 75 cm^2 T-flask with a total working volume of 25 ml. Both the serum enriched (10% FBS) and serum withdrawal (0% FBS) were supplemented with PtdCho to a final concentration of 100 μg/ml. The cultures without any PtdCho supplementation were used as controls. The cultures were then incubated at 37 °C. Samples were taken daily in order to assess viable cell number, viability and apoptosis levels as mentioned above.

3 Results and Discussion

In the present study, 100 μg/ml of PtdCho was supplemented to the hybridoma culture in the presence of serum and under serum withdrawal conditions. Under the serum withdrawal condition, the culture supplemented with PtdCho was able to maintain about 30% viability for over 6 days, while the viability of the culture without PtdCho supplementation has decreased to about 10% (Table 1). In the serum

Table 1 Influence of PtdCho Supplementation on the Growth and Survivability of the Hybridoma C_2E_7 Cells under Serum Withdrawal Conditions (0% FBS)

	With 100 μg/ml of PtdCho	Without PtdCho
Initial Cell Density (cells/ml)	1.95×10^5	1.95×10^5
Maximum Cell Density (cells/ml)	4.00×10^5	3.65×10^5
Viability (%) after 6 days of Cultivation	29	10

Table 2 Influence of PtdCho Supplementation on the Growth and Survivability of the Hybridoma C_2E_7 Cells under Serum Enriched Conditions (10% FBS)

	With 100 μg/ml of PtdCho	Without PtdCho
Initial Cell Density (cells/ml)	1.90×10^5	1.90×10^5
Maximum Cell Density (cells/ml)	1.50×10^6	1.42×10^6
Viability (%) after 6 days of Cultivation	35	2.5

supplemented culture, the presence of exogenous PtdCho was able to enhance the survivability of hybridoma at the death phase of the culture. The viability of the PtdCho culture was maintained at about 35% for over 8 days, while the viability of the control culture has dropped to about 2% (Table 2).

The majority of the dead cells in the control culture were identified as apoptotic cells (Tables 3 and 4). Hence, the supplementation of PtdCho in the medium has delayed the apoptotic cell death that induced by serum withdrawal. The results of the current study is in good agreement with that reported by other researchers who used

Table 3 Cell Fraction of Hybridoma C_2E_7 Cells after 6 Days of Cultivation under Serum Withdrawal Conditions (0% FBS)

Cell Type	With 100 μg/ml of PtdCho	Without PtdCho
Viable (%)	20.8	7.3
Early Apoptotic (%)	3.8	5.4
Late Apoptotic (%)	70.2	83.4
Ghost (%)	5.2	3.9
Necrosis (%)	0	0

Table 4 Cell Fraction of Hybridoma C_2E_7 Cells after 8 Days of Cultivation under Serum Enriched Conditions (10% FBS)

Cell Type	With 100 μg/ml of PtdCho	Without PtdCho
Viable (%)	23	3.0
Early Apoptotic (%)	20	15.3
Late Apoptotic (%)	48.5	73.2
Ghost (%)	3.5	8.5
Necrosis (%)	5.0	0

PtdCho to suppress apoptosis induced by various apoptotic inducer such as purified pneumolysin and H_2O_2 [10], and drugs such as farnesol and chelerythrine [1]

4 Conclusion

The results of the present study showed that PtdCho is able to protect the hybridoma cells from apoptosis triggered by serum withdrawal. In addition, no effect on the specific growth rate, maximum cell density and monoclonal antibody production were observed in the culture supplemented with PtdCho. Therefore, PtdCho is a suitable component for the formulation of a serum free medium.

Acknowledgements This study was supported by the e-Science Fund (02-01-04-SF0763) from the Ministry of Science, Technology and Innovation; FRGS Grant (FRGS A-408) from the Ministry of Higher Education of Malaysia; and Japan Society for the Promotion of Science (JSPS).

References

1. Anthony, M.L., Zhao, M., and Brindle, K.M. (1999) Inhibition of phosphatidylcholine biosynthesis following induction of apoptosis in HL-60 cells. *J. Biol. Chem*. **274**: 19686–19692.
2. Fujita, T., Terada, S., Ueda, H., and Suzuki, E. (1996) Over-expression of Bcl-2 improved survival of COS-1 cells and enhanced transient protein production. *J. Ferment. Bioeng*. **82:** 589–591.
3. Lee, S.B., Cho, E.S., Yang, H.S., Kim, H., and Um, H-D. (2005) Serum withdrawal kills U937 cells by inducing a positive mutual interaction between reactive oxygen species and phosphoinositide 3-kinase. *Cell. Signal*. **17**: 197–204.
4. Moore, A., Donahue, C.J., Hooley, J., Stocks, D.L., Bauer, K.D., and Mather, J.P. (1995) Apoptosis in CHO cell batch cultures – examination by flow cytometry. *Cytotechnol*. **17**: 1–11.
5. Singh, R.P., Al-Rubeai, M., Gregory, C.D., and Emery, A.N. (1994) Cell-death in bioreactors – a role for apoptosis. *Biotechnol. Bioeng*. **44**: 720–726.
6. Tey, B.T., Singh, R.P., and Al-Rubeai, M. (2001) Programmed cell death – An overview of apoptosis in cell culture. *Asia Pac. J. Mol. Biol. Biotechnol*. **9**: 1–28.
7. Tey, B.T., Singh, R.P., Piredda, L., Piacentini, M., and Al-Rubeai, M. (2000a) Bcl-2 mediated suppression of apoptosis in myeloma NS0 cultures. *J. Biotechnol*. **79**: 147–159.
8. Tey, B.T., Singh, R.P., Piredda, L., Piacentini, M., and Al-Rubeai, M. (2000b) Influence of Bcl-2 on cell death during cultivation of a Chinese hamster ovary cell line expressing a chimeric antibody. *Biotechnol. Bioeng*. **68**: 31–43.
9. Zanghi, J.A., Fussenegger, M., and Bailey, J.E. (1999) Serum protects protein-free competent Chinese hamster ovary cells against apoptosis induced by nutrient deprivation in batch culture. *Biotechnol. Bioeng*. **64**: 108–119.
10. Zweigner, J., Jackowski, S., Smith, S.H., van der Merwe, M., Weber, J.R., and Tuomanen, E.I. (2004) Bacterial inhibition of phosphatidylcholine synthesis triggers apoptosis in the brain. *J. Exp. Med*. **200**: 99–106.

Monoclonal Antibody Productivity of Hybridoma Cells Under Active Hypothermic Growth Condition

Beng Ti Tey, Sun Li Chong, Michelle Y.T. Ng, Duen Gang Mou, Saw Hoon Lim, and Abdul Manaf Ali

1 Introduction

There is a great demand for the biopharmaceutical such as cytokines, vaccines, and monoclonal antibodies (mAb) that are produced from mammalian cells over the past few years. However, the productivity of recombinant proteins in animal cell is always lower compared to other microbial expression systems. Therefore, there is a need to increase the productivity of these biopharmaceutical proteins in mammalian cells in order to meet the market demand. Over the years, various strategies such as modification of the manufacturing facilities, genetically-modification of cell lines and optimization of the operating conditions have contributed greatly to the improvement of mammalian cell protein productivities. The strategy on the modification of operating parameters such as pH, osmolarity and temperature would be favoured by most pharmaceutical manufacturers due to its cost effectiveness and it is easy to implement.

Mammalian cell culture is normally performed at 37 °C, a temperature for the optimal cell growth and cellular activities. Under hypothermic condition, cellular adaptations in response to cold shock are necessary for survival of most organisms. Mammalian cells would normally experience an arrested growth when they were exposed to mild hypothermic conditions (between 37 and 30 °C). The growth arrested mammalian cells would normally have a longer life span in batch culture, and lower nutrient consumption, hence, would be expected to have a higher specific cellular protein productivity. Indeed, several researchers had reported that great positive impact towards the productivity of recombinant proteins had been achieved in CHO cell culture by lowering the cultivating temperature [4, 5, 9] However, due to the low cell density as a result of growth arrestment, the total hypothermic mAb productivity is somehow lower than that of normal temperature. In our previous study, the specific mAb productivity of hybridoma is increased proportionally to

B.T. Tey (✉)
Department of Chemical and Environmental Engineering, Faculty of Engineering, Universiti Putra Malaysia, 43400 UPM Serdang, Selangor, Malaysia
e-mail: btey@eng.upm.edu.my

M. Kamihira et al. (eds.), *Animal Cell Technology: Basic & Applied Aspects*, Animal Cell Technology: Basic & Applied Aspects 16, DOI 10.1007/978-90-481-3892-0_13,

the population of S-phase cells and inversely proportional to the population of G1-phase cells under mild hypothermic condition [2]. In another study, Fox et al [3]. also reported that the specific productivity of CHO cells under hypothermic condition was proportional to the population of cells in S phase. On the other hand, the specific productivity of NS0 cells in chemostat culture was reported to be correlated to the G2/M cells [7]. Hence, the active growth of cells may play an important role in mAb productivity. Therefore, the aim of the present study was to investigate the mAb productivity of hybridoma cells under active mild hypothermic growth.

2 Materials and Methods

2.1 Cell Line

Hybridoma clone C_2E_7 excreting mAb IgM reacted with human breast cancer cell line MCF7, T47-D and ductal and lobular carcinoma was used in this study [1].

2.2 Culture Conditions

RPMI 1640 (Gibco BRL, USA) consists of 2 g/l of sodium bicarbonate ($NaHCO_3$) was used in the present study. The batch culture of hybridoma cells was performed in 175 cm^2 T-flask containing 60 ml of fresh medium inoculated with mid exponential cells at a density of 2.5×10^5 cells/ml. The cultures were supplemented with 10 and 30% (v/v) of FBS in duplicate at each incubation temperature (37 and 32 °C). Samples were harvested daily for cell counting, viability, mAb concentration determinations and mRNA expression analysis.

2.3 Cell Density and Viability Determination

Cell density and viability was determined using haemocytometer (improved Neubauer–Haemocytometer) with trypan blue exclusion method.

2.4 Monoclonal Antibody Quantification

The mAb concentration was quantified using an ELISA kit (Bethyl Laboratories, Inc., Texas, USA) as been described in Chong et al. [2].

2.5 Total RNA Isolation and Quantitation

Sample containing at least 10^6 cells was used for total RNA isolation. The total RNA isolated using an RNeasy^{TM} Mini Kit (Qiagen Inc., Hilden, Germany) according to the manufacturer's protocol with some modification. The concentration of RNA was

quantitated by measuring the absorbance at 260 nm with Ultrospec-3000 UV-VIS Spectrophotometer (Amersham Biosciences UK Ltd, UK). The purity of RNA was determined by the ratio of the reading at 260 and 280 nm (A_{260}/A_{280}), in which pure RNA has an A_{260}/A_{280} ratio of 1.8–2.1.

2.6 Real Time PCR Quantification of IgM Expression Level

The PCR reaction was performed in 20 μl of total reaction volume containing 2 μl of cDNA template, 10 μl of 2x Quantitect SYBR Green PCR Master Mix (Qiagen Inc., Hilden, Germany), 0.5 μM of reverse and forward IgM1 primers (IgM1_F: 5'- AAATGTCTTCCCCCTCGTCTCCTGC; IgM1_R: 5'- CAGATCTCTGTTTTTGCCTCCGTAGTG) using Light Cycler 2.0 Instrument (Roche Diagnostics Corp., Indianapolis, USA).The reactions were performed with 35 cycles, each cycle consisted of denaturation without hold time at 90 °C, annealing at 63 °C for 30 second and extension for 45 min at 72 °C. After PCR cycling, melting curve analysis was performed. The cycle at which a given sample crosses a threshold fluorescence value (crossing point) is proportional to the amount of DNA template and was calculated using the LightCycler® Software 4.0 (Roche Diagnostics Corp., Indianapolis, USA). A plot of crossing point versus logarithm of concentration ranging from 10^2 to 10^8 copies was generated and can be interpolated to find the concentration of unknown sample. Both the sample and standards were prepared in duplicate.

2.7 Calculation

2.7.1 Specific Growth Rate

Specific growth rate, $\mu_{\max}$

$$\ln X_t = \mu_{\max} t + \ln X_0 \tag{1}$$

Where X_t is the viable cell density at time t, and X_0 is the initial viable cells density and t is the cultivation time.

2.7.2 Specific Monoclonal Antibody Productivity

Specific monoclonal antibody productivity, q_{mAb}

$$q_{mAb} = \left([mAb]_{t2} - [mAb]_{t1}\right) / \int X_v dt \tag{2}$$

Where $[mAb]_{t1}$ is the mAb concentration at $t1$, $[mAb]_{t2}$ is the final mAb concentration at $t2$, and $\int X_v$ dt is the integrated viable cells density (IVCD) from $t = t1$ to $t2$.

3 Results and Discussion

The growth of hybridoma under hypothermic condition (32 °C) was stimulated through the supplementation of high serum concentration (up to 30%) into the culture medium. The results showed that the specific and volumetric mAb productivity of hybridoma cultured at 32 °C and supplemented with 30% FBS (active hypothermic growth) was 1.34 and 1.38-folds higher than the control culture (37 °C and supplemented with 10% FBS) (Table 1). Higher serum dosage has been reported to increase the fraction of S-phase cells, and the specific growth rate in mammalian cell culture [3, 6]. This finding is in line with our previous study whereby the specific hypothermic productivity is found to be correlated to the fraction of S-phase cells [2].

Real time PCR quantification of mAb (IgM) expression level showed that the enhanced specific hypothermic productivity was found to be related to the elevated IgM mRNA level during lag and early exponential hypothermic growth (Table 2). Hence, higher viable cells density during the lag and early exponential phase of hypothermic growth is critical for improved total hypothermic productivity of mAb by hybridoma cells.

Table 1 Summary of specific growth rate, total production and specific productivity of IgM with varied dosage of FBS supplementation at 32 °C and 37 °C

	μ_{max} (day^{-1})		Maximum Cell Density ($\times 10^6$ cells/ml)		Total mAb Production (mg/l)		Specific mAb Productivity (pg/cells-hr)	
Growth Condition	32 °C	37 °C	32 °C	37 °C	32 °C	37 °C	32 °C	37 °C
Control – 10% FBS	0.65	0.78	1.23	1.25	3.57	3.94	0.0420	0.036
30% FBS	0.68	1.04	1.39	1.53	5.29	5.71	0.0490	0.041

Table 2 Monoclonal antibody (IgM) expression level in the mild hypothermic (32 °C) growth of hybridoma cells

	mRNA Conc. (Copies/10^6 cells)	
Day	10% FBS	30% FBS
0	0	0
1	2.24E + 07	4.86E + 07
2	1.58E + 07	2.56E + 07
3	1.07E + 07	1.25E + 07
4	2.86E + 06	8.52E + 06
5	2.21E + 06	1.10E + 07
6	2.05E + 06	1.41E + 07

4 Conclusion

The results of this study have demonstrated the possibility of promoting hypothermic growth with high dosage of serum supplementation. However, the application of serum that originated from animal is prohibited by the regulatory authority. Therefore, there is a need to seek other alternative to replace FBS usage to promote active hypothermic growth. Indeed, the over-expression of antiapoptotic gene such as Bcl-2 was reported able to reduce the serum dependency of NS0 cells [8].

Acknowledgements S.L. Chong is supported by a scholarship from Malaysia University of Science and Technology. This study was supported by the e-Science Fund (02-01-04- SF0763) from the Ministry of Science, Technology and Innovation; and FRGS Grant (FRGS A-408) from the Ministry of Higher Education of Malaysia, and Japan Society for the Promotion of Science (JSPS).

References

1. Ali, A.M., Ong, B.K., Yusoff, K., Hamid, M., Ali, A.S., and Azimahtol, H.L.P. (1996) Generation of stable hybridoma clones secreting monoclonal antibodies against breast carcinoma cell lines. *Asia Pac. J. Mol. Biol. Biotechnol*. **4**: 123–131.
2. Chong, S.L., Mou, D.G., Ali, A.M., Lim, S.H., and Tey, B.T. (2008) Cell growth, cell-cycle progress, and antibody production in hybridoma cells cultivated under mild hypothermic condition. *Hybridoma* **27**: 107–111.
3. Fox, S.R., Tan, H.K., Tan, M.C., Wong, S.C., Yap, M.G., and Wang, D.I.C. (2005) Detailed understanding of the enhanced productivity of interferon-γ by Chinese hamster ovary cells. *Biotechnol. Appl. Biochem*. **41**: 255–264.
4. Furukawa, K. and Ohsuye, K. (1998) Effect of culture temperature on a recombinant CHO cell line producing a C-terminal α-amidating enzyme. *Cytotechnol*. **26**:153–164.
5. Kaufmann, H., Mazur, X., Fussenegger, M., and Bailey, J.E. (1999) Influence of low temperature on productivity, proteome and protein phosphorylation of CHO cells. *Biotechnol. Bioeng*. **63**: 573–582.
6. Sherr, C.J. (1995) D-type cyclin. *Trends Biochem. Sci*. **20**: 187–190.
7. Tey, B.T. and Al-Rubeai, M. (2005a) Effect of Bcl-2 over-expression on cell cycle and antibody productivity in chemostat cultures of myeloma NS0 cells. *J. Biosci. Bioeng*. **100**: 303–310.
8. Tey, B.T. and Al-Rubeai, M. (2005b) Protective effect of Bcl-2 in NS0 myeloma cell culture is greater in more stressful environments. *Biotechnol. Biopro. Eng*. **10**: 564–570.
9. Yoon, S.K., Song, J.Y., and Lee, G.M. (2003) Effect of low culture temperature on specific productivity, transcription level and heterogeneity of erythropoietin in Chinese hamster ovary cells. *Biotechnol. Bioeng*. **82**: 289–298.

Efficient Selection of Cell Clones with Higher Productivity in the Production of Recombinant Human Monoclonal Antibodies

Ayako Ohshima, Yumiko Takamatsu, Koichi Yamamot, and Hiroyuki Saitoh

1 Introduction

To achieve a high production level of recombinant human monoclonal antibody (rhMAb) through inoculation and cultivation of Chinese hamster ovary (CHO) cells, it is absolutely necessary to select the clones that show superior performance under manufacturing conditions [1]. However, during the phase of cell development, a huge number of clones have to be handled at once. Figure 1 shows an example of a process flow diagram of cell clone screening. The clone selection process begins with the transfection, followed by a series of screening methods using a tissue culture plate. The performances of the selected clone are then evaluated under actual manufacturing culture conditions using shake flasks and bioreactors. During the screening stage, however, is very difficult to quickly choose from among a huge number of tested clones (>5,000) using a culture plate. One of the main reasons for this difficulty is the difference in culture methods between the screening stage and the production stage. In the screening stage, the culture method is kept very simple in order to allow the efficient handling of so many clones. On the other hand, the process for production is highly optimized to increase cell growth and rhMAb production [2]. In most cases, a fed-batch culture is used to supply cells with nutrients on demand over the course of several weeks during the production stage. This change in the cultivation conditions (e.g., the production medium, feed medium and feeding strategy) between the two stages can lead to changes in the production level or cell growth level. Therefore, in terms of selecting the most efficient clones, it would be preferable if the conditions used to screen and produce the antibodies were more similar.

In this study, we tried to establish a cell selection method that can solve these issues—i.e., the difficulty of selecting from among a huge number of clones in the screening stage and the use of different culture methods for screening and

A. Ohshima (✉)
Bio Process Research and Development Laboratories, Production Division,
Kyowa Hakko Kirin Co., Ltd., Takasaki-shi, Gunma 370-0013, Japan
e-mail: ayako.ohshima@kyowa-kirin.co.jp

M. Kamihira et al. (eds.), *Animal Cell Technology: Basic & Applied Aspects*, Animal Cell Technology: Basic & Applied Aspects 16, DOI 10.1007/978-90-481-3892-0_14,

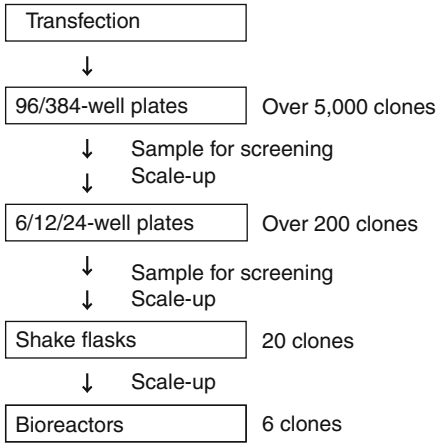

Fig. 1 Diagram of clone screening process

production. To bridge the gap between the screening culture and production culture, we adopted a simplified production culture to minimize the effort expended in the cell clone screening stage and the variety of cell culture conditions. We performed the experiments with the following goals in mind: (1) fast screening, (2) simple operation, (3) the ability to evaluate many clones simultaneously and (4) a consistency of the titer level between the screening and a large-scale production.

2 Materials and Methods

2.1 Culture Condition of Flasks and Plates

The cells used in this study were CHO cells expressing rhMAb A and rhMAb B.

Batch culture with 125 mL Erlenmeyer flasks and with tissue culture plates (12, 24, and 96-well plate) was carried out. Cell culture was started by inoculating the cells at 2.0×10^5 cells mL^{-1} in serum-free medium. The inoculated flasks and culture plates were placed on a rotary shaker and cultured in a humidified incubator at 37°C with 5% CO_2. The shaking speed was 120 rpm for flasks and 180 rpm for plates. The glucose concentration of the culture medium was set at 8 g L^{-1} so that the batch culture could be continued for 7 days.

In a separate trial, a fed-batch culture was carried out for 17 days in 125 mL Erlenmeyer flasks. The initial cell concentration and the culture conditions were the same as those for the batch culture except that the initial concentration was 4 g L^{-1} glucose. Feed medium was added on days 4, 7, 10, and 13.

2.2 Analyses

The viable cell density was determined using an AlamarBlue™ assay [3]. The culture fluid was diluted in fresh medium to a concentration that fell within the bounds

of an analytical curve ($\sim 10^6$ cells mL^{-1}). 100 μL of diluted samples was incubated with 10 μL of AlamarBlue™ (Diagnostic Systems, Inc.) on 96-well plates for 3 h at 37°C with light shielding. The fluorescence of each well was detected using EnVision (PerkinElmer), and the viable cell densities of each sample were calculated by the ratio of absorbance at 595 nm/615 nm using the analytical curve. Culture fluids for which the viable cell densities were already known were used to generate the analytical curve.

The antibody productivity was measured using LANCE™ (PerkinElmer) [4] or Protein A HPLC. Supernatants were diluted in 20 mM Tris-HCl buffer (pH 7.2) including 10% Block Ace (Dainippon Sumitomo Pharma Co., Ltd.) (Buffer A) to a concentration that fell within the bounds of an analytical curve (~ 10 μg mL^{-1}). 2 μL of diluted samples was incubated with 12 μL of Buffer A including 2.9 μg mL^{-1} LANCE europium (Eu)-W1024 labeled mouse anti-human immunoglobulin G (Fc-specific, monoclonal antibody) (PerkinElmer), 25 μg mL^{-1} of biotin-conjugated mouse anti-human immunoglobulin G (kappa-specific, monoclonal antibody) (BD Biosciences), and 50 μg mL^{-1} Surelight allophycocyanin (APC) streptavidin (PerkinElmer) on 96-well half-area plates for 1 h at room temperature with light shielding. The fluorescence of each well was detected using EnVision (PerkinElmer), and the concentration of the antibody in the supernatant was calculated by the ratio of absorbance at 665 nm/615 nm using an analytical curve. The rhMAb was used as the standard to generate the analytical curve.

3 Results

3.1 Selection of a Culture Vessel for Simplified Production Culture in the Screening Stage

It is very convenient to evaluate cell performance using tissue culture plates, because their closely packed wells allow the handling of many clones. To compare the efficacy of cultures in Erlenmeyer flasks, we performed a simplified production culture using 12, 24, and 96-well plates for 7 days. The time course of the viable cell density and the antibody production level at day 7 are shown in Figs. 2 and 3, respectively.

As shown in Fig. 2, the time course of viable cell density in the 12-well plate and 24-well plate cultures were the same as that of the flask culture. On the other hand, the cell growth in the 96-well plate culture was much lower than that in the flask culture, presumably due to a lack of mixing efficiency caused by the small diameters of the wells. That is, the oxygen supply appeared to be insufficient in the 96-well cultivation due to the low mixing speed. The antibody production levels at day 7 in the 12-well and 24-well plate culture were the same as that of the flask condition (Fig. 3). In contrast, the production level in the 96-well plate culture decreased to 20% in accordance with the low cell growth. These results indicated that a 24-well plate could be used for the clone selection instead of a flask.

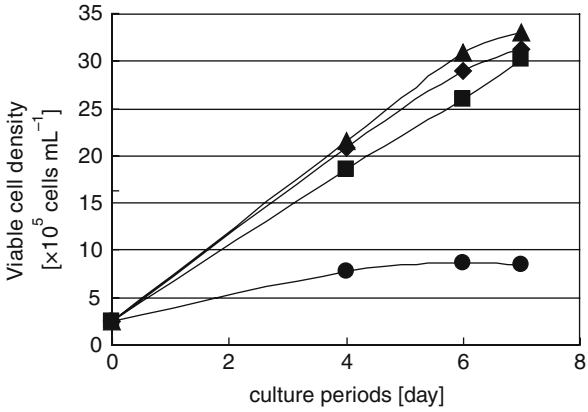

Fig. 2 Time course of viable cell density. Shake flask(♦), 12-well plate(■), 24-well plate(▲) and 96-well plate(●)

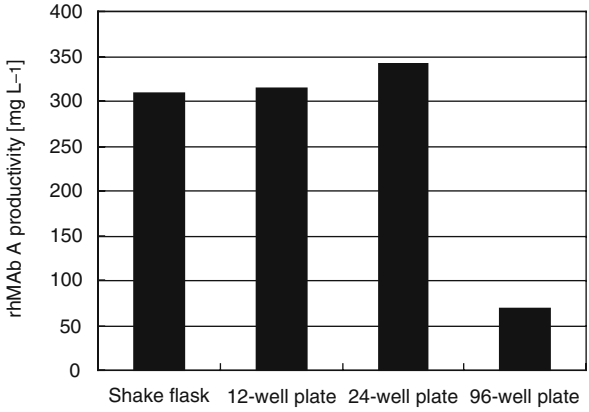

Fig. 3 Antibody production level at 7 days

3.2 Comparison of the Cell Clone Performance in a Production Culture Using an Erlenmeyer Flask and 24-well Tissue Culture Plate

It is very important to evaluate the effectiveness of tissue culture plates in the selection of clones showing high performance under manufacturing conditions. In this experiment, we compared 6 clones of CHO cells producing antibody B in production cultures using an Erlenmeyer flask and 24-well plate to evaluate the cell clone performance. Figure 4 shows the relative antibody production level of each clone. Although the production levels of the cells in the flasks and the 24-well plates were not the same (1800 mg L^{-1} and 600 mg L^{-1} for clone No. 4, respectively), this was attributed to the difference in the duration of cultivation (17 days for the flask culture and 7 days for the plate culture). Despite this difference, the production levels of the 6 clones were same in order. Clone No. 4 showed the highest production level,

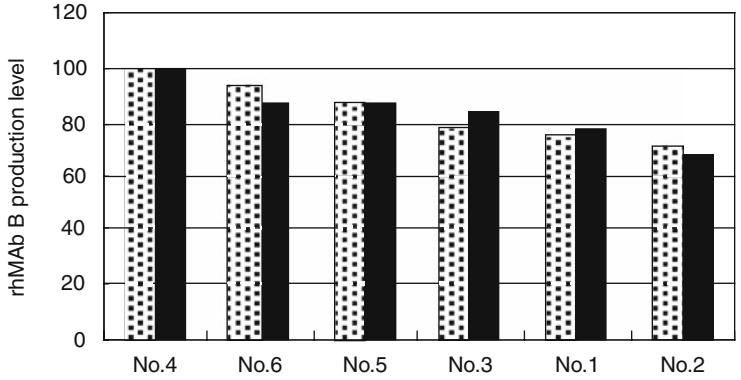

Fig. 4 Antibody production level of each clone. Shake flask (*black*) and 24-well plate (*mesh*). The titers of the No. 4 clone were 1800 mg L^{-1} and 600 mg L^{-1} using a shake flask and 24-well plate, respectively

and clone No. 2 showed the lowest. The same results were obtained in regard to cell growth profile (data not shown). Take together, these results indicated that a successful selection of clones with higher productivity was possible by 24-well plate culture.

4 Discussion

In order to establish an efficient procedure for the selection of cell clones that will exhibit superior performance under manufacturing conditions, the selection method should be simple, because it takes a long time to develop the rhMAb-producing CHO cells. Therefore, it is necessary to develop a culture method that is on a smaller scale than that using Erlenmeyer flasks, and tissue culture plates are ideal for this purpose. In our previous study, we demonstrated that the performance of a fed-batch culture using a flask was similar to that of a larger scale fed-batch culture using a bioreactor (data not shown).

In this study, we investigated to minimize the culture scale to evaluate a large number of clones. The screening was carried out with the same medium as used in the production culture. The batch culture with production medium for 7 days resulted in a similar production profile as the fed-batch culture for 17 days. In addition, the titer level of the 24-well plate culture was on the same order as that of the flask culture (Figs. 2 and 3). From these results, we concluded that a batch culture with 24-well plates was well correlated to a fed-batch culture with flasks in terms of the cell growth and titer level.

This novel scaled-down method using tissue culture plates instead of a bioreactor or flask could be fast, simple and consistent for the selection of cell clones that will exhibit superior performance under manufacturing conditions.

References

1. Browne, S.M. and Al-Rubeai, M. (2007) Selection methods for high-producing mammalian cell line. *Trends Biotechnol*. **25:** 425–432.
2. Oguchi, S., Saito, H., Tsukahara, M., and Tsumura, H. (2004) Control of temperrature and pH enhances human monoclonalantibody production in CHO cell culture. *Animal Cell Technol. Basic Appl. Aspects* **13:** 169–172.
3. Nakayama, G.R., Caton, M.C., Nova, M.P., and Parandoosh, Z. (1997) Assessment of the Alamar blue assay for cellular growth and viability in vitro. *J. Immunol. Methods* **204:** 205–208.
4. Kuroda, K., Kobayashi, K., Kitagawa, Y., Nakagawa, T., Tsumura, H., Komeda, T., Shinmi, D., Mori, E., Motoki, K., Fuji, K., Sakai, T., Nonaka, K., Suzuki, T., Ichikawa, K., Chiba, Y., and Jigami, Y. (2008) Efficient antibody production upon suppression of *O* mannosylation in the yeast *Ogataea minuta. Appl. Environ. Microbiol*. **74:** 446–453.

Continuous Cell Production from Three Dimensional Hematopoietic Microenvironment in Polyurethane Foam

Tadasu Jozaki, Kentarou Aoki, Hiroshi Mizumoto, and Toshihisa Kajiwara

1 Introduction

In adult humans, the bone marrow is the site for hematopoiesis. In this site, hematopoietic stem cells (HSCs) maintain, self-renew and differentiate into all blood cells [1]. HSCs adhere to the surface of trabecular bone through bone marrow stromal cells. The cell-cell or cell-extra cellar matrix (ECM) interactions maintain the physiological hematopoietic environment [2].

The suitable culture conditions for hematopoietic cell activity in vitro are provided by co-culture with stromal cells and addition of cytokines [3–5]. In stromal-dependent culture, the stromal cell layer provides physical support and some cytokines to hematopoietic cells. Dexter et al. reported that HSCs maintain colony-forming ability on a 2 dimensional stromal cell layer for 3 months [3]. Several cytokines such as stem cell factor (SCF), thrombopoietin (TPO), and flt-3 ligand were reported to partially regulate hematopoiesis [6, 7]. We can standardize and maintain cells more easily in a stromal-free culture than in a stromal-dependent culture. But, a stromal-free culture requires a higher concentration of cytokines than a stromal-dependent culture [8].

Stromal-dependent culture in a monolayer such as the Dexter culture system requires the addition of a large amount of cytokines for proliferation of HSCs and hematopoietic progenitors [9, 10]. So, to use cell-cell or cell-ECM interaction more effectively, 3D culture systems have been developed as follows: polyvinyl formal, nonwoven disks, porous micro spheres, and so on [9, 11, 12]. These 3D porous carriers have a larger surface area than the conventional monolayer culture system and promote a high cell density culture [13, 14].

In these reports, the contribution to maintenance or proliferation of HSCs and hematopoietic progenitor cells has been documented. But, a 3-D culture is required to establish continuous blood cell production system from cultured HSCs. A suitable

T. Kajiwara (✉)
Department of Chemical Engineering, Kyushu University, Nishi-ku, Fukuoka, Japan
e-mail: kajiwara@chem-eng.kyushu-u.ac.jp

M. Kamihira et al. (eds.), *Animal Cell Technology: Basic & Applied Aspects*, Animal Cell Technology: Basic & Applied Aspects 16, DOI 10.1007/978-90-481-3892-0_15,

carrier and culture method are required for the reconstruction of the hematopoietic microenvironment in vitro.

We focused on polyurethane foam (PUF) as a porous scaffold for hematopoietic cell culture. It has a sponge-like macro porous structure with each pore comprised of smooth thin films and thick skeletons. PUF can achieve sufficient mass transfer and high cell density culture because the pores are partially opened and connected with each other. Moreover, the floating cells generated from the hematopoietic microenvironment in the PUF can be harvested easily.

We employed two kinds of PUF, which have different contact angles and hydrophilic properties. We investigated the effect of the scaffold on reconstruction of the hematopoietic microenvironment in vitro.

2 Methods

2.1 Cell Culture

C57BL6/J male mice (6–8 week-old) were purchased from Kyudo Co., Ltd (Kumamoto, Japan). Mouse bone marrow cells were isolated from their femur and tibia by flushing with CMF-PBS using a 1 ml syringe and 26 gauge needles [12]. Mouse bone marrow mononuclear cells (mBMMNCs) were separated by density gradient separation on percoll (1.077 g/ml, Sigma) [15]. mBMMNCs were cultured in IMDM (Iscove's Modified Dulbecco's Medium, Sigma) supplemented with 20% Horse serum (Gibco), 5 U/ml Penicillin and 5 μg/ml Streptomycin (Gibco).

We investigated 2-D and 3-D culture. For 2-D culture, mBMMNCs were cultured in a monolayer culture as previously described [3]. For 3-D, we employed PUF as a scaffold.

2.2 Preparation of Polyurethane Form as a scaffold

PUF was kindly donated by Inoac (Nagoya, Japan). It has a sponge like macro porous structure with each pore consisting of smooth thin films and thick skeletons [16]. The PUF block was cut into a flat disk (with radius 11 mm, thickness of 1.0 mm). We used two kinds of PUF (W1, R4) with different surfaces and structural properties (Table 1).

Table 1 Physical parameters of two types of PUF

PUF type	W1	R4
Contact angle (degree)	85.2 ± 2.3	47.8 ± 4.5
Pore size (μm)	500	250

2.3 PUF 3D Culture

Each PUF disk was placed in a 12 well plate for static culture. Medium containing 3.2×10^6 mBMMNCs (1.6 ml) was inoculated into each well and incubated in a humidified incubator at 5% CO_2 and a temperature of 37°C.

After day 12, rotational culture was started to isolate mature blood cells from PUF pores (Fig. 1). Then, the PUF disks were transferred to a new 12-well plate with fresh culture medium at 3 days intervals. At the same time, non adherent cells were harvested from old medium and counted as "Produced cells". On the other hand, adherent cells on PUF surface were harvested as "Adherent cells".

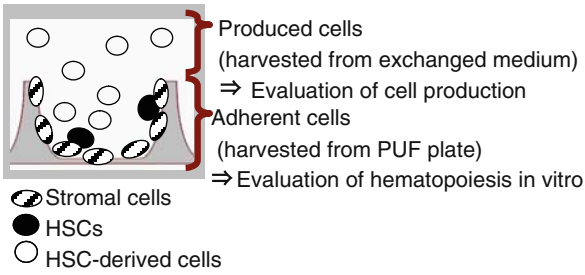

Fig. 1 Schematic diagram of 3D culture configuration in PUF pores

2.4 Phenotype Analysis of Produced Cells

We evaluated lineage-specific surface markers for the Produced cells by MACS (Miltenyi Biotec) at day 21–24. The cells released from PUF culture were labeled with Ter-119 MicroBeads or CD45 MicroBeads (Miltenyi Biotec) as recommended by the manufacturer. And, $Ter119^+$ or $CD45^+$ cells were isolated from the magnet-retained fraction with a MACS separation unit (Miltenyi Biotech).

2.5 Colony Forming Unit (CFU) Assay

The cultured cells were washed and resuspended at a density of 1.0×10^5 cells /ml in IMDM containing 1% FBS. The CFU samples (0.3 ml) were added to the suspended medium to form a 3.0 ml HSC-CFU complete with erythropoietin and tested in accordance with the manufacturer's protocol (Miltenyi Biotec).

3 Result

3.1 Distinctive Efficiency of PUF in Cell Growth of mBMMNC Cultivation

We counted the number of cells produced from PUF or monolayer culture as an indicator of cell production (Fig. 2a). In monolayer culture, cell production ceased by day 21. In both PUF cultures, the cell production from PUF increased until day 33 and then began to decrease. The number of cells produced in W1 culture was higher than that of R4 culture.

From the population of Ter119 or CD45 positive cells at day 21–24, almost 99% of produced cells were hematopoietic cells and 21.8–34.9% differentiated into the erythroid line without the addition of erythropoietin (Table 2).

Figure 2b showed changes in the adherent cell number. Adherent cell proliferation was obviously occurring in PUF culture after day 14. And, the number of adherent cells remained fairly constant between day 14 and day 21.

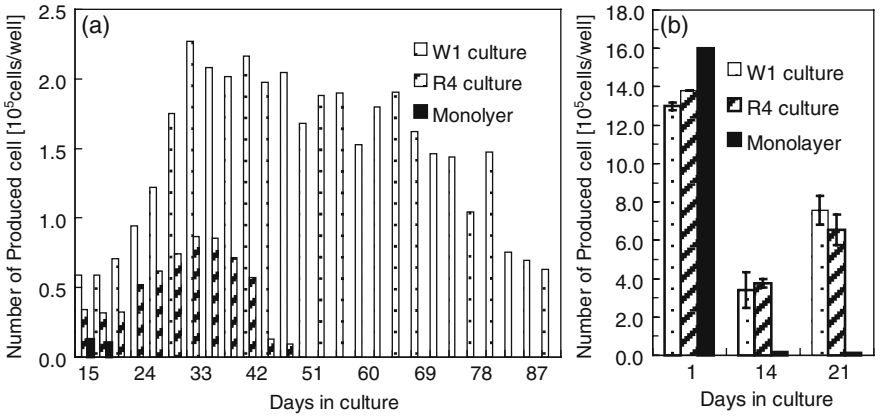

Fig. 2 Hematopoietic cell proliferation (**a**) Produced cells (**b**) Adherent cell

Table 2 Evaluation of lineage specific surface markers of produced cell in PUF culture

Culture system	%Ter119$^+$	%CD45$^+$
Fresh mBMMNC (day 0)	40.9	39.0
W1 culture (day 21–24)	21.8	99.2
R4 culture (day 21–24)	34.9	99.1

3.2 Colony-Forming Ability is Associated with Cell Density in Culture Space and the Surface Characteristic

The number of colony-forming units (CFUs) in PUF culture was larger than in the monolayer culture (Table 3). In comparison of PUF cultures, colony-forming ability was maintained in R4 culture better than in W1 culture. These results might be due to differences in cell density within each culture or surface characteristics of each carrier.

Table 3 Compsrison of CFUs among various culture system

Culture system	Day 14 ([CFU/well])	Day 21 ([CFU/well])
W1 culture	345.4 ± 298.8	62.5 ± 5.7
R4 culture	259.5 ± 228.0	127.0 ± 36.5
Monolayer	21.8 ± 14.3	9.8 ± 0.8

4 Discussion

The purpose of this work was to investigate the effect of scaffold type on reconstruction of the hematopoietic microenvironment in vitro. In this study, we showed that PUF pores might contribute to hematopoietic cell production. In comparison of PUF and monolayer culture, PUF culture exceeded monolayer culture in adherent cell proliferation and maintenance of colony-forming ability (Fig. 2 and Table 2). The cell proliferation suggests that stromal cells support the hematopoietic cells, but the stromal cells in 2-D culture were not sufficient to continue cell production in comparison with 3-D culture. In both PUF cultures, cell production increased and decreased similarly. Therefore, PUF cultures might benefit from the structural characteristic of the pores, but the surface characteristic influences cell productivity.

W1 culture exceeded R4 culture in nonadherent cell production, while R4 culture exceeded W1 culture in maintenance of colony-forming ability (Fig. 2). These results might be due to surface characteristics. So, different cells in each PUF culture might adhere, and they are likely to generate different cytokine effects.

These results indicate that an optimum environment for HSCs consists of high cell density co-culture with a stromal cell line in PUF pores. The surface characteristic that influences the cell activity for reconstructing a HSC niche in vitro needs to be investigated further.

References

1. Emerson, S.G. (1996) Ex vivo expansion of hematopoietic precursors, progenitors, and stem cells: The next generation of cellular therapeutics. *Blood* **87**: 3082–3088.
2. Panoskaltsis, N., Mantalaris, A., and David Wu, J.H. (2005) Engineering a mimicry of bone marrow tissue ex vivo. *J. Biosci. Bioeng.* **100**(1): 28–35.

3. Dexter, T.M., Allen, T.D., and Lajtha, L.G. (1977) Conditions controlling the proliferation of haemopoietic stem cells in vitro. *J. Cell Physiol.* **91**: 335–344.
4. Koller, M., Bender, J.G., Papoutsakis, E.T., and Miller, W.M. (1992) Effects of synergistic cytokine combinations, low oxygen, and irradiated stroma on the expansion of human cord blood progenitors. *Blood* **80**: 403–411.
5. Kanai, M., Hirayama, F., Yamaguchi, M., Ohkawara, J., Sato, N., Fukazawa, K., Yamashita, K., Kuwabara, M., Ikeda, H., and Ikebuchi, K. (2000) Stromal cell-dependent ex vivo expansion of human cord blood progenitors and augmentation of transplantable stem cell activity. *Bone Marrow Transplant.* **26**: 837–844.
6. Yoshida, M., Tsuji, K., Ebihara, Y., Muraoka, K., Tanaka, R., Miyazaki, H., and Nakahata, T. (1997) Thrombopoietin alone stimulates the early proliferation and survival of human erythroid, myeloid and multipotential progenitors in serum-free culture. *Br. J. Haematol.* **98**: 254–264.
7. Ebihara, Y., Tsuji, K., Lyman, S.D., Sui, X., Yoshida, M., Muraoka, K., Yamada, K., Tanaka, R., and Nakahata, T. (1997) Synergistic action of Flt3 and gp130 signalings in human hematopoiesis. *Blood* **90**: 4363–4368.
8. Mutsumi, T. (2005) Cell processing engineering for ex-vivo expansion of hematopoietic cells. *J. Biosci. Bioeng.* **99**(3): 189–196.
9. Tomimori, Y., Takagi, M., and Yoshida, T. (2000) The construction of an in vitro three-dimensional hematopoietic microenvironment for mouse bone marrow cells employing porous carriers. *Cytotechnol.* **34**: 121–130.
10. Bennaceur-Griscelli, A., Tourino, C., Izac, B., Vainchenker, W., and Coulombel, L. (1999) Murine stromal cells counteract the loss of long-term culture-initiating cell potential induced by cytokines in $CD34^{+}CD38^{low/neg}$ human bone marrow cells. *Blood* **94**: 529–538.
11. Naughton, B.A., Preti, R.A., and Naughton, G.K. (1987) Hematopoiesis on nylon mesh templates. I. Long-term culture of rat bone marrow cells. *J. Med.* **18**(3–4): 219–250.
12. Tun, T., Miyoshi, H., Aung, T., Takahashi, S., Shimizu, R., Kuroha, T., Yamamoto, M., and Ohshima, N. (2002) Effect of growth factors on ex vivo bone marrow cell expansion using three-dimensional matrix support. *Artif. Organs* **26**: 333–339.
13. Li, Y., Kniss, D.A., Yang, S.-T., and Lasky, L.C. (2001) Human cord cell hematopoiesis in three-dimensional nonwoven fibrous matrices: In vitro simulation of the marrow microenvironment. *J. Hematother. Stem Cell Res.* **10**: 355–368.
14. Naughton, B.A. and Naughton, G. K. (1989) Hematopoiesis on nylon mesh templates. Comparative long-term bone-marrow culture and the influence of stromal support cells. *Ann. NY. Acad. Sci.* **554**: 125–140.
15. Palsson, B.O., Paek, S.H., Schwartz, R.M., Palsson, M., Lee, G.M., and Emerson, S.G. (1993) Expansion of human bone marrow progenitor cells in a high cell density continuous perfusion system. *Biotechnology* **11**(3): 368–372.
16. Ijima, H., Nakazawa, K., Mizumoto, H., Matsushita, T., and Funatsu, K. (1998) Formation of a spherical multicellular aggregate (spheroid) of animal cells in the pores of polyurethane foam as a cell culture substratum and its application to hybrid artificial liver. *J. Biomater. Sci. Polymer Ed.* **9**(7): 765–778.

A New Approach for Drug Discovery and Differentiation Study Using Cutting-Edge 3d Cell Culture System

Fujiko Ozawa, Yoshitaka Miyagawa, Masami Hiroyama, Nobutaka Kiyokawa, Akihiro Umezawa, Akito Tanoue, and Satoru Tanaka

1 Introduction

Cell-cell interactions are important in numerous biological processes, including tumor growth [1], and stem cell differentiation and self-renewal [2–5]. In addition, cell-cell interactions have been proven to be crucial for generating functional tissues in vitro [6, 7], which can be achieved by 3D cell culture [8]. Therefore, 3D cell culture model is crucial to understand biological events in a living body such as normal organs and tumor tissues.

To date, various 3D cell culture systems have been applied to a variety of cell types, Several examples are: (i) mouse embryonic stem cells (mESC) cultured on 3D cell culture system showed greatly enhanced proliferation and self-renewal in comparison with 2D cell culture [9]; (ii) preadipocytes undergo a sequential differentiation in respond to insulin signaling, synthesize and store triglyceride deposits, and express functionally important adipokines within a 3D environment that is rich in extracellular matrix (ECM) [10–12]; (iii) bone marrow stromal cells (BMSCs) cultured within the 3D scaffolds can be easily adjusted for bone replacement [13], and (iv) hepatocytes sandwiched between two layers of hydrated rat tail tendon collagen gel maintain a variety of hepatocyte functions.

In regard to tumor cells, the groups of Kerbel and Teicher demonstrated a multicellular mediated resistance to alkylating drugs. Drug resistance induced in EMT6 tumors in mice was completely lost when the cancer cells were isolated and grown in monolayers but could be fully recapitulated when cells cultures as multicellular spheroid [14, 15]. Furthermore, it is recently reported the comparison of the sensitivity to trastuzumab between 2D and 3D depending on the tyrosine phosphorylation, and that the sensitivity is increased in 3D culture [16].

M. Hiroyama (✉)
SCIVAX Corporation Kanagawa Science Park East 502, Kawasaki-shi, Kanagawa 213-0012, Japan; Department of Pharmacology, National Research Institute for Child Health and Development, Setagaya-ku, Tokyo, Japan
e-mail: m-hiroyama@scivax.com

M. Kamihira et al. (eds.), *Animal Cell Technology: Basic & Applied Aspects*, Animal Cell Technology: Basic & Applied Aspects 16, DOI 10.1007/978-90-481-3892-0_16,

Here we investigate the effects of 3D environment on tumor drug sensitivity, hepatocyte function and adipose differentiation of stem cell using a NanoCulture plate (NCP). The plate has approximately 2~3 μm diameter of uneven microfabrications on a culture surface and the system is able to generate uniform spheroids using conventional techniques without addition of any animal compounds.

2 Materials and Methods

2.1 Cell Culture and Spheroid Formations

All types of cell were seeded on 96-well NanoCulture® plates (NCP) (SCIVAX Corp.) at 1×10^4 cells/well using SCIVAX media (SCIVAX Corp.). To optimize the condition for spheroid formation, two types of plate patterns and two kinds of media were used. To compare with other 3D cell culture systems, ultra low attachment plate (Corning), Ez-BindShut (Iwaki), Vecell-3D Insert (Nikkyo) and matrigel (BD Biosciences) were used, and the same density of HepG2 hepatocarcinoma cell were seeded on those culture plates.

2.2 Immunoblot

Total cell lysates from 2D and 3D cell cultures were applied on SDS-PAGE and transferred to PVDF membrane. The membranes were stained with antibodies against HIF-1α (SantaCruz), VEGF and Akt.

2.3 Drug Susceptibility Test

For a drug susceptibility test, three kinds of drugs (5-FU, tegafur) were added into the culture media of two types of cell, hepatocarcinoma (HepG2) and colon cancer cell lines after spheroid formation or 3D culture experiment on NCP. On the other hand, cells were seeded on polystyrene plate (Corning) for 2D culture experiment in the same manner followed by addition of the drugs. The cell number was evaluated using CellTiter-Glo (Promega).

2.4 Measurement of Albumin Secretion

HepG2 cells and immortal hepatocytes (Nosan) were seeded on collagen-coated polystyrene and NCP plates for 2D and 3D cell cultures, respectively. The culture media were collected, and the albumin concentrations in the media were measured by an ELISA using anti-human albumin.

2.5 Adipocytes Culture and Oil-red O Staining

Preadipocytes (Primary Cell Co.) from rats mesenteric adipose were seeded using Visceral fat differentiation medium (Primary Cell Co.), and then the cells were fixed with 10% formalin for 1 h and then soaked in 3 mg/ml oil-red O in 60% isopropanol for 1 h. Then cells were washed with 60% isopropanol for 2 min.

2.6 Spheroid Formation of Human Adipose-Derived Stem Cell

Human mesenchymal stem cells (hMSC) were seeded using maintaining medium and adipocyte differentiation medium. Then, the cells were stained with oil-red O as described above.

3 Results and Discussion

3.1 Spheroid Formation on NCP

The two kinds of pattern of NCP include honeycomb and square shapes. The spheroid formation on NCP depends on the NCP pattern, medium types and cell types. Therefore, HCC1954 breast cancer cells were seeded on two kinds of NCP using two kinds of media (NCM-M and -L) and spheroid formation was monitored. The spheroid formation of HCC1954 cells was optimal on honeycomb pattern of NCP and NCM-M medium compared to square pattern of NCP and NCM-L medium (Fig. 1).

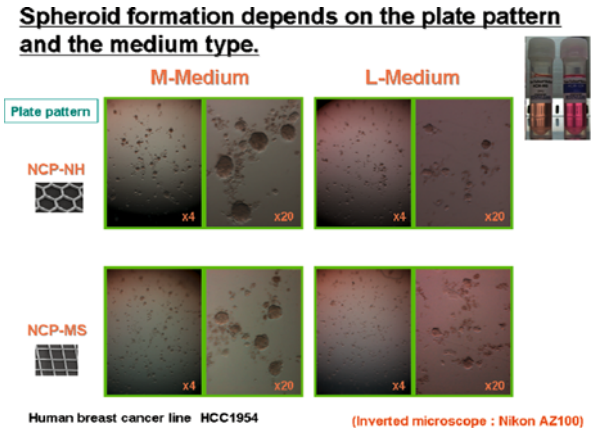

Fig. 1 Spheroid formation depends on the plate pattern and the medium type

3.2 Comparison of Spheroid Formation among 3D Cell Culture Systems

To compare NCP with other commercially available 3D system, HepG2 cells were used. On Ez-BindShut and Vecell-3D Insert systems, HepG2 cells did not form spheroid. On an ultra low attachment plate, the cells formed non-uniform spheroid. On the hand, HepG2 cells formed uniform spheroids using NCP and matrigel, however those spheroids were different in size and number reflecting the difference in spheroid formation mechanisms in these 3D cell culture systems (Fig. 2). On NCP cells migrate and proliferate (http://www.scivax.com/cell/english/index.html), while in matrigel spheroids are formed by proliferation of a single cell. Among these 3D systems, only NCP suited to high-though put screening (HTS).

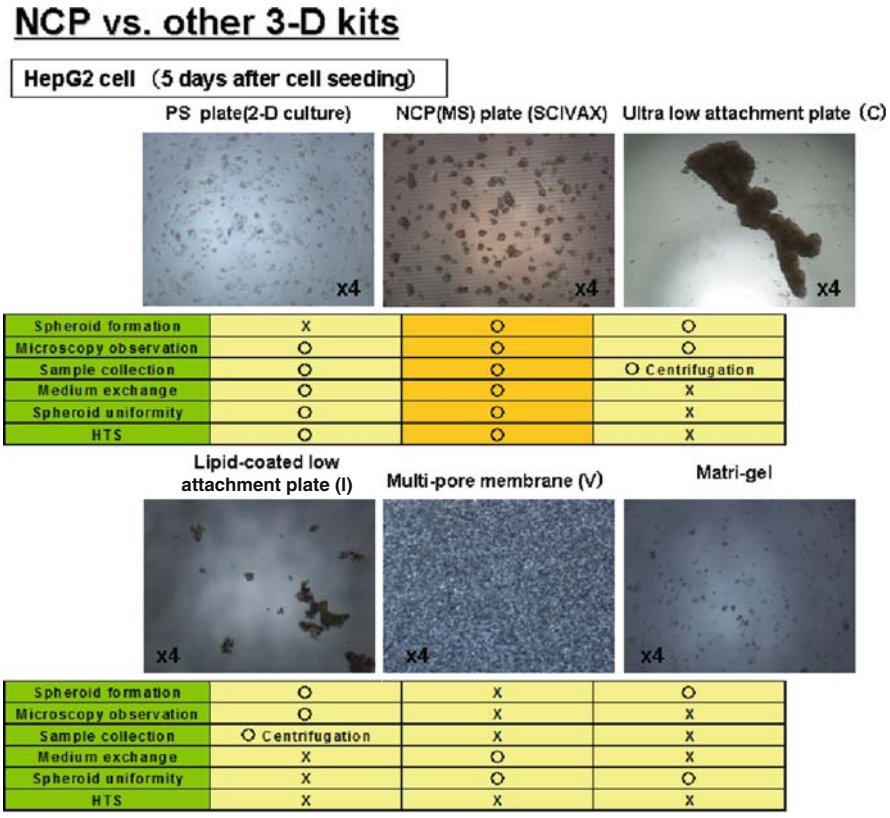

Fig. 2 NCP vs. other 3-D kits

3.3 The Expressions of Related Proteins to Hypoxia and Survival

Hypoxia-inducible factor-1a (HIF-1a) is a transcription factor for many genes that control the delivery of oxygen and nutrients via the induction of angiogenesis and

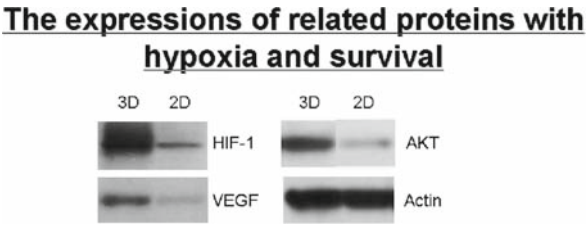

Fig. 3 The expressions of related proteins with hypoxia and survival

glycolysis. HIF-1α activates the transcription of vascular endothelial growth factor (VEGF), a key factor in tumor angiogenesis, and the expression of glucose transporters, glycolytic enzymes, and growth factors, which may promote tumor cell survival under hypoxic conditions [17]. Therefore, we investigated the expression levels of these proteins in spheroids cultured on NCP. The expressions of hypoxic marker, HIF-1α and the downstream molecule, VEGF were increased in 3D cell culture using NCP more than in 2D cell culture (Fig. 3). In addition, survival signal molecule, Akt was increased in NCP compared to 2D culture. These differences in protein expressions indicate that hypoxic condition may be present in the spheroids grown on NCP, similarly to in vivo tumor tissue.

3.4 Evaluation of Drug Susceptibility Difference between 2D and 3D Cell Cultures

It is known that the drug susceptibility can differ in 3D culture compared to a cell monolayer [14–16]. Thus, drug susceptibilities were compared between 2D and 3D cell culture using polystyrene and NCP plates, respectively. The 5-FU and the prodrug, tegafur drugs were added into the culture medium of hepatocarcinima cell line (HepG2), and mitomycin C was added into the culture medium of colon cancer cells. In case of 5-FU, the drug susceptibility of 3D cell culture was higher than that of 2D. Furthermore, the drug susceptibility to tegafur was more enhanced in 3D than in 2D cell culture. On the other hand, the drug susceptibility to mitomycin C of 3D cell culture was lower than that of 2D (Fig. 4). The differences in drug susceptibilities might be drug specific and depend on parameters like drug permeability, drug transporter (MDR1) expression, target protein expression, and protein phosphorylation state. Especially, the result from tegafur experiment indicates that the expressions of enzymes.

Such as CYP2A6 in liver or thymidine kinase in tumor, which catalyze tegafur to 5-FU were increased in 3D cell culture.

3.5 Enhanced Albumin Secretion Form Hepatocytes on NCP

To compare the ability of liver function between 2D and 3D cell cultures, the albumin secretion from HepG2 cell and immortal cells were measured. The albumin secretion from immortal hepatocytes in 3D cell culture was 10~25 –folds of that

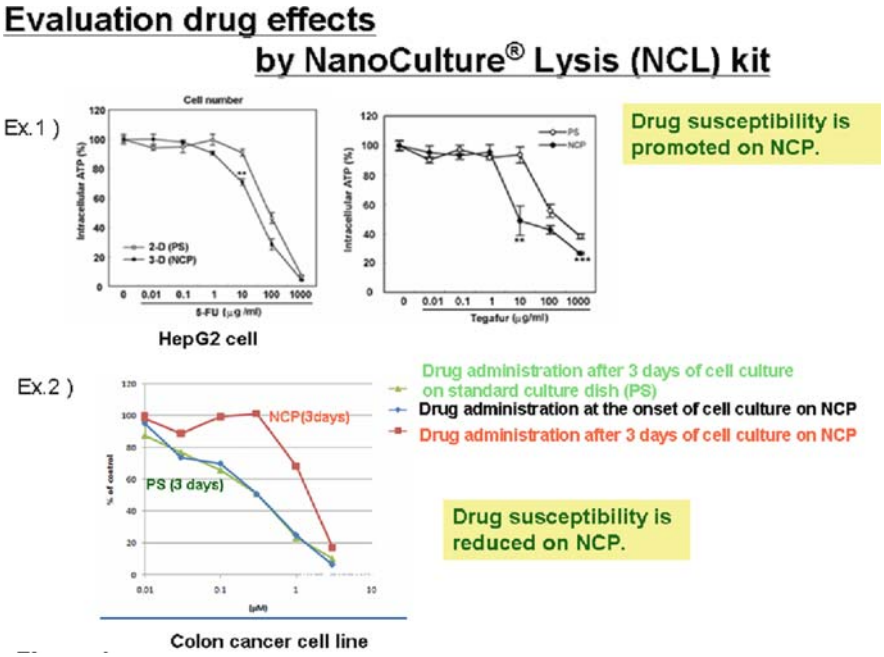

Fig. 4 Evaluation drug effects by NanoCulture® lysis (NCL) kit

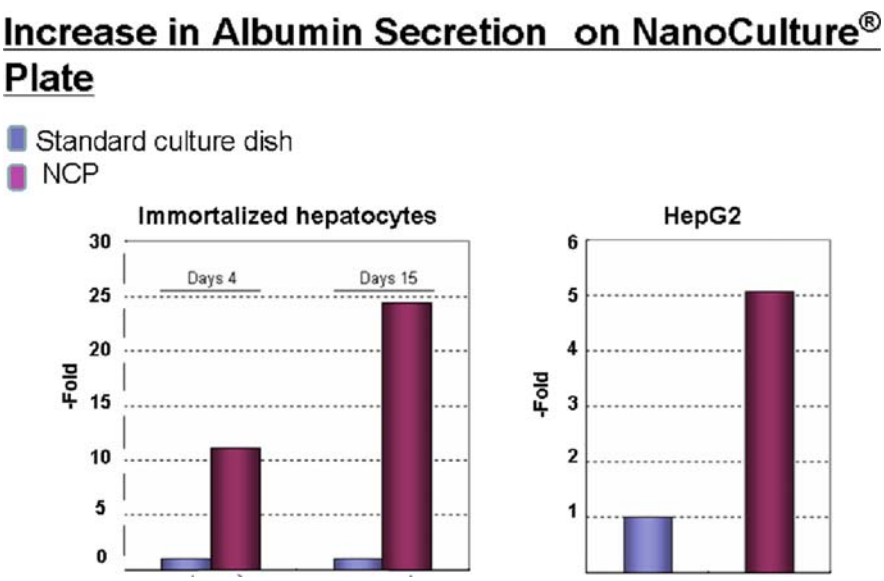

Fig. 5 Increase in albumin secretion on NanoCulture® plate

in 2D cell culture (Fig. 5). Similarly, the albumin secretion from HepG2 in 3D cell culture was approximately 5–folds in 2D cell culture (Fig. 5). These results indicate that 3D system using NCP promotes the ability of liver function of hepatocytes in vitro. To date, sandwiched culture of hepatocytes was used to maintain hepatocyte functions. However, we here show that NCP could be an alternative technology for sandwiched culture of hepatocytes.

3.6 Lipids Accumulation in Adipocyte Spheroids on NCP

Preadipocytes were seeded and differentiated to adipocytes using differentiation medium. Both cells in 2D and 3D cell cultures accumulated lipids, especially single droplet was observed in 3D cell culture using NCP (Fig. 6). Similarly, hMSCs were also cultured with same manners and stained with oil-red O (Data not shown). The cells also accumulated lipids in the cytoplasm.

Our results indicated that functional abilities and ability to differentiate are promoted and preserved in 3D cell culture using NCP. Over the decades, there have been an increasing number of publications on 3D cell culture system. Such a research effort reflects the common need of 3D culture system for in vitro

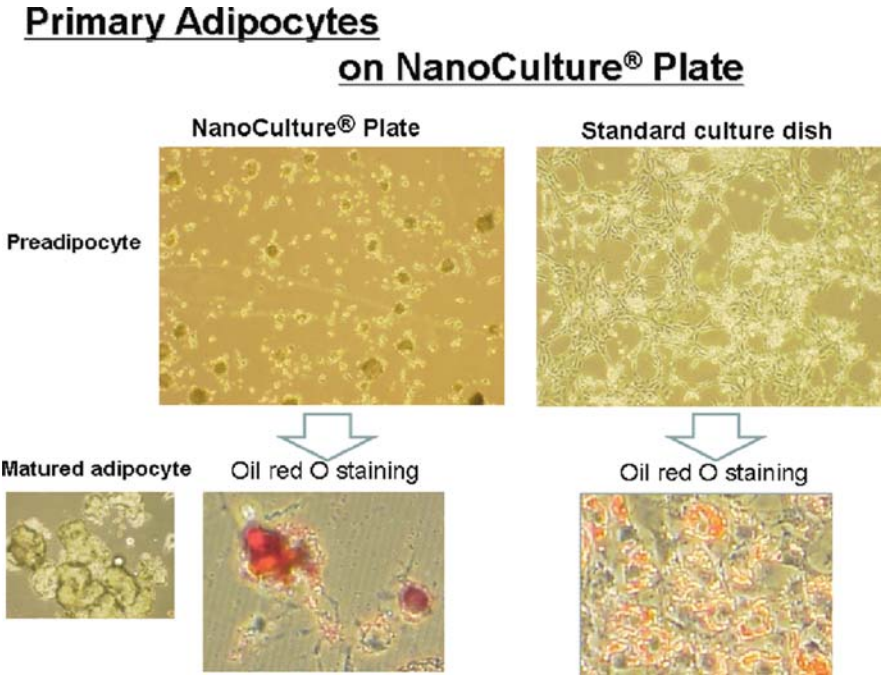

Fig. 6 Primary adipocytes on NanoCulture® plate

model mimicking whole organisms in vivo. NCP could be the most advanced and convenient technology, which can result in reproducible results.

References

1. Heasley, L.E. (2001) Autocrine and paracrine signaling through neuropeptide receptors in human cancer. *Oncogene* **20**(13): 1563–1569.
2. Tsai, R.Y.L. and McKay, R.D.G. (2000) Cell contact regulates fate choice by cortical stem cells. *J. Neurosci*. **20**(10): 3725–3735.
3. Purpura, K.A., Aubin, J.E., and Zandstra, P.W. (2003) Sustained in vitro expansion of bone progenitors is cell density dependent. *Stem Cells* **22**(1): 39–50.
4. Javazon, E.H., Colter, D.C., Schwarz, E.J., and Prockop, D.J. (2000) Rat marrow stromal cells are more sensitive to plating density and expand more rapidly from single-cell-derived colonies than human marrow stromal cells. *Stem Cells* **19**(3): 219–225.
5. Zandstra, P.W., Le, H.V., Daley, G.Q., Griffith, L.G., and Lauffenburger, D.A. (2000) Leukemia inhibitory factor (LIF) concentration modulates embryonic stem cell self-renewal and differentiation independently of proliferation. *Biotechnol. Bioeng*. **69**(6): 607–617.
6. Bhatia, S.N., Balis, U.J., Yarmush, M.L., and Toner M. (1998) Microfabrication of hepatocyte/fibroblast co-cultures: Role of homotypic cell interactions. *Biotechnol. Progr*. **14**(3): 378–387.
7. Albrecht, D.R., Underhill, G.H., Wassermann, T.B., Sah, R.L., and Bhatia, S.N. (2006) Probing the role of multicellular organization in three-dimensional microenvironments. *Nat. Methods* **3**(5): 369–375.
8. Glicklis, R., Shapiro, L., Agbaria, R., Merchuk, J.C., and Cohen, S. (2000) Hepatocyte behavior within three-dimensional porous alginate scaffolds. *Biotechnol. Bioeng*. **67**: 344–354.
9. Nur-E-Kamal, A., Ahmed, I., Kamal, J., Schindler, M., Meiners, S. (2006) Three-dimensional nanofibrillar surfaces promote self-renewal in mouse embryonic stem cell. *Stem cell* **24**: 426–433.
10. Rosen, E.D. and Spiegelman, B.M. (2000) Molecular regulation of adipogenesis. Annu. *Rev. Cell Dev. Biol*. **16**: 145–171. Review.
11. Napolitano, L. (1963) The differentiation of white adipose cells. An electron microscope study. *J. Cell Biol*. **18**: 663–679.
12. Saltiel, A.R. and Kahn, C.R. (2001) Insulin signaling and the regulation of glucose and lipid metabolism. *Nature* **414**(6865): 799–806.
13. Shimizu, K., Ito, A., and Honda, H. (2007) Mag-seeding of rat bone marrow stromal cells into porous hydroxyapatite scaffolds for bone tissue engineering. *J. Biosci. Bioeng*. **104**: 171–177.
14. Graham, C.H., Kobayashi, H., Stankiewicz, K.S., Man, S., Kapitain, S.J., and Kerbel, R.S. (1994) Rapid acquisition of multicellular drug resistance after a single exposure of mammary tumor cells to antitumor alkylating agents. *J. Natl. Cancer Inst*. **86**: 975–982.
15. Kobayashi, H., Man, S., Graham, C.H., Kapitain, S.J., Teicher, B.A., and Kerbel, R.S. (1993) Acquired multicellular-mediated resistance to alkylating agents in cancer. *Proc. Natl. Acad. Sci. USA* **90**: 3294–3298.
16. Pickl, M. and Ries, C.H. (2008) Comparison of 3D and 2D tumor models reveals enhanced HER2 activation in 3D associate with an increased response to trastuzumab. *Oncogene*. 1–8. Doi: 10.1038/onc.2008.394.
17. Akakura, N., Kobayashi, M., Horiuchi, I., Suzuki, A., Wang, J., Chen, J., Niizeki, H., Kawamura, K., Hosokawa, M., and Asaka, M. (2001) Constitutive expression of hypoxia-inducible factor – I alpha renders pancreatic cancer cells resistant to apoptosis induced by hypoxia and nutrient deprivation. *Cancer Res*. **61**: 6548–6554.

Dimensional Cell Culture Dish for In Vivo-Like Cell Culture

VECELL® of Cell Adhesive ePTFE Membrane

Y. Furutani, T. Tamura, and M. Kodama

1 Introduction

Culturing cells on flat plastic dish results in artificial 2-dimensional sheets of cells and there are the strong interactions between cells and plastic dish surfaces to induce excess differentiation, because the cell shape is so stretched out on the surface. The experiments in vitro on monolayer of cells on plastic substrates may not reflect faithfully important aspects of cell behavior in vivo [1, 2].

Normal cells in the human body at a 3-D (3-D) environment are surrounded by other cells, membranes, fibrous layers, and adhesion proteins. Living tissues and cells reside in a complex 3-D microenvironment formed by other cells and extracellular matrix. We have engineered 3-D scaffolds of expanded polytetrafluoroethylene (ePTFE) for 3-D cell culture as VECELL®. In this study, we will examine the differences between normal plastic dish and VECELL® in cellular attachment, proliferation, and differentiation.

2 Materials and Methods

2.1 Preparation of VECELL® Membrane

The surface of VECELL® membrane is shown in Fig. 1, of which the fibril length is 20–50 μm, the porosity about 80–90%, the thickness 50–70 μm. The ePTFE membrane is coated with amphiphilic polymer – PAU (poly amino-acid and urethane copolymer – Mitsubishi Chemical Corporation) and ocean collagen (salmon collagen – Air Water Inc.) to be very hydrophilic and cell adhesive. However, the coating layer is so thin and homogeneous that it cannot be easily recognized as shown in Fig. 1.

M. Kodama (✉)
Vessel Inc., Kitakyushu City, Fukuoka Japan
e-mail: kodama@vessels.co.jp

M. Kamihira et al. (eds.), *Animal Cell Technology: Basic & Applied Aspects*, Animal Cell Technology: Basic & Applied Aspects 16, DOI 10.1007/978-90-481-3892-0_17,

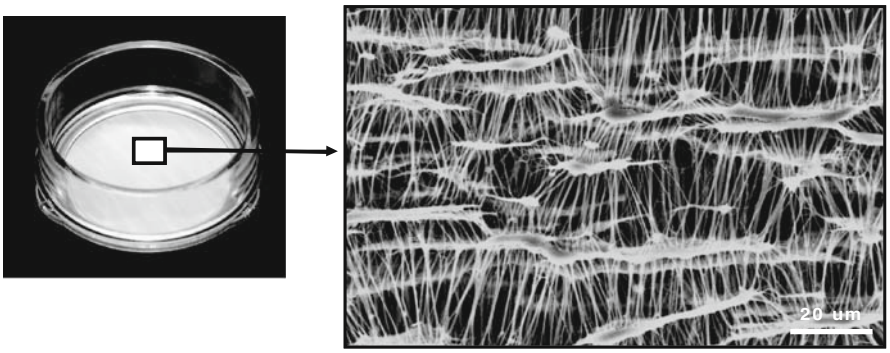

Fig. 1 Membrane structure of VECELL® coated with PAU and collagen

VECELL® allows cell adhesion and proliferation in physiological conditions without any stress unlike surface of normal plastic cell culture surfaces. Cells on VECELL® can adhere on membrane in a 3D fashion as shown in Fig. 2.

Cells adhere to surface coated fibers and there are no excess stretch faces to cells from membrane surface. Cells proliferate on the membrane keeping at the native state to form tissue layer with extra-cellular matrix (ECM). We think it is real 3-D cell culture.

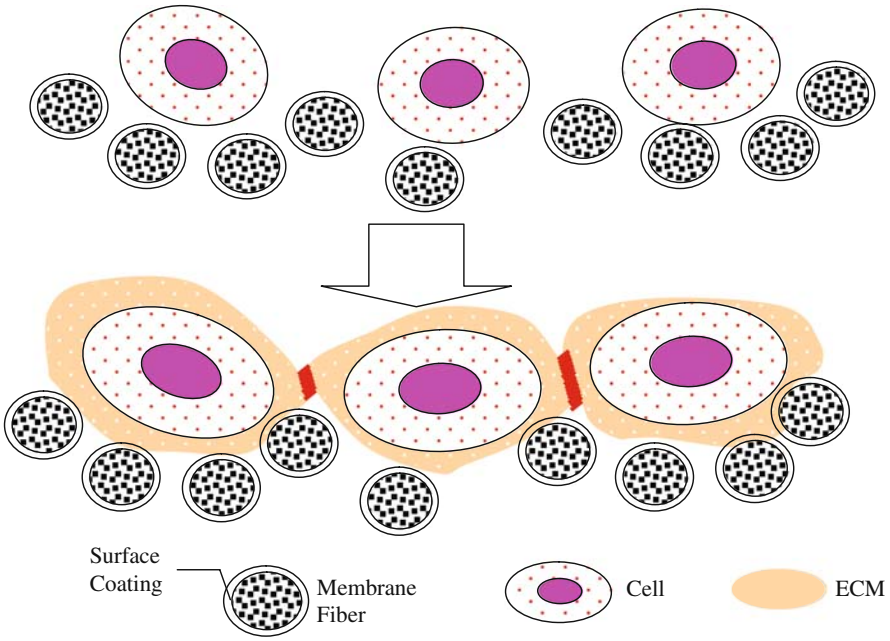

Fig. 2 Schematic illustration of cell adhesion and tissue formation on VECELL®

2.2 Cell Preparation and Culture

L929, Caco-2 cells, and Mouse ES cells (C3Hfc-1) were purchased from Riken Cell Bank (Tsukuba, Japan). Primary hepatocytes were isolated from adult male Wister rats (180–220 g) by collagenase perfusion. The viability was 80%, determined by trypan blue exclusion.

L929 cells were sub-cultured in Dulbecco's modified Eagle's medium (DMEM) containing 10% heat-inactivated FBS. Caco-2 cells were sub-cultured in DMEM containing 20% FBS and 0.1 mM NEAA.

Mouse ES cells were in DMEM containing 20% FBS, Nucleosides, 0.1 mM NEAA, 1000 U/ml LIF and 0.05 mM 2-Mercaptoethanol.

Rat hepatocytes were culture in Williams medium E (WE) containing 10% FBS, 100 μm Insulin, 10 ng/ml effects of epidermal growth factor (EGF) ,and 5 mM Dexamethasone.

3 Results

Cell Culture and Proliferation – on Plastic Dish or on VECELL®

3.1 Caco-2 Cell Culture

For Fig. 2 example, Caco-2 cell culture results are shown in Fig. 3. Adhered cells in 3 Days culture are changed into cell-tissue layer in 26 Days culture, where ECM can be easily observed.

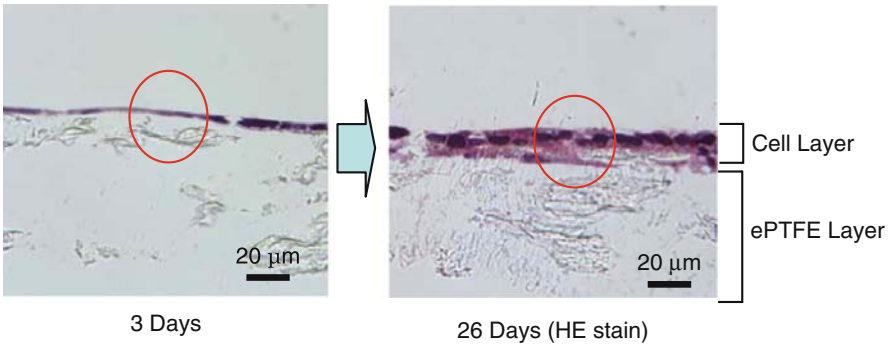

Fig. 3 Cross sectional views of Caco-2 cell culture

3.2 Long Period Stability of L929 Cell Culture

The cells cultured on VECELL® can be visualized by a phase contrast microscope and very stable and maintained native state shape for a long cell culture period up

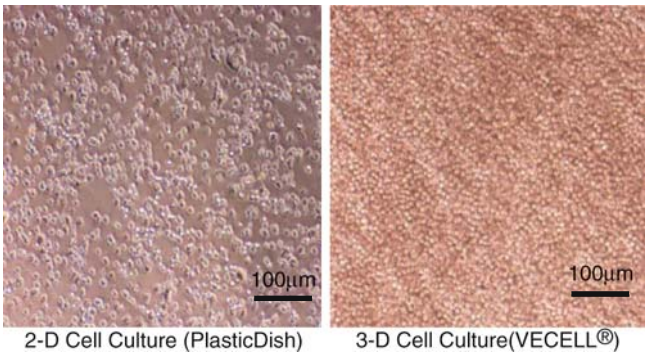

Fig. 4 L929 Cell culture for 264 h – reverse phase contrast microscope observation

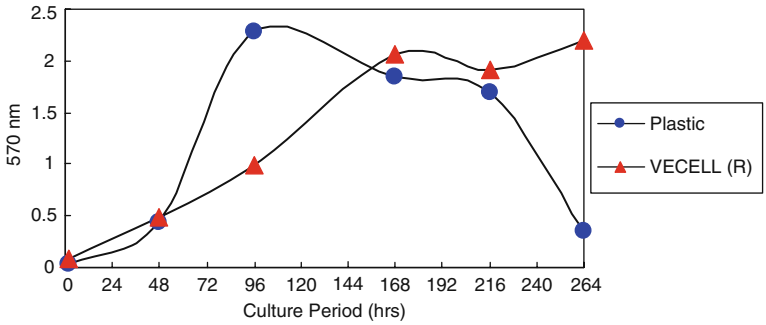

Fig. 5 Cell proliferation on plastic dish and on VECELL® – MTT assays

to 2 weeks (L929) as shown in Fig. 4. In Caco-2 cell culture, stable monolayer formation of cell and tissue organization was observed. These results suggest that VECELL® can be used for cell-based screening test.

The results of the cell proliferation rate determined by MTT assay in Fig. 5 show that indeed it on plastic dish is higher than on VECELL® within 144 h culture period, but after that, most of cells on plastic dish detach from the surface, and on the other hand cells on VECELL® are stable after 168 h culture period.

3.3 Rat Hepatocyte Cell Culture

Cells on VECELL® membrane can proliferate at native cell shape as shown in Fig. 6. Rat hepatocytes on plastic dish spread highly that the nuclears can be easily showed. However, rat hepatocytes shape is not changed after 6 Days culture period.

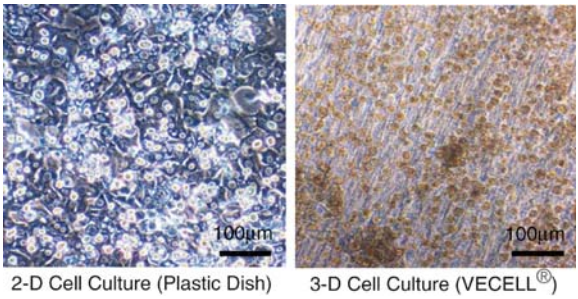

Fig. 6 Rat Hepatocyte culture for 6 Days – phase contrast views

3.4 ES (mouse C3Hfc-1) Cell Culture

VECELL® has so porous membrane and is expected to suppress excess differentiation process of ES cells and stem cells. On normal plastic dish, ES cells and stem cells change easily into differentiated state during cell culture. As shown in Fig. 3, ES cells were formed Embryoid Body like aggregates on VECELL®. Most of ES cells on VECELL® showed ALP strong positive activity to express undifferentiation state. But many of ES cells on gelatin coated plastic dish are changed into ALP weak activity as shown as circle (A) to express differentiation state (Fig. 7).

Indeed, the ES cell proliferation on VECELL® is not so high as compared with that of gelatin-coated dish, but on VECELL® most of cells are kept at undifferentiated condition as Fig. 8 shows.

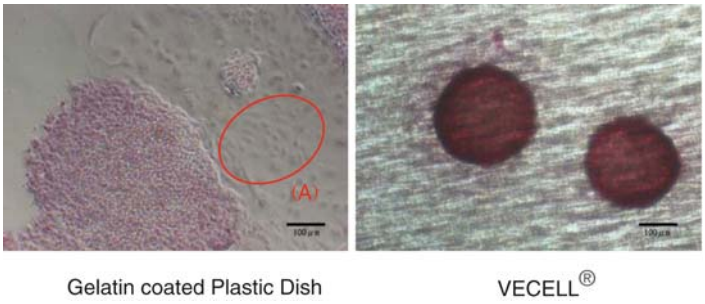

Fig. 7 Mouse ES cell (C3Hfc-1) culture for 7 days. – phase contrast views with ALP stain Circle (A) of the *left* is ALP negative area

4 Discussions

Advantages of 3-D cell culture are to reveal in vivo-like morphology, better intercellular interactions and more realistic biology and function. There is a need for a surface upon which cells behave as though in vivo, thus the surface provides a relevant in vitro model of cellular processes.

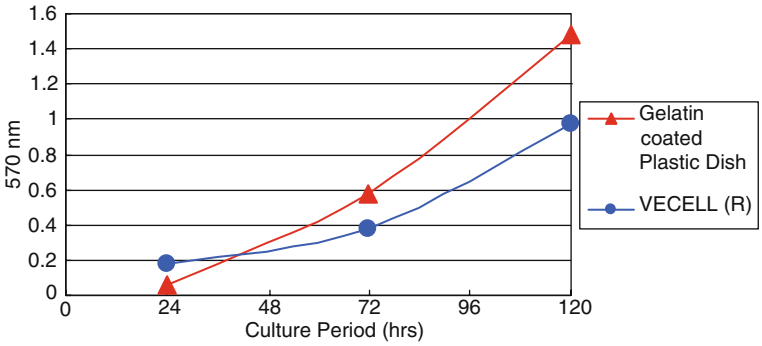

Fig. 8 ES cell (mouse C3Hfc-1) proliferation on gelatin-coated plastic dish and on VECELL® – MTT assay

Cell culture using permeable micro-porous membranes will become a standard method for culturing cells.

From our results, it seems that VECELL® can be used as 3-D cell culture dish. It is very clear that the porosity of membrane is so important for cell function and proliferation. This unique insert of very porous membrane can be applied for ES and stem cell culture including tissue culture as shown in our results.

References

1. Abbott, A. (2003) Biology's new dimension. *Nature* 424: 870–872.
2. Weaver, V.M., Petersen, O.W., Wang, F., Larabell, C.A., Briand, P., Damsky, C., and Bissell, M.J. (1997) Reversion of the malignant phenotype of human breast cells in 3-dimensional culture and in vivo using integrin blocking antibodies. *J. Cell Biol.* 137: 231–246.

Characterization of the Erythropoietin (EPO) Protein Production in the Recombinant Human Cultured Cells, in which the Exogenous EPO Gene was Introduced into Hypoxanthine Phosphoribosyl Transferase (HPRT) Gene Locus

Toshiaki Banzai, Yukiko Koyama, and Shuji Sonezaki

1 Introduction

Mammalian cell expression systems are widely used for production of therapeutic proteins [1, 2]. Industrial production of recombinant DNA-derived protein requires a large culture volume, and scale-up to this volume requires a long time: generally, at least 60 generations [3, 4]. Moreover, it is preferable that recombinant cell lines are cultured in the absence of the drugs used for selection of the recombinant cell lines, since the drugs are expensive and complicate downstream purification. Thus, it is very important for industrial purposes to obtain cell lines that maintain a stable production rate of recombinant DNA-derived protein during prolonged cultivation without selective pressure by drugs [5]. However, there are only a few reports in which stable cell lines for protein production have actually been [5, 6].

We previously reported that the green fluorescent protein (GFP) gene was expressed at a constant rate during 129 days without selective pressure in the human fibrosarcoma HT1080 cell line, when the GFP gene was site-specifically introduced into the hypoxanthine phosphoribosyl transferase (HPRT) gene locus, one of a constitutively expressed endogenous gene locus [7]. The GFP protein accumulates in cytosol, however most therapeutic proteins are secretory proteins. In this study, we examined whether the effect of stabilizing gene expression is applicable to secretory proteins by replacing GFP gene with human erythropoietin (EPO) gene, one of therapeutic and secretory proteins.

S. Sonezaki (✉)
Biotechnology Group, Research Institute, TOTO, LTD., Kitakyushu-city, Fukuoka 802-8601, Japan
e-mail: shuji-sonezaki@toto.co.jp

M. Kamihira et al. (eds.), *Animal Cell Technology: Basic & Applied Aspects*, Animal Cell Technology: Basic & Applied Aspects 16, DOI 10.1007/978-90-481-3892-0_18,

2 Materials and Methods

2.1 Vector Construction

Three EPO expression vectors was constructed (Fig. 1), named phprt-GT-EPO genome #41 (abbreviated as #41), phprt-GT-EPO cDNA #2 (abbreviated as #2) and phprt-GT-IVS-EPO cDNA #52 (abbreviated as #52), respectively. Homology arms (HA1 and HA2), complementary to *hprt* genomic sequences around exon 3, were cloned by PCR reaction from human genomic DNA (Fig. 1) by using a

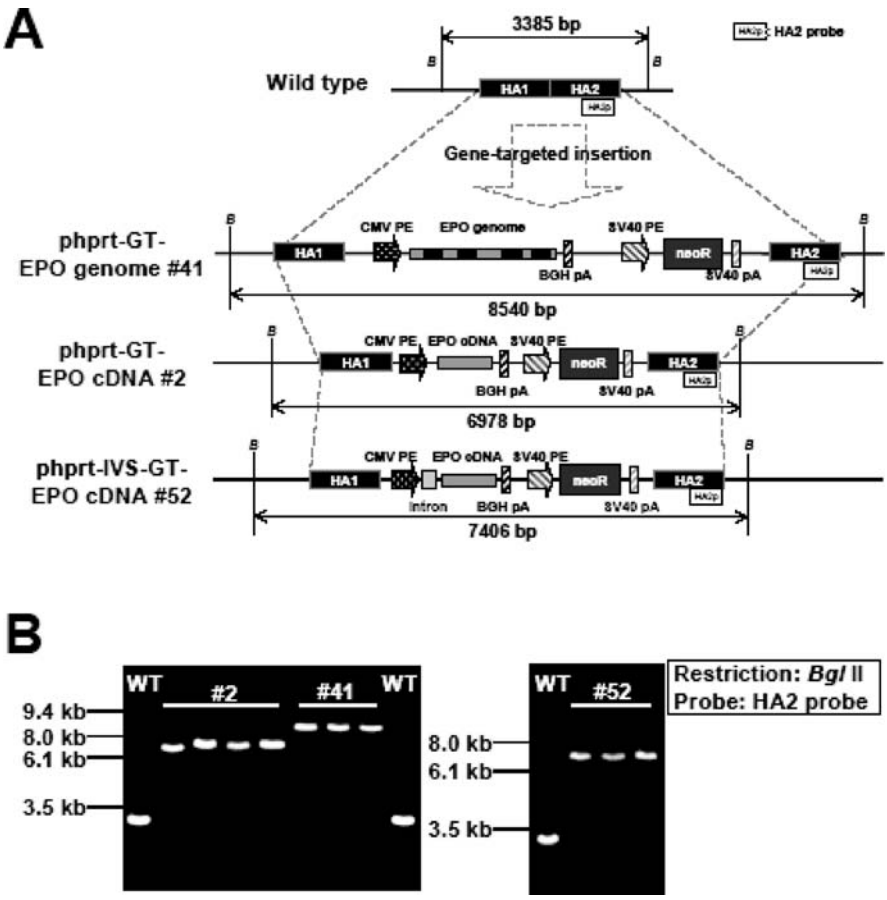

Fig. 1 (**a**) Schematic diagram of wild type HT1080 and gene-targeted HT1080 genomes. Gene-targeting results in the insertion of the vector sequence between HA1 and HA2. The region, where the HA2 probe hybridizes to in Southern analysis, is indicated as white square with annotation (HA2p). Recognition sites of Bgl II are indicated as b. (**b**) Example of the results of southern hybridization analysis was shown. The indicated sizes were estimated from DNA molecular weight marker

Table 1 Primer sequences

Primer name	Primer sequences (5′–3′ direction)
HA1 sense	cctgcaggtcgcgattggtacttgttcagctttattcaag
HA1 antisense	gtcgacaaggacgcgttctgataaaatctacagtcatagga
HA2 sense	Gtcgacctctagctagagcttggcgtaatcatggtctccggagactgaagagctattgtgtgagtat
HA2 antisense	acatgttctcttaagtcgcgaagtagtgttatgatgtatgggcata
HA2 probe sense	Aaactagtcaccttggagga
HA2 probe antisense	Ctcaagagagggtatctgtc
EPO sense	ccttgctagcatgggggtgcacggtgagta
EPO antisense	ccttgaattctcatctgtcccctgtcctgc

primer set of HA1 sense and HA1 antisense or a primer set of HA2 sense and HA2 antisense, respectively (Table 1). CMV promoter/enhancer was derived from pcDNA 3.1 (Invitrogen; #2 and #41) or pIRES (Promega; #52) plasmid. EPO coding sequence was cloned by PCR reaction from either genomic DNA (#41) or reverse-transcripted products of mRNA (#2 and #52) by using EPO sense and EPO antisense primers (Table 1).

2.2 Screening of Gene-Targeted Clones

Two μg of linearized vector was transfected to 1×10^6 cells of HT1080 cells (JCRB cell bank; Cat. No. IFO50354) by using the Nucleofector® device (WAKO) programmed to L-005 in Solution T. After the transfection, the cells were seeded in 96-well micro titer plates. Gene targeted clones were screened as described in previous report [7]. The cells grown in the medium containing both G418 and 6TG were discriminated by microscopic observation, and were scaled up. The cells picked up from one well of the 96-well micro titer plates were termed as clone.

2.3 Southern Analysis

All clones picked up and scaled up were subjected to southern analysis. Genomic DNA was digested by *Bgl* II restriction enzyme and probed with the HA2 probe, PCR amplified by using HA2 probe sense and antisense primer (Table 1). Detailed procedure was described in previous report [7].

2.4 EPO Specific Production Rates Assay

EPO specific production rates (spr) of 4–5 gene-targeted clones out of clones obtained by the one of the vectors described above were analyzed. Six culture dishes, in which 5×10^4 cells were seeded with the medium containing both G418 and 6TG, per one clone were prepared for the assay. After 3 and 4 days of the

seeding, the mediums were recovered for ELISA assay and the total numbers of the cells were counted by using a hemocytometer from three culture dishes. EPO spr [pg cell^{-1} day^{-1}] were calculated from the data by the following equation;

EPO spr = {(EPO at day 4) – (EPO at day 3)}/ [{(cell number at day 3) + (cell number at day 4)}/ 2]/(culture time)

Long-term stability of EPO spr were analyzed for 1 gene-targeted clone out of clones obtained by the one of the vectors described above. The clones were continuously cultured in the medium containing no selection drugs over 60 days by passageing every 4–5 days. The EPO spr of those clones were periodically assayed as described above.

3 Results and Discussion

3.1 Obtaining EPO Producer Clones by Gene-Targeting

All clones grown in the medium containing both G418 and 6TG were subjected to southern analysis for confirming gene-targeted insertion of the vector at the target *hprt* locus. Figure 1a shows the schematic diagram of genomic structures of either wild-type HT1080 cell or gene-targeted clones by each vector. In the southern analyses, in which each genomic DNA was digested by *Bgl* II restriction enzyme and probed with the HA2 probe, a fragment of 3385 bp in length will be detected in wild-type genome, while a fragment of 6978 bp, 8540 bp, and 7406 bp will be detected in gene-targeted clones by the #2, the #41 and the #52 vector, respectively. Figure 1b shows the example of results of the southern analyses. In the Fig. 1b, the restricted fragments in the expected sizes were detected. No trace of signal derived from wild-type genome (i.e. signals at 3385 bp) was detected in those clones, indicating that the insertion of the vector at the target *hprt* locus occurred.

Regardless of the kinds of the vector used, 1–7 gene-targeted clones were obtained in 1 transfection experiment, and the ratio of the number of gene-targeted clone obtained per the number of cells used for transfection experiment was ranged from 2.8 to 7.0 $\times$ 10^{-6}.

3.2 Diversity of EPO spr is Low in the Gene-Targeted Clones

EPO spr were assayed immediately after obtaining the clones in G418 and 6TG screening. The assays were performed in the medium containing both G418 and 6TG. The results are shown in Fig. 2. Gene-targeted clones obtained by transfection of either the #2, the #41, or the #52 vector showed low diversity of EPO spr as can be seen in Fig. 2. It also was represented as low CV value (#2; 15.2%, #41; 16.1%, and #52; 14.6%). While clones, where the #52 vector was randomly integrated into genome, showed relatively high CV value (59.1%). The low CV values in gene-targeted clones might represent that the expression level of exogenous gene

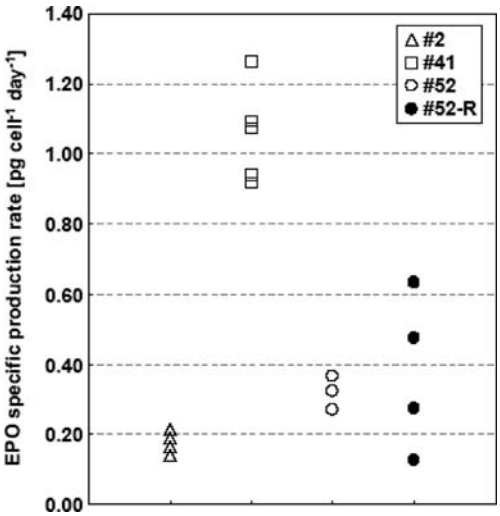

Fig. 2 EPO spr was evaluated. The *white dots* represent the EPO spr of gene-targeted clone (#2, #41, #52), the *black dots* represent randomly-integrated clones (#52-R)

is depending on the chromosomal position, where the exogenous gene is integrated. On the other hands, EPO spr levels were quietly different depending on the vector types even in the gene-targeted clones (spr average is 0.18, 1.13, and 0.32 pg cell^{-1} day^{-1} in gene-targeted clones by the #2, #41, or #52 vector, respectively). The results could suggest that by modifying the vector structures, specific protein production rate in gene-targeted clones could be enhanced more. The ability for producing EPO in spinner flask scale is to be evaluated for further characterization of those cell lines in respect to industrial use.

3.3 Long-Term Stability of EPO spr in the Gene-Targeted Clones

Three gene-targeted clones and two randomly-integrated clones were subjected to long-term culturing for analyzing the stability of EPO spr in the medium containing no selection drug. EPO spr of those clones were periodically assayed during long-term culture up to approximately 60 days, corresponding to approximately 102 generations. In gene-targeted clones analyzed, no decrease of EPO spr was observed, regardless of the vector types, during 60 days culturing without selective pressure (Fig. 3). While in randomly-integrated clones, EPO spr were decreased (Fig. 3). One of the randomly-integrated clones, #52-R 1E9, gradually decreased its EPO specific production rate for 80% at 30 days and 50% at 60 days.

The results would suggest that the exogenous gene, which is site-specifically introduced into the *hprt* locus, could retain its expression level at a constant level without selection drugs for long-term, even though its coding protein is a secretory one.

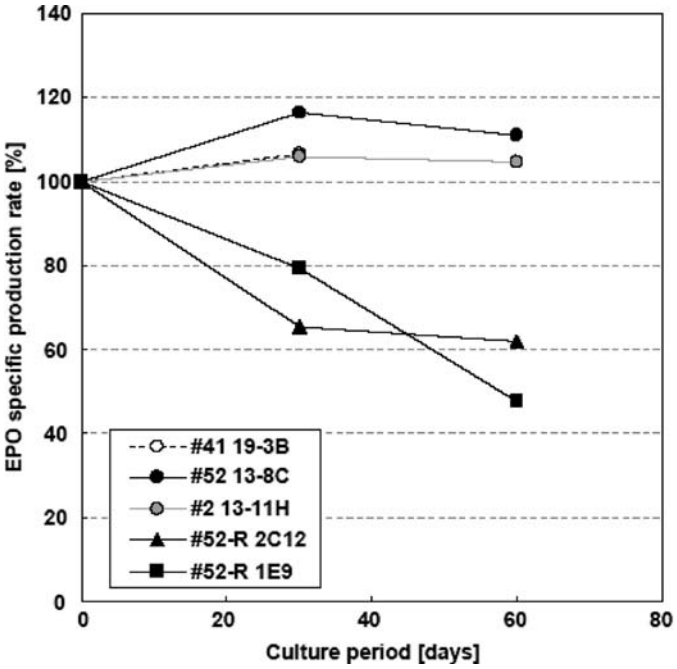

Fig. 3 Stability of EPO spr level during long-term culture in the medium without selection drugs (6TG and G418). Gene-targeted clone 19-3B (by the #41 vector), clone 13-8C (by the #52 vector), and clone 13-11H (by the #2 vector) were subjected to the analysis. Randomly-integrated clone 2C12 (#52-R) and 1E9 (#52-R) were also analyzed

References

1. Werner, R.G., Noé, W., Kopp, K., and Schlüter, M. (1998) Appropriate mammalian expression systems for biopharmaceuticals. *Arzneim.-Forsch./Drug Res*. **48**: 870–880.
2. Andersen, D.C. and Krummen, L. (2002) Recombinant protein expression for therapeutic applications. *Biochem. Eng*. **13**: 117–123.
3. Brown, M.E., Renner, G., Field, R.P., and Hassell, T. (1992) Process development for the production of recombinant antibodies using the glutamine synthetase (GS) system. *Cytotechnology* **9**: 231–236.
4. Birch, J. R., Bebbington, C.R., Field, R.P., Renner, G., Brand, H., and Finney, H. (1993) The production of recombinant antibodies using the glutamine synthetase (GS) systems. In: S. Kaminogawa, A. Ametani, and S. Hachimura (Eds.), *Animal cell technology: Basic and applied aspects* (Vol. 5, pp. 573–577). Netherlands: Kluwer Academic press.
5. Barnes, L.M., Bentley, C.M., and Dickson, A.J. (2003) Stability of protein production from recombinant mammalian cells. *Biotechnol. Bioeng*. **81**: 631–639.
6. Kim, N.S., Kim, S.J., and Lee, G.M. (1998) Clonal variability within dihydrofolate reductase-mediated gene amplified Chinese hamster ovary cells: stability in the absence of selective pressure. *Biotechnol. Bioeng*. **60**: 679–688.
7. Koyama, Y., Banzai, T., Sonezaki, S., and Kusano, K. (2006) Stable expression of a heterogeneous gene introduced via gene targeting into the HPRT locus of human fibrosarcoma cells. *Biotechnol. Bioeng*. **95**: 1052–1060.

Development of Protein High Expression System by Using Fructose Metabolism

Yuriko Tsukamoto, Shigeki Nakamura, Aiko Inoue, Norikazu Nishino, Yuichi Inoue, and Hiroharu Kawahara

1 Introduction

A fructose-based cell culture is suitable for the production of useful proteins because it decreases lactate production in culture medium, leading to cell and product stability [1, 3]. However, not all cell lines can be cultured in a fructose-based medium. Our previous study suggested that two fructose metabolism-related genes, glucose transporter 5 (GLUT5) and fructose 1,6-bisphosphatase (FBP) might be related to it [4, 5]. We attempted to develop high expression system of monoclonal antibodies (MAbs) in the fructose-based medium by using the fructose metabolism-related gene.

2 Materials and Methods

2.1 Cell Line and Cell Culture

The human hybridoma cell line AE6 and BD9 were generated by fusing peripheral blood lymphocytes from a healthy adult with a fusion partner A_4H_{12} derived from human Molt 4 cells using an in vitro immunization method [6]. The human cell line SC-01MFP was established from human myeloma cell line RPMI8226. Cells were maintained in RPMI1640 medium supplemented with 10% FBS (Thermo Fisher Scientific, USA), at 37°C in humidified 5% CO_2/95% air. Before fructose experiments, cells were adapted in the 10%FBS-RPMI1640 medium containing 2 g/L of fructose for one day.

Y. Tsukamoto (✉)
Graduate School of Life Science and Systems Engineering, Kyushu Institute of Technology, Kitakyushu-shi, Fukuoka 808-0196, Japan
e-mail: tsukamoto-yuriko@edu.life.kyutech.ac.jp

M. Kamihira et al. (eds.), *Animal Cell Technology: Basic & Applied Aspects*, Animal Cell Technology: Basic & Applied Aspects 16, DOI 10.1007/978-90-481-3892-0_19,

2.2 Vector Design for Protein Expression

The full length of GLUT5 and FBP was amplified by RT-PCR from the human hybridoma AE6, and inserted into the mammalian expression vector pTARGET^{TM} (Promega, USA) by the TA cloning method, respectively. After cloning, they were identified by DNA sequencing. The obtained expression vectors were referred to pGLUT5 and pFBP, respectively. To construct the vector expressing both IgG and GLUT5 genes, the NheI/SmaI fragment containing GLUT5 gene from pGLUT5 was inserted between the NheI and EcoRV sites of the expression vector pSecTag2C (Invtrogen, USA), and then the NruI/NaeI fragment containing CMV promoter, IgG heavy chain gene, and polyadenylation signal site from pC5-gamma [2] was inserted into the NruI site of the GLUT5-inserted pSecTag2C. The obtained IgG and GLUT5 expression vector was referred to pSec-IgG/GLUT5.

2.3 Transfection of Gene to Cells

Gene expression vector was transfected into cells with Lipofectamine 2000 (Invitrogen, USA) according to a common instruction. Transfection was done in 2 ml medium containing 4 μg of DNA, 10 μl of Lipofectamine 2000. The expression vector pGLUT5 or/and pFBP was transfected into AE6 cells. The expression vector pC5-gamma, pGLUT5, pSec-IgG/GLUT5, and their combination was transfected into SC-01MFP cells. After 48 h, cells were maintained in the 10% FBS-RPMI1640 medium containing G418 (pGLUT5, pFBP, and pC5-gamma) or Zeocin (pSec-IgG/GLUT5).

2.4 Measurement of Antibody Concentration and Viable Cell Density

The MAb concentrations in culture medium were measured by an enzyme-linked immunosorbent assay (ELISA) as described previously [8], using anti-human IgG antibody (Biosource International, Inc., USA) as the first antibody, and anti-human IgG peroxide conjugate antibody (Biosource International, Inc., USA) as the second antibody. Cell number was counted by using a hemacytometer, and viability was determined by the trypan blue dye exclusion method.

2.5 RT-PCR Analysis

Total RNA was recovered from cells using ISOGEN reagent (NIPPON GENE, Tokyo, Japan). Reverse transcription was done using random hexamer primers, as described in a common protocol (Invitrogen). To examine gene expression of the fructose transporter, GLUT5, the following primers were used: as forward primer, 5'-CCC CTG GTA ACA TAA CAA CA-3', and as reverse primer, 5'-TGA CAT

CAC ACC TTC CTA GA-3'. As a control, the beta-actin primers were used as forward primer, 5'-GAC TTA GAG CAA GAG ATG-3', and as reverse primer, 5'-GCC AGA CAG CAC TGT GTT-3'.

PCR amplification reactions were done in 50 μl reaction volumes containing 25 μl of 2× PCR buffer, 10 μl of 2 mM deoxynucleoside triphosphates, 3 μl of 10 pmol of each primer, 1 μl of first strand cDNA, and 1.0 units of KOD FX (Takara Biomedicals, Osaka, Japan). The mixture was denatured at 94°C for 2 min, followed by 30 cycles at 98°C for 10s, at 54°C for 30s, and at 72°C for 1 min. The amplified products were analyzed by electrophoresis on a 1.0% agarose gel and stained by ethdium bromide.

3 Results and Discussion

3.1 Improvement of Cell Proliferation by GLUT5 Gene Transfection

BD9 cells were not cultured in the fructose-based medium. To examine the effects of GLUT5 and FBP genes on cell proliferation, the GLUT5 expression vector pGLUT5 and the FBP expression vector pFBP were transfected into BD9 cells, respectively. GLUT5 gene showed a tendency to improve cell proliferation and viability (Fig. 1), while FBP gene did not change them (data not shown). These results suggest that GLUT5 gene may be involved in growth potential in the fructose-based medium.

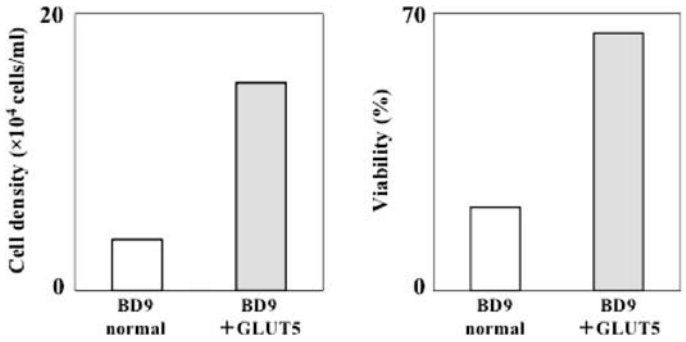

Fig. 1 Improvement of proliferation and viability by GLUT5 gene transfection in BD9 cells. Cells (1 × 104 cells/ml) were cultured in a fructose-based 10%FBS-RPMI1640 medium for 5 days. After 5 days, cell density and viability were measured

3.2 Improvement of IgG Productivity by GLUT5 Gene Transfection

To examine the effect of GLUT5 gene on IgG productivity, the GLUT5 expression vector pGLUT5 and the IgG expression vector pC5-gamma were cotransfected

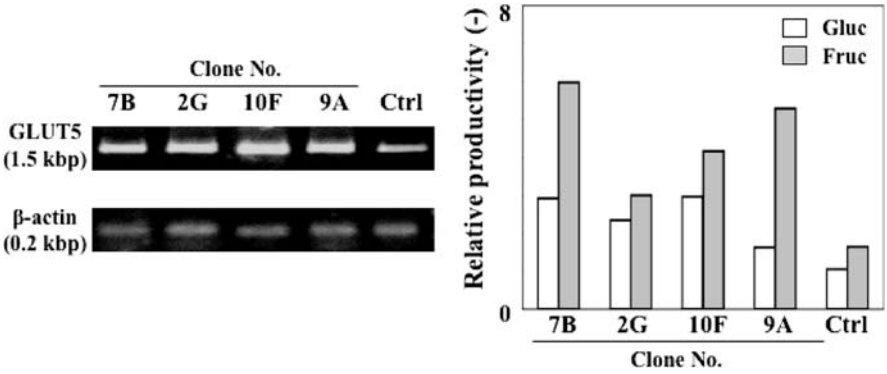

Fig. 2 GLUT5 gene expression and IgG productivity in the SC-01MFP cells. Gene expression was examined by RT-PCR. Cells (1×10^4 cells/ml) were cultured in glucose- and fructose-based 10%FBS-RPMI1640 medium for 5 days. After 5 days, antibody concentration in the medium was measured

into SC-01MFP cells. Four clones expressing both IgG and GLUT5 were obtained (Fig. 2). The pC5-gamma transfected control did not significantly increase IgG productivity, while two clones 7B and 9A showed higher IgG productivity in the fructose-based medium than the glucose-based medium. The IgG productivity of the clones may be enhanced by the suppression of endogenous GLUT5 expression with the inhibitor of the GLUT5 original promoter [7].

3.3 Improvement of IgG Productivity by GLUT5 and IgG Gene Cotransfection

To increase co-expression efficiency of IgG and GLUT5 genes, the IgG and GLUT5 expression vector pSec-IgG/GLUT5 was transfected into SC-01MFP cells. As a result, IgG production in the fructose-based medium was over 2.5 times higher than that in the glucose-based medium (Fig. 3). This result suggests that the relative position of IgG and GLUT5 genes integrated into genome may affect IgG productivity in SC-01MFP cells. Because IgG and GLUT5 gene expression was controlled by the CMV promoter, respectively, IgG expression might be coactivated when GLUT5 expression was activated in the fructose-based medium.

4 Conclusions

This study showed that the fructose transporter, GLUT5 improved cell proliferation and IgG productivity in human hybridoma and myeloma cell lines in the fructose-based medium. The increased IgG productivity might be involved in the relative position of GLUT5 and IgG genes integrated into genome in SC-01MFP cells.

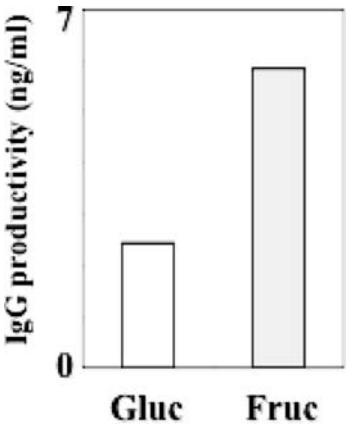

Fig. 3 IgG productivity of SC-01MFP cells transfected with the IgG and GLUT5 expression vector. Cells were cultured in glucose- and fructose-based 10%FBS-RPMI1640 medium for 3 days. After 3 days, IgG concentration in the medium was measured

References

1. Burant, C.F., Takeda, J., Brot-Laroche, E., Bell, G.I., and Davidson, N.O., (1992) Fructose transporter in human spermatozoa and small intestine is GLUT5. *J. Biol. Chem.* **267**: 14523–14526.
2. Haruta, H., Tachibana, H., Mochizuki, K., Hashizume, S., Kusakabe, K., Shirahata, S., and Murakami, H. (1997) Class-switching of the IgM type anti-adenocarcinoma human antibody HB4C5 into an IgG1 type resulted in the loss of the antigen binding ability. *Hum. Antibod.* **8**: 137–145.
3. Imamura, T., Crespi, C.L., Thilly, G.W., and Brunengraber, H. (1982). Fructose as a carbohydrate source yields stable pH and redox parameters in microcarrier cell culture. *Anal. Biochem.* **124**: 353–358.
4. Inoue, Y., Fujisawa, M., Kawamoto, S., Shoji, S., Hashizume, M., Fujii, S., Katakura, Y., and Shirahata, S. (1999). Effectiveness of vitamin A acetate for enhancing the production of lung cancer specific monoclonal antibodies. *Cytotechnology* **31**: 77–83.
5. Inoue, Y., Kawahara, H., Shirahata, S., and Sugimoto, S. (2006) Retinoic acid improves a hybridoma culture in a fructose-based medium by up-regulation of fructose incorporation via retinoid nuclear receptors. *Biosci. Biotechnol. Biochem.* **70**: 2248–2253.
6. Kawahara, H., Shirahata, S., Tachibana, H., and Murakami, H., (1992) In vitro immunization of human lymphocytes with human lung cancer cell line A549. *Hum. Antibod. Hybridomas* **3**: 8–13.
7. Kirchner, S., Kwon, E., Muduli, A., Cerqueira, C., Cui, X. L., and Ferraris, R.P. 2006. Vanadate but not tungstate prevents the fructose-induced increase in GLUT5 expression and fructose uptake by neonatal rat intestine. *Am. Soc. Nutr. J. Nutr*. **136**: 2308–2313.
8. Shoji, M., Kawamoto, S., Sato, S., et al., (1994) Specific reactivity of human antibody AE6F4 against cancer cells in tissuec and sputa from lung cancer patients. *Hum. Antibod. Hybridomas* **5**: 116–122.

Controlling Fucosylation Levels of Antibodies with Osmolality during Cell Culture

Yoshinobu Konno, Yuki Kobayashi, Ken Takahashi, Eiji Takahashi, Shinji Sakae, Masako Wakitani, Toshiyuki Suzawa, Keiichi Yano, Masamichi Koike, Kaori Wakamatu, and Shinji Hosoi

1 Introduction

Monoclonal antibodies (MAbs) are being used in an increasing number of therapeutic applications targeting conditions such as cancer, cardiovascular disease, inflammatory disease, macular degeneration, transplant rejection, multiple sclerosis, and viral infection. Since the production cost of MAbs is much higher than that of other biopharmaceuticals and low-molecular-weight compounds, it is critical to produce high-efficacy MAbs efficiently. One method to increase the effectiveness of a MAb, which in turn affects antibody-dependent cellular cytotoxicity (ADCC), is to consider the type of host cell employed. Since different host cell lines produce distinct glycosylation patterns (fucosylation in particular), MAbs produced in a particular host will demonstrate a specific ADCC activity. For example, MAbs produced in a rat myeloma cell line (YB2/0) exhibit higher ADCC activity than MAbs produced in Chinese hamster ovary cells (CHOs) or in NS0 myeloma cells. This is because YB2/0 cells produce MAbs with a lower fucose content. This finding led to the development of a CHO host cell line with α-1,6-fucosyltransferase gene knock out (Potelligent^{TM} cell, BioWa, NJ, USA) [1].

2 Materials and Methods

Cell culture: Rat hybridoma YB2/0 cells (ATCC CRL 1662, MD, USA) were used as the host cell line. A YB2/0 cell line expressing proprietary recombinant chimeric IgG_1 antibody was cultured in Hybridoma SFM or CD-Hybridoma medium (Invitrogen, CA, USA) with appropriate supplements in a 250-mL shaker flask (Corning, NY, USA) in 1-L (ABLE, Tokyo, Japan) and 5-L bioreactors (Marubishi-bioeng., Tokyo, Japan). The cultures were inoculated at a density of

Y. Konno (✉)
Bioprocess Research and Development Laboratories, Kyowa Hakko Kirin Co., LTD., Takasaki-shi, Gunma 370-0013, Japan
e-mail: Yoshinobu.Konno@kyowa-kirin.co.jp

M. Kamihira et al. (eds.), *Animal Cell Technology: Basic & Applied Aspects*, Animal Cell Technology: Basic & Applied Aspects 16, DOI 10.1007/978-90-481-3892-0_20,

at least of 2×10^5 cells/mL and cultivated at 37°C and pH 7.1 [2, 3] until the decline phase.

Assay: Viable cell density and viability was analyzed by Cedex^{TM} (Innovatis, Bielefeld, Germany) using the trypan blue dye exclusion method. The osmolality of the medium was measured by a Vogel osmometer OSMOMAT 030-D (Vogel, Giessen, Germany) using freezing-point depression. Glucose concentration was monitored by the glucose/lactate biosensor YSI2700 (YSI, OH, USA). Fucosylation levels were measured as a monosaccharide composition of each purified MAb, as previously described [4].

3 Results and Discussion

3.1 Dilution of Basal Medium

For the fed-batch culture in a 5-L bioreactor, the osmolality of the initial basal medium was maintained between 285 and 345 mOsm/kg by dilution with distilled water. The defucosylation level (deFuc%) of MAbs was found to be between 40 and 70%, depending on the medium osmolality (Fig. 1). Although protein production is affected by the osmolality of the culture medium in general, no significant changes were observed in the amount of MAb produced under the conditions employed.

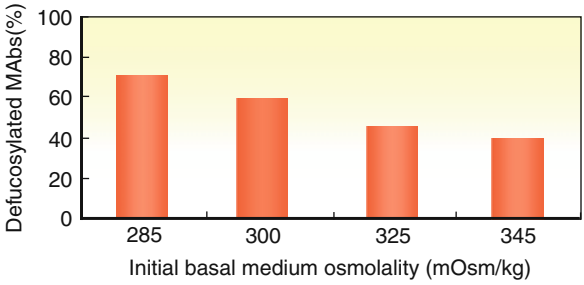

Fig. 1 Dependence of MAb defucosylation level (deFuc%) on medium osmolality. The fed-batch method was used in a 5-L bioreactor

3.2 Effects of Different Osmolality-Influencing Compounds on deFuc%

To evaluate the chemical structure of the compounds used for controlling osmolality, we first diluted the medium from 320 to 250 mOsm/kg, and then added either NaCl, KCl, fucose, fructose, creatine, or mannitol. Cells were cultured at 37°C for 11 days. deFuc% was linearly correlated with osmolality, with r^2 being as high as 0.92, irrespective of the identity of the compound added (Fig. 2). Both ionic and non-ionic compounds exhibited the same correlation, and fucose showed no effect on the strength of the correlation.

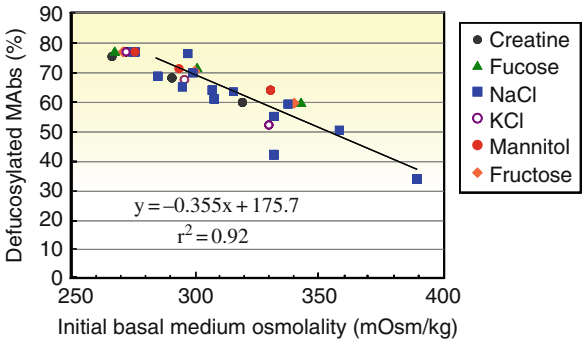

Fig. 2 Relative defucosylation levels (deFuc%) of MAbs produced in media with different osmolalities. Variation in osmolality was attained by supplementation of basal medium with one of the above-mentioned compounds. Cells were cultured in 250-mL shaker flasks (Corning, NY, USA) for 11 days

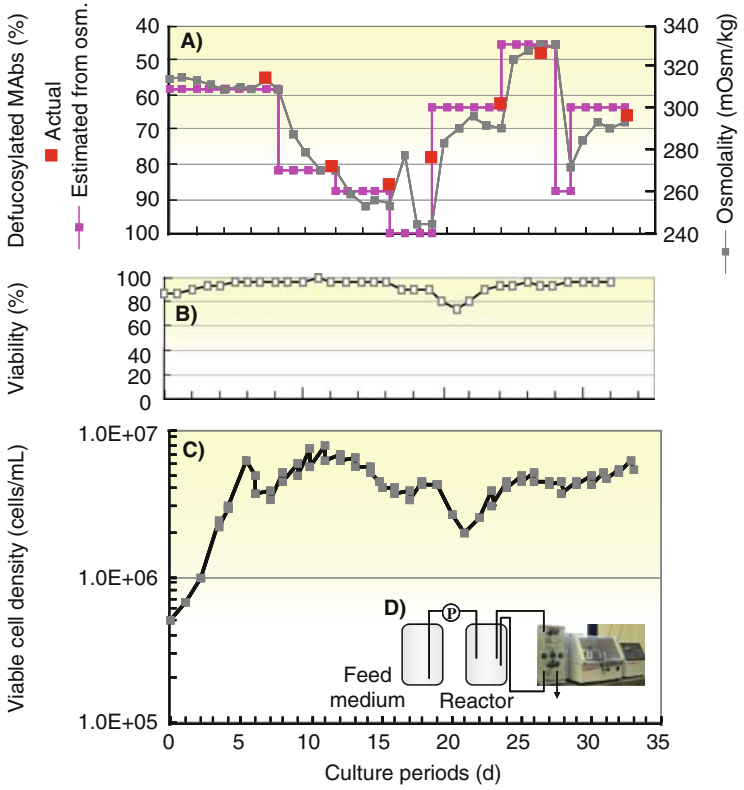

Fig. 3 Relative defucosylation level (deFuc%) of MAbs produced in different osmolalities. Cells were cultured by a perfusion method using a 1-L bioreactor (Centritech^{TM} LabII system). (**a**) Gray, pink, and red squares indicate medium osmolality, deFuc% estimated from the set point of osmolality, and the actual deFuc% observed, (**b**) cell viability, (**c**) viable cell density, (**d**) outline of the bioreactor system employed

3.3 Perfusion Culture

Perfusion with the Sorvall Centritech^{TM} Lab II system (Thermo, MA, USA) maintained medium osmolality so that we could arbitrarily and subsequently control deFuc% during cell culturing. The perfusion rate was set at 1 vvd. The osmolality of the medium was maintained by changing the culture medium at an interval of about four days. As a result, we succeeded in regulating deFuc% arbitrarily between 45% and 85% by controlling medium osmolality from 260 to 330 mOsm/kg (Fig. 3). At a lower osmolality (245 mOsm/kg), growth inhibition was observed.

3.4 Fed-Batch Culture

Fed-batch is the most common method used for MAb production. However, it is not easy to control medium osmolality throughout the culture period, because several cell by-products accumulate in the tank. Since the tank size limits the volume of

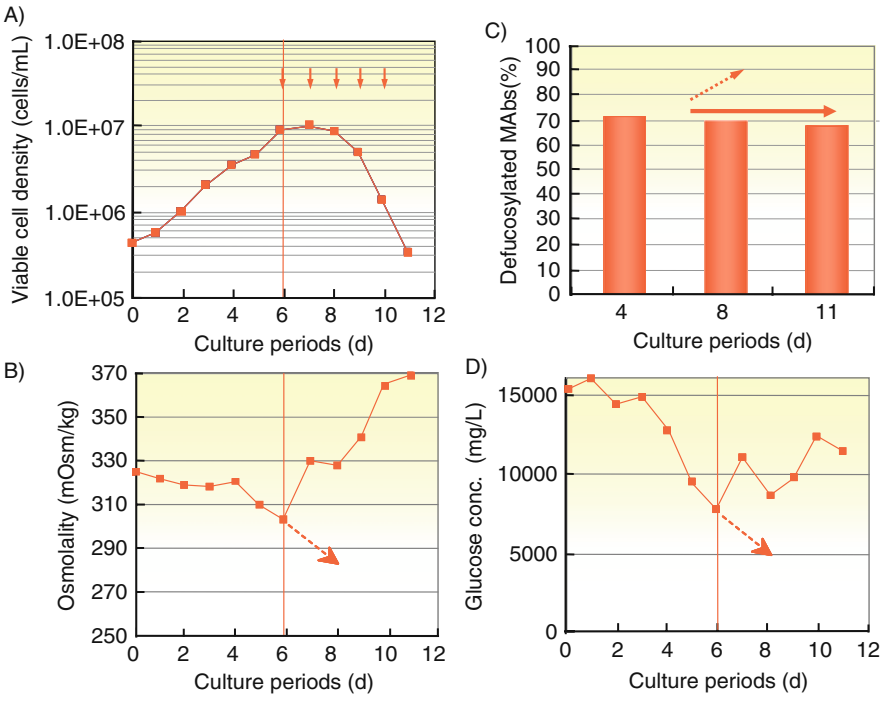

Fig. 4 Cells were cultured in a custom-made medium containing low NaCl concentration. The high initial osmolality decreased as glucose was consumed during fed-batch culturing; this led to a reduction in osmolality. Relative amount of defucosylation levels (deFuc%) of MAbs for the production of IgG_1 MAbs using 5-L bioreactor when the glucose feed solution was combined. (**a**) growth curves, (**b**) osmolality, (**c**) glucose concentration, (**d**) deFuc%

feed solutions, dilution is not practical for industry-level production. Furthermore, the initial osmolality cannot be maintained throughout the culture. Thus, the method employed was used to control the increase in osmolality during culture without requiring a dilution step. We used a custom-made medium containing a low concentration of sodium chloride. The osmolality was regulated by controlling glucose concentration, because glucose is a primary nutrient that is initially present in high concentration but is ultimately consumed by cells. Consumption of glucose results in an osmolality decrease; this was observed as expected (Fig. 4). The increase in osmolality was achieved by supplementation of glucose from day 6. Constant osmolality of the medium was attained by the addition of glucose.

4 Conclusion

- deFuc% was dependent on medium osmolality during culture.
- deFuc% was not affected by the type of compound used for controlling osmolality (creatine, fucose, NaCl, KCl, fructose or mannitol).
- Based on these results, we succeeded in controlling the deFuc% of MAbs arbitrarily between 45 and 85% by maintaining medium osmolality constant during perfusion of cultures.
- By using medium containing an initial low concentration of NaCl and a high concentration of glucose in combination with glucose solution feeding, we could maintain the low osmolality and high deFuc% during the fed-batch culturing.

Acknowledgements We are grateful to Drs. Mitsuo Sato, Kazuhisa Uchida, Mr. Hiroshi Takasugi, Mr. Kazutoshi Maki, and Mr. Noriyuki Takahashi for their helpful discussions and their technical assistance.

References

1. Yamane-Ohnuki, N., Kinoshita, S., Inoue, M., Kusunoki, M., Iida, S., Nakano, R. Wakitani, M., Niwa, R., Uchida, K., Shitara, K., and Satoh M. (2004) Establishment of FUT8 knockout Chinese hamster ovary cells: an ideal host cell line for producing completely defucosylated antibodies with enhanced antibody-dependent cellular cytotoxicity. Biotechnol. Bioeng. **87**: 614–622.
2. Ogawa, T., Narihisa, A., Konno, Y., Takasugi, H., Seiji, S., and Yano. K. (2001) Process for producing polypeptide. WO 01/29246.
3. Konno, Y., Aoki, M., Takagishi, M., and Takasugi. H. (2003) Process for producing substance. WO 03/046174.
4. Shinkawa, T., Nakamura, K., Yamane, N., Shoji-Hosaka, E., Hanai, N., Shitara, K. et al. (2003) The absence of fucose but not the presence of galactose or bisecting *N*-acetylglucosamine of human IgG1 complex-type oligosaccharides shows the critical role of enhancing antibody-dependent cellular cytotoxicity. *J. Biol. Chem*. **278**: 3466–3473.

Comparison of Immunoresponses Between Cecal Patch Cells and Peyer's Patch Cells Stimulated by Bacterial Components

Takuma Konno, Akira Hosono, Yasuhiro Hiramatsu, Satoshi Hachimura, Kyoko Takahashi, and Shuichi Kaminogawa

1 Introduction

The mucosa of the gastrointestinal tract is constantly exposed to various antigens, including commensal or pathogenic bacteria and dietary foods. In the Peyer's patches (PPs), one of the gut-associated lymphoid tissues (GALT), commensal and pathogenic bacteria are taken up into M cells via intracellular transport prior to stimulation of mucosal antigen-presenting cells (APCs). Next, APCs transmit this stimulus to T cells, thus promoting immunoresponses in the small intestine. Interestingly, commensal bacteria are able to exist in the gut without hypersensitivity, but pathogens induce remarkable immunoresponses leading to their removal by the gut immune system. On the other hand, more than 99% of intestinal commensal bacteria are localized in the large intestine in which lymphoid tissues including cecal patches (CPs) and colonic patches are located. Therefore, immune system in the large intestine is supposed to be stimulated by these various commensal bacteria, but the characteristics of the large intestinal immunoresponses to them have not been clarified.

In previous studies, it was reported that CPs in the large intestine had M cells in their follicle associated epithelium (FAE) and their histological character was similar to PPs [1, 2]. Furthermore, it was observed that the lymphoid population of T or B cells in CPs was similar to those in PPs [3]. Moreover, we previously reported that dietary *Bifidobacterium pseudocatenulatum* JCM 7041 (Bp) was taken up into the luminal side of PPs directly, and that the Bp was captured by $CD11c^+$ cells of PPs in the small intestine [4] and CPs in the cecum (unpublished data). It is assumed that the bacterial stimulation occurred in CPs as well as in PPs. However, it has not been clarified how CP cells trigger immune responses to the intestinal commensal bacteria.

A. Hosono (✉)
Department of Food Science and Technology, College of Bioresource Sciences, Nihon University, Fujisawa-shi, Kanagawa 252-8510, Japan
e-mail: hosono@brs.nihon-u.ac.jp

M. Kamihira et al. (eds.), *Animal Cell Technology: Basic & Applied Aspects*, Animal Cell Technology: Basic & Applied Aspects 16, DOI 10.1007/978-90-481-3892-0_21,

Consequently, this study aimed to clarify how immune responses are triggered to bacterial components in CPs in the large intestine compared to PPs, described as inductive sites of intestinal immunity in the small intestine.

2 Materials and Methods

2.1 Animals

Female BALB/c mice were purchased from CLEA Japan (Tokyo, Japan) and were used in experiments at 7 weeks of age. All animal experiments were performed in accordance with the guidelines for the care and use of laboratory animals of the College of Bioresource Sciences, Nihon University.

2.2 Preparation of Unfractionated Cells or Thy1.2$^-$ Cells as APCs from PPs and CPs

PPs and CPs were removed carefully from the small intestine and the cecum. Then PP and CP cells were obtained by treatment with collagenase and EDTA as described previously, and cultured at 2.0×10^6 cells/ml in 48-well flat-bottom plates with RPMI 1640 supplemented with 10% fetal calf serum, 2 mM L-glutamine, penicillin (50 U/ml), and streptomycin (50 μg/ml) [5].

Thy1.2 (CD90.2) negative cells as APCs from PP and CP cells were isolated by magnetic cell sorting system (MACS; Miltenyi Biotec, Bergisch Gladbach, Germany) with anti-mouse CD90.2-conjugated magnetic microbeads and LD column. The purity of Thy1.2$^-$ cells from PPs and CPs were >95% in all experiments (data not shown).

2.3 Cell Culture for Cytokine Production

Cytokine production was measured in unfractionated cells or Thy1.2$^-$ cells from PPs and CPs, cultured at 2.0×10^6 cells/ml in 48-well flat-bottom plates with sonicated *Bifidobacterium* (BIM) [5] or lipopolysaccharide (LPS) from *Eschelichia coli* B55:05 (*E.coli*) (Sigma, St. Louis, MO) for 24 h or 72 h. Concentrations of bacterial components in all samples were 1, 10, or 50 μg/well. Cytokine production was measured in APCs from PPs and CPs, cultured at 2.0×10^6 cells per ml with BIM or LPS from *E.coli* for 24 h. Concentrations of bacterial components in all samples were 0.1, 1 or 10 μg/well.

2.4 Enzyme-Linked Immunosorbent Assay (ELISA) for Cytokines

The culture supernatants were assayed for interleukin (IL)-12p40 and IL-10. The concentrations of cytokines in the supernatants were measured by BD OptEIA^{TM} ELISA kits for mouse IL-10 and IL-12p40 (BD Biosciences, Franklin Lakes, NJ).

2.5 Flow Cytometric Analysis

Surface markers were detected using anti-CD90.2 (BD Biosciences), and nonviable cells were detected using Propidium Iodide (PI) (Sigma). Flow cytometric analysis was performed by using FACSCanto (BD Biosciences); and data were analyzed using FlowJo ver. 8 software (Tree Star, Ashland, OR).

2.6 Statistical Analysis

Data were expressed as the mean ± SD. Analysis of the data was by one-way ANOVA. In addition, a comparison of the mean of each group was performed by Tukey's test. All the data were analyzed using SPSS ver. 13.0 (SPSS, Chicago, IL).

3 Results

First of all, we examined cytokine production by PP and CP unfractionated cells stimulated with bacterial components in vitro. We isolated whole cells from PPs and CPs from female 7-weeks-old BALB/c mice, and co-cultured them with BIM or LPS for 24 h or 72 h.

In Table 1, it can be seen that CP cells and PP cells produced almost equal levels of IL-10 following bacterial stimulation (BIM or LPS). In contrast, CP cells produced significantly lower levels of IL-12p40 than PP cells following bacterial stimulation ($p < 0.05$). IL-12p40 is a proinflammatory cytokine secreted by APCs, e.g. macrophages and dendritic cells. These data suggest that the immunoresponse following bacterial stimulation of APCs from CPs might be less than that following stimulation of APCs from PPs.

Therefore, we isolated Thy1.2^{-} cells as APCs and determined cytokine production by PP and CP APCs stimulated with bacterial components in vitro. The purity of Thy1.2^{-} cells from PP and CP were confirmed to be more than 95% in all experiments by flow cytometer (data not shown).

It was observed that APCs of CPs produced lower levels of IL-12p40 than those from PPs. This result was found to be similar to that with the unfractionated cells.

Table 1 Production of IL-12p40 and IL-10 by PP and CP whole cells co-cultured with bacterial components

	IL-12p40 production		IL-10 production	
Concentration of BIM or LPS (μg/ml)	PP	CP	PP	CP
1	+	±	++	++
10	++	±	++	++
50	+++	+	++	++

PP and CP whole cells were obtained and pooled from BALB/c mice. Cells were cultured with BIM or LPS for 24 h or 72 hours. IL-12p40 and IL-10 production was measured by ELISA. The determinations, "+++, ++, +, ±" were judged from the results based on three independent experiments compared to un-stimulated negative control.

Table 2 Production of IL-12p40 and IL-10 production by PP and CP APCs co-cultured with bacterial components

	IL-12p40 production		IL-10 production	
Concentration of BIM or LPS (μg/ml)	PP-APCs	CP-APCs	PP-APCs	CP-APCs
0.1	+	±	+	++
1	++	±	+	++
10	+++	+	+	++

APCs from PPs and CPs were obtained and pooled from BALB/c mice, and then cultured with BIM or LPS for 24 hours. IL-12p40 and IL-10 production was measured by ELISA. The determinations, "+++, ++, +, ±" were judged from the results based on three independent experiments compared to un-stimulated negative control.

However, considering IL-10 production, APCs of CPs tended to produce higher levels of IL-10 than those of PP (Table 2).

4 Discussion

It is supposed that CPs in the cecum can be stimulated by intestinal commensal bacteria, because there are huge numbers of bacteria in the large intestine including the cecum. In our recent work, we observed that luminal bacteria were taken up into the epithelial site of CPs directly (unpublished data). It has been reported that M cells were observed in the FAE in the cecum [1, 2]. This therefore suggests that the immune system of CPs could be stimulated by commensal bacteria constantly. We next hypothesized that the immunoresponses of CPs might be different from those of PPs, because large amounts of commensal bacteria are allowed to exist in the large intestine without hypersensitivity.

In this study, we found that the unfractionated cells of CPs produced lower levels of IL-12p40 and equal levels of IL-10 compared with PP cells. Additionally, APCs of CPs produced lower levels of IL-12p40 compared with those of PPs. In

contrast, APCs of CPs tended to produce higher levels of IL-10 compared with those of PPs. It is well known that IL-12p40 and IL-10 have opposite effects [6]. APCs of CPs might be more tightly regulated as regards IL-12p40 production stimulated by bacterial components compared with those of PP. This suggests that the down-regulation of IL-12p40 production by CP-APCs in response to bacterial components might be very important in the prevention of intestinal inflammation by commensal bacteria, because IL-12p40 is a proinflammatory cytokine inducing Th1 responses. Furthermore, the inverse correlation between IL-10 production and IL-12p40 production in CP-APCs was demonstrated. Therefore, lower production of IL-12p40 by CP-APCs might cause increased IL-10 production. In conclusion, these results suggest that the immunoresponses of CPs are different from those of PPs, and that APCs of CPs down-regulate immunoresponses to bacterial components compared with those of PPs. Thereby, the homeostasis of the large intestine may be maintained, in spite of the fact that large numbers of commensal bacteria are located there.

References

1. Kweon, M.N., Yamamoto, M., Rennert, P.D., Park, E.J., Lee, A.Y., Chang, S.Y., Hiroi, T., Nanno, M., and Kiyono, H. (2005) Prenatal blockage of lymphoyoxin beta receptor and TNF receptor p55 signaling cascade resulted in the acceleration of tissue genesis for isolated lymphoid follicles in the large intestine. *J. Immunol.* **174**: 4365–4372.
2. Clark, M.A., Jepson, M.A., and Hirst, B.H. (1995) Lectin binding defines and differentiates M-cells in mouse small intestine and caecum. *Histochem. Cell Biol.* **104**: 161–168.
3. Mizoguchi, A., Mizoguchi, E., Chiba, C., and Bhan, A.K. (1996) Role of appendix in the development of inflammatory bowel disease in TCR-alpha mutant mice. *J. Exp. Med.* **184**: 707–715.
4. Hiramatsu, Y., Hosono, A., Nakanishi, Y., Muto, M., Hachimura, S., Sato, R., Takahashi, K., and Kaminogawa, S. (2009) Immunomodulatory effects of orally administered *Bifidobacterium* components on intestinal lymphoid tissues. *Animal Cell Technol. Basic Appl. Aspects* **15**: 105–110.
5. Nakanishi, Y., Hosono, A., Hiramatsu, Y., Kimura, T., Nakamura, R., and Kaminogawa, S. (2005) Characteristic immune response in Peyer's patch cells induced by oral administration of *Bifidobacterium* components. *Cytotechnology* **47**: 69–77.
6. Watford, W.T., Moriguchi, M., Morinobu, A., and O'shea, J.J. (2003) The biology of IL-12: Coordinating innate and adaptive immune responses. *Cytokine Growth Factor Rev.* **14**: 361–368.

Conjugate of β-Lactoglobulin with Carboxymethyl Dextran Increased the Antigen-Specific IgG1 Production, While It Decreased IgE Production Compared with Native β-Lactoglobulin

Tadashi Yoshida, Yuko Shigihara, Manami Nakamura, and Makoto Hattori

1 Introduction

IgE is a critical factor of type I allergic diseases. IL-4 produced by Th2 cells is known as an essential cytokine to induce IgE [1, 2]. On the other hand, the regulating mechanism for the induction of IgE and IgG1 has not been clarified. IgG1 is not involved in type I allergy although it is induced by IL-4 as well as IgE. A fine understanding of the mechanism for inducing IgE would contribute to the prevention of allergic disorders.

Ig class switching is known to require two independent signals [3]. One is provided from cytokines and the other is from CD40. Among these signals, only the signal from cytokines could determine the class to switch, for example IL-4 induces IgG1 and IgE as described above. However, the influence of the signal from BCR on the class switching has not been investigated. It is considered that the signal from BCR would be involved in the regulation of the class switch because it is also an important factor to activate B cells as well as the signals from cytokines and CD40.

In this study, we examined the distinct activity of β-lactoglobulin (β-LG) and a conjugate of it with polysaccharides to induce IgE and IgG1. The results of this study would suggest that the surface structure of antigen is important for regulating IgE production.

T. Yoshida (✉)
Department of Applied Biological Science, Tokyo University of Agriculture and Technology, Fuchu, Tokyo 183-8509, Japan
e-mail: tyoshi@cc.tuat.ac.jp

M. Kamihira et al. (eds.), *Animal Cell Technology: Basic & Applied Aspects*, Animal Cell Technology: Basic & Applied Aspects 16, DOI 10.1007/978-90-481-3892-0_22,

2 Materials and Methods

2.1 Mice

Female BALB/c mice were purchased from Clea Japan (Tokyo, Japan). Female NC/Nga mice were purchased from Charles River Japan (Yokohama, Japan). These mice were used at 6–9 weeks old. All the mice used in this study were maintained and used in accordance with the guidelines for the care and use of experimental animals of Tokyo University of Agriculture and Technology.

2.2 Preparation of β-LG and Conj.162

Crude bovine β-LG (genotype AA) was prepared from fresh milk of a Holstein cow. Crude β-LG was purified with a DEAE-Sepharose Fast Flow column (Amersham Pharmacia Biotech, Buckinghamshire, UK). A conjugate of β-LG with carboxymethyldextran (CMD) was prepared as described previously [4]. In brief, Dextran 162 (Mw. 162000; Sigma Chemical Co., St. Louis, MO) was carboxymethylated with monochloroacetic acid under alkaline conditions. β-LG and CMD were dissolved in distilled water, and the pH of the solution was adjusted to 4.75 with 1 M HCl. EDC (1-ethyl-3-(3-dimethylaminopropyl)carbodiimide) solution was added in 30 min, and the pH was kept at 4.75 by addition of 1 M HCl. The reaction mixture was incubated at 25°C for 3 h, and then 2 M acetate buffer was gradually added over a period of 10 min to stop the reaction. After dialysis against distilled water at 4°C and lyophilization, the crude β-LG-CMD conjugate (Conj.162) was obtained.

2.3 Purification of Conj.162

Conj.162 was purified as described previously [4]. In brief, hydrophobic chromatography (Butyl-Toyopearl 650S, Tosoh, Tokyo, Japan) was applied to remove free CMD from the crude Conj.162. Then free β-LG and polymerized β-LG in the crude Conj.162 was removed by anion-exchange chromatography (QA-Cellulofine Q-800-m, Seikagaku Industry Co., Tokyo, Japan). After dialysis against distilled water and lyophilization, the purified Conj.162 was obtained.

2.4 Chemical Analysis of Conj.162

The amount of protein in Conj.162 was determined by measuring the absorbance at 280 nm. The amount of CMD bound to β-LG was determined by measuring the absorbance at 490 nm after coloring by the phenol-sulfuric acid method.

2.5 Immunization

BALB/c or NC/Nga mice were immunized i.p. with 100 μg (as protein) of β-LG or Conj.162 absorbed in Alum adjuvant. Two weeks after immunization, the mice were bled, and sera samples were collected from the mice.

2.6 ELISA

The amount of the β-LG-specific IgG1 and IgE antibody was measured by ELISA. Maxisorp immunoplates were coated with a 0.01% β-LG solution. After washing and blocking, the sample sera and standards were added to the plates. The bound antibody was detected with biotin-labeled goat anti-mouse IgG1 (A85-1, BD Pharmingen, San Diego, CA) or biotin-labeled rat anti-mouse IgE (R35-118, BD Pharmingen), before incubating with alkaline phosphatase-streptavidine. A substrate (p–nitrophenyl-phosphate) was then added, and the absorbance was determined at 405 nm. The titer of β-LG-specific IgG1 and IgE in each sample serum was calculated relative to that of β-LG-specific IgG1 and IgE in the standard serum, respectively.

2.7 Statistical Analysis

Differences between β-LG and Conj.162 immunized groups were analyzed by Student's *t* test. *P* values less than 0.01 were considered statistically significant and indicated as "∗" in the tables.

3 Results

3.1 Chemical Property of Conj.162

Conj.162 was prepared, and the chemical property of Conj.162 was analyzed as described above. As shown in Table 1, the molar ratio of β-LG to CMD in Conj.162 was determined to be 7:1, and weight ratio was 2:3.

Table 1 Chemical property of Conj.162

	β-LG : CMD	
	Molar ratio	Weight ratio
Conj.162	7:1	2:3

3.2 Conj.162 Induced Higher Level of IgG1 and Lower Level of IgE than Native β-LG

BALB/c mice were immunized with β-LG or Conj.162. β-LG-specific IgG1 and IgE titier in the sera from these mice were measured. β-LG-specific IgG1 titier in the sera from β-LG immunized mice was significantly lower than that from Conj.162 immunized mice (Table 2). Interestingly, β-LG-specific IgE titier in the sera from β-LG immunized mice was significantly higher than that from Conj.162 immunized mice contrary to IgG1 (Table 2). Similar result was obtained from the experiments of NC/Nga mice (data not shown).

Table 2 IgG1 and IgE induction in BALB/c mice immunized with β-LG or Conj.162

	β-LG-specific antibody (relative conc.)	
Immunized with	IgG1	IgE
β-LG	0.45±0.10	3.77±1.26
Conj.162	1.30±0.46*	0.54±0.16*

4 Discussion

Type I allergic reaction is a major mechanism for several allergic diseases, including food allergy and house dust asthma. IgE is a key molecule inducing type I allergy. Therefore, many previous studies have tried to suppress IgE production although the mechanism for inducing IgE has not been clearly understood [5–8]. Most such studies adopted the strategy of inhibiting the Th2 response [5–7], because IL-4 secreted from Th2 is known to be a critical factor to induce IgE class switching. On the other hand, Th2 and IL-4 are important for not only IgE production but also other several immune responses. Hence, the strong suppression of Th2 responses would result in the immune deficiency.

Our results in this study showed that Conj.162 induced lower level of IgE than native β-LG. On the other hand, IgG1 production induced by Conj.162 was significantly higher than that induced by β-LG. IgG1 is also an antibody induced by IL-4 as well as IgE, while it does not cause type I allergy. This result clearly indicates that the induction of IgE and IgG1 is distinctly regulated by the surface structure of antigen. It was considered that the structure of antigen directly affects B cells and influences their class switching because it has not been known any cytokines which enhance IgG1 but suppress IgE production. Actually, Taneichi *et al*. have reported that ovalbumin (OVA) surface-coupled with liposome induced IgE-selective unresponsiveness and that T cells were not involved in the inhibition of IgE induced by OVA-liposome [8]. This evidence strongly suggests the direct effect of OVA-liposome on B cells although the mechanism for distinct regulation of IgE and IgG1 by the property of antigen has not been revealed. Conj.162 might regulate

IgE and IgG1 production by a similar mechanism with OVA-liposome; for example, regulating intracellular signals from BCR.

In summary, we clearly demonstrated the distinct regulation of IgE and IgG1 class switching. Conj.162 preferentially induced IgG1 than IgE, while native β-LG was opposite. We are now conducting the work to identify the mechanism for regulating IgE and IgG1 production by the property of antigen. It is expected that the results of our study would contribute to the prevention and treatment of allergic diseases.

References

1. Mikita, T., Kurama, M., and Schindler, U. (1998) Synergistic activation of the germline ε promoter mediated by Stat6 and C/EBPβ, *J. Immunol*. **161:** 1822–1828.
2. Gascan, H., Gauchat, J.F., Aversa, G., Van Vlasselaer, P., and de Vries, J.E. (1991) Anti-CD40 monoclonal antibodies or $CD4^+$ T cell clones and IL-4 induce IgG4 and IgE switching in purified human B cells via different signaling pathways. *J. Immunol*. **147:** 8–13.
3. Purkerson, J. and Isakson, P. (1992) A two-signal model for regulation of immunoglobulin isotype switching. *FASEB J*. **6:** 3245–3252.
4. Kobayashi, K., Hirano, A., Ohta, A., Yoshida, T., Takahashi, K., and Hattori, M. (2001) Reduced immunogenicity of β-lactoglobulin by conjugation with carboxymethyl dextran differing in molecular weight. *J. Agric. Food Chem*. **49:** 823–831.
5. Shida, K., Takahashi, R., Iwadate, E., Takamizawa, K., Yasui, H., Sato, T., Habu, S., Hachimura, S., and Kaminogawa, S. (2002) *Lactobacillus casei* strain Shirota suppresses serum immunoglobulin E and immunoglobulin G1 responses and systemic anaphylaxis in a food allergy model. *Clin. Exp. Allergy* **32:** 563–570.
6. Ishida, Y., Nakamura, F., Kanzato, H., Sawada, D., Yamamoto, N., Kagata, H., Oh-ida, M., Takeuchi, H., and Fujiwara, S. (2005) Effect of milk fermented with *Lactobacillus acidophilus* strain L-92 on symptoms of Japanese cedar pollen allergy: a randomized placebo-controlled trial. *Biosci. Biotechnol. Biochem*. **69:** 1652–1660.
7. Fujiwara, D., Inoue, S., Wakabayashi, H., and Fujii, T. (2004) The anti-allergic effects of lactic acid bacteria are strain dependent and mediated by effects on both Th1/Th2 cytokine expression and balance. *Int. Arch. Allergy Immunol*. **135:** 205–215.
8. Taneichi, M., Naito, S., Kato, H., Tanaka, Y., Mori, M., Nakano, Y., Yamamura, H., Ishida, H., Komuro, K., and Uchida, T. (2002) T cell-independent regulation of IgE antibody production induced by surface-linked liposomal antigen. *J. Immunol*. **169:** 4246–4252.

Anti-Inflammatory Action of Epigallocatechin-3-Gallate at a Physiological Concentration through the 67-KDA Laminin Receptor in Lipopolysaccharide-Stimulated Raw264.7 Cells

Byun Eui Hong, Yoshinori Fujimura, Koji Yamada, and Hirofumi Tachibana

1 Introduction

Green tea (*Camellia sinensis L.*) is a popular beverage worldwide, and its possible health benefits have been the subject of considerable attention [1, 2]. Among the green tea polyphenols, EGCG constitutes approximately 60% of the catechins in tea and it is well known to have a variety of biological and pharmacological properties, including cancer-preventive, anti-virus, anti-oxidative effects, anti-inflammatory activities and to have anti-Alzheimer and anti-Parkinson disease properties [2–4]. In case of murine macrophage cell line, RAW 264.7 and in elicited BALB/c mouse peritoneal macrophages, EGCG have been reported to inhibit the activation of transcription factors, NF-κB and AP-1, induced by many pro-inflammatory stimuli such as UV and LPS [3, 4] resulting in the decrease in the expression of inflammatory gene products including lipoxygenase [5], cyclooxygenase [6], nitric oxide synthase [7], and TNF-α [4]. Furthermore, most experiments using EGCG requires high concentrations of EGCG (10–50 μM) to demonstrate a variety of biological activities although the peak plasma concentration of EGCG is less than 1 μM [8].

Recently, We have identified 67-kDa laminin receptor (67LR) as a cell surface EGCG receptor that mediates the anti-cancer action of physiologically achievable concentrations of EGCG (0.1–1 μM) [9]. Furthermore, this receptor has been shown to be responsible for modulation of immune systems based on anti-allergic effects of EGCG, and also found that the inhibition of myosin II regulatory light chain or extracellular signal-regulated kinase1/2 phosphorylation plays a critical role in the EGCG-induced degranulation inhibition or suppression of FcεRI expression, respectively [10, 11]. However, the relationship of 67LR and anti-inflammatory activity of EGCG at a physiological concentration in LPS-stimulated macrophage cells has not yet been reported.

B.E. Hong (✉)
Department of Bioscience and Biotechnology, Kyushu University, Higashi-ku, Fukuoka 812-8581, Japan
e-mail: hong3486@hanmail.net

M. Kamihira et al. (eds.), *Animal Cell Technology: Basic & Applied Aspects*, Animal Cell Technology: Basic & Applied Aspects 16, DOI 10.1007/978-90-481-3892-0_23,

Therefore, the present study reveals the information that relationship of suppression effects of EGCG at a physiological concentration and 67LR on the production of inflammatory mediators from LPS-stimulated RAW264.7 cells.

2 Materials and Methods

2.1 Reagents

(–)-Epigallocatechin-3-gallate (EGCG) was purchased from Kurita Water Industries (Tokyo, Japan). Lipopolysaccharide (LPS), anti-β-Actin polyclonal antibody, and horseradish peroxidase (HRP)-conjugated anti-rabbit antibody were derived from Sigma (St. Louis, MO). Anti-67LR (F-18) antibody, anti-iNOS polyclonal antibody, anti-COX-2 polyclonal antibody and horseradish peroxidase (HRP)-conjugated anti-goat (donkey) IgG antibody were obtained from Santa Cruz Biotechnology, Inc. (Santa Cruz, CA, USA), and HRP-conjugated anti-Rat IgG_{2a} antibody, HRP-conjugated anti-mouse IgG antibody were obtained from Zymed Laboratories (San Francisco, CA). HRP-conjugated anti-rabbit antibody was purchased from ICN Pharmaceuticals (Aurora, OH). An anti-mouse TNF-α antibody was obtained from Endogen (Woburn, MA). Biotinylated anti-mouse TNF-α antibody was obtained from Biosource (Camarillo, CA).

2.2 Cell Preparation

The RAW264.7 Cells were cultured in DMEM supplemented with antibiotics (100 U/mL penicillin and 100 U/mL streptomycin), and 10% (v/v) fetal calf serum. The cells were maintained at 37°C in a humidified incubator containing 5% CO_2. In all experiments, cells were allowed to acclimate for 24 h before any treatments.

2.3 Construction of 67LR-Suppressed Cells

The psiRNA-hH1 (G2) short hairpin RNA expression vector was purchased from InvivoGen. As the inserts for expressing short hairpin RNA, one insert was selected: shRNA1-sense (5'-TCCCGATCT TGACTTCCAGATGGAA TTCAAGAGATTCCATCTGGAAGTCAAGATTT-3') and sh RNA-antisense (5'-CAAAAA ATCTTGACTTCCAGATGGAATTCAAGAGTTCCATCTG GAAG-TCAAGATC-3'). This insert was annealed and subcloned into psiRNA-hH1 (G2), which was linearized with BbsI. Vector containing the 67LR gene-targeting shRNA expression was transfected into the RAW 264.7 cells by electroporation. Then, the clone with the neomycin resistance was selected and used for experiments.

2.4 Enzyme-Linked Immunosorbent Assay

The amount of TNF-α in culture medium was measured by sandwich enzyme-linked immunosorbent assay (ELISA). An anti-mouse TNF-α antibody was used to fix TNF-α. Antibody solution diluted at 500 times by PBS was added to a 96-well plate, and incubated for 2 h at 37°C. After washing with 0.05% Tween 20-PBS (T-PBS) three times, each well was blocked with 1% BSA-PBS for 2 h at 37°C. Then wells were washed again three times with wash buffer. Following blocking reaction, each well was treated with 50 μl of culture supernatant for 1 h at 37°C. The wells were then treated with biotinylated anti-mouse TNF-α antibody diluted at 1,000 times using 1% BSA-PBS solution for 1 h at 37°C. HRP-conjugated streptavidin solution diluted at 1000 times by 1% BSA-PBS solution was added to each well at 100 μl. Then, 0.6 mg/ml of 2,20-azinobis (ethylbenzothazoline-6-sulfonic acid diammonium salt) (ABTS) dissolved in 0.03% H_2O_2-0.05 M citrate buffer (pH 4.0) was added to the well at 100 ml, and the absorbance at 405 nm was measured after the addition of 1.5% oxalic acid to terminate the coloring reaction at 100 ml.

2.5 Measurement of NO

The concentration of NO in culture supernatant was determined as nitrite, a major stable product of NO, by the Griess reagent (1% sulfanilamide/0.1% naphtylethylenediamine dihydrochloride in 2.5% H_3PO_4) (Sigma, USA). Briefly, culture medium (100 μl) was incubated with 100 μl of Griess reagent. Absorbance of the mixture was then measured at 535 nm.

2.6 Reverse Transcription-Polymerase Chain Reaction (RT-PCR)

Total cellular RNA was extracted from appropriately treated RAW 264.7 cells with Trizol™(Sigma-Aldrich, St Louis, MO) according to the manufacturer's protocol. The resultant cDNA samples were subjected to 37 cycles of PCR amplification in the presence of specific sense and antisense primers. Mouse β-Actin cDNA was amplified as an internal control. Each cycle consisted of denaturation at 94°C for 1 min, annealing at 60°C for 1 min (β-Actin, IL-6 and TNF-α), and DNA synthesis at 72°C for 1 min. Sequences for the PCR primers sizes and expected amplification product sizes are as follows: for the β-Actin: sense 5'-GGAATCCTGTGGCAT CCATGAAAC-3', and antisense 5'-TAAAACGCAGCTCAGTAACAGTCCG-30'; for the TNF-α: sense 5'-TCCCCAAAGGGATGAGAAGTTC-3', and antisense 5'-TCATACCAGG GTTTGAGCTCAG-3'; for the IL-6: sense 5'-AAGTGCATCAT-CGTTGTTCATACA-3', and antisense 5'-AAGTGCATCATCGTTGTTCATACA-3'. Samples were subjected to electrophoresis on 1.5% agarose gels, stained with ethidium bromide, and photographed.

2.7 Western Blot Analysis

Whole cell protein lysates of RAW 264.7 cells were lysed in 100 μl of lysis buffer containing 50 mM Tris-HCl (pH 7.5), 150 mM NaCl, 1% Triton-X 100, 1 mM EDTA, 50 mM NaF, 30 mM $Na_4P_2O_7$, 1 mM phenylmethanesulfonyl fluoride (PMSF), 2 μg/ml aprotinin, and 1 mM pervanadate. Whole cell lysate samples were separated by 8% sodium dodecyl sulfate-polyacrylamide gel electrophoresis and electrotransferred to nitrocellulose membranes. The blotted nitrocellulose was incubated with primary antibodies for 2 h, and with HRP-conjugated secondary antibodies for 1 h at room temperature. Epitopes on proteins recognized specifically by antibodies were visualized by using enhanced chemiluminescence Advance kit (Amersham Biosciences, Piscataway, NJ).

3 Results and Discussion

To explore whether the effects of EGCG on cellular responses to the LPS stimulation are mediated through the 67LR, RAW264.7 cells were stably transfected with short hairpin RNA (shRNA) expression vector to reduce the 67LR expression. Western blot analysis showed that RAW264.7 cells expressed the 67LR, and this expression has been shown to be lowered in RAW264.7 cells transfacted with shRNA for 67LR (Fig. 1a).

Among a variety of inflammatory mediators, TNF-α and IL-6 are major inflammatory cytokines produced by macrophages, and have been reported to participate in regulating the immune response, acute-phase reaction, and hematopoiesis [4]. In addition, iNOS expression can be significantly induced by LPS and/or cytokines in a variety of immune cells, including macrophages, hepatocytes and endothelial cells, and COX-2 is another enzyme that plays a pivotal role in the mediation of inflammation [12]. Recently, a major green tea catechin, EGCG has been reported to decrease LPS-induced COX-2, iNOS, TNF-α and IL-6 expression in the murine macrophage cell line, RAW 264.7, and to similarly inhibit LPS-induced TNF-α and IL-6 production in elicited BALB/c mouse peritoneal macrophages [3, 4]. In this study, we examined whether the inhibitory effect of EGCG through the 67LR on TNF-α and NO production from LPS-stimulated RAW 264.7 cells culture media. The cells were pretreated with EGCG (1 μM) for 1 h, and then incubated with LPS (50 ng/mL) for 12 h. The TNF-α production levels in the culture medium were measured by ELISA and NO production levels in the culture medium were measured by Griess assay. The TNF-α and NO production was increased in the culture medium of LPS-stimulated RAW 264.7 cells, and these increased TNF-α and NO was significantly decreased upon treatment with EGCG in LPS-stimulated RAW 264.7 cells. However, the TNF-α and NO production in 67LR-downregulated cells treated with LPS plus EGCG were higher (relative intensive) than that of the control cells (Fig. 1b). These results suggest that the expression level of 67LR may be elevated in the cells that are sensitive to the effect of EGCG at a physiological concentration (1 μM) and suppressive effects of EGCG are mediated through binding to the 67LR.

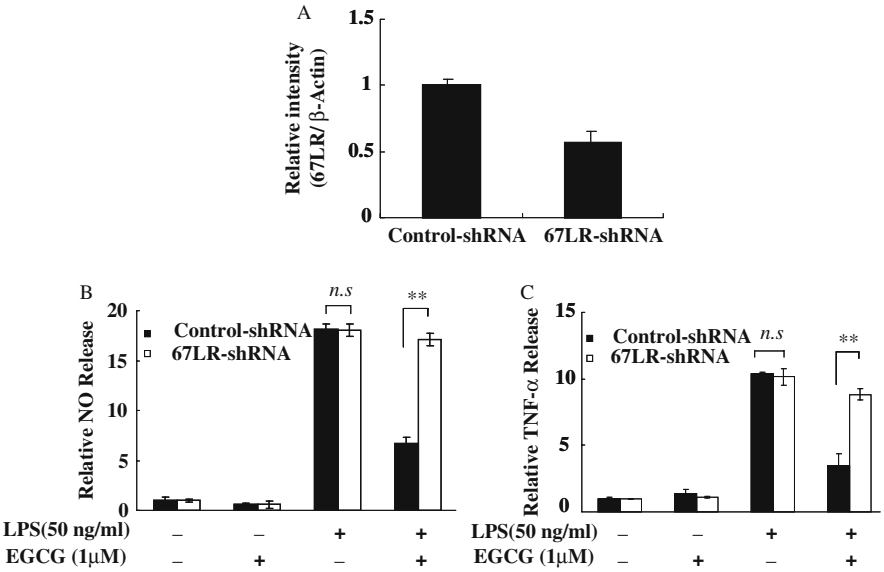

Fig. 1 Through binding to the cell-surface 67LR, the anti-inflammatory effect of EGCG in macrophage cells. (**a**) The cell-surface expression of 67LR in RAW 264.7 cells. (**b**) The Effect of 67LR-downregulation on the EGCG-induced reduction of NO and TNF-α production in RAW264.7 cells

We also investigated the inhibitory effects of EGCG through the 67LR on mRNA and protein expression of inflammatory mediators, such as TNF-α, IL-6, nitric oxide synthase and cyclooxygenase-2 from LPS-stimulated RAW 264.7 cells. The cells were pretreated with EGCG (1 μM) for 1 h, and then incubated with LPS (50 ng/mL) for 6 h. The TNF-α and IL-6 mRNA expression was determined by RT-PCR, and the iNOS and COX-2 protein expression was determined by Western immunoblot analysis. LPS increased expression of inflammatory mediators, such as TNF-α, IL-6, iNOS and COX-2, whereas EGCG inhibited expression of LPS-induced inflammatory mediators, such as TNF-α, IL-6, iNOS and COX-2 in control cells. However, the expression of inflammatory mediators, such as TNF-α, IL-6, iNOS and COX-2 in 67LR-downregulated cells treated with LPS plus EGCG were higher (relative intensive) then that of the control cells (date not shown). These results show that the ability of EGCG to decrease the expression of inflammatory mediators, such as TNF-α, IL-6, iNOS and COX-2 was mediated through binding to the 67LR. Taken together, 67LR may be the primary target for EGCG to mediate anti-inflammatory responses to the LPS stimulation and decide the accessibility of EGCG to the macrophage cells.

In summary, we showed the data for the first time that 67LR plays an important role in mediating anti-inflammatory actions of EGCG at a physiologically achievable concentration, and we have revealed a new mechanism by which EGCG suppresses inflammatory response through binding to the 67LR as a cell-surface receptor.

References

1. Yang, C.S., Chung, J.Y, Yang, G., Chhabra, S.K., and Lee, M.J. (2000) Tea and tea polyphenols in cancer prevention. *J. Nutr*. **130 :** 472S–478S.
2. Lin, J.K., Liang, Y.C., and Lin-Shiau, S.Y. (1999) Cancer chemoprevention by tea polyphenols through mitotic signal transduction blockade. *Biochem. Pharmacol*. **58:** 911–915.
3. Barthelman, M., Bair III W.B., Stickland, K.K., Chen, W., Timmermann, B.N., and Valcic S. (1998) (–)-Epigallocatechin-3-gallate inhibition of ultraviolet B-induced AP-1 activity. *Carcinogenesis* **19**: 2201–2204.
4. Yang, F., de Villiers, W.J., McClain, C.J., and Varilek, G.W. (1998) Green tea polyphenols block endotoxin-induced tumor necrosis factor-production and lethality in a murine model. *J. Nutr*. **128:** 2334–2340.
5. Yang, T.T. and Koo, M.W. (2000) Inhibitory effect of Chinese green tea on endothelial cell-induced LDL oxidation. *Atherosclerosis* **148**: 67–73.
6. Soriani, M., Rice-Evans, C., and Tyrrell, R.M. (1998) Modulation of the UVA activation of haem oxygenase, collagenase and cyclooxygenase gene expression by epigallocatechin in human skin cells. *FEBS Lett*. **439:** 253–257.
7. Lin, Y.L. and Lin, J.K. (1997) (–)-Epigallocatechin-3-gallate blocks the induction of nitric oxide synthase by down-regulating lipopolysaccharide-induced activity of transcription factor nuclear factor-kappaB. *Mol. Pharmacol*. **52:** 465–472.
8. Joshua, D. and Lambert Chung, S. (2003) Introduction to the proceedings of the third international scientiWc symposium on tea and human health: Role of Xavonoids in the diet. *J. Nutr. Suppl*. **10:** 3262–3267.
9. Tachibana, H., Koga, K., Fujimura, Y., and Yamada, K. (2004) A receptor for green tea polyphenol EGCG. *Nat. Struct. Mol. Biol*. **11**: 380–381.
10. Fujimura, Y., Yamada, K., and Tachibana, H. (2005) A lipid raft-associated 67 kDa laminin receptor mediates suppressive effect of epigallocatechin-3-O-gallate on FcεRI expression. *Biochem. Biophys. Res. Commun*. **336:** 674–681.
11. Umeda, D., Tachibana, H., and Yamada, K. (2005) Epigallocatechin-3-O-gallate disrupts stress fibers and the contractile ring by reducing myosin regulatory light chain phosphorylation mediated through the target molecule 67 kDa laminin receptor. *Biochem. Biophys. Res. Commun*. **333:** 628–635.
12. Ohshima, H. and Bartsch, H. (1994) Chronic infections and inflammatory processes as cancer risk factors: possible role of nitric oxide in carcinogenesis. *Mutat. Res*. **305:** 253–264.

Enhancement of Antibody Production using Solution after Antibody Purification: Application of Spent Medium for Antibody Production

Akiko Ogawa, Sadaharu Fukui, and Satoshi Terada

1 Introduction

Monoclonal antibodies are essential in fields of diagnostics and medicine. The market for antibody drugs is growing every year by 20% but antibody production has some risks including limited supply and high costs because antibodies are produced by mammalian cells such as hybridomas and Chinese hamster ovary (CHO) cells. These cells are cultured in expensive serum-free media containing growth factors in order to maintain cellular functions. In particular, transferrin and insulin are essential for the production of antibodies; transferrin functions as an iron transporter and a mitogen, while insulin improves glucose uptake [1]. However, as these growth factors remain after cell culture, the used culture media are typically discarded. Riese et al. have reported that used culture medium was effective for the production of mouse monoclonal antibodies when it was mixed with additional amino acids and glucose, after purification by microfiltration and ultra filtration [2].

In this study, we examined a recycling culture medium for antibody production, which was previously used for antibody production by CHO cells.

2 Materials and Methods

2.1 Cell Line and Cell Culture

CHO-DP12 cells (ATCC®CRL-12445™) were obtained from the American Type Culture Collection (Manassas, Virginia, USA) and used throughout this work. This

A. Ogawa (✉)
Department of Chemistry and Biochemistry, Suzuka National College of Technology, Suzuka, Mie 510-0294, Japan
e-mail: ogawa@chem.suzuka-ct.ac.jp

M. Kamihira et al. (eds.), *Animal Cell Technology: Basic & Applied Aspects*, Animal Cell Technology: Basic & Applied Aspects 16, DOI 10.1007/978-90-481-3892-0_24,

cell line produces recombinant human anti-IL-8 (Gonzalez, TN., et. al., Nucleic acids encoding humanized anti IL-8 monoclonal antibodies, US patent, 6025158 dated Feb. 15, 2000).

The subculture medium was DMEM medium (Nissui, Tokyo, Japan) supplemented with 5% (v/v) FBS (Biowest, Nuaillé, France), 0.2% sodium bicarbonate (Nacalai Tesque, Kyoto, Japan), 10 mM HEPES (Nacalai Tesque, Kyoto, Japan), 2 mM glutamine (Nacalai Tesque, Kyoto, Japan), 0.06 mg/mL kanamycin (Nacalai Tesque, Kyoto, Japan) and 200 μM MTX (Sigma Aldrich, MO, USA).

CHO-DP12 cells were grown in culture dishes (Sumitomo Bakelite, Tokyo, Japan) at 37°C in humidified air containing CO_2 at 5%.

2.2 Determination of Antibody Concentration

The amount of human IgG in the culture supernatant was determined by sandwich enzyme-linked immunosorbent assay (ELISA). For the ELISA, rabbit affinity purified antibody to human IgG (H+L, Bethyl Laboratories, Inc., TX, USA) was used as the capture antibody, goat antibody to human IgG (γ) conjugated with horseradish peroxidase (HRP) (American Qualex Antibodies, CA, USA) was used for detection, and o-phenylenediamine dihydrochloride (Nacalai Tesque, Kyoto, Japan) was used as the substrate. Human IgG concentration was calculated from optical density at 492 nm (Hitachi High-Technologies, Tokyo, Japan).

2.3 Production of Human Monoclonal Antibody and Preparation of Recovered Medium

In order to produce human monoclonal antibody, CHO-DP12 cells were seeded at 765,000 cells/dish on two 90 mm culture dishes (Sumitomo Bakelite, Tokyo, Japan) in DMEM medium containing 5% FBS. The next day, adhesion to the dish was confirmed, and the medium was removed. The cells were then washed with PBS four times in order to completely remove the FBS. Fresh ASF104 medium (Ajinomoto, Tokyo, Japan) containing 5 mg/L transferrin and 5 mg/L insulin was added to the dishes at 12 mL/dish and the cells were cultured for two days. When they reached confluency (viable cell number 4,178,000 cells/dish) on the fourth day, the culture supernatant was collected and the antibody was purified from it by affinity protein G column (GE Healthcare UK, Buckinghamshire, England). The flow-through fraction, which contained various materials that did not attach to the column, was collected and concentrated 18-fold by ultrafiltration using Amicon Ultra-15 centrifugal filter units (Millipore, MA, USA) and then it was diluted to one-eighteenth the concentration using fresh basal ASF104 medium. This is referred to as the recovered medium.

2.4 Proliferation Assay of CHO-DP12 Cells with Recovered Medium

CHO-DP12 cells were seeded at 16,400 cells/well on 24-well culture plates (Sumitomo Bakelite, Tokyo, Japan) in DMEM medium containing 5% FBS. The next day, adhesion to the dish was confirmed, and the medium was removed. These cells were then washed with PBS four times in order to completely remove the FBS. Each experimental medium was added to each well at 500 μL and then they were cultured for 70 h.

Final viable cell density and cell viability were determined by counting in a hemacytometer under a phase contrast microscope using the trypan blue exclusion assay.

2.5 SDS-Page

All samples were subjected to 20% PAGE in the presence of sodium dodecyl sulfate according to the method of Laemmli [3]. Separated proteins were stained with a commercialized silver stain kit (ATTO, Tokyo, Japan).

3 Results and Discussions

3.1 Detection of Proteins Including Transferrin and Metabolic Products of CHO-DP12 Cells

Generally, mammalian cells synthesize and release various autocrine and paracrine factors, which maintain cellular functions and promote cell differentiation. Used culture medium is rich in such factors and is often used as a conditioned medium. For example, human embryonic stem cells can be cultured in mouse embryonic fibroblast-conditioned medium [4]. Therefore it was possible that the culture supernatant of CHO-DP12 would have not only growth factors derived from medium but also autocrine or paracrine factors derived from CHO-DP12 cells. Figure 1 shows SDS-PAGE analysis of the culture supernatant of CHO-DP12 (lane 1) and the concentrated flow-through fraction of the affinity column (lane 2: one-tenth dilution; lane 3: no dilution). Transferrin was detected in both samples: the culture supernatant of CHO-DP12 and the concentrated flow-through fraction from the affinity column. Judging by the condensation of the band, the content of transferrin in the supernatant was nearly equal to that of the concentrated flow-through fraction. On the other hand, insulin was not detected in any sample. These results indicated that an abundant amount of transferrin remained after culture, antibody purification and condensation by ultrafiltration, and that insulin was consumed during the culture or the other processes including antibody purification and condensation.

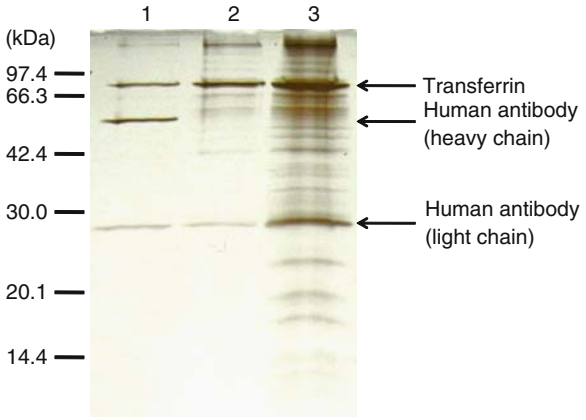

Fig. 1 SDS-PAGE analysis of the culture supernatant from CHO-DP12 cells and the concentrated flow-through fraction from affinity column followed ultrafiltration. Lane 1: supernatant of CHO-DP12 cells cultured in fresh ASF104 supplemented with 5 mg/L transferrin and 5 mg/L insulin; Lane 2 and 3: the concentrated flow-through fraction from the affinity column. The concentrated flow-through fraction of lane 2 was diluted with PBS to one-eighth of the absorbance

Additionally, several unidentified proteins were detected in both samples. They were likely produced by the CHO-DP12 cells.

3.2 Effect of the Recovered Medium on Cell Proliferation of CHO-DP12

To examine the effect of the recovered medium on cell proliferation, CHO-DP12 cells were cultured under several conditions: ASF104 basal medium only, supplemented with growth factors such as transferrin and insulin, respectively, at 0.625 or 5 mg/L, recovered medium only, and recovered medium supplemented with growth factors at 0.625 or 5 mg/L. Figure 2 shows the viable number of CHO-DP12 cells cultured under the conditions described above. When the cells were cultured in the presence of both the recovered medium and the growth factors (column 4 and 6), the viable cell numbers were higher than when they were cultured in the presence of supplemented growth factors only (column 2 and 5). Additionally, the viable cell number obtained from a combination of 0.625 mg/L of growth factors and recovered medium was equal to that obtained from supplementing with 5 mg/L of growth factors. In the presence of recovered medium only, the viable cell number was reduced compared with the seeding period (column 3). These results show that recovered medium has different growth factors which enhance the cell proliferation of CHO-DP12 cells but that use of recovered medium alone was not enough to support the proliferation of CHO-DP12 cells.

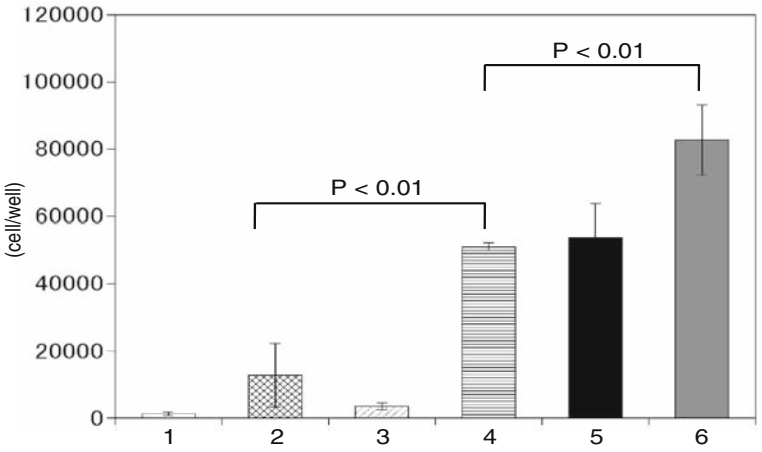

Fig. 2 The viable cell number of CHO-DP12 cells cultured under several media conditions for 70 h. CHO-DP12 cells were cultured under the following conditions: no growth factors (*column 1*), supplemented growth factors at 0.625 mg/L (*column 2*) or 5 mg/L (*column 5*), recovered medium (*column 3*), and recovered medium with growth factors at 0.625 mg/L (*column 4*) or 5 mg/L (*column 6*)

3.3 Effect of the Recovered Medium on the Human IgG Production of CHO-DP12

To examine the effect of recovered medium on antibody production, the final human IgG concentration in the culture supernatants of CHO-DP12 cells (see Section 3.2) was measured by ELISA. The supernatants were collected at the end of the culture period. When CHO-DP12 cells were cultured in the medium containing both recovered medium and growth factors (column 4 and 6), the human IgG concentration was higher than when they were cultured in the medium supplemented with growth factors only (column 2 and 5). Additionally, the combination of 0.625 mg/L of growth factors and recovered medium produced the same amount of IgG as the media containing 5 mg/L of growth factors. However, there were no significant differences in the antibody productivities per cell among these culture conditions. These results show that the combination of transferrin, insulin and recovered medium was sufficient for CHO-DP12 cells to produce more human antibody, but that the capacity of antibody production between the different culture conditions was nearly equal.

In conclusion, we studied the effect of recovered medium on cell proliferation and antibody production. The recovered medium improved cell proliferation of CHO-DP12 cells and increased the total amount of human IgG production, but did not enhance the overall antibody productivity. Furthermore, although some proteins produced by CHO-DP12 cells were detected in the culture supernatant and concentrated flow-through solution, it was assumed that they would have had the ability to enhance the cell proliferation of CHO-DP12, but this was not very defined in this study.

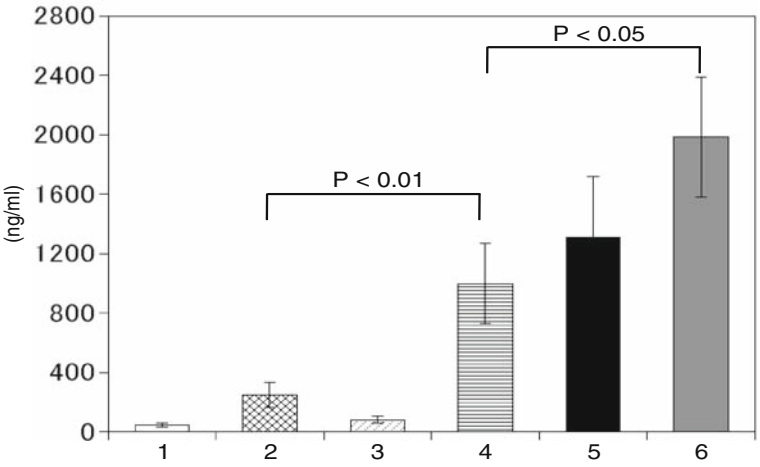

Fig. 3. The human IgG concentration of supernatants from CHO-DP12 cells cultured under several media conditions for 70 h. Each column indicates the final human IgG concentration of the culture supernatants from CHO-DP12 cells. They were cultured under the conditions detailed in the caption for Fig. 2 CHO-DP12 cells were cultured under the following conditions: no growth factors (*column 1*), supplemented growth factors at 0.625 mg/L (*column 2*) or 5 mg/L (*column 5*), recovered medium (*column 3*), and recovered medium with growth factors at 0.625 mg/L (*column 4*) or 5 mg/L (*column 6*)

References

1. Murakami, H., Masui, H., Sato, G.H., Sueoka, N., Chow, T.P., and KaNo-Sueoka, T. (1982) Growth of hybridoma cells in serum-free medium: Ethanolamine is an essential component. *Proc. Natl. Acad. Sci. USA* **79:** 1158–1162.
2. Riese, U., Lütkemeyer, D., Heidemann, R., Büntemeyer, H., and Lehmann, J. (1994) Re-use of spent cell culture medium in pilot scale and rapid preparative purification with membrane chromatography. *J. Biotech*. **34:** 247–257.
3. Laemmli, U.K. (1970) Cleavage of structural proteins during the assembly of the head of bacteriophage T4. *Nature* **227:** 680–685.
4. Mallon, B.S., Park, K.Y., Chen, K.G., Hamilton, R.S., and McKay, R.D.G. (2006) Toward xeno-free culture of human embryonic stem cells. *Int. J. Biochem. Cell Biol*. **38:** 1063–1075.

Production of Human Monoclonal Antibodies Against FC Epsilon Receptor I Alpha by Combining In Vitro Immunization with Phage Display

Kosuke Tomimatsu, Shin-ei Matsumoto, Makiko Yamashita, Kiichiro Teruya, Yoshinori Katakura, Shigeru Kabayama, and Sanetaka Shirahata

1 Introduction

Monoclonal antibodies (mAbs) have a great potential and hope for the treatment of various human diseases. The advent of mAbs was done using hybridoma technology, which was introduced by Köhler and Milstein [1]. However, owing to their murine origins, the first generation of mAbs evaluated in the clinic was limited by their immunogenicity [2–4]. Thus, increasing effort has been applied to engineer antibodies without a non-human structure to minimize such responses [5–7]. To overcome this problem, we developed an in vitro immunization (IVI) protocol [8–10], which elicits antigen-specific immune responses in peripheral blood mononuclear cells (PBMC). In antibody engineering, cell surface antigens are often targeted [11] as they play an increasingly important role. However the generation of antibodies against cell surface antigens is hard owing to the difficulty in obtaining sufficient amounts of antigen with high purity and in the native conformation for immunization [12].

In this study, we tried to generate antigen-specific monoclonal antibodies against membrane proteins using intact cells as the antigen. We focused on the high affinity IgE receptor epsilon alpha chain (FcεRIα), which triggers allergic reactions [13] and is expressed on human basophile cell line KU812F. We tried to obtain FcεRIα-specific human monoclonal antibody using a method combining IVI and phage display.

S. Shirahata (✉)
Faculty of Agriculture, Kyushu University, Higashi-ku, Fukuoka 812-8581, Japan
e-mail: sirahata@grt.kyushu-u.ac.jp

M. Kamihira et al. (eds.), *Animal Cell Technology: Basic & Applied Aspects*, Animal Cell Technology: Basic & Applied Aspects 16, DOI 10.1007/978-90-481-3892-0_25,

2 Experimental Procedure

2.1 Recombinant FcεRIα

Total RNA from KU812F cells was prepared by GenElute Mammalian Total RNA Kit (Sigma-Aldrich) and recombinant FceRIa was constructed as previously described [14].

2.2 In Vitro Immunization

The preparation of PBMCs and in vitro immunization were performed as previously described [15]. LLME-treated PBMCs were sensitized with KU812F cells fixed with 1% glutaraldehyde and cultured in eRDF medium (Invitrogen, Carlsbad, CA) supplemented with 10% heat-inactivated FBS, IL-2, IL-4, 2-mercaptoethanol and D-type CpG ODN (1 mM). After culture for 3 days, K-type CpG ODN (1 mM) was added and the cells were cultured for an additional 3 days. The total amounts of immunoglobulin secreted into the culture supernatant were determined by ELISA as previously described [16]. B cells producing antigen-specific antibodies were detected by the ELISPOT assay as previously described [10]. Experiments throughout this study were carried out in accordance with the principles of the Declaration of Helsinki and the regulations of the ethics committee of the Faculty of Agriculture at Kyushu University.

2.3 Generation of the Phage Antibody Library and Selection

The phage antibody library was constructed as previously described [15]. To select antigen specific phage antibody from the library, we demonstrated panning with streptavidin magnetic beads conjugated with biotinylated recombinant FcεRIα. Antigen specificity of the selected phage antibodies were evaluated by ELISA.

2.4 Production of Recombinant Human Monoclonal IgG in Chinese Hamster Ovary Cells

We amplified the VH and VL genes by PCR using vectors expressing scFv specific for FcεRIα as templates and appropriate primers. The VH and VL genes were cloned into the pSecTag2A/IgGc bearing heavy chain constant region (CH) gene and pSecTag2A/IgLc bearing light chain constant region (CL) gene respectively. Chinese hamster ovary (CHO) cells were transfected with these expression vectors using Lipofectamine (Invitrogen) according to the manufacturer's instructions. IgG in the supernatant was purified by affinity chromatography with protein G column

(GE Healthcare, Sweden). Specificity of these generated antibodies were assessed by competitive ELISA.

2.5 Flow Cytometric Analysis

KU812F cells were teated with C9 and-FcεRIα IgG. After treatment, the cells were washed with PBS and incubated with FITC-labeled human IgG for 30 min. The fluorescence intensity was measured with a FACSAria^{TM} Cell Sorter (BD Bioscience).

3 Results

3.1 KU812F-Specific Immune Response Elicited by In Vitro Immunization

Figure 1a shows that the PBMCs, immunized in vitro with fixed KU812F cells, augmented the cell-cell interactions and consequently formed numerous larger clusters than control cells. The PBMC immunized with fixed KU812F produced a large amount of IgM and IgG (data not shown) and KU812F-specific antibodies (Fig. 1b and c). These data indicate that the in vitro immunization method using fixed cell antigen could activate PBMCs and induce cell surface antigen-specific immune responses when sensitized with intact cells or lysate antigen.

3.2 Construction of the Phage Display Library and Selection

The variable region genes of antibody were amplified from cDNA prepared from PBMCs immunized in vitro by PCR using V region family specific primers. Next we constructed and obtained scFv phage display library contain 6.4×10^3 clones from PBMC immunized with cells and 2.4×10^4 clones from PBMC immunized with lysate. The antigen-specific scFv phages were selected from the phage libraries by panning.

3.3 Production of the IgG Type Antibody and Functional Analysis

Generated IgG genes were transfected into CHO cells and IgG were produced into the culture supernatants. The three FcεRIα specific individual clones (C9, C51 and L49) were obtained by purification with affinity chromatography and performed competitive ELISA to assess antigen specificity of purified IgGs (Fig. 2a). We found

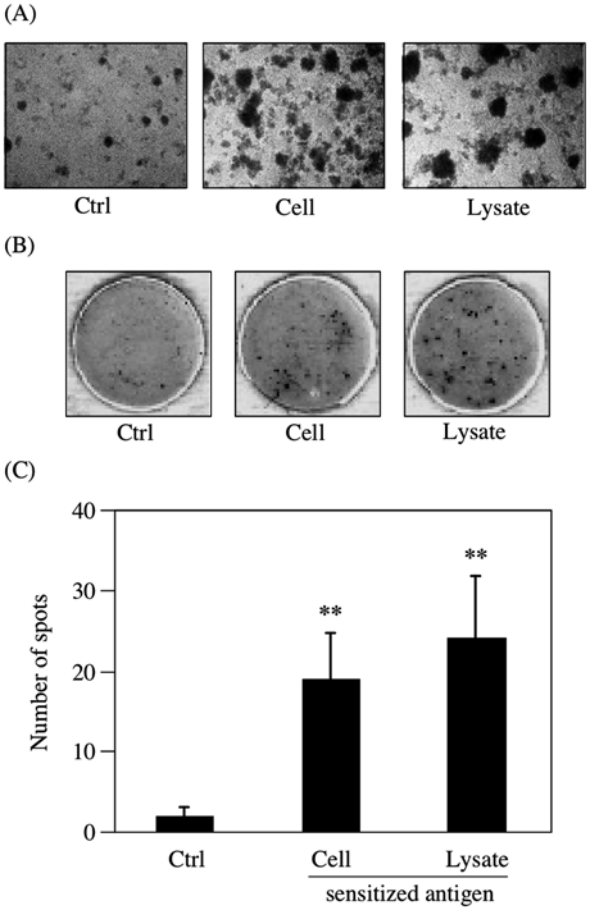

Fig. 1 Immune responses of lymphocytes augmented by in vitro immunization. LLME-treated PBMCs were cultured in eRDF medium supplemented with 10% FBS (ctrl), or sensitized with KU812F cells in eRDF medium supplemented with 10% FBS, IL-2, IL-4, and CpG ODN (Cell or Lysate). (**a**) After culture for 6 days, the PBMC were observed with a phase contrast microscope. (**b**, **c**) KU812F cell-specific IgM derived from PBMCs immunized in vitro were evaluated by ELISPOT assays

that all three IgGs could bind specifically to FcεRIα. Next we determined whether the generated recombinant FcεRIα specific IgG could recognize FcεRIα expressed on the KU812F cell surface membrane by flow cytometric analysis. C9 exhibited binding ability to FcεRIα expressed on the cell surface of KU812F cell (Fig. 2b); however, the other two IgG clones (C51 and L49) did not (data not shown). Next we investigated the ability of C9 anti-FcεRIα IgG to inhibit the binding of IgE to FcεRIα on KU812F. As shown in Fig. 3c, the C9 IgG inhibited the binding of IgE to FcεRIα on KU812F.

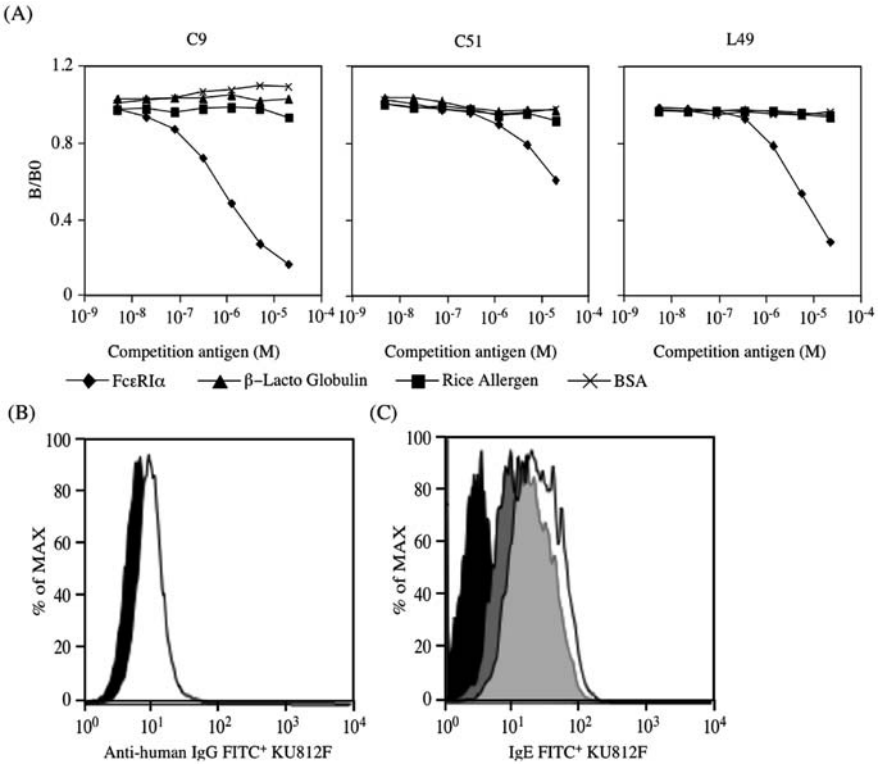

Fig. 2 Analysis of monoclonal IgG clones against FcεRIα. (**a**) Evaluation of antigen specificity of the purified mAbs (C9, C51 and L49) with competition ELISA. (**b**) Flow cytometric analysis of C9 binding to FcεRIα expressed on KU812F cell surfae. Filled peak, binding of human IgG for control. Open peak, binding of mAb C9. (**c**) Inhibition analysis of the IgE binding to FcεRIα by flow cytometry analisys. Filled peak, negative control. Open peak, binding with FITC-conjugated IgE. Gray peak, binding with FITC-conjugated IgE after treatment with mAb C9

4 Discussion

Here, we report a new method for generating human monoclonal antibody against cell surface antigens by combining in vitro immunization of human PBMCs with phage display. Fixed KU812F cells elicited antigen-specific antibody production from PBMCs by in vitro immunization as shown in Fig. 1, and the FcεRIα-specific phage antibody library constructed from cell immunized PBMCs seems to have better specificity than the library constructed from lysate immunized PBMCs. Additionally, in our previous study, we demonstrated that VH gene expression in PBMCs immunized in vitro was considerably enhanced compared with non-stimulated PBMCs [15]. These results suggest that an efficient immune response against cell surface membrane protein was induced by in vitro immunization with a fixed cell providing the antigen.

When receptor-bound IgE forms cross-links with a multivalent allergen, the resulting activation signal causes the release of inflammatory mediators. The C9 IgG generated bound to FcεRIα expressed on KU812F cells and blocked binding between FcεRIα and IgE. This suggests that the C9 IgG might inhibit allergic interactions at the molecular level. In summary, we have developed a human monoclonal antibody against a receptor protein using a small phage antibody library and PBMCs immunized in vitro with intact whole cells. These results indicate that combining in vitro immunization with phage display has advantages for generating human monoclonal antibody.

References

1. Köhler, G. and Milstein, C. (1975) Continuous cultures of fused cells secreting antibodies of predefined specificity. *Nature* **256**: 495–497.
2. Badger, C.C., Anasetti, C., Davis, J., and Bernstein, I.D. (1987) Treatment of malignancy with unmodified antibody. *Pathol. Immunopathol*. Res. **6**: 5–6.
3. Khazaeli, M.B., Conry, R.M., and LoBuglio, A.F. (1994) Human immune response to monoclonal antibodies. *J. Immunother. Emphasis Tumor Immunol*. **15**: 42–52.
4. Lee, J., Fenton, B.M., Koch, C.J., Frelinger, J.G., and Lord, E.M. (1998) Interleukin 2 expression by tumor cells alters both the immune response and the tumor microenvironment. *Cancer Res.* **58**: 1478–1485.
5. Co, M.S. and Queen, C. (1991) Humanized antibodies for therapy. *Nature* **351**: 501–502.
6. Hwang, W.Y.K. and Foote, J. (2005) Immunogenicity of engineered antibodies. *Methods* **36**: 3–10.
7. Leonald, G.P. (2006) Engineering of therapeutic antibodies to minimize immunogenicity and optimize function. *Adv. Drug Deliv. Rev.* **58**: 640–656.
8. Ichikawa, A., Katakura, Y., Teruya, K., Hashizume, S., and Shirahata, S. (1999) In vitro immunization of human peripheral blood lymphocytes: establishment of B cell lines secreting IgM specific for cholera toxin B subunit from lymphocytes stimulated with IL-2 and IL-4. *Cytotechnology* **31**: 133–141.
9. Xu, Q., Katakura, Y., Yamashita, M., Fang, S., Tamura, T., Matsumoto, S.E., Aiba, Y., Teruya, K., Osada, K., Nishikawa, R., and Shirahata, S. (2004) IL-10 augments antibody production in in vitro immunized lymphocytes by inducing a Th 2-type response and B cell maturation. *Biosci. Biotechnol. Biochem*. **68**: 2279–2284.
10. Matsumoto, S.E., Yamashita, M., Katakura, Y., Noguchi, E., Aiba, Y., Ichikawa, A., Teruya, K., and Shirahata, S. (2006) In vitro immunization can elicit the expansion of diverse repertoire of B cells from peripheral blood mononuclear cells. *Cytotechnology* **52**: 227–233.
11. Kim, S.J., Park, Y., and Hong, H.J. (2005) Antibody engineering for the development of therapeutic antibodies. *Mol. Cells* **20**: 17–29.
12. Grisshammer, R. and Tate, C.G. (1995) Overexpression of integral membrane proteins for structural studies. *Q. Rev. Biophys*. **28**: 315–422.
13. Ishizaka, T., Conrad, D.H., Schulman, E.S., Sterk, A.R., and Ishizaka, K. (1983) Biochemical analysis of initial triggering events of IgE-mediated histamine release from human lung mast cells. *J. Immuol*. **130**: 2352–2362.
14. Hashiguchi, S., Nakashima, T., Nitani, A., Yoshihara, T., Yoshinaga, K., Ito, Y., Maeda, Y., and Sugimura, K. (2003) Human Fc epsilon receptor I alpha-specific human single-chain Fv (scFv) antibody with antagonistic activity toward IgE/Fc epsilon receptor I alpha-binding. *J. Biochem*. **133**: 43–49.
15. Matsumoto, S.E., Yamashita, M., Katakura, Y., Aiba, Y., Tomimatsu, K., Kabayama, S., Teruya, K., and Shirahata, S. (2008) A rapid and efficient strategy to generate antigen-specific

human monoclonal antibody by in vitro immunization and the phage display method. *J. Immunol. Methods*, **332**: 2–9.

16. Yamashita, M., Katakura, Y., Shim, S.Y., Matsumoto, S.E., Tamura, T., Morihara, K., Teruya, K., Tsuchiya, T., and Shirahata, S. (2002) Different individual immune responses elicited by in vitro immunization. *Cytotechnology* **40**: 161–165.

Enhancement of Hepatocyte Function Through Heterotypic Cell-Cell Interactions Using E-Cadherin-Expressing NIH3T3 Cells

Akira Ito, Takehiko Kiyohara, Yoshinori Kawabe, Hiroyuki Ijima, and Masamichi Kamihira

1 Introduction

Heterotypic cell-cell interactions between epithelial and mesenchymal cells play crucial roles in living tissues and organs. Thus, these interactions are fundamentally important in tissues and organs, and have to be taken into account in replicating tissue functions in bioartificial organs and in tissue engineering. Tissue cells such as epithelial cells or hepatocytes can spontaneously form aggregates in vitro. During the aggregate formation, cells reconstruct tissue-like structures such as epithelial islands by connecting cells via the homophilic adhesion molecule, E-cadherin. The calcium-dependent, transmembrane molecules, cadherins directly regulate morphologic events [1]. The predominant cadherin of most epithelia including hepatocytes is E-cadherin. Because E-cadherin is a homophilic adhesion molecule, cells expressing different cadherin molecules such as E- and P-cadherins tend to distinguish between each other when artificially mixed in vitro. In the present study, in order to engineer heterotypic interactions between epithelial and mesenchymal cells via E-cadherin molecules, the E-cadherin gene was introduced into mesenchymal mouse fibroblast NIH3T3 cells, and the effects of co-culture of E-cadherin-expressing NIH3T3 cells with hepatocytes were investigated.

2 Materials and Methods

2.1 Establishment of E-Cadherin-Expressing NIH3T3 Cells

The fragment of full-length murine E-cadherin cDNA [2] obtained from RIKEN Bioresource Center (Tsukuba) was ligated into the pcDNA4 plasmid (Invitrogen,

A. Ito (✉)
Department of Chemical Engineering, Faculty of Engineering, Kyushu University, Nishi-ku, 744 Motooka, Nishi-ku, Fukuoka 819-0395, Japan
e-mail: akira@chem-eng.kyushu-u.ac.jp

M. Kamihira et al. (eds.), *Animal Cell Technology: Basic & Applied Aspects*, Animal Cell Technology: Basic & Applied Aspects 16, DOI 10.1007/978-90-481-3892-0_26,

Carlsbad, CA, USA), and NIH3T3 cells were transfected with the plasmid using Lipofectamine 2000 reagent (Invitrogen). Cells were selected in the medium containing 1 mg/ml zeocin (Sigma-Aldrich, St. Louis, MO, USA), and stable E-cadherin-expressing clones were established (designated as 3T3/E-cad).

2.2 Western Blot Analysis

The cell lysates (total protein, 15 μg) of NIH3T3 or 3T3/E-cad cells were subjected to SDS-PAGE on a 7.5% polyacrylamide gel, and the proteins were transferred onto a nitrocellulose membrane. After blocking using 5% skimmed milk, the membrane were incubated with a rabbit anti-E-cadherin monoclonal antibody (Santa Cruz Biotechnology, Santa Cruz, CA, USA) for 1 h, and probed with peroxidase-labeled anti-rabbit IgGs (Santa Cruz Biotechnology) for 1 h. The labeled antibodies were detected by the ECL detection system (GE Healthcare, Buckinghamshire, UK).

2.3 Co-Culture Experiment

Primary rat hepatocytes were obtained from Wistar rats by the two-step collagenase perfusion method. Details of the culture medium for hepatocytes and protocols were reported previously [3], except that the medium contained 10% fetal bovine serum in the present study. Co-culture of hepatocytes with NIH3T3 or 3T3/E-cad cells was performed firstly by seeding freshly isolated hepatocytes onto wells of 6-well collagen-coated tissue culture plates at 1.7×10^5 cells/well (day 0), followed by medium change after 24 h using cell suspension containing 3T3/E-cad or NIH3T3 cells at 1×10^5 cells per well in fresh medium. Co-culture was maintained by medium change every day.

2.4 Fluorescence Microscopy and Analysis

For fluorescence microscopy, 3T3/E-cad and NIH3T3 cells were pre-stained using CellTracker (red fluorescent probe, Molecular Probes, Eugene, OR, USA), and observed by fluorescence microscopy (Olympus, Tokyo) 1 d after the co-culture. Frequency of cell-cell contacts by co-culture was analyzed by using images of 5 fields in each of three separate wells per sample were captured by fluorescence microscope and saved to a disk for later analysis. Frequency of cell-cell contacts, which is defined as the number of cell-cell contacts divided by the number of 3T3/ E-cad or NIH3T3 cells, was measured using Photoshop software (Adobe Systems, San Jose, CA, USA).

2.5 Assay for Albumin Secretion Rate

Albumin secretion rate was determined as follows: A fixed population of hepatocytes (1×10^4 cells) was co-cultured with increasing number of 3T3 cells (1, 3, or 9×10^4 cells) corresponding to 1:3, 1:1, or 3:1 (3T3:hepatocyte), respectively, and the amount of albumin secreted from hepatocytes in culture medium on day 2 was quantified by enzyme-linked immunosorbent assay (ELISA) using commercially available kits (Bethyl Laboratory, Montgomery, TX, USA). Time course of albumin secretion rate was determined as follows: Hepatocytes (3×10^4 cells) were co-cultured with NIH3T3 or 3T3/E-cad cells (3×10^4 cells), and the amount of albumin secreted in the medium was quantified by ELISA on days 2, 3 and 6.

3 Results and Discussion

3.1 Establishment of E-Cadherin-Expressing NIH3T3 Cells

Western blot analysis revealed that 3T3/E-cad cells stably expressed E-cadherin [4]. E-cadherin was detected throughout the cell membrane of 3T3/E-cad cells by immunostaining with anti-E-cadherin antibodies. 3T3/E-cad cells grew to form cell islands like epithelial cells in culture, and were obviously different from parental NIH3T3 cells which showed more scattered and fibroblastic morphology. Although we established four 3T3/E-cad clones during antibiotic selection, identical morphological changes were observed for all the clones.

3.2 Co-Culture with Hepatocytes

In co-culture with hepatocytes, 3T3/E-cad cells were incorporated into the cell islands formed by hepatocytes, and the frequency of cell-cell contacts between 3T3/E-cad cells and hepatocytes was 1.8-fold more than that between parental NIH3T3 cells and hepatocytes (Fig. 1).

3.3 Effects of Co-Culture with Hepatocytes on Albumin Secretion Rate

It is known that homotypic and heterotypic cell-cell interactions play fundamental roles in proliferation and differentiation in the liver, and even *in vitro*, co-cultures of hepatocytes with nonparenchymal cells have been shown to be effective in the expression of liver-specific functions in cultured hepatocytes [5]. To investigate the effects of interaction with 3T3/E-cad cells on albumin secretion in cultured hepatocytes, a fixed population of hepatocytes was co-cultured with an increasing number

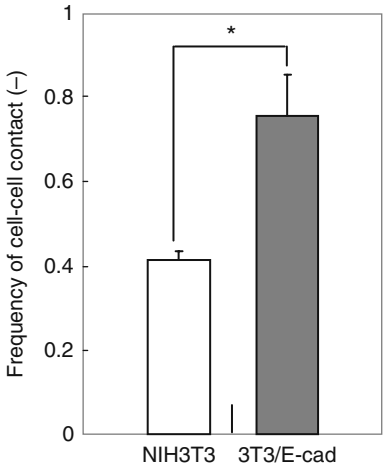

Fig. 1 Frequency of cell-cell contacts by co-culture on day 2. *P<0.05

of NIH3T3 or 3T3/E-cad cells (3T3:hepatocyte; 1:3, 1:1, or 3:1) (Table 1). As the ratio of parental NIH3T3 cells to hepatocytes increased from 1:1 to 3:1, the albumin secretion rate increased. For 3T3/E-cad cells, on the other hand, the higher level of albumin secretion rate was observed even with a low cell ratio (1:1) compared with that for NIH3T3 cells. These results suggest that the frequency of cell-cell interactions between hepatocytes and fibroblasts promoted the expression of liver-specific functions in cultured hepatocytes, and the liver function was enhanced by the reinforced adhesion between 3T3/E-cad cells and hepatocytes.

After 6 d of co-culture, the differences in albumin secretion rate between the cultures became more obvious (Fig. 2). When hepatocytes were cultured alone, the albumin secretion rate drastically decreased on day 6. In the co-culture with NIH3T3 cells, the albumin secretion rate was higher than in the culture of hepatocytes alone on days 3 and 6, but the overall albumin secretion rate decreased on day 6. On the other hand, when hepatocytes were co-cultured with 3T3/E-cad cells, the albumin

Table 1 Effects of interaction with 3T3/E-cad cells on albumin secretion rate on day 2

	Albumin secretion rate (μg/ml/d)
Hepatocyte alone	13.6 ± 2.1
NIH3T3: Hepatocyte	
1:3	16.9 ± 2.2
1:1	14.1 ± 1.2
3:1	21.5 ± 4.5
3T3/E-cad: Hepatocyte	
1:3	14.0 ± 1.9
1:1	20.9 ± 4.2
3:1	20.2 ± 4.1

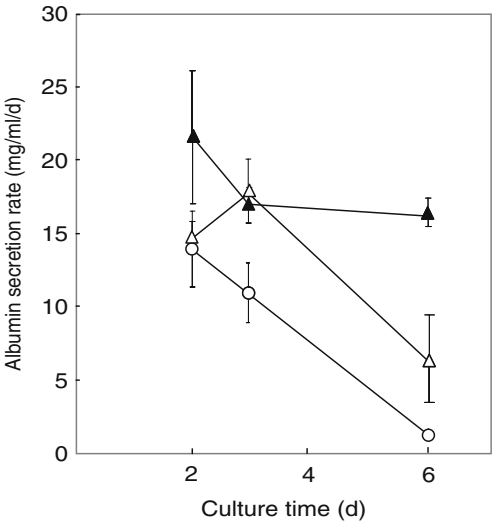

Fig. 2 Time course of albumin secretion rate. Open circle, hepatocyte alone; open traingle, hepatocyte + NIH3T3; closed traingle, hepatocyte + 3T3/E-cad. Data points are mean and SD of triplicate

secretion rate was maintained throughout the culture for 6 d, and the level was significantly higher than in the culture of hepatocytes alone or in the co-culture of hepatocytes and NIH3T3 cells.

In the present study, the interactions between parenchymal and nonparenchymal cells were artificially generated and enforced by using NIH3T3 cells expressing E-cadherin. These results indicate that 3T3/E-cad cells may be useful for co-culture-based bioartificial liver and liver tissue engineering.

References

1. Takeichi, M. (1991) Cadherin cell adhesion receptors as a morphogenetic regulator. *Science* **251**(5000): 1451–1455.
2. Nagafuchi, A., Shirayoshi, Y., Okazaki, K., Yasuda, K., and Takeichi, M. (1987) Transformation of cell adhesion properties by exogenously introduced E-cadherin cDNA. *Nature* **329**(6137): 341–343.
3. Ijima, H., Murakami, S., Matsuo, T., Takei, T., Ono, T., and Kawakami, K. (2005) Enhancement of liver-specific functions of primary rat hepatocytes co-cultured with bone marrow cells on tissue culture-treated polystyrene surface. *J. Artif. Organs* **8**(2): 104–109.
4. Ito, A., Kiyohara, T., Kawabe, Y., Ijima, H., and Kamihira, M. (2008) Enhancement of cell function through heterotypic cell-cell interactions using E-cadherin-expressing NIH3T3 cells. *J. Biosci. Bioeng*. **105**(6): 679–682.
5. Bhatia, S.N., Balis, U.J., Yarmush, M.L., and Toner, M. (1999) Effect of cell-cell interactions in preservation of cellular phenotype: Cocultivation of hepatocytes and nonparenchymal cells. *FASEB J*. **13**(14): 1883–1900.

Magnetic Cell-Patterning for Tissue Engineering

Hirokazu Akiyama, Akira Ito, Yoshinori Kawabe, and Masamichi Kamihira

1 Introduction

In normal tissues and organs, various cell types and cell layers are highly organized and interact with each other in micro-scale order, constructing and maintaining the three-dimensional (3D) structures. From a viewpoint of tissue engineering, it is essential to mimic natural microenvironment for the construction of functional tissue substitutes [7]. To this end, micro-scale cell patterning techniques have attracted great attention, and they have been applicable not only to tissue engineering field but also to cell biological studies [2, 10].

Lithographic approaches have been used widely for cell patterning due to their high resolution capacities [1, 6]. However, because substrates used in these methods are non-biodegradable, their application has been very limited in tissue engineering. Conversely, cell patterning technologies such as the 3D photopatterning [9] and ink-jet printing [13, 14] do not require specialized substrates. Although these techniques provide a potentially powerful method to create 3D cell patterns, the approaches currently have many problems. Therefore, the development of a new cell patterning procedure applicable to tissue engineering is still required.

In our previous study, we developed a novel cell-patterning procedure [5] using magnetite cationic liposomes (MCLs) which were designed to improve the accumulation of 10-nm magnetite nanoparticles into target cells for magnetic cell manipulation. The MCL-labeled cells could be micro-patterned using magnetic field concentrators, in which magnetized micron-thick steel plates were embedded. On the other hand, as the scaffold-free 3D tissue construction approach, multilayered cell sheets were also created by strongly depositing MCL-labeled cells on the culture surfaces by magnetic force [4]. In principle, using the magnetic cell manipulation technique, cell patterns can be created irrespective of surface conditions. In the present study, we applied the magnetic cell patterning technique to form cell patterns on a monolayer of cells and a magnetic tissue-engineered cell sheet. Based on these

H. Akiyama (✉)
Department of Chemical Engineering, Faculty of Engineering, Kyushu University, 744 Motooka, Nishi-ku, Fukuoka 819-0395, Japan
e-mail: hakiyama@chem-eng.kyushu-u.ac.jp

M. Kamihira et al. (eds.), *Animal Cell Technology: Basic & Applied Aspects*, Animal Cell Technology: Basic & Applied Aspects 16, DOI 10.1007/978-90-481-3892-0_27,

results, we also attempted to fabricate complex 3D tissue constructs by combining the magnetic force-based cell sheet formation and cell patterning procedures.

2 Materials and Methods

2.1 Cells and Culture

Human umbilical vein endothelial cells (HUVECs) obtained from the supplier (Kurabo, Osaka, Japan) were grown in commercially available growth media (Humedia-EG2; Kurabo). Mouse myoblast C2C12 cells were grown in Dulbecco's modified Eagle medium (DMEM; Sigma-Aldrich, St. Louis, MO, USA) supplemented with 10% fetal bovine serum. Cells were cultured at 37°C under a humidified atmosphere of 5% CO_2 and 95% air.

2.2 Preparation of Magnetite Cationic Liposomes

The magnetite (Fe_3O_4; average particle size, 10 nm) was obtained from Toda Kogyo (Hiroshima, Japan). MCLs were prepared as described previously [11]. For magnetic labeling of the cells, MCLs were added to the culture media at the concentration of 100 pg-magnetite/cell, and cells were cultured for 24 h (HUVECs) and 4 h (C2C12 cells), respectively.

2.3 Device Fabrication for Magnetic Cell-Patterning

Steel plates (thickness, 200 μm; Toyo koban, Tokyo, Japan) were used as magnetic field gradient concentrators. Cell patterning devices with steel plates for linear patterns [3] and arbitrary patterns (Fig. 2A; [5]) were manufactured as described previously. To magnetize steel plates to attract MCL-labeled cells, these devices were placed on neodymium cylindrical magnets (diameter, 30 mm; height, 15 mm; magnetic induction, 0.4T).

2.4 Magnetic Cell-Patterning onto Cell Layers

To fabricate cell patterns on a monolayer of cells, a 35-mm cell culture dish (hydrophilic lumox dish; film bottom thickness, 25 μm; Greiner bio-one, Frickenhausen, Germany), where C2C12 cells reached a confluent state, was placed on the cell patterning device. Then, MCL-labeled HUVECs (5×10^3 cells/dish) were seeded. For cell-patterning on a cell sheet, magnetic tissue-engineered C2C12 cell sheets were fabricated as described previously with a slight modification [4]. After 2 h cultivation of the cell sheet, the cell patterning device for arbitrary patterns, where the letter "G"-shaped steel plate was embedded, was positioned underneath the dish. Magnetically labeled HUVECs (1×10^4 cells/dish) were then seeded onto

the C2C12 cell sheet. To visualize the patterned HUVECs on a cell sheet, cells were stained using goat anti-mouse IgG alkaline phosphatase conjugate, nitro-blue tetrazolium chloride (NBT), and 5-bromo-4-chloro-3'-indolyl phosphatase *p*-toluidine salt (BCIP) (Tubule Staining Kit for CD31, Kurabo).

2.5 Construction of 3D Tissue Construct Incorporating Patterned HUVECs

The structure of 3D tissue construct, in which the micro-patterned HUVECs were embedded, was illustrated in Fig. 3A. C2C12 cell layer (1×10^6 cells/dish) was constructed, and magnetically labeled HUVECs (4.3×10^3 cells/dish) were patterned on the layer with the similar method as described above. Thereafter, magnetic cell layer formation of C2C12 cells and magnetic patterning of HUVECs were alternatively repeated twice and once, respectively. Cells were allowed to culture for layer formation and attachment of the patterned HUVECs to the cell layer for 1 h and 2 h, respectively.

2.6 Fluorescence Microscopy

Fluorescence microscopy of the cells was performed using Cell-Tracker (Molecular Probes, Eugene, OR, USA). HUVECs were pre-stained with the orange fluorescent probe. For 3D analysis, C2C12 cells were also pre-stained with the green fluorescent probe. The 3D tissue constructs were observed using a fluorescence microscope (BZ-9000, Keyence, Osaka, Japan) and processed with a BZ-Analyzer (Keyence).

3 Results

For the construction of in vivo-like complex 3D tissues, it is often necessary to fabricate cell patterns on the top of cell layers. Because the magnetic cell-patterning technique can control cell arrangements on any surfaces under sufficient magnetic force, we firstly attempted to pattern HUVECs on a monolayer of C2C12 cells. After C2C12 cells reached a confluent state, the dish was placed on the magnetic cell-patterning device (200 μm-thick steel plate with a magnet), and then MCL-labeled HUVECs were seeded. As shown in Fig. 1, HUVECs were patterned on the confluent C2C12 cell monolayer with a line width of almost 200 μm, which was consistent of the thickness of the steel plate.

Next, in order to demonstrate that the magnetic cell-patterning procedure is not limited on monolayer cells, we attempted to fabricate patterns of HUVECs on a magnetic tissue-engineered C2C12 cell sheet constructed by accumulating magnetically labeled C2C12 cells to the culture surface by applying magnetic force using the procedure developed in our previous study [4]. In this case, a

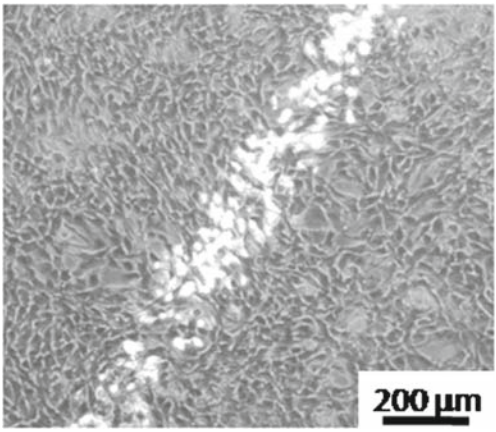

Fig. 1 Magnetic micro-patterned HUVECs on a monolayer of C2C12 cells. A merged image of the phase-contrast and fluorescence images. Patterned HUVECs were pre-stained with orange fluorescent probe

cell patterning device, in which the letter "G"-shaped steel plate with a thickness of 200 μm was embedded, was used (Fig. 2A). When the magnetically labeled HUVECs were seeded onto the C2C12 cell sheet, it was found that the line width of HUVEC patterns was consistent with the thickness of the steel plate by fluorescence microscopy (almost 200 μm). Moreover, CD31 staining revealed that HUVECs were successfully patterned in the letter of "G" according to the figuration of the device (Fig. 2B).

Based on the results described above, we finally attempted to create a complex C2C12 cell sheet, in which patterned HUVECs were incorporated. As illustrated in Fig. 3A, magnetic cell layer formation of C2C12 cells and magnetic patterning of HUVECs were alternately repeated, and each pattern of HUVECs was positioned at a right angle by perpendicularly rotating the cell patterning device. As shown in Fig. 3B and C, HUVECs were successfully patterned to form a cross line in C2C12 cell layers, and the cross pattern of HUVECs was embedded into the 3D tissue construct.

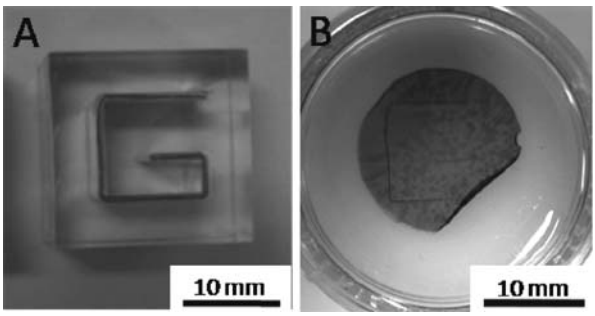

Fig. 2 Formation of the letter "G"-shaped HUVEC pattern on a C2C12 cell sheet. (**A**) Cell patterning device. (**B**) Patterned HUVECs were visualized by CD31 staining

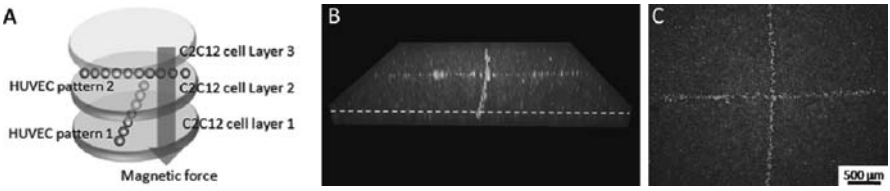

Fig. 3 Fabrication of 3D tissue constructs incorporating patterned HUVECs. HUVECs and C2C12 cells were pre-stained with orange and green fluorescent probes, respectively. (**A**) The structure of the 3D tissue construct. (**B**) The 3D view of the construct. (**C**) The cross-section of the dashed line in (**B**)

4 Discussion

In this study, we demonstrated effectiveness of the magnetic cell-patterning technique for the application to tissue engineering. The advantage of our method is that magnetically labeled cells can be patterned irrespective of surface conditions. We successfully patterned HUVECs on a monolayer of cells (Fig. 1) and a magnetic tissue-engineered cell sheet (Fig. 2). In these cases, conventional methods such as lithography-based approaches could not control cell placements. Moreover, line widths of the patterned HUVECs on these substrates were almost consistent with the thickness of magnetized steel plates (200 μm). Magnetic control of the widths of linearly arranged HUVECs on monolayer cells was also possible by using below 100 μm-thick steel plates including a 10 μm-thick plate (data not shown). These results indicated that line widths of cell patterns could be controlled by the thicknesses of magnetized steel plates in micro-scale order. However, because the magnetic inductive force of target cells is inversely proportional to the distance from magnetic source, it may be difficult to create magnetic arrangements of cells on a thick substrate, where sufficient magnetic force could not be provided. In this regard, we need further investigation of controllability of cell patterns on thick substrates using strong magnets.

We also demonstrated a successful fabrication of 3D tissue constructs, in which micro-patterned endothelial cells were incorporated, by combining the magnetic cell layer formation and magnetic cell patterning techniques (Fig. 3). Although the other groups developed procedures feasible to construct complex 3D tissues by transferring orderly arranged cells on micro-patterned substrates to a tissue matrix [8, 12], these methods required time-consuming and complicated processes for surface modification and transferring procedures. In contrast, our procedure is simple and easy, because target cells were directly arranged on a tissue matrix and magnetic force could induce to form a tissue layer again on the top of patterned cells, leading to cell arrangements within 3D tissue constructs. These results suggest that the magnetic cell-patterning procedure can be a key technology for construction of complex 3D tissue architectures required in tissue engineering.

References

1. Brock, A., Chang, E., Ho, C.C., LeDuc, P., Jiang, X., Whitesides, G.M., and Ingber, D.E. (2003) Geometric determinants of directional cell motility revealed using microcontact printing. *Langmuir* **19**: 1611–1617.
2. Hui, E.E. and Bhatia, S.N. (2007) Micromechanical control of cell-cell interactions. *Proc. Natl. Acad. Sci. U S A.* **104**: 5722–5726.
3. Ito, A., Akiyama, H., Kawabe, Y., and Kamihira, M. (2007) Magnetic force-based cell patterning using Arg-Gly-Asp (RGD) peptide-conjugated magnetite cationic liposomes. *J. Biosci. Bioeng*. **104**: 288–293.
4. Ito, A., Hayashida, M., Honda, H., Hata, K., Kagami, H., Ueda, M., and Kobayashi, T. (2004) Construction and harvest of multilayered keratinocyte sheets using magnetite nanoparticles and magnetic force. *Tissue Eng*. **10**: 873–880.
5. Ino, K., Ito, A., and Honda, H. (2007) Cell patterning using magnetite nanoparticles and magnetic force. *Biotechnol. Bioeng*. **97**: 1309–1317.
6. Jiang, X., Xu, Q., Dertinger, S.K., Stroock, A.D., Fu, T.M., and Whitesides, G. M. (2005) A general method for patterning gradients of biomolecules on surfaces using microfluidic networks. *Anal. Chem.* **15**: 2338–2347.
7. Khademhosseini, A., Langer, R., Borenstein, J., and Vacanti, J.P. (2006) Microscale technologies for tissue engineering and biology. *Proc. Natl. Acad. Sci. USA.* **103**: 2480–2487.
8. Kobayashi, A., Miyake, H., Hattori, H., Kuwana, R., Hiruma, Y., Nakahama, K., Ichinose, S., Ota, M., Nakamura, M., Takeda, S., and Morita, I. (2007) In vitro formation of capillary networks using optical lithographic techniques. *Biochem. Biophys. Res. Commun*., **358**: 692–697.
9. Liu Tsang, V., Chen, A.A., Cho, L.M., Jadin, K.D., Sah, R.L., DeLong, S., West, J.L., and Bhatia, S.N. (2007) Fabrication of 3D hepatic tissues by additive photopatterning of cellular hydrogels. *FASEB J*. **21**: 790–801.
10. Nelson, C.M., Jean, R.P., Tan, J.L., Liu, W.F., Sniadecki, N.J., Spector, A.A., and Chen, C.S. (2005) Emergent patterns of growth controlled by multicellular form and mechanics. *Proc. Natl. Acad. Sci. U S A*. **16**: 11571–11572.
11. Shinkai, M., Yanase, M., Honda, H., Wakabayashi, T., Yoshida, J., and Kobayashi, T. (1996) Intracellular hyperthermia for cancer using magnetite cationic liposomes: in vitro study Jpn. *J. Cancer Res*. **87**: 1179–1183.
12. Tsuda, Y., Shimizu, T., Yamato, M., Kikuchi, A., Sasagawa, T., Sekiya, S., Kobayashi, J., Chen, G., and Okano, T. (2007) Cellular control of tissue architectures using a three-dimensional tissue fabrication technique. *Biomaterials* **28**: 4939–4946.
13. Wilson, W.,C., Jr., and Boland, T. (2003) Cell and organ printing 1: protein and cell printers. *Anat. Rec. A Discov. Mol. Cell. Evol. Biol*. **272**: 491–496.
14. Xu, T., Gregory, C. A., Molnar, P., Cui, X., Jalota, S., Bhaduri, S.B., and Boland, T. (2006) Viability and electrophysiology of neural cell structures generated by the inkjet printing method. *Biomaterials* **27**: 3580–3588.

Magnetic Force-Based Tissue Engineering of Skeletal Muscle for Bio-Actuator

Yasunori Yamamoto, Masahiro Kato, Akira Ito, Yoshinori Kawabe, Kazunori Shimizu, Eiji Nagamori, and Masamichi Kamihira

1 Introduction

Micro-actuators have attracted considerable attention for applications in various fields such as micro-total analysis system (μ-TAS) and lab-on-a-chip. Recently, bio-actuators have been developed because biological cells may be powered without requiring external energy sources. For instance, there are some examples such as hydrogel micropillar [4] and cardiomyocyte sheet actuator [7]. Actuating principle of the hydrogel micropillar was powered by cultured primary neonatal rat cardiomyocytes. The fabricated polymer pillars were ~100 μm in length and cell adhesion peptides were immobilized on the hydrogel surface to promote attachment of cardiomyocytes to the pillars. Total natural contractile forces of single or a few cardiomyocytes attached to the pillar seemed to exceed 80 nN, as estimated from displacement of the micropillar. On the other hand, actuating principle of the cardiomyocyte sheet actuator was powered by a cultured primary neonatal rat cardiomyocyte sheet. Diaphragm and fluid in a chamber were driven by the attached cardiomyocyte sheet. Using micro-check valves, directional fluid flow was generated. The expected flow rate using ideal check valves to regulate the flow direction of the actuator without loss was estimated to be 0.24 μL/min.

Thus, primary neonatal rat cardiomyocytes may be a potent cell source to construct the actuators. On the other hand, the use of mouse myoblast C2C12 cells for bio-actuators has two advantages over primary cardiomyocytes; controllability of the actuators by electrical stimulation and ability of cell proliferation.

Magnetite nanoparticles have been used in an increasing number of biological and medical applications because of the unique responses to magnetic force. Magnetite cationic liposomes (MCLs), which are cationic liposomes containing 10-nm magnetite nanoparticles, were previously developed to improve accumulation of magnetite nanoparticles in target cells, using electrostatic interactions between MCLs and the cell membrane [6]. We have recently developed a tissue

Y. Yamamoto (✉)
Graduate School of Systems Life Sciences, Kyushu University, 744 Motooka, Nishi-ku, Fukuoka, 819-0395, Japan
e-mail: yyamamoto@chem-eng.kyushu-u.ac.jp

M. Kamihira et al. (eds.), *Animal Cell Technology: Basic & Applied Aspects*, Animal Cell Technology: Basic & Applied Aspects 16, DOI 10.1007/978-90-481-3892-0_28,

engineering technique using MCLs, based on the fact that cells labeled with MCLs can be manipulated using a magnet [1–3]. Thus, we have developed a novel methodology for tissue engineering using magnetite nanoparticles combined with magnetic force, and designated this methodology as "magnetic force-based tissue engineering (Mag-TE)".

In the present study, three-dimensional (3D) constructs composed of C2C12 cells were fabricated by the Mag-TE technique, for the application to bio-actuator.

2 Materials and Methods

Magnetite cationic liposomes (MCLs). MCLs were fabricated from a colloidal magnetite and lipid mixture consisting of N-(α-trimethylammonioacetyl)-didodecyl-D-glutamate chloride (TMAG), dilauroylphosphatidylcholine (DLPC) and dioleoylphosphatidyl-ethanolamine (DOPE) in a 1:2:2 molar ratio, as described previously [6]. A schematic model of MCL is illustrated in Fig. 1.

C2C12 cell culure. Mouse myoblast C2C12 cells were grown in Dulbecco's modified Eagle's medium (DMEM) supplemented with 10% fetal bovine serum (FBS) and were cultured at 37°C in a 5% CO_2 incubator.

Construction of C2C12 cell sheet. For magnetic labeling of cells, MCLs (net magnetite concentration, 100 pg/cell) were added to the culture medium of C2C12 cells, and the cells were incubated for 4 h to allow the uptake of MCLs. The MCL-labeled C2C12 cells were harvested by trypsin treatment and 2 or 4×10^6 cells were reseeded onto a well of 24-well ultra-low cell attachment culture plates (cat. no. 3473; Corning, NY, USA; culture area, 200 mm^2/well), whose surface is composed of a covalently bound hydrogel layer that is hydrophilic and neutrally charged. Then,

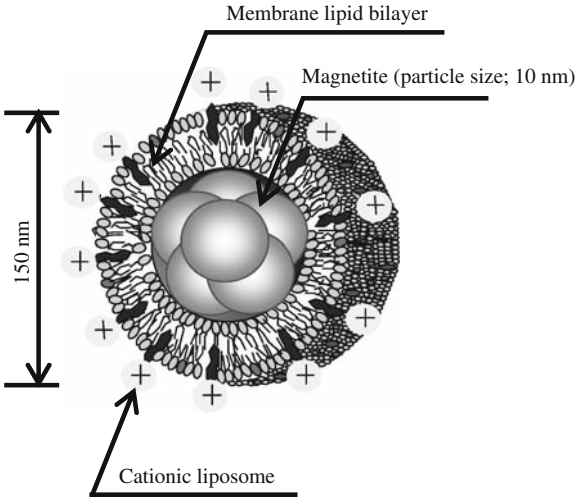

Fig. 1 Magnetite cationic liposomes (MCLs)

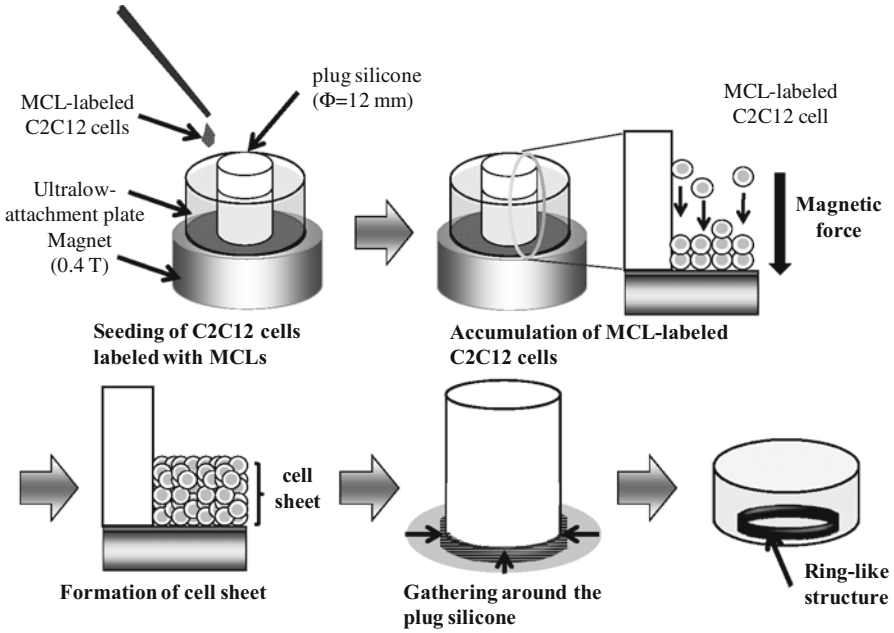

Fig. 2 Construction of C2C12 cell ring

a cylindrical neodymium magnet (diameter, 30 mm; height, 15 mm; magnetic induction, 0.4 T) was placed on the reverse side of the ultralow-attachment plate in order to apply magnetic force vertically to the plate, and cells were cultured for 1 d to form a C2C12 cell sheet.

Construction of C2C12 cell ring. A plug silicone (diameter, 12 mm) was positioned at the center of a well of 24-well ultra-low cell attachment culture plates, MCL-labeled C2C12 cells (6×10^5 cells) were seeded into the gap between the well wall and the plug silicone, and then a magnet (diameter, 30 mm; height, 15 mm; magnetic induction, 0.4 T) was placed under the well. The cells were attracted onto the bottom of the well by magnetic force and accumulated to form a multilayered cell sheet. One day after the beginning of culture, the cell sheet drastically shrank and the cells formed a ring-like structure by gathering around the plug silicone. The schematic drawing is shown in Fig. 2.

3 Results

C2C12 cell sheet fabricated by Mag-TE technique is shown in Fig. 3. When C2C12 cells labeled with MCLs were seeded onto 24-well ultra-low cell attachment culture plates, the cells were attracted onto the bottom of well by magnetic force and accumulated to form a multilayered cell sheet. As shown in Table 1, C2C12 cell

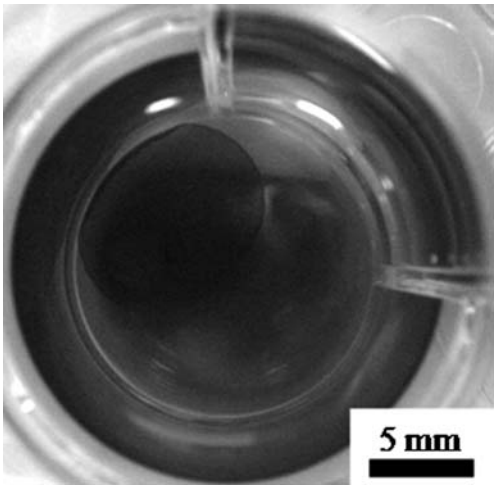

Fig. 3 C2C12 cell sheet (2×10^6 cells, 4 h)

Table 1 Shrinkage of C2C12 cell sheets

Culture time (h)	Shrinkage (%)	
	2×10^6 cells	4×10^6 cells
1	0	0
2	21.4 ± 4.8	0
4	60.6 ± 4.1	0
8	85.9 ± 1.3	22.6 ± 5.2
12	92.8 ± 0.5	28.8 ± 2.2
24	93.0 ± 1.9	67.3 ± 1.7

sheets started shrinking in several hours, and the area of cell sheets reduced to 93.0% (2×10^6 cells/well) and 67.3% (4×10^6 cells/well).

Next, we fabricated a ring-like structure by utilizing the feature of the shrinkage of C2C12 cell sheets. The structure of C2C12 cell ring and the cross-section are shown in Fig. 4. The ring-like structure was 12 mm in diameter and 119.8 ± 13.6 μm in thickness. Interestingly, histological study revealed that the cells were oriented in the direction of circumference by the tension generated within the structure. Thus, the 3D fibrous myoblast cell structure was induced by using MCLs and magnetic force.

4 Discussion

A significant characteristic of cell-based bio-actuators is that they are self-actuated, wireless and mechanochemical transducers requiring no externally coupled energy sources. Another characteristic is the complete integration of the cell-based actuator that encapsulates its energy source within a cellular, aqueous environment. C2C12

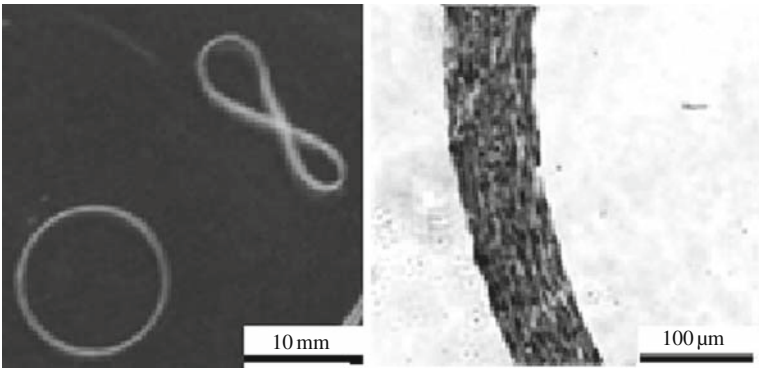

Fig. 4 C2C12 cell ring. *Left*: overview of a cell ring. *Right*: histological examination of fabricated C2C12 cell ring. Representative bright-field micrograph of hematoxylin/eosin-stained cross-sections of C2C12 cell ring

cell-based actuators may possess these characteristics, and, in the present study, we fabricated 3D constructs (cell sheet and cell ring) of C2C12 cells for the application to bio-actuator.

In this study, we showed that C2C12 cell sheets drastically shrank within a day (Fig. 3 and Table 1), which may be a specific feature of C2C12 myoblast cells because shrinking of NIH3T3 cell sheets was much slower than that of C2C12 cell sheets (data not shown). This feature would be a problem to fabricate bio-actuators, because the fabricated 3D constructs can not maintain their configuration. Since the end of muscular tissues attaches onto bone via tendon and myofibers in muscle receive a tensile force in vivo, the fabricated C2C12 cell constructs should be bound to a tendon-like structure even in vitro.

On the other hand, when a plug silicone was positioned at the center of a well, the cell sheet drastically shrank and the cells formed a ring-like structure by gathering around the plug silicone (C2C12 cell ring, Fig. 4). Histological study of the ring-like structure revealed that the cells were oriented in the direction of circumference, suggesting that cells received a tensile force and a plug silicone played a tendon-like role. Because some researchers reported that the differentiation of myoblast cells was promoted by the tension generates within the cell structure [5], this procedure by the Mag-TE technique may provide a novel strategy to fabricate bio-actuators using C2C12 cells.

References

1. Ito, A., Hayashida, M., Honda, H., Hata, K., Kagami, H., Ueda, M., and Kobayashi, T. (2004) Construction and harvest of multilayered keratinocyte sheets using magnetite nanoparticles and magnetic force. *Tissue Eng*. **10**(5–6): 873–880.
2. Ito, A., Shinkai, M., Honda, H., and Kobayashi, T. (2005) Medical application of functionalized magnetic nanoparticles. *J. Biosci. Bioeng.* **100**(1): 1–11.

3. Ito, A., Jitsunobu, H., Kawabe, Y., and Kamihira, M. (2007) Construction of heterotypic cell sheets by magnetic force-based 3-D coculture of HepG2 and NIH3T3 cells. *J. Biosci. Bioeng.***104**(5): 371–378.
4. Morishima, K., Tanaka, Y., Ebara, M., Shimizu, T., Yamato, M., Kikuchi, A., Okano, T., and Kitamori, T. (2006) Demonstration of a bio-microactuator powered by cultured cardiomyocytes coupled to hydrogel micropillars. *Sensor Actuator B Chem.* **119**: 345–350.
5. Okano, T., and Matsuda, T. (1998) Tissue engineered skeletal muscle: preparation of highly oriented hybrid muscular tissues, Cell Transplant, 7: 71–82.
6. Shinkai, M., Yanase, M., Honda, H., Wakabayashi, T., Yoshida, J., and Kobayashi, T. (1996) Intracellular hyperthermia for cancer using magnetite cationic liposomes: in vitro study. *Jpn. J. Cancer Res.* **87**: 1179–1183.
7. Tanaka, Y., Morishima, K., Shimizu, T., Kikuchi, A., Yamato, M., Okano, T., and Kitamori, T. (2006) An actuated pump on-chip powered by cultured cardiomyocytes. *Lab. Chip* **6**: 362–368.

Fabrication of Skeletal Muscle Tissue from C2C12 Myoblast Cell Towards the Use as Bio-Actuator

Hideaki Fujita, Kazunori Shimizu, and Eiji Nagamori

1 Introduction

Muscle develops active tension upon stimulation and is the only actuator in animals. Muscles work at relatively low temperature compared to combustion engine and are able to use glucose as energy source and considered to be highly efficient actuator. Thus, muscle can be decent candidate for bio-based actuators. Several studies report the use of cardiac cells as actuators and succeeded in producing sufficient force to power micro-devices [1, 2]. Because cardiac cells contract spontaneously, use of skeletal muscle will be more suitable for the use as bio-actuators. Fabrication of skeletal muscle tissue from established cell line is difficult due to the low cell-cell attachment, need of differentiation, and requirement of highly oriented myotubes. Recently, Dennis et al. reported the fabrication of muscle tissue from primary skeletal muscle cells and termed the construct "myooid" [3]. They reported that on their attempt to fabricate muscle tissue from mono-culture of murine myoblast cell line C2C12, muscle tissue could not be formed and only when fibroblast cell line 10T1/2 was co-cultured with C2C12, muscle tissue was formed [4]. Their myooid produced only ∼2.5% of active tension compared to the in vivo skeletal muscle, which may result from the presence of fibroblast in the myooid construct. In this study, we report the fabrication of myooid from mono-culture of C2C12 by the use of serum free medium AIM-V. Fabricated myooid produced active tension upon electric pulse stimulation and more active tension was generated compared with myooid formed by co-culture of C2C12 and 10T1/2, which demonstrates the increased capability as bio-actuators.

E. Nagamori (✉)
Toyota Central R&D Labs. Inc., Aichi 480-1192, Japan
e-mail: nagamori@mosk.tytlabs.co.jp

M. Kamihira et al. (eds.), *Animal Cell Technology: Basic & Applied Aspects*, Animal Cell Technology: Basic & Applied Aspects 16, DOI 10.1007/978-90-481-3892-0_29,

2 Materials and Methods

2.1 Cell Culture

C2C12 was purchased from Riken Cell Bank (Riken, Saitama, Japan) and maintained in GM (DMEM supplemented with 10% fetal bovine serum and antibiotics). C2C12 was differentiated in DM (DMEM supplemented with 2% horse serum and antibiotics) or in AIM-V (Invitrogen, Carlsbad, CA). Medium was exchanged daily.

2.2 Preparation of Laminin Coated PDMS Dish

Myooid was formed by culturing C2C12 on polydimethylsiloxane (PDMS) which was coated with laminin as reported previously [4]. Procedure for preparation of laminin coated PDMS dish is illustrated in Fig. 1. First, 2 g of PDMS was poured on 35 mm petri dish and polymerized at 50°C and cured for 2 weeks. Then, PBS containing 2 $\mu g/cm^2$ of laminin was poured on PDMS coated petri dish and air dried for 8 h. Laminin coated silk suture was prepared by immersing ~3 mm of silk suture in PBS containing 50 $\mu g/ml$ laminin for 1 h. Salt precipitation on PDMS coated dish was washed with PBS and laminin coated silk suture was pinned at 2 places 18 mm apart. Then GM containing 10 $\mu g/ml$ of laminin was poured and incubated for 1 week at 37°C.

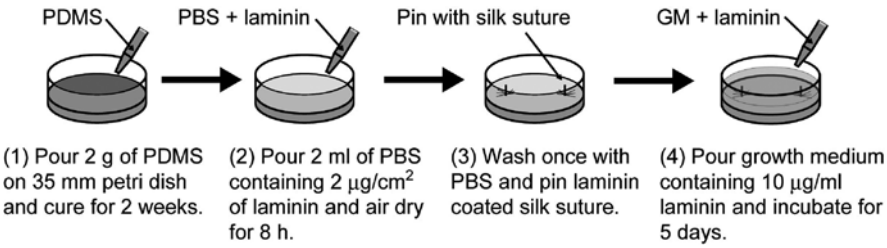

Fig. 1 Prepatation of laminin coated PDMS dish

3 Results

3.1 Differentiation of C2C12 by AIM-V

C2C12 was seeded on laminin coated PDMS dish at density of 2×10^4 cells/dish in GM and cultured in GM until confluence. Cells reached confluence 3 days after seeding. Then, cells were differentiated in DM or AIM-V. After 3 days in AIM-V, cells fused and formed multinucleated myotubes as reported previously [5]. Figure 2

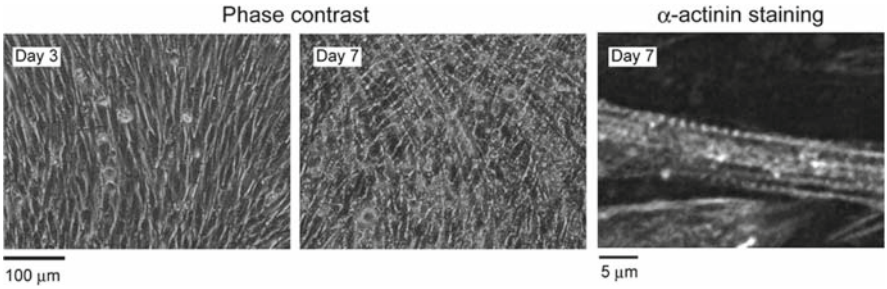

Fig. 2 Differentiation of C2C12 by AIM-V

shows phase contrast image of C2C12 differentiated by AIM-V, which show formation of myotubes after 1 week of differentiation (Fig. 2). Immuno-fluorescent microscopy revealed the presence of sarcomere structure (Fig. 2), indicating that myotubes formed by AIM-V possess contractile capability. Western blot analysis shows that myogenic transcription factor myogenin increased 3 days after differentiation, followed by increase in the amount of myosin heavy chain and myosin light chain both by DM and AIM-V (Fig. 5A). Amount of tropomyosin also increased slightly after differentiation. These results indicate that although differentiation is weaker compared to DM, AIM-V is capable of differentiating C2C12.

We have also evaluated the change in the amount of glucose and lactate in medium during cultivation in DM and AIM-V (Fig. 3). Amount of glucose decreased linearly in DM and AIM-V, and rate of glucose consumption did not change significantly. Amount of lactate in medium increased linearly and change was almost identical in DM and AIM-V.

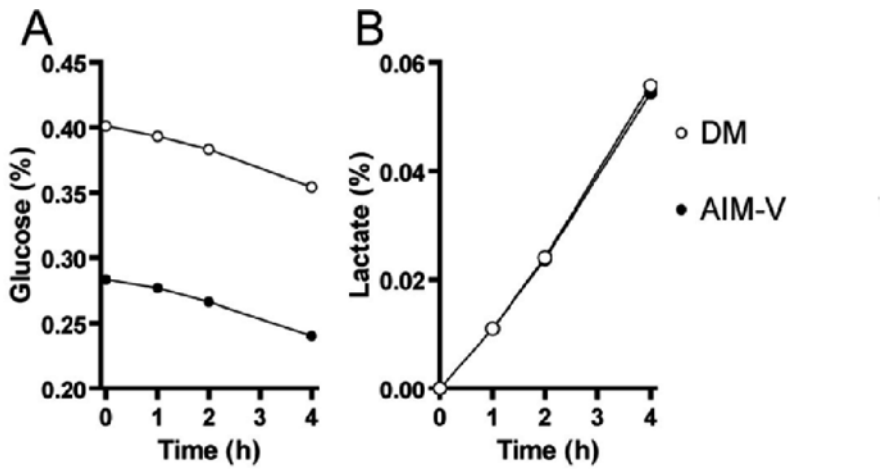

Fig. 3 Change in the amount of glucose (**a**) and lacate (**b**) in medium

3.2 Formation of Myooid by AIM-V

After 5–7 days of differentiation in DM and AIM-V, C2C12 started to dissociate from culture surface probably because of the de-lamination of the PDMS surface. When C2C12 was differentiated by DM, C2C12 dissociated in a patchy manner and did not form cylindrical construct, consistent with the previous report [4]. On the other hand, when C2C12 was differentiated in AIM-V, cells started to dissociate from PDMS surface in sheet-like manner and formed cylindrical construct after 1 week of cultivation (Fig. 4).

To evaluate the differentiation status of C2C12 by AIM-V, we performed Western blot analysis (Fig. 5A) and found that although C2C12 differentiate and express muscle proteins when differentiated by AIM-V, amount of muscle proteins decreased rapidly after formation of myooid (Fig. 5B). When medium was exchanged to DM after formation of myooid, muscle protein expression increased showing that AIM-V is not sufficient to maintain differentiation. Thus, we fixed our protocol to exchange the medium from AIM-V to DM just after the formation of myooid.

3.3 Active Tension Generation of Myooid

To evaluate the tension generation capability of myooid formed by AIM-V, we measured active tension generation by electric pulse stimulation. Myooid formed by AIM-V and cultured in DM for 1 week generated active tension when 1 V/mm, 10 ms duration electric pulse was applied (Fig. 6A). When myooid was activated by

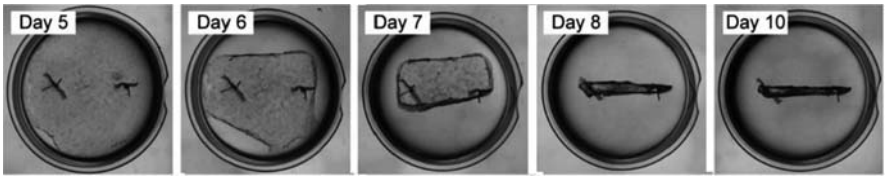

Fig. 4 Formation of myooid by AIM-V

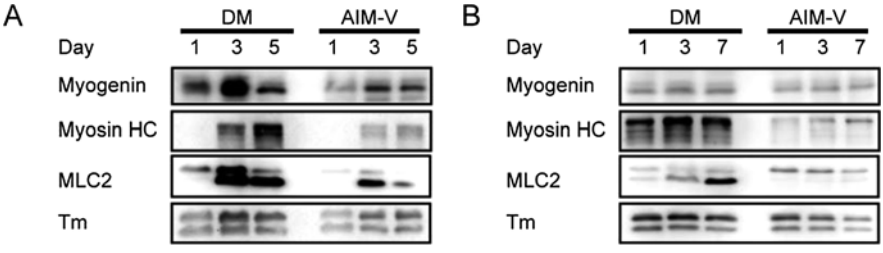

Fig. 5 Western blot analysis of C2C12 in (**a**) normal 2D culture, and (**b**) myooid

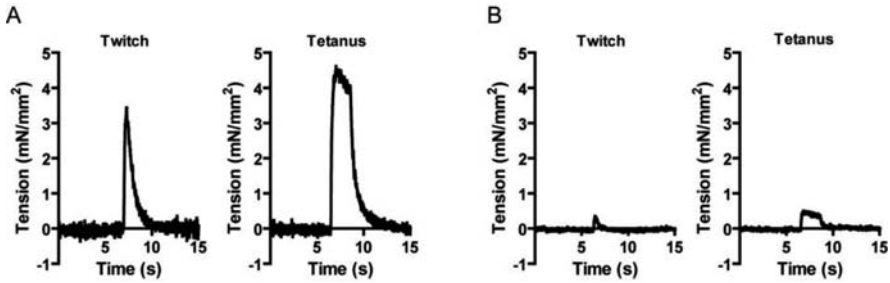

Fig. 6 Active tension generation of myooid cultured in (**a**) DM, and (**b**) AIM-V

50 Hz, 10 ms tetanus stimulation for 2 s, larger active tension was generated which is common characteristic of striated muscle. Myooid formed and cultured in AIM-V also generated active tension when stimulated with electric pulse, but amount of tension generation was smaller than that of myooid cultured in DM (Fig. 6b). These results indicate that change of medium to DM after formation of myooid is necessary to maintain contractile function of C2C12.

3.4 Passive Tension Generation of Myooid

Next we examined the passive property of myooid formed by AIM-V. Figure 7 shows increase in passive tension when myooid was subjected to stretch at constant speed of 0.5 mm/s to 15% of initial length. Both myooid cultured in DM and AIM-V generated passive tension when myooid was stretched, but passive tension was larger in myooid cultured in AIM-V than that of myooid cultured in DM. This result indicates that myooid cultured in AIM-V is rich in connective tissue than that cultured in DM.

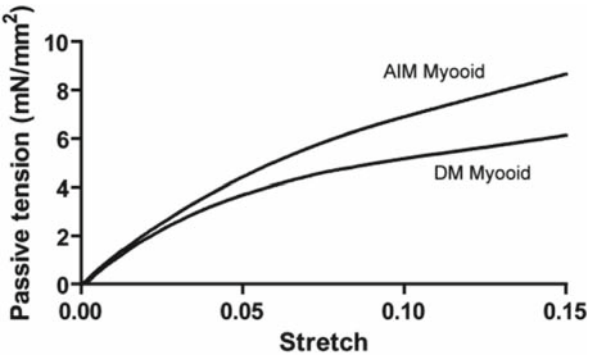

Fig. 7 Passive tension generation upon stretch at 0.5 mm/s

4 Discussion

We have succeeded in fabricating muscle tissue construct using mono-culture of murine myogenic cell line C2C12 by enhancing cell-cell attachment using AIM-V. It seems likely that AIM-V enhances production of extracellular matrix proteins such as collagen because we observed that medium became more viscous after cultivation when cultured in AIM-V. Although myooid was formed by AIM-V, continuous cultivation of myooid by AIM-V resulted in muscle tissue with less muscle protein and small active tension. By exchanging the medium from AIM-V to DM after the formation of myooid, muscle tissue with active tension generation capability was fabricated. Myooid formed from mono-culture of C2C12 produced 1.4× active tension than that formed from co-culture of C2C12 and 10T1/2 [4]. Thus, myooid formed using AIM-V will be more useful as bio-actuator than those previously reported.

Passive tension of myooid cultured in DM was smaller than that of myooid cultured in AIM-V. Smaller passive tension indicates that myooid cultured in DM maybe mechanically weaker than that cultured in AIM-V. On the other hand, smaller passive tension may be beneficial in fabricating bio-based machines because smaller passive tension will result in longer working stroke when two or more myooid were combined to power machines.

Recently several bio-based actuators were designed that use motor proteins as power source [6, 7], but because molecular motors are basically "On" at all times when ATP is present, control of the movement is difficult. In addition, ATP and molecular motor must be obtained before the use. Muscle cells intrinsically possess excitation-contraction mechanisms as well as metabolic function which can produce ATP from glucose, regeneration of motor proteins within the cell, and tissue repairing capability from myoblasts. Furthermore, myotubes are composed from massive amount of molecular motors, enabling higher output than using molecular motor itself. Thus, skeletal muscle tissue fabricated from C2C12 cell line will be ideal material for bio-actuators. This report will provide simple method for production of electrically controllable skeletal muscle based bio-actuator.

References

1. Xi, J., Schmidt, J.J., and Montemagno, C.D. (2005) Self-assembled microdevices driven by muscle. *Nat. Mater*. 4(2): 180–184.
2. Tanaka, Y., Morishima, K., Shimizu, T., Kikuchi, A., Yamato, M., Okano, T., et al. (2006) An actuated pump on-chip powered by cultured cardiomyocytes. *Lab. Chip*. 6(3): 362–368.
3. Dennis, R.G., and Kosnik, P.E., 2nd. (2000) Excitability and isometric contractile properties of mammalian skeletal muscle constructs engineered in vitro. *In Vitro Cell Dev. Biol. Anim*. 36(5): 327–335.
4. Dennis, R.G., Kosnik, P.E., 2nd, Gilbert, M.E., and Faulkner, J.A. (2001) Excitability and contractility of skeletal muscle engineered from primary cultures and cell lines. *Am. J. Physiol. Cell Physiol*. 280(2): C288–295.
5. Lawson, M.A., and Purslow, P.P. (2000) Differentiation of myoblasts in serum-free media: Effects of modified media are cell line-specific. *Cells Tissues Organs* 167(2–3): 130–137.

6. Soong, R.K., Bachand, G.D., Neves, H.P., Olkhovets, A.G., Craighead, H.G., and Montemagno, C.D. (2000) Powering an inorganic nanodevice with a biomolecular motor. *Science* 290(5496): 1555–1558.
7. Hiratsuka, Y., Tada, T., Oiwa, K., Kanayama, T., and Uyeda, T.Q. (2001) Controlling the direction of kinesin-driven microtubule movements along microlithographic tracks. *Biophys. J*. 81(3): 1555–1561.

Retroviral Vectors Pseudotyped with Chimeric Vesicular Stomatitis Virus Glycoprotein for Antibody-Dependent Gene Transduction

Yujiro Kameyama, Yoshinori Kawabe, Akira Ito, and Masamichi Kamihira

1 Introduction

Gene delivery technology has been essential for biotechnology since they have been used for establishing recombinant animal cell lines for the production of pharmaceutical agents, for the generation of transgenic animals, and for gene therapy. Among gene delivery procedures, retroviral vectors (including lentiviral vectors) derived from RNA viruses have been used widely when stable gene transfer is required both in vitro and in vivo, because of their ability to integrate the gene of interest into the genome of host cells including non-dividing cells [2].

Since the host range specificity of retroviral vectors is mainly determined by the envelope proteins, it can be altered by the substitution of these proteins. For example, viral vectors pseudotyped with ecotropic envelope protein can infect only rodent cells, whereas viral vectors pseudotyped with amphotropic envelope protein can infect most other mammalian cells. Recently, retroviral vectors pseudotyped with vesicular stomatitis virus glycoprotein G (VSV-G) have been used widely due to their broad host range specificity. These vectors can infect not only the mammalian cells, but also the non-mammalian cells such as the insect, avian and fish cells regardless of species (pantropic) because the receptors for VSV-G are phospholipids which are observed ubiquitously in membrane lipids. In addition, pseudotyping with VSV-G improves the mechanical strength of viral vectors, and viral titers can be increased up to 1000-fold by ultracentrifugation [3].

However, the in vivo use of pantropic viral vectors is limited due to the low transduction efficiency of target cells and possible side-effects. To overcome these problems, pantropic viral vectors could be modified by pseudotyping with chimeric envelopes [6, 9, 10, 11]. Despite the advantages of VSV-G, no studies have succeeded so far in modifying this protein for pseudotyping of viral vectors, whilst still

Y. Kawabe (✉)
Department of Chemical Engineering, Faculty of Engineering, Kyushu University,
744 Motooka, Nishi-ku, Fukuoka 819-0395, Japan
e-mail: kawabe@chem-eng.kyushu-u.ac.jp

M. Kamihira et al. (eds.), *Animal Cell Technology: Basic & Applied Aspects*, Animal Cell Technology: Basic & Applied Aspects 16, DOI 10.1007/978-90-481-3892-0_30,

satisfying the requirements for both efficient production of infectious viral particles and alteration of host specificity.

In the present study, VSV-G protein has been engineered genetically using the duplicated Z domain of Staphylococcal protein A, which can bind specifically to the Fc region of immunoglobulin G (IgG). Gammaretroviral (based on mouse stem cell virus, MSCV) and lentiviral (based on human immunodeficiency virus type 1, HIV-1) vectors pseudotyped with the VSV-G chimeric proteins were produced to achieve antibody-dependent infection by viral vectors.

2 Materials and Methods

2.1 Plasmid Construction

An expression vector (pZZ-VSV-G) for the chimeric VSV-G was constructed as described in our previous report [7]. The schematic drawing of the structure of plasmids is shown in Fig. 1.

2.2 Production of Viral Vectors

GP293-lacZ [8] cells were transfected with the VSV-G expression plasmids (pVSV-G, pZZ-VSV-G, or pZZ-VSV-G + pVSV-G) using lipofection reagent (Lipofectamine 2000; Invitrogen) to produce gammaretroviral vectors for the expression of bacterial β-garactosidase. Lentiviral vectors for the expression of enhanced green fluorescent protein (EGFP) were produced using a kit (ViraPower lentiviral expression systems; Invitrogen) and the VSV-G expression plasmids.

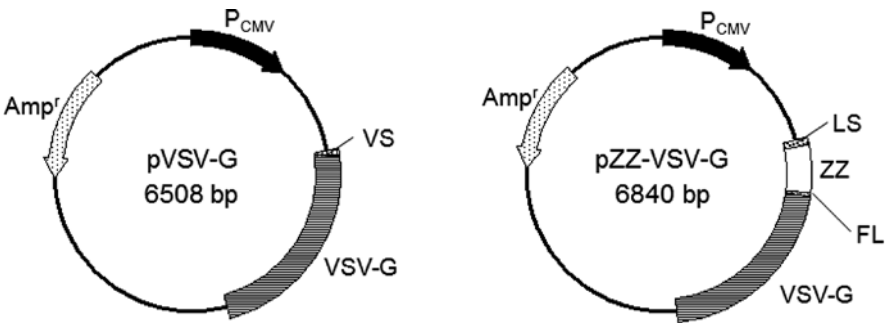

Fig. 1 Schematic drawing of pVSV-G (**a**) and pZZ-VSV-G (**b**) VS: secretion signal derived from VSV-G, LS: secretion signal derived from lysozyme, FL: flexible linker

2.3 Detection of Viral RNA by Reverse Transcription (RT)-PCR

The amount of viral particles was semi-quantified by amplifying virus-specific sequence (packaging signal sequence) by RT-PCR.

2.4 Western Blot Analysis for ZZ Fragments of Viral Particles

Western blotting was performed for the detection of ZZ fragments incorporated into the viral vectors using POD-conjugated rabbit antibodies.

2.5 Antibody-Dependent Infection of Viral Vectors

To confirm the antibody-dependent infectivity, the assay was performed as the cell transfection array assay using human IgG coated 96-well plates. The procedure is shown in Fig. 2. The 96-well plates coated with BSA were used as a negative control.

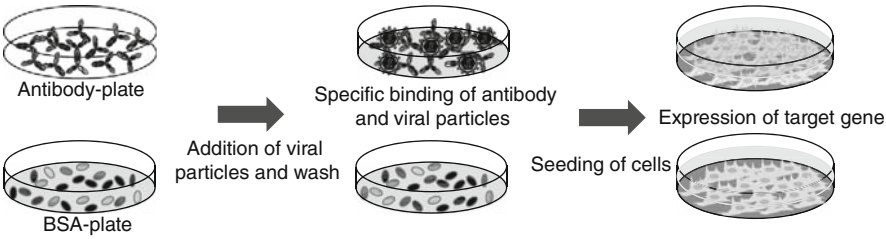

Fig. 2 Procedure of antibody dependent infection of viral vectors

3 Results

To confirm the expression of ZZ-VSV-G on the surface of cells, immunostaining of cells transfected with the expression vector plasmids was performed using anti-VSV antibodies conjugated with FITC (data not shown). Although cells transfected with ZZ-VSV-G plasmid alone were stained strongly, cell fusion was not observed. The strong staining with the anti-VSV antibodies seemed to be due to the interaction between ZZ fragment and Fc region of antibodies, indicating that ZZ-VSV-G protein was expressed on the cell surface. The staining intensity of cells co-transfected with VSV-G and ZZ-VSV-G plasmids was stronger than that of cells expressing ZZ-VSV-G alone. These results suggest that viral vectors pseudotyped with ZZ-VSV-G require native VSV-G for the efficient production of functional viral particles. Next,

Table 1 Productivity of gammaretroviral and lentiviral vectors

	Density of bands amplified by RT-PCR		
	pVSV-G	pZZ-VSV-G	pZZ-VSV-G + pVSV-G
Gammaretroviral vector	46212.421	35273.886	49986.271
Lentiviral vector	27030.409	14390.338	20465.702

RT-PCR was performed to evaluate the productivity of gammaretroviral and lentiviral vectors. The band density was estimated using an imaging software (Table 1). Although the band density was lower for the viral particles expressing ZZ-VSV-G alone, the band density of the viral particles co-expressing ZZ-VSV-G and VSV-G was comparable to that of VSV-G alone, indicating that VSV-G promoted virus production.

Western blotting was performed for the detection of ZZ fragments incorporated into the gammaretroviral and lentiviral vectors as the envelope. Bands corresponding to the expected molecular weight of ZZ-VSV-G were detected for ZZ-VSV-G and ZZ-VSV-G+VSV-G vectors (Fig. 3). The higher amount of ZZ-VSV-G proteins was detected for the samples of ZZ-VSV-G+VSV-G vectors.

Finally, we evaluated infectivity and antibody-binding activity of viral particles using plates coated with human IgG or BSA for gammaretroviral (Table 2a) and lentiviral vectors (Table 2b). When plates were coated with BSA as a negative control, the infectivity of the vectors was negligible in all samples. Although the viral vectors pseudotyped with native VSV-G or ZZ-VSV-G alone also exhibited very

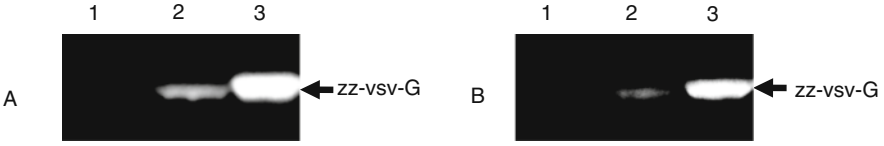

Fig. 3 Western blot analysis for ZZ fragment of gammaretroviral (**a**) and lentiviral (**b**) particles. Lane1, pVSV-G; lane2, pZZ-VSV-G; lane3, pZZ-VSV-G + pVSV-G

Table 2a Antibody-dependent. Infectivity of gammaretroviral vectors

		Viral titer (IU/well)			
Cell species		pVSV-G	pZZ-VSV-G	pZZ-VSV-G + pVSV-G (1:1)	pZZ-VSV-G + pVSV-G (1:5)
	IgG+	5.67	0	746	792
Neuro2a	BSA+	27.3	0	8.33	9.67
	Normal	1.86×10^5	0	5.21×10^4	8.62×10^4
COS7	IgG+	54.7	1.33	1330	1000
	BSA+	44	0.333	15.0	22.7
	Normal	4.70×10^5	0	8.31×10^4	1.11×10^5

Table 2b Antibody-dependent. Infectivity of lentiviral vectors

Cell species		pVSV-G	pZZ-VSV-G	pZZ-VSV-G + pVSV-G (1:1)	pZZ-VSV-G + pVSV-G (1:5)
HeLa	IgG+	21.7	4.00	168	119
	BSA+	3.67	0	8.00	3.67
Normal	1.00×10^5	1.40×10^2	3.40×10^4	5.70×10^4	
HaCaT	IgG+	0	0	41.7	57.0
	BSA+	0	0	2.00	1.67
Normal	4.15×10^3	0	1.06×10^3	2.93×10^3	

low or negligible infectivity in this assay, viral vectors pseudotyped with both ZZ-VSV-G and VSV-G exhibited infectivity only on the IgG-coated plates. Although the viral vectors pseudotyped with native VSV-G or ZZ-VSV-G alone also exhibited very low or negligible infectivity in this assay, viral vectors pseudotyped with both ZZ-VSV-G and VSV-G exhibited infectivity only on the IgG-coated plates.

4 Discussion

We constructed a genetically engineered VSV-G protein fused with a duplicated Z domain which can bind specifically to the Fc region of IgG. Although modified VSV-G often failed to express on the cell surface [11, 12], the expression of ZZ-VSV-G proteins was confirmed by the immunostaining, indicating that native VSV-G promoted the expression of ZZ-VSV-G on cell surface. The productivity of viral particles pseudotyped with ZZ-VSV-G alone was decreased, being consistent with the previous report [5]. However, the productivity of viral particles pseudotyped with ZZ-VSV-G increased by co-expressing with native VSV-G (Table 1). The incorporation of ZZ-VSV-G proteins into viral particles was confirmed by the western blot analysis for detection of ZZ fragments (Fig. 3). These results showed that the production of viral vectors pseudotyped with ZZ-VSV-G was promoted by the expression of native VSV-G, as shown in Table 1. Furthermore, the infectivity of viral vectors pseudotyped with ZZ-VSV-G alone was very low, even in the presence of antibodies. The similar results were reported previously [4, 5]. The infectivity of viral vectors pseudotyped with modified VSV-G was often lost due to deficiencies in virus production and/or the fusogenic ability of VSV-G. In order to induce fusogenic ability and improve infectivity, native VSV-G may be added to pseudotyped viral vectors using modified VSV-G, although non-specific infectivity is also induced. For gammaretroviral vectors pseudotyped with ZZ-VSV-G and VSV-G, the viral titer enhanced 470- and 140-fold for Neuro2a and COS7, respectively, compared with native VSV-G alone. In spite of the different procedure of viral production, lentiviral vectors pseudotyped with ZZ-VSV-G and VSV-G also exhibited the antibody-dependent infectivity (Table 2a and b).

In conclusion, we succeeded in the production of viral vectors with antibody-binding activity by using ZZ-VSV-G. The ZZ-VSV-G pseudotyped vectors exhibited antibody-dependent infectivity by the addition of native VSV-G. This viral vector system may be useful for genetic transduction of cells expressing specific proteins on their surface, and for screening of antibodies specific for cell surface receptors.

References

1. Aires da Silva, F., Costa, M.J., Corte-Real, S., and Goncalves, J. (2005) Cell type-specific targeting with sindbis pseudotyped lentiviral vectors displaying anti-CCR5 single-chain antibodies. *Hum. Gene Ther*. **16**: 223–234.
2. Baum, C., Schambach, A., Bohne, J., and Galla, M. (2006) Retrovirus vectors: Toward the plentivirus? *Mol. Ther*. **13**: 1050–1063
3. Burns, J.C., Friedmann, T., Driever, W., Burrascano, M., and Yee, J.K. (1993) Vesicular stomatitis virus G glycoprotein pseudotyped retroviral vectors: concentration to very high titer and gene transfer into mammalian and no mammalian cells. *Proc. Natl. Acad. Sci. USA* **90**: 8033–8037.
4. Dreja, H., and Piechaczyk, M. (2006) The effects of N-terminal insertion into VSV-G of an scFv peptide. *Virol. J*. **3**: 69–76.
5. Guibinga, G.H., Hall, F.L., Gordon, E.M., Ruoslahti, E., and Friedmann, T. (2004) Ligand-modofied vesicular stomatitis virus glycoprotein displays a temperature-sensitive intracellular trafficking and virus assembly phenotype. *Mol. Ther*. **9**: 76–84.
6. Hatziioannou, T., Delahaye, E., Martin, F., Russell, S.J., and Cosset, F.L. (1999) Retroviral display of functional binding domains fused to the amino terminus of influenza hemaggulutinin. *Hum. Gene Ther*. **10**: 1533–1544.
7. Kameyama, Y., Kawabe, Y., Ito, A., and Kamihira, M. (2008) Antibody-dependent gene transduction using gammaretroviral and lentiviral vectors pseudotyped with chimeric vesicular stomatitis virus glycoprotein. *J. Virol. Methods* **153**: 49–54.
8. Kamihira, M., Ono, K., Esaka, K., Nishijima, K., Kigaku, R., Komatsu, H., Yamashita, T., Kyogoku, K., Iijima, S. (2005) High-level expression of single-chain Fv-Fc fusion protein in serum and egg white of genetically manipulated chickens by using a retroviral vector. *J. Virol*. **79**: 10864–10874.
9. Morizono, K., Bristol, G., Xie, Y.M., Kung, S.K., and Chen, I.S. (2001) Antibody-directed targeting of retroviral vectors via cell surface antigens. *J. Virol*. **75**: 8016–8020.
10. Morizono, K., Xie, Y., Ringpis, G.E., Johnson, M., Nassanian, H., Lee, B., Wu, L., and Chen, I.S. (2005) Lentiviral vector retargeting to P-glycoprotein on metastatic melanoma through intravenous injection. *Nat. Med*. **11**: 346–352.
11. Schlehuber, L.D., and Rose, J.K. (2004) Prediction and identification of a permissive epitope insertion site in the vesicular stomatitis virus glycoprotein. *J. Virol*. **78**: 5079–5087.
12. Yu, J.H., and Schaffer, D.V. (2006) Selection of novel vesicular stomatitis virus glycoprotein variants from a peptide insertion library for enhanced purification of retroviral and lentiviral vectors. *J. Virol*. **80**: 3285–3292.

Improvement of CPP-RBD for siRNA Delivery

Rina Kuwabara, Tamaki Endoh, Masahiko Sisido, and Takashi Ohtsuki

1 Introduction

Small interfering RNA (siRNA) containing sequence homologous to specific gene causes sequence-specific gene silencing, which is termed RNA interference (RNAi). RNAi was first discovered in *Caenorhabditis elegans*, and its applicability to mammals was recently discovered. RNAi offers one of the most attractive methods for therapy of genetic diseases such as cancer and viral infections. At present, to deliver the siRNA into cells, virus vectors or polymers are used as siRNA carrier. However, these carriers are concerned about integration of viral RNA or high toxicity for cells. It is necessary to deliver siRNA into the cells safely and efficiently in order to apply the RNAi strategy for therapy.

Recently, we reported siRNA delivery and photo-induced RNAi by using fluorescently labeled carrier protein [1]. It consists of Alexa546 labeled cell permeable RNA binding protein, a fusion protein of HIV-1 Tat peptide, one of cell-penetrating peptides (CPP), and U1A RNA-binding domain (RBD). The constructed TatU1A-Alexa internalized into cells together with interacted siRNA, which contains U1A binding sequence, through endocytotic pathway. Then, it induced RNAi-mediated gene silencing without cytotoxicity caused by cytosolic diffusion in response to photostimulation.

In this study, we examined siRNA delivery and photo-induced RNAi using several CPP-RBPs to improve the RNAi effect. The RBP part in TatU1A was replaced with other RBP [RBD of drosophila Sex-lethal protein (Sxl) [2] or bacteriophage λN peptide (λNp) [3] derived from bacteriophage λN protein] to make Tat-RBP variants (TatSxl and Tatλ Np). Sxl recognizes a single-stranded RNA (5'-GUUGUUUUUU(U)-3'). λNp recognizes an RNA hairpin loop (5'-GCCCUGAAAAAGGGC-3'). Purified proteins were labeled with Alexa546 to make TatRBP-Alexa variants (TatSxl-Alexa and Tatλ Np-Alexa) for photo-induced RNAi.

R. Kuwabara (✉)
Graduate School of Natural Science and Technology, Okayama University, Okayama, Japan
e-mail: gen20908@cc.okayama-u.ac.jp

M. Kamihira et al. (eds.), *Animal Cell Technology: Basic & Applied Aspects*, Animal Cell Technology: Basic & Applied Aspects 16, DOI 10.1007/978-90-481-3892-0_31,

siRNA containing a short 3'-extension that binds to the Sxl (*Sxl*siRNA) or λNp (λ*Np*siRNA) was also prepared as a cargo partner. Constructions of protein/RNA complexes (TatSxl/*Sxl*siRNA and Tatλ Np/λ*Np*siRNA) were confirmed by gel mobility shift assay. Then, fluorescent labeled siRNAs were applied to the cells with TatRBP-Alexa variants to evaluate sequence specific delivery of corresponding siRNA. Finally, to induce the RNAi mediated gene silencing, cells incubated with protein/RNA complex were irradiated by light at 540 nm, which excites the Alexa546 entrapped in endocytotic compartments.

2 Experiment

2.1 Plasmid Construction

The coding sequence for the Sxl protein was amplified from Drosophila Sxl cDNA clone (Open Biosystems) using the following primers: 5'-CCGCTCGAGTTAGGATCCCTTGCCATGCTCCTCAG-3' and 5'-CGCGCTAGCGGCGCAAGCAACACCAACCTG-3'. Double-stranded DNA encoding λNp was prepared by primer extension using the following primers: 5'-CCGCTCGAGTTAGGATCCAGGGCGGTTAACTGGTTTTGCGCTTACCCCAACCAACAGGGGATTTGCTGCTTTCCATTG-3' and 5'-CGCGCTAGCGGCCTGGATGCACAAACACGCCGCCGCGAACGTCGCGCAGAGAAACAGGCTCAATGGAAAGCAGCAAATCC-3'.

Expression vectors for TatSxl and Tatλ Np, which contains C-terminal Cys for later modification of Alexa546, were constructed by inserting the coding sequence of Sxl or λNp into the Nhe I-Xho I site of previously constructed pET-TatU1A-C [1]. The coding sequences of constructed vectors (pET-TatSxl and pET-Tatλ Np) were confirmed by sequencing analysis with an ABI PRISM 310 genetic analyzer.

2.2 Preparation and Fluorescent Labeling of Protein

BL21(DE3) was transformed with prepared vectors, pET-TatU1A, pET-TatSxl or pET-Tatλ Np, which express Tat-RBP variants with N-terminal His-tags. Protein expression was induced by IPTG (1 mM) at 25°C for 16 h. Cells were harvested by centrifugation, and lysed by sonication in buffer A [50 mM HEPES-KOH (pH 7.5), 150 mM $(NH_4)_2SO_4$, 7 mM $MgCl_2$, 20% glycerol, 7 mM β-mercaptoethanol, and 100 μM phenylmethylsulfonyl fluoride]. Then protein was purified by His-tag purification. Buffer B [50 mM HEPES-KOH (pH 7.5), 1 M NH_4Cl, 10 mM imidazole and 20% glycerol] was used to wash the Ni-NTA column, and Buffer C [50 mM HEPES-KOH (pH 7.5), 100 mM $(NH_4)_2SO_4$, 150 mM imidazole, and 20% glycerol] was used to elute the His-tagged protein. To label the Alexa Fluor 546, eluted proteins were mixed with Alexa Fluor 546 C5 maleimide (Molecular Probes) in Buffer C and incubated at room temperature. The Alexa-modified proteins (TatU1A-Alexa, TatSxl-Alexa, and Tatλ Npepide-Alexa)

were purified by using Centri-Sep spin column (Princeton Separations), which was preliminarily equilibrated with T buffer [20 mM HEPES-KOH (pH 7.4), 115 mM NaCl, 5.4 mM KCl, 1.8 mM $CaCl_2$, 0.8 mM $MgCl_2$, and 13.8 mM glucose]. Concentrations of all Alexa546-labeled proteins were quantified using Protein Assay Kit (Bio-Rad). The labeling efficiency of Alexa546 was calculated from absorbance of Alexa546 (Abs_{556}) measured by ND-1000 Spectorophotometer (NanoDrop), and adjusted to 50% using separately prepared unlabeled proteins in order to compare the difference between Tat-RBP variants.

2.3 Preparation of RNAs

In order to construct a siRNA-type cargo RNAs, antisense and sense strands were dissolved in distilled water at final concentration of 20 μM and annealed by incubation at 90°C for 1 min followed by 60 min-incubation at 37°C. The antisence strand targeting EGFP mRNA was (5'-UGCGCUCCUGGACGUAGCCUU-3'). The sense strands contain 5' short extensions, which bind to respective RBP, to make *U1A*siGFP (5'-GGGCAUUGCACUCCGCCCUCUGGCUACGUCCAGGAGCGCAUU-3'), *Sxl*-siGFP (5'-GGUUGUUUUUUUUCUGGCUACGUCCAGGAGCGCAUU-3') and λ*Np*-siGFP (5'-GGCCCUGAAAAAGGGCCUCUGGCUACGUCCAGGAGCGCAUU-3'). Underlined sequences were RBP binding sequence. FAM-labeled antisense strand was purchased from Japan Bio Services Co., Ltd., and annealed with the sense strands to make FAM-labeled siRNAs.

2.4 Gel Mobility Shift Assay

Purified proteins (0–5 μM) were mixed with 200 nM of FAM-labeled siRNAs in T buffer. After 10-min incubation at 37°C, protein-RNA mixtures were analyzed in 8% native polyacrylamide gels with Gel-Shift buffer (50 mM Tris-HCl [pH 6.8], 10 mM $Mg(OAc)_2$, 65 mM NH_4OAc, 1 mM EDTA) at 4°C. The FAM-labeled siRNAs in the gel were detected by FMBIO III fluorescence image analyzer (Hitachi) using a 488 nm excitation laser and 520 nm emission filter set.

2.5 RNA Delivery and Photoaccelerated Endosomal Escape

For RNA delivery experiments, TatRBP-Alexa variants and cargo RNA were mixed in 50 μL of T buffer and incubated at 37°C for 10 min. Cells in 96-well culture plates were overlaid with the mixture. After 3 h incubation at 37°C, cells were treated twice with culture medium containing RNase for 1 h at 37°C to remove RNAs adhering to the extracellular surface of the cells. The supernatant medium was replaced to normal culture medium (200 μL), and cells were irradiated by light at 540 ± 10 nm passed through 4× objective lens (IX51/IX2-FL-1/MP5Mc/OL-2, Olympus). The

intensity of the irradiated light was 10 J/cm^2 to induce photoaccelerated endosomal escape of the internalized complex.

2.6 Induction of RNAi-mediated EGFP Silencing

One day prior to RNA delivery, dEGFP-CHO cells were plated in a 96-well culture plate at a density of 2×10^4 cells per well. siRNA was delivered into the cells using TatRBP-Alexa variants, and photoaccelerated endosomal escape was induced as described above. The cells were continuously cultured at 37°C. The RNAi-mediated EGFP silencing was evaluated according to previous report [1]. Briefly, at 22 h after the photostimulation, cell proliferation was evaluated by using Cell Counting Kit-8 (Dojindo). Then, the culture medium was replaced with T buffer followed by two washes, and EGFP intensity of adhering dEGFP-CHO cells was directly quantified by FLUOstar OPTIMA (BMG Labtech) using a 480 nm excitation and 540 nm emission filter set. The effect of RNAi-mediated EGFP silencing was normalized by subtracting the values of the wells without cells and dividing by cell proliferation value. Cellular fluorescence images were subsequently obtained using a fluorescence microscope.

3 Results and Discussion

3.1 Gel Mobility Shift Assay

Construction of complex between Tat-RBP and corresponding cargo siRNA was confirmed by gel mobility shift assay. In the case of TatλNp, λ*Np*-siGFP bands became faint by addition of TatλNp, and definite shifted band was not observed (data not shown). Since the similar result was observed when TatλNp was mixed with *Sxl*-siGFP, a negative partner for TatλNp, the results suggested that TatλNp nonspecifically interacted with λ*Np*-siGFP mediated by electrostatic interaction between positive charge of Tat-peptide and negative charge of RNA.

In contrast, in the case of TatSxl, shifted *Sxl*-siGFP was observed when TatSxl was mixed at 2 μM (Fig. 1). Although the shifted band was considerably weak, original RNA band was almost disappeared, and λ*Np*-siGFP, a negative partner for TatSxl, was remained at original position at the same condition (2 μM TatSxl). The results indicated specific interaction between TatSxl and *Sxl*-siGFP. When the TatSxl was mixed at 5 μM, both *Sxl*-siGFP and λ*Np*-siGFP became fainter, and shifted *Sxl*-siRNA was also disappeared. From the results, TatSxl interacted with *Sxl*-siGFP mediated by both specific Sxl interaction and nonspecific electrostatic interaction.

TatSxl was further modified with Alexa546 to compare with TatU1A for inducing RNAi-mediated gene silencing. TatλNp did not indicate specific interaction with λ*Np*-siGFP, which was modified with Alexa546 only low efficiency (data not shown).

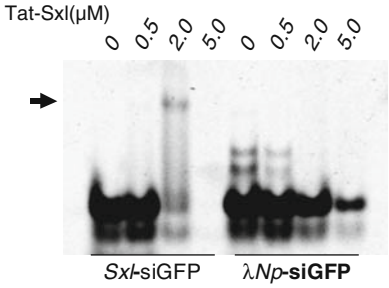

Fig. 1 Construction of TatSxl/*Sxl*-siGFP complex. FAM labeled cargo RNAs, Sxl-siGFP or λ*Np*siRNA, was mixed with varied concentrations of Tat-Sxl, and analyzed in 8% native polyacrylamide gel. FAM signal was imaged by fluorescence image analyzer

3.2 EGFP Silencing by TatRBP/siRNA

TatSxl-Alexa and TatU1A-Alexa (2 μM) were mixed with Sxl-siGFP and U1A-siGFP (200 nM), and applied to dEGFP-CHO cells, which express destabilized EGFP. The EGFP silencing was evaluated according to the EXPERIMET section. Figure 2) shows cellular relative EGFP intensities after 24 h from the photostimulation. In the case of TatU1A-Alexa, moderate EGFP silencing was observed with specific cargo RNA (*U1A*-siGFP), and non specific control RNA (*Sxl*-siGFP and normal siRNA) indicated weaker EGFP silencing. The results indicated preferential delivery of *U1A*-siGFP by TatU1A-Alexa and effective induction of RNAi-mediated gene silencing in response to the photostimulation, which agrees with our previous report [1].

However, in contrast, TatSxl-Alexa did not indicate any EGFP silencing irrespective of cargo RNA, specific *Sxl*-siGFP or non specific *U1A*-siGFP. The efficiency

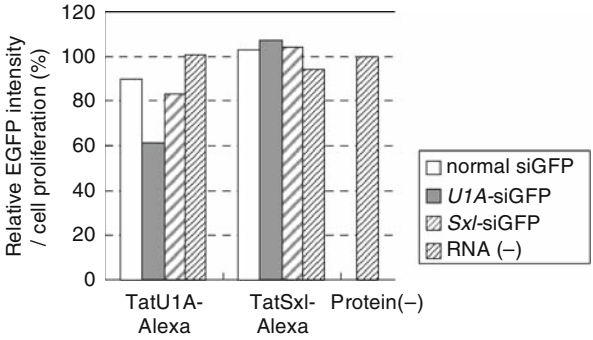

Fig. 2 Photo-induced EGFP silencing by using TatRBD-Alexa variants. siRNA variants (200 nM) were delivered into dEGFP-CHO cells using TatRBD-Alexa variants (2 μM), and photostimulation (10 J/cm^2) was applied. Cellular EGFP intensity was evaluated after 24 h from the photostimulation

of cytosolic diffuse of TatSxl-Alexa in response to the photostimulation was also lower than that of TatU1A-Alexa when Alexa546 signal was observed after photostimulation (data not shown). It suggests that absolute amount of internalized TatSxl-Alexa/*Sxl*-siRNA complex was insufficient to indicate photoaccelerated endosomal escape and induce RNAi-mediated gene silencing at 10 J/cm^2-photostimulation. Higher concentration of TatSxl-Alexa or stronger intensity of photostimulation might be required to induce RNAi.

4 Conclusion

We could delivery siRNA into the cells and induce RNAi by using a cell-penetrating peptide (CPP) and RNA-binding proteins (RBPs). The result indicated that TatU1A as siRNA carrier was superior to that of TatSxl.

At present, we are making CPP-RBP variants to induce RNAi more efficiently.

We expect that siRNA delivery using a cell-penetrating peptide and RNA-binding domain will be a useful method in treating some gene diseases.

References

1. Endoh, T., Sisido, M., and Ohtsuki, T. (2008) Cellular siRNA delivery mediated by a cell-permeant RNA-binding protein and photoinduced RNA interference. *Bioconjug. Chem.* **19**: 1017.
2. Handa, N., Nureki, O., Kurimoto, K., Kim, I., Sakamoto, H., Shimura, Y., Muto, Y. and Yokoyama, S. (1999) Structural basis for recognition of the tra mRNA precursor by the Sex-lethal protein. *Nature* **398**: 579.
3. Scharpf, M., Sticht, H., Schweimer, K., Boehm, M., Hoffmann, S., and Rosch, P. (2000) Antitermination in bacteriophage lambda. The structure of the N36 peptide-boxB RNA complex. *Eur. J. Biochem.* **267**: 2397.

Production of Recombinant Human EPO and EPO/Fc Fusion Proteins by Chinese Hamster Ovary Cells

Carlos Alberto Penno, Yoshinori Kawabe, Akira Ito, and Masamichi Kamihira

1 Introduction

Recombinant human erythropoietin (hEpo), the best-selling single drug in the US biotech drug market accounting for $10 billion sales in 2006, is the most successful therapeutic agent empowered by the advent of recombinant DNA technology [1, 2]. hEpo is a glycoprotein hormone produced mainly by kidney cells whose production is stimulated by a reduction in the oxygen content into renal circulation [3]. Its mechanism of action is based on the proliferation of erythroid progenitors in the bone marrow, resulting in replication and maturation towards functional erythrocytes [4, 5]. hEpo has widely been used to treat chronic kidney disease, anemia of cancer and anemia associated with chemotherapy [6, 7]. Carbohydrates attached to hEpo molecule have a central role modulating its in vivo activity, particularly prolonging its serum half-life [8]. In fact, a glyco-engineered version of hEpo trade name Darboepoetin® presenting three-fold longer half-life enables dosing frequency reduction [8]. Paradoxically, sialic acid carbohydrates play an inhibitory role on hEpo-receptor binding [8].

Presently, the redesign of proteins prolonging their serum half-lives is a main goal in pharmaceutical industries, because their uncomfortable and painful administration is a major hindrance placing a burden in patients and caregivers [9]. There are numerous strategies for therapeutics redesign which include PEGylation, Fc-fusion, incorporation of *N*-linked oligosaccharide motifs and albumin-fusion [9]. In the present study, we succeeded to establish CHO cell lines producing hEpo and hEpo/Fc by retroviral vector transduction. Moreover, the productivities of the proteins were enhanced with a sequence derived from the woodchuck hepatitis virus post-transcriptional regulatory element (WPRE) inserted downstream of the target genes. hEpo and hEpo/Fc produced were biochemically characterized and their in vitro activities were also assessed.

Y. Kawabe (✉)
Department of Chemical Engineering, Faculty of Engineering, Kyushu University, 744 Motooka, Nishi-ku, Fukuoka 819–0395, Japan
e-mail: kawabe@chem-eng.kyushu-u.ac.jp

M. Kamihira et al. (eds.), *Animal Cell Technology: Basic & Applied Aspects*, Animal Cell Technology: Basic & Applied Aspects 16, DOI 10.1007/978-90-481-3892-0_32,

2 Materials and Methods

Plasmid construction. Totally four retroviral plasmids were constructed according to Fig. 1. The construction of the plasmids pMSCV/GΔAEpo and pMSCV/GΔAEpoW are described in our previous report [10]. A gene for Fc fragment derived from human IgG2 was amplified from pMSCV/GΔAscFv-Fc2 [11] and fused to hEpo sequence in either plasmid through the hinge region.

Transient protein production. The effect of WPRE insertion into the vectors on protein production was investigated by the transient transfection (Lipofectamine 2000; Invitrogen) of plasmids into CHO cells. At 24 h post-transfection, the medium was replaced with serum-free medium (CHO-S-SFM; Invitrogen) and culture broths were collected after 48 h. The concentrations of hEpo and Fc-fusion proteins were determined by ELISA (EPO ELISA; Roche Diagnostics).

Retroviral vector production and establishment of clones. VSV-G pseudotyped pantropic retroviral vectors were produced by DNA transfection into GP293 cells. The viral particles produced in the medium were concentrated by ultracentrifugation and used to infect CHO cells. GFP-positive clones were isolated by the limiting dilution method. Viral titration was determined by visual expression of GFP in 3T3-infected cells. Further biochemical characterization was carried out by Western blot using antibodies against hEpo and Fc region (hIgG).

In vitro activity. Ba/F3 cells expressing the murine Epo receptor (mEpoR) [12] were exposed to various concentration of hEpo and hEpo/Fc. Cell proliferation was

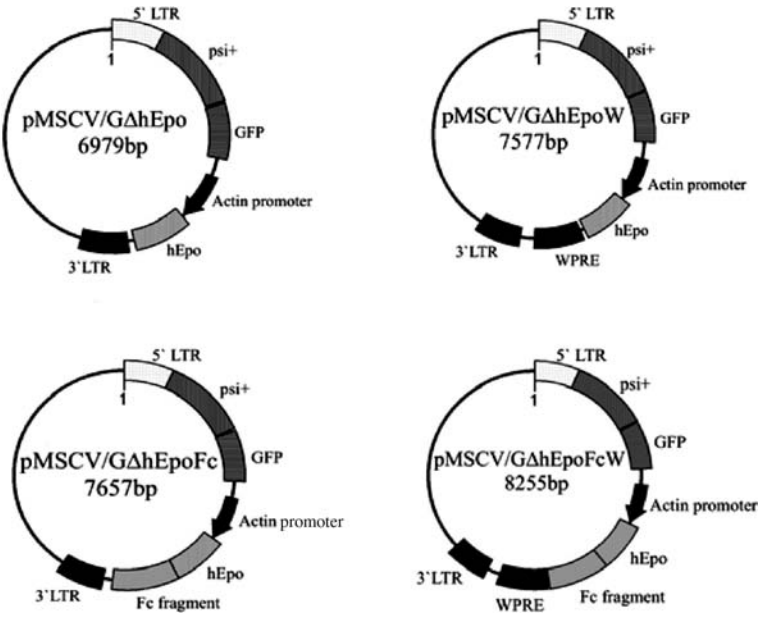

Fig. 1 Schematic drawings of retroviral vector plasmids

measured by employing cell counting kit (WST-8; Dojindo). Data analysis and EC_{50} values for samples were obtained by the use of Prism (GraphPad Software Inc.). Statistical significance was assessed by unpaired Student's *t*-test. A value of $p < 0.05$ was considered to be significant.

3 Results

First, the effect of WPRE insertion to the vectors on the recombinant protein production in CHO cells was determined. WPRE sequence was located at downstream of hEpo and hEpo/Fc sequences and these cassettes were ligated into the retroviral vector plasmids based on murine stem cell virus (MSCV) (Fig. 1). CHO cells transfected transiently with the WPRE-containing plasmids resulted in an increase in protein productivity (Fig. 2). The enhancements by WPRE were approximately 6-fold and 2-fold for hEpo and hEpo/Fc respectively.

Subsequently, CHO cell lines producing hEpo and hEpo/Fc were established. The structure of synthesized proteins were analyzed by Western blot employing two different antibodies (against hEpo and Fc region of IgG; Fig. 3). SDS-PAGE under reducing (Fig. 3a) and non-reducing conditions (Fig. 3b) were performed using culture broths of the cells. Proteins were synthesized within their expected molecular weights either under reducing (hEpo 34–39 kDa; hEpo/Fc 63–68 kDa; hIgG 65 kDa) or non-reducing conditions (hEpo/Fc 126–136 kDa; hIgG 150 kDa).

Finally, the proteins produced by CHO cells were characterized by in vitro activities in a proliferation assay using Ba/F3 cells expressing the murine Epo receptor. The concentrations of samples were determined by solid-phase ELISA and cells were exposed to various concentrations of agonists. Figure 4 shows that hEpo/Fc retained biological activity although with a lower potency ($EC_{50} = 1.3$) than hEpo itself ($EC_{50} = 0.6$).

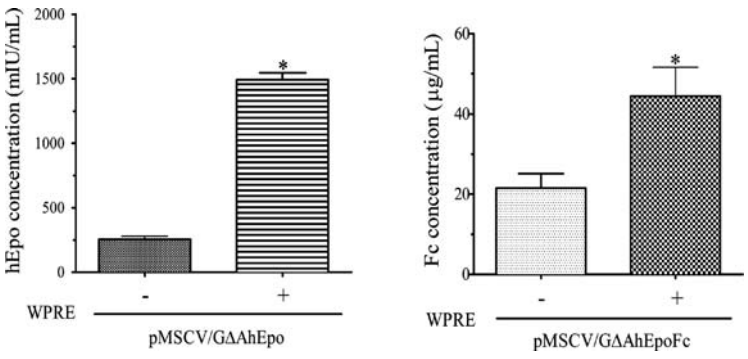

Fig. 2 WPRE increases protein productivity in CHO cells

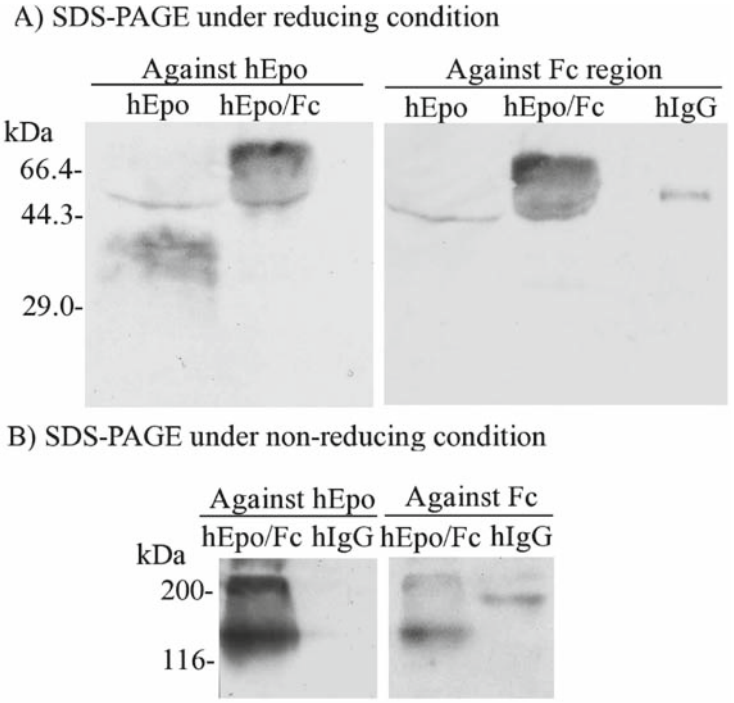

Fig. 3 Western blot analysis of hEpo and hEpo/Fc fusion proteins

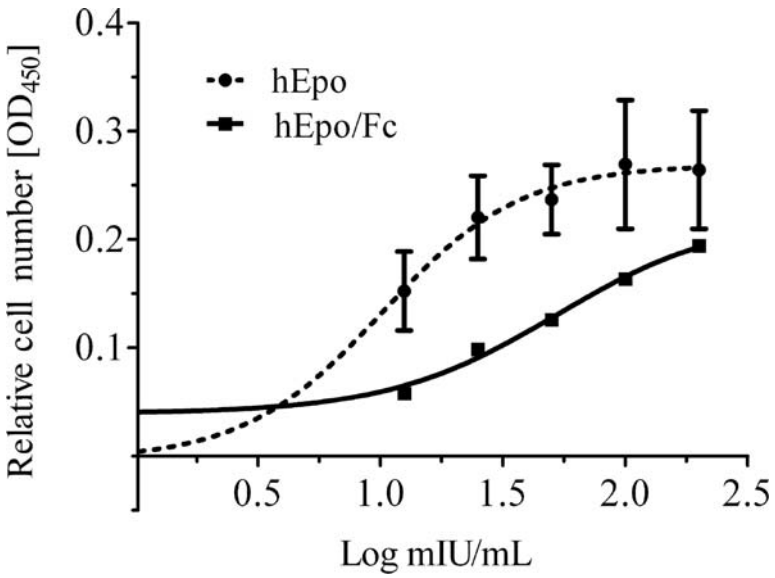

Fig. 4 In vitro biological activities of hEpo and hEpo/Fc

4 Discussion

Here we report the production of recombinant hEpo and hEpo/Fc proteins. The effect of WPRE located at downstream of the target cDNA sequences on protein productivity was also investigated. The presence of WPRE sequence in the vectors enhanced both hEpo and hEpo/Fc production to 6- and 2-fold respectively. On the other hand, WPRE did not influenced protein productivity in HEK293 cells when transfected with identical plasmids (data not shown). At present, the reason for this inconsistency remains unclear; however, it may be related to distinct regulatory effects of WPRE on the context of different cells lines and promoters. Supporting this evidence, Klein et al. [13]. have demonstrated that although WPRE elicited marked improvements in terms of EGFP expression when transfected into viral vector packaging cells, the effect of WPRE was promoter and cell line dependent. Taking these data together, it is uncertain whether or not WPRE might be useful to increase biopharmaceuticals production in broad range of cell lines and/or promoters contexts. We generated CHO cell lines stably producing hEpo and hEpo/Fc using viral transduction. Our clones have synthesized proteins within their expected molecular weights as observed by Western blot (Fig. 3). Furthermore, in vitro biological activities were assessed: hEpo ($EC_{50} = 0.6$) provided a higher proliferative performance than hEpo/Fc ($EC_{50} = 1.3$). In agreement with this result Bitonti et al. [14]. have constructed hEpo/Fc (Fc-derived from IgG1) dimers and monomers (comprised of a single Epo conjoined to a dimeric Fc subunit) aiming at it pulmonary delivery. Despite the fact that the protein structure differs from our construct (Fc-derived from IgG2) the results showed that hEpo/Fc monomers presented improved pharmacokinetics parameters including 2-fold improved receptor affinity and enhanced efficacy in vivo over hEpo/Fc dimer and Epogen® [14]. In a different study, Way et al.[9] have shown that Epo/Fc half-life by intraperitoneal administration in mice was lower than hEpo itself. The engineering of hEpo by mean of Fc-fusion may not be a successful strategy to enhance hEpo activity, although Fc-fusion facilitates purification of target proteins using affinity columns.

In this study, we succeeded to increase hEpo and hEpo/Fc productivity by using the WPRE sequence in CHO cells. The proteins were correctly synthesized and in vitro studies revealed that hEpo/Fc partially retained the biological activity of hEpo. Nevertheless, our research to create a novel erythropoietic agent that may allow a superior performance is in progress.

References

1. Aggarwal, S., (2007) What's fueling the biotech engine? *Nat. Biotechnol*. **25**(10): 1097–1104.
2. Bunn, H.F. (2007) New agents that stimulate erythropoiesis. *Blood* **109**(3): 868–873.
3. Jelkmann, W. (1992) Erythropoietin: structure, control of production, and function. *Physol Rev* **72**, 449–489.
4. D'Andrea, A.D., Lodish, H.F., and Wong, G.G. (1989) Expression cloning of the murine erythropoietin receptor. *Cell* **57:** 277–285.
5. Lacombe, C., and Mayeux, P. (1998) Biology of erythropoietin. *Haematologica* **83:** 724–732.

6. Eschbach, J.W., Egrie, J.C., Downing, M.R., Browne, J.K., and Adamson, J.W. (1987) Correction of the anemia of end-stage renal disease with recombinant human erythropoietin. Results of a combined phase I and II clinical trial. *N. Engl. J. Med*. **316**: 73–78.
7. Abels, R.I. (1992) Use of recombinant human erythropoietin in the treatment of anemia in patients who have cancer. *Semin. Oncol*. **19**(3 suppl 8): 29–35.
8. Elliott, S., Egrie, J., Browne, J., Lorenzini, T., Busse, L., Rogers, N., and Ponting, I. (2004) Control of rHuEPO biological activity. The role of carbohydrate. *Exp. Hematol*. **32**: 1146–1155.
9. Way, J.C., Lauder, S., Brunkhorst, B., Kong, S., Qi, A., Webster, G., Campbell, I., McKenzie, S., Lan, Y., Marelli, B., Nguyen, L.A., Degon, S., Lo, K.M., and Gillies, S.D. (2005) Improvement of Fc-erythropoietin structure and pharmacokinetics by modification at a disulfide bond. *Protein Eng. Des. Sel*. **18**(3): 111–118.
10. Kodama, D., Nishimiya, D., Iwata, K., Yamaguchi, K., Yoshida, K., Kawabe, Y., Motono, M., Watanabe, H., Yamashita, T., Nishijima, K., Kamihira, M., and Iijima, S. (2008) Production of human erythropoietin by chimeric chickens. *Biochem. Biophys. Res. Commun*. **367**(4): 834–839.
11. Kamihira, M., Ono, K., Esaka, K., Nishijima, K., Kigaku, R., Komatsu, H. Yamashita, T., Kyogoku, K., and Iijima, S. (2005) High-level expression of single-chain Fv-Fc fusion protein in serum and egg white of genetically manipulated chickens by using a retroviral vector. *J. Virol*. **79**: 10864–10874.
12. Ueda, H., Kawahara, M., Aburatani, T., Tsumoto, K., Todokara, K., Suzuki, E., Nishimura, H., Schueler, P.A., Winter, G., Mahoney, W.C., Kumagai, I., and Nagamune, T. (2000) Cell-growth control by monomeric antigen: The cell surface expression of lysozyme-specific Ig V domains fused to truncated Epo receptor *J. Immunol. Methods* **241**(1–2): 159–170.
13. Klein, R., Ruttkowski, B., Knapp, E., Salmons, B., Günzburg, W.H., and Hohenadl, C. (2006) WPRE mediated enhancement of gene expression is promoter and cell line specific. *Gene* **372**: 153–161.
14. Bitonti, A.J., Dumont, J. A., Low, S.C., Peters, R.T., Kropp, K. E., Palombella, V.J., Stattel, J.M., Lu, Y., Tan, C.A., Song, J.J., Garcia, A.M., Simister, N.E., Spiekermann, G.M., Lencer, W.I., and Blumberg, R.S. (2004) Pulmonary delivery of an erythropoietin Fc fusion protein in non-human primates through an immunoglobulin transport pathway, *Proc Natl Acad Sci U S A* **101**(26): 9763–9768.

Development of Oviduct-Specific Gene Expression System for Transgenic Avian Bioreactor

Yoshinori Kawabe, Kensaku Numata, Masashi Teramori, Akira Ito, and Masamichi Kamihira

1 Introduction

Transgenic animal bioreactors have been proposed to be the next generation production system for biopharmaceuticals [1, 2]. Avian systems using chickens and quails have several advantages in that they rapidly reach sexual maturity and have a small space requirement for breeding and a high production yield of egg proteins over mammalian expression systems including goats and sheep [3, 4]. We have developed various techniques to generate transgenic chickens and quails which express the target genes throughout the body including the eggs [4–9]. However, since the target proteins have the possibility of a detrimental effect in animal health, tissue-specific expression is desired. In case of avian, oviduct where egg white proteins such as ovalbumin and conalbumin are produced can be a site for recombinant protein production. For the oviduct-specific expression, the regulatory sequences of white protein genes such as ovalbumin, lyzosome and conalbumin have been characterized [10–12] but the whole region of original promoter required for the tissue-specificity and high-level expression is too long to transfer to plasmid-based expression vectors, and the expression level of target proteins often decreases when promoter regions are partially used.

Here we report to develop a synthesis promoter system to realize oviduct-specific expression by combining the Tet system [13] and the minimal regulatory sequences of the *ovalbumin* (*OVA*) and *conalbumin* (*conA*) genes.

2 Materials and Methods

Plasmid construction The expression vector plasmids for the evaluation of positive feedback expression are shown as Fig. 1. pΔA-tTA includes the expression unit of a tetracycline transactivator (tTA) under the control of a chicken β-actin

Y. Kawabe (✉)
Department of Chemical Engineering, Faculty of Engineering, Kyushu University, 744 Motooka, Nishi-ku, Fukuoka 819-0395, Japan
e-mail: kawabe@chem-eng.kyushu-u.ac.jp

M. Kamihira et al. (eds.), *Animal Cell Technology: Basic & Applied Aspects*, Animal Cell Technology: Basic & Applied Aspects 16, DOI 10.1007/978-90-481-3892-0_33,

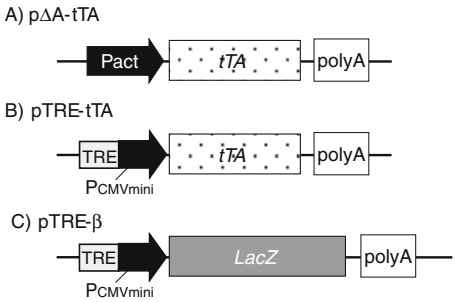

Fig. 1 Vector constructs

promoter. pTRE-tTA and pTRE-β include the expression units of tTA and bacterial β-galactosidase under the control of TRE harboring CMV minimal promoter, respectively.

Transient plasmid transfection The plasmids were transfected into the NIH-3T3 cells using a lipofection reagent (LF2000) and the transfected cells were assayed by β-galactosidase activity as described below.

β-Gal activity. For quantification of β-galactosidase activity, the cells tansfected with expression vector plasmids or transducted with retroviral vectors were collected, washed with PBS and the β-galactosidase activity of cell lysates was measured using ONPG as a substrate as described previously [6, 7].

Retroviral vector production The regulatory sequences of the *OVA* (-140 ∼ +41) and *conA* (-107 ∼ +62) genes were amplified from the chicken genomic DNA by PCR. The retroviral vector plasmids for the evaluation of positive feedback expression are shown in Fig. 2. The production of retroviral vectors and

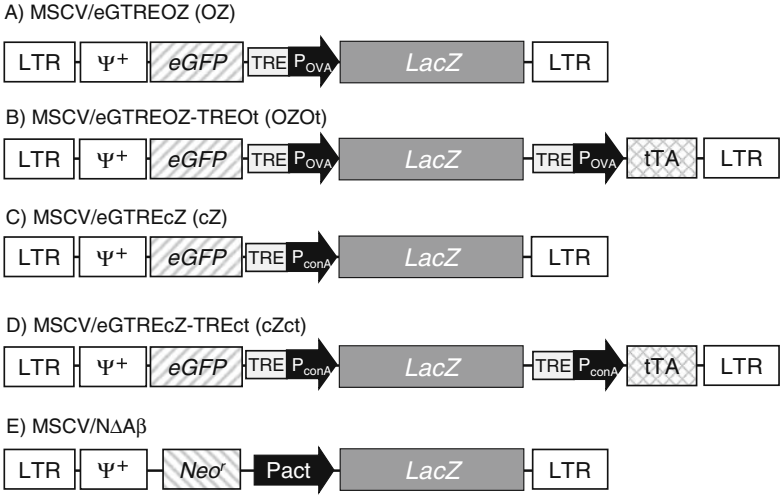

Fig. 2 Retroviral vector constructs

concentration of viral vectors by ultracentrifugation were performed as described previously [6, 7].

Primary culture of chicken oviduct cells and gene transduction Oviduct cells were isolated from magnum portion of diethylstilbestrol (DES) -treated chickens by the method of Sanders and McNight [14], except that DES dissolved in ethanol was injected intramuscularly at a dose of 1 mg/d. Cells were seeded at a density of 1–5 $\times$ 10^5 cells per well of a 96-well collagen type-I coated plate in 0.1 ml of D-MEM/F12 medium supplemented with 0.1% BSA, 0.1 μM 17β-estradiol, 1.0 μM dexamethasone, 50 ng/ml insulin and antibiotics (penicillin and streptomycin). After 1–2 h, the supernatants were transferred into other well to remove the fibroblast cells. After cultivating the primary cells for 1–2 d, the viral solutions were infected into the cell. After 48 h of post-infection, the cells were collected and β-galactosidase activity was measured for cell lysates.

3 Results

We firstly evaluated the enhanced expression by positive feedback system which the tTA expression vector (pTRE-tTA) was added into a Tet system in animal cells. The expression vector plasmids were transfected into NIH3T3 cells by lipofection method and the expression level of the transgene in the cells was measured by β-galactosidase activity. The plasmids (Tet system; pΔA-tTA and pTRE-β, Positive feedback system; pΔA-tTA, pTRE-tTA and pTRE-β) were co-transfected into NIH3T3 cells. The expression level of *LacZ* gene was 25-fold higher compared to without the tTA expression vector (Fig. 3), indicating that the positive feedback system worked effectively for the enhanced expression. However, since the CMV minimal promoter is located downstream of the tetracycline-responsive element, the automatic leak expression derived from the CMV minimal promoter was observed even in the absence of tetracycline and the leak expression triggered the positive feedback when the two expression vector plasmids (pTRE-tTA and pTRE-β) were co-transfected into cells (data not shown). Consequently, to suppress the leak expression of *tTA* and *LacZ* genes, the plasmid in which the region of the

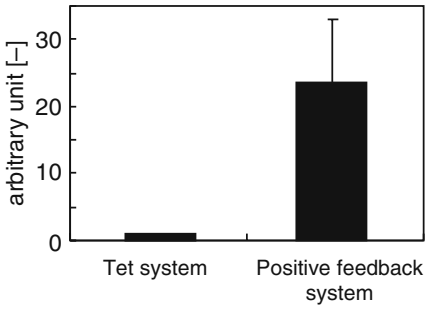

Fig. 3 Evaluation of positive feedback system

CMV minimal promoter was deleted (pTREΔ-β) was constructed and assayed. As the result, the leak expression became negligible, suggesting that the choice of minimal promoter is important and the tissue-specific expression may be controlled in this region. To demonstrate tissue-specific expression using this region, synthetic promoters containing a TATA-box neighboring regulatory regions derived from *OVA* and *conA* genes located downstream of the TRE sequence (TREO and TREc, respectively) were constructed. The enhanced expression by a positive feedback was not observed in non-oviduct cells, when the tTA expression vector plasmids under the control of TREO and TREc synthetic promoters (pTREO-tTA and pTREc-tTA) were introduced (data not shown), suggesting that the enhanced expression by the positive feedback may occur in oviduct cells using the synthetic promoter.

Finally, retroviral vectors were infected to oviduct cells isolated from magnum portion of DES-treated chickens. Chicken embryonic fibroblasts (CEF) were isolated from a 10-day embryo and used as non-oviduct cells for a negative control. Retroviral vectors encoding expression cassettes for *LacZ* gene under the control of synthetic promoters (OZ and cZ) were produced and infected to oviduct cells and CEF cells. The β-galactosidase activity measured were normalized by the retroviral titer determined using NIH3T3 cells (Table 1). The expression level for cZ was higher than that for OZ in oviduct cells, while the expression was negligible in CEF cells for both retroviral vectors. To confirm the enhanced expression by the positive feedback, one-packed retroviral vectors where both *LacZ* and *tTA* genes were introduced (OZOt and cZct, respectively) were produced and infected to oviduct cells. The enhanced expression was observed for cZct, and the expression level was 8.2-fold higher than that for cZ and comparable for using the ubiquitous promoter. These results suggest that by combining the synthetic promoter and Tet system, the oviduct-specific and high-level expression could be achieved.

Table 1 Relative activity of β-galactosidase

	Relative β-galactosidase activity (mU/mg-protein)				
Cells	OZ	OZOt	cZ	cZct	β-actin
Oviduct primary cells	0.053 ± 0.015	ND	0.83 ± 0.027	6.8 ± 1.0*	6.7 ± 1.4
CEF	0.018 ± 0.011	0.13 ± 0.013	0.052 ± 0.013	0.36 ± 0.16	2.2 ± 0.90

*$P<0.05$ (cZ vs cZct), ND: not detected

4 Discussion

We successfully developed the oviduct-specific and enhanced expression system by combining a positive feedback expression system of tTA and a synthetic promoter comprised of TRE and TATA-box neighboring regulatory regions derived from oviduct protein genes. Although some research groups have generated the

transgenic [15] and chimeric [16] chickens expressing the recombinant genes in an oviduct-specific manner, the expression level is not high. In many cases, it is difficult to achieve high-level expression using a limited control region. The requirements for oviduct-specific gene expression system in pharmaceutical protein production are (1) strict oviduct specificity, (2) high-level expression, (3) compactness in size and (4) robustness. In this study, the enhanced expression was observed for primary oviduct cells but not for non-oviduct cells using the cZct retroviral vector. The expression level was comparable to that using chicken β-actin promoter. Previously, when a recombinant antibody gene under the control of a chicken β-actin promoter was expressed in the egg white of genetically manipulated chickens and quails, the expression level was ∼ mg/ml [6, 7]. The retroviral vector incorporated the gene expression system developed in this study may be a useful tool for generation of genetically manipulated avian with oviduct-specific and high-level expression.

References

1. Rudolph, N.S., (1999) Biopharmaceutical production in transgenic livestock. *Trends. Biotechnol*. **17**: 367–374.
2. Kues, W.A., and Niemann, H. (2004) The contribution of farm animals to human health. *Trends. Biotechnol*. **22**: 286–294.
3. Sang, H.M. (2004) Prospects for transgenesis in the chick. *Mech. Dev*. **121**: 1179–1186.
4. Ivarie, R. (2003) Avian transgenesis: progress towards the promise. *Trends. Biotechnol*. **21:** 14–19.
5. Mizuarai, S. Ono, K. Yamaguchi, K. Nishijima, K., Kamihira, M., and Iijima, S. (2001) Production of transgenic quails with high frequency of germ-line transmission using VSV-G pseudotyped retroviral vector. *Biochem. Biophys. Res. Commun*. **286:** 456–463.
6. Kamihira, M. Ono, K. Esaka, K. Nishijima, K., Kigaku, R., Komatsu, H., Yamashita, T., Kyogoku, K., and Iijima, S. (2005) High-level expression of scFv-Fc fusion protein in serum and egg white of genetically manipulated chickens using a retroviral vector. *J. Virol*. **79:** 10864–10874.
7. Kawabe, Y., Kamihira, M., Ono, K., Kyogoku, K., Nishijima, K., and Iijima, S. (2006) Production of scFv-Fc fusion protein using genetically manipulated quails. *J. Biosci. Bioeng*. **102:** 297–303.
8. Kodama, D., Nishimiya, D., Iwata, K., Yamaguchi, K., Yoshida, K., Kawabe, Y., Motono, M., Watanabe, H., Yamashita, T., Nishijima, K., Kamihira, M., and Iijima, S. (2008) Production of human erythropoietin by chimeric chickens. *Biochem. Biophys. Res. Commun*. **367:** 834–839.
9. Kyogoku, K., Yoshida, K., Watanabe, H., Yamashita, T., Kawabe, Y., Motono, M., Nishijima, K., Kamihira, M., and Iijima, S. (2008) Production of recombinant tumor necrosis factor receptor/Fc fusion protein by genetically manipulated chickens. *J. Biosci. Bioeng*. **105**: 454–459.
10. Park, H.M., Haecker, S.E., Hagen, S.G., and Sanders, M.M. (2000) COUP-TF plays a dual role in the regulation of the ovalbumin gene. *Biochemistry* **39**: 8537–8545.
11. Huber, M.C., Jägle, U., Krüqer, G., and Bonifer, C. (1997) The developmental activation of the chicken lysozyme locus in transgenic mice requires the interaction of a subset of enhancer elements with the promoter. *Nucleic. Acids. Res*. **25:** 2992–3000.
12. Dierich, A., Gaub, M. P., LePennec, J.P, Astinotti, D., and Chambon, P. (1987) Cell-specificity of the chicken ovalbumin and conalbumin promoters. *EMBO J*. **6:** 2305–2312.

13. Gossen, M., and Bujard, H. (1992) Tight control of gene expression in mammalian cells by tetracycline-responsive promoters. *Proc. Natl. Acad. Sci. USA*. **89:** 5547–5551.
14. Sanders, M.M., and McKnight, G.S. (1985) Chicken egg white genes: multihormonal regulation in a primary cell culture system. *Endocrinology* **166:** 398–405.
15. Lillico, S.G., Sherman, A. McGrew, M.J., Robertson, C. D., Smith, J., Haslam, C., Barnard, P., Radcliffe, P.A., Mitrophanous, K.A., Elliot, E.A., and Sang, H.M. (2007) Oviduct-specific expression of two therapeutic proteins in transgenic hens. *Proc. Natl. Acad. Sci. USA*. **104**(6): 1771–1776.
16. Zhu, L., van de Lavoir, M. C., Albanese, J., Beenhouwer, D. O., Cardarelli, P.M., Cuison, S. Deng, D.F., Deshpande, S., Diamond, J. H., Green, L., Halk, E.L., Heyer, B. S., Kay, R.M., Kerchner, A., Leighton, P.A., Mather, C.M., Morrison, S. L., Nikolov, Z.L., Passmore, D.B., Pradas-Monne, A., Preston, B.T., Rangan, V. S., Shi, M., Srinivasan, M., White, S. G., Winters-Digiacinto, P., Wong, S., Zhou, W., and Etches, R.J. (2005) Production of human monoclonal antibody in eggs of chimeric chickens. *Nat. Biotechnol*. **23**(9): 1159–1169.

Production of Therapeutic Proteins Composed of Seven Dominant Human T Cell Epitopes Derived from the Japanese Cedar Pollen Allergens

Yoshinori Kawabe, Yoshifumi Hayashida, Kensaku Numata, Akira Hishigae, Akira Ito, and Masamichi Kamihira

1 Introduction

About 23 million people suffer from Japanese cedar (*Cryptomeria japonica*) pollen allergy in Japan [1, 2] and the number of pollen allergy patients is steadily increasing. Histamine receptor antagonists have been mainly used for the treatment of this disease as the symptomatic treatment. Although the allergen-specific immunotherapy has attracted great attention, the use of intact native allergens has a risk of systemic anaphylaxis. To avoid side effect, the peptide immunotherapy using dominant T-cell epitopes has been expected as an effective treatment for allergic diseases. The effectiveness of this strategy has been proven in animal model and also described in humans [3, 4]. Recently, Takaiwa and co-workers developed transgenic plants expressing dominant T cell epitope peptides of Cry j 1 and Cry j 2 allergens of Japanese cedar pollen [5, 6]. Zhu et al. also reported that a chimeric protein composed of human IgG Fcγ and allergen might be effective for the immune therapy of allergic disease [7].

On the other hand, we have generated the transgenic avian species such as chickens and quails for the production of recombinant proteins by using retroviral vectors for gene transfer [8–11]. If T-cell epitope peptides are expressed in the eggs of transgenic avian, it may be possible to induce successful oral immune tolerance to these allergens by eating the eggs. Moreover, while the transgenic plants cannot produce complex recombinant proteins with post-translational modifications, transgenic avian system may be superior choice.

Here we report the production of chimeric fusion proteins for human T-cell epitopes derived from the Japanese cedar pollen allergens (7crp; Fig. 1) in animal cells and genetically manipulated chickens.

Y. Kawabe (✉)
Department of Chemical Engineering, Faculty of Engineering, Kyushu University,
744 Motooka, Nishi-ku, Fukuoka 819-0395, Japan
e-mail: kawabe@chem-eng.kyushu-u.ac.jp

M. Kamihira et al. (eds.), *Animal Cell Technology: Basic & Applied Aspects*, Animal Cell Technology: Basic & Applied Aspects 16, DOI 10.1007/978-90-481-3892-0_34,

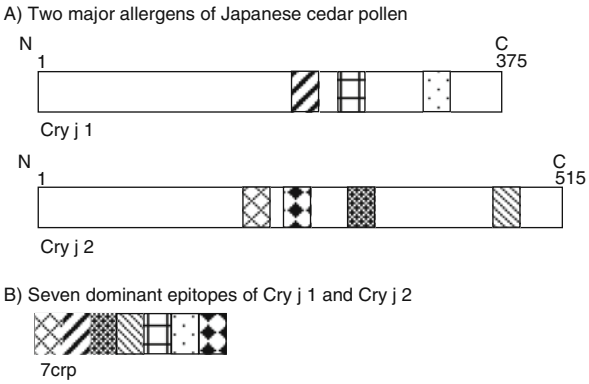

Fig. 1 Two major allergens of Japanese cedar pollen and the structure of 7 crp

2 Materials and Methods

Plasmid Construction Oligonucleotides corresponding to sequences of a seven dominant human T cell-epitope peptide derived from the Japanese cedar pollen allergens were synthesized according to chicken codon usage (Fig. 2). Total RNA was extracted from oviduct cells isolated from magnum portion of

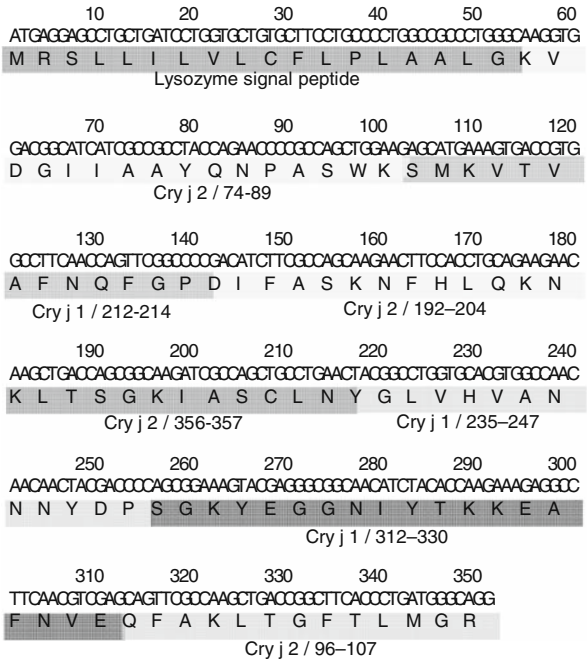

Fig. 2 Nucleotide and deduced amino acid sequences of 7crp

diethylstilbestrol-treated chicks [12] using a kit (QuickPrep^{TM} total RNA extraction kit) and the RNA samples were converted to cDNA using a reverse transcriptase (ReverTra Ace^{TM}). Chicken egg white lysozyme gene was amplified by PCR from cDNAs. mFcα and mFcγ genes were amplified by PCR. hFcγ gene was amplified by PCR from the plasmid pMSCV/GΔAscFvFc [9] and hFcα gene was obtained from the RIKEN gene bank. Retroviral vector plasmids including an expression cassette of seven dominant human T-cell epitopes derived from the Japanese cedar pollen allergens (7crp) fused with the Fc region of immunoglobulin A or G, or chicken lysozyme were constructed (Fig. 3).

Production of fusion proteins by transient transfection CHO-K1 cells were transfected with the retroviral vector plasmids. After 48 h of post-transfection, the cells were harvested. Western blot analysis for cell lysates was carried out to confirm the production of fusion proteins using anti- lysozyme, Fc and 7crp antibodies, as described below.

Expression of 7crp in E. coli and antisera production The coding region of 7crp+His-tag was amplified by PCR and the PCR product was subcloned into pGEX-6P-2. *E. coli* Rossettta transformed with the recombinant plasmid were cultured and the protein production was induced with IPTG. After sonication of the cells, cell lysates were dissolved with 8M Urea. The recombinant protein was purified using a Ni^{+}-chelate column. Antisera against 7crp were obtained by immunizing the protein to BALB/c mice.

Retroviral vector production, injection into chicken embryos and cultivation of embryos Production of VSV-G pseudotyped pantropic retroviral vectors, injection

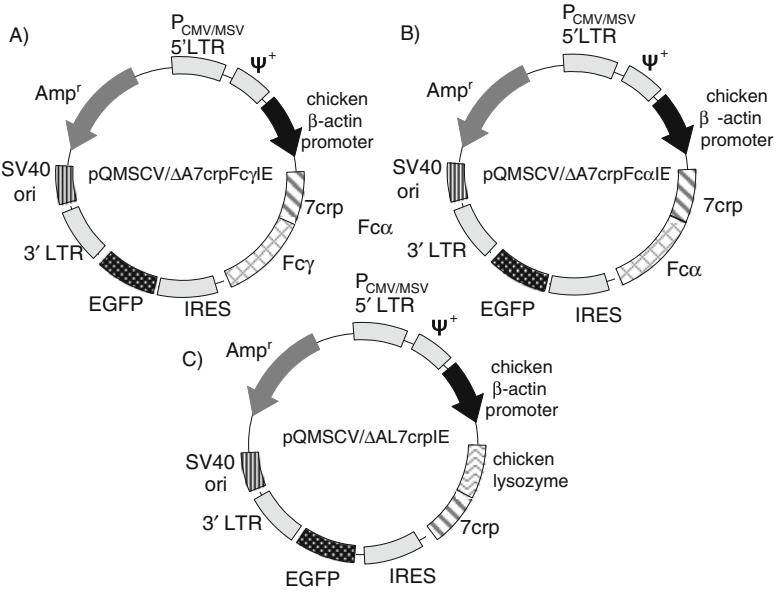

Fig. 3 The retroviral vector plasmids

of viral solution into embryos and culture of manipulated embryos were performed as described previously [9].

Analysis of manipulated chickens Genomic DNAs were extracted from the blood cells and some tissues of genetically manipulated chickens using a genomic DNA preparation kit (MagExtractor). The fluorescence was confirmed by microscopic observation. For Western blotting of cLys-7crp, samples were prepared from some tissues of genetically manipulated chickens.

3 Results

Since Cry j 1 and Cry j 2 allergens of Japanese cedar pollen are originally produced in plants, a 7crp gene optimized for chicken codon and a secretion signal sequence derived from chicken egg white lysozyme were chemically synthesized (Fig. 2). We firstly examined the production of the chimeric fusion proteins in mammalian cells. The retroviral vector plasmids including the expression units of chimeric fusion proteins (7crp-Fc,α 7crp-Fcγ and cLys-7crp) under the control of a chicken β-actin promoter were transfected into CHO-K1 cells. Retroviral vectors produced using the same plasmids were also infected to GP293 and NIH3T3 cells. After 48 h of post–transfection or infection, cells were harvested and production of the target proteins was analyzed by Western blotting. For the chimeric 7crp-Fc fusion proteins, they were detected as major bands, but a few bands with lower molecular weight were also detected. On the other hand, the chimeric chicken lysozyme-7crp fusion protein was detected as single band. These results indicate that the chimeric fusion proteins were properly expressed in mammalian cells.

In order to generate genetically manipulated chickens expressing the chimeric fusion proteins, retroviral vectors were concentrated by ultracentrifugation. The viral titer was determined for NIH3T3 cells. Among the retroviral vectors tested, titer was increased up to $0.9–3.8\times10^8$ infectious units (IU)/ml for the cLys-7crp retroviral vector after concentration. Thus, the viral vector was injected into total 32 of chicken embryos in the two experiments, and the hatchability of manipulated embryos was 44% (11/25). The chickens that hatched exhibited no apparent abnormality. A retroviral sequence was detected by PCR using genomic DNA extracted from blood cells of the chickens (Fig. 4a lane 1–5). PCR primers for amplification of the retroviral packaging signal were used for detection of the viral sequence. pMSCV/eGΔAL7crpIE plasmid as positive control and genomic DNA extracted

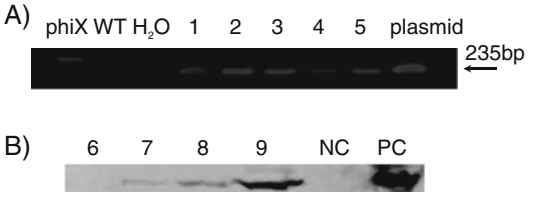

Fig. 4 Analysis of genetically manipulated chickens (**a**) PCR (**b**) Western blotting

from wild-type chicken as negative control were also used for PCR. EGFP expression in blood cells of manipulated chickens was observed microscopically. Target genes were expressed under a constitutive β-actin promoter and the EGFP expression was driven by IRES-dependent translation. Next, cLys-7crp expression was analyzed by Western blotting using anti-7crp antibodies. The cell lyastes of NIH3T3 cells transduced with the same viral vector as the positive control and heart tissues of a wild-type chicken as the negative control were used. cLys-7crp protein was detected in heart of manipulated chickens (Fig. 4 b; lane 6–9), but not in other tissues including blood cells (data not shown).

4 Discussions

We examined the expression of chimeric fusion proteins for human T-cell epitopes derived from the Japanese cedar pollen allergens in animal cells and genetically manipulated chickens. Three types of chimeric fusion proteins (7crp-Fcα, 7crp-Fcγ and cLys-7crp) could be expressed in animal cells (CHO-K1, NIH3T3 and GP293 cells). When the three retroviral vectors were produced, the cLys-7crp retroviral vector gave higher titer. We have generated transgenic chickens and quails using retroviral vector for gene transfer [8–11]. Through these studies, it was found that at least 10^8 IU/ml is necessary for a high-level expression of the transgene [9, 10]. Since the retroviral vector for cLys-7crp reached to a titer of around 10^8 IU/ml after ultracentrifugation, retroviral solution was injected into chicken embryos. The hatchability of manipulated embryos was almost the same level as those of our previous report [9–11]. For Western blotting, cLys-7crp was detected in the heart of manipulated chickens, but not in other tissues. Since β-actin promoter used for the transgene expression drives a gene strongly in muscular tissues [10] and retroviral solution were directly injected into the heart of embryos, the detection of transgene expression in heart may be attributable to promoter activity and/or higher copy number of transgene. Since the synthetic peptide consisting of the seven dominant human T cell epitopes (7crp) includes some hydrophobic amino acids, it may be possible that the target protein is retained and degraded in the cells. Further investigation is necessary to design chimeric T cell epitope proteins for effective form and efficient production.

References

1. Savage, J. and Roy, D. (2005) Allergic rhinitis: an update. *J.R. Soc. Promot. Health* **125**(4): 172–175.
2. Okuda, M. (2003) Epidemiology of Japanese cedar pollinosis throughout Japan. *Ann. Allergy Asthma Immunol*. **91**(3): 288–296.
3. Tsunematsu, M., Yamaji, T. Kozutsumi, D. Murakami, R. Kimura, S., and Kino, K. (2007) Establishment of an allergic rhinitis model in mice for the evaluation of nasal symptoms. *Life Sci*. **80**: 1388–1394.

4. Hirahara, K. Tatsuta, T. Takatori, T. Ohtsuki, M. Kirinaka, H. Kawaguchi, J., Serizawa, N. Taniguchi, Y. Saito, S. Sakaguchi, M., Inouye, S., and Shiraishi, A. (2001) Preclinical evaluation of an immunotherapeutic peptide comprising 7 T-cell determinants of Cry j 1 and Cry j 2, the major Japanese cedar pollen allergens. *J. Allergy Clin. Immunol*. **108**(1): 94–100.
5. Takagi, H., Hiroi, T., Yang, L., Tada, Y., Yuki, Y., Takamura, K., Ishimitsu, R., Kawauchi, H., Kiyono, H., and Takaiwa, F. (2005) A rice-based edible vaccine expressing multiple T cell epitopes induces oral tolerance for inhibition of Th2-mediated IgE responses. *Proc. Natl. Acad. Sci. USA* **102**(48): 17525–17530.
6. Takaiwa, F. Takagi, H. Hirose, S., and Wakasa, Y. (2007) Endosperm tissue is good production platform for artificial recombinant proteins in transgenic rice. *Plant Biotechnol. J*. **5**(1): 84–92.
7. Zhu, D., Kepley, C.L., Zhang, K., Terada, T., Yamada, T., and Saxon, A. (2005) A chimeric human-cat fusion protein blocks cat-induced allergy. *Nat. Med*. **11**(4): 446–449.
8. Mizuarai, S. Ono, K. Yamaguchi, K. Nishijima, K. Kamihira, M., and Iijima, S. (2001) Production of transgenic quails with high frequency of germ-line transmission using VSV-G pseudotyped retroviral vector. *Biochem. Biophys. Res. Commun.* **286**(3): 456–463.
9. Kamihira, M., Ono, K., Esaka, K., Nishijima, K., Kigaku, R., Komatsu, H., Yamashita, T., Kyogoku, K., and Iijima, S. (2005) High-level expression of single-chain Fv-Fc fusion protein in serum and egg white of genetically manipulated chickens by using a retroviral vector. *J. Virol*. **79**(17): 10864–10874.
10. Kawabe, Y., Kamihira, M., Ono, K., Kyogoku, K., Nishijima, K., and Iijima, S. (2006) Production of scFv-Fc fusion protein using genetically manipulated quails. *J. Biosci. Bioeng*. **102**(4): 297–303.
11. Kodama, D., Nishimiya, D., Iwata, K., Yamaguchi, K., Yoshida, K., Kawabe, Y., Motono, M., Watanabe, H., Yamashita, T., Nishijima, K., Kamihira, M., and Iijima, S. (2008) Production of human erythropoietin by chimeric chickens. *Biochem. Biophys. Res. Commun.* **367**(4): 834–839.
12. Sanders, M.M. and McNight, G.S. (1985) Chicken egg white genes: multihormonal regulation in a primary cell culture system, *Endocrinology* **116**(1): 398–405.

The Differentiation of C2C12 Cells to Myotube by Paraquat

Masaaki Okabe, Koichi Akiyama, Sogo Nishimoto, Takuya Sugahara, and Yoshimi Kakinuma

1 Introduction

Paraquat (1, 1'-dimethyl-4, 4'-bypiridinium) is one of herbicide, often used in many counties. However, in some case with wrong usage of paraquat, paraquat shows toxicity against human, especially on framer [1–4]. In these cases, paraquat produces reactive oxygen species (ROS) to show its toxicity.

One of important toxicity in paraquat against mammal is to induce Parkinsonism. 1-methyl-4-phenylpyridinium (MPP+), the structure is similar to paraquat have been known to induce Parkinsonism [5, 6]. MPP+ is metabolized from 1-methyl-4-phenyl-1,2,3,6-tetrahydropyridine (MPTP), impurity in stimulant. Because paraquat and MPP+ have similar structure, paraquat also is concerned with Parkinson's disease [M]. It is also known that paraquat activates Mitogen-activated protein kinase kinase (MEK) – extracellular signal-regulated kinases (ERK) and c-Jun N-terminal kinases (JNK) in brain neuroblasts [7]. These kinases are known to concerned with the differentiation of cells to macrophages [8], adipocytes [9] and muscle [10, 11], suggesting the importance of these kinases in the differentiation of these kind of tissues.

Paraquat is known to induce injury on the lungs [12]. Then paraquat induces the differentiation of interstitial cells into muscle cells in the lung of monkeys [13] suggesting that paraquat perturbs the differentiation of muscle cells.

C2C12 cells are mouse myoblast cell line and have an ability to differentiate into skeletal muscle cells [14]. C2C12 cells have been often used to study about the differentiation of skeletal muscle cells. In this paper, we examined the effect of paraquat on the differentiation of C2C12 cells. To show the manner of paraquat on the modulation of the differentiation in C2C12 cells, we studied the role of ROS from paraquat and the activity of MEK-ERK and JNK on the differentiation in C2C12 cells.

M. Okabe (✉)
Center for Marine Environmental Studies (CMES), Ehime University, Tarumi, Matsuyama 790-8577, Japan; Ehime University, Tarumi, Matsuyama 790-8566, Japan
e-mail: okabema@agr.ehime-u.ac.jp

M. Kamihira et al. (eds.), *Animal Cell Technology: Basic & Applied Aspects*, Animal Cell Technology: Basic & Applied Aspects 16, DOI 10.1007/978-90-481-3892-0_35,

2 Materials and Methods

2.1 Cell Culture

C2C12 cells were bought from Riken Bioresource Center. C2C12 cells were maintained under 5% CO_2 at 37°C in DMEM (Nissui Pharmaceutical) supplemented with 10% fatal bovine serum (JRH bioscience), 100,000 unit/L penicillin and 10 mg/L streptomycin (Nakarai Tesque).

To study the effect of paraquat on the differentiation of C2C12 cells, C2C12 cells were plated at 5×10^4 cells/well, and cultured for 24 h. Then the medium was changed to DMEM with 10% fatal bovine serum and paraquat (0.1~1000 ng/mL, Wako). The cells were cultured in each period, taken photos and harvested to apply to each examination.

In future experiment, 10 or 100 μM ascorbic acid, 0.1 ~ 100 μM H_2O_2, was add to the medium and C2C12 cells were cultured in the medium with the condition above.

2.2 Western Blotting

After the culturing in each condition, C2C12 cells were harvested and applied to and washed twice with phosphate-buffered saline and lysed in the buffer containing 50 mM Tris-HCl (pH 7.5), 150 mM HaCl, 1% Triton-X 100, 1 mM EDTA, 50 mM NaF, 30 mM $Na_4P_2O_7$, 1 mM phenylmethylsulfonyl fluoride, 2.0 μg/mL aprotinin and 1 mM pervanadate. The whole-cell lysate was incubated at 4°C for 30 min and then contributed at $12{,}000 \times g$ for 30 min. The supernatant was mixed with a sodium dodecyl sulfate-polyacrylamide gel electrophoresis (SDS-PAGE) sample buffer. The mixture was loaded onto 8% SDS-PAGE gel, and electrophoresis was performed under reducing conditions. The sample was then electrotransferred onto a PVDF membrane. The blotted membrane was probed for monoclonal mouse anti-myosin antibody M4276 (Sigma) or anti-actin antibody produced in rabbit A2066 (Sigma). The secondary antibody used was horseradishperoxidase-conjugated anti-mouse immunoglobulin (Ig) G, and the detection of each protein was performed using ECL Plus Western Blotting Detection System (GE Healthcare) and Lumino Imaging Analyzer FAS-1000 (Toyobo).

2.3 Measurement of TBARS Level in C2C12 Cells

TBARS levels in C2C12 cells were measured with a commercial kit (Cayman Chemical) according to Yagi's method [15].

3 Results and Discussions

C2C12 cells were cultured for 12 days in the medium containing 0.1~100 ng/mL paraquat and 10% FBS, undifferentiating condition. However, depending on the concentration of paraquat, many cells changed to myotube-like form. Furthermore, cells became ticker depending on the concentration of paraquat (Fig. 1a).

MHC is a marker protein for the differentiation of muscle cells. As shown in Fig. 1b, the effect of paraquat on MHC increased depending on the concentration of paraquat. Especially, the concentration of MHC increased in the cells cultured with 100 and 1000 ng/mL paraquat. There was no effect on the amount of MHC in other concentration.

The main function of paraquat is to product reactive oxygen species (ROS). To study the rule of ROS on the differentiation of C2C12 cells by paraquat, C2C12 cells were cultured in the medium with paraquat and ascorbic acid. In the presence of ascorbic acid, C2C12 cells changed their forms (Data not shown).

Moreover, Culturing with each concentration of H_2O_2 (0.1~100 μM) showed no effect on the differentiation of C2C12 cells.

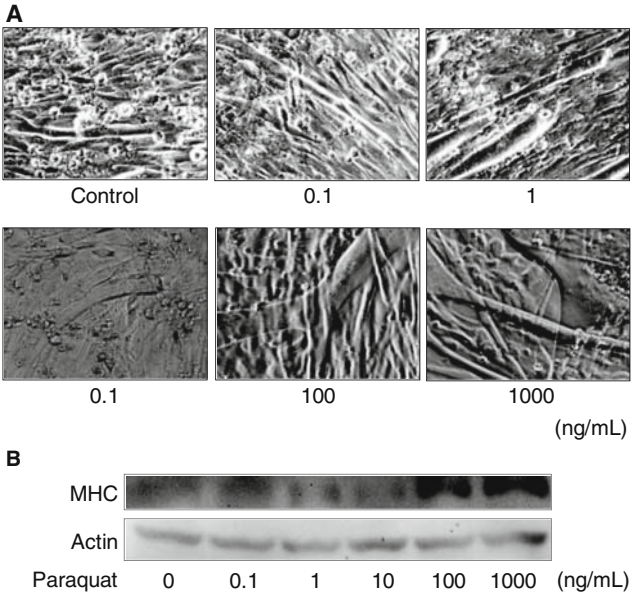

Fig. 1 Effect of paraquat on the differentiation of C2C12 cells. C2C12 cells were cultured in 10% FBS-containing DMEM with each concentration of paraquat for 12 days. (**a**) Effect of paraquat on the morphology of C2C12 cells. (**b**) Effect of paraquat on the amount of myosin heavy chain in C2C12 cell

To discuss the role of ROS come from paraquat on the differentiation of C2C12 cells, it is important to measure ROS level in each sample. In this study, TBARS level was measured as a marker of ROS level. There was no significant differences between control and 100 ng/mL paraquat-add cells in TBARS level. This suggests ROS from paraquat is not concerned in the differentiation of C2C12 cells.

When paraquat induces inflammation in the lungs, the differentiation of cells to muscle is shown [13]. This suggests the possibility that paraquat perturbs the differentiation of muscle cells. Usually C2C12 cells differentiate in the medium with 2% house serum [14]. However, in this study C2C12 cells showed the morphologically change to myotube and the increasing of MHC and MyoD level with 100 or 1000 ng/mL paraquat even in the medium with 10% FBS, undifferentiating condition. These results suggest that paraquat perturbs the differentiation of C2C12 cells to myotube.

The activity of paraquat as a herbicide was given by ROS producing activity for weed control. In many cases, the toxicity of paraquat is dependent on the ROS from paraquat in mammals. For instance, it has been reported that paraquat and MPP+, the structure is similar to paraquat, are the cause of Parkinson disease-like symptoms [16–20] by the ROS produced by paraquat or MPP+. ROS induces apoptosis on nerve cells of substantia nigra. It is important to know the role of ROS produced by paraquat to clarify the perturbing-mechanism of muscle-differentiation by paraquat. In our study, ascorbic acid, one of anti-oxidative substances showed no effect on the differentiation-perturbing by paraquat. H_2O_2, one of ROS did not cause the differentiation. Moreover, 100 ng/mL of paraquat did not increase TBARS level compare with control. These results suggest that paraquat induces the confusion of differentiation on C2C12 cells in ROS-independent manner.

References

1. Rahman, M., Lewis, D.M., and Allison, K. (2007) A case of paraquat burns following an industrial accident. *Emerg. Med. J*. **24**(11): 777.
2. Gear, A.J., Ahrenholz, D.H., and Solem, L.D. (2001) Paraquat poisoning in a burn patient. *J. Burn. Care Rehabil*. **22**(5): 347–351.
3. Wesseling, C., van Wendel de, J.B., and Monge, P. (2001) Pesticide-related illness and injuries among banana workers in Costa Rica: A comparison between 1993 and 1996. *Int. J. Occup. Environ. Health* **7**(2): 90–97.
4. Christakis-Hampsas, M., Tutudakis, M., Tsatsakis, A.M., Assithianakis, P., Alegakis, A., Katonis, P.G., and Michalodimitrakis, E.N. (1998) Acute poisonings and sudden deaths in Crete: A five-year review (1991–1996). *Vet. Hum. Toxicol*. **40**(4): 228–230.
5. Langston, J.W., Langston, E.B., and Irwin, I. (1984) MPTP-induced parkinsonism in human and non-human primates–clinical and experimental aspects. *Acta. Neurol. Scand. Suppl*. **100**: 49–54.
6. Langston, J.W., Irwin, I., Langston, E.B., and Forno, L.S. (1984) Pargyline prevents MPTP-induced parkinsonism in primates. *Science* **225**(4669): 1480–1482.
7. Niso-Santano, M., Morán, J.M., García-Rubio, L., Gómez-Martín, A., González-Polo, R.A., Soler, G., and Fuentes, J.M. (2006) Low concentrations of paraquat induces early activation of extracellular signal-regulated kinase 1/2, protein kinase B, and c-Jun N-terminal kinase 1/2 pathways: Role of c-Jun N-terminal kinase in paraquat-induced cell death. *Toxicol. Sci*. **92**(2): 507–515.

8. Li, C., Yu, Y., Wang, Y., Liu, L., Zhang, M., Sugano, S., Wang, Z., and Chang, Z. (2008) Both ERK and JNK are required for enhancement of MD-2 gene expression during differentiation of HL-60 cells. *Biol. Cell* **100**(6): 365–375.
9. Kim, K.A., Kim, J.H., Wang, Y., and Sul, H.S. (2007) Pref-1 (preadipocyte factor 1) activates the MEK/extracellular signal-regulated kinase pathway to inhibit adipocyte differentiation. *Mol. Cell Biol*. **27**(6): 2294–2308.
10. Mauro, A., Ciccarelli, C., De, C.P., Scoglio, A., Bouché, M., Molinaro, M., Aquino, A., and Zani, B.M. (2002) PKCalpha-mediated ERK, JNK and p38 activation regulates the myogenic program in human rhabdomyosarcoma cells. *J. Cell Sci*. **115**(Pt 18): 3587–3599.
11. Ishrath, A., Kumar, N., and Dey, C.S. (2002) Differential activation of ERK and JNK by arsenite in mouse muscle cells. *Comp. Biochem. Physiol. C Toxicol. Pharmacol*. **132**(3): 375–384.
12. Manktelow, B.W. (1967) The loss of pulmonary surfactant in paraquat poisoning: A model for the study of the respiratory distress syndrome. *Br. J. Exp. Pathol*. **48**(3): 366–369.
13. Fukuda, Y., Ferrans, V.J., Schoenberger, C.I., Rennard, S.I., and Crystal, R.G. (1985) Patterns of pulmonary structural remodeling after experimental paraquat toxicity. The morphogenesis of intraalveolar fibrosis. *Am. J. Pathol*. **118**(3): 452–475.
14. Yaffe, D. and Saxel, O. (1977) Serial passaging and differentiation of myogenic cells isolated from dystrophic mouse muscle. *Nature* **270**: 725–727.
15. Yagi, K. (1976) A simple fluorometric assay for lipoperoxide in blood plasma. *Biochem. Med*. **15**: 212–216.
16. Hertzman, C., Wiens, M., Bowering, D., Snow, B., and Calne, D. (1990) Parkinson's disease: A case-control study of occupational and environmental risk factors. *Am. J. Ind. Med*. **17**(3): 349–355.
17. Hubble, J.P., Cao, T., Hassanein, R.E., Neuberger. J.S., and Koller, W.C. (1993) Risk factors for Parkinson's disease. *Neurology* **43**; 1693–1697.
18. Jimenez-Jimenez, F.J., Mateo, D., and Gimenez-Roldan, S. (1992) Exposure to well water and pesticides in Parkinson's disease: A case-control study in the Madrid area. *Mov. Disord*. **7**: 149–152.
19. Liou, H.H., Tsai, M.C., Chen, C.J., Jeng, J.S., Chang, Y.C., Chen, S.Y., and Chen, R.C. (1997) Environmental risk factors and Parkinson's disease: A case control study in Taiwan. *Neurology* **48**: 1583–1588.
20. Wang, F., Semchuk, K.M., and Love, E.J. (1992) An assessment of the usefulness of demographic data provided by surrogate respondents in a case-control study of Parkinson's disease. *J. Clin. Epidemiol*. **45**; 1219–1227.

Molecular Cloning and Characterization of a Novel Canine Sulfotransferase

Katsuhisa Kurogi, Yoichi Sakakibara, Shin Yasuda, Ming-Cheh Liu, and Masahito Suiko

1 Introduction

The cytosolic sulfotransferases (SULTs) are enzymes that catalyze the transfer of a sulfonate group from the active sulfate, 3'-phosphoadenosine 5'-phosphosulfate (PAPS), to a hydroxyl or an amino group of an acceptor compound [1]. Sulfonation represents an important mechanism *in vivo* for the metabolism/detoxification of the drugs and other xenobiotics, as well as endogenous compounds such as steroids and thyroid hormones, catecholamine neurotransmitters, and bile acids in mammals [2–4]. It has been proposed that all cytosolic SULTs constitute a gene superfamily [5], within which several SULT gene families have been classified. It is generally accepted that members of the same SULT gene family share at least 45% amino acid sequence identity, while members of a subfamilies further divided within each SULT gene family are greater than 60% identical in amino acid sequence [6, 7]. Presently, there are six SULT gene families: SULT1 (phenol sulfotransferases), SULT2 (hydroxysteroid sulfotransferases), SULT3 (amine sulfotransferases), SULT4, SULT5, and SULT6. Tissue/organ-specific distribution and ontogenetic expression of some cytosolic SULTs have been studied in human, mouse, and rat, and the results showed that different SULTs may differ in tissue/organ and developmental stage distribution [8–10].

Many xenobiotics and endogenous compounds undergo sulfonation and are excreted via the kidney or bile. Notably, some cytosolic SULTs are expressed in kidney as well as in liver. It seems therefore that kidney is not only an excretion organ but may actively participate in detoxification via the sulfonation pathway. Madin-Darby canine kidney (MDCK) cells have been widely used as a model system for investigating the excretion/detoxification mechanism of kidney. However, little is known with regard to the cytosolic SULTs that may be involved in the detoxification mechanism of MDCK cells. Moreover, although sulfonation has been studied

K. Kurogi (✉)
Department of Biochemistry and Applied Biosciences, University of Miyazaki, Miyazaki 889-2192, Japan
e-mail: ng2801u@student.miyazaki-u.ac.jp

M. Kamihira et al. (eds.), *Animal Cell Technology: Basic & Applied Aspects*, Animal Cell Technology: Basic & Applied Aspects 16, DOI 10.1007/978-90-481-3892-0_36,

in many mammalian species including rat, mouse and human, similar information is lacking concerning the dog, where only SULT1A1, SULT1B1, and SULT1D1 have been identified and characterized [11–13]. For these reasons, MDCK cells may serve as an excellent host for the discovery of new canine cytoslic SULTs and for investigating the functional relevance of these enzymes in kidney.

In this paper, we report the molecular cloning, expression, purification, and characterization, as well as tissue distribution, of a novel canine cytosolic SULT, which is apparently an orthologue of the human SULT1C4 [14].

2 Materials and Methods

2.1 Materials

Acetaminophen, *o*-bromophenol, eugenol, minoxidil, *p*-nitrophenol (*p*NP), vanillin, and L-p-tyrosine were products of Wako Pure Chemical Industries, Ltd. 1-Naphthol was purchased from KATAYAMA CHEMICAL INDUSTRIES Co., Ltd. 2-Naphthol was from Nacalai Tesque. 1,3-Bis[tris(hydroxymethyl) methylamino]propane (bis-tris propane), dehydroepiandrosterone (DHEA), dopamine, 17β-estradiol (E_2), estrone, pregnenolone were products of Sigma Chemical Company Industries. 2-(N-morpholino) ethanesulfonic acid, monohydrate (MES) was purchased from DOJINDO. 3,3',5-Triiodothyronine (T_3) was from MP Biomedicals. 4-octylphenol and 1-naphthylamine (1-NA) were from Aldrich Chemical Company. TRIzol was obtained from Invitrogen. ReverTra Ace, KOD FX, and all restriction endonucleases were from TOYOBO. Isopropyl β-D-thiogalactopyranoside (IPTG) was purchased from TAKARA. Ligation-Convenience Kit was from NIPPON GENE. Oligonucleotide primers were synthesized by NIPPON EGT. pBluescript II SK(+) and XL1-Blue MRF' and BL21 *Escherichia coli* host strain were from Stratagene. pGEX-4T-1 prokaryotic GST fusion vector and glutathione Sepharose 4B were from GE Healthcare Biosciences. MDCK II cells (CCL-34) were from American Type Culture Collection. Cellulose thin-layer chromatography (TLC) plates were products of Merck. All other chemicals were of the highest grade commercially available.

2.2 Molecular Cloning of a Novel Canine Cytosolic SULT

MDCK II cells were routinely maintained in MEM containing 5% FBS at 37°C and 5% CO_2. Total RNA was extracted from MDCK II cells using TRIzol according to manufacturer's instructions [15], and the cDNA encoding the novel canine SULT was amplified by employing the RT-PCR technique. With the total RNA from MDCK II cells as the template and oligo (dT) as the primer, the first-strand cDNA was synthesized using a First-Strand cDNA Synthesis Kit (TOYOBO). Using gene-specific sense (5'-GCGCGGATCCATGGCCTTAAACAAAATGG AG-3')

and antisense (5'-CCCTCGAGGGTTATGAGAATTGGAAGTGAAA-3') oligonucleotideprimers, a PCR reaction in a 20 μl reaction mixture was carried out under the action of KOD-FX, with the first-strand cDNA prepared as template. Amplification conditions were 2 min at 94°C, followed by 30 cycles of 30 s at 94°C, 30 s at 50°C, 1.5 min at 68°C. The PCR product isolated by spin-filtration, upon digestion by Bam HI/Xho I, was subcloned into the Bam HI/Xho I site of pBluescript II SK(+) and transformed into *E. coli* XL1-Blue MRF'. To verify its authenticity, the cDNA insert was subjected to nucleotide sequencing [16].

2.3 Bacterial Expression and Purification of the Recombinant Canine Cytosolic SULT1C4

pBluescript II SK(+) harboring the canine *SULT* cDNA was digested by *Bam* HI/*Xho* I, and subcloned into the *Bam* HI/*Xho* I site of pGEX-4T-1 prokaryotic expression vector. pGEX-4T-1. pGEX-4T-1 harboring the canine *SULT1C4* cDNA was transformed into competent *E. coli* BL21 cells. Transformed BL21 cells were grown to $OD_{600\ nm} = \sim 0.4$ in 200 ml LB medium and induced with 0.1 mM IPTG. After a 4-h induction at 25°C, the cells were collected by centrifugation and homogenized in ice-cold lysis buffer (50 mM Tris-HCl, pH 8.0, 150 mM NaCl, and 1 mM EDTA) using an Ohtake French Press. The crude homogenate containing the GST fusion protein was subjected to centrifugation at 20,400*g* for 20 min at 4°C. The purification procedure for the recombinant canine cytosolic SULT1C4 was carried out by affinity gel fractionation using glutathione Sepharose 4B at 4°C. The recombinant protein was eluted by a 3-h digestion at 4°C using 500 μl of a thrombin digestion buffer (50 mM Tris-HCl, pH 8.0, 150 mM NaCl, and 2.5 mM $CaCl_2$) containing 5 unit/ml bovine thrombin.

2.4 Enzymatic Assay

The sulfonation activity was assayed using PAP[^{35}S] (synthesized from ATP and [^{35}S]sulfate using recombinant human bifunctional ATP sulfurylase/adenosine 5'-phosphosulfate kinase as described previously) as the sulfate donor [17]. The standard assay mixture, with a final volume of 25 μl, contained 50 mM bis-tris propane buffer (pH 7.00), 0.2 μM PAP[^{35}S] (45 Ci/mmol), and 1, 10, or 100 μM substrates. The reaction was started by the addition of the enzyme, allowed to proceed for 10 min at 37°C, and terminated by heating at 100°C for 3 min. The final assay mixture was subjected to the analysis of [^{35}S]sulfated product using the previously developed thin-layer chromatography procedure [18], with *n*-butanol/isopropanol/formic acid/water (3:1:1:1; by volume) as the solvent system. Upon completion of TLC, the plate was analyzed using a Fluoro Image Analyzer (FLA-3000G).

2.5 Analysis of the Tissue Specific Distributions of Canine SULT1C4

RT-PCR was employed to examine the expression of SULT1C4 mRNA in different canine tissues. For use as templates in PCR, first-strand cDNAs were first reverse-transcribed from total RNA, isolated from eight canine tissues of male or female beagle, using random hexamers according to the manufacturer's instruction (TOYOBO). Using gene-specific sense (*5'-TCCCATCCATTGGATCTGGT-3'*) and antisense (*5'-CAGGTCCTCATAGAAGAGGT-3'*) oligonucleotide primers, PCR reactions in 20 μl reaction mixtures were carried out under the action of *Taq* DNA polymerase, with different (heart, thyroid grand, liver, spleen, stomach, small intestine, kidney, testis, or ovary) first-strand cDNA prepared as template. Reaction conditions were 2 min at 94°C, followed by 30 cycles of 30 s at 94°C, 30 s at 45°C, and 60 s at 72°C. The final reaction mixture was applied onto a 2.5% agarose gel, separated by electrophoresis, and visualized by ethidium bromide staining.

3 Results and Discussion

3.1 Molecular Cloning of a Novel Canine Cytosolic SULT

Using the nucleotide sequence of canine SULT1D1 (GenBank accession no. AY004331) as a search tool, a novel canine *SULT* gene (LOC474542) was identified in the dog genome database (NCBI). The cDNA encoded by this newly identified canine *SULT* gene was amplified by RT-PCR with the total RNA isolated from MDCK II cells as the template, and was subjected to nucleotide sequencing. Figure 1 shows the nucleotide and deduced amino acid sequences of this novel canine SULT. The open reading frame encompasses 912 nucleotides and encodes a 303 amino acid polypeptide. Similar to other cytosolic SULTs, this newly identified canine SULT contains sequences resembling the so-called ''5'-phosphosulfate binding (5'-PSB) motif'' (YPKSGTxW in the N-terminal region) and "3'-phosphate binding (3'-PB) motif" (YxYRNPKDVLISxFH in the central region) [19] which are proposed to be involved in the binding of PAPS, a co-substrate for the SULT-catalyzed sulfonation reactions [1]. Sequence analysis revealed that the newly identified canine SULT displays highest (82.8%) amino acid sequence identity to human SULT1C4. It is generally accepted that members of the same SULT gene family share at least 45% amino acid sequence identity, whereas members of subfamilies further divided within each SULT gene family are greater than 60% identical in amino acid sequence [6, 7]. Based on these criteria, the newly cloned canine SULT clearly belongs to the same gene subfamily as human SULT1C4, and was thus designated the canine SULT1C4 (see Table 1) [5, 15].

```
atggccttaaacaaaatggaggattttaaatttgatggaacaacacgcctacctgtcgct  60
M  A  L  N  K  M  E  D  F  K  F  D  G  T  T  R  L  P  V  A   20
tatgtggaggggattttacaacccacacctacctgtgacatctgggaccagatctggaat  120
Y  V  E  G  I  L  Q  P  T  P  T  C  D  I  W  D  Q  I  W  N   40
ttccaagccaagtctgatgatctgcttattgccacctatcctaaagcaggaacaacatgg  180
F  Q  A  K  S  D  D  L  L  I  A  T  Y  P  K  A  G  T  T  W   60
actcaggagatagtggacttaatacaaaatgaaggggatgttgacaaaagtcaaagagca  240
T  Q  E  I  V  D  L  I  Q  N  E  G  D  V  D  K  S  Q  R  A   80
cctattcatgtacgaattcctttcattgaatggataatcccatccattggatctggtttg  300
P  I  H  V  R  I  P  F  I  E  W  I  I  P  S  I  G  S  G  L   100
gaaagagctaatgaaatgccctcaccacggaccctgaaaacacatcttcccatccatttg  360
E  R  A  N  E  M  P  S  P  R  T  L  K  T  H  L  P  I  H  L   120
ctgccaccatccttcatagaaaaaaactgcaagataatctatgtggcaagaaatccaaag  420
L  P  P  S  F  I  E  K  N  C  K  I  I  Y  V  A  R  N  P  K   140
gacaatatggtgtcttattaccatttccaaagaatgaataaatctcttcctgctccagga  480
D  N  M  V  S  Y  Y  H  F  Q  R  M  N  K  S  L  P  A  P  G   160
acctgggaagagtattttgagaattttctggctgggaaagtatgctggggttcttggtat  540
T  W  E  E  Y  F  E  N  F  L  A  G  K  V  C  W  G  S  W  Y   180
gaccacgtgaaaggatggtggaaagccaaagaccaacaccgcattctctacctcttctat  600
D  H  V  K  G  W  W  K  A  K  D  Q  H  R  I  L  Y  L  F  Y   200
gaggacctgaagaagaatacaaagcatgaaattcagaaggtggcagagtttattggaaaa  660
E  D  L  K  K  N  T  K  H  E  I  Q  K  V  A  E  F  I  G  K   220
aacctagatgatgaaatcctagataaaattgtccatcacacttcatttgatgttatgaag  720
N  L  D  D  E  I  L  D  K  I  V  H  H  T  S  F  D  V  M  K   240
gagaatccaatgtcaaactattcatcagttcctgctaaaatcatgaaccactctgtgtct  780
E  N  P  M  S  N  Y  S  S  V  P  A  K  I  M  N  H  S  V  S   260
ccattcatgagaaaagggatagttggagactggaagaatcactttaccgtggctcagaat  840
P  F  M  R  K  G  I  V  G  D  W  K  N  H  F  T  V  A  Q  N   280
gaaagatttaatgaagactacaagaagaaaatggctgataccaatctaacttttcacttc  900
E  R  F  N  E  D  Y  K  K  K  M  A  D  T  N  L  T  F  H  F   300
caattctcataa                                                  912
Q  F  S  *                                                    303
```

Fig. 1 Nucleotide and deduced amino acid sequences of canine SULT1C4 5'-PSB motif and 3'-PB motif located, in the N-terminal and middle regions are underlined

Table 1 Amino acid sequence comparison of canine SULT1C4 with other SULTs

Enzyme	GeneBank accession number	Identity* (%)
cSULT1A1	D29807	50
cSULT1B1	AY004332	52
cSULT1D1	AY004331	53.5
hSULT1C1	XM497863	53.1
hSULT1C2	U66036	62.2
hSULT1C4	AF055584	82.8

*Identity (%) of the amino acid sequence of cSULT1C4 to other SULTs are shown.

3.2 Tissue-Specific Expression of Canine SULT1C4

We were interested in the expression patterns of SULT1C4 in different dog tissues/organs. RT-PCR was employed to examine the expression of mRNA encoding SULT1C4 in 8 tissues from male and female dog (see Section 2). Interestingly,

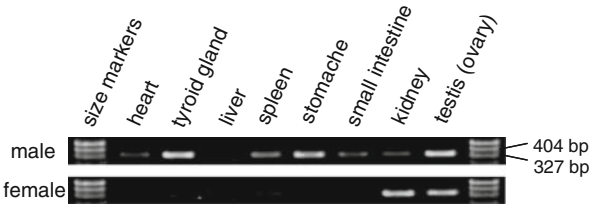

Fig. 2 Tissue distributions of the canine SULT1C4 mRNA expression analysis of SULT1C4 was performed using RT-PCR

male dog expressed SULT1C4 mRNA in every tested tissue except the liver, whereas female dog expressed SULT1C4 mRNA only in spleen, kidney and ovary. These results suggested that SULT1C4 may play a role in not only kidney but also other tissue, and with a gender difference. A previous study demonstrated that human SULT1C4 was expressed in ovary, kidney, fetal heart, fetal lung, fetal kidney, but not in thyroid grand, stomach, and small intestine [15]. It therefore appears that the expression of SULT1C4 may vary between different species (Fig. 2).

3.3 Characterization of a Recombinant Canine SULT1C4

Recombinant canine SULT1C4 was expressed and purified using the pGEX-4T-1 GST gene fusion system. Purified recombinant canine SULT1C4 was subjected to functional characterization with respect to their sulfonating activities. A pH-dependence experiment was first carried out using *o*-bromophenol as the substrate. Results showed that canine SULT1C4 displayed a pH optimum at 7.00 (data not shown).

To study the substrate specificity of the purified SULT1C4, representative endogenous and xenobiotic compounds were tested as substrates. The activity data compiled in Table 2 revealed that SULT1C4 enzyme displayed sulfonating activities toward a variety of xenobiotic compounds, especially xenobiotic phenols including phenol, *o*-bromophenol, vanillin, *p*-nitrophenol (*p*NP), 1-naphthol and 2-naphthol. It is therefore possible that the canine SULT1C4 may play a role on the metabolism and/or detoxification of those xenobiotic phenols. The enzyme, however, is probably not involved in the sulfonation of endogenous compounds such as dopamine, E_2 (17β-estradiol), pregnenolone, DHEA (dehydroepiandrosterone), T_3 (3,3',5-triidothyronine). It should be noted that human SULT1C4 [15, 20] shares with canine SULT1C4 the sulfonating activities toward simple phenols.

Table 3 shows the kinetic constants of canine SULT1C4 with the phenol, *o*-bromophenol, vanillin, eugenol, *p*NP, 1-naphthol and 2-naphthol as substrates. In comparison with those determined with phenol as substrate, canine SULT1C4 displayed lower K_m (and therefore higher affinity) with *o*-bromophenol. It was noted that the V_{max}/K_m value of canine SULT1C4 with *o*-bromophenol is 82.9-fold greater than that with phenol, indicating the higher catalytic efficiency of the enzyme with

Table 2 Specific activities of the canine SULT1C4 toward endogenous and xenobiotic compounds

	Specific activity (nmol/min/mg)		
Substrate conc. (μM)	1	10	100
Phenol	0.24 ± 0.01	2.36 ± 0.08	7.08 ± 0.19
o-Bromophenol	7.09 ± 0.32	10.27 ± 0.48	3.64 ± 0.11
Vanilin	2.29 ± 0.12	8.86 ± 0.51	9.05 ± 0.54
Eugenol	0.18 ± 0.01	1.65 ± 0.06	6.83 ± 0.47
4-Octyphenol	0.06 ± 0.01	0.43 ± 0.10	0.20 ± 0.01
p-NP (*p*-Nitrophenol)	0.05 ± 0.03	0.31 ± 0.02	0.29 ± 0.25
Dopamine	N.D.*	N.D.	N.D.
Tyrosine	N.D.	N.D.	N.D.
Tyramine	N.D.	N.D.	N.D.
Acetaminophen	N.D.	N.D.	N.D.
1-naphthol	0.83 ± 0.10	8.31 ± 0.20	9.59 ± 0.30
2-naphthol	0.27 ± 0.02	2.71 ± 0.21	7.75 ± 0.16
E_2 (17β-Estradiol)	N.D.	N.D.	N.D.
Pregnenolone	N.D.	N.D.	N.D.
DHEA (Dehydroepiandrosterone)	N.D.	N.D.	N.D.
T_3 (3,3′,5-Triiodothylamine)	0.01 ± 0.00	0.07 ± 0.01	0.01 ± 0.00
1-NA (1-Naphthylamine)	N.D.	N.D.	N.D.
Minoxidil	N.D.	N.D.	N.D.

Data shown represent means ± SD from three determinations.
*N.D. refers to activity not detected.

Table 3 Kinetic constants of canine SULT1C4

	K_m* (μM)	V_{max}** (nmol/min/mg)	V_{max}/k_m (nmol/min/mg/μM)
Phenol	25.66	9.02	0.35
o-Bromophenol	0.63	18.28	29.02
Vanilin	19.87	17.18	0.86
Eugenol	42.28	7.85	0.19
*p*NP	72.95	3.59	0.05
1-Naphthol	8.29	15.63	1.89
2-Naphthol	27.36	9.6	0.35

*K_m and **V_{max} values were determined from Lineweaver-Burk plots.

o-bromophenol as the substrate. In contrast, it was observed that the V_{max}/K_m value with *p*NP was less than that with phenol, indicating the lower catalytic efficiency of the enzyme for *p*NP. These results suggest that canine SULT1C4 prefers bromo group at *ortho-* to nitro group at *para-* position. Moreover, it is an interesting feature that canine SULT1C4 prefers 1-naphthol over 2-naphthol with a 5.4-fold greater V_{max}/K_m value.

In conclusion, we have cloned, expressed, purified and characterized a novel canine cytosolic SULT, SULT1C4. Recombinant canine SULT1C4 resembled the orthologous human SULT1C4 with regard to enzymatic properties particularly substrate specificity. However, RT-PCR analysis showed that, unlike human SULT1C4, canine SULT1C4 was expressed mainly in spleen, kidney and testis/ovary, indicating their tissue/organ-specific differences between human and dog. Collectively, the results obtained suggested that the newly identified canine SULT1C4 may be involved in the sulfonation of xenobiotic phenols such as phenol, *o*-bromophenol. vanillin, 1-naphthol in kidney as well as other tissues. These results provide a foundation for further studies on the catalytic mechanism underlying phenols sulfonation.

Acknowledgements This work was supported by a Grant-in-Aid for Scientific Research (B), (C) (M.S. and Y.S.), a Grant-in Aid for Encouragement of Young Scientists (Y.S.) from the Ministry of Education, Culture, Sports, Science and Technology of Japan, Health and Sciences Research Grants (Toxicogenomics) from the Ministry of Health, Labor and Welfare of Japan (Y.S.) and start-up funds from College of Pharmacy, The University of Toledo (M.C.L.). We also thank Satoshi Miyazaki, Saki Takahashi, Dr Madhyasha Harish Kumar for great help of this study and manuscript.

References

1. Lipmann, F. (1958) Biological sulfate activation and transfer. *Science* **128**: 575–580.
2. Mulder, G.J. and Jakoby, W.B. (1990) In: Mulder, G.J. (Ed.), *Conjugation Reactions in Drug Metabolism* (pp. 107–161). London: Taylor and Francis Ltd.
3. Falany, C. and Roth, J.A. (1993) In: Jeffery, E.H. (Ed.), *Human Drug Metabolism: From Molecular Biology to Man* (pp. 101–115). BocaRaton, FL: CRC Press, Inc.
4. Weinshilboum, R.M. and Otterness, D.M. (1994) In: Kaufmann, F.C. (Ed.), *Conjugation-Deconjugation Reactions in Drug Metabolism and Toxicity* (pp. 45–78). Berlin: Springer-Verlag, Inc.
5. Blanchard, R.L., Freimuth, R.R., Buck, J., Weinshilboum, R.M., and Coughtrie, M.W.H. (2004) A proposed nomenclature system for the cytosolic sulfotransferase (SULT) superfamily. *Pharmacogenetics* **14**: 199–211.
6. Yamazoe, Y., Nagata, K., Ozawa, S., and Kato, R. (1994) Structural similarity and diversity of sulfotransferases. *Chem. Biol. Interact*. **92**: 107–117.
7. Weinshilboum, R.M., Otterness, D.M., Aksoy, I.A., Wood, T.C., Her, C.T., and Raftogianis, R.B. (1997) Sulfation and sulfotransferases 1: Sulfotransferase molecular biology: cDNAs and genes. *FASEB J*. **11**: 3–14.
8. Pacifici, G.M., Franchi, M., Colizzi, C., Giuliani, L., and Rane, A. (1988) Sulfotransferase in humans: Development and tissue distribution. *Pharmacology* **36**: 411–419.
9. Alnouti, Y. and Klaassen, C.D. (2006) Tissue distribution and ontogeny of sulfotrasnferase enzymes in mice. *Toxicol. Sci*. **93**: 242–255.
10. Dunn II, R.T. and Klaassens, C.D. (1998) Tissue-specific expression of rat sulfotransferase messenger RNAs. *Drug. Metab. Dispos*. **26**: 598–604.
11. Tsoi, C., Morgenstern, R., and Swedmark, S. (2002) Canine sulfotransferase SULT1A1: Molecular cloning, expression, and characterization. *Arch. Biochem. Biophys*. **401**: 125–133.
12. Tsoi, C., Falany, C.N., Morgenstern, R., and Swedmark, S. (2001) Molecular cloning, expression, and characterization of a canine sulfotransferase that is a human ST1B2 ortholog. *Arch. Biochem. Biophys*. **390**: 87–92.

13. Tsoi, C., Falany, C.N., Morgenstern, R., and Swedmark, S. (2001) Identification of a new subfamily of sulphotransferases: Cloning and characterization of canine SULT1D1. *Biochem. J*. **356**: 891–897.
14. Chomczynski, P. and Sacchi, N. (1987) Single-step method of RNA isolation by acid guanidinium thiocyanate-phenol-chloroform extraction. *Anal. Biochem*. **162**: 156–159.
15. Sakakibara, Y., Yanagisawa, K., Katafuchi, J., Ringer, P.D., Takami, Y., Nakayama, T., Suiko, M., and Liu, M.-C. (1998) Molecular cloning, expression, and characterization of novel human SULT1C sulfotransferases that catalyze the sulfonation of N-hydroxy-2-acetylaminofluorene. *J. Biol. Chem*. **273**: 33929–33935.
16. Sanger, F., Nicklen, S., and Coulson, A.R. (1977) DNA sequencing with chain-terminating inhibitors. *Proc. Natl. Acad. Sci USA*. **74**: 5463–5467.
17. Yanagisawa, K., Sakakibara, Y., Suiko, M., Takami, Y., Nakayama, T., Nakajima, H., Takayanagi, K., Natori, Y., and Liu, M.-C. (1998) cDNA Cloning, expression, and characterization of the human bifunctional ATP sulfurylase/adenosine 5'-phosphosulfate kinase enzyme. *Biosci. Biotechnol. Biochem*. **62**: 1037–1040.
18. Liu, M.-C. and Lipmann, F. (1984) Decrease of tyrosine-*O*-sulfate-containing proteins found in rat fibroblasts infected with Rouse sarcoma virus or Fujinami sarcoma virus. *Proc. Natl. Acad. Sci. USA*. **81**: 3695–3698.
19. Kakuta, Y., Pedersen, L.G., Pedersen, L.C., and Negishi, M. (1998) Conserved structural motifs in the sulfotransferase family. *Trends Biochem. Sci*. **23**, 129–130.
20. Allali-Hassani, A., Pan, P.W., Ludmila, D., Rafael, N., Wolfram, T., Aiping, D., Peter, L., Fernando, M., Janet, T., Aled, E.M., Alexey, B., Alexander, P.N., Masoud, V., and Cheryl, A.H. (2007) Structural and chemical profiling of the human cytosolic sulfotransferases. *PLoS. Biol*. **5**: 1–16.

In Vitro Analysis of the Interaction Between Human Intestinal Epithelial Cells and Macrophage-Like Cells

Yoko Ishimoto, Hideo Satsu, Tetsunosuke Mochizuki, Mamoru Totsuka, and Makoto Shimizu

1 Introduction

In addition to the function of absorbing nutrients, intestines have many defense mechanisms against exogenous substances such as bacteria and chemicals. Intestinal epithelial cells, which cover the surface of intestines function to keep intestinal homeostasis not only by acting as a barrier but also by interacting with immune cells located in the intestinal epithelium via soluble factors. But, in the intestines of the patients suffering from intestinal inflammation, hyperproduction of inflammatory cytokines, especially TNF-α, from immune cells such as activated macrophages, and damage of intestinal epithelial cells is observed. This is one of the causes of intestinal inflammation.

There are many types of bowel diseases such as infectious enteritis and inflammatory bowel disease (IBD) and recently the number of IBD patients has been increasing probably due to westernization of the food style. But the therapeutic method has not yet been established since the diseases are induced by a lot of complicated factors.

Previously, we constructed an in vitro model using a coculture system to analyze the effect of macrophages on intestinal epithelial cells [1]. We showed that coculturing with macrophage-like THP-1 cells induced cell damage to intestinal epithelial-like Caco-2 cells, which was caused by TNF-alpha secreted from THP-1 cells. We also showed occurrence of apoptosis and necrosis in the disrupted Caco-2 cells, and involvement of NF-κB and ERK pathway in THP-1-induced cell damage of Caco-2 cells.

In this study, we further analyzed this phenomenon to reveal the pathogenic mechanism of the intestinal inflammation.

M. Shimizu (✉)
Department of Applied Biological Chemistry, Graduate School of Agricultural and Life Sciences, The University of Tokyo, 1-1-1 Yayoi, Bunkyo-ku, Tokyo 113-8657, Japan
e-mail: ams316@mail.ecc.u-tokyo.ac.jp

M. Kamihira et al. (eds.), *Animal Cell Technology: Basic & Applied Aspects*, Animal Cell Technology: Basic & Applied Aspects 16, DOI 10.1007/978-90-481-3892-0_37,

2 Material and Methods

2.1 Coculture Experiment

For a coculture system, human intestinal epithelial-like Caco-2 cell monolayers and macrophage-like THP-1 cells were used as previously described [1]. Briefly, Caco-2 cells were cultured for 14 days on a semi-permeable support, and THP-1 cells were differentiated with phorbol myristate acetate (PMA) for 4 days in 12-well plates. Then, the semi-permeable support membrane in which Caco-2 cells had been cultured was placed on the 12-well plates on which THP-1 has been cultured.

2.2 Determination of Cell Damage

The viability of the Caco-2 cell monolayers was mainly assessed by their ability to maintain lactate dehydrogenase (LDH) inside the cells as measured with an LDH-cytotoxic test kit (Wako, Japan).

2.3 RNA Preparation and DNA Microarray

Total RNA in Caco-2 cells which had been cocultured with THP-1 cells over the time periods of 0, 1, 3, 6, 24, and 48 h was extracted by using Isogen (Nippon Gene, Japan) according to the manufacturer's instructions. cRNA synthesis using 20 μg total RNA and hybridization to the HG-U133 plus 2.0 GeneChip was performed following the manufacturer's recommended instruction (Affymetrix, Santa Clara, CA). GeneChip Operating software was used to determine the presence, marginal, or absence of mRNA for specific genes in each sample. Affymetrix microarray Analysis Suite (MAS) 5.0 was used for chip-to-chip normalization and gene expression value determination. Based on the duplicate DNA microarray results, genes that were more than 4-fold up-regulated were selected.

2.4 Real Time RT-PCR

Reverse transcription of the RNA was performed using ExScript^{R} RT reagent Kit (TaKaRa, Japan) according to the manufacturer's instruction. Quantitative real-time RT-PCR analysis was performed with a Lightcycler (Roche, Japan). One-twentieth of the first strand cDNA was used as a template for detection of each gene of interest using SYBR Green PCR assay (TaKaRa, Japan). The gene expression levels were normalized to the level of the housekeeping gene (GAPDH). Relative gene expression changes were calculated as number-fold changes compared to the control samples.

3 Results and Discussion

We have previously reported that both apoptotic and necrotic cell death were induced in Caco-2 cells cocultured with THP-1 cells by morphorgical analysis. It is suggested that the expression of various genes changed in Caco-2 cells cocultured with THP-1 cells. Caco-2 cells which had been cocultured with THP-1 cells over the time periods of 0, 1, 3, 6, 24, and 48 h were therefore exhaustively analyzed with a DNA microarray to detect the changes of gene expression. As a result, the expression of 24,000 genes including a number of unknown genes out of 55,000 probe sets on a chip was observed.

Table 1 is the list of the selected genes whose signal intensity levels were more than 200 and which increased 4-folds compared with the gene expression in Caco-2 cells cocultured for 0 h. It showed that the expression of genes related to immunity and apoptosis was increased.

Genes of chemokines, such as IL-8, CXCL1, CXCL3 and CCL20, and Decay-Accelerating Factor (DAF or CD55) were among the immunity-related genes in Table 1. Puleston et al. reported that gene expression of CXCL1, CXCL2, CXCL3 and CCL20 was up-regulated in active colonic IBD, compared with uninflamed area or tissues from control [2]. DAF is one of the complement regulating proteins, and its expression is up-regulated during inflammation [3]. For example, an increased expression (or surface levels) of DAF on colon epithelium of IBD patients was reported [4, 5]. It has also been reported that a proportion of DAF-deficient (Cromer INAB) patients develop IBD [6]. These reports strongly support that Caco-2 cells cocultured with THP-1 cells are under inflammatory conditions. The apoptosis-related genes in Table 1 include not only pro-apoptotic genes but also anti-apoptotic genes, such as TNFAIPs and Mcl-1, suggesting that the increases in the anti-apoptotic genes are protective responses of the cells to avoid apoptosis.

Table 1 The up-regulated gene expression* in Caco-2 cells cocultured with THP-1 cells

	Gene	1 h	3 h	6 h	24 h	48 h
Immune	IL-8	5.9	5.9	6.7	4.5	NC
	CXCL1	5.4	4.8	4.5	2.9	NC
	CXCL3	3.4	3.2	3.3	2.3	NC
	CCL20	3.2	3.7	3.7	3.1	1.7
	CXCR4	NC	1.2	2.1	1.4	0.9
	DAF	1.0	1.8	2.1	1.9	2.1
Apoptosis	PHLDA2	2.9	2.7	2.9	2.4	1.5
	TNFRS10B	0.6	1.8	2.4	2.3	1.6
	IEX-1	3.2	3.1	2.8	1.6	0.4
Anti-apoptosis	TNFAIP3	3.1	3.0	3.1	1.9	0.9
	TNFAIP8	NC	1.5	2.1	1.5	1.0
	MCL-1	1.9	2.6	2.6	1.1	0.7

*The number is fold change ($\log_2$ ratio)

The increase in gene expression in Caco-2 cells was then confirmed by real time RT-PCR. The expression of 4 apoptosis-related genes, Mcl-1, TNFAIP8, TNFSF10B and IEX-1genes, was observed to be changed as detected by a DNA microarray (data not shown).

We focused on IEX-1 whose changes in the mRNA expression was the highest among the genes, and analyzed whether IEX-1 was involved in THP-1 -induced cell damage in Caco-2 cells. IEX-1 is an immediate early response gene and induced by various stimuli such as irradiation, growth factors, LPS and inflammatory cytokines including TNF-α and IL-1β [7]. Several reports indicate that IEX-1 is involved in the regulation of apoptosis, although contradicting results regarding the pro-apoptotic or anti-apoptotic properties of IEX-1 have also been reported [8–11].

To investigate the effect of TNF-α secreted from THP-1 cells on IEX-1 mRNA expression, Caco-2 cells were treated with anti-TNF-α monoclonal antibody. After coculturing for 1 h, RNA was extracted from Caco-2 cells and measured IEX-1 mRNA expression using real time RT-PCR. Induction of IEX-1 expression in cocultured Caco-2 cells was suppressed, suggesting that TNF-α was involved in an increase of IEX-1 mRNA level in Caco-2 cells (Fig. 1).

The fact that cell damage in Caco-2 cells was suppressed by anti-TNF-α monoclonal antibody indicates that adding recombinant TNF-α on the basal side may reproduce this phenomenon. Three culture models were therefore constructed to investigate this hypothesis (Fig. 2). Model-(I) contained non-treated Caco-2 cells cultured on semi-permeable support membranes and was used as a control. Model-(II) contained Caco-2 cells treated with TNF-α (25 ng/ml), and Model-C contained Caco-2 cells cultured with THP-1 cells. Some factors as well as TNF-α might be present in the basal side of Model-(III). The large quantity of LDH released from damaged cells was observed only in the Caco-2 cells cocultured with THP-1 cells, which suggested some factors other than TNF-α seemed to be involved in the damage in Caco-2 cells (Fig. 2a). And, the highest IEX-1 mRNA level was observed in Caco-2 cocultured with THP-1 cells (Fig. 2b).

The difference in the IEX-1 mRNA level of the three models would be due to the different quantity and types of factors present in the basal side. Secretion of several

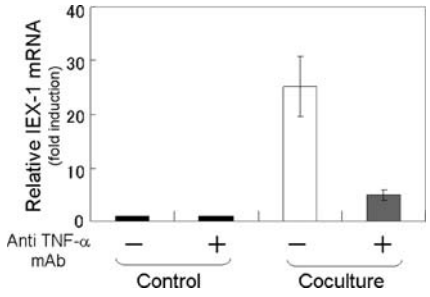

Fig. 1 Effect of the anti-TNF-α antibody on IEX-1 mRNA expression in Caco-2 cells cocultured with THP-1 cells. For real-time RT-PCR, Caco-2 cells cocultured for 1 h in the absence or presence of anti-TNF-α antibody (3.2 μg/ml) were used

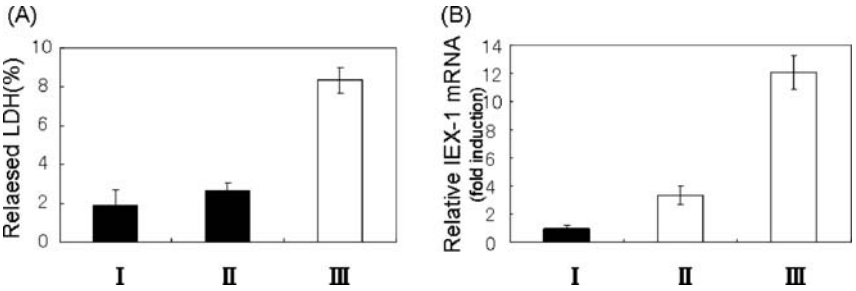

Fig. 2 LDH leakage (**a**) and IEX-1 mRNA expression (**b**) of Caco-2 cells cultured in three culture models. Model-(I), control; Model-(II), cultured with TNF-α; Model-(III), cocultured with THP-1 cells

cytokines known to be produced by THP-1 cells was therefore measured using a sandwich-ELISA method. The results showed that IL-1β production was increased in THP-1 cells cocultured with Caco-2 cells (data not shown).

To investigate the effect of IL-1β secreted from THP-1 cells on the IEX-1 mRNA expression, Caco-2 cells were treated with anti-IL-1β monoclonal antibody (8.0 μg/ml). After coculturing for 1 h, the induction of IEX-1 expression in cocultured Caco-2 cells was partly suppressed, suggesting that IL-1β was involved in the increased IEX-1 mRNA expression in Caco-2 cells (data not shown).

In conclusion, we showed that the expression of genes related to immunity and apoptosis was increased in Caco-2 cells by coculturing with THP-1 cells. The apparent increase in IEX-1 mRNA expression would be, at least partly, due to TNF-α and IL-1β secreted from THP-1 cells. The role of IEX-1 in Caco-2 cell damages induced by THP-1 cells should be revealed.

These results suggest that the phenomenon observed in this system is similar in some respects to that observed with intestinal inflammation such as IBD, supporting the previous suggestion that this coculture system would be useful to analyze the interaction between the cells upon intestinal inflammation.

References

1. Satsu, H., Ishimoto, Y., Nakano, T., Mochizuki, T., Iwanaga, T., and Shimizu, M. (2006) Induction by activated macrophage-like THP-1 cells of apoptotic and necrotic cell death in intestinal epithelial Caco-2 monolayers via tumor necrosis factor-alpha. *Exp. Cell Res*. **312**: 3909–3919.
2. Puleston, J., Cooper, M., Murch, S., Bid, K., Makh, S., Ashwood, P., Bingham, A.H., Green, H., Moss, P., Dhillon, A., Morris, R., Strobel, S., Gelinas, R., Pounder, R.E., and Platt, A. (2005) A distinct subset of chemokines dominates the mucosal chemokine response in inflammatory bowel disease. *Aliment. Pharmacol. Ther*. **21**: 109–120.
3. Andoh, A., Kinoshita, K., Rosenberg, I., and Podolsky, D.K. (2001) Intestinal trefoil factor induces decay-accelerating factor expression and enhances the protective activities against complement activation in intestinal epithelial cells. *J. Immunol*. **167**: 3887–3893.
4. Berstad, A.E. and Brandtzaeg, P. (1998) Expression of cell membrane complement regulatory glycoproteins along the normal and diseased human gastrointestinal tract. *Gut* **42**: 522–529.

5. Uesu, T., Mizuno, M., Inoue, H., Tomoda, J., and Tsuji, T. (1995) Enhanced expression of decay accelerating factor and CD59/homologous restriction factor 20 on the colonic epithelium of ulcerative colitis. *Lab Invest*. **72**: 587–591.
6. Daniels, G. (1989) Cromer-released antigens–blood group determinats on decay-accelerating factor. *Vox Sang*. **56**: 205–211.
7. Wu, M.X. (2003) Roles of the stress-induced gene IEX-1 in regulation of cell death and oncogenesis. *Apoptosis* **8**: 11–18.
8. Zhang, Y., Schlossman, S.F., Edwards, R.A., Ou, C.N., Gu, J., Wu, M.X. (2002) Impaired apoptosis, extended duration of immune responses, and a lupus-like autoimmune disease in IEX-1-transgenic mice. *Proc. Natl. Acad. Sci. USA* **99**: 878–883.
9. Osawa, Y., Nagaki, M., Banno, Y., Brenner, D.A., Nozawa, Y., Moriwaki, H., and Nakashima, S. (2003) Expression of the NF-kappaB target gene X-ray-inducible immediate early response factor-1 short enhances TNF-alpha-induced hepatocyte apoptosis by inhibiting Akt activation. *J. Immunol*. **170**: 4053–4060.
10. Shen, L., Guo, J., Santos-Berrios, C., and Wu, M.X. (2006) Distinct domains for anti-and pro-apoptotic activities of IEX-1. *J. Biol. Chem*. **281**: 15304–15311.
11. Sebens Muerkoster, S., Rausch, A.V., Isberner, A., Minkenberg, J., Blaszczuk, E., Witt, M., Folsch, U.R., Schmitz, F., Schafer, H., and Arlt, A. (2008) The apoptosis-inducing effect of gastrin on colorectal cancer cells relates to an increased IEX expression mediating NF-kappaB inhibition. *Oncogene* **27**: 1122–1134.

Role of Ubiquitination Promoted During Restimulation in the Induction of T Cell Anergy

Yohei Mizuguchi, Ai Yamamoto, Makoto Hattori, and Tadashi Yoshida

1 Introduction

The immune system is a mechanism for preventing us from the infection by pathogens. Immune reaction is activated to remove antigens when the pathogens invade us. T cells play important roles in activating B cells, macrophages, T-cytotoxic cells by secreting cytokines or surface molecules. On the other hand, immune reaction against self and food antigens causes autoimmune disease and food allergy. Therefore, immune tolerance is induced against such antigens as food and self. One of the major mechanisms of immunological tolerance is T cell anergy [1]. T cell anergy is a condition of T cells unable to react against antigen.

Recent studies have demonstrated that some E3 ubiquitin ligases were upregulated in anergic T cells [2–5]. These observations suggested that the ubiquitination and degradation of intracellular proteins are required for the T cell anergy. The degradation of specific proteins would therefore occur actively during the induction of T cell anergy, and such proteins are considered to play important roles in the induction of immunological tolerance [2–5]. However, the role and mechanism of ubiqutination in the induction of T cell anergy has not been clarified.

In this study, we examined the kinetics of the ubiquitination in the induction of T cell anergy. The results of our study clearly demonstrated that the restimulation of anergic T cells is required for the ubiquitination of intracellular proteins.

2 Materials and Methods

2.1 Mice

T cell receptor transgenic mice DO11.10 were used at 6–9 weeks old. T cells of these mice recognize ovalbumin (OVA). BALB/c mice were purchased from Clea

T. Yoshida (✉)
Department of Applied Biological Science, Tokyo University of Agriculture and Technology, Fuchu, Tokyo 183-8509, Japan
e-mail: tyoshi@cc.tuat.ac.jp

M. Kamihira et al. (eds.), *Animal Cell Technology: Basic & Applied Aspects*, Animal Cell Technology: Basic & Applied Aspects 16, DOI 10.1007/978-90-481-3892-0_38,

Japan (Tokyo, Japan). All the mice used in this study were maintained and used in accordance with the guidelines for the care and use of experimental animals of Tokyo University of Agriculture and Technology.

2.2 Preparation of OVA-Specific Th1 Cells

Naïve splenocytes isolated from DO11.10 were stimulated with OVA supplemented with IL-12 for inducing the differentiation to Th1 cells. Th1 cells were used for the experiments 7 days after stimulation.

2.3 Anergy Induction

Th1 cells were incubated in the wells precoated with the anti-CD3 monoclonal antibody (145-2C11, Cedarlane, Ontario, Canada) for 24 h. These wells had been coated overnight with anti-CD3 antibody 1 μg/ml. The T cells were collected and moved to another well without the antibody to rest. After resting for 3 days, Th1 cells were collected and used for restimulation.

2.4 Restimulation

For analyzing the ubiquitinated proteins, collected Th1 cells were restimulated in the wells precoated with the anti-CD3 antibody 5 μg/ml and anti-CD28 monoclonal antibody (37.51, eBioscience, San Diego, CA) 5 μg/ml. After 30 min, cell lysates were prepared and applied for Western blotting. For analyzing the proliferation, collected Th1 cells were restimulated with OVA (100 μg/ml) in the presence of antigen-presenting cells (APC). APC was prepared from the splenocytes of BALB/c mice by treating with mitomycin C. After 3 days, the proliferation was measured by ELISA.

2.5 ELISA

Proliferation of anergic Th1 cells and normal Th1 cells were measured by BrdU ELISA Kit (Roche Diagnostics, Basel, Switzerland).

2.6 Western Blotting

SDS-PAGE was performed according to the method of Laemmli [6] with 4% of concentrating gel and 10% of running gel. After transferring the proteins to PVDF

membrane, ubiquitinated proteins were detected by using rabbit anti-ubiquitin antibody (CALBIOCHEM, La Jolla, CA) as a primary antibody.

2.7 Statistical Analysis

Differences between the control Th1 cell and anergic Th1 cell groups were analyzed by Student's *t* test. *P* values less than 0.05 were considered statistically significant and indicated as "*" in the figure.

3 Results

3.1 Proliferation of Anergic T cells

We examined proliferation of anergic T cells compared to normal T cells.

We used Th1 cells prepared from OVA-specific TCR transgenic mice because Th1 cells are more sensitive than naïve T cells and Th2 cells [7, 8]. T cell anergy was induced by the stimulation of anti-CD3 antibody. It is known that anti-CD3 antibody induces T cell anergy in vitro. Figure 1 shows that proliferation of anergic Th1 cells was reduced compared to the control T cells.

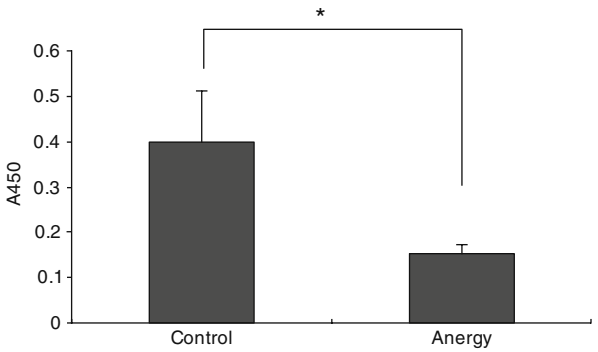

Fig. 1 Proliferation of anergic T cells

3.2 Ubiquitination of Intracellular Proteins

Next we analyzed the kinetics of ubiquitination of intracellular proteins in the induction of T cell anergy. The cells were treated with anti-CD3 antibody for induction of anergy. These cells were restimulated and detected ubiquitinated proteins by immunoblotting. Figure 2 shows that ubiquitination of intracellular proteins remarkably increased after the restimulation only in the T cells that had been induced

anergy (lane 2). The level of ubiquitinated proteins in the anergic T cells (lane 1) was equal to that in the normal T cells (lane 3) before the restimulation. In addition, the level of ubiquitinated proteins of the normal T cells did not change before and after the restimulation (lane 3 and lane 4).

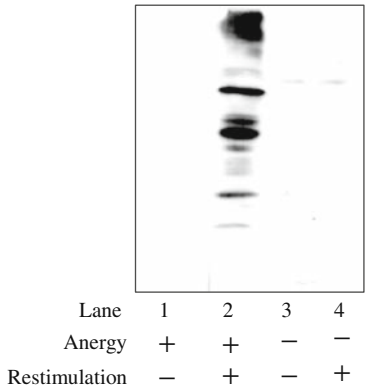

Fig. 2 Western blotting analysis of ubiquitinated proteins in anergy-induced Th1 cells

4 Discussion

Recent studies have demonstrated that several E3 ubiquitin ligases were upregulated in anergic T cells [2–5]. It suggested that the ubiquitination and degradation of intracellular proteins are involved in the T cell anergy. Our result showed that ubiquitinated proteins remarkably increased after the restimulation. Previous studies have demonstrated that several E3 ligases upregulated in the early phase of anergy induction. For example, the expression of GRAIL mRNA increased after the TCR stimulation in the absence of costimulation [9]. Together with these observation and our results, it was suggested that E3 ligases are upregulated by anergic stimulation but they work after the restimulation. This hypothesis is supported by a previous study which showed the increased ubiquitination of PLC-γ1 and PKC-θ in the anergic T cells that had been restimulated [2].

It has been known that E3 ligases such as Cbl-b, GRAIL are upregulated in the anergic T cells. Substrate proteins of Cbl-b are considered to be p85, CrkL, PLC-γ and PKC-θ. It has been also reported that these proteins are ubiquitinated in the anergic T cells [2]. These reports proposed that the degradation of such proteins results in the inability of T cells to respond to antigen. On the other hand, the proteins ubiquitinated in the anergic T cells have not been completely clarified. Our results demonstrated that many other proteins than those reported previously would be ubiquitinated and might be involved in the T cell anergy. Identifying these proteins would contribute to the clarifying the mechanism of T cell anergy. We are conducting the proteomic analysis of ubiquitinated proteins induced after the restimulation in the anergic T cells.

We have shown that the induction of anergy and activation is controlled by the intensity and length of calcium signal [10]. This finding suggests that the intensity and length of calcium signal would regulate the expression of E3 ligases. NF-AT is an important transcription factor for T cell activation and known to be activated by the calcium signal. The absolute amount of NF-AT or the ratio of NF-AT to unidentified other factors might affect the induction of E3 ligases. A fine understanding of the mechanism for inducing E3 ligases by the anergic stimulation is expected.

In summary, we demonstrated that ubiquitination of intracellular proteins increased remarkably after the restimulation. This result indicates that the ubiquitination of intracellular proteins is necessary for T cells to unrespond against antigen but not to become anergic state. It is expected that the results of our study would contribute to the prevention and treatment of allergic diseases.

References

1. Melamed, D. and Friedman, A. (1993) Direct evidence for anergy in T lymphocytes tolerized by oral administration of ovalbumin. *Eur. J. Immunol*. **23:** 935–942.
2. Heissmeyer, V., Macian, F., Im, S.H., Varma, R., Feske, S., Venuprasad, K., Gu, H., Liu, Y.C., Dustin, M.L., and Rao, A. (2004) Calcineurin imposes T cell unresponsiveness through targeted proteolysis of signaling proteins. *Nat. Immunol*. **5:** 255–265.
3. Seroogy, C.M., Soares, L., Ranheim, E.A., Su, L., Holness, C., Bloom, D., and Fathman, C.G. (2004) The gene related to anergy in lymphocytes, an E3 ubiquitin ligase, is necessary for anergy induction in CD4 T cells. *J. Immunol*. **173:** 79–85.
4. Jeon, M.S., Atfield, A., Venuprasad, K., Krawczyk, C., Sarao, R., Elly, C., Yang, C., Arya, S., Bachmaier, K., Su, L., Bouchard, D., Jones, R., Grouski, M., Ohashi, P., Wada, T., Bloom, D., Fathman, C.G., Liu, Y.C., and Penninger, J.M. (2004) Essential Role of the E3 ubiquitin ligase Cbl-b in T cell anergy induction. *Immunity* **21:** 167–177.
5. Anandasabapathy, N., Ford, G.S., Bloom, D., Holness, C., Paragas, V., Seroogy, C., Skrenta, H., Hollenhorst, M., Fathman, C.G., and Soares, L. (2003) GRAIL: An E3 ubiquitin ligase that inhibits cytokine gene transcription is expressed in anergic $CD4^+$ T cells. *Immunity* **18:** 535–547.
6. Laemmli, U.K. (1970) Cleavage of structural proteins during the assembly of the head of bacteriophage T4. *Nature* **227:** 680–685.
7. Ebihara, M., Hattori, M., and Yoshida, T. (2007) Distinctly different sensitivity in the induction and reversal of anergy of Th1 and Th2 cells. *Biosci. Biotechnol. Biochem*. **71:** 130–137.
8. Andris, A., Denanglaire, S., de Mattia, F., Urbain, J., and Leo, O. (2004) Naïve T cells are resistant to anergy induction by anti-CD3 antibodies. *J. Immunol*. **173:** 3201–3208.
9. Fang, D., Elly, C., Gao, B., Fang, N., Altman, Y., Joazeiro, C., Hunter, T., Copeland, N., Jenkins, N., and Liu, Y.C. (2002) Dysregulation of T lymphocyte function in itchy mice: A role for Itch in TH2 differentiation. *Nat. Immunol*. **3:** 281–287.
10. Yamamoto, T., Hattori, M., and Yoshida, T. (2007) Induction of T-cell activation or anergy determined by the combination of intensity and duration of T-cell receptor stimulation, and sequential induction in an individual cell. *Immunology* **121:** 383–391.

Expression Analysis of Senescence-Associated Genes: Their Possible Involvement in Diabetes

Miyako Udono, Kaori Mukae, Tsukasa Fujiki, Zhang Ping Bo, Hiroshi Fujii, Sanetaka Shirahata, and Yoshinori Katakura

1 Introduction

Accumulation of errors and damages concomitant with aging would cause not only physiologic dysfunction but also diseases such as cancer, diabetes and hypertension. In this study, we tried to clarify factors involved in senescence programs by proteomics approach and assumed their involvements in the aging-associated diseases.

2 Experimental Procedures

2.1 Cell Culture

TIG-1 cells (Institute of Development, Aging and Cancer, Tohoku University, Miyagi, Japan) were cultured in MEM medium (Nissui, Tokyo, Japan) supplemented with 10% FBS at 37°C in 5% CO_2.

2.2 Senescence-Associated β-Galactosidase Assay

Senescence-associated β-galactosidase (SA-β-Gal) assay was performed according to the method described by Dimiri et al. [1]. Staining was carried out at 37°C for 10 h.

Y. Katakura (✉)
Faculty of Agriculture, Kyushu University,
Higashi-ku, Fukuoka 812-8581, Japan
e-mail: katakura@mac.com

M. Kamihira et al. (eds.), *Animal Cell Technology: Basic & Applied Aspects*, Animal Cell Technology: Basic & Applied Aspects 16, DOI 10.1007/978-90-481-3892-0_39,

2.3 Isolation of Membrane Proteins

We used Cell Surface Protein Biotinylation and Purification Kit (PIERCE).

2.3.1 Cell Biotinylation

TIG-1 cells were prepared from 90 to 95% confluent culture in 150 mm plate. After aspirating medium, cells were washed twice with 8 ml of cold PBS. Then, sulfo-NHS-SS-Biotin solution (10 ml) was added to dishes and shaked for 30 min at 4°C. Cells were scraped and transferred to 50 ml tube. Cell were extensively washed with TBS.

2.3.2 Cell Lysis

Lysis buffer was added to cell pellets and transferred to 1.5 ml tube, and cells were sonicated on ice. After centrifugation, supernatant was transferred to fresh 1.5 ml tube.

2.3.3 Isolation of Labeled Proteins

Column was equilibrated with NeutrAvidin Gel solution. Cell lysates were added to this column, and incubated for 60 min with shaking at room temperature. After this incubation, column was washed with wash buffer containing protease inhibitor.

2.3.4 Elution of Proteins

Sample buffer containing 50 mM DTT was added to the column and incubated for 60 min at room temperature. The column was centrifuged at $100 \times g$ for 2 min. Eluted proteins were stored at –20°C.

2.4 Protein Assay

Protein concentration in cell lysate was determined by Bradford method using Protein Assay Dye (BIO-RAD Lab.).

2.5 SDS-PAGE

Cell lysates were applied to 1D/2D SDS-PAGE using 10% acrylamide gel.

2.6 MALDI TOF-MS ANALYSIS

After silver-staining of the gel, spots and bands were cut down and subjected to MALDI TOF-MS analysis.

2.7 PCR

2.7.1 Total RNA Preparation

Total RNA form TIG-1 cells were prepared by using TRIzol reagent according to the manufacturer's protocol.

2.7.2 cDNA Synthesis

Total RNA (2.5 μg) was used as template for cDNA synthesis reaction using M-MLV reverse transcriptase, RNase H^- (Promega).

2.7.3 Realtime PCR

cDNA derived from human muscle and pancreas tissues of diabetes patients (Toyobo) were used as template for realtime PCR analysis. Realtime PCR was done using SYBR Premix Ex Taq kit (Takara).

3 Results

We identified 16 candidates for senescence-associated genes by proteomics approach. Next we investigated the expression profiles these genes in replicative senescence of TIG-1 cells by quantitative realtime PCR. As a result, 14 genes were identified as senescence-associated genes. Further, we investigated the involvement of these genes in the onset of diabetes that is known to be one of aging-related diseases by using cDNA derived from muscle and pancreas tissues of diabetes patients by quantitative realtime PCR. Among these 14 senescence-associated genes, expression of 13–14 genes were augmented in muscle and/or pancreas tissues of diabetes patients (Table 1).

4 Discussion

All these results suggested that these senescence-associated genes can be novel markers and/or targets for life-style related diseases including diabetes, and further that life-style related diseases can be elicited by cellular senescence programs [2].

Table 1 Expression profiles of senescence-associated genes

	Replicative senescence	Diabetes	
		Muscle	Pancreas
Band 1	↑	↑	↑
Band 2	↓	–	↑
Band 3	–	↑	↑
Band 4	↓	↑	↑
Band 5	↑	↑	↓
Band 6	↓	↑	↑
Band 10	↓	–	↑
Band 11	↑	↑	↑
Spot 1	↑	↑	↑
Spot 4	↑	↑	↑
Spot 7	↑	↑	↑
Spot 8	↑	↑	↓
Spot 10	↑	–	↑
Spot 13	↓	↑	↑
Spot 23	↑	↑	↑
Spot 27	–	↑	↑
p16	↑	↑	↑
p21	↑	↑	↑

References

1. Dimiri, G.P., Lee, X., Basile, G., Acosta, M, Scott, G., Roskellery, C., Medrano, E.E., Linskens, M., Rubelj, I., and Pereira-Smith, O. (1995) A biomarker that identifies senescent human cells in culture and in aging skin in vivo. *Proc. Natl. Acad. Sci. USA* **92**: 9363–9367.
2. Wajapeyee, N., Serra, R.W., Zhu, X., Mahalingam, M., and Green, M.R. (2008) Oncogenic BRAF induces senescence and apoptosis through pathways mediated by the secreted protein IGFBP7. *Cell* **132**: 363–374

Study of Butyrate Signal Transduction Pathways in Rat Hepatic Stem-Like Cells

Toshihiko Saheki, Yusuke Mukai, Ken'ichi Saito, Emi Tajima, Kentaro Katakura, Atsuyoshi Nishina, Mikiko Kishi, Takashi Izumi, Toshihiro Sugiyama, and Itaru Kojima

1 Introduction

Short-chain fatty acids (SCFAs), acetate, propionate and butyrate, are the major anions in the lumen of the large intestine. They are produced by bacterial fermentation of undigested carbohydrates. Luminal SCFAs are not only absorbed as nutrients across the intestinal epithelium, but also influence various physiological functions of the intestinal system. Butyrate is also known as a histone deacetylase inhibitor and acts as a differentiation-promoting agent for a wide variety of cell types [5]. In 2003, two groups independently described that one of the G protein-coupled receptors (GPCRs), GPR43, is a receptor for SCFAs [2, 4]. There are many studies about butyrate induced differentiation, while there is little information about intracellular signal transduction mechanisms through the receptor.

To reveal the molecular mechanisms of the physiological activity of butyrate, it is necessary to study the intracellular molecular event owing butyrate signal transduction. We have reported some proteins which expression decreased after sodium butyrate treatment for rat hepatic stem-like (HSL) cells by two-dimensional electrophoresis and mass-spectrometer. HSL cells were established from healthy adult rats, and have a potential of self-renewal and an ability to differentiate to hepatocytes, biliary duct cells and pancreatic endocrine cells [3, 7].

In this study, we cultured HSL cells with 20 mM sodium butyrate and examined GPR43 mRNA expression and mitogen-activated protein (MAP) kinase cascade activation.

T. Saheki (✉)
Department of Biological and Chemical Engineering, Gunma University, Kiryu, Japan
e-mail: saheki@chem-bio.gunma-u.ac.jp

M. Kamihira et al. (eds.), *Animal Cell Technology: Basic & Applied Aspects*, Animal Cell Technology: Basic & Applied Aspects 16, DOI 10.1007/978-90-481-3892-0_40,

2 Materials and Methods

2.1 Materials

Butyrate sodium salt was purchased from Wako Pure Chemical Industries, Ltd. (Osaka, Japan). Dulbecco's Modified Eagle's Medium (DMEM) and Micro-to-Midi Total RNA Purification System were purchased from Invitrogen Corp. (Carlsbad, CA, USA). Fetal calf serum (FCS) was purchased from Biofluids (Rockville, MD, USA). Rabbit anti-phospho extracellular signal-regulated kinase 1/2 (ERK1/2), anti-ERK1/2, anti-phospho Akt and anti-Akt polyclonal antibodies and secondary alkaline-phosphatase (ALP)-conjugated anti-rabbit IgG were obtained from Cell Signaling Technology Inc. (Bererly, MA, USA). Complete Mini EDTA Free was obtained from Roche Diagnostics GmbH (Mannheim, Germany) and Phosphatase Inhibitor Cocktail 2 was obtained from Sigma-Aldrich (St. Louis, MO, USA).

2.2 Cell Culture

HSL cells were cultured in DMEM with 10% FCS at 37°C in a 5% CO_2 atmosphere. Cells were used for experiment at 80% confluence.

2.3 RNA Preparation and RT-PCR

Total RNA was prepared from scraped HSL cells (10^7 cells) using Micro-to-Midi Total RNA Purification System according to manufacturer's instruction. Reverse transcription and polymerase chain reaction were performed as described [6]. PCR was made as below: pre-denaturation 95°C, 2 min, 30 cycles of denaturation 95°C, 30s, annealing 60°C, 30s, elongation 72°C, 3 min, and post elongation 72°C, 10 min. The primers used were: rat GPR40 forward 5'-tggctatatgggcccttgtc-3', rat GPR40 reverse 5'-cctgagcttccgtttgtggt-3', rat GPR43 forward 5'-catcatcgttcagtacctgaactc-3', rat GPR43 reverse 5'-ggcattgagggaactgaacac-3' glyceraldehyde-3-phosphate dehydrogenase (GAPDH) forward; 5'-ccatcaccatcttccaggag-3', GAPDH reverse; 5'-cctgctcaccaccttcttg-3'. The primer sequence was selected using "Primer3" software. GAPDH was used as internal control. Amplified DNAs were separated on 2% agarose gel electrophoresis and stained with 0.5 μg/ml ethidium bromide.

2.4 Phosphoprotein Preparation and pERK and pAkt Western Blot Analysis

HSL cells were incubated with 20 mM sodium butyrate for independent time periods as shown in Fig. 3. HSL cells in 100 mm culture dish were lysed and homogenized in 0.5 mL of RIPA buffer (50 mM Tris-HCl, pH 8.0, 150 mM NaCl, 1% Triton X-100,

0.5% Sodium Deoxycholate, 0.1% SDS, 2 mM EDTA) with 130 μL Complete Mini EDTA free and 9 μL Phosphatase Inhibitor Cocktail 2. Equal amounts of protein samples (14 μg/lane) were subjected to 12% SDS-PAGE before being transferred to Immobilon-P (Millipore Co., Billerica, MA, USA). The samples were then exposed to the following primary antibodies: rabbit anti-phosphoERK1/2, anti-ERK1/2, anti-phosphoAkt or anti-Akt polyclonal antibodies.

3 Results

3.1 Effect of Butyrate is Reversible to HSL Cells

Butyrate was described to differentiate many cell types, however, the effects were reversible. In HSL cells, butyrate changed shape of HSL cells and induced cell death (Fig. 1a, b). After 2 days, butyrate was washed out in the medium (Fig. 1c), HSL cells shapes were returned as before and the cells proliferated (Fig. 1d). When butyrate added again, much more cells changed their shapes and were alive than after the first treatment of butyrate (Fig. 1e).

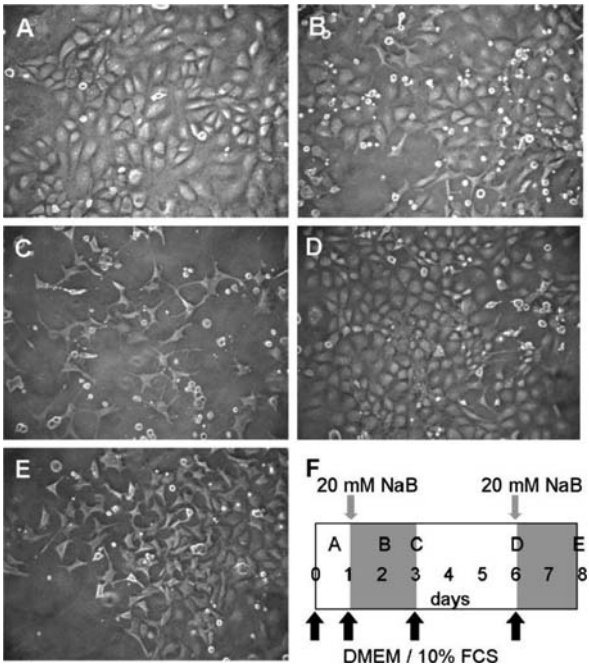

Fig. 1 Two treatments of butyrate to HSL cells. Before (**a**) and after incubation with 20 mM butyrate for 1 day (**b**). Two days after incubation, butyrate was washed out (**c**). Another four days culture in the medium without butyrate, HSL cells proliferated and the shape was back to the beginning (**d**). Second incubation with 20 mM butyrate for 2 days (**e**). Time schedule of butyrate treatment (**f**)

3.2 Existence of GPR43 G Protein-Coupled Receptor in HSL Cells

GPR43 and GPR40, long-chain fatty acids receptor [1], mRNA expression in HSL cells were evaluated by RT-PCR analysis using specific primers and were detected at the expected size (Fig. 2). Rat GAPDH primer designed from the region containing an intron did not amplify any products except a single 575 bp product, indicating that there was no contamination of the genomic DNA. The expression levels of GPR43 were quantified using quantitative-RT-PCR. GPR43 expression levels were almost same between before and after butyrate treatment (data not shown).

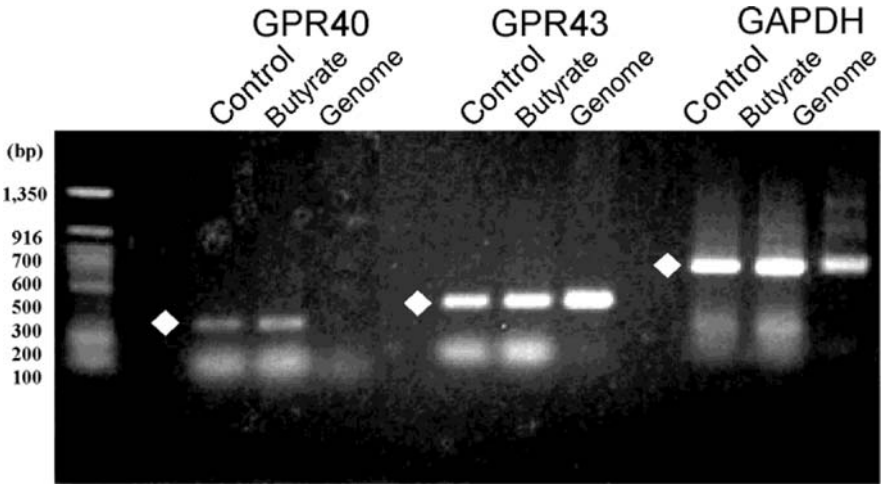

Fig. 2 GPR40 and GPR43 mRNA expression in HSL cells. RT-PCR was performed as described in Section 2. The PCR products were separated on a 2% agarose gel and stained with ethidium bromide. GAPDH is an internal control. The diamond indicates expected bands

3.3 Butyrate Selectively Affected the Phosphorylation of ERK

In order to determine whether butyrate activated classical GPCR signals via GPR43, we examined the effects of butyrate on the phosphorylation of MAP kinases ERK1/2 and Akt. As shown in Fig. 3, incubation of cells with 20 mM butyrate increased phosphorylation of ERK, which reached its maximum by 10 min, then reduced time-dependently until 1 h, finally returned the original level after 24 h. Butyrate had no effect on the phosphorylation of Akt.

4 Discussion

We are interested in proliferation activity of HSL cells and performed two-dimensional electrophoresis to identify the proteins statistically more abundant in rapidly growing undifferentiated HSL cells than in sodium butyrate-treated differentiated HSL cells [6]. One of the identified proteins, prohibitin, was described

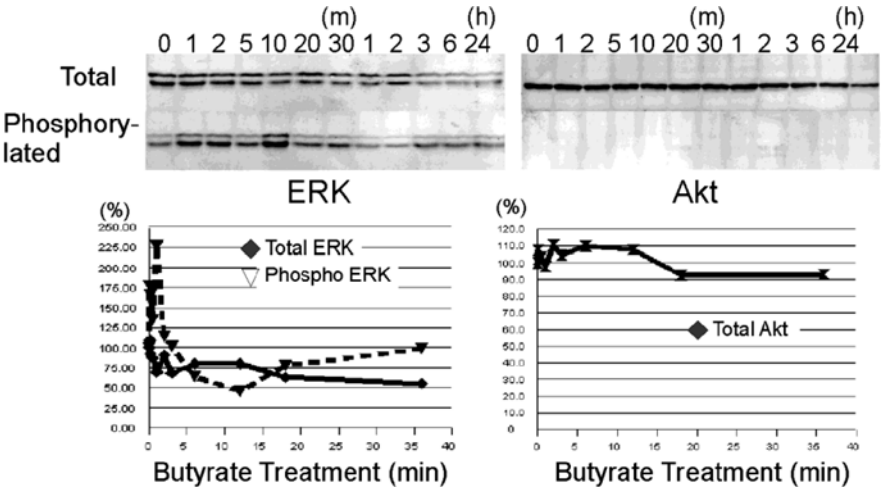

Fig. 3 Effects of butyrate on the phosphorylation of ERK1/2 and Akt. Cells were stimulated with 20 mM butyrate for the indicated times. Cell lysates were analyzed by immunoblotting using an antibody that was phosphor-specific or specific for total ERK1/2 (*upper left*) or Akt (*upper right*), respectively. Images were analyzed to compare the relative intensity of the bands (*lower panels*). For ERK, upper bands were analyzed

to control MAP kinase pathway. GPR43 is described to couple with Gq and Gi/o, it is possible that MAP kinase pathway is activated by butyrate in HSL cells. According to these reports, we studied whether HSL cells response against butyrate treatment dependent GPR43.

Our results showed that the mRNAs for GPR43 and GPR40 are expressed in the rat HSL cells. Quantitative RT-PCR demonstrated that the expression level of GPR43 mRNA was not affected by butyrate treatment (data not shown). Le Poul et al. showed that propionate activated ERK1/2 in CHL-K1 cells that expressed GPR41 or GPR43 [2]. Yonezawa et al. showed that p38/hsp27 path way was activated via GPR43 in the MCR-7 human breast cancer cell line [8]. They reported that SCFAs selectively induced the phosphorylation of p38 within 10 min. Our results showed that butyrate rapidly and selectively stimulated ERK1/2 phosphorylation, while, Ark phosphorylation was not detected. The results obtained were contrary to our intention, because much cell death was observed after sodium butyrate treatment. Although intracellular signal molecules that activated by SCFAs were varied with cell lines used, these effects of butyrate may have been mediated, in part, via GPR43.

References

1. Briscoe, C.P., Tadayyon, M., Andrews, J.L., et al. (2003) The orphan G protein-coupled receptor GPR40 is activated by medium and long chain fatty acids. *J. Biol. Chem*. **278**: 11303–11311.
2. Le Poul, E., Loison, C., Strnyf, S., et al. (2003) Functional characterization of human receptors fro short chain fatty acids and their role in polymorphonuclear cell activation. *J. Biol. Chem*. **278**: 25481–25489.

3. Nagai, H., Terada, K., Watanabe, G., et al. (2002) Differentiation of liver epithelial (stem-like) cells into hepatocytes induced by coculture with hepatic stellate cells. *Biochem Biophys. Res. Commun*. **293**: 1420–1425.
4. Nilsson, N.E., Kotarsky, K., Owman, C., et al. (2003) Identification of a free fatty acid receptor, FFA2R, expressed on leukocytes and activated by short-chain fatty acids. *Biochem. Biophys. Res. Commun*. **303**: 1047–1052.
5. Riester, D., Hildmann, C., and Schwienhorst, A. (2007) Histone deacetylase inhibitors turning epigenic mechanisms of gene regulation into tools of therapeutic intervention in malignant and other diseases. *Appl. Microbiol. Biotechnol*. **75**: 499–514.
6. Saheki, T., Ito, H., Sekiguchi, A., et al. (2008) Proteomic analysis identifies proteins that continue to grow hepatic stem-like cells without differentiation. *Cytotechnol*. **57**:137–143.
7. Yamada, S., Terada, K., Ueno, Y., et al. (2005) Differentiation of adult hepatic stem-like cells into pancreatic endocrine cells. *Cell Transplant*. **14**: 647–653.
8. Yonezawa, T., Kobayashi, Y., and Obara, Y. (2007) Short-chain fatty acids induce acute phosphorylation of the p38 mitogen-activated protein kinase/heat shock protein 27 pathway via GPR43 in the MCF-7 human breast cancer cell line. *Cell Signal*. **19**: 185–193.

Growth Control of Mammalian Cells via a Human Artificial Chromosome Harboring a Chimeric Receptor

Masahiro Kawahara, Toshiaki Inoue, Xianying Ren, Takahiro Sogo, Hidetoshi Yamada, Motonobu Katoh, Hiroshi Ueda, Mitsuo Oshimura, and Teruyuki Nagamune

1 Introduction

Cytokines play pivotal roles in controlling cell fate for maintenance of homeostasis in the body. Therefore, mimicry of cytokine functions with artificial ligands is a promising strategy for realizing artificial control of the fates of specific cell populations. To this end, we have designed several antibody/cytokine receptor chimeras that can transduce a growth signal in response to the cognate antigens [1]. An anti-fluorescein single-chain Fv (ScFv) tethered to extracellular D2 domain of the erythropoietin receptor (EpoR) and transmembrane and cytoplasmic domains of gp130 resulted in marked cell growth promotion in the presence of fluorescein-conjugated BSA (BSA-FL) or a series of fluorescein dimers connected by an oligo-DNA linker in factor-dependent hematopoietic cell lines [2]. This chimeric receptor could be employed to specifically amplify gene-transduced cells in an antigen-dependent manner, a technique known as antigen-mediated genetically modified cell amplification (AMEGA).

However, all the previous studies have used plasmid or retroviral vectors for expression of the gene of interest as well as chimeric receptors. Therefore, random integration of the transgene into the host genome is inevitable for its stable expression. This could lead to disruption of the host-genomic genes and subsequent clonal variability of the transgene expression induced by positional effects. Furthermore, the sizes of such transgenes are limited to several kilobases, especially for retroviral vectors that need to be packaged into a viral capsid.

To solve these problems, we employed human artificial chromosome (HAC) vectors in the present study, because they replicate and segregate in a similar manner to natural chromosomes. In our previous study, we constructed a novel HAC vector, 21ΔqHAC, from human chromosome 21 by telomere-directed chromosome truncation [3]. 21ΔqHAC contains a single loxP sequence for site-specific insertion of

M. Kawahara (✉)
Department of Chemistry and Biotechnology, School of Engineering, The University of Tokyo, Bunkyo-ku, Tokyo 113-8656, Japan
e-mail: kawahara@bio.t.u-tokyo.ac.jp

M. Kamihira et al. (eds.), *Animal Cell Technology: Basic & Applied Aspects*, Animal Cell Technology: Basic & Applied Aspects 16, DOI 10.1007/978-90-481-3892-0_41,

a circular DNA via the Cre/loxP system. Furthermore, 21ΔqHAC was mitotically stable in human cells and achieved long-term reproducible transgene expression, representing features that would be feasible for a transgene-regulation system. In the present study, we introduced a fluorescein-responsive ScFv-gp130 (Sg) chimeric receptor as well as a model transgene, enhanced green fluorescent protein (EGFP), into the 21ΔqHAC vector to investigate the HAC stability, maintenance of transgene expression and possibility of BSA-FL-dependent growth control of interleukin (IL)-6-dependent hybridoma cells.

2 Materials and Methods

2.1 Plasmid Construction

The construction of the chimeric receptor, ScFv-gp130 (Sg) gene was as described [2]. pBS226-PGK-SgIG was constructed by subcloning the PGK promoter, Sg, IRES-EGFP and the SV40 early polyA signal sequences into pBS226 vector (Invitrogen).

2.2 Cell Culture, Transfection and Microcell-Mediated Chromosome Transfer (MMCT)

A murine IL-6-dependent hybridoma cell line, 7TD1, was cultured in RPMI 1640 medium (Nissui) supplemented with 10% FBS (Biowest) and 1 ng/ml of murine IL-6 (Genzyme). CHO/21Δq, which is a CHO cell variant with 21ΔqHAC, was cultured in F12 medium (GibcoBRL) supplemented with 10% FBS and 8 μg/ml blasticidin S (Kaken Pharmaceutical).

CHO/21Δq-SgIG cells were established by transfecting pBS226-PGK-SgIG and Cre recombinase expression plasmid pBS185 (Invitrogen) into CHO/21Δq cells using Lipofectamine2000 (Invitrogen), followed by selection and cloning with 560 μg/ml G418 (Calbiochem) and 8 μg/ml blasticidin S. Microcells containing 21Δq-SgIG HAC were prepared as described [4], and fused with 7TD1 cells using polyethylene glycol 1000 (Wako). The cells selected in the presence of 450 μg/ml G418 were named 7TD/21Δq-SgIG and used for further study.

2.3 Fluorescence In Situ Hybridization (FISH)

Digoxigenin-labeled human Cot-1 DNA (Invitrogen) was hybridized with the chromosome spreads on the slide glasses at 37°C overnight. The probe was further labeled with a rhodamine-labeled anti-digoxigenin antibody Fab fragment (Roche). The chromosomes were counterstained with DAPI (Sigma). Images were captured with a microscope (Nikon) equipped with a photometric CCD camera, digitally processed, and visualized with Argus system (Hamamatsu photonics).

2.4 Cell Proliferation Assay

Cells were washed twice with PBS and seeded in 24-well plates containing various concentrations of BSA-FL. The initial cell concentration was adjusted to 10^4 cells/ml. Cell number and viability were determined by the trypan blue exclusion assay using a hemocytometer.

2.5 Flow Cytometry

Cells were washed once and resuspended with PBS. Green fluorescence intensity was measured using FACS Calibur flow cytometer (Becton Dickinson) at 488 nm excitation and fluorescence detection at 530 ± 15 nm.

3 Results

3.1 Establishment of an HAC Donor Cell Line with a Chimeric Receptor

The overall experimental scheme is shown in Fig. 1. The 21ΔqHAC is maintained in a CHO cell line, CHO/21Δq [3]. To introduce the chimeric receptor into the HAC vector, CHO/21Δq cells were cotransfected with the expression plasmid (pBS226-PGK-SgIG) and a Cre recombinase expression plasmid (pBS185) followed by G418 selection. Site-specific insertion of the targeting construct into the loxP site of the HAC vector generates a functional neo gene on the HAC vector. The resulting HAC construct and CHO transfectants were designated 21Δq-SgIG and CHO/21Δq-SgIG, respectively. Flow cytometric analysis revealed that CHO/21Δq-SgIG cells exhibited distinct green fluorescence compared with untransfected CHO/21Δq cells (Fig. 2a). In a FISH analysis, a human Cot1 DNA probe was detected in a small

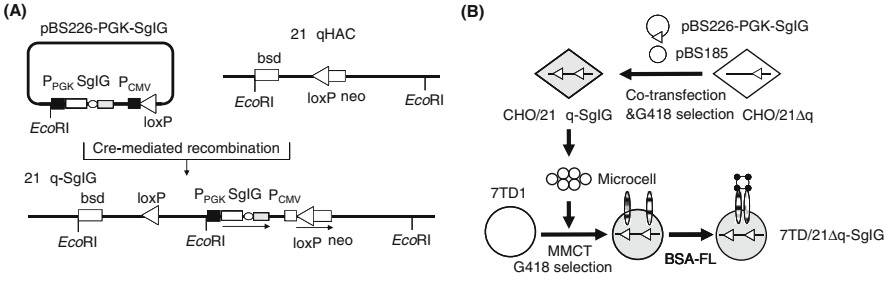

Fig. 1 Schematic diagram of the experimental scheme used in this study. (**a**) Site-specific insertion of ScFv-gp130-IRES-EGFP (SgIG) into the loxP site on the 21ΔqHAC vector. (**b**) Creation of donor cells and microcell-mediated chromosome transfer into recipient cells

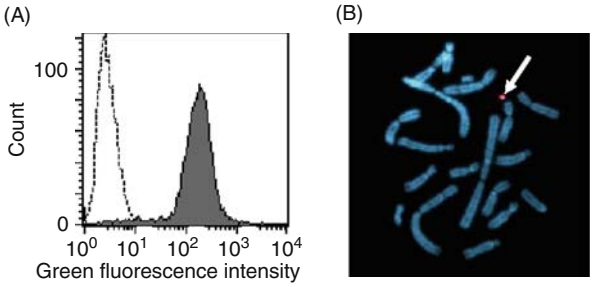

Fig. 2 (**a**) Flow cytometric analysis to confirm EGFP expression. The histograms for parental CHO/21Δq cells (*dotted line*) and CHO/21Δq-SgIG cells (*gray histogram*) are shown. (**b**) FISH analysis. A representative metaphase spread of a CHO/21Δq-SgIG clone is shown. A HAC fragment hybridized to the human Cot-1 DNA probe is indicated by an *arrow*

independently segregating minichromosome, and neither insertion nor translocation to the host chromosome was observed (Fig. 2b). These results indicate that CHO/21Δq-SgIG cells can be used for further studies as a donor cell line for transferring 21Δq-SgIG to recipient cells.

3.2 BSA-FL-Dependent Cell Growth, Stable EGFP Expression and Stable HAC Maintenance in 7TD/21Δq-SgIG Cells

Microcell-mediated chromosome transfer followed by G418 selection resulted in proliferating cells, designated 7TD/21Δq-SgIG cells. As a control, 7TD/21Δq-IG cells were also created from CHO/21Δq cells transfected with a plasmid lacking the Sg chimeric receptor gene (pBS226-PGK-IG), followed by G418 selection. To investigate whether the G418-resistant cells could respond to BSA-FL, cell growth assays were performed. As a result, 7TD/21Δq-SgIG cells showed BSA-FL-dependent cell growth and an anti-apoptotic effect, while parental 7TD1 and 7TD/21Δq-IG cells exhibited no BSA-FL dependency (Fig. 3). The growth was dependent on FL molecules conjugated on BSA because unconjugated BSA did not induce cell growth of 7TD/21Δq-SgIG cells. These results indicate that cell growth of 7TD1 cells harboring 21ΔqHAC can be successfully controlled by the addition of BSA-FL.

To investigate whether 7TD/21Δq-SgIG cells stably express the model transgene EGFP, flow cytometric analysis was performed. Consequently, 7TD/21Δq-SgIG cells after BSA-FL selection for 129 days exhibited significantly higher green fluorescence intensity than parental 7TD1 cells (Fig. 4a), indicating that the EGFP expression was stably maintained during BSA-FL selection. To examine whether 21Δq-SgIG exists as an independent minichromosome in 7TD/21Δq-SgIG cells cultured in BSA-FL for 21 days, a FISH analysis using a human Cot1 DNA probe was performed. The 21Δq-SgIG was detected as a small independent minichromosome, and the copy number was either one (75%) or two (25%) in the 50 metaphase

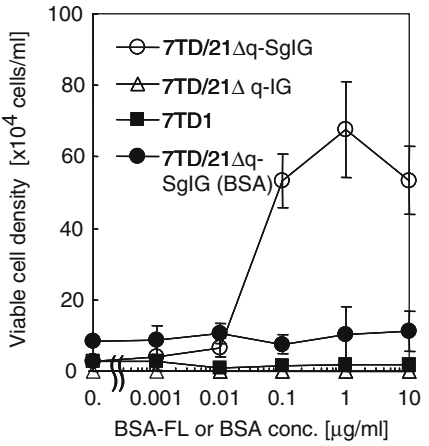

Fig. 3 BSA-FL-dependent cell growth of 7TD/21Δq-SgIG cells. Cells (1×10^4 cells/ml) were inoculated into 24-well plates with various concentrations of BSA-FL or BSA at day 0. The viable cell concentration of triplicate cultures after 7 days is plotted as the mean and 1 SD

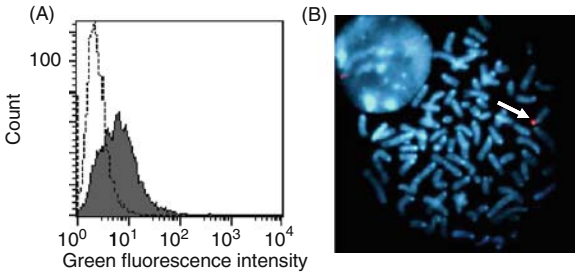

Fig. 4 (**a**) Flow cytometric analysis to confirm EGFP expression. The histograms for parental 7TD1 cells (*dotted line*) and 7TD/21Δq-SgIG cells after G418 selection, followed by a 129-day culture with BSA-FL (*gray histogram*) are shown. (**b**) FISH analysis. A representative metaphase spread of 7TD/21Δq-SgIG cells after G418 selection, followed by a 21-day culture with BSA-FL is shown. A HAC fragment hybridized to the human Cot-1 DNA probe is indicated by an *arrow*

spreads examined. Neither insertion into the host chromosome nor apparent amplification of 21Δq-SgIG was observed. These results indicate that 21Δq-SgIG is stably maintained in 7TD/21Δq-SgIG cells.

4 Discussion

In this study, we constructed a novel HAC vector carrying an antibody/receptor chimera gene to demonstrate growth control of HAC-introduced cells by a cognate antigen. This is the first study in which our chimeric gene has been introduced into cells via microcell-mediated transfer of an HAC, since all our previous studies utilized transfection or transduction of plasmids or retroviruses, respectively. The distribution of the EGFP fluorescence intensity in 7TD/21Δq-SgIG cells was

more uniform in histograms obtained by flow cytometry than that in retrovirally-transduced 7TD/SgIG cells (data not shown) [4]. This could be due to the nature of 21Δq-SgIG HAC, which is independent of the host chromosome, such that expression of the transgene can be sustained without suffering any positional effects from its neighboring sequences on the host genome. In addition, FISH analysis revealed that the majority of 7TD/21Δq-SgIG cells retained a single copy of the HAC, further contributing to the stability of the expression level. These results clearly indicate the merit of an HAC-based vector in obtaining gene-transduced cells with uniform and predictable characteristics.

Here we introduced the 21Δq-SgIG HAC into a factor-dependent hybridoma cell line. Since the HAC is functional in human bone marrow mononuclear cells and mesenchymal stem cells, application to other cell types with appropriate factor dependencies should not be difficult. Modification of the Sg chimeric receptor, including the use of other antigen-antibody pairs and alternative intracellular domains, could realize concurrent inputs of distinct signals or different signal outputs, such as cell growth and death signals, at different time points. HAC vectors, which can accommodate even megabase-range inserts, could show great advantages for coexpression of such a series of antigen-responsive chimeric receptors that could artificially control specific cell fates. Thus, our system may be promising as a versatile method for specifically modifying cellular processes both in vitro and in vivo.

References

1. Ueda, H. et al. (2000) Cell-growth control by monomeric antigen; The cell surface expression of lysozyme-specific IgV-domains fused to truncated Epo receptor. *J. Immunol. Methods* **241**: 159–170.
2. Kawahara, M. et al. (2004) Selection of genetically modified cell population using hapten-specific antibody/receptor chimera. *Biochem. Biophys. Res. Commun*. **315**: 132–138.
3. Katoh, M. et al. (2004) Construction of a novel human artificial chromosome vector for gene delivery. *Biochem. Biophys. Res. Commun*. **321**: 280–290.
4. Kawahara, M. et al. (2007) Antigen-mediated growth control of hybridoma cells via a human artificial chromosome. *Biochim. Biophys. Acta* **1770**: 206–212.

The Impact of Redox State on Regulation of the High-Affinity IgE Receptor Expression

Yoshinori Fujimura, Hayato Higo, Satomi Yano, Koji Yamada, and Hirofumi Tachibana

1 Introduction

IgE-mediated stimulation of mast cells and basophils is an important initial event in the IgE-dependent allergic reactions [1]. The crosslinking of allergen-specific IgE bound to the high-affinity IgE receptor FcεRI expressed on these cells with multivalent allergens results in a release of bioactive chemical mediators such as histamine, proteases, chemotactic factors and arachidoic metabolites. Therefore, FcεRI is required for mast cells and basophils to initiate the IgE-mediated allergic reaction such as atopic dermatitis, bronchial asthma, and food allergy. The FcεRI is a multisubunit receptor with a ligand binding α subunit, a signal modifying membrane-tetraspanning β subunit, and a homodimeric disulfide-linked γ subunit that provides the signaling ability of this receptor. Among the three subunits forming the FcεRI, the α chain is the specific component of FcεRI that mostly extends out to the extracellular region and directly binds to IgE. The study using α chain-deficient mice demonstrated that IgE was unable to bind to the cell surface of mast cells thereby failing to induce degranulation through IgE-binding [2]. Thus, it is expected that the IgE-mediated allergic symptoms may be attenuated by downregulating the FcεRI expression in mast cells and basophils.

Peroxisome proliferator-activated receptor-γ (PPARγ) are activated by the prostaglandin (PG) D2 metabolite 15-deoxy-Δ[12, 14]-PGJ_2 (15d-PGJ_2), which is able to suppress the expression of pro-inflammatory genes and tumor cell growth [3–6]. Moreover, it has been reported that PPARγ ligands can negatively regulate the activation of mouse and human mast cells such as histamine release and cytokine production [7, 8]. Previously we have found that natural ligands for PPARγ, 15d-PGJ_2, have the ability to suppress FcεRI expression in the human basophilic KU812 cells [9]. Generally, it has been known that there are both PPARγ-dependent

Y. Fujimura (✉)
Innovation Center for Medical Redox Navigation, Kyushu University, Higashi-ku, Fukuoka 812-8582, Japan
e-mail: fujimu@agr.kyushu-u.ac.jp

M. Kamihira et al. (eds.), *Animal Cell Technology: Basic & Applied Aspects*, Animal Cell Technology: Basic & Applied Aspects 16, DOI 10.1007/978-90-481-3892-0_42,

and -independent pathways mediating pleiotropic effects of 15d-PGJ_2 [10]. Which pathway is involved in 15d-PGJ_2-induced suppression of FcεRI expression still remains unclear. In the present study, we investigated the mechanism for the effect of 15d-PGJ_2 on the expression of FcεRI.

2 Materials and Methods

2.1 Reagents

Mouse anti-human FcεRI α chain antibody CRA-1 was obtained from Kyokuto seiyaku (Tokyo, Japan). Mouse IgG2b, used as negative control, was bought from Dako Cytomation (Glostrup, Denmark). Fluorescein isothiocyanate (FITC)-conjugated goat anti-mouse IgG antibody was purchased from Protos Immunoresearch (Burlingame, CA). Mouse anti-phosphorylated ERK1/2 antibody, rabbit anti-ERK1/2 antibody, and rabbit anti-PPARγ antibody were obtained from Santa Cruz Biotechnology, Inc. (Santa Cruz, CA). Horseradish peroxidase (HRP)-conjugated anti-mouse IgG antibody and HRP-conjugated anti-rabbit antibody were obtained from Zymed Laboratories, Inc. (San Francisco, CA) and ICN Pharmaceuticals, Inc. (Costa Mesa, CA), respectively. 15-deoxy-Δ [12, 14]-prostaglandin J_2 (15d-PGJ_2) was purchased from Cayman chemical Co. (Ann Arbor, MI). Catalase, hydrogen peroxide, *N*-acetylcysteine (NAC), and anti-β-actin antibody were obtained from Sigma Co. (St Louis, MO). H_2DCF-DA was obtained from Invitrogen (Carlsbad, CA).

2.2 Cell Culture

KU812 cells were obtained from the Japanese Cancer Research Resources Bank (Tokyo, Japan) and were maintained in RPMI-1640 (Nissui, Tokyo, Japan) supplemented with 10% fetal bovine serum (PAA Laboratories GmbH, Austria), 100 units/mL penicillin G, 100 μg/mL streptomycin, and 10 mM HEPES buffer. KU812 cells were cultured at 37°C in a humidified atmosphere with 5% CO_2. For stimulation with 15d-PGJ_2, KU812 cells were first centrifuged and washed with RPMI-1640 medium. Then the cells were cultured in serum-free RPMI-1640 medium with or without 2 μM 15d-PGJ_2.

3 Construction of PPARγ-siRNA Expression Plasmids and Transient Transfection

The psiRNA-hH1hygro G2 short hairpin RNA (shRNA) expression vector was purchased from InvivoGen (San Diego, CA). As the inserts for expressing short hairpin RNA, the following insert was selected: shRNA-sense (5'-GTACCGTTTGAG-

TTTGCTGTGAAGTTCAAGAGA CTTCAC AGCAAACTCAAACT TTTTGG-AAA-3') and shRNA-antisense (5'-AGCTTTTC CAAAAAGTTTGAGTTTGC-TGTGAAGTCTCTTGAACTTCACAGCAAACTCAAACG-3'). This insert was annealed and subcloned into Acc65 I/Hind III sites in psiRNA-hH1. PPARγ gene-targeting shRNA expression vector was transfected into the KU812 cells by electroporation. Then, the clone with the hygromycin B (Roche Diagnostics, Basel, Switzerland) resistance was selected and used for experiments.

3.1 Western Blot Analysis

KU812 cells treated with or without 15d-PGJ_2 were washed and lysed in cell lysis buffer containing 50 mM Tris-HCl (pH 7.5), 150 mM NaCl, 1% Triton-X 100, 1 mM EDTA, 50 mM NaF, 30 mM Na_4PO_7, 1 mM phenylmethanesulfonyl fluoride, 2.0 μg/ml aprotinin, and 1 mM pervanadate. Whole cell lysate samples were loaded onto 10% sodium dodecyl sulfate-polyacrylamide gel (SDS-PAGE), and electrophoresis was done under reducing condition. The samples were then electrotransferred onto a nitrocellulose membrane. The blotted nitrocellulose was probed using phosphorylated ERK1/2, FcεRI α chain, or PPARγ antibody, and the secondary antibody used here was the HRP-conjugated anti-mouse IgG or anti-rabbit IgG, and detection was done using the ECL kit (GE Healthcare, Buckinghamshire, UK). For detection of total ERK1/2 or β-actin, the same filter was blotted again with anti-ERK1/2 or anti-β-actin antibody.

3.2 Analysis of the Cell Surface FcεRI Expression

The cell surface expression of FcεRI was assessed by flow cytometry. In brief, cells were incubated with the anti-FcεRI α chain antibody CRA-1. Then cells were exposed to the FITC-conjugated anti-mouse IgG and subjected to flow cytometry (FACSCalibur; Becton Dickinson, Sunnyvale, CA). As a negative control, the mouse subclass-matched IgG2b antibody was used. The extent of FcεRI expression is represented as the relative percentage of the mean fluorescence intensity of CRA-1 to non-treated cells.

3.3 Measurement of Reactive Oxygen Species (ROS) Generation

KU812 cells were first centrifuged and washed with PBS. Then the cells (1×10^6) were incubated in PBS containing 2 μM H_2DCF-DA for 30 min at 0°C. After washing twice with PBS, the intensity of H_2DCF-DA fluorescence was determined by using a flow cytometer, with an excitation wavelength of 480 nm and an emission wavelength of 530 nm.

4 Results and Discussion

To elucidate whether PPARγ is involved in the suppressive effect of 15d-PGJ_2 on the expression of FcεRI, we tried the construction of PPARγ-kockdowned cells by a RNA interference method. KU812 cells were transfected with the PPARγ-siRNA expressing vector or control-siRNA vector by electroporation. For selecting stable clones, transfected cells were grown in medium containing hygromycin B. Lysate derived from the cells with hygromycin resistance were fractionated by SDS-PAGE, and then immunoblotted using the PPARγ antibody. KU812 cells transfected with control-siRNA vector expressed PPARγ, but this protein level was clearly reduced by transfecting with PPARγ-siRNA vector (data not shown). Stable siRNA expressing cells were cultured with 15d-PGJ_2 (2 μM) for 24 h under serum-free conditions. The cell surface expression of FcεRI was measured by flow cytometric analysis using the specific antibody against FcεRI. As shown in Fig. 1a, RNA interference-mediated downregulation of PPARγ expression did not affect the suppressive effect of 15d-PGJ_2 on the FcεRI expression. This result suggests that 15d-PGJ_2-induced downregulation of FcεRI expression may be due to the PPARγ-independent mechanism.

It has been reported that 15d-PGJ_2 are potential inducers of intracellular oxidative stress [11]. To examine whether the redox alteration based on the pro-oxidant effect of 15d-PGJ_2 is involved in its suppressive effect on the FcεRI expression, the intracellular ROS level was measured. KU812 cells were treated with 15d-PGJ_2 (2 μM) in the presence or absence of catalase (1000 U/ml) or NAC (10 mM) for 2 h. ROS generation was assayed by flow cytometer using H_2DCF-DA, and expressed as relative ROS level (%) to the non-treatment group. As seen in Fig. 1b, the intracellular ROS level was elevated upon treatment with 15d-PGJ_2, and this elevation was abrogated in the presence of ROS scavengers such as catalase and NAC. The ROS scavenging activity of catalase was higher than that of NAC. We next examined the effect of catalase on the suppression of FcεRI expression by 15d-PGJ_2. KU812 cells were cultured with 15d-PGJ_2 (2 μM) for 24 h in the presence of catalase (1000 U/ml) under serum-free conditions. A catalase treatment caused an inhibition of suppressive effect of 15d-PGJ_2 on the FcεRI expression (Fig. 1c). Catalase is known to function to catalyze the decomposition of hydrogen peroxide to water and oxygen. Suppression of the FcεRI expression was observed in hydrogen peroxide-treated cells (data not shown). These facts and the result of Fig. 1b suggest that 15d-PGJ_2-induced ROS generation such as hydrogen peroxide may be responsible for downregulation of FcεRI expression by 15d-PGJ_2.

We have reported that the reduction of ERK1/2 phosphorylation caused a downregulation of FcεRI expression [12]. To further elucidate the molecular basis for 15d-PGJ_2-induced suppression of FcεRI expression, we examined the effect of 15d-PGJ_2 on ERK1/2 phosphorylation (Fig. 1d). KU812 cells were treated with 15d-PGJ_2 for 6 h in the presence or absence of catalase. ERK1/2 was separated on a 10% SDS-PAGE and immunoblotted with the anti-phosphorylated ERK1/2 antibody. Immunoblot analysis revealed that 15d-PGJ_2 was able to reduce the phosphorylation of ERK1/2. In addition, a catalase treatment prevented the inhibitory

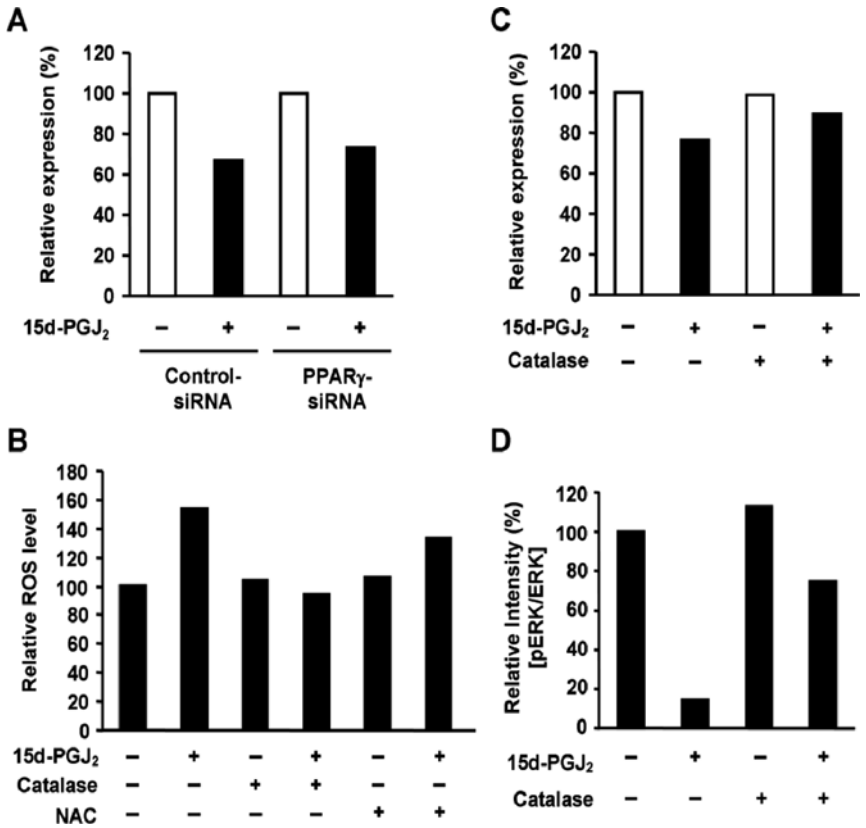

Fig. 1 Involvement of ROS in 15d-PGJ_2-induced suppression of FcεRI expression. (**a**) Stable siRNA expressing cells were cultured with 15d-PGJ_2 (2 μm) for 24 h under serum-free conditions. The cell surface expression of FcεRI was measured by flow cytometric analysis using the specific antibody against FcεRI. (**b**) KU812 cells were treated with 15d-PGJ_2 (2 μm) in the presence or absence of catalase (1000 U/ml) or NAC (10 mM) for 2 h. ROS generation was assayed by flow cytometer using H_2DCF-DA, and expressed as relative ROS level (%) to the non-treatment group. (**c**) KU812 cells were cultured with 15d-PGJ_2 (2 μm) for 24 h in the presence of catalase (1000 U/ml) under serum-free conditions. The cell surface expression of FcεRI was measured by flow cytometric analysis using the specific antibody against FcεRI. (**d**) KU812 cells were treated with 15d-PGJ_2 for 6 h in the presence or the absence of catalase. ERK1/2 was separated on a 10% SDS-PAGE and immunoblotted with the anti-phosphorylated ERK1/2 antibody

effect of 15d-PGJ_2 on the ERK1/2 phosphorylation. These results suggest that 15d-PGJ_2-induced generation of ROS such as hydrogen peroxide may contribute to the reduction of ERK1/2 phosphorylation, followed by the downregulation of FcεRI expression.

It has been known that degranulation stimulated by IgE/antigen was accompanied by production of intracellular ROS, and the inhibition of ROS production led to reduced degranulation [13]. However, possible roles of ROS elevation in

downregulation of mast cell or basophil activation, including FcεRI expression, degranulation, and cytokine production, still remains unclear. Our present data are the first report showing the involvement of redox state in the downregulation of FcεRI expression. This finding may shed new light on a negative role of ROS in basophil and mast cell activations.

References

1. Blank, U., Ra, C., Miller, L., White, K., Metzer, H., and Kinet, J.P. (1989) Complete structure and expression in transfected cells of high affinity IgE receptor. *Nature* **337**: 187–189.
2. Dombrowicz, D., Flamand, V., Brigman, K., Koller, B.H., and Kinet, J.P. (1993) Abolition of anaphylaxis by targeted disruption of the high affinity immunoglobulin E receptor alpha chain gene, *Cell* **75**: 969–976.
3. Ricote, M., Li, A.C., Willson, T.M., Kelly, C.J., and Glass, C.K. (1998) The peroxisome proliferator-activated receptor-γ is a negative regulator of macrophage activation. *Nature* **391**: 79–82.
4. Elstner, E., Muller, C., Koshizuka, K., Williamson, E.A., Park, D., Asou, H., Shintaku, P., Said, J.W., Heber, D., and Koeffler, H.P. (1998) Ligands for peroxisome proliferator-activated receptor γ and retinoic acid receptor inhibit growth and induce apoptosis of human breast cancer cells in vitro and in BNX mice. *Proc. Natl. Acad. Sci. USA* **95**: 8806–8811.
5. Kubota, T., Koshizuka, K., Williamson, E.A., Asou, H., Said, J.W., Holden, S., Miyoshi, I., and Koeffler, H.P. (1998) Ligand for peroxisome proliferator-activated receptor γ (troglitazone) has potent antitumor effect against human prostate cancer both in vitro and in vivo. *Cancer Res*. **58**: 3344–3352.
6. Sarraf, P., Mueller, E., Jones, D., King, F.J., De Angelo, D.J., Partridge, J.B., Holden, S.A., Chen, L.B., Singer, S., Fletcher, C., and Spiegelman, B.M. (1998) Differentiation and reversal of malignant changes in colon cancer through PPARγ *Nat. Med*. **4**: 1046–1052.
7. Sugiyama, H., Nonaka, T., Kishimoto, T., Komoriya, K., Tsuji, K., and Nakahata, T. (2000) Peroxisome proliferator-activated receptors are expressed in human cultured mast cells: A possible role of these receptors in negative regulation of mast cell activation. *Eur. J. Immunol*. **30**: 3363–3370.
8. Sugiyama, H., Nonaka, T., Kishimoto, T., Komoriya, K., Tsuji, K., and Nakahata, T. (2000) Peroxisome proliferator-activated receptors are expressed in mouse bone marrow-derived mast cells. *FEBS Lett*. **467**: 259–262.
9. Fujimura, Y., Tachibana, H., and Yamada, K. (2002) Peroxisome proliferator-activated receptor ligands negatively regulate the expression of the high-affinity IgE receptor Fc epsilon RI in human basophilic KU812 cells. *Biochem. Biophys. Res. Commun*. **297**: 193–201.
10. Scher, J.U. and Pillinger, M.H. (2005) 15d-PGJ_2: The anti-inflammatory prostaglandin? *Clin. Immunol*. **114**: 100–109.
11. Kondo, M., Oya-Ito, T., Osawa, T., and Uchida, K. (2001) Cyclopentenone prostaglandins as potential inducers of intracellular oxidative stress. *J. Biol. Chem*. **276**: 12076–12083.
12. Fujimura, Y., Tachibana, H., and Yamada, K. (2004) Lipid raft-associated catechin suppresses the FcεRI expression by inhibiting phosphorylation of the extracellular signal-regulated kinase1/2. *FEBS Lett*. **556**: 204–210.
13. Swindle, E.J. and Metcalfe, D.D. (2007) The role of reactive oxygen species and nitric oxide in mast cell-dependent inflammatory processes, *Immunol. Rev*. **217**: 186–205.

The Characteristic of Chimeric Receptors Based on Erythropoietin Receptor

Wenhai Liu, Masahiro Kawahara, Hiroshi Ueda, and Teruyuki Nagamune

1 Introduction

Cytokines are small secretory proteins, which bind to their cognate receptors expressed on the surface of target cells to control cell fate [1]. The erythropoietin receptor (EpoR) belongs to the cytokine receptor superfamily and is the primary regulator of mammalian erythropoiesis [2, 3]. Epo-binding to the extracellular D1 domains activates EpoR for signaling. Numerous studies have examined the roles of transmembrane (TM) and intracellular domains of the wild-type EpoR [4–6]. They did not examine the influence of the extracellular domains on signal transduction. Therefore, in this study, we designed a series of antibody/EpoR chimeras containing a hemagglutinin (HA)-tagged anti-fluorescein ScFv tethered to different combinations of EpoR D1/D2 domains in the extracellular domain. Furthermore, we also inserted one to four Ala residues at the intracellular juxtamembrane region of each chimeric receptor to modulate the orientation of the intracellular domain. Overall, such receptor engineering would offer more systematic analysis to elucidate the importance of conformation in EpoR. To test the signal-transduction ability of each chimeric receptor, the IL-3-dependent pro-B cell line Ba/F3 was transduced with a vector encoding each chimeric receptor. The transduced cells were stimulated with BSA-FL to examine the ligand-dependent cell growth. We evaluated the influence of the individual combinations of extracellular and intracellular domains on the signal transduction in EpoR.

2 Methods and Results

To analyze the influence of conformation of extracellular and intracellular domains on the signal transduction in EpoR, we developed a series of vectors for chimeric

W. Liu (✉)
Department of Chemistry and Biotechnology, The University of Tokyo, Tokyo 113-8656, Japan
e-mail: wenhai@bio.t.u-tokyo.ac.jp

M. Kamihira et al. (eds.), *Animal Cell Technology: Basic & Applied Aspects*, Animal Cell Technology: Basic & Applied Aspects 16, DOI 10.1007/978-90-481-3892-0_43,

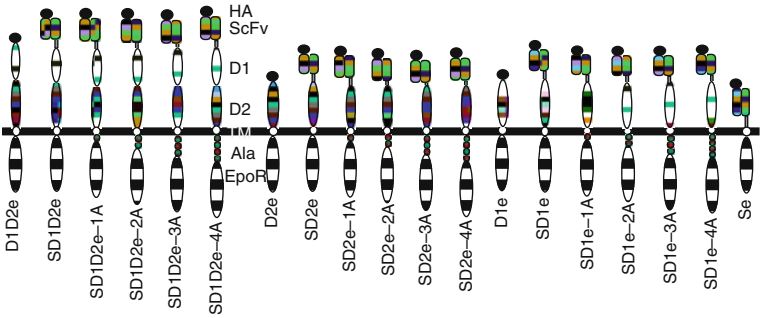

Fig. 1 Schematic diagrams of the chimeric receptor constructs and vectors. A series of chimeric receptor constructs with different combinations of the domains containing the anti-FL ScFv clone 31IJ3, extracellular D1/D2, transmembrane and intracellular domains of EpoR. A HA-tag was fused to the extracellular N-terminus of each chimeric receptor

receptors containing a HA-tagged anti-fluorescein ScFv tethered to different combinations of the extracellular D1/D2, TM and the intracellular domains of EpoR (Fig. 1).

A murine IL-3-dependent pro-B cell line, Ba/F3, was retrovirally transduced with the expression vector for chimeric receptors. EGFP-positive cells were selected by FACS sorting or by AMEGA [7] in the presence of 152 nM BSA-FL. The expression levels of chimeric receptors were analyzed by Western blotting (data not shown). The results confirmed that all of the constructed chimeric receptors were expressed in the transduced cells.

A cell growth assay was performed to examine whether the cells expressing the chimeric receptors could grow in response to BSA-FL, which could bind to the ScFv domain of the chimeric receptors. This assay was used to characterize the contribution of extracellular and intracellular domains to the signal transduction in the chimeric receptors. Cells were washed and cultured in a series of concentrations of BSA-FL for 3 days, and viable cell concentrations were measured (Fig. 2). As expected, chimeric receptors without ScFv, which were used as negative controls, failed to induce cell growth.

BSA-FL showed agonism at the constructs containing both D1 and D2 domains. SD1D2e succeeded in cell proliferation, but the growth activity was markedly reduced by inserting one to three Ala residues into the intracellular juxtamembrane domain. It was surprising that the growth activity recovered remarkably after insertion of four Ala residues, which also elevated the level of constitutive activation relative to that with SD1D2e.

On the other hand, BSA-FL showed inverse agonism at the constructs containing only the D2 domain. The constitutively active growth induced by SD2e, SD2e-2A and SD2e-3A was inhibited by the addition of BSA-FL. Although SD2e showed strong constitutive activation, the insertion of two or three Ala residues weakened the growth activity, which was nearly abolished by the insertion of one or four Ala residues.

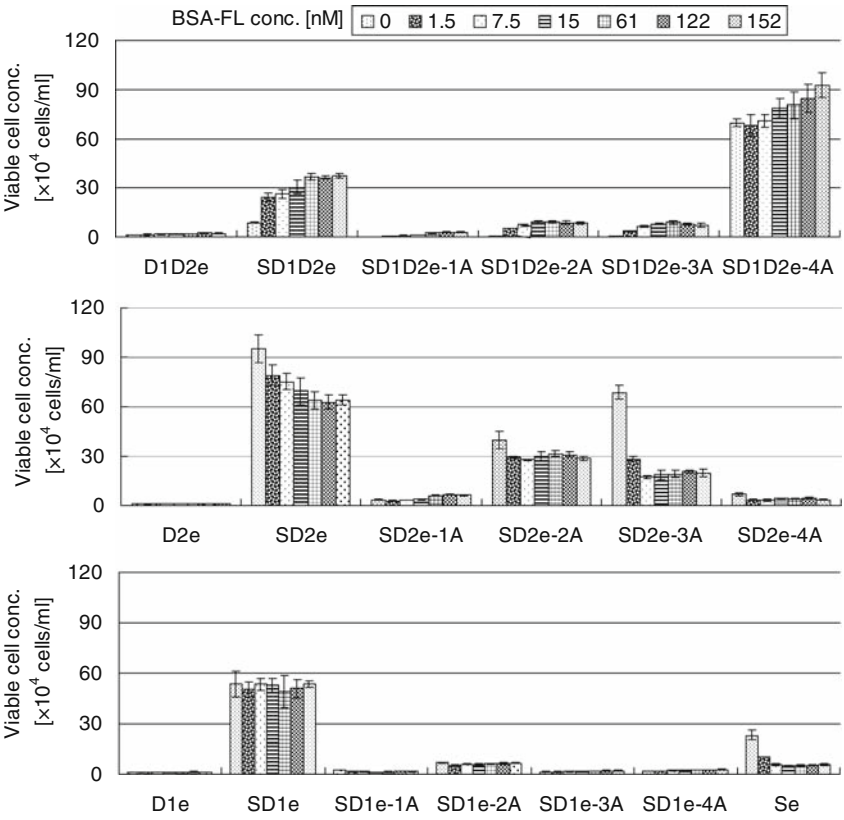

Fig. 2 Ligand-dependent cell growth induced by chimeric receptors. The EGFP-positive cells cultured in IL-3 were washed three times with PBS and seeded in 96-well plates at 1000 cells in 100 μl per well containing various concentrations of BSA-FL. Viable cell concentrations were determined using Cell Counting Kit-8 on day 3. The data from triplicate cultures are plotted as the mean ± S.D.

Of the constructs that contained only the D1 domain, only SD1e showed growth activity, which was constitutively active and unaffected by BSA-FL. However, the growth activity was abolished by the insertion of Ala residues. BSA-FL showed strong inverse agonism at Se, which contains neither the D1 nor D2 domain.

To confirm the ligand-specificity of the BSA-FL-responsive chimeric receptors, we performed a cell proliferation assay using a different set of ligands for the chimeric receptors. Besides BSA-FL, we also tested fluorescein-conjugated OVA (OVA-FL) as a specific ligand, while unconjugated ligands (BSA, OVA and free FL) or specific ligands in the presence of excess free FL (BSA-FL + free FL, OVA-FL + free FL) were tested to investigate the specificity of the chimeric receptors. BSA-FL and OVA-FL contain, on average, two FL molecules on each carrier protein, which would be expected to induce receptor dimerization, a prerequisite for triggering

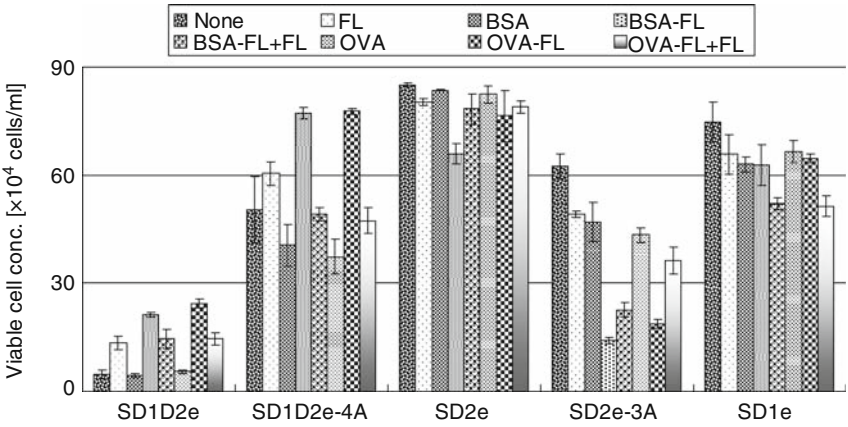

Fig. 3 Cell growth assay to test ligand specificity. The EGFP-positive cells cultured in IL-3 were washed three times with PBS and seeded in 96-well plates at 1000 cells in 100 μl per well without any ligands or with 60 nM BSA, 18 μM free FL, 60 nM BSA-FL, 60 nM BSA-FL with 18 μM free FL, 60 nM OVA, 60 nM OVA-FL or 60 nM OVA-FL with 18 μM free FL. BSA-FL and OVA-FL contain approximately two FL molecules per protein, which was determined from absorbance at 280 nm and 495 nm. Viable cell concentrations of triplicate cultures after 3 days are plotted as the mean ± S.D.

signal transduction. On the other hand, inclusion of excess free FL would be expected to inhibit the signal induced by BSA-FL or OVA-FL, since free FL is monomeric and could not induce receptor dimerization. We chose SD1D2e, SD1D2e-4A, SD2e, SD2e-3A and SD1e as representative chimeric receptors that responded to BSA-FL. As expected, all chimeric receptors showed no response to the unconjugated ligands (Fig. 3). The growth responses to OVA-FL were as strong as those to BSA-FL in all of the transduced cell lines. Furthermore, the cell proliferation in response to BSA-FL or OVA-FL was markedly affected in the presence of excess free FL. These results indicate that the chimeric receptors specifically recognize FL molecules on the carrier proteins.

3 Discussion

In this study, we designed a series of HA-tagged anti-FL ScFv-EpoR chimeras containing the EpoR extracellular D1 or D2 domain alone (D1 chimeras or D2 chimeras, respectively), both D1 and D2 domains (D1D2 chimeras), or no extracellular domains (Se). We also inserted one to four Ala residues into the intracellular juxtamembrane region to alter the orientation of the intracellular domain. These chimeras were individually expressed in the murine pro-B cell line Ba/F3. We used a FACS-based assay, in which the HA-tag in each chimeric receptor is stained with mouse anti-HA antibody and PE-labeled secondary antibody to measure the expression level of chimeric receptors on the cell surface (Table 1). As a result, all of the

Table 1 Surface expression level of chimeric receptors

Chimeric receptor	Expression level	Chimeric receptor	Expression level	Chimeric receptor	Expression level
D1D2e	84	D2e	58	D1e	8
SD1D2e	59	SD2e	50	SD1e	16
SD1D2e-1A	48	SD2e-1A	44	SD1e-1A	20
SD1D2e-2A	62	SD2e-2A	29	SD1e-2A	13
SD1D2e-3A	47	SD2e-3A	30	SD1e-3A	8
SD1D2e-4A	54	SD2e-4A	34	SD1e-4A	8

chimeric receptors were expressed on the cell surface. However, the levels of expression varied between chimeric receptors. Median fluorescence derived from the PE spanned from 8 (SD1e-3A) to 84 (D1D2e).

There was a statistically significant difference in the surface expression level between D1D2 chimeras, D1 chimeras and D2 chimeras (Fig. 4). The cell surface expression of D1D2 chimeras was higher than that of the D1 chimeras as well as the D2 chimeras; in particular, the expression of D1 chimeras was very low. These results suggest that the D2 domain is intrinsically important for the cell-surface expression of the chimeric receptors. Therefore, the domain structure in the extracellular domain is a key determinant for the surface expression level of these chimeras. At the primary sequence level, the extracellular domain, including the four cysteine

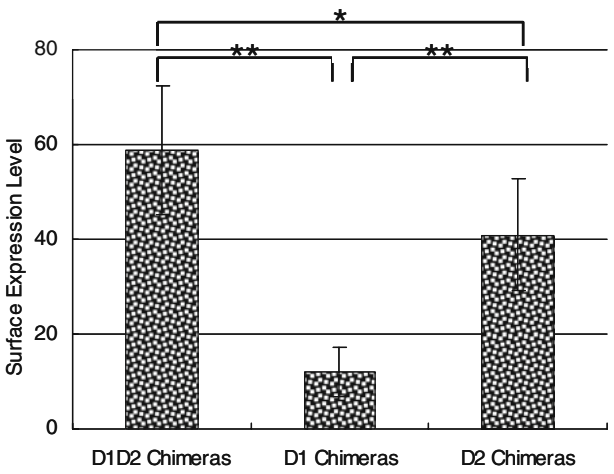

Fig. 4 Comparison of the surface expression levels of D1D2 chimeras, D1 chimeras and D2 chimeras. The surface expression level of D1D2 chimeras was calculated using the median fluorescence intensities of PE derived from SD1D2e, SD1D2e-1A to SD1D2e-4A. The surface expression levels of D1 chimeras and D2 chimeras were also calculated using the corresponding data. The calculated values are plotted as the mean ± S.D. **: $p < 0.01$; *: $0.01 < p < 0.05$

residues, the spacing of which is conserved, and the five-amino acid motif Trp-Ser-Xaa-Trp-Ser (WSXWS) are well conserved and very similar among cytokine receptors. The WSXWS motif or the WSXWS equivalent motif has been shown to be critical for the folding and transport of cytokine receptors to the cell surface [8, 9]. In fact, an A234E mutation in the WSAWS motif of EpoR was found to improve the efficiency of the processes [8]. Since the WSAWS motif is located in the D2 domain of EpoR, the folding and transport of the D1 chimeras to the cell surface might be severely impaired. The difference of the extracellular domain of the chimeras affected not only the surface expression level but also the ligand dependency. BSA-FL showed agonism at the D1D2 chimeras, inverse agonism at the D2 chimeras, and no effect on the D1 chimeras.

In addition to the modification of the extracellular domain, the orientation of the intracellular domain in the chimeras was modulated by the insertion of alanine residues. The cell growth assay to examine BSA-FL-dependency revealed that these subtle modifications could greatly affect the signaling activity of the chimeras. In the D1D2 chimeras, the cell proliferation signal was significantly reduced by inserting one to three Ala residues, but was strongly recovered by inserting four Ala residues. In the D2 chimeras, SD2e-2A and SD2e-3A stimulated cell growth, while SD2e-1A and SD2e-4A failed to stimulate cell growth. The growth signal was lost after inserting the Ala residues in the D1 chimeras.

In summary, here we developed a series of chimeric EpoRs. The results of our cell growth assay experiments indicate that EpoR signal transduction is affected by the conformations of both extracellular and intracellular domains.

References

1. Ihle, J.N. (1995) *Nature* 377: 591–594.
2. Constantinescu, S.N. et al. (1999) *Trends Endocrinol. Metab*. 10: 18–23.
3. D'Andrea, A.D. et al. (1989) *Cell* 58: 1023–1024.
4. Constantinescu, S.N. et al. (2001) *Proc. Natl. Acad. Sci. USA* 98: 4379–4384.
5. Gurezka, R. et al. (1999) *J. Biol. Chem*. 274: 9265–9270.
6. Livnah, O. et al. (1998) *Nat. Struct. Biol*. 5: 993–1004.
7. Kawahara, M. et al. (2004) *J. Immunol. Methods* 284: 187–194.
8. Baumgartner, J.W. et al. (1994) *J. Biol. Chem*. 269: 29094–29101.
9. Druhan, L.J. et al. (2005) *Blood* 105: 584–591.

Anti-Cancer and Structure-Activity Relationship of Natural Polyacetylenes

Soninkhishig Tsolmon, Yui Kurita, Si Won Hong, Parida Yamada, Hideyuki Shigemori, and Hiroko Isoda

1 Introduction

Plants contain many secondary metabolites; polyacetylenes are example of such metabolites. Polyacetylenic compounds are synthesized in plants in response to different stresses and play important role in plant "self-defense" against insects, fungi and other microorganisms [1]. In our recent studies we investigated a novel polyacetylenic compound 1 reduced cell growth and induced granulocytic differentiation in HL-60 cell lines [2].

Compound 1 possesses four acetylenic carbons, four olefin carbons, and six methylene carbons in polyacetylenic chain structure (Fig. 1). The most distinct structure of compound 1 is IAA at C-8, and compound 1 is the only reported compound including polyacetylenic chain and IAA in one structure [3].

Besides, three different polyacetylenic compounds were isolated from sun flower seeds. Compound A, B and C possess similar structures, including four acetylenic carbons, six olefin carbons, and three methylene carbons in polyacetylenic chain structure, on the other hand, compounds A-C possess different functional groups at C-8 (Fig. 2). Compounds A and B have a β-glucose and an acetoxy group at C-8, respectively, while compound C possesses a free hydroxyl group at C-8 [4].

In this study, we used K562 cell line to detect anti-cancer and structure-activity relationships of natural polyacetylenes. The K562 cell line was established from the pleural effusion of a patient with chronic myelogenous leukemia in blast crisis. It had been known that K562 cells have the capacity to express characteristics of erythrocytic, monocytic, and megakaryocytic differentiation when exposed to various agents, also provides an excellent model system for investigating process involved in cellular differentiation [5].

S. Tsolmon (✉)
Graduate School of Life and Environmental Sciences, University of Tsukuba, Tsukuba, Ibaraki 305-8572, Japan
e-mail: tssonio@yahoo.com

M. Kamihira et al. (eds.), *Animal Cell Technology: Basic & Applied Aspects*, Animal Cell Technology: Basic & Applied Aspects 16, DOI 10.1007/978-90-481-3892-0_44,

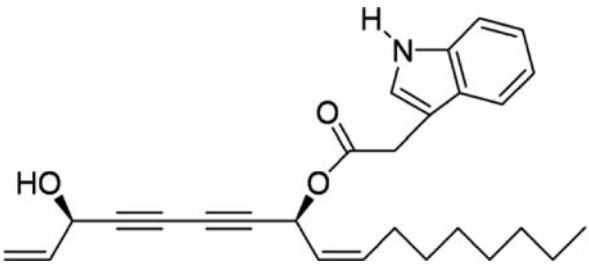

Fig. 1 Chemical structure of compound 1

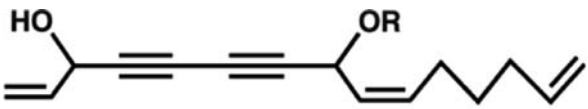

A: R = β-D-Glucose
B: R = Ac
C: R = H

Fig. 2 Chemical structure of compound A, B and C

2 Materials and Methods

2.1 Cell Culture

K562 cells were grown in the RPMI1640 medium supplemented with 10% fetal bovine serum (FBS). The cells were kept in an incubator at 37°C in a humidified atmosphere of 5% CO_2 in air.

2.2 Materials

Compound A, B and C were isolated from the acetone extract of seedlings of sunflower, *Helianthus annuus L. cv Russia*. The extract was subjected to silica gel column chromatography and reversed-phase HPLC to give compound A, B and C.

Compound 1 was isolated from the acetone extract of flower bud of *Hedera rhombea*. The extract was separated using silica gel column chromatography and reversed-phase HPLC to get compound 1.

2.3 MTT Assay

The time-dependent change in cell viability and proliferation was determined using the MTT tetrazolium assay. K562 cells were seeded onto a 96-well plate at 2×10^3 cells per well in 90 μl of RPMI1640 medium (Gibco) and then preincubated for 24 h. Compound 1, A, B and C diluents were added at 10 μl per well, followed by incubation for 12, 24, 48 and 72 h at 37°C in a humidified atmosphere of 5% CO_2. MTT (5 mg/ml) was then added at 10 μl per well, followed by 24 h of incubation at

37°C; 100 μl of 10% SDS was added to each well to solubilize the MTT formazan product. After 24 h of incubation at 37°C, the absorbance at 570 nm was determined with a POWERSCAN HT multidirectional microplate reader.

3 Results and Discussion

The time- and dose- dependent change in K562 cell viability was determined using the MTT assay. The viability of cells incubated with compound A and C (Fig. 3 and 5) were not significantly changed, and the viability of cells treated with compound B (Fig. 4) were slightly increased. On the other hand, cells incubated with compound 1 showed significant change of viability (Fig. 6). The viability of cells incubated with the highest concentration of compound 1 (10 μM) were decreased time- dependently, at 1.0 μM concentration compound 1 slightly suppress K562 cell growth compared with not treated cells, and at low concentration it (0.1 μM) had no effect on K562 cell viability.

From these results, polyacetylenes with β-glucose (compound A), free hydroxyl group (compound C) and acetoxy group (compound B) at C-8 did not show cytotoxic effect on K562 cell growth during up to 10 μM treatment concentrations. But compound A and B could induce cell growth inhibition in higher concentration (50 μM), compound B being more potent than compound A (data not shown). Compound 1 which had IAA at C-8 was the most effective in suppressing tumor cell growth among tested polyacetylenes. We suggest that IAA is the most important structure for growth inhibitory effect. Recently combination of IAA and horseradish

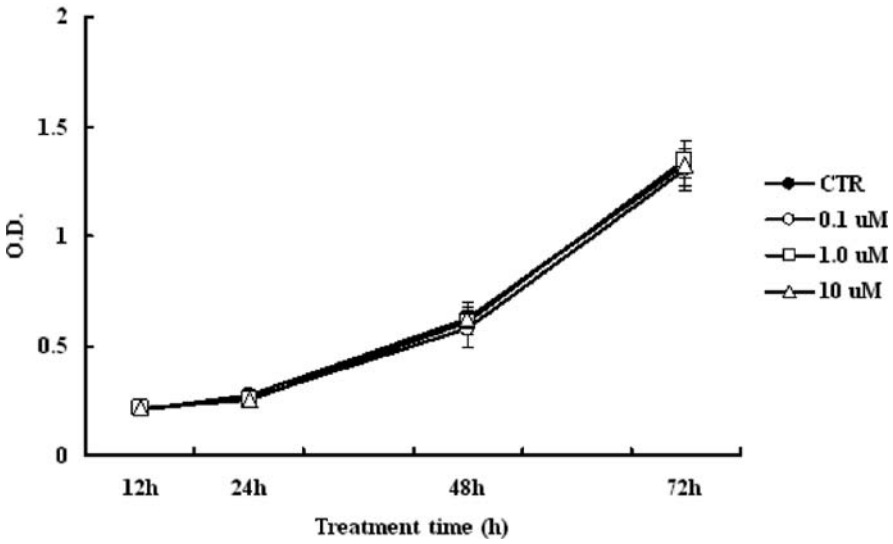

Fig. 3 Compound A treated K562 cell viability

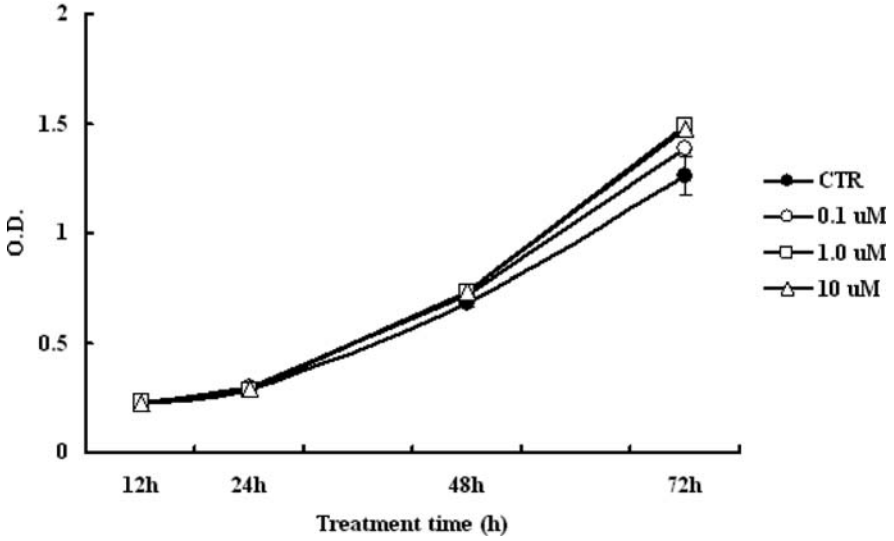

Fig. 4 Compound B treated K562 cell viability

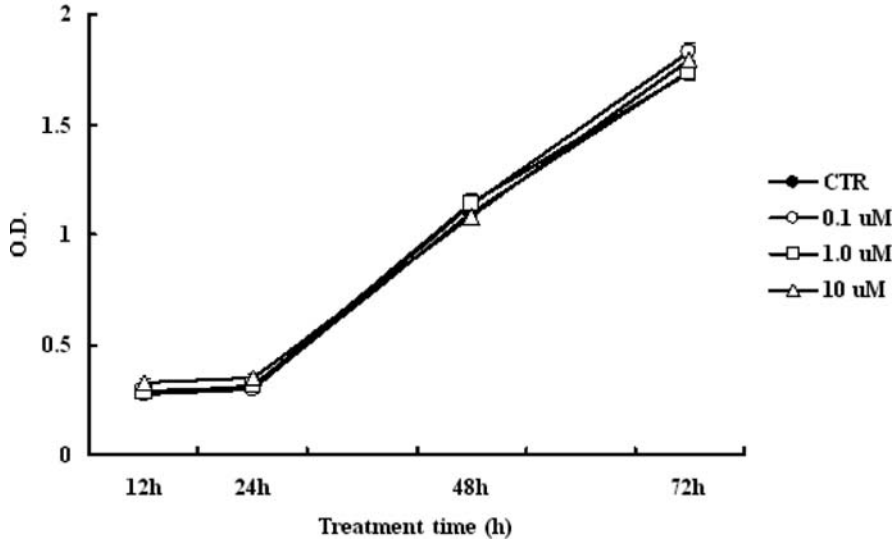

Fig. 5 Compound C treated K562 cell viability

peroxidase had been shown to be cytotoxic towards human tumor cells, and are targeted as anew produrg in cancer therapy due to radical forming ability of IAA reactive towards DNA and other biomolecules [6]. Besides, the growth inhibitory effect on K562 cells, polyacetylenic chain also may be involved to strengthen the

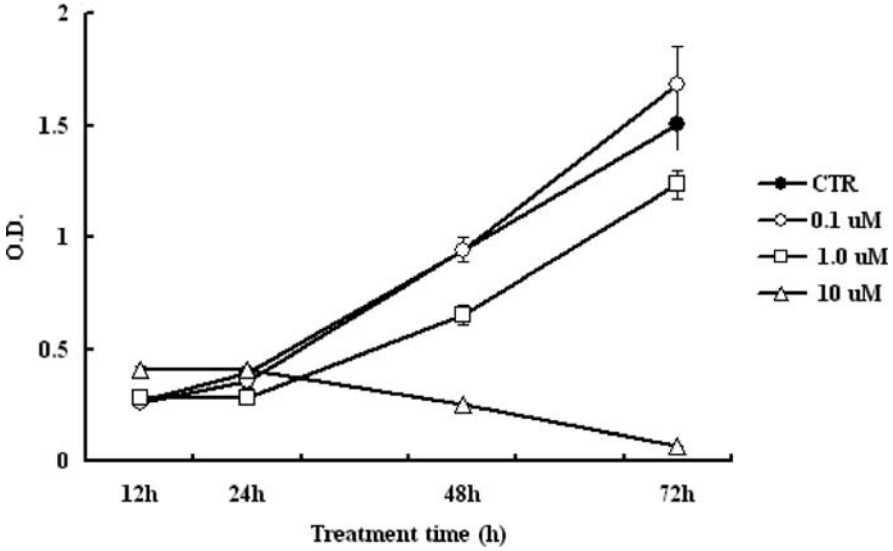

Fig. 6 Compound 1 treated K562 cell viability

effect. The unsaturated terminal of compound 1 may induce more effect, compare with the saturated terminal of compound A, B and C.

At 1.0 μM compound 1 treatment K562 cell growth was slightly decreased to compare to control cells but obvious cytotoxicity was not indicated. This result suggests that compound 1 may have differentiation inducing effect on K562. further studies are needed to elucidate this hypothesis.

References

1. Zidorm, C., Johrer, K., Ganzera, M., Schubert, B., Sigmund, E.M., and Mader, J. (2005) Polyacetylenes from the Apiaceae vegetables carrot, celery, fennel, paseley, and parsnip and their cytotoxic activites. *J. Agri. Food Chem*. **53**: 2518–2523.
2. Tsolmon, S., Kurita, Y., Yamada, P., Shigemori, H., and Isoda, H. (2009) Indole acetic acid falcarindiol ester induces granulocytic differentiation of human leukemia cell line HL-60. *Planta Medica*. **1**.
3. Yamazoe, S., Hasegawa, K., and Shigemori, H. (2007) Growth inhibitory indole acetic acid polyacetylenic ester from Japanese ivy (Hedera rhombea bean). *Phytochemical* **68**: 1706–1711.
4. Hong, S.W., Hasegawa, K., and Shigemori, H. (2008) Plant growth regulating activity of three polyacetylenes from helianthus annuus L. *Nat. Prod. Comm*. **3**(0): 1–4.
5. Kang, C.D., Lee, B.K., Kim, K.W., Kim, C.M., Kim, S.H., and Chung, B.S. (1996) Signaling mechanism of PMA-induced differentiation of K562 cells. *Biochem. Biophys. Res. Comm*. **221**: 95–100.
6. Rossiter, S., Folkes, L.K., and Wardman, P. (2002) Halogenated indol-3-acetic acids as oxdatively activated prodrug with potential for targeted cancer therapy. *Bioorg. Med. Chem. Lett*. **12**: 2523–2526.

Effect of Mongolian Medicinal Plant *Stellera Chamaejasme* on Chronic Leukemia Cells K562

Soninkhishig Tsolmon, Parida Yamada, and Hiroko Isoda

1 Introduction

Programmed cell death comprises apoptosis which is manifested by caspases activations and subsequent nuclear fragmentation. However, accumulating morphological and biochemical evidence suggests that programmed cell death is not confined only to apoptosis. Recently the cell's suicide program has been found to involve autophagic compartment. Autophagy is a process where cytoplasmic material, including organelles, is segregated into a double-membrane bound vesicle and then delivered to the lysosomal compartment for degradation. Although autophagy is considered as a cell survival mechanism, a number of studies describe it as a possible death pathway of cancer cells [1], [2], [3]. Cancer cell lines often have lower autophagic capacity than their normal counterparts and fail to respond to serum/amino acid deprivation or high cell density [3].

The root of *Stellera chamaejasme* L. (Thymelaeaceae) is one of the main substitutes of traditional Mongolian medicine. The clinical applications of this plant were supported by its pharmacological properties, such as tumor suppression and bactericidal action as demonstrated by a number of experimental studies conducted in the past decade [4]. Despite a long history of its clinical use, little is known about the mechanisms underlying its therapeutic effects. There have been continued efforts in investigating how *S. chamaejasme* L. regulates cellular responses in cancer and other diseases.

In this study we investigated anticancer effect of the ethanol extract of *S.chamaejasme* using chronic leukemia cell line K562. Our data suggests that the extract of this plant may induce autophagic cell death in chronic leukemia cells.

S. Tsolmon (✉)
Graduate School of Life and Environmental Sciences, University of Tsukuba, Tsukuba, Ibaraki 305-8572, Japan
e-mail: tssonio@yahoo.com

M. Kamihira et al. (eds.), *Animal Cell Technology: Basic & Applied Aspects*, Animal Cell Technology: Basic & Applied Aspects 16, DOI 10.1007/978-90-481-3892-0_45,

2 Materials and Methods

2.1 Cell Lines, Chemicals and Biochemicals

Human promyelocytic leukemia cell line K562 was purchased from Riken Cell Bank (Tsukuba, Ibaraki, Japan) and grown in RPMI 1640 medium supplemented with 10% of heat-inactivated fetal bovine serum at 37°C in a 5%CO_2 incubator. Acridine orange (AO) was purchased from Sigma Aldrich.

2.2 Extract Preparation

10*g* of dried plant of St.chamaejasme was extracted in 100 ml 99.8% EtOH for 1 week. The extract was filtered by 0.45 mm membrane filter and membrane-sterilized by 0.2 μm membrane. Extract was stored at –80°C.

2.3 Cell Viability Assay

The viability of cells was determined by MTT assay. Briefly, K562 cells were seeded onto 96-well plates for MTT assay at 2000 cells in 90 μL medium. After 24 h incubation, 10 μL extract diluents with medium were added to obtain final concentrations from 0.5% to 0.002% and the cells were cultured for 24, 48 and 72 h, followed by the addition of 10 μL of 5.0 mg/mL of 3-(4,5-dimethythiazol-2-yl)-2,5-diohenyl-2H-tetrazolium bromide. After another 24 h of incubation, 100 μL of 10% sodium dodecyl sulfate (SDS) was added and incubated for 24 h to completely dissolve the formazan produced by the cells. The absorbance was spectrophotometrically determined at 570 nm using a multidetection microplate reader (Powerscan HT, Dainippon Pharmaceutical, USA). Blanks were prepared at the same time to correct for the absorbance caused by sample color and by the inherent ability of the samples to reduce MTT in the absence of cells.

2.4 DNA Fragmentation Assay

K562 cells were plated onto Petri plates at 10^6 cells/plate in 9.5 ml of medium and incubated at 37°C for 24 h. The extract was added at 0.2%, 0.02%, 0.002% final concentration and the cells were incubated for 24 h and 48 h. The DNA extraction was carried out using the genomic DNA purification kit (Promega, Tokyo, Japan). The DNA purity was determined by measuring the absorbance ratios (A260/A280) using a spectrophotometer (Beckman, Fullerton, CA, USA). A 1% agarose gel was prepared using electrophoresis-grade agarose (Nippon Gene, Tokyo, Japan). The DNA samples well as molecular weight marker solution (DNA Ladder, Toyobo, Co. Ltd.) were mixed thoroughly with loading buffer (Wako) and loaded onto the gel in

1×TAE buffer solution. Electrophoresis was carried out for 30 min at 100 V. The gel was stained with ethidium bromide and directly photographed under ultraviolet illumination.

2.5 Detection of Autophagic Vacuoles by Acridine Orange Staining

Cell staining with acridine orange (Sigma Aldrich) was performed according to published procedure [5]. Briefly, cells were treated with 0.02% of the extract for 48 h, washed with PBS and incubated with 1 μg/ml acridine orange for 15 min at room temperature. Photographs were obtained with fluorescent microscope (Leica Microsystems, Germany). In acridine orange stained cells the cytoplasm and nucleolus fluoresce bright green and dim red, whereas acidic compartments fluoresce bright red. We also measured the autophagy by the intensity of the red fluorescence which is proportional to the degree of acidity of autophagic vacuoles by Guava PCA flow cytometry (GE Healthcare, USA).

3 Results and Discussion

To asses the anticancer effect of traditional medicinal plant *St.Chamaejasme* on K562 chronic leukemia cells we used MTT assay. MTT is a yellow water-soluble tetrazolium dye that is reduced by mitochondrial enzymes of live, but not dead, cells to purple formazan, which can be measured spectophotometricaly. During the treatment of K562 cells with ethanolic extract of the plant the cell growth was inhibited dose and time dependently compared to control after 48 h and 72 h of treatment with the highest inhibition rate of 70% at 0.5% extract treatment. Phase contrast microscopy revealed membrane blebbing and cell aggregation in the treated cells whereas vehicle treated cells did not differ from non treated controls.

Since the extract had cytotoxic effect on cancer cells we tried to elucidate the cause of cell death in the sample treated cells. The most common death pathway in cells is apoptosis. Most drugs used nowdays in cancer treatment are known for their induction of apoptotic death pathways in cancer cells. Many techniques have been developed to detect apoptotic programmed cell death. One of the most commonly used techniques is identification of DNA ladders. Our DNA fragmentation analysis results showed that treated cells did not produce any ladder, thus suggesting that the cell death could not be due to apoptosis.

Recently the cell's suicide program has been found to involve autophagic compartment. Autophagy is characterized by an increase in the number of vacuoles surrounded by a double membrane called autophagosomes, that sequester cytoplasm or organelles. Subsequently, autophagosomes fuse with lysosomes to form autolysosomes, where sequestered material is digested before nuclear collapse [6]. During physiological conditions, autophagy plays an important role in normal protein and organelle turnover. Furthermore, autophagy can be enhanced by several

cancer-related stimuli, for example, starvation, radiation as well as several anti-cancer agents [7]. Our further morphological observations showed extract-treated K562 cells display a dramatic increase in intracellular vacuoles. This evidence prompted us to study the possible role of autophagy in cancer cell death.

Autophagy can be detected by acridine orange staining. Acridine orange (AO) moves freely to cross biological membranes and accumulates in acidic compartment, where it is seen as fluorescence bright red. Vital staining of cells treated with plant extract have shown accumulation of AO indicated by bright red dot punctures in the cell cytoplasm, whereas in control cells, less accumulation of AO was observed. Autophagosome formation rate at 24 h treatment was 70% in 0.2% extract treated cells, while at 0.02% and 0.002% the rate was 35 and 18% respectively measured by flow cytometry (Guava).

Our results suggest that anticancer effect of traditional medicinal plant *St.Chamaejasme* could be due to induction of autophagy in malignant cells. Genetic links between defects in autophagy regulation and cancer have been reported. Thus, mice with decreased autophagy were more prone to the development of spontaneous tumours including lymphomas, lung carcinomas, hepatocellular carcinomas, and mammary precancerous lesions. suggest that autophagy is a true tumour suppressor pathway [7]. However, autophagy mechanisms underlying tumour suppression effect remain largely undetermined. Understanding those mechanisms and regulation of autophagy will be most apparent in medical aspects of many diseases such as cancer.

References

1. Chen, Y., McMillan-Ward, E., Kong, J., Israels, S.J., and Gibson, S.B. (2008) Oxidative stress induces autophagic cell death independent of apoptosis in transformed and cancer cells. *Cell Death Differ*. **15**: 171–182.
2. Cui, Q., Tashiro, S., Onoder, S., Minami, M., and Ikejima, T. (2007) Autophagy preceded apoptosis in oridonin-treated human breast cancer MCF- cells. *Biol. Pharm. Bull*. **30**(5): 859–864.
3. Comes, F., Matrone, A., Lastella, P., Nico, B., Susca, F.C., Bagnulo, R., Ingravallo, G., Modica, S., Lo Sasso, G., Moschetta, A., Guante, G., and Simona, C. (2007) A novel cell type-specific role of p38a in the control of autophagy and cell death in colorectal cancer cells. *Cell Death Diff*. **14**: 693–702.
4. Tian, Q., Li, J., Xie, X., Sun, M., Sang, H., Zhou, C., An, T., Hu, L., Ye, R D., and Wang, M. (2005) Stereospecific Induction of Nuclear Factor-kB Activation by Isochamaejasmin. *Mol. Pharmacol*. **68**(6).
5. Kanazawa, T., Kondo, Y., Ito, H., Kondo, S., and Germano, I. (2003) Induction of autophagic cell death in malignant glioma cells by arsenic trioxide. *Cancer Res*. **63**.
6. Yang, C., Kaushal, V., Shah SV., and Kaushal G.P. (2008) Autophagy is associated with apoptosis in cisplatin injury to renal tubular epithelial cells. *Am. J. Physiol. Renal. Physiol*. **294**: 777–787.
7. Mizushima, N., Levine, B., Cuervo A.M., and Klionsky, D.J. (2008) Autophagy fights disease through cellular self-digestion. *Nature* **451**: 28.

Capsaicin Induced the Upregulation of Transcriptional and Translational Expression of Glycolytic Enzymes Related to Energy Metabolism in Human Intestinal Epithelial Cells

Junkyu Han and Hiroko Isoda

1 Introduction

Capsaicin (8-methyl-N-vanillyl-6-nonennamide) is the pungent compound of number of structurally related moieties characterized by their pungent flavor. Capsaicin has been widely studied because of its importance in spices, food additives and drug [1]. Studies indicate that capsaicin alters thermogenesis and energy metabolism through sympathetic nervous system activation. The sympathetic nervous system activation by capsaicin induced reduction of body weight and suppression of body fat accumulation [2, 3]. Also capsaicin inhibits adipocyte differentiation via activation of AMPK (AMK-activated kinase).

Recently, it was reported that capsaicin and capsaicin receptor play an important role in increasing in metabolic rate: the metabolic rates of capsaicin receptor knockout mice and normal mice were measured by oxygen consumption [4]. The oxygen consumption of normal mice, which have the capsaicin receptor, was increased by injection of capsaicin into intestine, but the oxygen consumption of knockout mice was not.

2 Materials and Methods

2.1 Cells and Culture

Caco-2 cells were maintained in Dulbecco's modified Eagle's medium (DMEM, Sigma, St Louis, MO) supplemented with 10% fetal calf serum (Sigma), 1% penicillin-streptomycin (Sigma), and 1% nonessential amino acids (Cosmo Bio Co. Ltd., Tokyo, Japan). They were incubated in an atmosphere of 5% CO_2 at 37°C. The cells were passaged at a split ratio of 4–8 every 3 or 4 days.

J. Han (✉)
Graduate School of Life and Environmental Sciences, University of Tsukuba, Tsukuba, Ibaraki 305-8572, Japan
e-mail: jhan@sakura.cc.tsukuba.ac.jp

M. Kamihira et al. (eds.), *Animal Cell Technology: Basic & Applied Aspects*, Animal Cell Technology: Basic & Applied Aspects 16, DOI 10.1007/978-90-481-3892-0_46,

2.2 Proteomics

Proteins from capsaicin-treated or untreated cells were resuspended in 350 μl of 8 M urea, 2% (w/v) 3-[(3-Cholamidopropyl) dimethylammonio]-1-propanesulfonate (CHAPS), 0.5% (v/v) immobilized pH gradient (IPG) buffer, and 10 mM DTT. Solubilized proteins were electrophoresed in the first dimension using a commercial flatbed electrophoresis system and 18 cm IPG dry strips with a pH 3–10 linear range. Cytotoxicity assay. The IPG strip was rehydrated for approximately 14 h at room temperature and the proteins were electrophoresed in gradient mode using an EPS 3501 XL power supply (GE Healthcare) under the following conditions: 150 V, 1 mA for 30 min; 300 V, 1 mA for 30 min; 500 V, 1 mA for 1 min; 3,500 V, 1 mA for 1.5 h; 3,500 V, 1 mA for 7.8 h. After isoelectric focusing, the IPG strips were reequilibrated for 20 min in 2% (w/v) sodium dodecyl sulfate (SDS), 6 M urea, 30% (v/v) glycerol, 0.05 M Tris-HCl (pH 8.8), and 2% (w/v) DTT and for 20 min in 2% (w/v) SDS, 6 M urea, 30% (v/v) glycerol, 0.05 M Tris-HCl (pH 8.8), and 5% (w/v) iodoacetamide. The strip was placed on a gradient SDS-PAGE gel (12–14% (w/v) polyacrylamide) and run at 1000 V, 20 mA for 45 min and at 1000 V, 40 mA for 160 min.

3 Results and Discussion

3.1 Proteomics Analysis

The proteins overexpressed following treatment with capsaicin (100 μM) in Caco-2 cells were identified by proteomics technologies (Fig. 1). Proteins from capsaicin-treated cells and control cells were separated on immobilized pH gradient strips followed by SDS-PAGE (Fig. 2). Stained gels were analyzed with image analysis soft. We focused on the spots, overexpressed more than 1.7 folds. The two protein spots that showed a significant change; Spot 1 was upregulated 2.1-fold and Spot 2

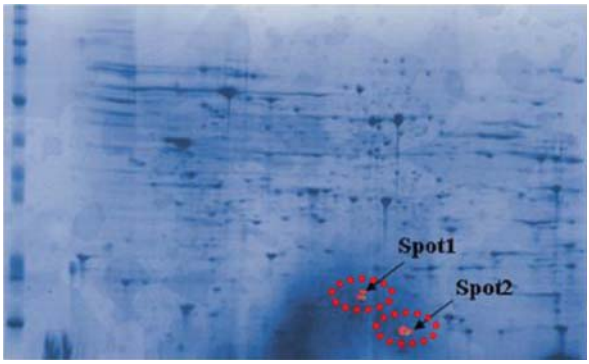

Fig. 1 Two-dimensional gel electrophoresis of capsaicin-treated Caco-2 cells

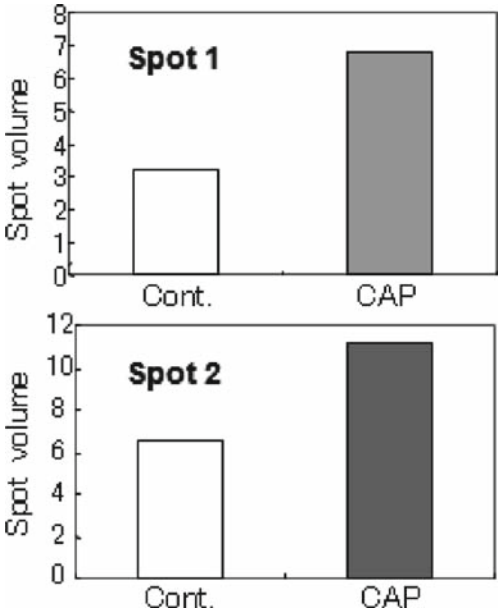

Fig. 2 Spot volume of spot 1 and spot 2

was upregulated 1.7-fold in intensity compared to that of controls had been excised and analyzed by MALDI-TOF mass spectrometry, which gave sufficient confirmation of protein identity for both spots. Proteins that were induced in Caco-2 cells treated with capsaicin were identified as phosphoglycerate mutase (PGM; Spot 1) and triosephosphate isomerase (TPI; Spot 2). PGM is an enzyme that catalyzes step 8 of glycolysis. It catalyzes the internal transfer of a phosphate group from C-3 to C-2 which results in the conversion of 3-phosphoglycerate to 2-phosphoglycerate through a 2,3-bisphosphoglycerate intermediate. TPI is an enzyme that catalyzes the reversible interconversion of the triose phosphate isomers dihydroxyacetone phosphate and D-glyceraldehyde 3-phosphate. TPI plays an important role in glycolysis and is essential for efficient energy production. These proteins are glycolytic enzymes that activate a central glycolytic ATP-producing pathway.

References

1. Chancellor, M.B. and Groat, W.C. (1999) Intravesical capsaicin and resiniferatoxin therapy: Spicing up the ways to treat the overactive bladder. *J. Urol.* **162**: 3–11.
2. Chung, K.F. and Chang, A.B. (2002) Therapy for cough: Active agents. *Pulmon. Pharmacol. Therapeut*. **15**: 335–338.
3. Olzer, P. (2004) TRPV1 and the gut: From a tasty receptor for a painful vanilloid to a key player in hyperalgesia. *Eur. J. Pharmacol*. **500:** 231–241.
4. Szolcsányi, J. (2004) Forty years in capsaicin research for sensory pharmacology and physiology. *Neuropeptides* **38:** 377–384.

Effect of Novel Compounds from *Thymelaea Hirsuta* on Melanogenesis

Myra O. Villareal, Yusaku Miyamae, Junkyu Han, Yamada Parida, Hideyuki Shigemori, and Hiroko Isoda

1 Introduction

The human skin color is imparted by the type and amount of melanin produced by melanocytes. Melanins are the end-product of complex multistep transformations of L-tyrosine, are polymorphous and multifunctional biopolymers [1]. Melanins have very diverse roles and functions in various organisms. It gives color to the skin and hair and protect the skin against harmful UV light. A large number of skin diseases, which include acquired hyperpigmentation, such as melasma and solar lentigo, are caused by increased production and accumulation of melanins [2].

Hyperpigmentation is treated using a wide array of depigmenting or skin lightening agents such as magnesium-L-ascorbyl-2-phosphate (MAP), hydroxyanisole, N-acetyl-4-S-cysteaminylphenol, arbutin (hydroquinone-beta-D-glucopyranoside) and hydroquinone (HQ). However, with reports of potential mutagenicity and unwanted side effects, there has been an increasing demand for alternative herbal and pharmaceutical depigmenting agents [3]. In our search for a safe but effective antimelanogenesis compound from a natural source, we discovered that extract of Tunisian *Thymelaea hirsuta* has antimelanogenesis properties [4]. This study was conducted to determine the possible anti-melanogenesis effects of novel compounds from *T. hirsuta* extract on melanogenesis of B16 murine melanoma cells.

2 Materials and Methods

2.1 Cells and Culture

B16 murine melanoma cells were obtained from the Riken Cell Bank (Tsukuba, Japan) and were maintained as a monolayer culture in Dulbecco's modified Eagle's

M.O. Villareal (✉)
Graduate School of Life and Environmental Sciences, University of Tsukuba, Tsukuba, Ibaraki 305-8572, Japan
e-mail: mye_o@yahoo.com

M. Kamihira et al. (eds.), *Animal Cell Technology: Basic & Applied Aspects*, Animal Cell Technology: Basic & Applied Aspects 16, DOI 10.1007/978-90-481-3892-0_47,

medium (DMEM) (Sigma, St Louis, MO, USA), supplemented with 10% fetal bovine serum (Sigma), 50 unitsml penicillin and 50 lg ml streptomycin (Cambrex, East Rutherford, NJ, USA) at 37°C with 5% CO_2.

2.2 Isolation of Compounds from Thymelaea Hirsuta

Thymelaea hirsuta leaves (100 g) were extracted with eight (8) liters of methanol (MeOH) and evaporated to dryness in vacuo at 30°C. The crude extract was subjected to MeOH and EtOAc extraction and subjected to a series of fractionation using silica gel column and elutions with $CHCl_3$/MeOH applied to a Sep-Pak Cartridge. The fractions containing daphnane was further separated and purified by reverse-phase HPLC and the novel compounds were obtained from that fraction.

2.3 Cytotoxicity Assay

To determine the general viability of cultured cells, 3-(4,5-dimethylthiazol-2-yl)-2,5-diphenyl-tetrazolium bromide (MTT) assay, based on the protocol first described by Mossman [5], was carried out.

2.4 Melanin Assay

B16 melanoma cells were seeded at a density of 5×10^5 cells per 100-mm petri dish and cultivated by the method described above. The cells were treated with 0.1 μM novel compounds and 100 μM arbutin and incubated for 48 h. The melanin content was measured following Hosoi et al.'s [6] method, with some modifications. The total melanin content was estimated using the standard curve for synthetic melanin and expressed as melanin content per viable cell.

3 Results and Discussion

3.1 Cytotoxicity Test

The MTT assay is considered as a reliable means of measuring cell proliferation in vitro. The results we obtained show that the novel daphnane compounds are not in any way cytotoxic to the cells but rather appear to have proliferative effects between concentrations of 0.1–2 μM.

3.2 Effect on Cell Melanin Content

To determine the effect of the compounds on melanogenesis, melanin content per viable cell was determined. B16 cells were treated with 0.1 μM NC1 and NC2

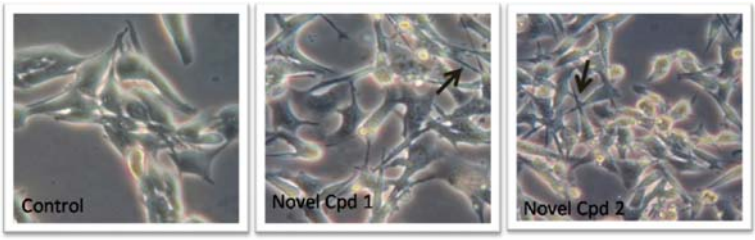

Fig. 1 B16 murine melanoma cells treated with novel compounds from *Thymelaea hirsuta*. *Arrows* pointing to long dendrites not observed in untreated cells (control)

compounds. The compounds induced a noticeable change in the cell morphology (Fig. 1).

B16 cells treated with novel compounds had lower melanin content compared with the control. NC1's ability to reduce the melanin content of B16 cells, at 0.1 μM concentration, is the same as that of 100 μM arbutin, a known depigmenting agent [7, 8].

The results of the MTT assay in addition to the melanin assay suggest that the compounds are strong melanogenesis inhibitors and thus may be considered as promising candidates for novel skin depigmenting agents.

References

1. Slominski, A., Tobin, D., Shibahara, S., and Wortsman, J. (2004) Melanin pigmentation in mammalian skin and its hormonal regulation. *Physiol. Rev*. **84**: 1155–1228.
2. Archambault, M., Yaar, M., and Gilchrest, B.(1995) Keratinocytes and fibroblasts in a human skin equivalent model enhance melanocyte survival and melanin synthesis after ultraviolet irradiation. *J. Invest. Dermatol*. **104**: 859–867.
3. Parvez, S., Kang, M., Chung, H., Cho, C., Hong, M., Shin, M., and Bae, H. (2006) Survey and mechanism of skin depigmenting and lightening agents. *Phytother. Res*. **20**(11): 921–934.
4. Kawano, M., Matsuyama, K., Miyamae, Y., Shinmoto, H., Kchouk, M., Morio, T., Shigemori, H., and Isoda, H. (2007) Antimelanogenesis effect of Tunisian herb *Thymelaea hirsuta* extract on B16 murine melanoma cells. *Experim. Dermatol*. **16**: 977–984.
5. Mossman, T. (1983) Rapid colorimetric assay for cellular growth and survival. *J. Immunol. Methods* **65**: 55–63.
6. Hosoi, J., Abe, E., Suda, T., and Kuroki, T. (1985) Regulation of melanin synthesis of B16 mouse melanoma cells by 1a, 25-dihydroxyvitamin D3 and retinoic acid. *Cancer Res*. **45**: 1474–1478.
7. Chakraborty, A., Funasaka, Y., Komoto, M., and Ichihashi, M. (1998). Effect of arbutin on melanogenic proteins in human melanocytes. *Pigment Cell Res*. **11**: 206–212.
8. Jun, S.Y., Park, K.M., Choi, K.W., Jang, M.K., Kang, H. L., Lee, S.H., Park, K.H., and Cha, J. (2008) Inhibitory effects of arbutin-b-glycosides synthesized from enzymatic transglycosylation for melanogenesis. *Biotechnol. Lett*. **30**: 743–748.

Electrolyzed Reduced Water Prolongs *Caenorhabditis elegans'* Lifespan

Hanxu Yan, Huaize Tian, Takeki Hamasaki, Masumi Abe, Noboru Nakamichi, Kiichiro Teruya, Yoshinori Katakura, Shinkatsu Morisawa, and Sanetaka Shirahata

1 Introduction

Electrolysis of water produces two types of water: electrolyzed reduced water (ERW) in the cathode site and electrolyzed oxidized water (EOW) in the anode site. ERW has attracted much attention because of its therapeutical effects. ERW has been shown to exhibit inhibitory effects on pancreatic cell damage in HIT-T15 cells [1] and anti-diabetic effects on type 2 diabetes model mice (*db/db*) [2]. ERW reduced hemodialysis-induced oxidative stress in end-stage renal disease (ESRD) patients [3]. Shirahata et al. [4]. first demonstrated that ERW exhibiting high pH, low dissolved oxygen, and extremely high dissolved molecular hydrogen showed ROS scavenging activity and protected oxidative damage to DNA.

According to the free radical theory of ageing, ageing is the result of the accumulation of molecular damage caused by free radicals. Free radicals, particularly reactive oxygen species (ROS), such as singlet oxygen ($^1O_2$), superoxide ($O_2^{\bullet -}$), hydrogen peroxide (H_2O_2), and hydroxyl radical ($OH^{\bullet}$) are considered to cause extensive oxidative damage to biological macromolecules such as DNA, proteins and lipids. The correlation between delayed ageing progression and oxidative stress resistance has been testified many times over the years in *Caenorhabditis elegans* (*C. elegans*) and many other model organisms. It has been shown that vitamin E [5], tocotrienols [6], EGB761, which is an extract of *Ginkgo biloba* leaves [7] and CoQ10 [8] can prolong the lifespan of *C. elegans* by increasing resistance to oxidative stress. Recently the antioxidative and anti-ageing properties had also been found in platinum nano-particle solution [9].

Based on those former works and the free radical theory of aging, we investigated effect of ERW on lifespan of *C. elegans*. In the present study, we developed a new culture method using a special culturing medium called water medium and compared the effects of ERW on the lifespan of *C. elegans* strains in both water

S. Shirahata (✉)
Faculty of Agriculture, Kyushu University, Higashi-ku, Fukuoka 812-8581, Japan
e-mail: sirahata@grt.kyushu-u.ac.jp

M. Kamihira et al. (eds.), *Animal Cell Technology: Basic & Applied Aspects*, Animal Cell Technology: Basic & Applied Aspects 16, DOI 10.1007/978-90-481-3892-0_48,

medium and conventional S medium. We found that ERW was able to significantly extend *C.elegans* lifespan in water medium, but not in S medium.

2 Methods and Materials

2.1 Elegans Strains and Growth Condition

The wild-type N2 strain was provided by Dr. K. Nomura, Department of Biology, Faculty of Sciences of Kyushu University. The worms were maintained at 20ºC, according to the procedures established by Brenner [10]. Age-synchronous populations were prepared, as previously described by Emmons et al. [11]. Briefly, collected eggs were hatched overnight at 20ºC in S-basal buffer, which consisted of 100 mM NaCl, 0.01 mM cholesterol, and 50 mM potassium phosphate (pH 6.0), on nematode growth medium (NGM) agar plates [12]. Hatched worms (L1-stage larvae) were transferred to fresh NGM agar plates and cultured at 20ºC or 25ºC with *Escherichia coli* strain OP50 (*E. coli* OP50) as a food source, until they reached L4 larval stage.

2.2 Preparation of ERW

ERW (pH 11.57; DH, 0.928 ppm; DO, 6.15 ppm; ORP, -659 mV) and EOW (pH 11.06; DH, 0.005 ppm; DO, 12.3 ppm) were produced by the batch type TI-200 electrolyzing device equipped platinum-coated titanium electrodes set in the 4 L chamber separated by semi-permeable membrane (Nihon Trim Co., Osaka, Japan). 0.002 M NaOH solution (pH 11.34; DH, 0.001 ppb; DO, 7.67 ppm; ORP, +350 mV) was electrolyzed for 1 hr at a 100 DC voltage. 0.002 M NaOH as well as ERW and EOW was neutralized with HEPES as control and expressed as Milli Q. Freshly prepared electrolyzed water was immediately used for preparation of medium.

2.3 Preparation of Water Medium

In order to test the effect of ERW, we used 2 kinds of culturing media. One was the traditional *C.elegans* culturing medium called S medium [S-basal medium supplemented with 3 mM $CaCl_2$, 3 mM $MgSO_4$, 50 μM EDTA, 25 μM $FeSO_4$, 10 μM $MnCl_2$, 10 μM $ZnSO_4$, 1 μM $CuSO_4$, and 10 mM KH_2PO_4 (pH 6.0)] with *E. coli* OP50.

The other one, called water medium, was designed especially for electrolyzed water. Water samples were adjusted to pH 7.0 with HEPES, and heat killed *E. coli* OP50 (2×10^9 bacterial cells/ml) was added in the medium as a food resource. We also added 50 μM FUdR into the culture mediums during the assays to prevent worm death due to internal hatching. Dishes were shaken in a gyratory shaker at 120 oscillations/min [13].

2.4 Lifespan Assay

For the lifespan assay, L4 larvae were transferred to each culture medium. The transfer day was designated as Day 0. The worms were transferred to fresh culture medium every second day and the surviving worms were counted at the same time. The mortality data were derived from Kaplan–Meier survival curves, and statistical comparisons of mean lifespan values between the control and ERW group worms were analyzed by log-rank test.

2.5 ROS Detection

Nematodes were cultured with ERW medium or MQ medium until Day 5. After Day 5, worms were picked up and washed extensively with M9 buffer (22 mM Na_2HPO_4, 22 mM KH_2PO_4, 85 mM NaCl, 1 mM $MgSO_4$, 0.02% gelatin), then incubated with 0.4 M paraquat (Supelco, USA) for 5 h. The worms were washed three times with M9 buffer and then transferred to 2 ml of Hank's solution (0.44 mM KH_2PO_4, 5.37 mM KCl, 0.34 mM Na_2HPO_4, 137 mM NaCl, and 5.55 mM D-glucose) that contained 10 mM DCHFDA (Invitrogen, USA) and incubated for 30 min at 20ºC. Finally, the worms were fixed with 4% formaldehyde and subjected to laser scanning confocal microscopy (OLFV-32U2/XE; Olympus Co., Japan, excitation at 488 nm and emission at 510 nm) [9]. The relative fluorescence of the whole worm body was determined densitometrically using the Olympus FV10-ASW 1.4 software. The statistical significance of differences between the control and treated groups were determined by one-way ANOVA.

3 Results

3.1 Lifespan

Wild-type nematodes cultured in TI-200 ERW medium resulted in increases in average-lifespans of 7% ($P < 0.05$) while worms cultured in TI-200 EOW medium showed a significant shortened lifespan of 29% ($P < 0.05$) (Fig. 1).

3.2 Detection of ROS

Ageing is associated with intracellular damage, which is caused by endogenous and exogenous oxidative stress. We measured the effects of ERW medium on the intracellular accumulation of ROS induced by paraquat. Worms cultured in TI-200 ERW medium reduced the level of ROS generated by 0.4 M paraquat-induced oxidative stress compared with the control ($74.95 \pm 7.8\%$, $p < 0.01$) (Fig. 2).

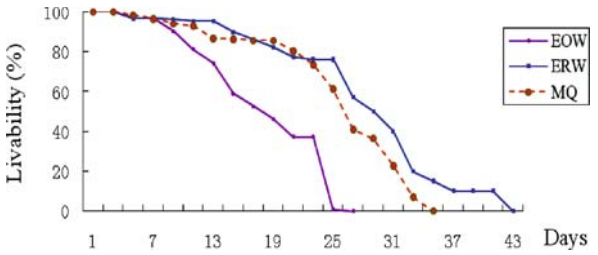

Fig. 1 Survival curves of *C.elegans* cultured in TI-200 ERW, TI-200 EOW or MQ media. N2 worms were cultured in each water medium at 20ºC. Worms were scored as dead when they failed to respond to repeated touching with a platinum wire pick. The number of worms used per each lifespan assay experiment was 58–125 ($n = 58 - 125$) and three to six independent experiments were repeated ($N = 3 - 6$). MQ means 0.002 M NaOH solution neutralized to pH 7.0 with HEPES as well as EOW and ERW

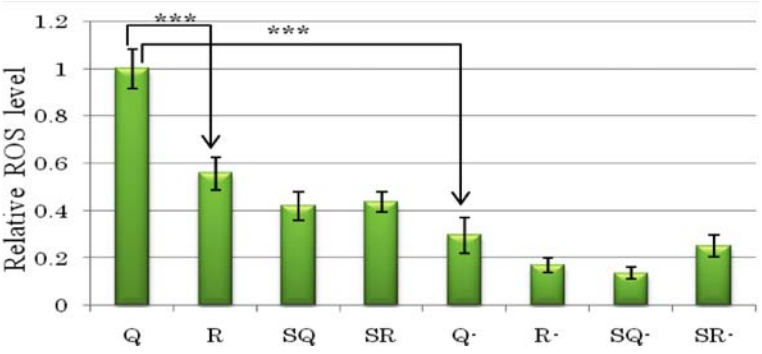

Fig. 2 Effects of ERW media and on ROS accumulation in *C.elegans*. Worms were cultured in TI-200 for 5 days ($n = 5 - 12$). The intensity of fluorescence of worms was detected by Olympus FV10-ASW 1.4 software. The average intensity is presented as mean ± S.E.M., in relation to the MQ water medium worms. Q, R, SQ, SR means the relative intensity of fluorescence of paraquat-treated-worms in MQ medium, TI-200 ERW medium, S medium (MQ), S medium (TI-200 ERW) respectively. Q-, R-, SQ-, SR- means the relative intensity of fluorescence of none-paraquat-treated-worms in MQ medium, TI-200 ERW medium, S medium (MQ), S medium (TI-200 ERW). *** $p < 0.001$, * $p < 0.5$

4 Discussion

Our former research showed ERW has an ability to scavenge the intracellular ROS in multiple types of cultured animal cells. Since ERW medium can significantly extend the nematode lifespan, we assumed that the ROS scavenging ability of ERW is responsible to the prolonged lifespan of *C.elegans* we have observed. In order to confirm the assumption, we detected the ROS level in *C.elegans*, and the results showed that in the conditions of water medium, ERW significantly alleviated the

accumulation of ROS induced by the paraquat compared to Milli Q. ERW also suppressed the ROS level in nematodes without treatment of paraquat. On the other hand, nematodes showed much lower levels of ROS in S medium than in water medium. ERW did not exhibit suppressive effect of ROS level in S medium. Taken together, it is reasonable to believe that ERW have benefits to animals' lifespan by at least in part by the scavenging ability of ROS.

References

1. Li, Y.P., Nishimura, T., Teruya, K., Tei, M., Komatsu, T., Hamasaki, T., Kashiwagi, T., Kabayama, S., Shim, S.-Y., Katakura, Y., Osada, K., Kawahara, T., Otsubo, K., Morisawa, S., Ishii, Y., Gadek, Z., and Shirahata, S. (2002) Protective mechanism of reduced water against alloxan-induced pancreatic β-cell damage: Scavenging effect against reactive oxygen species. *Cytotechnology* **40**: 139–140.
2. Kim, M.-J., Jung, K.H., Uhm, Y.K., Leem, K.-H., and Kim, H.K. (2007) Preservative effect of electrolyzed reduced water on pancreatic beta–cell mass in diabetic *db/db* mice. *Biol. Pharm. Bull*. **30**: 234–236.
3. Huang, K.-C., Yang, C.-C., Hsu, S.-P., Lee, K.-T., Kiu, H. W., Morisawa, S., Otsubo, K., and Chen, C.-T. (2006) Electrolyzed-reduced water reduced hemodialysis-induced erythrocyte impairment in end-stage renal disease patients. *Kidney Int*. **70**: 391–398.
4. Shirahata, S., Kabayama, S., Nakano, M., Miura, T., Kusumoto, K., Gotoh, M., Hayashi, H., Otsubo, K., Morisawa, S., and Katakura, Y. (1997) Electrolyzed–reduced water scavenges active oxygen species and protects DNA from oxidative damage. *Biochem. Biophys. Res. Commun*. **234**: 269–274.
5. Harrington, L.A. and Harley, C.B. (1988) Effects of vitamin E on lifespan and reproduction in *Caenorhabditis elegans*. *Mech. Ageing Dev*. **43**: 71–78.
6. Adachi, H. and Ishii, N. (2000) Effects of tocotrienols on life span and protein carbonylation in *Caenorhabditis elegans*. *J. Gerontrol. A Biol. Sci*. **55**: B280–B285.
7. Wu, Z., Smith, J.V., Paramasivam, V., Butko, P., Khan, I., Cypser, J.R., and Luo, Y. (2002) *Ginkgo biloba* extract EGB 761 increases stress resistance and extends lifespan of *Caenorhabditis elegans*. *Cell. Mol. Biol*. **48**: 725–731.
8. Ishii, N., Senoo-Matsuda, N., Miyake, K., Yasuda, K., Ishii, T., Hartman, P.S., and Furukawa, S. (2004) Coenzyme Q10 can prolong *C. elegans* lifespan by lowering oxidative stress. *Mech. Ageing Dev*. **125**: 41–46.
9. Kim, J., Takahashi, M., Shimizu, T., Shirasawa, T., Kajita, M., Kanayama, A., and Miyamoto Y. (2008) Effects of a potent antioxidant, platinum nanoparticle, on the lifespan of *Caenorhabditis elegans*. *Mech. Ageing Dev*. **129**: 322–331.
10. Brenner, S. (1974) The genetics of *Caenorhabditis elegans*. *Genetics* **77**: 71–94.
11. Emmons, S.W., Klass, M.R., and Hirsh, D. (1979) Analysis of the constancy of DNA sequenced during development and evolution of the nematode *Caenorhabditis elegans*. *Proc. Natl. Acad. Sci. USA* **76**: 1333–1337.
12. Sulston, J.E. and Brenner, S. (1974) The DNA of *Caennorhabditis elegans*. *Genetics* **77**: 95–104.
13. Houthoofd, K., Braeckman, B.P., Johnson, T.E., and Vanfleteren, J.R. (2003) Life extension via dietary restriction is independent of the Ins/IGF-1 signalling pathway in *Caenorhabditis elegans*. *Exp. Gerontol*. **38**: 947–954.

Anti-Cancer Effects of Enzyme-Digested Fucoidan Extract from Seaweed Mozuku

Yoshiko Matsuda, Kiichiro Teruya, Sakiko Matsuda, Ayumi Nakano, Takuya Nishimoto, Masashi Ueno, Akitomo Niho, Makiko Yamashita, Hiroshi Eto, Yoshinori Katakura, and Sanetaka Shirahata

1 Introduction

Fucoidan is a unique sulfated polysaccharide found in the cell walls of several types of brown seaweed. Recently, fucoidan has attracted a lot of clinical attention due to its strong anti-tumor potential, which has been intensively investigated. Fucoidan suppresses the growth of tumor cells in vivo and activates the immune system against tumors [1–6]. Sulfation of fucoidan enhanced its antitumor activity [2]. Koyanagi et al. reported that fucoidan inhibited tube formation following migration of human umbilical vein endothelial cells [7]. Ye et al. reported that enzyme-digested fucoidan extract inhibited invasion and angiogenesis of tumor cells [8]. Aisa et al. reported that fucoidan induced apoptosis HS-Sultan cells accompanied by caspase-3 activation and down-regulation of ERK pathway [9].

In this study, we examined that anti-cancer effects of enzyme-digested fucoidan extract derived from *Mozuku* of *Cladosiphon novae-caledoniae* Kylin, which originates in the Kingdom of Tonga, inducing the apoptosis of tumor cells.

2 Materials and Methods

2.1 Preparation of Fucoidan and Treatment

The abalone glycosidase-digested fucoidan extract prepared from seaweed *Mozuku* of *Cladosiphon novae-caledoniae* Kylin from the Kingdom of Tonga, commercially available as a product named 'Power fucoidan', was donated for the study by the Daiichi Sangyo Corporation (Osaka, Japan) [8]. An undiluted solution (pH 3.7) was

K. Teruya (✉)
Department of Genetic Resources Technology, Faculty of Agriculture, Kyushu University, Fukuoka, Japan
e-mail: kteruya@grt.kyushu-u.ac.jp

M. Kamihira et al. (eds.), *Animal Cell Technology: Basic & Applied Aspects*, Animal Cell Technology: Basic & Applied Aspects 16, DOI 10.1007/978-90-481-3892-0_49,

neutralized to pH 7.0 with NaOH. The precipitants were removed by centrifugation at 2,200×*g* for 15 min. The supernatants were then autoclaved, and stored as 'fucoidan extract (2.8 mg/ml)' at 4°C. The fucoidan extract was mixed with culture medium, and treatments to various cells were performed.

2.2 Cell Culture and Anti-proliferative Assay

The human fibrosarcoma cell line HT1080, human uterine carcinoma cell line HeLa, human lung adenocarcinoma and human normal fibroblast TIG-1 were cultured in Minimum Eagle's medium (MEM) supplemented with 10% fetal bovine serum (FBS), 10 mM HEPES, 100 units/ml penicillin and 100 μg/ml streptomycin (10% FBS/MEM). Human leukemic cell lines HL60, U937 and K562 cells were cultured in RPMI 1640 medium supplemented with heat-inactivated 10% FBS, 10 mM HEPES, 100 units/ml penicillin and 100 μg/ml streptomycin. All cell culture was performed in a humidified atmosphere with 5% CO_2 at 37°C.

Cells were inoculated at a final concentration of 1×10^5 cells/ml in culture medium in 35 mm culture dishes. After 24 h pre-incubation, the cells were exposed to various concentrations of the fucoidan extract. After cultivation, the cell number in each culture dish was measured using automated hematology analyzer (Sysmex Co., Kobe, Japan).

2.3 Caspase-3/7 Activity Assay and Analysis of Cell Cycle and Apoptosis

To examine caspase activity, HL60 cells were inoculated at a density of 2.0×10^4 cells in 100 μl culture medium with the fucoidan extract and cultured in a 96-well microplate. After 24 h culture, caspase-3/7 activity was measured with Apo-ONE^{TM} Homogeneous Caspase-3/7 Assay kit (Promega Co., Madison, WI).

Cell cycle was determined by PI staining and flow cytometry as described [10]. Mitochondrial membrane potential was determined by Rhodamine 123 staining using a flowcytomer, as previously reported [11].

3 Results

3.1 Anti-proliferative Activity of the Fucoidan Extract to Cancer Cells

The treatment of the enzyme-digested fucoidan extract suppressed the proliferations of various cancer cells (Fig. 1). The fucoidan extract suppressed the proliferations of anchorage-dependent human cancer cells such as cervix adenocarcinoma HeLa,

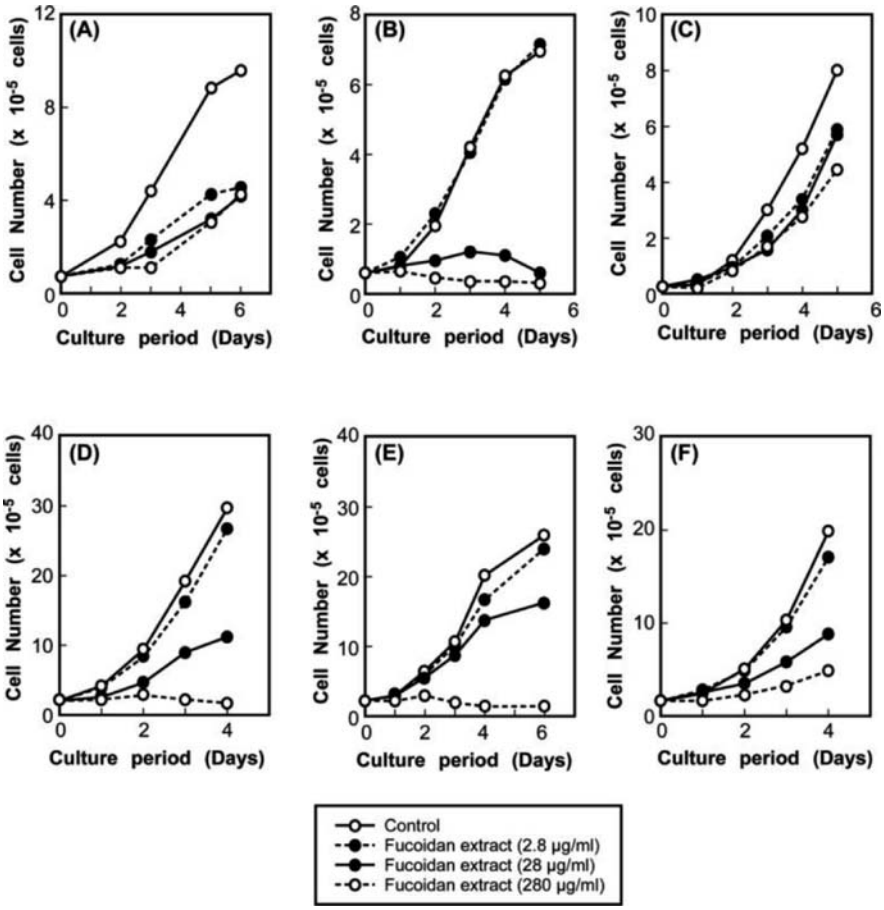

Fig. 1 Anti-proliferative activity of the fucoidan extract to human cancer cells. (**a**) HeLa (cervix adenocarcinoma), (**b**) HT1080 (connective tissue fibrosarcoma), (**c**) A549 (lung adenocarcinoma), (**d**) HL60 (acute promyelocytic leukemia), (**e**) U937 (histiocytic lymphoma), (**f**) K562 (chronic myelogenous leukemia)

connective tissue fibrosarcoma HT1080 and lung adenocarcinoma A549 cells. Anchorage-independent human cancer cells, typical leukemic cells, such as acute promyelocytic leukemia HL60, histiocytic lymphoma U937 and chronic myelogenous leukemia K562 cells were also suppressed the proliferations by the fucoidan extract treatment. The anti-proliferation effect of cancer cells was enhanced by treatment with the fucoidan extract in a dose-dependent manner.

On the other hand, the fucoidan extract did not induce apoptosis to human peripheral blood lymphocytes even at the highest dose of 560 μg/ml. At the highest dose, HL60 and U937 cells were induced 33.2 and 34.5% sub-G1 population, respectively (data not shown). It was suggested that the fucoidan extract specifically suppressed the proliferation of cancer cells.

3.2 The Fucoidan Extract Induced Apoptosis in HL60 Cells

The cell cycle analysis of human leukemic HL60 cells was analyzed using a flow-cytometer. The percentage of sub-G1 fraction was increased in a time- and dose-dependent manner after treatment with the fucoidan extract (data not shown). Pretreatment of HL60 cells with pan-caspase inhibitor, Z-VAD-FMK, inhibited the augmentation of sub-G1 population induced by the fucoidan extract (Fig. 2a). This result indicated that the caspase activity played the important role for the augmentation of sub-G1 population in the fucoidan extract treated HL60 cells. To evaluate the involvement of the activation of caspase-3/7, the activity of caspase-3/7 was determined. After 3 h treatment of the fucoidan extract, the caspase-3/7 activity

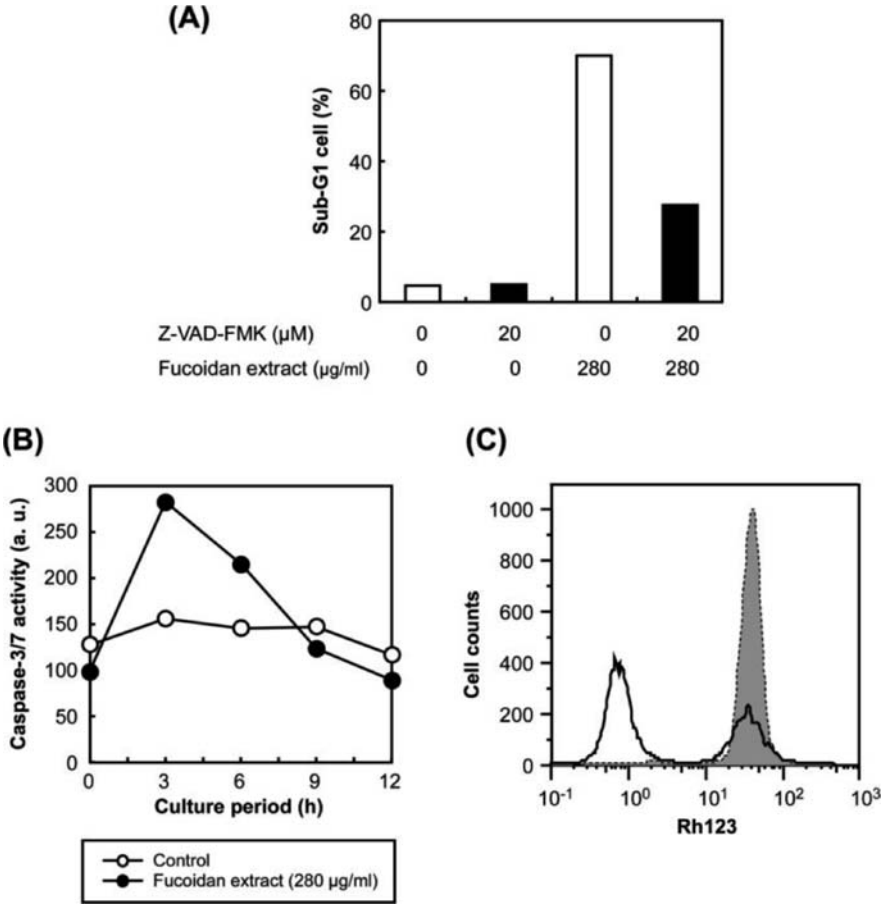

Fig. 2 The fucoidan extract induced apoptosis in human leukemic HL60 cells. (**a**) Detection of sub-G cells treated with or without the fucoidan extract and pan-caspase inhibitor Z-VAD-FMK. (**b**) Detection of caspase-3/7 activation in the fucoidan extract treated HL60 cells. (**c**) Analyses of mitochondrial electric potential. Control; a *dotted line* and *gray* filling. Fucoidan extract treatment (280 μg/ml, 24 h); a *solid line*

reached the maximum value (Fig. 2b). The mitochondrial membrane potential of HL60 cells was decreased by the fucoidan extract treatment for 24 h (Fig. 2c). These results showed that the treatment of the fucoidan extract induced apoptosis in HL60 cells via caspase-3/7 activation and the mitochondrial depolarization.

4 Discussion

Fucoidan is reported to induce apoptosis of tumor cells [9, 12, 13]. However, the mechanism by which of fucoidan induces the apoptosis of tumor cells has not been clearly elucidated. We used fucoidan derived from the seaweed *Cladosiphon novae-caledoniae* Kylin and digested with abalone glycosidase [8]. The fucoidan extract was found to consist mostly of fucose (73%) by sugar composition analysis, and digested small MW fraction (72%, MW: < 500) by size-exclusion chromatography; therefore, fucoidan extract consists mostly of digested fucoidan. In this study, we tried to evaluate the apoptosis inducing activity of the fucoidan extract as one of the anti-tumor effects.

First, anti-proliferative activity of the fucoidan extract was indicated. It was shown that the fucoidan extract inhibited the proliferation of all human cancer cell lines we tested. The fucoidan extract suppressed the proliferations of anchorage-dependent and anchorage-independent human cancer cells in a dose-dependent manner (Fig. 1), and an enzymatic digestion of fucoidan was not an obstacle to suppress the proliferation of cancer cells. In another experiment, a cell death was not induced in human peripheral blood lymphocytes even at the highest dose of 560 μg/ml. At the highest dose, HL60 and U937 cells exhibited 33.2% and 34.5% sub-G1 population, respectively. It was suggested that the fucoidan extract specifically suppressed the proliferation of cancer cells. The cell cycle analysis revealed that the percentage of sub-G1 fraction was increased after treatment with the fucoidan extract. The augmentation of sub-G1 fraction was suppressed by pan-caspase inhibitor Z-VAD-FMK. The treatment of the fucoidan extract stimulated the caspase-3/7 activation and the mitochondrial membrane depolarization (Fig. 2). These results strongly suggested that the suppression of cell proliferation in HL60 cells induced by the fucoidan extract was the apoptosis.

In conclusion, the enzyme-digested fucoidan extract suppressed the growth of anchorage-dependent and anchorage-independent cancer cells. The enzyme-digested fucoidan extract stimulated the caspase-3/7 and mitochondrial pathways to induce apoptosis. The enzyme-digested fucoidan extract enhanced Con A binding of cancer cells and Con A-induced apoptosis.

References

1. Usui, T., Asari, K., and Mizuno, T. (1980). Isolation of highly purified ‘fucoidan’ from Eisenia bicyclis and its anticoagulant and antitumor activities. *Agri. Biol. Chem.* **44**: 1965–1966.
2. Yamamoto, I., Takahashi, M., and Suzuki, T. (1984) Antitumor effect of seaweeds. IV. Enhancement of antitumor activity by sulfation of a crude fucoidan fraction from sargassum kjellmanianum. *Jpn. J. Experi. Med.* **54**: 143–151.

3. Noda, H., Amano, H., Arashima, K., and Nisizawa, K. (1990) Antitumor activity of marine algae. *Hydrobiologia* **204–205**: 577–584.
4. Itoh, H., Noda, H., Amano, H., Zhuaug, C., Mizuno, T., and Ito, H. (1993) Antitumor activity and immunological properties of marine algal polysaccharides, especially fucoidan, prepared from Sargassum thunbergii of phaeophyceae. *Anticancer Res.* **13**: 2045–2052.
5. Zhuang, C., Itoh, H., Mizuno, T., and Ito, H. (1995) Antitumor active fucoidan from the brown seaweed, umitoranoo (Sargassum thunbergii). *Biosci. Biotech. Biochem.* **59**: 563–567.
6. Maruyama, H., Tamauchi, H., Hashimoto, M., and Nakano, T. (2003) Antitumor activity and immune response of Mekabu fucoidan extracted from Sporophyll of Undaria pinnatifida. *In Vivo* **17**: 245–249.
7. Koyanagi, S., Tanigawa, N., Nakagawa, H., Soeda, S. and Shimeno, H. (2003) Oversulfation of fucoidan enhances its anti-angiogenic and antitumor activities. *Biochem. Pharmacol.* **65**: 173–179.
8. Ye, J., Li, Y., Teruya, K., Katakura, Y., Ichikawa, A., Eto, H., Hosoi, M. Nishimoto, S., and Shirahata, S. (2005) Enzyme-digested fucoidan extracts derived from seaweed *Mozuku* of *Cladosiphon novaecaledoniae kylin* inhibit invasion and angiogenesis of tumor cells. *Cytotechnology* 47: 117–126
9. Aisa, Y., Miyakawa, Y., Nakazato, T., Shibata, H., Saito, K., Ikeda, Y. and Kizaki, M. . (2005) Fucoidan induces apoptosis of human HS-sultan cells accompanied by activation of caspase-3 and down-regulation of ERK pathways. *Am. J. Hematol.* 78:7–14.
10. Nicoletti, I., Migliorati, G., Pagliacci, M. C., Grignani, F. and Riccardi, C. (1991) A rapid and simple method for measuring thymocyte apoptosis by propidium iodide staining and flow cytometry. *J. Immun. Meth.* **3**: 271–279.
11. Ito, K., Nakazato, T., Miyakawa, Y., Yamato, K., Ikeda, Y., and Kizaki, M. (2003) Caffeine induces G2/M arrest and apoptosis via a novel p53-dependent pathway in NB4 promyelocytic leukemia cells. *J. Cell. Physiol.* **196**: 276–283.
12. Haneji, K., Matsuda, T., Tomita, M., Kawakami, H., Ohshiro, K., Uchihara, J. N., Masuda, M., Takasu, N., Tanaka, Y., Ohta, T., and Mori, N. (2005) Fucoidan extracted from *Cladosiphon okamuranus* Tokida induces apoptosis of human T-cell leukemia virus type 1-infected T-cell lines and primary adult T-cell leukemia cells. *Nutr. Cancer* **52**: 189–201.
13. Teruya, T., Konishi, T., Uechi, S., Tamaki, H., and Tako, M. (2007) Anti-proliferative activity of oversulfated fucoidan from commercially cultured *Cladosiphon okamuranus* TOKIDA in U937 cells. *Inter. J. Biol. Macromol.* **41**: 221–226.

The Downregulation of Mast Cell Activation Through the Suppression of the High-Affinity IgE Receptor Expression by Green Tea Catechin Egcg

Hirofumi Tachibana, Yoshinori Fujimura, Yusuke Hasegawa, Satomi Yano, and Koji Yamada

1 Introduction

IgE-mediated stimulation of mast cells and basophils is an important initial event in the IgE-dependent allergic reactions [1]. The crosslinking of allergen-specific IgE bound to the high-affinity IgE receptor FcεRI expressed on these cells with multivalent allergens results in a release of bioactive chemical mediators such as histamine, proteases, chemotactic factors and arachidoic metabolites. Therefore, FcεRI is required for mast cells and basophils to initiate the IgE-mediated allergic reaction such as atopic dermatitis, bronchial asthma, and food allergy. The FceRI is a multisubunit receptor with a ligand binding α subunit, a signal modifying membrane-tetraspanning β subunit, and a homodimeric disulfide-linked γ subunit that provides the signaling ability of this receptor. Among the three subunits forming the FcεRI, the α chain is the specific component of FcεRI that mostly extends out to the extracellular region and directly binds to IgE. The study using α chain-deficient mice demonstrated that IgE was unable to bind to the cell surface of mast cells thereby failing to induce degranulation through IgE-binding [2]. Thus, it is expected that the IgE-mediated allergic symptoms may be attenuated by downregulating the FcεRI expression in mast cells and basophils.

Tea (*Camellia sinensis* L.) is one of the most widely consumed beverages in the world, and it is known to contain various beneficial constituents. It has been demonstrated that these tea constituents exhibit various biological and pharmacological properties, and have been reported to act in several ways that are antioxidative [3, 4], and antimutagenic or anticarcinogenic [5, 6]. Catechins apparently have an essential role in these actions, and (-)-epigallpcatechin-3-*O*-gallate (EGCG), which is the major catechin in tea leaves, is believed to be most responsible for their beneficial effects. We have previously reported that EGCG has the suppressive effect of the expression of FcεRI in human basophilic cells [7]. However, whether EGCG can

H. Tachibana (✉)
Bio-Architecture Center, Kyushu University, Fukuoka 812-8581, Japan
e-mail: tatibana@agr.kyushu-u.ac.jp

M. Kamihira et al. (eds.), *Animal Cell Technology: Basic & Applied Aspects*, Animal Cell Technology: Basic & Applied Aspects 16, DOI 10.1007/978-90-481-3892-0_50,

reduce the FcεRI expression in mast cells remains unclear. In the present study, we investigated the effect of EGCG on the FcεRI expression in mast cells.

2 Materials and Methods

2.1 Reagents

(-)-Epigallocatechin-3-*O*-gallate (EGCG) was purchased from Sigma Co. (St Louis, MO). Mouse anti-human FcεRI α chain antibody CRA-1 was obtained from Kyokuto seiyaku (Tokyo, Japan). Mouse IgG2b, used as negative control, was bought from Dako (A/S, Denmark). Fluorescein isothiocyanate (FITC)-conjugated goat anti-mouse IgG antibody was purchased from Protos Immunoresearch (Burlingame, CA, USA). Mouse anti-phosphorylated ERK1/2 antibody and rabbit anti-ERK1/2 antibody were obtained from Santa Cruz Biotechnology,Inc. (Santa Cruz, CA, USA). Antimouse IgG antibody, horseradish peroxidase (HRP)-conjugated antimouse IgG antibody, and HRP-conjugated anti-rabbit antibody were obtained from Zymed Laboratories, Inc. (San Francisco, CA, USA) and ICN Pharmaceuticals,Inc. (Aurora, OH, USA), respectively.

2.2 Cell Preparation

Bone marrow cells were maintained in RPMI-1640 medium (Nissui, Tokyo, Japan) supplemented with 10% fetal calf serum (FCS; PAA Laboratories GmbH, Austria), 2 mM L-glutamine, 100 U/ml penicillin, 100 μg/ml streptomycin and 10 mM HEPES buffer. The cells were cultured at 37°C in a humidified atmosphere with 5% CO_2. Bone marrow cells were isolated from the femurs of 8 weeks old C57BL/6 mice. Bone marrow cells were cultured to >99% homogeneity in RPMI containing interleukine-3 and stem cell factor at a concentration of 10 ng/ml over a four-week period. Bone marrow derived mast cell (BMMC) phenotype and homogeneity were confirmed by flow cytometry for mast cell surface marker such as FcεRI, and by histological staining with toluidine blue (data not shown).

2.3 Western Blot Analysis

BMMC cells treated with or without EGCG were washed and lysed in cell lysis buffer containing 50 mM Tris-HCl (pH 7.5), 150 mM NaCl, 1% Triton-X 100, 1 mM EDTA, 50 mM NaF, 30 mM Na4PO7, 1 mM phenylmethanesulfonyl fluoride (PMSF), 2.0 μg/ml aprotinin, and 1 mM pervanadate. Whole cell lysate samples were loaded onto 10% sodium dodecyl sulfate-polyacrylamide gel, and electrophoresis was done under reducing condition. The samples were then electrotransferred onto a nitrocellulose membrane. The blotted nitrocellulose was probed

using phosphorylated ERK1/2 antibody, and the secondary antibody used was the HRP-conjugated anti-mouse IgG, and detection was done using the ECL kit (Amersham Pharmacia Biotech). For detection of total ERK1/2, the same filter was blotted again with anti-ERK1/2 antibody.

2.4 Flow Cytometric Analysis

The cell surface expression of FcεRI was assessed by flow cytometry. In brief, cells were incubated with the anti-FcεRI α chain antibody CRA-1. Then cells were exposed to the FITC-conjugated anti-mouse IgG and subjected to flow cytometry (FACSCalibur; Becton Dickinson, Sunnyv ale, CA, USA). As a negative control, the mouse subclass-matched IgG2b antibody was used. The extent of FcεRI expression is represented as the mean fluorescence intensity of CRA-1, and the value is indicated in each panel. The vertical line in the figure indicates the peak point for CRA-1 in non-treated cells.

2.5 Surface Plasmon Resonance Biosensor Assay

Analysis of the interaction between EGCG and BMMC cells was performed using the SPR biosensor SPR670 (Moritex, Nagoya, Japan). BMMC cells were immobilized on the sensor chip and then this chip was equilibrated in SPR running bu¡er, phosphate-buffered saline (pH 7.4, 30 μl/min). EGCG was diluted at 0 or 50 μM in SPR running buffer in 60 μl injection volumes and at a flow rate of 30 μl/min. Binding was measured at 25°C for 2 min, followed by dissociation.

2.6 Histamine Release Assay

BMMC (1×10^6 cells/mL) cultured with or without 25 μM EGCG for 24 h, were sensitized with IgE anti-DNP. The treated cells were washed and suspended in 200 μL of histamine release buffer (pH 7.2), containing 2.7 mM KCl, 1.8 mM $CaCl_2$, 1.1 mM $MgCl_2$, and 11.9 mM NaH_2PO_4, and then DNP-HSA was challenged at 37°C for 30 min. After centrifugation at 300*g* for 5 min, the histamine content of the supernatant or cell lysate was measured by means of a fluorometric assay.

2.7 RT-PCR

Total RNA was isolated using the TRIZol reagent (Invitrogen, Carlsbad, CA, USA) and was reverse transcribed. The resultant cDNA samples were subjected to 25 cycles of PCR amplification in the presence of specific sense

and antisense primers. Human glyceraldehyde-3-phosphate dehydrogenase (G3PDH) cDNA was amplified as an internal control. Temperatures were 94°C for denaturation, 60°C for annealing,and 72°C for polymerizations. Sequences for the PCR primers are as follows: for the FcεRI α chain: sense 5'-TGTGCCTAGCACTGCTGTTCATG-3', and antisense 5'-ACCTTGCGGACATT CCAG TTC-3'; for the FcεRI β chain: sense 5'-CCCAAATCCACAAGAATC CTCC-3', and antisense 5'-GCTACTGACAATGTTTGCTCCCAG-3'; for the FcεRI γ chain: sense 5'-AGCCGTGATCTTGTTCTTGCTCC-3', and antisense 5'-TTCAAAGCACAGAGGTGACC AAG-3'; for G3PDH: sense 5'-CGCATCTTCTTGTGCAGTGCC-3', and antisense 5'-TCCA CGAC ATACTCAGCACCG-3'.

3 Results and Discussion

To examine the effect of EGCG (Fig. 1a) on the FcεRI expression of mast cells, we used the mouse bone marrow-derived mast cells (BMMC) as a mast cell model. Flow cytometric analysis showed that EGCG was able to decrease the cell-surface expression of FcεRI in BMMC after a 24-h treatment in a dose-dependent manner (Fig. 1b, the data of 25 μM EGCG treatment). To assess whether the reduction of FcεRI expression by EGCG is associated with a functional change, especially histamine release, BMMC, cultured with or without EGCG (25 μM) for 24 h, were sensitized with IgE anti-DNP, and then DNP-HSA was challenged. Histamine released from the cells was determined using a fluorometric assay. In non-treated cells with the catechins, the value of histamine release was 22%, and the value was reduced to 16% in EGCG-treated cells (data not shown). This observation indicated that the reduction of histamine release was caused by the suppression of the cell surface FcεRI expression by EGCG.

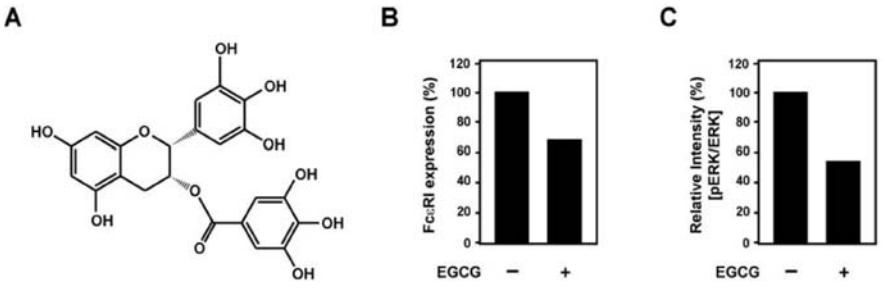

Fig. 1 EGCG suppresses the FcRI expression. (a) The chemical structure of EGCG. (b) The murine immature cultured cells BMMC were treated with EGCG. Then the cells were stained with anti-FcεRI α chain antibody CRA-1. The mean fluorescence intensity was determined using FACSalibur. FcεRI expression (%) was represented as relative mean fluorescence intensity of EGCG(+) to EGCG(–). (**c**) BMMC were stimulated with EGCG, and then lysed and ERK1/2 was separated on a SDS-PAGE. Immunoblot analysis using anti-phosphorylated ERK1/2 antibody was performed

We also examined whether the suppressive effect of EGCG on the FcεRI expression is due to the inhibition of mRNA expression for the FcεRI α, β, γ chain genes. BMMC were cultured for 24 h with or without 25 μM of EGCG, and total RNA was isolated from the cells. The mRNA levels for the α chain as well as the β and γ chains were measured by RT-PCR. All subunits of FcεRI mRNA of non-treated cells were clearly detected, and the corresponding mRNA levels in the EGCG-stimulated cells were shown to be significantly reduced (data not shown). Thus, it was suggested that the suppressive effect of EGCG on the cell surface expression of FcεRI is related to the down-regulation of the expression of the FcεRI α, β, and γ mRNA.

For investigating the cell-surface interaction of EGCG with BMMC, SPR assay was performed. This experiment showed that the SPR signal significantly increased by the injection of EGCG, and the strength of SPR signal was sustained just after the termination of the EGCG exposure (data not shown). The strength of SPR signals were increased in a dose-dependent manner. These results suggested that the SPR signal of EGCG may be due to a result of the binding to the cell surface of BMMC.

We have recently reported that the inhibition of ERK1/2 phosphorylation was responsible for the suppressive effect elicited by EGCG on the FcεRI expression [8]. To elucidate further mechanism for EGCG's action in BMMC, the cells were treated with 25 μM EGCG for 3 h to examine the level of phosphorylated ERK1/2. Immunoblot analysis showed that the suppressive effect of EGCG on phosphorylated ERK1/2 level was observed (Fig. 1c), suggesting that reduction of ERK1/2 phosphorylationis involved in EGCG-induced suppression of FcεRI expression.

Taken together, the present results suggest that EGCG has the ability to down-regulate FcεRI expression of mast cells, and that both the cell-surface binding and the reduction of ERK1/2 phosphorylation are involved in the activity of EGCG to suppress the FcεRI expression. These findings indicate that EGCG-induced suppression of FcεRI expression is effective for inhibiting mast cell activation induced by antigen/IgE stimulation.

Currently, we have identified a cell surface receptor that mediates the anticancer activity of EGCG [9]. Expression of the metastasis-associated 67 kDa laminin receptor (67LR) conferred EGCG responsiveness to cancer cells. The 67LR is a nonintegrin receptor for laminin, fibronectin, and type IV collagen [10, 11]. Expression of the 67LR has been shown to be upregulated in neoplastic cells compared with their normal counterparts and directly correlate with an enhanced invasive and metastatic potential in many malignancies [12, 13]. The receptor has been implicated in laminin-induced tumor cell attachment and migration, as well as in tumor angiogenesis, invasion, and metastasis [14–16]. It has been reported that the expression of 67LR in mast cells is related to the adhesion to laminin and may contribute to the tissue distribution of mast cells and to mast cell accumulation at sites of tissue injury and inflammation [17, 18]. The appearance of both FcεRI and 67LR may be important for mast cells to localize to areas of inflammation and respond to IgE-mediated stimuli [18]. However, a possible role for 67LR in the IgE-mediated allergic reactions and in suppressive effects of EGCG on FcεRI expression still remained unknown. For best understanding the molecular basis for the

downregulation of mast cell activation by EGCG, further study on involvement of 67LR in the action of EGCG is needed.

References

1. Blank, U., Ra, C., Miller, L., White, K., Metzer, H., and Kinet J.P. (1989) Complete structure and expression in transfected cells of high affinity IgE receptor. *Nature* **337:** 187–189.
2. Dombrowicz, D., Flamand, V., Brigman, K., Koller, B.H., and Kinet, J.P. (1993) Abolition of anaphylaxis by targeted disruption of the high affinity immunoglobulin E receptor alpha chain gene. *Cell* **75:** 969–976.
3. Yoshino, K., Hara, Y., Sano, M., and Tomita, I. (1994) Antioxidative effects of black tea theaflavins and thearubigin on lipid peroxidation of rat liver homogenates induced by tert-butyl hydroperoxide. *Biol. Pharm. Bull*. **17:** 146–149.
4. Sano, M., Takahashi, Y., Yoshino, K., Shimoi, K., Nakamura, Y., Tomita, I., Oguni, I., and Konomoto, H. (1995) Effect of tea (*Camellia sinensis* L.) on lipid peroxidation in rat liver and kidney: a comparison of green and black tea feeding. *Biol. Pharm. Bull*. **18:** 1006–1008.
5. Yamane, T., Nakatani, H., Kikuoka, N., Matsumoto, H., Iwata, Y., Kitao, Y., Oya, K., and Takahashi, T. (1996) Inhibitory effects and toxicity of green tea polyphenols for gastrointestinal carcinogenesis. *Cancer* **77:** 1662–1667.
6. Yen G.C. and Chen, H.Y. (1996) Relationship between antimutagenic activity and major components of various teas. *Mutagenesis* **11:** 37–41.
7. Fujimura, Y., Tachibana, H., and Yamada, K. (2001) A tea catechin suppresses the expression of the high-affinity IgE receptor FceRI in human basophilic KU812 cells. *J. Agric. Food Chem*. **49:** 2527–2531.
8. Fujimura, Y., Tachibana, H., and Yamada, K. (2004) Lipid raft-associated catechin suppresses the FcεRI expression by inhibiting phosphorylation of the extracellular signal-regulated kinase1/2. *FEBS Lett*. **556:** 204–210.
9. Tachibana, H., Koga, K., Fujimura, Y., and Yamada, K. (2004) A receptor for green tea polyphenol EGCG. *Nat. Struct. Mol. Biol*. **11:** 380–381.
10. Narasimhan, S., Armstrong, M.Y., Rhee, K., Edman, J.C., Richards, F.F., and Spicer, E. (1994) Gene for an extracellular matrix receptor protein from Pneumocystis carinii. *Proc. Natl. Acad. Sci. USA* **91:** 7440–7444.
11. Iwabuchi, K., Nagaoka, I., Someya, A., and Yamashita, T. (1996) Type IV collagen-binding proteins of neutrophils: possible involvement of L-selectin in the neutrophil binding to type IV collagen. *Blood* **87:** 365–372.
12. Menard, S., Tagliabue, E., and Colnaghi, M.S. (1998) The 67 kDa laminin receptor as a prognostic factor in human cancer. *Breast Cancer Res. Treat*. **52:** 137–145.
13. Sanjuan, X., Fernandez, P.L., Miquel, R., Munoz, J., Castronovo, V., Menard, S., Palacin, A., Cardesa, A., and Campo, E.(1996) Overexpression of the 67-kD laminin receptor correlates with tumour progression in human colorectal carcinoma. *J. Pathol*. **179:** 376–380.
14. Mafune, K.I. and Ravikumar, T.S. (1992) Anti-sense RNA of 32-kDa lamininbinding protein inhibits attachment and invasion of a human colon carcinoma cell line. *J. Surg. Res*. **52:** 340–346.
15. Vande Broek, I., Vanderkerken, K., De Greef, C., Asosingh, K., Straetmans, N., Van Camp, B., and Van Riet, I. (2001) Laminin-1-induced migration of multiple myeloma cells involves the high-affinity 67 kDa laminin receptor. *Br. J. Cancer* **85:** 1387–1395.
16. Tanaka, M., Narumi, K., Isemura, M., Abe, M., Sato, Y., Abe, T., Saijo, Y., Nukiwa, T., and Satoh, K. (2000) Expression of the 37-kDa laminin binding protein in murine lung tumor cell correlates with tumor angiogenesis. *Cancer Lett*. **153:** 161–168.
17. Thompson, H.L., Burbelo, P.D., Segui-Real, B., Yamada, Y., and Metcalfe, D.D. (1989) Laminin promotes mast cell attachment. *J. Immunol*. **143:** 2323–2327.
18. Thompson, H. L., Burbelo, P.D., and Metcalfe, D.D. (1990) Regulation of adhesion of mouse bone marrow-derived mast cells to laminin. *J. Immunol*. **145:** 3425–3431.

Anti-Diabetes Effects of Hita Tenryou-Sui Water®, a Natural Reduced Water

Kazuhiro Osada, Yuping Li, Takeki Hamasaki, Masumi Abe, Noboru Nakamichi, Kiichiro Teruya, Yoshitoki Ishii, Ying Wang, Yoshinori Katakura, and Sanetaka Shirahata

1 Introduction

Diabetes mellitus is an endocrine disorder in which glucose metabolism is impaired because of total loss of insulin after destruction of pancreatic β-cells, inadequate release of insulin from pancreatic β-cells or insensitivity of target tissues to insulin. Diabetes is classified mainly into two types. Type 1 diabetes (insulin-dependent diabetes mellitus; IDDM) is due primarily to autoimmune-mediated destruction of pancreatic β-cell islets, resulting in absolute insulin deficiency. On the other hand, type 2 diabetes (non-insulin-dependent diabetes mellitus; NIDDM) is a complex disorder with a strong genetic background and made up of different forms each of which is characterized by variable degrees of insulin resistance and β-cell dysfunction, and which together lead to hyperglycemia. Recently it has been revealed that reactive oxygen species (ROS) are deeply related to both IDDM and NIDDM [1].

Water has no calorie and can easily be taken everyday. Thus, natural reduced water (NRW), which can scavenge ROS will be beneficial to prevent and improve ROS-related diseases including diabetes mellitus. Previously, we reported that a natural mineral water derived from a deep well in Japan (trademark, Hita Tenryousui water®, Nakanoshima, Hita City, Oita, Japan) was one of NRW and could scavenge intracellular ROS and suppress oxidative damage of pancreatic β cells induced by alloxan, a type 1 diabetes inducer [2]. Here we report that Hita Tenryosui water® can improve the symptoms of alloxan-induced type 1 diabetes model mice. The water also stimulated the glucose uptake into myotubes by activation of insulin signaling pathway. Open clinical test revealed that Hita Tenryosui water® improved blood sugar, triglycerol and total cholesterol levels of diabetes and hyperlipemia patients.

S. Shirahata (✉)
Faculty of Agriculture, Kyushu University, Higashi-ku, Fukuoka 812-8581, Japan
e-mail: sirahata@grt.kyushu-u.ac.jp

M. Kamihira et al. (eds.), *Animal Cell Technology: Basic & Applied Aspects*, Animal Cell Technology: Basic & Applied Aspects 16, DOI 10.1007/978-90-481-3892-0_51,

2 Materials and Methods

2.1 Cell Culture and Waters

L6 rat skeletal muscle myoblasts were grown and maintained in DME medium supplemented with 10% fetal bovine serum (FBS), 100 IU/ml penicillin and 100 μg/ml streptomycin. The cells were reseeded in the appropriate culture dishes and, after reaching sub-confluence, the medium was changed to DME medium supplemented with 2% FBS. The medium was then exchanged every 2 days until the cells were fully differentiated into myotubes, typically after 7–10 days. All experiments were carried out in the stage of myotubes. Hita Tenryosui water® (Hita T. W.; pH 8.3; Na, 23 mg/l; K, 8.5 mg/l; Ca, 9.2 mg/l; Mg, 1.6 mg/l) was obtained from Hita Tenryosui Water Co. Ltd., Hita city, Japan. A commercial natural mineral water from company A as control water (natural mineral water A; mineral water; pH 7.3; Na, 28 mg/l; K, 0.6 mg/l; Ca, 7.4 mg/l; Mg, 4.0 mg/l) was purchased in the market of Japan. Culture media were prepared with these waters instead of ultra pure water (Milli Q water, Millipore; UPW).

2.2 Determination of 2-Deoxyglucose Uptake

Uptake of 2-deoxy-[^{3}H] D-glucose into L6 myotubes was determined as reported previously [3]. Briefly, fully differentiated L6 myotubes were incubated in 2% FBS/DMEM prepared with various waters for 3 days. L6 myotubes were deprived of serum for 4 h by incubation in DMEM. After the medium was removed, cells were placed in HBSS for 30 min containing 25 mM glucose. During the final 20 min, 100 nM insulin was added to determine glucose uptake.

2.3 Analysis of Insulin Receptor (IR) Phospho-Rylation

After fully differentiated L6 myotubes were incubated in 2% FBS/DMEM with or without Hita Tenryousui water® for 72 h, L6 myotubes were deprived of serum for 4 h in DMEM and washed twice with warm PBS. Cells were incubated subsequently at 37°C in HBSS for 30 min. During the last 20 min, 100 nM insulin was added. Myotubes were then lysed in dishes using ice-cold lysis buffer. Aliquots of the cell lysates (50 μg of protein) from each group were separated by SDS-PAGE (7.5% acrylamide), immunoprecipitated with anti-IR β-subunit, and then immunobloted with anti-phospho-IR (pY1158) antibody. Immunoreactive proteins were visualized by enhanced chemiluminescence method, followed by densitometory. The cellular protein content in each sample was determined using Bio-Rad protein assay dye reagent concentrate according to the manufacturer's instructions.

2.4 Assay for PTPase Activity

Fully differentiated L6 myotubes were treated as described above. To establish a positive control, cells were treated with 10 mM vanadate for 20 min, which is known to inhibit the PTPase activity. Myotubes were washed three times with ice-cold PBS, and then collected in 100 μl lysis buffer by using a cell scraper. Cells were passed through a 25-gauge needle 10 times and centrifugation. PTPase activity in the cell extracts (50 μg protein) was determined by measuring the hydrolysis of p-nitrophenyl phosphate (pNPP) as described by Chen H. et al [4].

2.5 Animal Experiments

Adult male ICR (CD-1 strain) mice (5 weeks age, ca. 30 g of body weight) were acclimated for 7 days and randomly assigned into 6 groups of mice; Group 1 was treated with Ultra pure water (Milli-Q water) and citrate buffer as control; Group 2 with Milli-Q water and alloxan; Group 3 with Hita Tenryosui water® and alloxan; Group 4 with commercial natural mineral water and alloxan. Normal ICR mice were also administered daily with fresh water for 4 weeks. To induce type 1 diabetes, mice submitted to fasting for 18 h were administered alloxan by three i.p. injections. Alloxan was dissolved in citrate buffer (0.05 M, pH 4.0) and administered at intervals of 48 h, in a dose of 100 mg/kg body weight each. The control group received only the citrate buffer. Various waters were administered daily to the end of study. All mice treated with alloxan were observed for behavioral changes like polydipsia, polyphagia and polyurea. Four weeks after alloxan injection, blood samples from tail vein were collected for determination of blood glucose by Glucose auto-analyzer.

Type 2 diabetes mice (C57BL/KsJ-db^+/db^+) exhibit the symptoms of type 2 diabetes due to obesity. The sugar tolerance test was performed on the mice administrated tap water or Hita Tenryousui water® freely. After fasting for 18 h, glucose (1 mg/30 g weight) was administrated i.p. and blood glucose levels were determined after 0, 30 and 60 min.

2.6 Open Clinical Test

The open clinical test was performed to study changes in the relevant tests parameters of 65 diabetes patients and 50 hyperlipemia patients who drunk Hita Tenryousui water® in the Center Hospital in Changchun city, Jilin, China. The average age of the subjects (male, 56; female, 24) was 62±9.5 year old and the daily consumption of drinking water was as much as 2 l per day for 2 months. The diagnostic parameters such as blood sugar, triglycerol, and total cholesterol concentration were tested twice – at the beginning and at the end of 2 months.

3 Results and Discussion

We reported that Hita Tenryosui water® scavenged intracellular ROS of hamster pancreatic beta HIT-T15 cells with or without alloxan treatment, previously [2]. Here, the effect of the water on alloxan-induced type 1 diabetic mouse was investigated. Starved blood glucose levels of the normal mice administrated natural mineral water A or Hita Tenryousui water® were not changed significantly compared to those of control Milli Q water-administrated mice. The blood glucose levels of alloxan-induced diabetic mice administrated with Milli-Q water and natural mineral water A gradually elevated and reached about 450 mg/dl 4 weeks after final alloxan injection. Hita Tenryousui water® partially prevented hyperglycemia (Fig. 1).

Concerning to anti-type 2 diabetes effect, we investigated whether NRW exerted a direct effect on glucose transport. L6 myotubes were exposed to Hita Tenryousui water® for 3 days, followed by the addition of 100 nM insulin for 20 min. Hita Tenryousui water® but not mineral water A increased both basal and insulin-stimulated glucose transport ($p < 0.01$) (Fig. 2).

To determine whether NRW is associated with changes in the first steps of the insulin signaling cascade, IR protein level was assessed in total cell lysates by immunoprecipitation with anti-IR β-subunit antibodies and western blotting with anti-phosphotyrosine antibodies. NRW treatment increased the phosphorylated IR protein level (Fig. 3). This result indicates that NRW treatment activated the first steps of the insulin signaling by inducing phosphorylation of the insulin receptor.

Since the level of tyrosine-phosphorylated proteins in the cell depends upon the balanced activity of tyrosine kinase and tyrosine phosphatase, we measured total PTPase activity of L6 myotubes lysate after treatment with NRW. After treatment

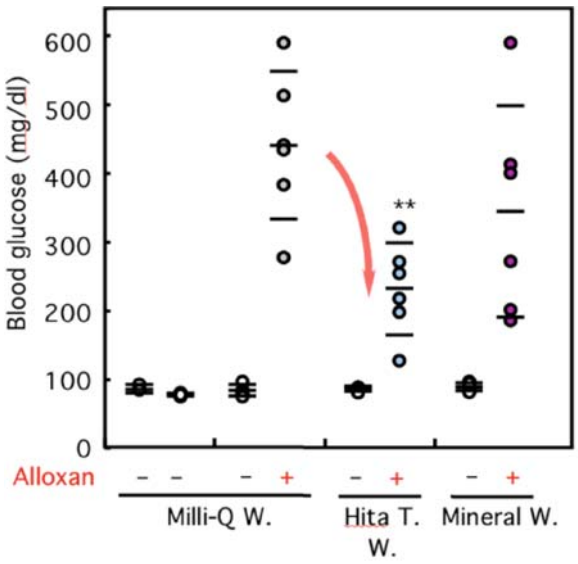

Fig. 1 Effects of various waters on fasted blood glucose levels of normal and alloxn-induced diabetic CD-1 mice. Each value was shown as circle and bars denote the mean ± S.E.M. and n was 6 for each value. **, $p < 0.01$ compared to alloxan-treated group

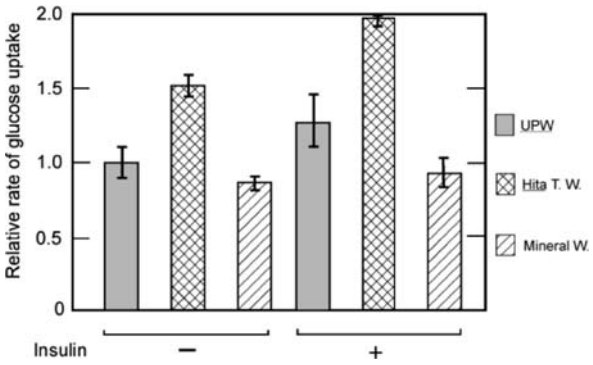

Fig. 2 Effects of Hita Tenrousui water® on 2-deoxyglucose uptake in L6 myotubes. After fully differentiated L6 myotubes were incubated with various waters for 3 days, 100 nmol/l insulin was added in HBSS and incubated for 20 min. At the end of the incubation, 2-deoxyglucose uptake was measured

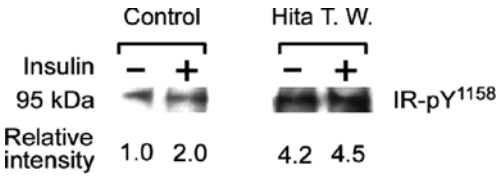

Fig. 3 Stimulatory effect of Hita Tenryosui water on phospho-rylation of insulin receptor (IR) β-subunit in L6 myotubes

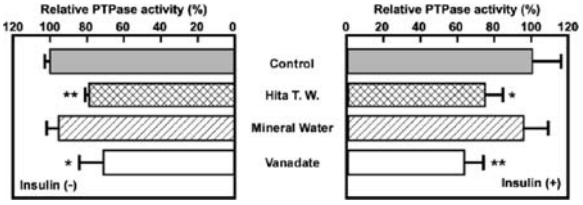

Fig. 4 Inhibition of PTPase activity by Hita Tenryousui water®. Fully differentiated L6 myotubes were incubated with various waters for 3 days and PTPase activity in the cell lysate was determined

with this water, the PTPase activity was reduced as well as 10 mM vanadate treatment as positive control in both absence and presence of insulin (Fig. 4). The results suggest that the Hita Tenryousui water®-induced stimulation of tyrosine phosphorylation may be partially mediated by the inhibition of PTPase.

When Hita Tenryousui water® was administrated to type 2 diabetes model mice, significant differences were not observed in body weights, amounts of food and drinking water and fasted blood sugar levels compared to tap water-administrated mice. However, Hita Tenryousui water® showed a tendency to improve the impaired glucose tolerance compared to tap water (Fig. 5).

The open clinical test was performed to investigate changes in the relevant tests parameters of 65 diabetes patients and 50 hyperlipemia patients who drunk 2 l of Hita Tenryousui water® per day for 2 month.

Given all the results of the clinical trials (Table 1), it can be said that the natural reduced water consumption improves average values of fasting blood sugar at 89% of 65 diabetes patients after 2 month. Roughly 92% of responders showed the high statistically significant improvement at their trigrlycerol and total cholesterol

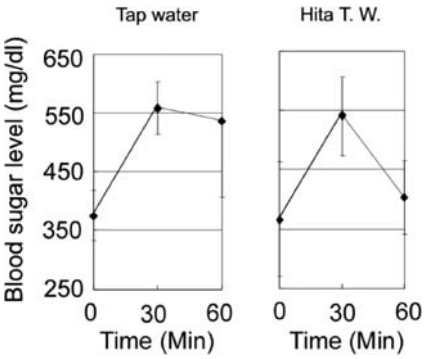

Fig. 5 Effects of tap water and Hita Tenryousui water® on the impaired glucose tolerance of type 2 diabetes model mice (C57BL/KsJ-db^+/db^+). Blood glucose levels were determined after intraperitoneal injection of glucose into the mice of 17 weeks age. Tap water was supplied from Kyushu University, Hakozaki, Fukuoka, Japan

Table 1 Suppressive effect of Hita Tenryosui water® on fasting blood sugar, triglycerol, and total cholesterol levels of 65 diabetes patients and 50 hyperlipemia patients

	Case	Blood marker levels before consumption (mmol/l)	Blood marker levels after consumption for 2 months (mmol/l)	*P* value
Fasting blood sugar	65	8.14 ± 1.25	6.99 ± 1.45	$P<0.05$
Triglycerol	50	3.15 ± 0.74	2.35 ± 0.88	$P<0.05$
Total cholesterol	50	5.32 ± 0.91	4.38 ± 0.76	$P<0.05$

concentration values, which can be also beneficial to other diseases like high blood pressure, circulatory disturbance, renal insufficiency or atherosclerotic dementia. The randomized double blind clinical tests with 29 patients performed in Fukuoka Tokusyukai Hospital also demonstrated that Hita Teryousui water® significantly increased blood HDL-cholesterol and decreased the amount of 8-OH dG, an oxidative marker, in urea of type 2 diabetes patients after drinking about 1 l per day for 6 months [5].

Taking account of all the experimental facts in vitro and in vivo, it can be said that NRW will be considered as a useful complementation to the usual medication of ROS-associated diseases.

References

1. Fridlyand, L.E. and Philipson, L.H. (2005) Oxidative reactive species in cell injury mechanisms in diabetes mellitus and therapeutic approaches. *Ann. NY. Acad. Sci*. **1066**: 136–151.
2. Ye, J., Li, Y., Hamsaki, T., Nakamichi, N., Komatsu, T., Kashiwagi, T., Teruya, K., Nishikawa, R., Kawahara, T., Osada, K., Toh, K., Abe, M., Tian, H., Kabayama, S., Otsubo, K., Morisawa, S., Katakura, Y., and Shirahata, S. (2008) Inhibitory effect of electrolyzed reduced water on tumor angiogenesis. *Biol. Pharm. Bull*. **31**: 19–26.
3. Teruya, K., Yamashita, M., Tominaga, R., Nagira, T., Shim, S.-Y., Katakura, Y., Tokumaru, S., Tokumaru, K., Barnes, D., and Shirahata, S. (2002) Fermented milk, Kefram-Kefir enhances glucose uptake into insulin-responsive muscle cells. *Cytotechnology* **40**: 107–116.

4. Chen, H., Wertheimer, S.J., Lin, C.H., Katz, S.I., Amrein, K.E., Burn, P., and Quton, M.J. (1997) Protein-tyrosine phosphatases PTP1B and syp are moulators of insulin-stimulated translocation of GLUT4 in transfected rat adipose cells. *J. Biol. Chem*. **272**: 8026–8031.
5. Matsubayashi, N., Hisamoto, T., Murao, N., and Hara, T. (2008) Effect of so called reduced water on diabetes patients. The abstract book of the 46th Kyushu Regional Meeting of Japan Diabetes Society. IB–9.

Suppressive Effect of ERW on Lipid Peroxidation and Plasma Triglyceride Level

Masumi Abe, Shunpei Sato, Kazuko Toh, Takeki Hamasaki, Noboru Nakamichi, Kiichiro Teruya, Yoshinori Katakura, Shinkatsu Morisawa, and Sanetaka Shirahata

1 Introduction

Oxidative stress is produced as a result of imbalance due to excess formation of free radicals and decreased activity of antioxidant defense systems. All oxidative reactions are continuous sources of potentially cytotoxic reactive oxygen species (ROS), which play important roles in living systems both through their beneficial and detrimental effects. Electrolyzed reduced water (ERW) generated nearby the cathode exhibited anti-oxidative properties, and suppressed tumor angiogenesis [1]. Here we investigated whether ERW prevents arteriosclerosis arisen from low-density lipoprotein (LDL) oxidation. We revealed that ERW inhibited LDL oxidation in vitro by macrophage cells. Furthermore, the effect of ERW on lipid peroxidation in tissues and lipid metabolism in plasma were examined in vivo.

2 Materials and Methods

2.1 Preparation of Electrolyzed Reduced Water (ERW)

ERW (pH 11.6; DH, 0.928 ppm; DO, 6.15 ppm; ORP, –659 mV) was prepared by electrolyzing ultra pure water (MilliQ, Millipore) containing 2 mM NaOH (pH 11.3; DH, 0.001 ppb; DO, 7.67 ppm; ORP, +350 mV) at 100 V for 60 min using a batch-type electrolyzing device equipped with platinum-coated titanium electrodes (TI-200s, Nihon Trim Co., Osaka, Japan). ERW typically contained 0.2–2.5 ppb Pt nanoparticles (Nps) when assayed with ICP-MS spectrometer.

S. Shirahata (✉)
Faculty of Agriculture, Kyushu University, Higashi-ku, Fukuoka 812-8581, Japan
e-mail: sirahata@grt.kyushu-u.ac.jp

M. Kamihira et al. (eds.), *Animal Cell Technology: Basic & Applied Aspects*, Animal Cell Technology: Basic & Applied Aspects 16, DOI 10.1007/978-90-481-3892-0_52,

2.2 Measurement of lipid peroxidation

Thiobarbituric acid reactive substances (TBARS) in plasma and LDL were determined as a measurement of lipid peroxidation by the fluorescent method [2]. TBARS in RBC was measured as described by Yagi et al [3]. TBARS was calculated from [*A*532–*A*600], referred to tetraethoxypropane standard. TBARS in liver and aorta were measured as described by Ohkawa et al [4]. The fluorescent intensity (Ex 515 nm and Em 553 nm) of the *n*-butanol layer, separated from the mixture by centrifugation at 600 × g for 10 min, was measured. TBARS was calculated from the fluorescent intensity by standardization against tetraethoxypropane.

2.3 Cell Culture

The macrophage-like cell line J774.A1 was obtained from Cell Resource Center for Biomedical Research, Institute of Development, Aging and Cancer, Tohoku University (Sendai, Japan). The J774.A1 cells were cultured in DMEM, which contained 10% (vol/vol) fetal bovine serum, 5 mM HEPES, 1.0 mM sodium bicarbonate. For each experiment, the cells were cultured in the 24-well culture plate (Falcon) at 37 °C at an atmosphere of 5% CO_2/95% air.

2.4 LDL Oxidation in the Culture Supernatant of J774.A1 Cells

LDL was oxidized in J774.A1cells-cultured DMEM prepared with various waters in the presence of 10 μM copper (II) sulfate ($CuSO_4$). A hundred ng/ml LDL was added to DMEM for 24 h in CO_2 incubator at 37 °C and oxidation reaction was terminated by addition of 20 mM ethylenediaminetetraacetic acid. Peroxidation of LDL was measured by the TBARS described above.

2.5 DiI-LDL Uptake by Macrophages in the Presence of Cu^{2+} ion

DiI-LDL, a fluorescent labeled LDL (Biomedical Technologies Inc.) was incubated with 10 μM Cu^{2+} ion in DMEM prepared with various waters at 37 °C for 24 h in dark. J774.A1-derived macrophages were incubated with the test substance or vehicle control (0.1% v/v DMSO) for 48 h and then incubated with DiI-oxLDL (100 ng/mL) for another 24 h. The cells were washed and then investigated in triplicates by flow cytometry. Data were acquired from 10,000 cells (events), and the DiI-oxLDL uptake was determined and expressed as the geometric mean fluorescence intensity (MFI).

2.6 Animal Experiments

Male Wistar rats, 4 weeks old, were purchased from KBT oriental Inc. (Tokyo, Japan). After acclimatization for 1 week using commercial diet (CRF-1, Oriental

Yeast Co. Ltd., Tokyo, Japan), the animals were divided into six groups including seven rats each.

Experimental groups: MQ, ultrapure water from Millipore; MQ+H_2; MQ+H_2+2 ppm Pt; MQ+2 ppm Pt; ERW; ERW+Pt. The rats were housed individually in stainless wire netting cages for 3 weeks. All rats were given free access to the experimental diet and each water, and their body weights were monitored daily. After an experimental period of 3 weeks, the rats were fasted for 20 h, and blood was collected from the abdominal artery under ether anesthesia. The heparinized blood was immediately separated into plasma and red blood cells (RBC) by centrifugation at 1600 × g for 10 min. The plasma samples for oxidation were stored on ice until oxidation, and the other plasma samples were frozen at –80°C. After blood collection, physiological saline was perfused, and then the liver and aorta were removed, weighed, and stored at –80 °C.

2.7 Lipid Analysis

Total cholesterol (T-CHO), free cholesterol (FCHO), high-density lipoprotein-cholesterol (HDL-CHO), LDL-cholesterol (LDL-CHO), triglyceride (TG), phospholipid (PL), and nonesterified fatty acid (NEFA) in plasma were analyzed by SRL company (Tokyo, Japan).

2.8 Statistical Analyses

Data were analyzed by two-way ANOVA followed by Tukey's post hoc tests. Differences were considered to be statistically significant for $P > 0.05$.

3 Results and Discussion

3.1 Effect of Various Waters on Lipid Peroxidation In Vitro

Measurement of oxidized LDL in various waters after 7 days' incubation. The generation of malonyldialdehyde (MDA) equivalents during LDL oxidation was estimated by thiobarbituric acid reactive substances (TBARS) assay. ERW suppressed lipid peroxide significantly compared with MQ on the 7th day (Fig. 1). There was significantly difference between MQ and ERW. ERW suppressed LDL peroxdation in vitro. Tap water oxidized LDL three folds in ERW.

3.2 Measurement of LDL Oxidation in Supernatant of Macrophage-Like Cells

Figure 2 shows the amount of oxidized LDL in J774.A1 cells cultured in ERW medium was significantly decreased compared with MQ medium in the presence of

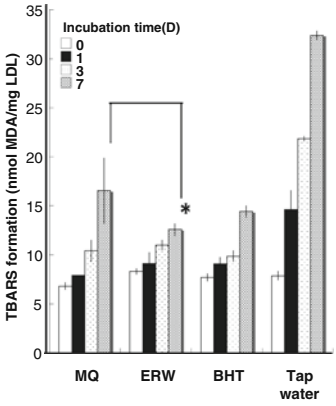

Fig. 1 Measurement of LDL peroxidation by TBARS. LDL incubated in various waters at 37°C for 1 week. LDL contained in each solution 100 ng/ml. * $=P<0.05$ compared to MQ control. BHT: Buthylated hydroxytoluene is lipidic antioxidant

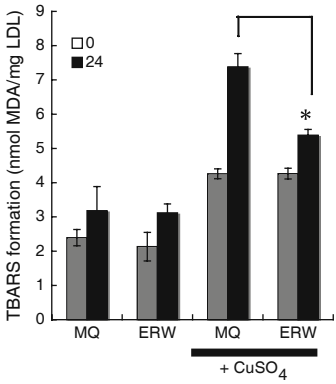

Fig. 2 Measurement of oxidized LDL in supernatant of J774.A1 cells cultured DMEM made from various waters in the presence of Cu^{2+} ion. Oxidized LDL measured by TBARS assay. Copper–mediated LDL oxidation was performed at 37°C for 24 h in CO_2 incubator. +$CuSO_4$ means 10 μM $CuSO_4$-added each medium. * $=P<0.05$ compared to MQ control

10 μM $CuSO_4$. There was no significant correlation between MQ and ERW medium in the absence of Cu^{2+} ion. Under drastic oxidation (presence of Cu^{2+}), ERW suppressed lipid peroxidate in J774A1 cells. It suggested that ERW was helpful to prevent oxidative stress of lipid peroxidation.

3.3 774A1 Uptake Fluorescence Oxidized LDL

The incorporation of DiI-LDL into J774.A1 cells were enhanced by the presence of Cu^{2+} ion (data not shown). To determine whether Cu^{2+} ion could induce the uptake of DiI-LDL by macrophage-like cells cultured in media prepared using various waters. However, there was no difference on the uptake of DiI-oxLDL between MQ and ERW group. However, the incorporation of DiI-oxLDL increased in tap water medium compared with ERW medium (Fig. 3).

Table 1 Measurement of lipid peroxide in plasma, RBC, liver and aorta by TBARS formation

nmol/mg protein

tissue	MQ	MQ + H_2	MQ + H_2 + Pt	MQ + Pt	ERW	ERW + Pt
plasma	0.16 ± 0.03	0.14 ± 0.02	0.15 ± 0.01	0.16 ± 0.02	0.14 ± 0.01	0.14 ± 0.02
RBC	1.57 ± 0.23	1.72 ± 0.21	0.89 ± 0.47	0.72 ± 0.01	0.82 ± 0.01	0.70 ± 0.54
liver	4.36 ± 0.84	4.42 ± 0.82	5.14 ±1.30	3.71 ± 0.75	4.62 ± 0.80	4.78 ± 0.72
aorta	10.86 ± 1.10	12.38 ± 0.85	11.24 ± 1.66	11.37 ± 1.80	10.99 ± 1.09	11.32 ± 1.32

RBC: red blood cell

3.4 Measurement of Lipid Peroxide in Plasma, RBC, Liver and Aorta

The plasma, RBC, hepatic, and aortic concentrations of TBARS in rats fed the natto fraction diets for 3 weeks are shown in Table 1. Lipid peroxide level in RBC was significantly lowered in the groups of MQ+H_2+Pt, MQ+Pt, ERW and ERW+Pt. However, nhibition of lipid oxidation of plasma, and a reduction in lipid peroxidation in liver and aorta were not observed. The antioxidant effect in the body was not of similar order to the inhibitory effect on the oxidation of plasma and LDL by $CuSO_4$ ex vivo. In this study, although the rats were given cholesterol as a substrate for oxidation, they were not subjected to oxidative stress. Therefore, it is suggested that the difference in the order of inhibitory effect of ERW on oxidation between in vitro and ex vivo was caused by a difference in their active ingredient, absorption, and metabolism.

3.5 Analysis of Lipid Concentration in Plasma

To investigate the mechanism of lipid metabolism of the ERW in the body, lipids such as total cholesterol, free cholesterol, high-density lipoprotein, low-density lipoprotein, triglyceride, phospholipid, nonesterified fatty acid were determined. Plasma concentrations of T-CHO, F-CHO, HDL-CHO, LDL-CHO, TG, NEFA, and PL in high cholesterol fed rats are shown in Table 2. Triglyceride level in the ERW group was significantly lower than that in the control group. No significant differences in other lipids were observed in the six groups. These results suggest that although the addition of CHO to the diet increased lipids, ingestion of ERW appeared to decrease TG. However, there was no difference of body weights and liver weights (data was not shown) between MQ control and ERW groups. This phenomenon suggests that ERW suppressed absorption of lipids. As these lipids are not only dangerous factors in arteriosclerosis [5], but also cause overweight, ERW may have a useful effect on lipid metabolism.

The results suggest that ERW inhibits absorption of excessive lipids. It was suggested that ERW might help to prevent hyperlipidemia and arteriosclerosis, because ERW reduced lipid peroxidation in vitro and improved lipid metabolism in vivo.

Table 2 Analysis of lipid concentration in plasma

	MQ	MQ + H_2	MQ + H_2 + Pt	MQ + Pt	ERW	ERW + Pt
T-CHO (mg/dL)	71.85 ± 11.81	70.14 ± 7.60	65.43 ± 8.72	70.71 ± 14.35	75.00 ± 8.23	65.57 ± 11.07
F-CHO (mg/dL)	11.14 ± 2.035	10.71 ± 1.11	10.14 ± 1.57	11.00 ± 1.40	10.29 ± 2.29	13.71 ± 6.26
HDL-CHO (mg/dL)	20.29 ± 3.638	18.00 ± 2.31	19.71 ± 3.15	20.00 ± 3.06	20.29 ± 1.38	19.29 ± 3. 45
LDL-CHO (mg/dL)	15.71 ± 4.271	18.00 ± 4.83	14.57 ± 2.30	15.86 ± 3.67	18.57 ± 5.32	14.14 ± 3.34
TG (mg/dL)	65.0 ± 13.13	52.0 ± 27.67	56.83 ± 4.76	45.83 ± 13.39	36.5 ± 11.94	49.14 ± 24.3
PL (mg/dL)	105.43 ± 11.073	97.71 ± 9.12	100.43 ± 12.38	104.71 ± 15.18	103.29 ± 4.72	99.57 ± 10.64
NEFA (mg/dL)	700.00 ± 178.98	793.57 ± 234.42	779.57 ± 128.31	732.29 ± 170.41	742.29 ± 177.28	764.29 ± 172.61

*$P < 0.05$ vs MQ group control

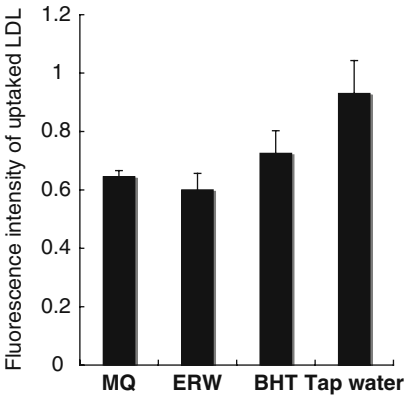

Fig. 3 Macrophage-like J774.A1 cells uptaked oxidized DiI-LDL. J774.A1 cells cultured DMEM made from various waters in the presence of 10 μM $CuSO_4$. Oxidized DiI-LDL uptake to cells. DiI-oxLDL measured by flow cytometry. Copper–mediated LDL oxidation was performed 37°C for 24 h in a CO_2 incubator. DiI: 1,1'-dioctadecyl-3,3,3',3'-tetramethylindo-carbocyanine perchlorate (fluorescent dye)

References

1. Ye J., Li Y.-P., Hamsaki T., Nakamichi N., Komatsu T., Kashiwagi T., Teruya K., Nishikawa R., Kawahara T., Osada K., Toh K., Abe M., Tian H., Kabayama S., Otsubo K., Morisawa S., Katakura Y., and Shirahata S. (2008) Inhibitory effect of electrolyzed reduced water on tumor angiogenesis. *Biol. Pharm. Bull*. **31**: 19–26.
2. Ihm S.H., Yoo H.J., Park S.W., and Ihm J. (1999) Effect of aminoguanidine on lipid peroxidation in streptozotocin-induced diabetic rats. *Metabolism* **48**: 1141–1145.
3. Yagi K. (1976) A simple fluorometric assay for lipoprotein in blood plasma. *Biochem Med*. **15**: 212–216.
4. Ohkawa H., Ohishi N., and Yagi K. (1979) Assay for lipid peroxides in animal tissues by thiobarbituric acid reaction. *Anal Biochem*. **95**: 351–358.
5. Iwai K., Nakaya N., Kawasaki Y., and Matsue H. (2002) The inhibitory effect of natto, a kind of fermented soybeans, on LDL oxidation in vitro. *J. Agric. Food Chem*. **50**: 3592–3596.

Growth Suppression of HL60 and L6 Cells by Atomic Hydrogen

Kensuke Nakanishi, Takeki Hamasaki, Takuro Nakamura, Masumi Abe, Kiichiro Teruya, Yoshinori Katakura, Shinkatsu Morisawa, and Sanetaka Shirahata

1 Introduction

We previously reported ERW which is produced near the cathode by electrolysis has a reductive activity and tumor-suppressive activity [1–3]. We also revealed that ERW contains both molecular hydrogen and Pt nanoparticles (nps) derived from platinum-coated titanium electrodes. Synthesized Pt nps have catalytic activity converting molecular hydrogen to atomic hydrogen. Consequently, there is a possibility that the atomic hydrogen is produced in ERW. Thus, we synthesized Pt nps to construct a model water of ERW containing both molecular hydrogen and Pt nps, and then we examined the effect of the model water on the cell viability and Sub-G1 analysis in this study.

2 Experimental Procedure

2.1 Cell Culture and Measurement of Cell Proliferation

Premyeloblastic cell lines (HL60; JCRB0085), skeletal muscle myoblast cell lines (L6; JCRB9081) were obtained from the Japanese Collection of Research Bioresources (JCRB, Osaka, Japan). HL60 Cells were cultured in RPMI 1640 medium (Nissui Pharmaceutical Co., Ltd., Tokyo, Japan) supplemented with 10% fetal bovine serum (FBS) (Invitrogen Japan K. K., Tokyo Japan) at 37°C in a 95% air/ 5% CO_2 atmosphere (10% FBS/MEM).L6 cells were cultured in Dulbecco's Modified Eagle Medium supplemented with 10% FBS at 37°C in a 95% air/ 5% CO_2 atmosphere. Briefly, cells were seeded (floating cells, 1.0×10^5 cells/cm^2 and adherent cells, 2.0×10^4 cells/cm^2) in 6-well plates. The cultures were incubated with different concentrations of Pt nps for 2 h in serum-free medium, washed two times with PBS, exchanged with fresh serum containing medium and incubated with

S. Shirahata (✉)
Faculty of Agriculture, Kyushu University, Higashi-ku, Fukuoka 812-8581, Japan
e-mail: sirahata@grt.kyushu-u.ac.jp

M. Kamihira et al. (eds.), *Animal Cell Technology: Basic & Applied Aspects*, Animal Cell Technology: Basic & Applied Aspects 16, DOI 10.1007/978-90-481-3892-0_53,

a gas incubator at 37°C in a 75% H_2/ 20% O_2/ 5% CO_2 atmosphere for 24 h. Dissolved helium solution was used as control. The number of cells was counted by a cell counter.

2.2 Cell Cycle Analysis by Flowcytometer

Cells were harvested 2 h after treatment with or without H_2/Pt nps solution. After washing with PBS, 1×10^6 cell pellets were suspended in 0.5 ml of hypotonic fluorochrome solution, containing 50 μg/ml propidium iodide (PI; Sigma, MO). Cells were stained overnight in the dark at 4°C and examined by a flowcytometer (EPICS XL ADC System, Beckman Coulter, Inc. Ca, USA).

3 Results and Discussion

Cells were incubated with dissolved H_2 solution after treatment with Pt nps at 2 h in FBS-free medium. The cell viability was decreased on both HL60 and L6 cells when supplemented with both Pt nps and H_2 (Fig. 1). The result of trypan blue dye assay shows that this suppression of cell viability was caused by cell death (data not shown). Thus, we next examined the cell death by Sub G-1 analysis using flowcytometer.

Increasing of Sub-G1 phase is one of the indications of apoptosis. Analysis of cell cycles was performed 24 h after Pt nps supplement. In the condition of dissolved hydrogen solution supplemented with 3.0–5.0 ppm Pt nps in HL60 cells and L6 cells, 20–37% of Sub-G1 phase are increased compared to control medium. The result suggests that atomic hydrogen induced apoptosis of both L6 and HL60 cells (Fig. 2).

The H-transfer reaction in vitro by antioxidants has been well investigated so far. There are many reports about the activities of antioxidants. However, there are few

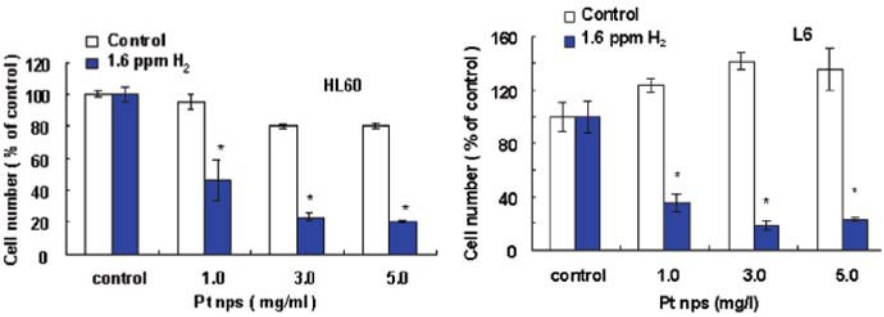

Fig. 1 Dissolved hydrogen solution supplement with Pt nps suppresses the growth of HL60 cells and L6 cells. Bars represent means ±SD. *P<0.01 in comparison with control

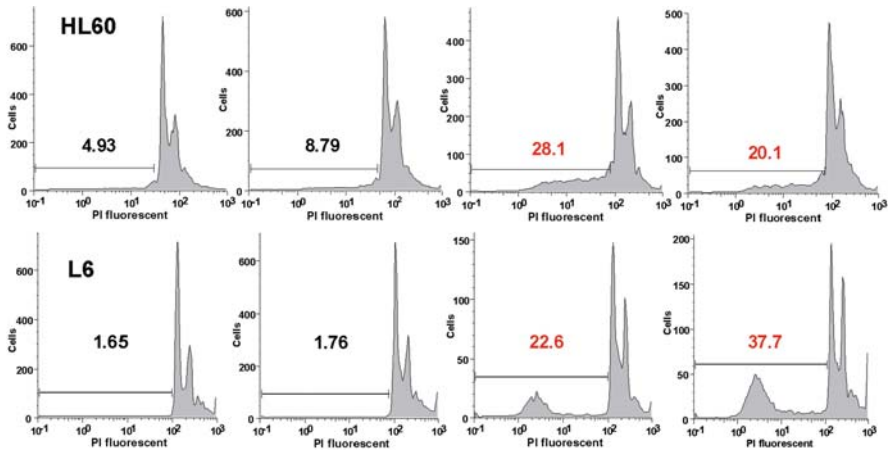

Fig. 2 Cell cycle analysis of HL60 and L60 cells cultured in medium supplemented with H_2 and Pt nps

reports about effects in a living organism of atomic hydrogen itself. We expect that physiological effects of atomic hydrogen itself will be figured out in the future.

References

1. Shirahata, S., Kabayama, S., Nakano, M., Miura, T., Kusumoto, K., Gotoh, M., Hayashi, H., Otsubo, K., Morisawa, S., Katakura, Y. (1997). Electrolyzed-reduced water scavenges active oxygen species and protects DNA from oxidative damage. *Biochem. Biophys. Res. Commun.* **234**: 269–274.
2. Shirahata, S. Reduced water for prevention of diseases. In: Shirahata, S. Teruya, K. Katakura, Y., (Eds.) (2002) *Animal Cell Technology: Basic & Applied Aspects* (Volume 12, pp. 25–30). Netherlands: Dordrecht. Kluwer Academic Publishers.
3. Huang, K. C., Yang, C. C., Lee, K. T., Chien, C. T. (2003) Reduced hemodialysis-induced oxidative stress in end-stage renal disease patients by electrolyzed reduced water. *Kidney Int.* **64**: 704–714.

Insulin-Mimetic Activity of Inositol Derivatives Depends on Phosphorylation of PKCζ/λ in L6 Myotubes

Nhung Thuy Dang, Masanori Yamaguchi, Tadashi Yoshida, Ken-ichi Yoshida, and Hitoshi Ashida

1 Introduction

Insulin plays an important role in the maintenance of postprandial glucose homeostasis. Insulin stimulates glucose transport into the striated skeletal muscle and cardiac muscle cells, and fat cells in adipose tissue through the translocation of glucose transporter 4 (GLUT4). GLUT4 is translocated from the storage sites of endoplasmic reticulum to the plasma membrane surface upon stimulation by insulin [1], resulting in increased glucose uptake from the bloodstream into target tissue cells [2]. Therefore, a defect of this regulatory machinery in muscle and fat cells causes insulin resistance and pathogenesis of type 2 diabetes [3].

Inositol (1, 2, 3, 4, 5, 6-cyclohexanehexol) is a class of compounds which could form nine distinct stereoisomers through epimerization of the six hydroxyl groups. Some inositol derivatives, such as D-*chiro*-inositol (DCI) and 3-*O*-methyl-D-*chiro*-inositol (pinitol, PI) [4–6], have been shown to possess insulin-like effect, and are potential therapeutics in the prevention and treatment of diabetes. However, the mechanism by which the inositol derivatives act on the insulin signaling pathway is not fully understood yet. Therefore, we investigated the effect of selected inositol derivatives on the insulin signaling pathway in a model system using L6 myotubes.

2 Materials and Methods

2.1 Materials

Modified Eagle's medium (MEM) was purchased from Nissui pharmaceutical (Tokyo, Japan). Fetal bovine serum (FBS) was obtained from Equitech-Bio, Inc.

N.T. Dang (✉)
Graduate School of Agriculture Science, Kobe University, Nada-ku, Kobe, Hyogo 657-8501, Japan
e-mail: nhungthuydang@yahoo.ca

M. Kamihira et al. (eds.), *Animal Cell Technology: Basic & Applied Aspects*, Animal Cell Technology: Basic & Applied Aspects 16, DOI 10.1007/978-90-481-3892-0_54,

(Kerrville, TX). PI, DCI, L-*chiro*-inositol (LCI), and *myo*-inositol (MI) were products of Hokko Chemical Industry Co., Ltd (Tokyo, Japan). Anti-GLUT4 and anti-goat IgG antibodies were purchased from Santa Cruz Biotechnology (Santa Cruz, CA). Anti-Akt and anti-phospho PKCζ/λ, anti-phosphoAkt, and anti-PKCζ/λ were from Cell Signaling Technology (Beverly, MA), Sigma Chemical Co. (St. Louis, MO), and Transduction Laboratories Ltd. (San Diego, CA), respectively. Blocking-One^{TM} and Blocking One-P^{TM} were obtained from Nacalai Tesque (Kyoto, Japan). Immuno-Blot PVDF membrane and ECL plus used for Weatern blotting were purchased from Pall Gelman Laboratory (Tokyo, Japan) and GE Healthcare Bio-Science Corp. (Piscataway, NJ), respectively.

2.2 Cell Culture

L6 myoblasts were grown and maintained in MEM supplemented with 10% FBS in a 5% CO_2 humidified atmosphere at 37°C. When myoblasts were grown to confluence, the medium was replaced with MEM containing 2% FBS, and the cells were cultured up to 7 days to induce the differentiation into myotubes. The degree of the differentiation of L6 myotubes at differentiated days was confirmed by detection of the expression level of GLUT4 in cell lysates (data not shown). Fully differentiated myotubes were serum-starved for 18 h in MEM containing 0.2% bovine serum albumin prior to the experiments.

2.3 Preparation of Cell Lysate

The fully differentiated and serum-starved L6 myotubes were incubated with Krebs-Ringer HEPES (KRH) buffer (50 mM HEPES, pH 7.4, 137 mM NaCl, 4.8 mM KCl, 1.85 mM $CaCl_2$, and 1.3 mM $MgSO_4$) for 10 min at 37°C and then treated with 100 nM insulin or 1 mM inositol derivatives in KRH buffer for 15 min. After being washed twice with ice-cold KRH buffer, the cells were harvested and lysed with RIPA buffer (50 mM Tris-HCl, pH 8.0, 150 mM NaCl, 1% Nonidet® P-40, 0.5% sodium deoxycholate, 0.1% SDS, 1 mM Na_3VO_4, 10 μg/ml leupeptin, 10 mM sodium fluoride, and 1 mM phenylmethylsulfluoride) for 1 h at 4°C. The lysate was collected by centrifugation at 10,000 × *g* for 20 min at 4°C.

2.4 Preparation of the Plasma Membrane Fraction From Myotubes

The plasma membrane of L6 myotubes was prepared as described previously [7]. Briefly, the fully differentiated L6 myotubes were treated with 100 nM insulin or 1 mM inositol derivatives as described above. The cells were washed twice with ice-cold KRH buffer, and harvested with buffer A (10 mM Tris, pH 7.8, 10 mM

KCl, 1.5 mM $MgCl_2$, 1 mM phenylmethylsulfonylfluoride, 0.5 mM dithiothreitol, 5 μg/ml aprotinin, 1 mM Na_3VO_4, and 10 μg/ml leupeptin) containing 0.1% Nonidet® P-40. The cells were then homogenized by passing through a 27-gauge needle three times, and homogenates were spun at 1,000 $\times g$ for 10 min at 4°C. The pellet was washed with buffer A without Nonidet® P-40 and spun at 1,000 $\times g$ for 10 min at 4°C. The plasma membrane fraction was obtained by resuspending the resulting pellet in buffer A containing 1% Nonidet® P-40 and centrifuging at 10,000 $\times g$ for 20 min at 4°C. The resulting supernatant containing the plasma membrane fraction was collected and subjected to immunoblot analysis.

2.5 Immunoblot Analysis

For detection of GLUT4, aliquots of the plasma membrane fraction (3 μg protein) and cell lysate (10 μg protein) were separated by 10% SDS-polyacrylamide gel electrophoresis (SDS-PAGE), and transferred onto a PVDF membrane. The membrane was soaked in 5% (w/v) non-fat dry milk in TBST (10 mM Tris-HCl, pH 8.0, 150 mM NaCl and 0.05% Tween 20), and incubated with anti-GLUT4 for 1 h at room temperature. After being washed, the membrane was then incubated with horseradish peroxidase-conjugated anti-goat antibody for 1 h at room temperature. For detection of Akt and PKC expression and their phosphorylation, aliquots of the cell lysate (30 μg protein) were separated by 8% SDS-PAGE gels, and transferred onto the PVDF membrane. The membrane was treated with Blocking-One™ or Blocking-One-P™, incubated with primary antibody for 1 h at room temperature, and then incubated with horseradish peroxidase-conjugated secondary antibody for 1 h at room temperature. Specific immuno-complex was detected by enhanced using the ECL plus™ detection kit.

3 Results

3.1 Inositol Derivatives Stimulate Translocation of GLUT4 to Plasma Membrane

GLUT4 is mainly expressed in muscle and adipose tissues and plays an important role in glucose homeostasis [8]. Insulin stimulates the translocation of GLUT4 from intracellular storage sites to the plasma membrane surface [1], resulting in the increased glucose uptake from the bloodstream into the cells of target tissues [2]. In this study, we selected four inositol derivatives, namely PI, DCI, LCI, and MI. Structures of them are shown in Fig. 1. We investigated the effects of four inositol derivatives on GLUT4 translocation in vitro using a model system of L6 myotubes. We found that three inositol derivatives other than MI stimulated the translocation of GLUT4 to plasma membrane (Table 1).

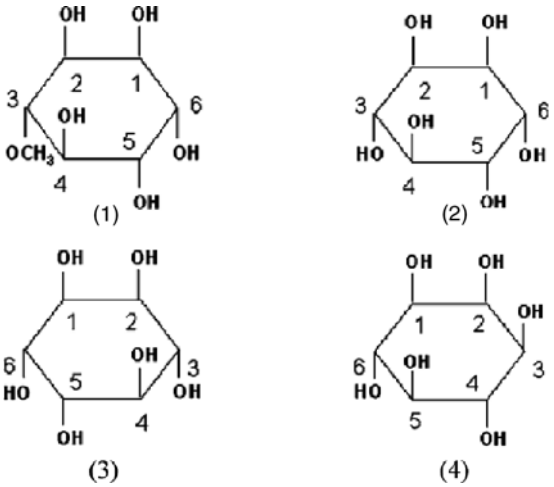

Fig. 1 Structure of inositol derivatives, PI (1), DCI (2), LCI (3), and MI (4)

Table 1 Summarized results of assays to determine effects of inositol derivatives on L6 myotubes

	Compounds				
	Insulin (100 nM)	PI (1 mM)	DCI (1 mM)	LCI (1 mM)	MI (1 mM)
GLUT4 translocation	+	+	+	+	–
PKCζ/λ phosphorylation	+	+	+	+	–
Akt phosphorylation	+	–	–	–	–

3.2 Inositol Derivatives Activate PKCζ/λ Phosphorylation but not Akt Phosphorylation

aPKC isoforms ζ/λ and Akt are known as the mediators involved in the insulin-stimulated glucose transport in muscle and adipocytes [1, 9]. To understand a mechanism by which three inositol derivatives stimulated the translocation of GLUT4, we investigated phosphorylation status of PKCζ/λ and Akt. Three inositol derivatives other than MI stimulated phosphorylation of PKCζ/λ at 1 mM, but none of them enhanced phosphorylation of Akt at Ser473 (Table 1).

4 Discussion

In this study, we confirmed that three inositol derivatives, namely PI, DCI, and LCI, stimulated the translocation of GLUT4 to plasma membrane surface in the model system of L6 myotubes (Table 1), well coinciding with the previous reports [4, 6, 10]. In addition, it was also reproduced that MI failed to stimulate the GLUT4

translocation (Table 1), as previous studies demonstrated that MI possessed no anti-hyperglycemic effect [6, 11, 12]. It was reported that some of MI can be converted to DCI in the body [12], but the conversion might be too limited to exert the insulin-mimetic effect, which could be the case in the L6 myotube system as well. In any case, it is intriguing that such a simple alternation in structure of inositols epimerizing a hydroxyl group results in the dramatic change in their biological activity. The L6 myotube system can be regarded as an ideal model to work with the mysterious mechanism by which the inositols exert the activity, since the present study actually enabled us to find the striking fact that inositol derivatives provoked the differential phosphorylation status of the kinases, such as aPKCζ/λ and Akt, which are involved in the insulin signaling pathway. Although obviously further study is still required, the L6 myotube system will help us to understand the mechanism underlying the insulin-mimetic activity of inositol derivatives.

References

1. Wang, Q., Somwar, R., Bilan, P.J., Liu, Z., Jin, J., Woodgett, J.R., and Klip, A. (1999) Protein kinase B/Akt participates in GLUT4 translocation by insulin in L6 myoblasts. *Mol. Cell. Biol*. **19**(6): 4008–4018.
2. Tsuru, M., Katagiri, H., Asano, T., Yamada, T., Ohno, S., Ogihara, T., and Oka, Y. (2002) Role of PKC isoforms in glucose transport in 3T3-L1 adipocytes: Insignificance of atypical PKC. *Am. J. Physiol. Endocrinol. Metab*. **283**(2): 338–345.
3. Chen, J., Lu, G., and Wang, Q.J. (2005) Protein kinase C-independent effects of protein kinase D3 in glucose transport in L6 myotubes. *Mol. Pharmacol*. **67**(1): 152–162.
4. Bates, S.H., Jones, R.B., and Bailey, C.J. (2000) Insulin-like effect of pinitol. *Br. J. Pharmacol*. **130**(8): 1944–1948.
5. Weeks, C.E. and Albany, N. (2003) Stimulating transport of glucose into animal tissue by the administration of pinitol. US Patent 6, 518, 318 B1.
6. Yap, A., Nishiumi, S., Yoshida, K., and Ashida, H. (2007) Rat L6 myotubes as an in vitro model system to study GLUT4-dependent glucose stimulated by inositol derivatives. *Cytotechnol*. **55**(2–3): 103–108.
7. Nishiumi, S. and Ashida, H. (2007) Rapid preparation of a plasma membrane fraction from adipocytes and muscle cells: Application to detection of translocated glucose transporter 4 on the plasma membrane. *Biosci. Biotechnol. Biochem*. **71**(9): 2343–2346.
8. Ramm, G., Larance, M., Guilhaus, M., and James, D.E. (2006) A role for 14-3-3 in insulin-stimulated GLUT4 translocation through its interaction with the RabGAP AS160. *J. Biol. Chem*. **281**(39): 29174–29180.
9. Farese, R.V., Sajan, M.P., and Standaert, M.L. (2005) Insulin-sensitive protein kinases (atypical protein kinase C and protein kinase B/Akt): Actions and defects in obesity and type II diabetes. *Exp. Biol. Med*. **230**(9): 593–605.
10. Khan, A.H. and Pessin, J.E. (2002) Insulin regulation of glucose uptake: A complex interplay of intracellular signaling pathways. *Diabetologia* **45**(11): 1475–1483.
11. Ostlund, R.E. and Sherman, W.R. (1998) Pinitol and derivatives thereof for the treatment of metabolic disorders, US Patent 5, 827, 896.
12. Ortmeyer, H.K., Huang, L.C., Zhang, L., Hansen, B.C., and Larner, J. (1993) Chiroinositol deficiency and insulin resistance. II. Acute effects of D-chiroinositol administration in streptozotocin-diabetic rats, normal rats given a glucose load, and spontaneously insulin-resistant rhesus monkeys. *Endocrinology* **132**(2): 646–651.

Enhancement of Phagocytic Activity by a Crude Polysaccharide from Tea (*Camellia sinensis*) Extract

Manami Monobe, Kaori Ema, Keiko Azuma, and Mari Maeda-Yamamoto

1 Introduction

Tea, from the plant *Camellia sinensis* L., is one of the most popular beverages consumed worldwide in its green, black, or oolong form. Tea polyphenols and tea polysaccharides are the main components in tea extracts. Epigallocatechin gallate (EGCG), a major polyphenolic compound in tea extracts, is well-known to have antioxidant [1], antibacterial [2], and immunomodulatory effects [3]. Tea polysaccharides are also reported to have the ability to inhibit pathogenic bacterial adhesion [4]. Wang et al [5]. reported that tea polysaccharides enhanced immunization of rats. In general, it is known that food polysaccharides in mushrooms and plants activate macrophage immune responses and lead to immunomodulation, antitumor activity, and so on [6]; however, there are still only few reports on the immunostimulating effect of tea polysaccharides, and furthermore, the dependence of immunostimulating activity on the level of leaf maturation has never been reported. In this study, we found that the immunostimulating activity of crude polysaccharide from immature tea leaves was higher than that of TPS from mature tea leaves, and we conclude that the catechin-polysaccharide complex is a potential immunostimulator.

2 Materials and Methods

2.1 Preparation of TPS

Tea cultivars were harvested at the plantation of the National Institute of Vegetable and Tea Science in Kanaya, Shizuoka, Japan. Tea leaves were dried in a microwave oven, pulverized, and stored at 4°C before analysis. The pulverized tea leaves were boiled in distilled water (DW) for 30 min and centrifuged for 30 min (1200*g*).

M. Monobe (✉)
National Institute of Vegetable and Tea Science, NARO, Shizuoka, Japan
e-mail: monobe@affrc.go.jp

M. Kamihira et al. (eds.), *Animal Cell Technology: Basic & Applied Aspects*, Animal Cell Technology: Basic & Applied Aspects 16, DOI 10.1007/978-90-481-3892-0_55,

The tea extract was precipitated by using ethanol (final 70% concentration). The sediment was washed with ethanol and acetone alternately and dried (crude polysaccharide, TPS). Separation of high- and low-molecular weight TPS fractions was performed by a dialysis membrane (Slide-A-Lyzer 20 k MWCO, Pierce, Rockford, IL) and a centrifugal filter device (Microcon YM-100, Millipore Co., Bedford, MA, USA) (TPS-F1 and TPS-F2), respectively. To remove the substances that conjugated with TPS from buds, such as polyphenols and proteins, 100 mg of precipitate was dissolved in 10 mL of 0.1 M NaOH; 1 mL of a NaClO solution (available chlorine >5%) was added. The mixture was then incubated at 4°C overnight [7]. The reaction mixture was dialyzed (Slide-A-Lyzer 20 k MWCO, Pierce) with DW, precipitated by using acetone (final 70% concentration) at room temperature, and dried. A precipitate was dissolved in DW and centrifuged for 30 min (1200*g*), and this solution was divided into a clear supernatant (TPS-F3) and brown precipitate. The clear supernatant was precipitated by using ethanol (final 70% concentration). The sediment was washed with ethanol and acetone alternately and dried.

2.2 Catechin Assay

Catechins were analyzed by the procedure of Maeda-Yamamoto et al [8]. The tea was diluted 3- to 5-fold with DW, and 20 μL of the filtrate after filtration through a membrane filter (DISMIC-13-HPPTFE, pore size 0.45 μm, ADVANTEC, Tokyo, Japan) was injected into the HPLC apparatus (Shimadzu Class VP HPLC system). Epicatechin (EC), catechin (C), EGCG, epicatechin gallate (ECG), catechin gallate (CG), and epigallocatechin-3-*O*-(3-*O*-methyl) gallate (EGCG3''-Me) were measured at 272 nm and epigallocatechin (EGC) at 242 nm. Quantification of catechins was performed after data acquisition by using an LC workstation (Class VP system, Shimadzu).

2.3 Molecular Weight of TPS

The molecular weight of tea polysaccharides was determined by HPLC equipped with a refractive index detector (RID-10A, Shimadzu) and a Shodex OHpak SB-806 M HQ column (8.0 mm × 300 mm). The elutions of the standard molecular weight of dextran (Pharmacia AB, Uppsala, Sweden) and pullulans (Showa Denko Co. Ltd., Tokyo, Japan) were carried out in the same manner.

2.4 Phagocytesis Assay

The phagocytosis assay was performed as previously described [9]. Briefly, to differentiate cells along the monocytic pathway, HL60 cells (American-type

Culture Collection, Rockville, MD) were cultured in RPMI 1640 medium (Gibco-Invitrogen, Burlington, ON, Canada) supplemented with 120 nM VD3 (Wako Pure Chemical Industries, Ltd.). Differentiated HL60 cells were seeded in 48-well plates (BD Biosciences, Franklin Lakes, NJ). Cells were treated with 25 μL of TPS, a catechin mixture (polyphenone E, Mitsui-Norin Co., Ltd., Shizuoka, Japan), or lipopolysaccharide (LPS, Calbiochem, San Diego, CA). Next, 25 μL of a 1% suspension of YG-labeled microspheres (Polysciences, Inc., Warrington, PA) was added, and the solution was incubated at 37°C in 5% CO_2 for 16 h. The cells were fixed with 2% formaldehyde and resuspended in phosphate-buffered saline. The rate of phagocytosis was measured with an EPICSXL-flow cytofluorometer (Beckman Coulter, Fullerton, CA).

2.5 Statistical Analysis

All data were derived from at least three experiments. Data are expressed as the means ± standard deviation (SD). The efficiency of phagocytosis was compared by using the paired *t*-test. The parameter n represents the number of experiments.

3 Results

3.1 Immunostimulation Activity of TPS

Phagocytosis by macrophages is used as an important indicator of immune function activation; thus, we estimated the immunostimulation activity of TPS by using VD3-differentiated HL60 cells in which phagocytosis is activated by various immune-enhancing polysaccharides. As shown in Fig. 1, TPS from various cultivars stimulated VD3-differentiated HL60 cells. Although data are not shown, the immunostimulating activity of TPS from buds to second leaves was higher than that of TPS from other leaves and stems (data not shown).

3.2 Polyphenol Content and Immunostimulating Activity

A good correlation was obtained between the percentage of phagocytosis and total catechin (Fig. 2); however, no correlation was obtained between the percentage of phagocytosis and each catechin, such as EGCG.

3.3 Molecular Weight Distribution of TPS

The molecular weight of TPS is calculated by using the molecular standard fitting equation. TPS has three major peaks of around 200, 1, and 0.1 ($\times 10^4$) M.W. TPS

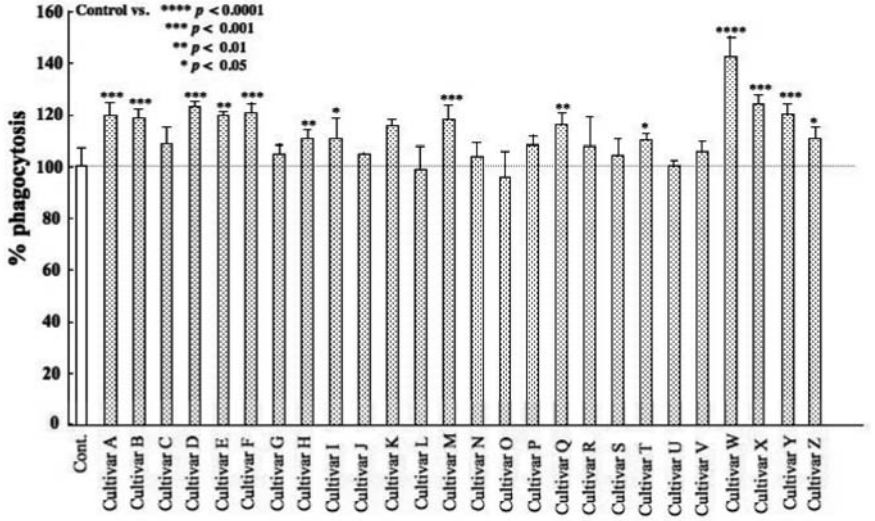

Fig. 1 Phagocytic activities by TPS from various cultivars. VD3-differented HL60 cells were incubated with beads in the presence of TPS (100 μg/mL). Phagocytosis activity in the absence of TPS (control) is normalized to 100%. Values are the means, $n = 3$

was separated into two fractions (TPS-F1 and TPS-F2) by a dialysis membrane and a centrifugal filter device, and the phagocytic activities were measured. TPS-F1 (more than 200×10^4 M.W.) ($p < 0.05$), but not TPS-F2 (less than 1×10^4 M.W.), significantly increased the phagocytic activity (Fig. 3).

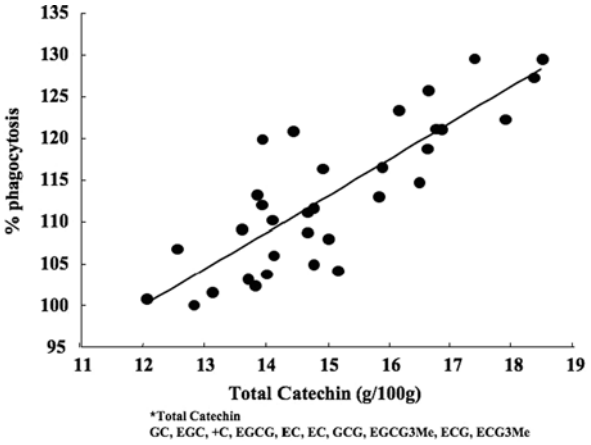

Fig. 2 Relationship between the percentage of phagocytosis and total catechin. $Y = 4.3868X + 47.047$ and $r^2 = 0.6946$, where Y and X are the percentage of phagocytosis and the total catechin, respectively

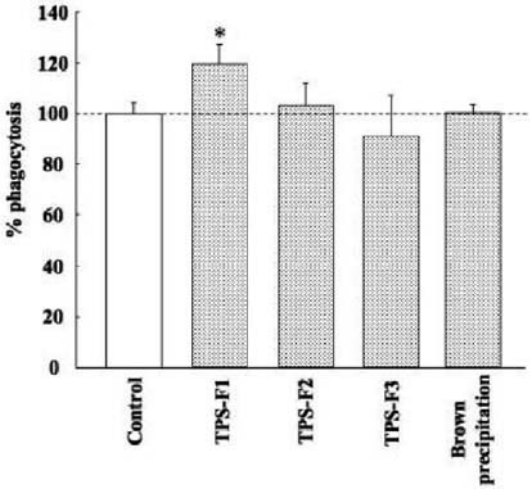

Fig. 3 Phagocytic activities of TPS-1, 2, 3 and brown precipitation. VD3-differented HL60 cells were incubated with beads in the presence of TPS (100 μg/mL). Phagocytosis activity in the absence of TPS (control) is normalized to 100%. Values are the means, $n = 3$. $^{*}p < 0.05$ versus the control

3.4 Immunostimulating Activity of TPS that Removed Polyphenols (TPS-F3) and the Brown Precipitate

Neither TPS-F3 nor the brown precipitation stimulated VD3-differentiated HL60 cells (Fig. 3).

3.5 Immunostimulating Activity of the Catechin Mixture

The catechin mixture (the catechin content was more than 90%, and the EGCG content was more than 60%) did not stimulate VD3-differentiated HL60 cells (data not shown).

4 Discussion

In this study, we found that the immunostimulating activity of TPS was dependent on the content of total catechin in the leaf extract (Fig. 2), and the activity of TPS from immature tea leaves was higher than that of TPS from mature tea leaves. Furthermore, high-molecularweight TPS was the main substance with an immunostimulating activity, and TPS that removed polyphenols (TPS-F3) did not stimulate VD3-differentiated HL60 cells (Fig. 3). Also, tea catechins have been reported to have immunomodulatory effects [3], but in this study, a catechin mixture did not stimulate VD3-differentiated HL60 cells. These results suggest that the polyphenol-polysaccharide complex is a potential immunostimulator. Nakamura

et al [10]. reported that a complex mixture of tannins with polyphenols and polysaccharides inhibited tumor promotion and carcinogenesis in mice and mice cell lines. These results were similar to ours. However, the mechanism underlying these activities is still not clear. Tannin such as catechins and strictinin are the main polyphenols in green tea extract. This suggests that the tannin-polysaccharide complex is a very important molecule in the immunomodulating activity of tea extracts. Further studies and data are needed to clarify the mechanism of immunomodulation by tannin-polysaccharide complexes.

References

1. Katiyar, S.K., and Elmets, C.A. (2001) Green tea polyphenolic antioxidants and skin photoprotection (Review). *Int. J. Oncol*. **18**(6): 1307–1313.
2. Matsunaga, K., Klein, T.W., Friedman, H., and Yamamoto, Y. (2001) Legionella pneumophila replication in macrophages inhibited by selective immunomodulatory effects on cytokine formation by epigallocatechin gallate: A major form of tea catechins. *Infect. Immun*. **69**(6): 3947–3953.
3. Mantena, S.K., Meeran, S.M., Elmets, C.A., and Katiyar, S.K. (2005) Orally administered green tea polyphenols prevent ultraviolet radiation-induced skin cancer in mice through activation of cytotoxic T cells and inhibition of angiogenesis in tumors. *J. Nutr*. **135**(12), 2871–2877.
4. Lee, J.H., Shim, J.S., Lee, J.S., Kim, J.K., Yang, I.S., Chung, M.S., and Kim, K.H. (2006) Inhibition of pathogenic bacterial adhesion by acidic polysaccharide from green tea (*Camellia sinensis*). *J. Agric. Food Chem*. **54**(23): 8717–8723.
5. Wang, D.W., Wang, C.W., Li, J.L., and Zhao, G.Z. (2001) Components and activity of polysaccharides from coarse tea. *J. Agric. Food Chem*. **49**(1): 507–510.
6. Schepetkin, I.A., and Quinn, M.T. (2006) Botanical polysaccharides: Macrophage immunomodulation and therapeutic potential. *Int. Immunopharmacol*. **6**(3): 317–333.
7. Ohno, N., Uchiyama, M., Tsuzuki, A., Tokunaka, K., Miura, N.N., Adachi, Y., Aizawa, M.W., Tamura, H., Tanaka, S., and Yadomae, T. (1999) Solubilization of yeast cell-wall beta-(1–>3)-D-glucan by sodium hypochlorite oxidation and dimethyl sulfoxide extraction. *Carbohydr. Res*. **316**(1–4): 161–172.
8. Maeda-Yamamoto, M., Nagai, H., Suzuki, Y., Ema, K., Kanda, E., and Mitsuda, H. (2005) Changes in *O*-methylated catechin and chemical component contents of "Benifuuki" green tea (*Camellia sinensis* L.) beverage under various extraction conditions. *Food Sci. Technol. Res*. **11**(3): 248–253.
9. Monobe, M., Ema, K., Kato, F., Hirokane, H., and Maeda-Yamamoto, M. (2007) Technique for screening immune-enhancing polysaccharides in food using 1, 25-dihydroxyvitamin D3-differentiated HL60 cells. *J. Agric. Food Chem*. **55**(7): 2543–2547.
10. Nakamura, Y., Kawase, I., Harada, S., Matsuda, M., Honma, T., and Tomita, I. (1997) In: Ohigashi, H., Osawa, T., Terao, J., Watanabe, S., and Yoshikawa, T. (Eds.), *Food Factors for Cancer Prevention* (pp. 138–141). Tokyo: Springer Verlag.

Effects of Lupeol on Melanoma In Vitro and In Vivo: Fundamental and Clinical Trials

Keishi Hata, Kikumi Ogihara, Saori Takahashi, Takeshi Tsuka, Saburo Minami, and Yoshiharu Okamoto

1 Introduction

The studies on tumor cell differentiation provide useful information for the preclinical evaluations of potent anticancer agents [3, 11]. Malignant melanoma is known to be one of difficult tumor to cure. Lupeol, a lupane triterpene, is widely distributed in plant kingdom, and recently found to suppress the tumor progressions in vitro and in vivo [8, 9, 5]. We previously reported that lupeol induced mouse melanoma cell differentiation, and inhibited the proliferation and motility of melanoma cells in vitro [4]. In the present study, we examined the differentiation-inducing activities of lupeol against melanoma cells in vitro and its clinical effects on the dogs with spontaneous melanoma.

2 Materials and Methods

2.1 Transmission Electron Microscopy (TEM)

B16 2F2 cells treated without or with 10 μM lupeol for 48 h, were fixed with 0.25% glutaraldehyde/phosphate buffer saline (PBS), and rinsed with PBS. Then the cells were set in 4% agar noble and post-fixed with 1% osmium tetroxide. The cells were dehydrated by ethyl alcohol according to the routine technique, displaced with QY-1, and embedded in Epon. Ultra thin sections of cells were carried out, and the cells were double-stained with uranyl acetate and lead citrate, and observed under an electron microscope.

K. Hata (✉)
Institute for Food and Brewing, Akita Prefectural Agricultural, Forestry, and Fisheries Research Center, Araya-machi, Akita 010-1623, Japan
e-mail: hata@arif.pref.akita.jp

M. Kamihira et al. (eds.), *Animal Cell Technology: Basic & Applied Aspects*, Animal Cell Technology: Basic & Applied Aspects 16, DOI 10.1007/978-90-481-3892-0_56,

2.2 Fluorescence Microscopy

Cells grown on glass coverslips pre-coated with fibronectin were cultured with or without lupeol for 12 h. The cells were rinsed twice with PBS, fixed in 4% formaldehyde, and permealized with 0.1% Triton X-100 for 10 min. For the detection of stress fibers, the cells were stained with Alexa-488-conjugated phalloidin.

2.3 Western Blotting

Aliquots of B16 2F2 cells were incubated with or without a stimulant for an appropriate period. The cells were collected by pipetting, washed twice with PBS, and then lysed with 5 mM Tris-HCl buffer, pH 6.8, containing 1% SDS, 1 mM EDTA and 10% sucrose. The proteins were separated by SDS-polyacrylamide gel electrophoresis, and then transferred to a nitrocellulose membrane. The membrane was immersed in 20 mM Tris-HCl, pH 7.5, 0.15 M NaCl, and 0.05% Tween 20 (TBST) containing 5% skim milk, and then incubated with primary antibodies for 2 h at room temperature, washed three times with TBST, and then incubated with HRP-conjugated secondary antibodies for 1 h at room temperature. The membrane was washed three times with TBST, and the signals were visualized using enhanced chemiluminescence reagents.

2.4 Migration Assay

Cancer cell migration assays were performed using Transwell cell culture chambers [6]. The Transwell cell culture chambers contained polyvinylpyrrolidone-free polycarbonate filters with a pore size of 8.0 μm were pre-coated with 2 μg of fibronectin on the lower surface. Cancer cells (5×10^4 cells) in enriched RDF medium supplemented with 0.1% BSA were added to the upper compartment, the chambers were and incubated at 37°C for 6 h. The cells on the lower surface of the filter were fixed with methanol and stained with hematoxylin. The cells on the upper surface were removed by wiping with cotton swabs. The average number of migrated cells in 4 areas was counted manually under a microscope, and each assay was repeated four times.

3 Results and Discussion

3.1 Differentiation Markers of Melanoma

Briefly, we studied the effects of lupeol on morphological changes in B16 2F2 cells. The observations with TEM revealed that the mature melanosomes in B16

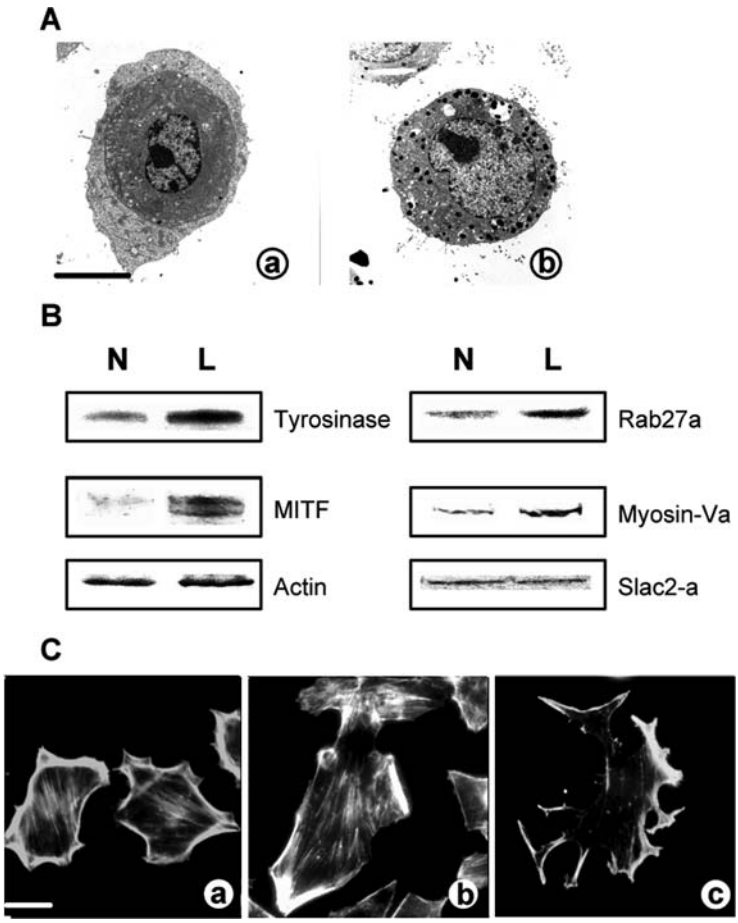

Fig. 1 Biomarkers of melanoma cell differentiation (**A**): B16 2F2 cells were stimulated without (a) or with 10 μM lupeol (b) for 48 h, and the intracellular melanosomes were observed under a transmission electron microscope (bar, 5 μm). (**B**): B16 2F2 cells were incubated without (N) or 10 μM lupeol (L) for 48 h, and the proteins in cell lysates were separated by SDS-PAGE, and subjected to Western blotting. Three independent experiments were performed. (**C**): B16 2F2 cells were cultured on coverslips pre-coated with fibronectin for 24 h, and treated with 10 μM lupeol for 0 h (a), 4 h (b) and 8 h (c). The cells were labeled with Alexa-Fluor 488-phalloindin (bar, 40 μm)

2F2 cells treated with 10 μM lupeol for 48 h significantly increased, when compared to the untreated cells (Fig. 1A). Therefore, we investigated the events involved in melanosome transports such as the expressions of Myosin-Va/Rab27a/Slac-2a by observations with fluorescence microscopy and Western blotting. The exposure to 10 μM lupeol for 48 h markedly elevated the expressions of tyrosinase, MITF, a transcriptional factor of tyrosinase, Rab27a and myosin-Va in B16 2F2

cells (Fig. 1B). It was reported that Rab27a and myosin-Va, but not Slac2-a was stimulated in forskolin-induced B16 cell differentiation [7]. We examined the levels of Slac2-a in B16 2F2 cells treated with lupeol for 48 h, but lupeol did not modulate the expression of Slac2-a. We examined dendrite formations in B16 2F2 cells by lupeol. Following treatment with 10 μM lupeol for 4 h, actin stress fibers remained in the cytoplasm in B16 2F2 cells, and dendrites of the cells were not formed (Fig. 1C–a and b). By the lupeol treatment for 8 h, the disassembly of actin stress fibers in B16 2F2 cells and dendrite outgrowth were observed (Fig. 1C–c). Rearrangement of the actin cytoskeleton by inhibition of Rho signaling was found to trigger dendritic formation in melanoma cells [1, 4, 10]. These results suggested that lupeol attenuated the actin fiber assembly for 4–8 h, and this event caused dendritic formation in B16 2F2 cells.

3.2 Melanoma Cell Motility

It has been reported that disruptions in actin fiber assembly are involved in cancer cell motility and invasion [2]. We investigated the effects of lupeol on human cancer cell motilities. The results are summarized in Table 1. At 10 μM, lupeol did not influence the growth of nine types of cancer cells, and weakly inhibited HeLa cell proliferation. Lupeol at 10 μM markedly suppressed G361 melanoma and NB-1 neuroblastoma cell migration, and weakly suppressed A549 lung adenocarcinoma cell migration. However, lupeol at the same concentration did not inhibit the migration of other types of human cancer cells. These findings suggested that lupeol selectively suppressed the migration of melanoma and neuroblastoma cells, which are derived from the neural crest.

Table 1 Effects of Lupeol on growth and migration of cancer cells

Cell line (origin)	Cell growth (%)	Migration index (%)
G361 (melanoma)	97.5 ± 3.8	40.5 ± 3.1
NB-1 (neuroblastoma)	96.0 ± 2.5	39.7 ± 6.1
A549 (lung adenocarcinoma)	100.1 ± 7.4	87.3 ± 5.0
ACHN (renal adenocarcinoma)	106.3 ± 6.9	103.4 ± 4.8
HeLa (cervical carcinoma)	72.4 ± 2.3	101.4 ± 4.1
HT1080 (fibrosarcoma)	91.6 ± 6.5	100.6 ± 10.8
MIA Paca2 (pancreatic cancer)	99.1 ± 4.9	93.1 ± 4.7
Saos2 (osteogenic sarcoma)	100.0 ± 9.8	101.3 ± 5.0
SH-10-TC (stomach cancer)	99.6 ± 5.2	94.6 ± 4.1
T24 (urinary bladder carcinoma)	90.7 ± 5.5	101.5 ± 2.3

The effects of 10 μM lupeol on cell growth for 72 h and migration for 6 h were examined. The values represent percentages, relative to the control ($n = 4$).

3.3 Clinical Tests

In the cases I-III, in which melanoma cells metastasized to mandibular lymph nodes, we topically injected lupeol (0.75–1.5 mg per site in one time) at the metastatic sites. The melanoma at the metastatic sites was completely disappeared by injection of lupeol, but the primary melanomas progressed (cases I and II). In case III, lupeol induced the increase of melanosome in vivo, which is a hallmark of melanoma cell differentiation. In other 4 cases (cases IV-VII), we topically injected lupeol around primary sites after extirpations of melanoma areas at primary site without keeping surgery margins. In case IV, the tumor progression was suppressed and the focal lysis of tumor tissues was observed by lupeol alone. In cases V-VII, we took other therapies together lupeol including hyperthermia and immunotherapy. As the results, lupeol regulated the tumor progression in two (cases V and VI), and the melanoma in case V was completely disappeared; however, melanomas metastasized to whole body in one (case VII). In the present clinical tests, it was demonstrated that the repeat treatments with lupeol took some actions on 6 cases of 7 dogs with malignant melanomas. Especially, lupeol seemed to be more effective against the melanomas metastasizing to mandibular lymph nodes than those at primary sites. In the present point, we cannot explain exactly the phenomenon. However, one possible reason is that lupeol diffuse sufficiently in the lymph node when lupeol is injected into the lymph node. On the other hand, in primary tumor site, lupeol does not diffuse sufficiently around the tumor site because the tissue around the tumor site is rigid. In this point, we must investigate regarding interval of administration, concentration of lupeol, and range of injection area.

This work was supported in part by a Grant-in-aid for Scientific Research (20580352) from the Ministry of Education, Culture, Sports, Science and Technology.

References

1. Busca, R., Bertolotto, C., Abbe, P., Engalo, W., Ishizaki, T., Narumiya, S., Boquet, P., Ortonne, J.P., and Balotti, R. (1998) Inhibition of Rho is required for cAMP-induce melanoma cell differentiation. *Mol. Cell. Biol*. **9**: 1367–1378.
2. Byers, H.R., Etoh, T., Vink, J., Franklin, N., Gattoni-Celli, S., and Mihm, M.C. Jr. (1992) Actin organization and cell migration of melanoma cells relate to differential expression of integrins and actin-associated proteins. *J. Dermatol*. **19**: 847–852.
3. Garattini, E., Gianni, M., and Terao, M. (2007) Retinoids as differentiating agents in oncology: A network of interactions with intracellular pathways as the basis for rational therapeutic combinations. *Curr. Pharm. Des*. **13**: 1375–1400.
4. Hata, K., Hori, K., Murata, J., and Takahashi, S. (2005) Remodeling of actin cytoskeleton in lupeol-induced B162F2 cell differentiation. *J. Biochem*. **138**: 467–472.
5. Lee, T.K., Poon, R.T., Wo, J.Y., Ma, S., Guan, X.Y., Myers, J.N., Altevogt, P., and Yuen, A.P. (2007) Lupeol suppresses cisplatin-induced nuclear factor-kappaB activation in head and neck squamous cell carcinoma and inhibits local invasion and nodal metastasis in an orthotopic nude mouse model. *Cancer Res*. **67**: 8800–8809.

6. Murata, J., Ayukawa, K., Ogasawara, M., Watanabe, H., and Saiki, I. (1999). Induction of autocrine factor inhibiting cell motility from murine B16-BL6 melanoma cells by a-melanocyte-stimulating hormone. *Int. J. Cancer* **80**: 889–895.
7. Passeron, T., Bahadoran, P., Bertolotto, C., Chiaverini, C., Busca. R., Valony, G., Bille, K., Ortonne, J.P., and Ballotti, R. (2004) Cyclic AMP promotes a peripheral distribution of melanosomes and stimulates melanophilin/Slac2-a and actin association. *FASEB J*. **18**: 989–991.
8. Saleem, M., Kaur, S., Kweon, M.H., Adhami, V.M., Afaq, F., and Mukhtar, H. (2005) Lupeol, a fruit and vegetable based triterpene, induces apoptotic death of human pancreatic adenocarcinoma cells via inhibition of Ras signaling pathway. *Carcinogenesis* **26**: 1956–1964.
9. Saleem, M., Maddodi, N., Abu Zaid, M., Khan, N., bin Hafeez, B., Asim, M., Suh, Y., Yun, J.M., Setaluri, V., and Mukhtar, H. (2008) Lupeol inhibits growth of highly aggressive human metastatic melanoma cells in vitro and in vivo by inducing apoptosis. *Clin. Cancer Res*. **14**: 2119–2127.
10. Scott, G. and Leopardi, S. (2003) The cAMP signaling pathway has opposing effects on Rac and Rho in B16F10cells: Implications for dendrite formation in melanocyte cells. *Pigment. Cell Res*. **16**:139–148.
11. Zanardi, S., Serrano, D., Argusti, A., Barile, M., Puntoni, M., and Decensi, A. (2006) Clinical trials with retinoids for breast cancer chemoprevention. *Endocr. Relat. Cancer* **13**: 51–68.

The Effect of Secoisolariciresinol on 3t3-L1 Adipocytes and the Relationship Between Molecular Structure and the Activity

Shiori Tominaga, Takuya Sugahara, Sogo Nishimoto, Manami Yamawaki, Yuki Nakashima, Taro Kishida, Koichi Akiyama, Masafumi Maruyama, and Satoshi Yamauchi

1 Introduction

Secoisolariciresinol (SECO) is one of the most abundant dietary lignans. It occurs predominantly in a glycosylated form in food products. SECO is the major lignan found in flaxseed (*Linum usitatissimum* L.) and is present in a polymer containing secoisolariciresinol diglucoside (SDG). SECO, SDG and the polymers are known to have a number of health benefits, including reduction of serum cholesterol levels, delay in the onset of type II diabetes and decreased formation of breast, prostate and colon cancers. Research on the isolation and synthesis of SECO compounds has been continued by organic chemists. However, the relationship between the molecular structure and biological activity has not been elucidated. On the other hand, *meso*-SECO is not common and there is no report about the stereoselective synthetic research and biological investigation on *meso*-SECO.

In this article, the effects of three types of SECOs on adipogenesis were compared by using of mouse 3T3-L1 adipocytes.

2 Materials and Methods

2.1 SECO Compounds

(+)- and (–)-SECO were synthesized by the previously reported methods. (+)-SECO: colorless crystals, mp, 111–112°C (CHCl3-(*iso*-Pr), 114-115°C in literature, [α] 20D = +31 (c 0.3, acetone). NMR data agreed with those of literature. (–)-SECO: mp, 111–112°C (CHCl3-(*iso*-Pr) 2O). [α] 20D = -32 (c 0.3, acetone). Lit. [α] 20D = -35.5 (c 1.07, acetone). Purity of these compounds was checked by

S. Tominaga (✉)
Ehime University, Matsuyama, Ehime 790-8566, Japan
e-mail: shiori-t@agr.ehime-u.ac.jp

M. Kamihira et al. (eds.), *Animal Cell Technology: Basic & Applied Aspects*, Animal Cell Technology: Basic & Applied Aspects 16, DOI 10.1007/978-90-481-3892-0_57,

silica gel TLC (EtOAc/hexane = 1/1) and HPLC analysis by DAICEL chiral column AD-H revealed that the optical purity of each SECO was more than 95%ee. *meso*-SECO was also synthesized by the method as we previously reported [3].

2.2 Cells and Cell Culture

3T3-L1 preadipocytes obtained from ATCC were subcultured in ERDF medium (Kyokuto Pharmaceutical, Tokyo, Japan) supplemented with 10% fetal bovine serum (FBS) at 37°C in a humidified atmosphere of 5% CO_2. The differentiation of 3T3-L1 preadipocytes into adipocytes was initiated by the addition of 0.25 μM DEX, 0.5 mM IBMX and 5 μg/ml of insulin, followed by the cultivation of cells without DEX and IBMX until differentiation after 2 days. The media were changed every 2 days.

The estrogen-responsive cell line T47D-KBluc cells were obtained from ATCC. T47D-KBluc cells were used for assay of estrogen-like activity of SECO compounds. T47D-KBluc cells express lucifarase by stimulation of the potent estrogen or well-characterized weaker environmental estrogens. T47D-KBluc cells were subcultured in ERDF medium supplemented with 10% of FBS at 37°C in a humidified atmosphere of 5% CO_2. The culture media was replaced to ERDF medium with 10% charcoal-treated FBS 7 days before experiments to eliminate trace estrogens in FBS.

2.3 Assay of Adiponectin Production of 3T3-L1 Adipocytes

3T3-L1 adipocytes were cultured in 10% FBS-ERDF medium supplemented with each SECO compound at 0.3 mM. Two days after, the amount of adiponectin secreted in culture medium was determined by mouse adiponectin ELISA kit.

2.4 Reveres Transcription-Polymerase Chain Reaction (RT-PCR) Analysis

After 3T3-L1 adipocytes were differentiated, the cells were cultured in 10% FBS-ERDF medium supplemented with each SECO for 2 days. Cells were harvested and washed twice with PBS. Total RNA was prepared by using Sepasol RNA-I super (Nacalai Tesque, Kyoto, Japan) according to manufacture's instruction. One microgram of total RNA was used as a template for the cDNA synthesis reaction performed using MMLV-reverse transcriptase and an oligo-dT primer (Toyobo, Osaka, Japan). The resultant cDNA samples were subjected to 30 cycles of PCR amplification performed under the following conditions: denaturation at 98°C for 10 s, annealing at 60°C for 2 s, and DNA synthesis at 74°C for 30 s,

according to the manufacture's recommendation. The PCR reaction was performed using Takara Taq DNA polymerase (Kyoto, Japan). Mouse β-actin cDNA was amplified as an internal control. The PCR primer sequences were as follows: for mouse β-actin sense, 5'- TGG AAT CCT GTG GCA TCC ATG AAA C-3', and antisense, 5'- TAA AAC GCA GCT CAG TAA CAG TCC G-3'; for mouse Adiponectin sense, 5'- AGT GGA TCT GAC GAC ACC -3', and antisense, 5'- CTG TCA TTC CAA CAT CTC C-3'; for mouse PPARγ sense, 5'- GCT GTT ATG GGT GAA ACT CTG -3', and antisense, 5'- ATA AGG TGG AGA TGC AGG TTC -3'. The amplified PCR products were subjected to electrophoresis on a 1.0% agarose gel, and stained using SYBR Gold (Molecular Probes, Eugene, OR, USA).

2.5 Oil Red O Staining

3T3-L1 preadipocytes were grown to confluence in 48-well culture plate in ERDF medium supplemented with 10% FBS. The differentiation was induced 10% FBS-ERDF with 5 μg/ml of insulin, 0.25 μM DEX and 0.5 mM IBMX, and each SECO and E2 were added at 0.15 μM at the initiation of differentiation. At day 2 after induction, medium was changed to adipogenesis progression media; 10% FBS-ERDF medium supplemented with 5 μg/ml of insulin and 0.15 μM SECOs without DEX and IBMX, and the media were changed every 2 days. Two weeks after inoculation, oil red staining performed by using lipid assay kit (Primary Cell; Hokkaido, Japan) according to manufacture's instructions. Briefly, oil red O dissolved in isopropanol was kept overnight at room temperature, filtered, mixed with distilled water, kept overnight in the cold, and finally filtered twice before use. The final staining solution was 0.2% oil red O in 60% isopropanol. Cells were washed twice with PBS, and fixed for at least 15 min with fixed buffer containing formalin. The cells were washed twice with PBS, then stained for 15 min in a filtered oil red O solutions. After washing with distilled water, the stained cells were observed with a microscope. Following microscopic observation, cells were lysed with lysis buffer and TG accumulation was measured by absorbance at 540 nm.

2.6 Assay of Estrogen-Like Activity

The T47D-KBluc cells were seeded at 1 × 104 cells per well in 96-well plates and cultured in 10% FBS-ERDF medium with various concentrations of SECO compounds and 0.1 nM 17β-estradiol (E2). After 48 h, the cells were washed twice with PBS, and then lysis buffer (Promega, Wisconsin, USA) was added at 20 μl per well and incubated until cells were lysed (15–30 min) at room temperature. Luciferase assay was performed by using of luciferase reporter gene assay

kit (Promega). Luciferase activity was determined by Luminessencer-JNR AB 2100 (ATTO, Tokyo, Japan), and quantified as relative luciferase units (RLU).

3 Result

3.1 Effects of SECOs on the Adiponectin Production by 3T3-L1 Adipocytes

3T3-L1 adipocytes were stimulated by SECO compounds in 10% FBS-ERDF medium for 2 days. As shown in Fig. 1, only (–)-SECO accelerated adiponectin production by 3T3-L1 adipocytes 1.6-fold. In contrast, (+)- and meso-SECO depressed the adiponectin production. Thus, these facts indicated difference in structures of the SECO compounds have different influence on the adiponectin production.

3.2 Effects of SECOs on mRNA Expression of Adiponectin

To examine the mode of regulation of each SECO on adiponectin production, the mRNA level for adiponectin in 3T3-L1 cells treated with each SECO was examined. As a result, (–)-SECO up-regulated the expression of adiponectin mRNA level. On the other hand, (+)- and *meso*-SECO down-regulated the expression level. This result was correlated with the adiponectin production levels of 3T3-L1 cells treated with each SECO. In both cases, SECO affected mRNA expression level to regulate adiponectin production of 3T3-L1 cells.

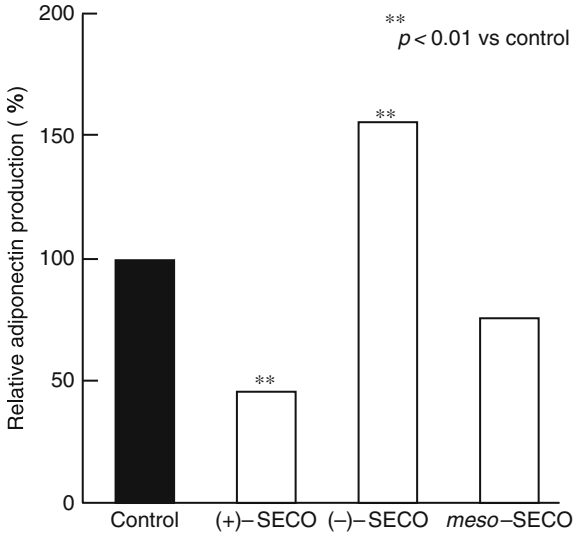

Fig. 1 Effects of SECOs on the adiponectin production by 3T3-L1 adipocytes

3.3 Effects of SECOs on Triglyceride Accumulation in 3T3-L1 Adipocytes

The differentiation was induced 10% FBS-ERDF with 5 μg/ml of insulin, 0.25 μM DEX, 0.5 mM IBMX, and 0.15 μM each SECO added to the medium at the initiation of differentiation. Two days after induction, medium was changed to adipogenesis progression media; 10% FBS-ERDF medium supplemented with 5 μg/ml insulin and 0.15 μM SECOs or E2, and the media were changed every 2 days. As shown in Fig. 2a, all SECOs and E2 significantly suppressed triglyceride (TG) accumulation. Especially, (–)-SECO obviously suppressed TG accumulation, and the oil droplets were much smaller than those in cells treated with other SECOs or E2. In addition, cytotoxicity of these substances was not observed at this concentration, and there was no difference in the rate of differentiation to adipocytes among these substances.

The quantitative analysis of TG content in 3T3-L1 adipocytes treated with SECO or E2 was performed by oil red O assay. As indicated in Fig. 2b, TG accumulation in 3T3-L1 cells stimulated with (–)-SECO was obviously lower than that in control cells.

3.4 Estrogen-Like Activity of SECOs

It is well known that SECO has estrogen activity. However, the activity was evaluated by using of the mixture of (+)- and (–)-SECO. To consider the structure-activity

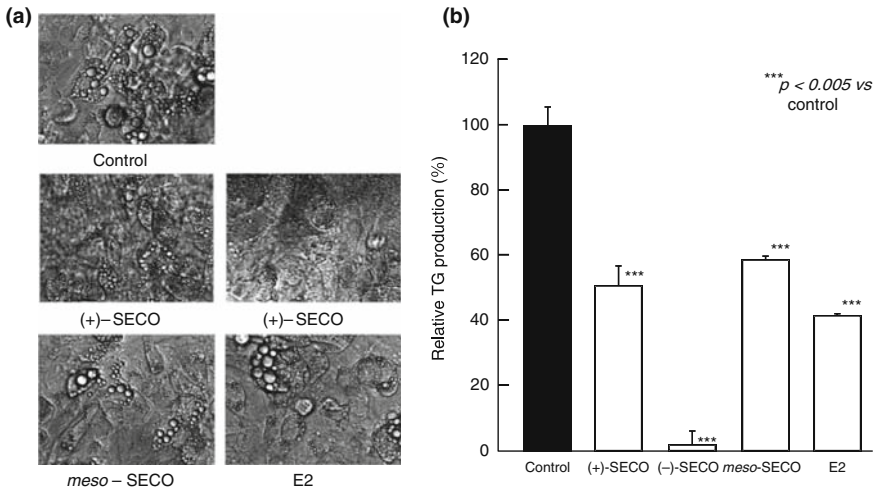

Fig. 2 Effects of SECOs on triglyceride accumulation in 3T3-L1 adipocyte

relationship of SECO on estrogen activity, estrogen activities of SECO compounds were compared. Estrogen-responsible lusiferase reporter gene assay using T47D-KBluc cells was performed. As a result, only (–)-SECO possessed estrogen activity. However, the activity was much lower than that of E2. The specific estrogen activity of (–)-SECO was less than 1/1000 of E2. In contrast, (+)- and meso-SECO did not have estrogen activity. This result suggests that estrogen activity of SECO from natural resources comes from only (–)-SECO.

4 Discussion

The research on the biological functions of SECO and SDG have been performed many researchers. In addition, it has been reported that SECO was converted to enterodiol and enterolactone, which are the compounds postulated to have anticarcinogenic properties, by intestinal microbes to mammalian lignans in body. However, the relationship between stereochemistry and biological activity has not been clear. We previously revealed the difference in biological functions such as immunological function, cytotoxic activity, and antioxidant activity [3]. The result showed that each optical isomer possesses different biological activities. This fact means that it is important to separate each optical isomer for precise analysis of the biological function of SECO. Recently, Fukumitsu et al [1]. reported that SDG reduced fat accumulation in mice, adiponectin mRNA expression level. In this report, we revealed that the structure-activity relationship between of SECO isomers on adipogenesis. As the result, (–)-SECO showed most beneficial effects on lipid metabolism. As shown in Fig. 2, adiponectin production was stimulated only by (–)-SECO, and (–)-SECO completely depressed lipid production without cytotoxicity. E2 also suppressed TG accumulation in 3T3-L1 cells, as much as (+)- and *meso*-SECO.

In addition, our previous study revealed that cell growth of human breast cancer MCF-7 cells was stimulated by (–)-SECO at 5 μM [3]. MCF-7 cells have estrogen receptor (ER) and the growth is stimulated by E2 or estrogen-mimicking compounds. It is supposed from these facts that (–)-SECO has estrogen-like activity and stimulates cell growth of MCF-7 cells via estrogen receptor. In fact, (–)-SECO exclusively had estrogen-like activity among SECO isomers. Our data indicated that E2 suppressed TG accumulation in 3T3-L1 cells. (–)-SECO strongly suppressed TG accumulation than E2. Matured 3T3-L1 cells are expressing both ERα and β, and ERα regulates insulin sensitivity [2]. ERs may concern with regulation of TG accumulation in 3T3-L1 adipocytes. However, (+)- and *meso*-SECO also suppressed TG production without estrogen activity. These facts suggest that although beneficial effects on lipid metabolism in 3T3-L1 cells partly come from estrogen-like activity of (–)-SECO, there are other pass ways except for estrogen-like activity for depressing TG accumulation by (–)-SECO. In addition, the concentration of (–)-SECO for suppression of TG accumulation was significantly lower than that for stimulation of adiponectin production. It is supposed from this fact that there are different pass ways for the adipogenesis in 3T3-L1 adipocytes induced by (–)-SECO.

References

1. Fukumitsu, S., Aida, K., Ueno, N., Ozawa, S., Takahashi, Y., and Kobori, M. (2008) Flaxseed lignan attenuates high-fat diet-induced fat accumulation and induces adiponectin expression in mice. *Br. J. Nutr*. **100**: 1–8.
2. Muraki, K., Okuya, S., and Tanizawa, Y. (2006) Estrogen receptor α regulates insulin sensitivity through IRS-1 tyrosine phosphorylation in mature 3T3-L1 adipocytes. *Endocr. J*. **53**: 841–851.
3. Sugahara, T., Yamauchi, S., Kondo, A., Ohno, F., Tominaga, S., Nakashima, Y., Kishida, T., Akiyama, K., and Maruyama, M. (2007) First stereoselective synthesis of *meso*-secoisolariciresinol and comparison of its biological activity with (+) and (–)-secoisolariciresinol. *Biosci. Biotechnol. Biochem*. **71**: 2962–2968.

Detection of Anti-Allergic Factors in Strawberry Extracts

Kazuhiro Mitsuda, Aiko Inoue, Norikazu Nishino, Yuichi Inoue, and Hiroharu Kawahara

1 Introduction

Pollinosis is well known as one of allergic problems in modern society. Many people are suffering from this disease every year from the end of February to the beginning of April. Allergies such as pollinosis are occurred by IgE antibodies. IgE produced when balance of type 1 helper T (Th1) and type 2 helper T (Th2) cells are inclined to Th2 cells. SOCS3 and SOCS5 are predominantly expressed in Th2 and Th1 cells, respectively, and they reciprocally inhibit the Th1 and Th2 differentiation processes [3, 4]. Therefore, we examined the effect of strawberry extracts on IgE production and gene expression for helper T cell differentiation.

Strawberry is rich in vitamin C, polyphenols including anthocyanin, flavonoid, phenylpropanoid and xylitol. It also contains the allergen Fra a1 homologue to the major birch pollen allergen Bet v1 [1]. The health-promoting functions of strawberry have been broadly investigated. But, the anti-allergic effects of strawberry have not well been studied. We reported here the anti-allergic action of their strawberry extracts.

2 Materials and Methods

2.1 Isolation of Lymphocytes from Whole Blood

Ficoll-Paque Plus (GE Healthcare, Sweden) is used for isolation of mononuclear cells from human peripheral blood by rapid centrifugation. Human blood samples were obtained from a healthy donor, and peripheral blood lymphocytes (PBL) were separated from each blood sample with Ficoll-Paque Plus. PBL were cultured in 5% FBS (Thermo Fisher Scientific, USA) –10% human plasma-ERDF

K. Mitsuda (✉)
Graduate School of Life Science and Systems Engineering, Kyushu Institute of Technology, Wakamatsu-ku, Kitakyushu-shi, Fukuoka 808-0196, Japan
e-mail: mitti_mitimiti@yahoo.co.jp

M. Kamihira et al. (eds.), *Animal Cell Technology: Basic & Applied Aspects*, Animal Cell Technology: Basic & Applied Aspects 16, DOI 10.1007/978-90-481-3892-0_58,

medium (Kyokuto Pharmaceutical Industrial Co., Tokyo, Japan). Human plasma was separated from the heparinized blood original donor.

2.2 Preparation of Strawberry Extracts

Strawberry extracts were prepared as follows. Strawberries were homogenized at 6,000 rpm for 30 s at 0°C, and equal amount of PBS was added to it. The homogenate was centrifuged at 8,300×g for 60 min at 4°C, and the supernatant was sterilized by a 0.22 μm filter. The obtained filtrate was used for the experiments as the strawberry extracts.

2.3 Effect of Strawberry Extracts on IgE Production

To investigate the effects of strawberry extracts on IgE production, an in vitro IgE inducing method was used [2]. 2.5×10^6 cells/ml of PBL were cultured in 5% FBS-10% human plasma-ERDF medium containing 10 ng/ml of recombinant human IL-2, IL-4, IL-6 (R&D systems, USA), 10 μg/ml of Muramyl dipeptide (MDP) (SIGMA, USA), and 100 ng/ml of the ceder pollen antigen Cryj1 (HAYASHIBARA, Japan), with or without 5% (v/v) of strawberry extracts. As a positive control, 100 ng/ml of epicatechin gallate (ECg) derived from tea leaves were used. After 10 days, the concentration of total IgE antibody in the supernatant was measured by an enzyme-linked immunosorbent assay (ELISA) and compared between control and sample containing strawberry extracts. Cells were recovered and used for RT-PCR abalysis.

2.4 Measurement of Total IgE Concentration

Total IgE concentrations in culture medium were measured by ELISA, using anti-human IgE antibody (#AHI0510; Biosource International., USA) as the first antibody, and anti-human IgE peroxidase-conjugated antibody (#AHI 0504; Biosource International Inc., USA) as the second antibody.

2.5 RT-PCR Analysis

Total RNA was recovered from PBL using ISOGEN (NIPPON GENE, Japan). Reverse transcription was done using Thermo Script RT-PCR System as described in a common protocol (GE Healthcare). The following primers were used to amplify the genes for helper T cell differentiation and the beta-actin gene as a control. Forward primer (5'-CAAGACCTT CAGCTCCA-3') and reverse primer (5'-CAGAGCTACAG GACTCTCTC-3') were used to amplify SOCS3 (suppressor of cytokine signaling 3). Forward primer (5'-AGTA GAATTGTATTGAAAGGC-3')

and reverse primer (5'-CATTTACAAGAGAAATTGTTG-3') were used to amplify SOCS5. Forward primer (5'-GACTTCGAGCAAGAGATG -3') and reverse primer (5'-GCCAGACAGCACTGTGTT -3') were used to amplify beta-actin. The amplification conditions used for SOCS3 (720 bp) and SOCS5 (870 bp) were 40 cycles for 94°C for 40 s, 57°C for 40 s, 72°C for 1 min. The PCR condition of beta-actin (240 bp) was 20 cycles for 94°C for 40 s, 52°C for 40 s, 72°C for 1 min. Amplified bands are analyzed as gene expression level by NIH image.

2.6 Biacore Analysis

Binding of the strawberry extracts to Cryj1 was measured using Biacore X instrument. Briefly, Cryj1 (20 μg/ml) in 10 mM sodium acetate, pH 3.0 was immobilized to the Sensor Chip CM5 surface by amine coupling according to a common protocol (GE Healthcare). CM5 surface were coupled to final resonance values of 12500 response units (RU) for Cryj1. HBS EP buffer, pH 7.4 (10 mM HEPES, 150 mM NaCl, 3.4 mM EDTA, 0.005% surfactant P20, pH 7.4) was used for immobilization and binding assays. Strawberry A extract and PBS were injected to the Cryj1 immobilized chip at 20 μl/min and monitored until equilibrium. Representative curves were indicated for the association and the dissociation phase.

3 Results and Discussion

3.1 Suppressive Effects of Strawberry Extracts on IgE Production

To investigate the anti-allergic effects of strawberry extracts, we used 18 breeds of strawberries. Most strawberry extracts suppressed IgE production and their suppressive effects were different among the breeds tested (Fig. 1). Strawberry A extract was the best in the decrease of IgE production and it effects was as much as an anti-allergic factor ECg. However, vitamin C, which is abundantly included in strawberries, was little effect. This suggested that the decreased IgE production was not caused by anti-oxidant action.

3.2 RT-PCR Analysis of Gene Expression for Helper T Cell Differentiation

Gene expression for helper T cell differentiation was examined by RT-PCR. As a result, SOCS3 gene expression that is related to Th2 differentiation was found to be significantly decreased by strawberry A extracts when compared with control (Fig. 2 left). This corresponded to total IgE production (Fig. 2 right). However, SOCS5 gene expression that is related to Th1 differentiation did not change. These findings suggest that strawberry extracts may suppress IgE production by decreased Th2 differentiation.

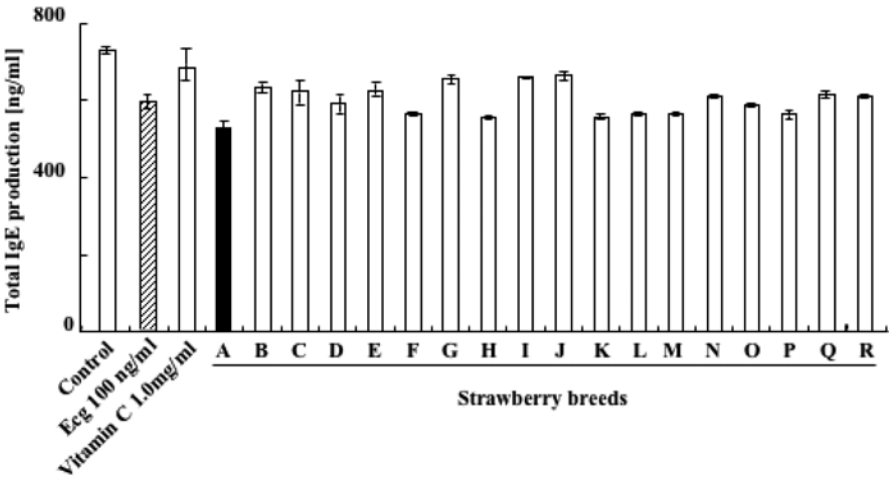

Fig. 1 Suppressive effects of strawberry extracts on IgE production

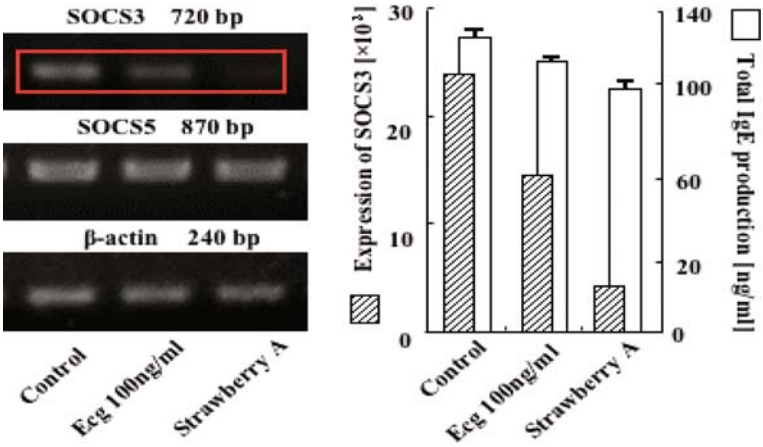

Fig. 2 Gene expression for helper T cell differentiation and its relation to IgE production

3.3 Interaction of Strawberry Extracts with Cryj 1

The binding of strawberry A extract to Cryj1 was examined by Biacore analysis. It revealed that there is a factor with the ability to bind with Cryj1 in the extracts. Cryj1 has the pectate lyase like activity that can degrade pectin, a component of plant cell walls [5]. Strawberry also includes many pectin components. This means that they may bind to Cryj1 as a substrate. But, apple pectin did not bind with Cryj1 (data not shown). Therefore, the strawberry-derived factor binding to Cryj1 need to be further investigated (Fig. 3).

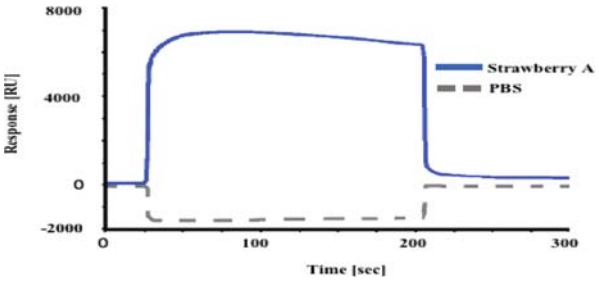

Fig. 3 Interaction of strawberry a extracts with Cryj1 by biacore analysis

4 Conclusions

We reported here that strawberry had anti-allergic effects. Our results suggest that the strawberry extracts may suppress the allergic reaction by acting on both Th2 cells and Cryj1 allergen. However, further study is needed to identify anti-allergic factors in strawberry extracts.

References

1. Hjerno, K., Alm, R., Canback, B., et al. (2006) Down-regulation of the strawberry Bet v 1-homologous allergen in concert with the flavonoid biosynthesis pathway in colorless strawberry mutant. *Proteomics* **6**(5): 1574–1587.
2. Inoue, H. and Kubo, M. (2004) SOCS protein in T helper cell differentiation : Implication for allergic disorder. *Expert Rev. Mol. Med*. **6**:1–11.
3. Kawahara, H., et al. (2000) Effective induction and acquisition of human monoclonal IgE antibodies reactive with house-dust mite extracts. *J. Immunol. Methods* **233**: 33–40.
4. Kubo, M., Hanada, T., and Yoshimura, A. (2003) Suppressors of cytokine signaling and immunity. *Nat. Immunol*. **4**: 1169–1176.
5. Midoro-Horiuti, T., Mathura, V., Schein, C.H., et al. (2003) Major linear IgE epitopes of mountain cedar pollen allergen Jun a 1 map to the pectate lyase catalytic site. *Mol. Immunol*. **43**: 555–562.

Anti-Melanogenic Activity of Yacon Leaves in Mouse Melanoma Cells

Anti-Melanogenic Activity of Traditional Andean Food Yacon

Tomoyuki Ishikawa, Toshio Hyakutake, Yasuaki Gondou, Mitsuhiro Sakai, Reiko Kinoshita, Jyunji Tottori, Hiroshi Kunitake, and Ken-Ichi Kusumoto

1 Introduction

Traditional food yacon (*Smallanthus sonchifolius*), a plant of asteraceae, is originally cultivated in the Andean of South America. Yacon contains beta-1, 2-oligofructans and polyphenols abundantly. Yacon leaves are used as a tea and the roots can be eaten raw. The leaves are known to contain components that led to a suppressing rise in blood glucose levels. Kurume city is one of the municipalities that an agricultural output is high in Japan. Although a number of agricultural products are cultivated in Kurume city, there isn't unique one. Therefore, we focused on a specialty product yacon as an attractive healthy vegetable. In the present, we have cultivated yacon to introduce functional yacon tea and confectionery.

Natural compounds known to exhibit anti-meanogenic activity such as arbutin or vitamin C are widely used in medical and cosmetic fields. Tyrosinase, a key enzyme of melanin synthesis, is targeted for anti-melanogenic activity. The mechanisms of suppression of melanin synthesis differ depending on the chemical structure of natural compounds. Most major mechanism is to directly inhibit activity of tyrosinase. Also, it is known to inhibit intracellular expression of tyrosinase by affecting a factor of signaling on melanin synthesis or to positively regulate proteasome mechanism to degrade tyrosinase.

In this report, we demonstrate that yacon leaf extracts have an anti-melanogenic activity to suppress melanin synthesis in mouse B16 melanoma cells. Natural components to exhibit anti-melanogenic activity were extracted and purified from yacon leaves by using an ethanol extraction, a silica-gel column, and reverse-phase high-pressure liquid chromatography C-18 column. Our results suggest that this approach can propose a novel biological function of traditional food yacon for suppressing melanin synthesis.

T. Ishikawa (✉)
Department of Biological Chemistry, Biotechnology and Food Research Institute, Fukuoka Industrial Technology Center, Kurume, Fukuoka 839-0861, Japan
e-mail: tishikawa@fitc.pref.fukuoka.jp

M. Kamihira et al. (eds.), *Animal Cell Technology: Basic & Applied Aspects*, Animal Cell Technology: Basic & Applied Aspects 16, DOI 10.1007/978-90-481-3892-0_59,

2 Materials and Methods

2.1 Yacon Leaf

Fresh leaves of yacon were supplied by Nomura's Farm in Kurume city. Yacon leaves were immediately freeze-dried and stored at –30°C (Fig. 1).

Fig. 1 Photograph of yacon cultivated by Nomura's Farm in Kurume city, Fukuoka, Japan; leaves (*left*) and roots (*right*)

2.2 Cell Culture and Cell Culture

Mouse melanoma B16 cells (American Type Culture Collection) were cultured in Dulbecco's modified Eagle's Medium (DMEM, Invitrogen) with 10% fetal bovine serum (FBS) at 37°C in a humidified atmosphere containing 5% CO_2.

2.3 Extraction of Yacon Leaves with Various Solvents

Freeze-dried yacon leaves were incubated for 24 h at 4°C in the following solvent (50 mg/ml); distilled water, ethanol, methanol, chloroform, ethyl acetate, hexane, and acetone. Samples extracted with four kinds of solvents (ethyl acetate, chloroform, hexane, and acetone) were evaporated and then dissolved with equal volume of methanol. In addition, the freeze-dried products were incubated for 1 h at 95°C in distilled water.

2.4 Anti-Melanogenic Analysis in Mouse B16 Melanoma Cells

B16 cells were precultured in 96-well plate at a density of 2.0×10^4 cells/well in 0.1 ml DMEM with 10% FBS. Culture medium was changed to DMEM with 10% FBS and 2 mM theophyline (Sigma). Each extract was added in the cells in the

presence of theophyline and the cells were incubated for a week at 37°C. After treatment, the cells were lysed by 0.9% Triton X-100 and incubated for 1 h at room temperature. Anti-melanogenic activity was measured by the absorbance of 414 nm and expressed as the percentage of decreasing amounts of melanin via total amounts of control cells and positive control cells treated with 1.64 mM Phenylthiourea (PTU, Sigma).

2.5 Purification of Ethanol Extracts from Yacon Leaves Using a Silica-Gel Column and a Reverse-Phase High-Pressure Liquid Chromatography C-18 Column

Freeze-dried products of yacon leaves (10 g) were incubated overnight in 200 ml of ethanol at 4°C (termed as Ethanol extracts). Ethanol extracts (20 ml) were loaded on a silica-gel column with methanol and a flow-through was collected (termed as Flow-through fraction with methanol). After the flow-through fractions were evaporated, the residues were dissolved in a solution of chloroform:methanol = 40:1 (v/v). The dissolved solution was loaded on a silica-gel column with chloroform-methanol solution (40:1) and flow-through fractions were collected (termed as 40:1 fraction). Subsequently, the column was subjected with chloroform-methanol solution (20:1) and the eluates were collected as a fraction at 25 ml. Finally, the column was eluted with chloroform-methanol solution (5:1) and then methanol in turn, in which these eluates were collected (termed as 5:1 fraction and 0:1 fraction, respectively).

Fractions having anti-melanogenic activity (termed as T3 fraction) were collected and subjected on a reverse-phase high-pressure liquid chromatography C-18 column, Sunfire (Waters Corporation). After the T3 fraction was injected, the column was washed for 20 min with the solvent of methanol-water (7:3), eluted for 15 min with a gradient from methanol-water (7:3) to methanol, and eluted for 20 min with methanol. In all steps, a flow rate was 1 ml/min and fraction volume was 2 ml. Each fraction was resolved by thin-layer chromatography (TLC) analysis that is developed with chloroform-methanol solution (20:1) and detected by phosphomolybdic acid.

3 Results and Discussion

3.1 Anti-Melanogenic Activity of Yacon Leaf Extracts with Various Solvents in Mouse B16 Melanoma Cells

We tried to estimated anti-melanogenic activity in crude extracts of yacon leaves with various solvents in mouse B16 melanoma cells (Fig. 2). Extracts from five kinds of solvents; ethanol, methanol, ethyl acetate, chloroform, and acetone, exhibited anti-melanogenic activity at 500 μM, whereas, extracts from three kinds of solvents; cold water, hot water, and hexane, had no effects at 500 μM. Ethanol

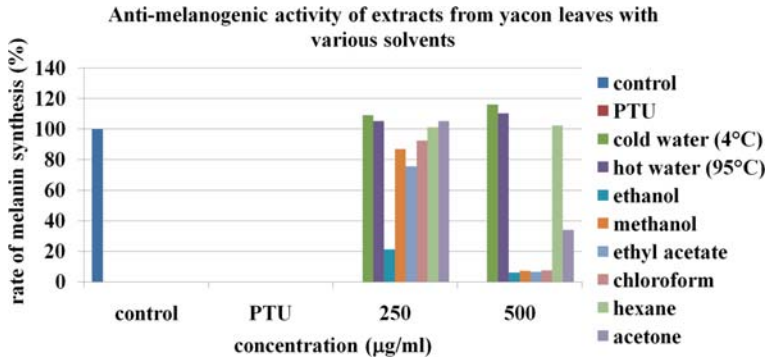

Fig. 2 Anti-melanogenic activity of yacon leaf extracts with various solvents; cold water, hot water, ethanol, methanol, ethyl acetate, chloroform, hexane, and acetone. B16 cells were treated with extracts from eight kinds of solvents or with PTU as a positive control for a week in 96-well plate. After incubation, the cells were lysed with Triton X-100, and then absorbance of 414 nm was read. Control of no treatment and positive control treated with PTU were calculated as 100% and 0% of the rate of melanin synthesis respectively, and each extracts was calculated at the rate of melanin synthesis against control and PTU

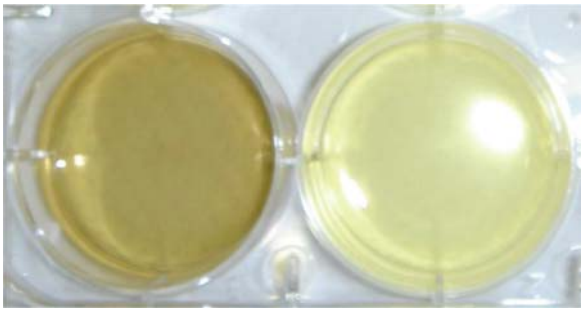

Fig. 3 Photograph of mouse B16 cell-cultured plate. B16 cells were cultured at the presence of yacon extracts. *Left*; control, treatment with 2 mM theophyline to induce melanin synthesis. *Right*; yacon leaves, treatment with ethanol extracts in the presence of theophyline

extracts only exhibited anti-melanogenic activity at 250 μM. These results showed that natural compounds of yacon leaves to be exhibiting anti-melanogenic activity in B16 cells are effectively extracted by using ethanol (Fig. 3).

3.2 Purification of Natural Compound from Ethanol Extracts of Yacon Leaves to be Exhibiting Anti-Melanogenic Activity in B16 Cells by Using a Silica-Gel Column and a Reverse-Phase High-Pressure Liquid Chromatography C-18 Column

We first attempted fractionation of the ethanol extracts from yacon leaves by using a silica-gel column. In this method, ethanol extracts of yacon leaves were generated

a precipitation by dissolving with organic solvent such as chloroform. Therefore, ethanol extracts were loaded on a silica-gel column with methanol to get rid of the precipitation generated in a hydrophobic environment. A flow through fraction was recovered by 83.9% of ethanol extracts. The relative activity of this flow through fraction elevated at 1.08-fold than that of ethanol extracts. Again, this flow through fraction was loaded on a silica-gel column with chloroform-methanol solution (40:1). The relative activity of 40:1 fraction elevated at 2.58-fold than that of ethanol extracts, which suggested that this fraction still contains compounds having anti-melanogenic functions. The relative activity of 20:1 fraction (T3 fraction) decreased at 0.311-fold than that of ethanol extracts. T3 fraction was homogeneously detected by TLC analysis. The 5:1 fraction eluted with chloroform-methanol (5:1) and 0:1 fraction eluted with methanol had little anti-melanogenic activity. Subsequently, T3 fraction was further purified by using a reverse-phase high-pressure liquid chromatography C-18 column. Each fraction separated on C-18 column was developed by TLC analysis. T3 fraction purified (termed as T3) was examined both in anti-melanogenic activity and in the preventive effects of intracellular tyrosinase in B16 cells. The identification and characterization of this compound as a melanogenic inhibitor will be presented in the future.

3.3 Anti-Melanogenic Activity by T3 Fraction in Mouse B16 Melanoma Cells

The purity of T3 was confirmed by TLC analysis (Fig. 5) and nuclear magnetic resonance (NMR) spectroscopy. T3 was evaluated in anti-melanogenic activity in B16 cells. A concentration suppressing half amount of melanin synthesis against control was 45.7 μM (Fig. 4). These results showed that anti-melanogenic mechanisms of T3 are to inhibit tyrosinase on melanin synthesis as well as that of arbutin.

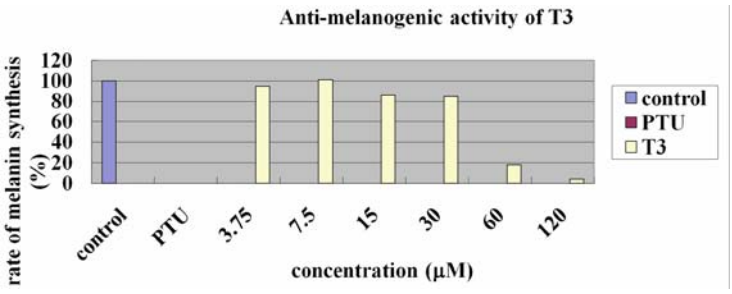

Fig. 4 Anti-melanogenic activity of T3 purified on C-18 column. B16 cells were treated with each concentration of T3 or with PTU as a positive control for a week in 96-well plate. After incubation, cells were lysed with Triton X-100, and then absorbance of 414 nm was read. Control of no treatment and positive control treated with PTU were calculated as 100% and 0% of the rate of melanin synthesis respectively, and each concentration of T3 was calculated at the rate of melanin synthesis against control and PTU

Fig. 5 TLC analysis of T3 purified on C-18 column. T3 was resolved and confirmed the purity by TLC analysis that is developed with chloroform-methanol solution (20:1) and then detected by phosphomolybdic acid

In summary, we extracted by using various types of solvents and purified natural component from yacon leaves to be exhibiting anti-melanogenic activity in B16 cells. T3 purified from ethanol extracts exhibited anti-melanogenic activity at 45.7 μM, a concentration suppressing half amount of melanin synthesis. Arbutin, a well-known compound for exhibiting anti-melanogenic activity, suppressed melanin synthesis to about 39% at 50 μM. Thus, these results are suggested that the anti-melanogenic activity of T3 is strong as well as that of arbutin. The elucidation of mechanism that T3 suppresses melanin synthesis needs further study. In the present, we are determining the chemical structure of T3. The chemical structure of T3 may be contributed to medical and cosmetic fields.

Cytokine Responses of Splenocytes of Female and Male Non-Obese Diabetic Mice Induced by Lactic Acid Bacteria

Atsushi Enomoto, Mohd Azraai Bin Jamal, Hiromi Mitsui, Hiromi Kimoto-Nira, Chise Suzuki, and Koko Mizumachi

1 Introduction

It has been well recognized that the incidences of autoimmune diseases such as insulin-dependent diabetes mellitus (IDDM) and rheumatoid arthritis (RA) are largely influenced by genetic factors [1, 2]. For example, non-obese diabetic (NOD) mice, an animal model for spontaneous IDDM, show a clear female predilection [3]. Genetic defects alone are not, however, sufficient to cause autoimmune diseases, and environmental factors including drug, food and microbial conditions are also involved [4–6], although their precise mechanisms are not clear at present. To find useful probiotics capable of effectively suppressing the onset of IDDM, we here examined and compared cytokine responses of spleen cells of female and male NOD mice induced by 2 strains of lactic acid bacteria, *Lactococcus lactis* subsp. *lactis* G50 and *Lactobacillus acidophilus* JCM1132.

2 Materials and Methods

2.1 Lactic Acid Bacteria

Lc. lactis G50 is maintained in the International Patent Organism Depository (FERM P-18415; Tsukuba, Japan) and has the immunomodulatory activity such as reduction of IgE level in mouse serum [7]. *Lb. acidophilus* JCM1132^{T}, a reference strain for probiotics [8], was obtained from the Japan Collection of Microorganisms (Wako Pure Chemical Industries, Saitama, Japan).

A. Enomoto (✉)
Department of Chemistry and Chemical Biology, Gunma University, Kiryu, Gunma 376-8515, Japan
e-mail: enomoto@chem-bio.gunma-u.ac.jp

M. Kamihira et al. (eds.), *Animal Cell Technology: Basic & Applied Aspects*, Animal Cell Technology: Basic & Applied Aspects 16, DOI 10.1007/978-90-481-3892-0_60,

2.2 Cytokine Responses

Female and male NOD mice were purchased from Clea Japan, Tokyo, and used at 10–11 weeks of age. Spleen cells from the prediabetic mice were cultured at a concentration of 1.0×10^7 cells/well with or without 10 μg/ml of a peptide fragment of glutamic acid decarboxylase 65, from amino acid residues 524 through 543 (GAD 524–543) and 5 μg/ml of the heat-killed lactic acid bacteria, *Lc. lactis* G50 or *Lb. acidophilus* JCM1132, in HL-1 medium (Cambrex Bio Science Walkersville, MD) in a flat-bottom 24-well culture plate (Asahi Techno Glass, Tokyo, Japan) for 3 days. In some experiments, splenocytes of BALB/c mice (Clea Japan) were used in the place of NOD mice. The culture supernatants were collected at day 1, 2 and 3, and then tested for production of various cytokines such as IL-4, 6, 10, 12, IFN-γ and TGF-β by ELISA, according to the manufacture's instructions (BD Biosciences Pharmingen, San Diego, CA).

The use and care of the animals in this study were approved by Animal Care and Experimentation Committee of Gunma University (No. 07–110).

3 Results and Discussion

In female NOD mice, both strains of lactic acid bacteria were usually found to induce the secretion of IL-6, 10, 12 and IFN-γ among the above 6 cytokines, although none of the cytokines could be detected in the supernatants without the bacterial stimulation, even in the presence of GAD 524–543, an important epitope of the autoantigen [9] (Figs. 1, 2, 3, and 4). The magnitude of each cytokine response elicited by the lactic acid bacteria was, however, different between the 2 strains.

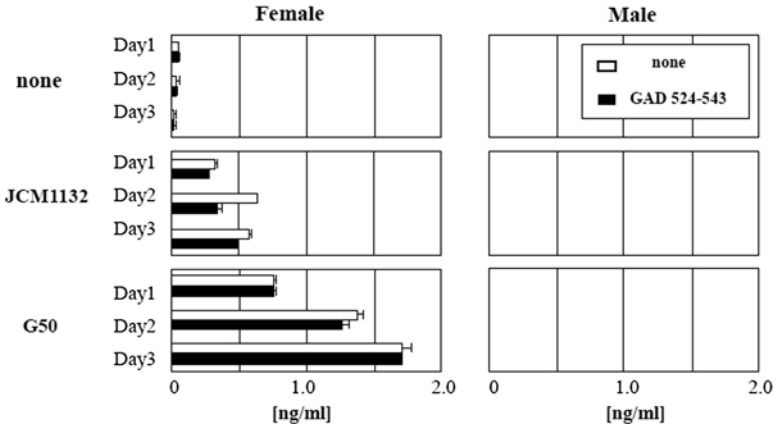

Fig. 1 IL-6 production of splenocytes of female (*left panel*) and male (*right panel*) NOD mice in response to *Lb. acidophilus* JCM1132 (*middle panel*) and *Lc. lactis* G50 (*lower panel*) in the presence (*closed bar*) or absence (*opened bar*) of GAD 524–543

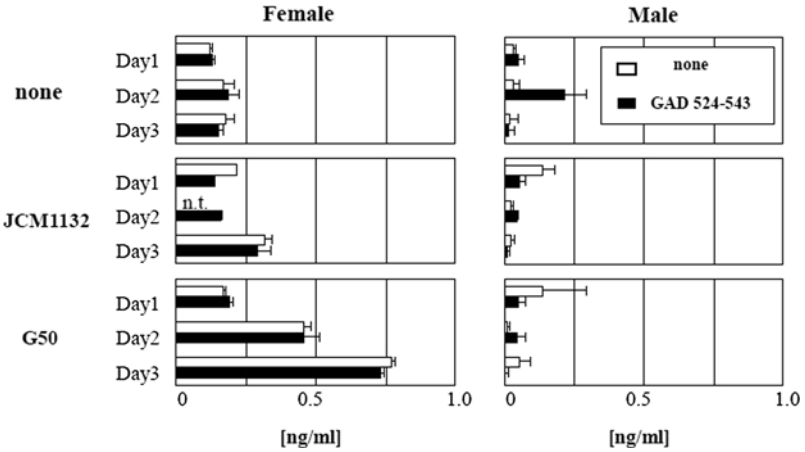

Fig. 2 IL-10 production of splenocytes of female (*left panel*) and male (*right panel*) NOD mice in response to *Lb. acidophilus* JCM1132 (*middle panel*) and *Lc. lactis* G50 (*lower panel*) in the presence (*closed bar*) or absence (*opened bar*) of GAD 524–543. n.t. = not tested

For example, the spleen cells secreted large quantities of IL-12, a cytokine for Th1 differentiation, but slight amounts of IL-10 in response to *Lb. acidophilus* JCM1132, while *Lc. lactis* G50 induced extremely high production of IL-10, an immunosuppressive cytokine, but low level of IL-12 (Figs. 1, 2, 3, and 4). These results suggest that *Lc. lactis* G50 might protect the female NOD mice from spontaneously developing IDDM, because both Th1 and Th17 cells are considered to mediate the induction and exacerbation of IDDM [10, 11].

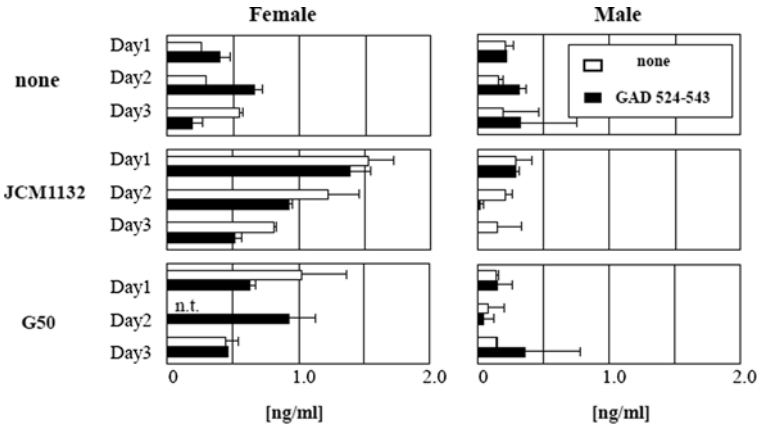

Fig. 3 IL-12 production of splenocytes of female (*left panel*) and male (*right panel*) NOD mice in response to *Lb. acidophilus* JCM1132 (*middle panel*) and *Lc. lactis* G50 (*lower panel*) in the presence (*closed bar*) or absence (*opened bar*) of GAD 524–543. n.t. = not tested

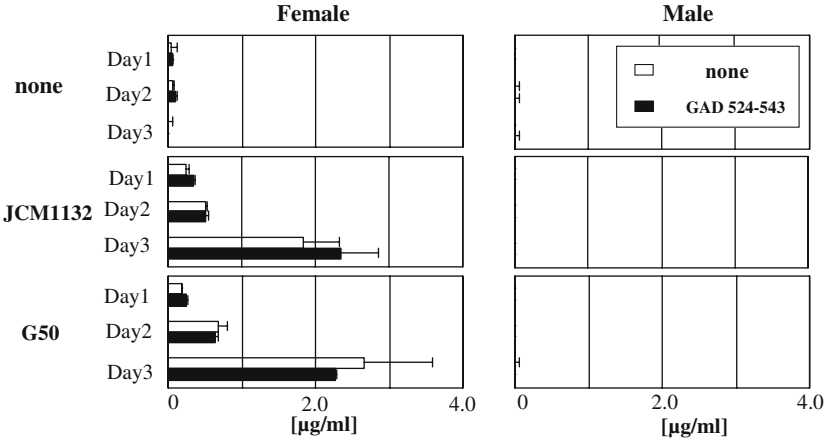

Fig. 4 IFN-γ production of splenocytes of female (*left panel*) and male (*right panel*) NOD mice in response to *Lb. acidophilus* JCM1132 (*middle panel*) and *Lc. lactis* G50 (*lower panel*) in the presence (*closed bar*) or absence (*opened bar*) of GAD 524–543

Interestingly, the splenocytes of male NOD mice with low susceptibility to IDDM did not produce all the cytokines tested in this study in response to the lactic acid bacteria (Figs. 1, 2, 3 and 4). Such sex differences were not so clear in the case of BALB/c mice, but IL-6, 12 and IFN-γ responses were shown to be somewhat higher in the female mice, as compared with those in the male mice (Figs. 5 and 6). From these results, it is suggested that female NOD mice with high sensitivity to IDDM tend to elicit more vigorous T cell activation in response to the lactic acid bacteria than the male mice.

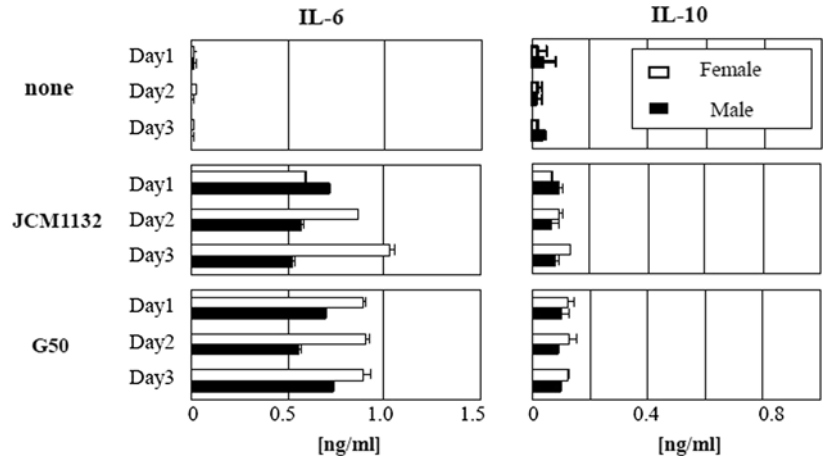

Fig. 5 IL-6 (*left panel*) and IL-10 (*right panel*) production of splenocytes of female (*opened bar*) and male (*closed bar*) BALB/c mice in response to *Lb. acidophilus* JCM1132 (*middle panel*) and *Lc. lactis* G50 (*lower panel*)

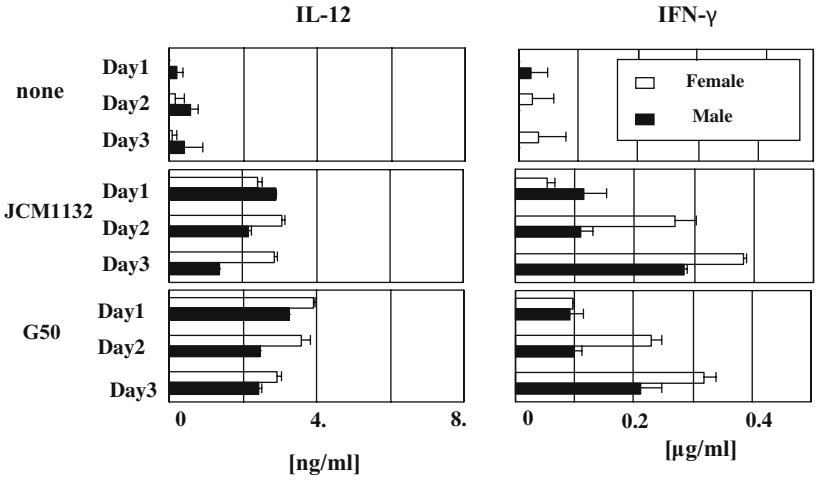

Fig. 6 IL-12 (*left panel*) and IFN-γ (*right panel*) production of splenocytes of female (*opened bar*) and male (*closed bar*) BALB/c mice in response to *Lb. acidophilus* JCM1132 (*middle panel*) and *Lc. lactis* G50 (*lower panel*)

Acknowledgments The authors thank Mr. Takahiro Takeuchi of Gunma University for his experimental assistance.

References

1. Gonzalez, A., Katz, J.D., Mattei, M.G., Kikutani, H., Benoist, C., and Mathis, D. (1997) Genetic control of diabetes progression. *Immunity* **7**: 873–883.
2. McDevitt, H.O. (2000) Discovering the role of the major histocompatibility complex in the immune response. *Annu. Rev. Immunol*. **18**: 1–17.
3. Whitacre, C.C. (2001) Sex differences in autoimmune diseases. *Nature Immunol*. **2**: 777–780.
4. Bach, J.-F. and Chatenoud, L. (2001) Tolerance to islet autoantigens in type 1 diabetes. *Annu. Rev. Immunol*. **19**: 131–161.
5. Ermann, J. and Fathman, C.G. (2001) Autoimmune diseases: genes, bugs and failed regulation. *Nature Immunol*. **2**: 759–761.
6. Kamradt, T., Goggel, R., and Erb, K. J. (2005) Induction, exacerbation and inhibition of allergic and autoimmune diseases by infection. *Trends Immunol*. **26**: 260–267.
7. Kimoto, H., Mizumachi, K., Okamoto, T., and Kurisaki, J. (2004) New *Lactococcus* strain with immunomodulatory activity: enhancement of Th1-type immune response. *Microbiol. Immunol*. **48**: 75–82.
8. Lidbeck, A., Geltner-Allinger, U., Orrhage, K.M., Ottova, L., Brismar, B.J., Gustafsson, A., Rafter, J.J., and Nord, C.E. (1991) Impact of *Lactobacillus acidophilus* supplements on the faecal microflora and soluble faecal bile acids in colon cancer patients. *Microbiol. Ecol. Health Disease* **4**: 81–88.
9. Kaufman, D.L., Clare-Salzler, M., Tian, J., Forsthuber, T., Ting, G.S.P., Robinson, P., Atkinson, M.A., Sercarz, E.E., Tobin, A.J., and Lehmann, P.V. (1993) Spontaneous loss of T-cell tolerance to glutamic acid decarboxylase in murine insulin-dependent diabetes. *Nature* **366**: 69–72.

10. Jain, R., Tartar, D.M., Gregg, R.K., Divekar, R.D., Bell, J.J., Lee, H.-H., Yu, P., Ellis, J.S., Hoeman, C.M., Franklin, C.L., and Zaghouani, H. (2008) Innocuous IFNγ induced by adjuvant-free antigen restores normoglycemia in NOD mice through inhibition of IL-17 production. *J. Exp. Med*. **205**: 207–218.
11. Spolski, R., Kashyap, M., Robinson, C., Yu, Z., and Leonard, W.J. (2008) IL-21 signaling is critical for the development of type 1 diabetes in the NOD mouse, *Proc. Natl. Acad. Sci. USA* **105**: 14028–14033.

Development of a High-Throughput Evaluation System for Antiviral Activities of Food Factors By Using Bioinformatics

Nozomu Eto, Kiyoko Nagahama, Shohei Miyamoto, Osayoshi Yamaguchi, Sayumi Miyauchi, Takako Iwata, Asuka Uchida, and Kunihito Yamamori

1 Introduction

To elucidate food functionality maintaining health is one of the most expected things in science activity for the human. Various physiological functions of food factors are being evaluated and the most are for the purpose of prevention of life-style related diseases or to raise biophylaxis ability. An estimated 170 million individuals in the world are infected with hepatitis C virus (HCV), a serious cause of chronic liver disease [4]. Although the acute phase of infection is usually associated with mild symptoms, approximate 80% of HCV infection results in chronic infection that frequently leads to severe chronic liver disease; 20–30% of infected individuals may develop cirrhosis and 1–3% may develop liver cancer. Therefore, screening a new food factor for chronic HCV is a major public health objective. A point of view of phylaxis for viruses such as influenza is important as well as a HCV, too. There are many functions which should be measured, for example, as well as above, antioxidation activity, anti-metastatic activity, anti-angiogenic activity, anti-inflammatory activity and so on. However, to measure all necessary bioactivity makes serious demands upon investigator's time. Therefore we want to suggest a new method to evaluate plural functions at the same time by applying artificial neural network [1, 2]. Neural networks, with their remarkable ability to derive meaning from complicated or imprecise data, can be used to extract patterns and detect trends that are too complex to be noticed by either humans or other computer techniques. In this study, we chose anti-HCV activity and natural killer (NK) cell activation activity as the plural bioactivities for simultaneous evaluation, and demonstrated that those bioactivities was able to be predicted with high precision at the same time.

N. Eto (✉)
University of Miyazaki, Miyazaki 889-2192, Japan
e-mail: neto@cc.miyazaki-u.ac.jp

M. Kamihira et al. (eds.), *Animal Cell Technology: Basic & Applied Aspects*, Animal Cell Technology: Basic & Applied Aspects 16, DOI 10.1007/978-90-481-3892-0_61,

2 Materials and Methods

2.1 Cells

HepG2 cells were maintained in DMEM medium supplemented with 10% FCS. HCV replicon cells were maintained in a MEM medium with 10% FCS. For HCV replicon cells, the culture medium was additionally supplemented with 500 μg/ml G418. KHYG-1 cells were maintained in a RPMI1640 medium with 10% FCS and 20 unit/ml of IL-2 (rIL-2, PeproTech EC, London, UK). Every cells were maintained in humidified atmosphere containing 5% CO_2.

2.2 Food Factors and Drugs for Construction of Artificial Neural Network

The food factors tested were as follows, 3 flavonols, quercetin, kaempferol and galangin; 3 anthocyanidins, delphinidin, cyanidin and perargonidin; 2 isoflavones, daidzein and glycitein; 6 other polyphenols, epigallocatechin gallte (EGCG), curcumin, resveratrol, chlorogenic acid, rosmarinic acid and capsaicin; 3 unsaturated fatty acids, arachidonic acid, 9*c*, 11*t*-conjugated linoleic acid (CLA) and linoleic acid; others, lipoic acid, gamma-aminobutyric acid (GABA) and benzyl isothiocyanate (BITC). The drugs tested include 2 anti-viral drugs; interferon-alpha (IFN-alpha) and ribavirin, 4 statins; atorvastatin, simvastatin, lovastatin and pravastatin.

2.3 Measurement of an Expression Level of Marker Proteins of HepG2 cells

Marker proteins of HepG2 cells were measured by ELISA to detect cellular reactiveness for a food factor. Measured proteins are as follows: IFN-inducible antiviral protein Mx (MxA), heat shock protein 90 (HSP90), heat shock protein 70 (HSP70), thioredoxin, thioredoxin reductase 1 (TXNRD1), NAD(P)H dehydrogenase (quinone) 1 (NQO1), Fas-associated death domain protein (FADD), Cellular tumor antigen p53 (p53), X-linked inhibitor of apoptosis protein (XIAP), baculoviral IAP repeat-containing protein 5 (survivin), apoptosis regulator Bcl-2 (Bcl-2), tumor-associated hydroquinone oxidase (tNOX), mitogen-activated protein kinase 1 (ERK2), and glyceraldehyde-3-phosphate dehydrogenase (GAPDH).

2.4 Anti-HCV Assay

Anti-virus activities of food factors were determined by luciferase assays and cell proliferation assay on HCV replicon cells. The luciferase assay was performed by

using the Steady-Glo or Bright-Glo luciferase assay systems (Promega, Madison, WI) according to the manufacturer's protocol. The cell proliferation was measured by metabolic conversion of WST-8 with a Cell Counting Kit-8 (Wako, Tokyo, Japan) according to the manufacturer's protocol. The value of luciferase activity was calculated by relative value in comparison with the solvent control. Antiviral activity defined as follows: Viral replication rate = (relative luciferase activity) / (cell proliferation rate)

2.5 NK Cell Activation Activity Assay

Natural immunity activation activities of food factors were determined by IFN-gamma production amount of human NK cell line, KHYG-1 cells. IFN-gamma included in culture supernatant of the NK cell was measured by using ELISA kit (PeproTech, London, UK).

2.6 Construction of Artificial Neural Network

The network consists of three groups, or layers, of units: a layer of "input" units is connected to a layer of "hidden" units, which is connected to a layer of "output" units. Each layer consists of 13 units, 6 units, and 1 unit respectively. An Error back propagation learning method was used for training of the neural network. Values of 13 marker proteins expression level that were obtained when a certain food factor was added in HepG2 cells, were input into an each "input" unit. The activity of each hidden unit was determined by the activities of the input units and the weights on the connections between the input and the hidden units. The behavior of the output units depended on the activity of the hidden units and the weights between the hidden and output units. An actual value of physiological functions was assumed teacher signal, and each weight was revised to shrink an error between teacher signal and output signal, namely the estimate of physiological function value. The network was trained repeatedly till error became less than 10% or till repetition number reached to 40,000.

2.7 Food Factors for Verification of Reliability of the Trained Neural Network Model

The food factors, drug and crude extract from plant tested were as follows, 10*t*, 12*c*-CLA, genistein, epigallocatechin (EGC), fluvastatin and blueberry leaf extract with hot water.

3 Results and Discussion

It is desirable to replace physiological function values into a common code to estimate plural different bioactivities from one set of experimental data. Because it is thought that every internal event is associated with behavior of proteins in a cell level, all physiological functions may be translatable in cellular protein expression pattern as a common code. If this supposition is right, plural physiological functions should be able to calculate from the same data of protein expression pattern by applying suitable translation method depending on kind of physiological functions, in the process translating expression patterns of protein into physiological function value. We planned to perform such a computation in artificial neural network. Since neural networks are the best at identifying patterns or trends in data, they are well suited for prediction or forecasting needs including sales forecasting, industrial process control, customer research, data validation, risk management, and target marketing [3].

In order to train a neural network to perform the task, the weights of each unit must be adjusted in such a way that the error between the output signal and the teacher signal is reduced (Fig. 1). This process requires that the neural network computes the error derivative of the weights. The error back propagation algorithm is the most widely used method for determining the error derivative of the weights.

Because the data sets of the scale that could perform error back propagation learning was too large, we couldn't prepare for these by a biochemical experiment. Therefore we composed learning data in assuming raw data dispersing, and the neural network became to be trained by this new data sets. The learning of neural network was completed within 5 min, and a network was built for every physiological function. It was needed only 0.1 sec to calculate of functionalities of a food factor by built neural networks.

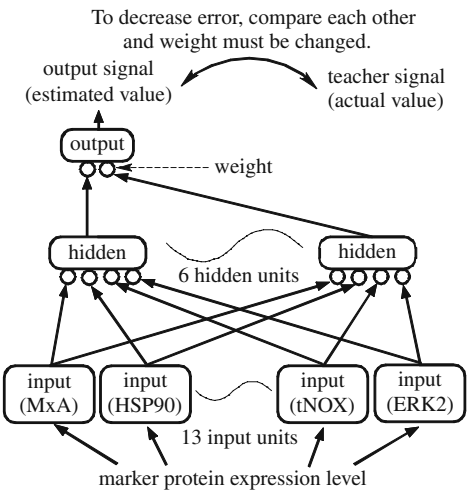

Fig. 1 Architecture of feed-forward type neural network

Table 1 Verification of reliability of the trained neural network model

	Anti-HCV activity		NK cell activation activity	
	estimated	actual (SD)	estimated	actual (SD)
CLA12*c*	0.09	0.95 (0.071)	0.77	0.86 (0.085)
genistein	1.04	1.03 (0.119)	1.34	1.17 (0.110)
EGC	1.10	1.12 (0.260)	0.92	2.09 (0.546)
fluvastatin	0.12	0.02 (0.001)	2.51	2.61 (0.304)
blueberry leaf extract	0.16	0.15 (0.036)	0.52	0.44 (0.063)

To verify reliability of the trained neural network model as a evaluation system for food functions, we applied to the system three food compositions, one drug, and one plant extract as follows: 10*t*, 12*c*-CLA which is a kind of conjugated linoleic acid included in bovine milk and dairy products, genistein which is a kind of soy bean isoflavones, EGC which is a catechin component in green tea, fluvastatin which is a high cholesterol lowering drug, and a blueberry leaf extract. Then these estimates were compared with actual values obtained by traditional methods. Of course, ingredients used for the system verification were not ones used to train the neural network. Table 1 shows actual value of anti-HCV activities by viral replication rate and NK cell activation activities by IFN-gamma production rate. The table also shows estimated values that calculated by the trained neural network. In the case of anti-HCV activity, low estimated values which mean high activities are obtained with fluvastatin and the leaf extract. On the other hand, in the case of NK cell activation activity, high estimated values which mean high activities are obtained with fluvastatin and EGC. These estimates are close to the measured actual values obtained by traditional assay methods, and their range of error is within 0.2. From these results, we conclude that the system proposed here is useful as a high-throughput evaluation system, which can estimate plural antiviral functions simultaneously in a high accuracy.

In general, an effect for human being must be finally measured. However, this system, which utilizes culture cells, is extremely effective for primary screening of useful food compositions, because plural functionalities can be estimated by just one ELISA experiment.

Acknowledgements This study was supported by Miyazaki prefecture collaboration of regional entities for the advancement of technological excellence (create) from the Japan science and technology agency.

References

1. Eto, N., Nishiyama, K., Sakakibara, Y., Yamamori, K., Nagahama, K., Iwata, T., Morinaga, H., Uchida, A., Kawahara, S., Yamasaki, M., Madhyastha, H.K., Furutani, H., Yoshihara, I., and Suiko, M. (2007) Development of a high-throughput evaluation system for food functions, Proceedings of the university of Miyazaki and Sunchon national university academic exchange agreement 15th anniversary symposium, 87–90.

2. Nagahama, K., Nishiyama, K., Eto, N., Sakakibara, Y., Yamasaki, M., Yoshihara, I., Yamamori, K., Iwata, T., Uchida A., and Suiko, M. (2007) Development of high-throughput assay for evaluation of food function *J. Clin. Biochem. Nutr*. **41s**: 167.
3. Papadopulos, G., Edwards, P.J., and Murray, A.F. (2001) Confidence estimation methods for neural networks: a practical comparison. *IEEE Trans. on Neural Network* **12**: 1278–1287.
4. Wasley, A., and Alter, M.J. (2000) Epidemiology of hepatitis C: geographic differences and temporal trends, *Semin. Liver Dis*. **20**: 1–16.

The Effects of Pesticides on Immune Cells

Sogo Nishimoto, Kota Kanda, Masaaki Okabe, Koichi Akiyama, Yoshimi Kakinuma, and Takuya Sugahara

1 Introduction

The wide spread of the environmental pollution caused by the chemical substances such as pesticides is a serious problem for creatures including human [1–3]. Various chemical substances taken in the body are carried to the organs responsible for detoxification such as liver and kidney, and excreted from the body. On the other hand, some hydrophobic substances among these chemicals are accumulated in our body [4].

In this study, we focused on the pesticidal chemicals used for the efficient cultivation of farm products for food. Many of pesticides prohibited production and/or use in Japan are still used in other countries and the farm products dusted such pesticides are imported. Therefore, we cannot deny the possibility of the exposure to these prohibited pesticides via residuals on cereals, vegetables and fruits that harvested in foreign countries.

In some previous reports, the influences of these risky pesticides on reproductive system have been studied [5, 6]. However, the influences on immune system have not been well uncovered yet. We chose two pesticides for investigation; methoxychlor possessing similar structure to DDT [7], and endosulfan (also referred as benzoepin) possessing similar characteristic property as endrin [8].

To examine the influences of these two pesticides on mammalian immune system, the effects on immunoglobulin production of human hybridoma cells and mouse splenic lymphocytes were evaluated. Human hybridoma cells and mouse splenic lymphocytes were cultured in the medium containing each pesticide at several concentrations. Moreover, to investigate the effect of pesticides on the body, mice were orally administrated each them at several concentrations for 2 week. In the present study, we investigate the effect of pesticides on mice in detail.

S. Nishimoto (✉)
Center for Marine Environmental Studies (CMES), Faculty of Agriculture, Ehime University, Matsuyama, Ehime 790-8577, Japan
e-mail: niss@agr.ehime-u.ac.jp

M. Kamihira et al. (eds.), *Animal Cell Technology: Basic & Applied Aspects*, Animal Cell Technology: Basic & Applied Aspects 16, DOI 10.1007/978-90-481-3892-0_62,

2 Materials and Methods

2.1 Reagents

Pesticides chemical substances, methoxychlor, α-endosulfan and β-endosulfan were purchased from Wako Pure Chemicals (Osaka, Japan). Briefly, 10 mM of each pesticide were prepared by dissolving in ethanol. For assays, each pesticide was diluted with ethanol at various concentrations.

Goat anti-human IgM, goat anti-human IgM-HRP (Biosource International), rabbit anti-mouse IgM, goat anti-mouse IgG, rabbit anti-mouse IgA, goat anti-mouse IgM-HRP, goat anti-mouse IgG-HRP conjugated, goat anti-IgA-HRP (Zymed) were used for quantitative analysis by ELISA.

2.2 Cells and Cell Culture

Human-human hybridoma, HB4C5 cells producing monoclonal IgM were used for the assay of Ig production-stimulating activity. HB4C5 cell line was a fusion product of a human B lymphocyte from a lung cancer patient and human fusion-partner NAT-30 cells [9].

Splenic lymphocytes were prepared from mice. Briefly, mice were killed by cervical dislocation, and spleens were excised from the cavity. Spleens were strained with 100 nM-pore nylon meshes, and collected cells were hemolyzed with hemolysis buffer (155 mM NH_4Cl, 15 mM $NaHCO_3$, 1 mM EDTA-2Na, pH 7.3). After wash twice with PBS, lymphocytes in spleen were obtained. HB4C5 cells and splenic lymphocytes were cultured in ERDF medium (Kyokuto Pharmaceutical, Tokyo, Japan) supplemented with 10 μg/mL of insulin (Sigma), 20 μg/mL of transferrin (Sigma), 20 μM ethanolamine (Sigma), and 25 nM selenite (Sigma) (ITES-ERDF) [10]. HB4C5 cells and lymphocytes were incubated at 37°C under humidified 5% CO_2-95% air.

2.3 Animals

Albino mice were purchased from the Japan SLC, Inc (Hamamatsu, Japan). Mice were housed in a room maintained at 24 on a 12 h light/dark cycle in a specific pathogen-free facility, and provided tap water and diet ad libitum. Animal experiments using mice described herein were approved by the Ehime University Animal Care and Use Committee and were performed in accordance with applicable guidelines and regulations.

2.4 Oral Administration

For oral administration, three mice per group were administrated each pesticide or ethanol as a control. The administration was performed against 8-week-old female

mice. Mice were administrated with 20 μL volume (1 mL/kg) of pesticides at high concentration (1 mM) everyday for 14 days [11]. After measurement of body weight, mice were killed by cervical dislocation, and spleens were excised at day 15. Following washing with PBS twice, the weight of spleen was measured. The mean tissue weight of the three control mice was calibrated as 100%, and relative weight rate was then calculated as occupation of spleen weight against body weight of control.

2.5 Assay for Ig Production Activity of Pesticides

The Ig production activity of each pesticide was examined by measuring the amount of IgM secreted by HB4C5 cells or of IgA, IgG and IgM secreted by splenic lymphocytes from mice into the culture medium. HB4C5 cells and splenic lymphocytes were inoculated into medium supplemented with each pesticide at various concentrations. The assay of the Ig production activity was performed in a 96-well culture plate, and HB4C5 cells and splenic lymphocytes were inoculated at a density of 2×10^5 cells/mL and 7.5×10^5 cells/mL, respectively. After cultivating for 24 h, the amount of Igs secreted into culture medium was determined by an enzyme-linked immunosorbent assay (ELISA).

2.6 Enzyme-Linked Immunosorbent Assay (ELISA)

ELISA was performed as a previously described [12, 13]. Briefly, 1.0 μg/mL of a anti-human IgM and anti-mouse Igs antibody was added to a 96-well plate at 100 μL/well, and incubated for 2 h at 37°C. After washing with 0.05% Tween20-PBS (T-PBS) three times, each well was blocked with 1.0% bovine serum albumin (BSA)-PBS solution for 2 h at 37°C. Following the blocking reaction, each well was treated with 50 μL of culture supernatant for 1 h at 37°C. Then, 100 μL/well of the HRP-conjugated anti-human IgM antibody or HRP-conjugated anti-mouse Igs that had been diluted 1,000 times by 1.0% BSA-PBS was added and incubated for 1 h at 37°C. Following this, 0.6 mg/ml of 2,2-azino-bis(ethylbenzothazoline-6-sulfonic acid diammonium salt) (ABTS) dissolved in a 0.03% H_2O_2-0.05 M citrate buffer (pH 4.0) was added to the wells at 100 μL/well, and the absorbance at 415 nm was measured after addition to 100 μL/well of 1.5% oxalic acid to terminate the coloring reaction. The IgM concentration was quantitatively determined by a standard curve, using a standard solution for human IgM, mouse IgA, mouse IgG and mouse IgM, respectively.

3 Results

To examine the effect of pesticides on Ig production activity of immune cells when we were taken in our body, we chose two kinds of pesticides, methoxychlor and endosulfan (Fig. 1a, b). Endosulfan has two different forms, α- and β-form.

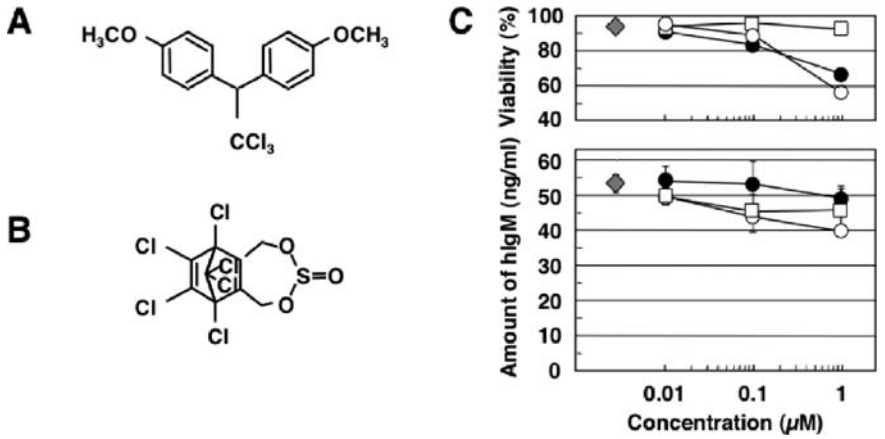

Fig. 1 Chemical structures and immune responses on HB4C5 cells. (**a**, **b**) Chemical structures of methoxychlor and endosulfan, respectively. (**c**) HB4C5 cells were cultured with methoxychlor (●) α-endosulfan (□) and β-endosulfan (○) at various concentrations for 24 h. Control is diamond shape. It is indicated that upper and lower phase are cell viability and hIgM production, respectively

To assess these pesticides on human IgM production, HB4C5 cells were cultured with methoxychlor and endosulfan at various concentrations for 24 h. As shown in Fig. 1c, methoxychlor and β-endosulfan indicated cytotoxicity against HB4C5 cells. On the other hand, only α-endosulfan had almost never toxicity between 0.1 and 1 μM. IgM production level was slightly decreased in α- and β-endosulfan treated cells. We found from this result that methoxychlor and endosulfan at concentration range in this experiment had not obviously affect on HB4C5 cells.

Next, we investigated whether mouse immune response of methoxychlor and endosulfan are similar with HB4C5 cells. Spleen cells were prepared from young female mouse according to above section. In spite of splenic lymphocytes treated by all pesticides were alive, it was down-regulated the IgA and IgG production at dose-dependent manner (Fig. 2). On the other hand, IgM production level was slightly increase and/or constant.

These results suggest that each pesticide control Ig production except for IgM and inhibit Ig secretion.

To observe the histological effect, each pesticide at 1 mM concentration was administrated to mice for 14 days. The administrated concentration was determined as reference to LD50 value [14]. Methoxychlor and endosulfan was set up one-two thousandth and one-fortieth of LD50, respectively. We could not observe the body weight loss of mice for experiment periods.

As shown in Table 1, spleen enucleated from high concentration pesticides-administrated mice became atrophied. All pesticides were induced the weight loss of spleen for 14 days; its rate was approximately 60% against control.

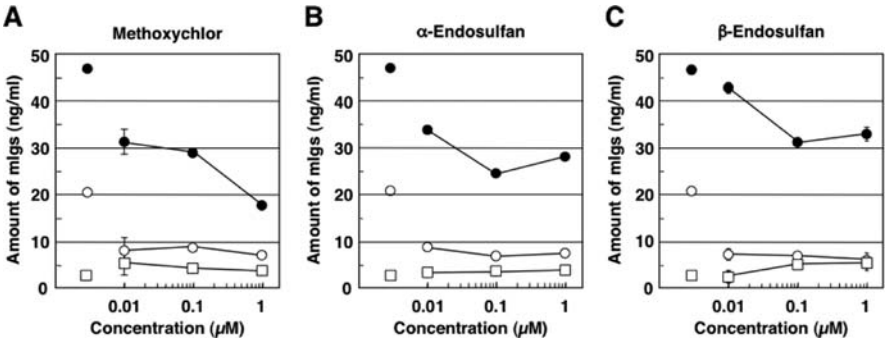

Fig. 2 Ex vivo effects of methoxychlor and endosulfan of Ig production on mouse spleen lymphocytes. It is indicated that the amount of IgA (●), IgG (○) and IgM (□) production on spleen cells cultured with methoxychlor (**a**), α-endosulfan (**b**) and β-endosulfan (**c**). Control was indicated to left side in each figure

Table 1 Relative weight rate of spleen on pesticides administrated mice

Methoxychlor	α-Endosulfan	β-Endosulfan	Control
0.30±0.04	0.30±0.02	0.28±0.02	0.53±0.01

The values (%) were calculated by spleen weight per body weight.

4 Conclusions

In human hybridoma cells, methoxychlor, α- and β-endosulfan were slightly decreased and/or constant human IgM production in culture medium and cell viability at high dose. The toxic effects of these pesticides did not be observed at between 0.01 and 1 μM. However, the toxicity of them may be increased in response to higher concentration.

In mouse splenic lymphocytes, each pesticide was markedly decreased in IgA and IgG production level except for IgM. Splenic lymphocytes treated with each pesticide at low dose were reduced in IgA and IgG production whereas they were lived. These pesticides may have suppression effect on secretion mechanism. In addition, we found that the atrophy of spleen was happened by each pesticide-administration.

IgG plays an important role in infectious diseases against viruses or bacterium [15, 16]. Hence, we may suffer from opportunistic infectious diseases by decline of immune response when methoxychlor or endosulfan was chronically taken and accumulated in our body.

References

1. McClure, G.Y., Helm, R.M., Stine, K., Burks, A.W., Jones, S.M., and Gandy, J. (2001) Evaluation of immune parameters in propanil-exposed farm families. *Arch. Environ. Contam. Toxicol*. **41:** 104–111.
2. McKinlay, R., Plant, J.A., Bell, J.N., and Voulvoulis, N. (2008) Calculating human exposure to endocrine disrupting pesticides via agricultural and non-agricultural exposure routes. *Sci. Total Environ*. **398:** 1–12.
3. Boobis, A.R., Ossendorp, B.C., Banasiak, U., Hamey, P.Y., Sebestyen, I., and Moretto, A. (2008) Cumulative risk assessment of pesticide residues in food. *Toxicol. Lett*. **180:** 137–150.
4. Somogyi, A. and Beck, H. (1993) Nurturing and breast-feeding: exposure to chemicals in breast milk, *Environ. Health Perspect*. **101**: 45–52.
5. Welshons, W.V., Nagel, S.C., Thayer, K.A., Judy, B.M., and Vom Saal, F.S. (1999) Low-dose bioactivity of xenoestrogens in animals: fetal exposure to low doses of methoxychlor and other xenoestrogens increases adult prostate size in mice. *Toxicol. Ind. Health* **15:** 12–25.
6. Bretveld, R., Brouwers, M., Ebisch, I., and Roeleveld, N. (2007) Influence of pesticides on male fertility. *Scand. J. Work Environ. Health* **33:** 13–28.
7. Coats, J.R. (1983) Structure-activity relationships among DDT derivatives. *J. Environ. Sci. Health B* **18**: 173–188.
8. Gegiou, D. (1974) Structural analysis of some chlorinated pesticides by nuclear quadrupole resonance spectrometry. *Talanta* **21:** 889–892.
9. Murakami, H., Masui, H., Sato, G.H., Sueoka, N., Chow, T.P., and Kono, T. (1982) Growth of hybridoma cells in serum-free medium. *Proc. Narl. Acad. Sci. USA* **79**: 1158–1562.
10. Murakami, H., Hashizume, S., Ohashi, H., Shinohara, K., Yasumoto, K., Nomoto, K., and Omura, H. (1982) Human-human hybridomas secreting antibodies specific to human lung carcinoma. *In Vitro Cell Develop. Boil*. **21**: 593–596.
11. Breinholt, V., Hossaini, A., Svendsen, G.W., Brouwer, C., and Nielsen, S.E. (2000) Estrogenic activity of flavanoids in mice. The importance of estrogen receptor distribution, metabolism and bioavailability. *Food Chem. Toxicol*. **38:** 555–564.
12. Sugahara, T., Ueno, M., Goto, Y., Shiraishi, R., Doi, M., Akiyama, K., and Yamauchi, S. (2006) Immunostimulation effect of the jellyfish collagen. *Biosci. Biotechnol. Biochem*. **70:** 2131–2137.
13. Nishimoto, S., Goto, Y., Morishige, H., Shiraishi, R., Doi, M., Akiyama, K., Yamauchi, S., and Sugahara, T. (2008) Mode of action of the immunostimulatory effect of collagen from jellyfish. *Biosci. Biotechnol. Biochem*. **72:** 2806–2814 (2008).
14. Gupta, P.K., Murthy, R.C., and Chandra, S.V. (1981) Toxicity of endosulfan and manganese chloride: cumulative toxicity rating. *Toxicol. Lett*. **7:** 221–227.
15. Insel, R.A., Amstey, M., Woodin, K., and Pichichero, M. (1994) Maternal immunization to prevent infectious diseases in the neonate or infant. *Int. Technol. Assess. Health Care* **10:** 143–53.
16. Nimmerjahn, F. and Ravetch, J.V. (2008) Fcgamma receptors as regulators of immune responses. *Nat. Rev. Immunol*. **8:** 34–47.

Co-Cultured Hepatocyte-Spheroid Chip Constructed Using the Microfabrication Technique

Yusuke Sakai and Kohji Nakazawa

1 Introduction

The liver is the main metabolic organ in the body; it plays important roles such as protein synthesis and drug metabolism. Hence, hepatocytes have often been used for research involving pharmacokinetics and toxicity assays. The conventional method involves culturing the hepatocytes as a monolayer. However, this results in the loss of the tissue-like organization of the hepatocytes and the rapid deterioration of liver-specific functions. In contrast, cultured hepatocyte spheroids (spherical multicellular aggregates) can maintain a high level of liver function in vitro, which is attributable to their resemblance to tissues in terms of the presence of abundant cytoplasmic organelles and close cell-cell contact [1–3]. Therefore, the spheroid culture system has been advocated as a useful technique to replace monolayer culture. Numerous reports have suggested that the hepatocyte spheroids can be cultured using various methods [4, 5] such as rotation culture and non-adhesion culture. We have also developed a microchip technique that can generate uniform hepatocyte spheroids in a regularly arrangement [6, 7]. However, the expression of hepatocyte functions in vitro is limited, even in the spheroid culture system.

On the other hand, in addition to parenchymal cells (hepatocytes), the liver is composed of non-parenchymal cells such as stellate cells, endothelial cells, fibroblasts, and so on. These non-parenchymal cells play an important role in hepatocyte function [8]. Therefore, the co-cultured spheroids comprising hepatocytes and non-parenchymal cells are useful models for the maintenance of high hepatic functions.

In this study, we established a spheroid co-culture technique by using our original microchip technique. Furthermore, the effects of mixture ratios of hepatocytes and non-parenchymal cells in the spheroids on the expression of hepatocyte functions were examined.

K. Nakazawa (✉)
Department of Life and Environment Engineering, University of Kitakyushu, Kitakyushu, Fukuoka 808-0135, Japan
e-mail: nakazawa@env.kitakyu-u.ac.jp

M. Kamihira et al. (eds.), *Animal Cell Technology: Basic & Applied Aspects*, Animal Cell Technology: Basic & Applied Aspects 16, DOI 10.1007/978-90-481-3892-0_63,

2 Materials and Methods

2.1 Hepatocyte Spheroid Chip

Figure 1 shows the construction of a hepatocyte spheroid chip. The chip comprises 672 circular microwells in a triangular arrangement (pitch, 400 μm) on a polymethyl methacrylate (PMMA) plate (24 × 24 mm); each circular microwell was 300 μm in diameter and 200 μm in depth. In the center of each circular microwell, an area with a diameter of 100 μm was modified with collagen to create a cell-adhesion area; the remaining area of the microwell was modified with polyethylene glycol (PEG) to create a non-adhesive area. The chip was prepared by using the microfabrication and microcontact printing techniques described in our previous studies [6, 7].

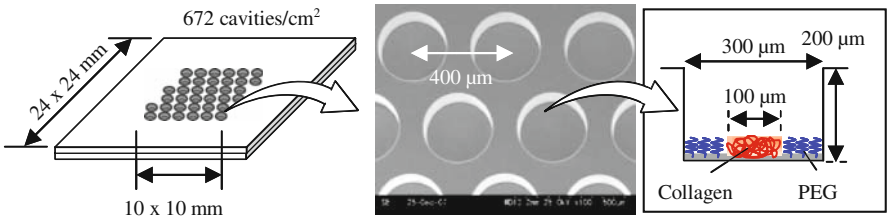

Fig. 1 Schematic representation of the spheroid chip

2.2 Isolation of Hepatocytes and Non-Parenchymal Cells

Hepatocytes and non-parenchymal cells were isolated as described in previous reports [9, 10]. The whole liver of adult Wistar rats (male, 7–8 weeks old, weighing approximately 200 g) was perfused with 0.05% collagenase solution. The liver minced after treatment with collagenase solution for approximately 10 min at 37°C, and large tissue fragments ware removed by filtration through a gauze mesh. The dense cell suspension thus obtained was passed through a stainless mesh with a pore size of 45 μm. For the isolation of hepatocytes, the resultant cell suspension was washed thrice with a culture medium by centrifuging at 50*g* for 90 s. For the isolation of non-parenchymal cells, the supernatant obtained from first centrifugation procedure was collected and centrifuged at 50*g* for 90 s to remove any residual hepatocytes. The supernatant thus obtained was washed twice with the culture medium by centrifuging at 60*g* for 60 s. The supernatant obtained after the third centrifugation procedure was passed through a stainless mesh with a pore size of 20 μm, and the resultant cell suspension was filtered through a filter paper with a pore size of 11 μm. Finally, the cell suspension obtained after filtrations was washed twice with the culture medium using centrifugation at 150*g* for 3 min. The cell viability was

determined by using the trypan blue exclusion method, and cells with more than 85% viability were used for this study.

In this study, we used Dulbecco's modified Eagle's medium (DMEM) supplemented with 10 mg/L insulin, 7.5 mg/L hydrocortisone, 50 μg/L epidermal growth factor, 60 mg/L proline, 50 μg/L linoleic acid, 0.1 μM $CuSO_4 \cdot 5\ H_2O$, 3 μg/L H_2SeO_3, 50 pM $ZnSO_4 \cdot 7\ H_2O$, 58.8 μg/mL penicillin, and 100 μg/mL streptomycin.

2.3 Homo- and Co-cultured Spheroids

In this study, the effect of several mixture ratios of hepatocytes and non-parenchymal cells in the spheroid culture were evaluated (Table 1).

Hepatocytes and non-parenchymal cells were mixed before they were inoculated onto the spheroid chip. Homo (hepatocytes only) – or 3 types of hetero (hepatocytes + non-parenchymal cells in varying ratios)- cell suspensions were inoculated into the culture area of the spheroid chip. The chip was placed in a polystyrene dish (diameter, 35 mm) containing 2 mL of culture medium. The medium was replaced at 4 h and 24 h after inoculation and subsequently, at 1-day intervals. All cells were cultured under a humidified atmosphere of 5% CO_2 and 95% air at 37°C.

Table 1 Culture condition for spheroids

Condition	Mixture ratio [cells/chip] (Hepatocyte: non-parenchymal cell)
Homo-culture	1.7×10^5: –
Co-culture-9:1	1.7×10^5: 0.19×10^5
Co-culture-7:3	1.7×10^5: 0.73×10^5
Co-culture-5:5	1.7×10^5: 1.7×10^5

2.4 Morphology and Liver-Specific Function

Phase-contrast micrographs were used to measure the diameters of the spheroids. A phase-contrast microscope was used to obtain photographic images of the spheroids with several mixture ratios on day 14 of culture. The diameters of the 50 spheroids in each chip were estimated from images by using a two-dimensional image-analysis program. The diameter was calculated using the equivalent circle diameter (ECD) method whereby the spheroid area was expressed in terms of ECD.

Albumin secretion by the spheroids on the chip was evaluated on day 14 of culture under each inoculation condition. The concentration of albumin into the culture medium during a 24-h of culture period was determined by performing an enzyme-linked immunosorbent assay (ELISA).

3 Results

3.1 Spheroid Morphology and Diameter

Figure 2 shows the phase-contrast micrographs of the chips containing homo- and co-cultured spheroids on day 14 of culture. Under all conditions, the cells spontaneously formed spheroids with the smooth surfaces and the uniform diameters in the center of each microwell on day 3 of culture. However, the circular conformation and smooth surfaces of the spheroids of the homo-culture, co-culture-9:1, and co-culture-7:3 gradually deteriorated after approximately 10 days of culture

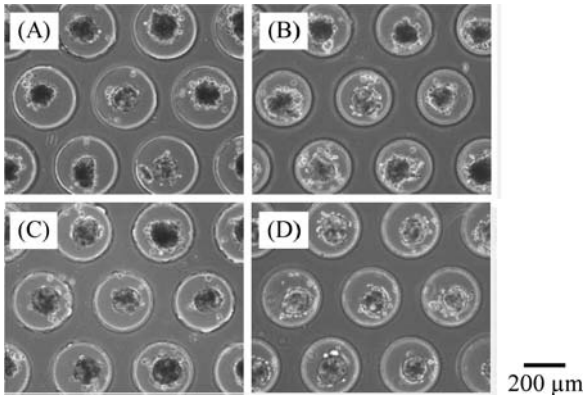

Fig. 2 Cell morphology of the mono- and co-cultured spheroids in day 14 of culture (**a**) Homo culture, (**b**) Co-culture-9:1, (**c**) Co-culture-7:3, and (**d**) Co-culture-5:5

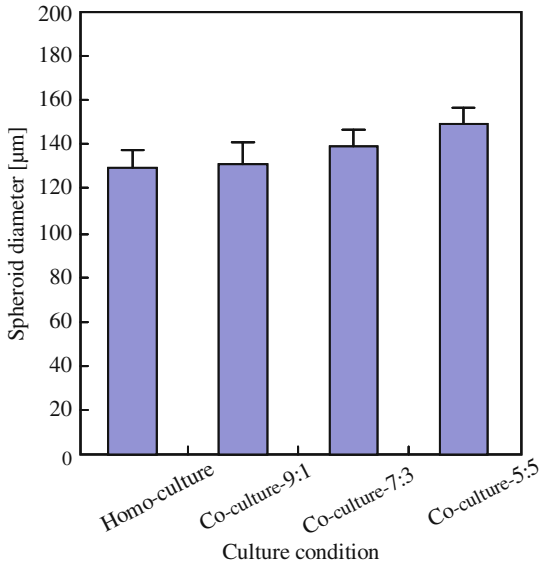

Fig. 3 Spheroid diameters on day 14 of culture. Error bars represent SD

(Fig. 2 A–C). In contrast, the conformation of co-cultured spheroids containing hepatocytes and non-parenchymal cells at a ratio of 1:1 (co-culture-5:5) was maintained for at least 14 days of culture (Fig. 2D).

Figure 3 shows the diameters of spheroids on 14 days of culture under each culture condition. The diameters of the spheroids were uniform for each of condition. The results showed that the size of the spheroids depends on the proportion of non-parenchymal cells.

3.2 Albumin secretion

Figure 4 shows the rates of albumin secretion on day 14 of culture. The albumin-secretion rates were higher in the case of co-cultured spheroids than in the case of homo-cultured spheroids. Furthermore, the activity of the spheroids depended on the proportion of non-parenchymal cells. The activities under the co-culture-9:1, co-culture-7:3, and co-culture-5:5 conditions were 2-, 3-, and 4-times higher than the activity under the homo-culture condition, respectively.

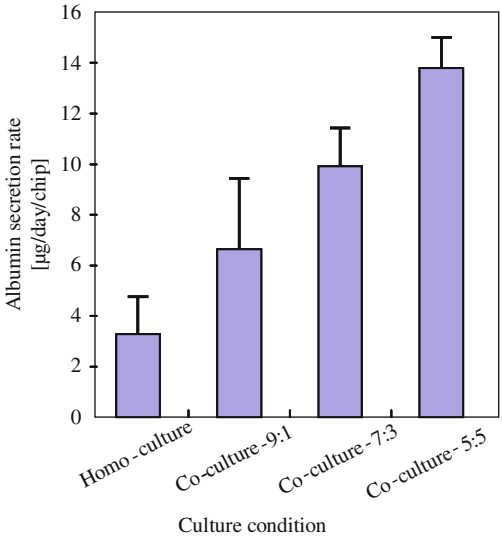

Fig. 4 Albumin-secretion rates of spheroids on day 14 of culture. Error bars represent SD. (N = 4; 2 independent cell preparations.)

4 Discussion

Some researchers have reported that compared to homo-cultured spheroids, co-cultured spheroids comprising hepatocytes and non-parenchymal cells or hepatocytes and fibroblasts such as 3T3 cells can enhance and maintain the hepatocyte functions [11, 12]. However, in the preciously used spheroid co-culture techniques,

it was difficult to control the diameter of the spheroid and the cell mixture ratio in individual spheroids. The controls of spheroid diameter and the cell mixture ratio in the spheroid are important items to evaluate the interaction between hepatocytes and non-parenchymal cells. Because of the structure of the microwells in our chip, our microchip technique could be used to control the number of cells in a single spheroid. Furthermore, the spheroids formed on the chip did not fuse to each other, because each spheroid was immobilized in the collagen area of the microwells in the chip. Therefore, our microchip technique may be a useful tool for the evaluation of the effects of co-cultured spheroids.

In this study, spheroid conformation and function were compared among homo-cultured spheroids and co-cultured spheroids under the co-culture-9:1, co-culture-7:3, and co-culture-5:5 conditions. Under all 4 conditions, the size of the spheroids depended on the proportion of non-parenchymal cells, but the spheroid size differ only slightly (Fig. 3). This may be attributable to the fact that non-parenchymal are smaller than hepatocytes and these cells did not proliferate throughout the culture duration because in this study, fetal bovine serum (FBS) was not added to the culture medium. On the other hand, the circular conformation and smooth surfaces of the spheroids were maintained stably because of the presence of non-parenchymal cells. This effect depended on the mixture ratio of hepatocytes and non-parenchymal cells, and was frequently observed under the co-culture-5:5 condition (Fig. 2). Furthermore, the albumin-secretory activity of the hepatocytes also depended on the mixture ratio of the hepatocytes and non-parenchymal cells (Fig. 4). Non-parenchymal cells produce various cytokines and extracellular matrices, which affect the hepatocytes [11]. Thus, the co-culture condition may reconstruct a suitable culture environment for hepatocytes.

In conclusions, we developed a simple technique for producing co-cultured spheroids. The spheroid conformation and hepatocyte function were maintained by increasing the proportion of non-parenchymal cells in the co-cultured spheroids. This technique may be applicable as a cellular platform for biological researches, such as that on hetero cell-cell interactions and reconstruction of tissues.

Acknowledgments This work was partly supported by grants from the knowledge cluster initiative and the nanotechnology network project implemented by the ministry of education, culture, sports, science and technology (mext).

References

1. Peshwa, M.V., Wu, F.J., Sharp, H.L., Cerra, F.B., and Hu, W.H. (1996) Mechanistics of formation and ultrastructural evaluation of hepatocyte spheroids. *In Vitro Cell Biol Anim*. **32**: 197–203
2. Abu-Absi, S.F., Friend, J.R., Hansen, L.K., and Hu, W.H. (2002) Structural polarity and functional bile canaliculi in rat hepatocyte spheroids. *Exp Cell Res*. **274**(1): 56–67
3. Depreter, M., Walker, T., De Smet, K., Beken, S., Kerckaert, I., Rogiers, V., and Roels, F. (2002) Hepatocyte polarity and the peroxisomal compartment: a comparative study. *Histochem J*. **34**(3–4): 139–151

4. Glicklis, R., Merchuk, J.C., and Cohen, S. (2004) Modeling mass transfer in hepatocyte spheroids via cell viability, spheroid size, and hepatocellular functions. *Biotechnol Bioeng*. **86**(6): 672–680
5. Koide, N., Sakaguchi, K., Koide, Y., Asano, K., Kawaguchi, M., Matsushima, H., Takenami, T., Shinji, T., Mori, M., and Tsuji, T. (1990) Formation of multicellular spheroids composed of adult rat hepatocytes in dishes with positively charged surfaces and under other nonadherent environments. *Exp Cell Res*. **186**(2): 227–235
6. Fukuda, J., Sakai, Y., and Nakazawa, K. (2006) Novel hepatocyte culture system developed using microfabrication and collagen/polyethylene glycol microcontact printing. *Biomaterials* **27**(7): 1061–1070
7. Mori, R., Sakai, Y., and Nakazawa, K. (2008) Micropatterned organoid culture of rat hepatocytes and HepG2 cells. *J Biosci Bioeng*. **106**(3): 237–242
8. Koike, M., Matsushita, M., Taguchi, K., and Uchino, J. (1996) Function of culturing monolayer hepatocytes by collagen gel coating and coculture with nonparenchymal cells. *Artif Organs*. **20**(2): 186–192
9. Seglen, P.O. (1976) Preparation of isolated rat liver cells. *Methods Cell Biol*. **13**: 29–83
10. Shimaoka, S., Nakamura, T., and Ichihara, A. (1987) Stimulation of growth of primary cultured adult rat hepatocytes without growth factors by coculture with nonparenchymal liver cells. *Exp Cell Res*. **172**(1): 228–242
11. Thomas, R.J., Bhandari, R., Barrett, D.A., Bennett, A.J., Fry, J.R., Powe, D., Thomson, B.J., and Shakesheff, K.M., (2005) The Effect of Three-Dimensional Co-Culture of Hepatocytes and Hepatic Stellate Cells on Key Hepatocyte Function in Vitro. *Cells Tissues Organs* **181**(2): 67–79
12. Lu, H.F., Chua, K.N., Zhang, P.C., Lim, W.S., Ramakrishna, S., Leong, K.W., and Mao, H.Q., (2005) Three-dimensional co-culture of rat hepatocyte spheroids and NIH/3T3 fibroblasts enhances hepatocyte functional maintenance. *Acta Biomater*. **1**(4): 399–410

Micropatterned Hepatocyte Culture Using Microstencil Technique

Yukako Shinmura, Ami Higuchi, Yusuke Sakai, and Kohji Nakazawa

1 Introduction

A cell chip, in which the cells are micropatterned on a culture plate, is expected to apply various cell-based assays, such as drug screening, cell transfection, cell differentiation studies, and fundamental cell biological studies, because it can facilitate the observation of cell responses, including high-throughput screening [1–3]. To develop such a cell chip, the formation of equal cell patterns on the culture plate is a key technology. Several cell patterning techniques for accelerating or inhibiting cell attachments have been reported, such as lithography, photo-reactive polymers, microcontact printing, and so on [4–7]. However, these techniques involve the use of especial devices for microfabrication or surface modification and complicated processes in chip preparation. Therefore, a simple technique that can form the cell pattern on the culture plate will have advantages over previous methods.

On the other hand, among the various mammalian cells, primary hepatocytes are one of the target cells for the cell-based assay, because the liver plays many essential roles in maintaining normal physiology. Therefore, cell chip micropatterning primary hepatocytes have attracted attention as a cell-based assay system for studying liver functions, including drug metabolism and hepatotoxicity [8–12].

In this study, we established a simple technique for a micropatterned culture of rat hepatocytes using a microstencil, which was a thin membrane with orderly through-microholes. Furthermore, the expression of hepatocyte functions in the micropatterned culture was compared with that in the randomly distributed culture.

K. Nakazawa (✉)
Department of Life and Environment Engineering, University of Kitakyushu, Kitakyushu, Fukuoka 808-0135, Japan
e-mail: nakazawa@env.kitakyu-u.ac.jp

M. Kamihira et al. (eds.), *Animal Cell Technology: Basic & Applied Aspects*, Animal Cell Technology: Basic & Applied Aspects 16, DOI 10.1007/978-90-481-3892-0_64,

2 Material and Methods

2.1 Preparation of a Microstencil Chip

A poly-dimethylsiloxane (PDMS) microstencil (wherein a thin membrane comprised 724 through-microholes (500 μm in diameter) in a triangle arrangement of 800 μm pitch) was fabricated by peeling the microstencil off from a microfabricated mould of poly-methylmethacrylate (PMMA). To prepare the microstencil chip, the fabricated microstencil was sealed onto the surface of a glass plate (24 × 24 mm) (Fig. 1). The surface of the microstencil chip was coated with type IV collagen in order to encourage cell adhesion.

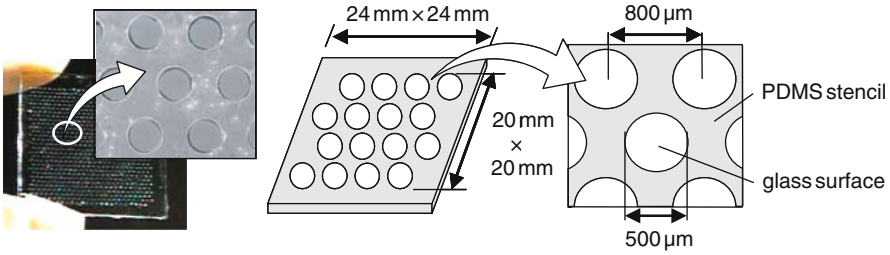

Fig. 1 Schematic diagram of the microstencil chip

2.2 Hepatocytes Preparation and Culture Medium

Rat hepatocytes were isolated from the whole liver of an adult Wistar rat (male, 7–8 wk old and weighing approximately 200 g) by performing liver perfusion using 0.05% collagenase [13]. The cell viability was determined using the trypan blue exclusion method, and cells exhibiting more than 80% viability were used for the subsequent analyses.

The culture medium comprised Dulbecco's modified Eagle's medium (DMEM) supplemented with 10 mg/L insulin, 7.5 mg/L hydrocortisone, 50 μg/L epidermal growth factor, 60 mg/L proline, 50 μg/L linoleic acid, 0.1 μM $CuSO_4 \cdot 5\ H_2O$, 3 μg/L H_2SeO_3, 50 pM $ZnSO_4 \cdot 7\ H_2O$, 58.8 μg/mL penicillin, and 100 μg/mL streptomycin.

2.3 Hepatocyte Culture

Figure 2 shows the process of creating the micropatterned culture of hepatocytes using the microstencil chip. Hepatocytes (1.0×10^6) were inoculated onto the microstencil chip that was placed in a polystyrene dish (diameter, 35 mm) containing a 2-mL culture medium. After 24 h, the stencil was deliberately peeled off the chip, and the chip with micropatterned hepatocytes was transferred to another

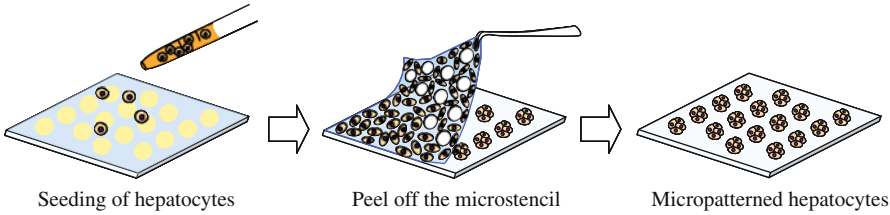

Fig. 2 Process of creating the micropatterned culture of hepatocytes using the microstencil chip

polystyrene dish containing a 2-mL fresh culture medium. To obtain a randomly distributed culture of cells as the control experiment, hepatocytes (5.0×10^5) were inoculated onto a 35-mm dish coated with type IV collagen. The culture medium was changed at intervals of 1 day. All the cells were cultured at 37°C in a humidified atmosphere of 5% CO_2 and 95% air.

2.4 Evaluation of Liver-Specific Functions

Albumin secretion and ammonia removal were evaluated as typical liver functions. The concentrations of albumin, which were secreted into the culture medium during 24 h of culture, were determined by performing an enzyme-linked immunosorbent assay (ELISA). To evaluate ammonia removal, the culture medium was replaced with a fresh culture medium containing 1 mM ammonium chloride. The ammonia concentration was measured using a commercial kit. The ammonia removal activity was calculated based on the decrease in ammonia concentration occurring during 24 h of culture, following the replacement of the culture medium. These functions were evaluated at 5 days of culture, and their values were normalized with the cell number in the culture on the same day.

3 Results

3.1 Hepatocyte Morphology

In the randomly distributed culture, rat hepatocytes adhered to the collagen-coated dish and formed a monolayer; however, the cell distribution was heterogeneous throughout the culture duration (Fig. 3A). Although the hepatocytes inoculated onto the microstencil chip adhered to the surface of the microstencil and the glass surface in through-microholes of the microstencil and formed a monolayer conformation within 1 day of culture, the micropatterned spots of hepatocytes were formed by peeling off the stencil (Fig. 3B). The conformation of micropatterned hepatocytes was maintained within 5 days of culture; however, the circular pattern of hepatocytes gradually decayed after 5 days of culture.

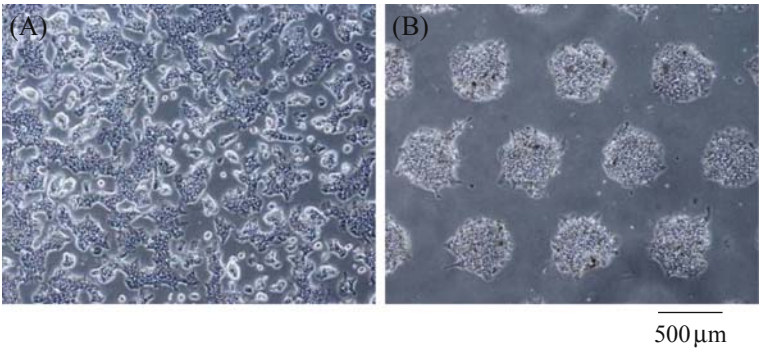

Fig. 3 Hepatocyte morphology on 3 days of culture (**A**) Randomly distributed culture, (**B**) Micropatterned culture

3.2 Liver-Specific Functions

Figure 4 shows the activities of albumin secretion and ammonia removal in hepatocytes on 5 days of culture. The activities of albumin secretion and ammonia removal in the micropatterned culture were approximately 3.3- and 1.6-times higher than those in the randomly distributed culture, respectively.

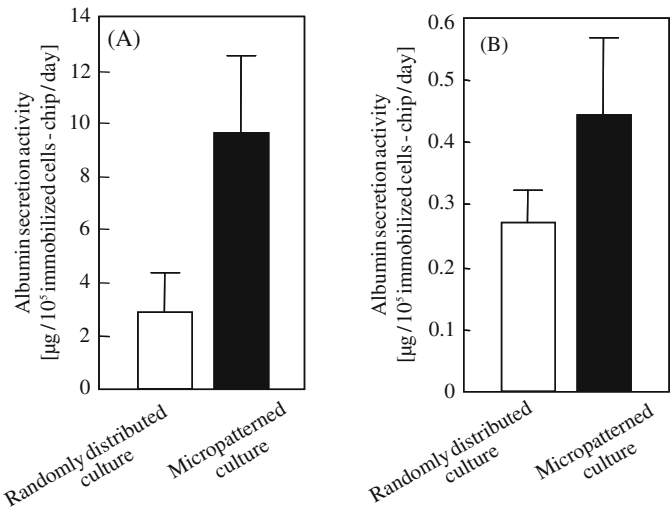

Fig. 4 Functional expression of hepatocyte on 5 days of culture (**A**) albumin secretion activity, (**B**) ammonia removal activity

4 Discussion

In this study, we established a simple technique to micropattern rat hepatocytes, that is, by peeling off the stencil from the chip. Previous methods for the micropatterned cell culture require the formation of the cell adhesion area and non-adhesion area on the culture chip prior to cell inoculation. In contrast, this method can form the micropatterned cell culture after cell inoculation. Thus, the concept of this method is quite different from previous methods. Furthermore, this method has potential for application to a micropatterned co-culture.

Although the conformation of micropatterned hepatocytes was maintained for 5 days of culture (Fig. 3B), subsequently, the circular pattern of hepatocytes gradually decayed, because the cells spread to the chip surface that was removed by the stencil. Therefore, this method may be available to the micropatterned culture for several days. The albumin section and ammonia removal activities of hepatocytes in a micropatterned culture were higher than those in randomly distributed culture (Fig. 4 A and B). The micropatterned culture may be able to maintain stable cell-cell interactions for the expression of functions in comparison with the randomly distributed culture, because the cells on the particular areas of patterned spot were gathered higher density than those of randomly distributed culture.

In conclusion, we established a simple technique for creating a micropatterned culture of rat hepatocytes using a microstencil and demonstrated that micropatterned hepatocytes could express higher functions in comparison with randomly distributed hepatocytes. This simple technique for micropatterned culture may be applicable as a cellular platform for a cell-based assay system.

Acknowledgments This work was partly supported by grants from the Knowledge Cluster Initiative and the Nanotechnology Network Project implemented by the Ministry of Education, Culture, Sports, Science and Technology (MEXT).

References

1. Baily, S.N., Wu, R.Z., and Sabatini, D.M. (2002) Applications of transfected cell microarrays in high-throughput drug discovery. *Drug Discov Today*. **7**(18 Suppl): S113–S118
2. Fico, A., Manganelli, G., Simeone, M., Guido, S., Minchiotti, G., and Filosa, S. (2008) High-throughput screening-compatible single-step protocol to differentiate embryonic stem cells in neurons. *Stem Cells Dev*. **17**(3): 573–584
3. Akagi, Y., Rao, S.R., Morita, Y., and Tamiya, E. (2004) Optimization of fluorescent cell-based assays for high-throughput analysis using microchamber array chip formats. *Sci.Technol. Adv. Mater*. **5**(3): 343–349
4. Kaji, H., Kanada, M., Oyamatsu, D., Matsue, T., and Nishizawa, M. (2004) Micro electrochemical Approach to Induce Local Cell Adhesion and Growth on Substrates. *Langmuir*. **20**(1): 16–19
5. Bhatia, S.N., Balis, U.J., Yarmush, M.L., and Toner, M. (1998) Microfabrication of hepatocyte/fibroblast co-cultures: role of homotypic cell interactions. *Biomaterial Prog*. **14**(3): 378–387
6. Kane, R.S., Takayama, S., Otsuni, E., Ingber, D.E., and Whitesides, G.M. (1999) Patterning proteins and cells using soft lithography. *Biomaterials*. **20:** 2363–2376

7. Falconnet, D., Csucs, G., Grandin, H.M., and Textor, M. (2006) Surface engineering approaches to micropattern surfaces for cell-based assays. *Biomaterials*. **27**(16): 3044–3063
8. Otsuka, H., Hirano, A., Nagasaki, Y., Okano, T. Horiike, Y., and Kataoka, K. (2004) Two-dimensional multiarray formation of hepatocyte spheroids on a microfabricated PEG-brush surface. *ChemBioChem*. **5**(6): 850–855
9. Powers, M.J., Janigian, D.M., Wack, K.E., Baker, C.S., Stolz, D.B., and Griffith, L.G. (2002) Functional behavior of primary rat liver cells in a 3D perfused microarray bioreactor. *Tissue Eng*. **8**(3): 513–527
10. Fukuda, J. and Nakazawa, K. (2005) Orderly arrangement of hepatocyte spheroids on a microfabricated chip. *Tissue Eng*. **11**(7–8): 1254–1262
11. Sakai, Y. and Nakazawa, K. (2007) Technique for the control of spheroid diameter using microfabricated chips. *Acta Biomater*. **3**(6): 1033–1040
12. Mori, R., Sakai, Y., and Nakazawa, K. (2008) Micropatterned organoid culture of rat hepatocytes and HepG2 cells. *J Biosci. Bioeng*. **106**(3): 237–242
13. Seglen, P.O. (1976) Preparation of isolated rat liver cells. *Methods Cell Biol*. **13**: 29–83

Structural Features of Totally Designed Lipidic Materials for Small Interfering RNA Delivery System

Glutamate-Based Lipidic Materials as Potential siRNA Carriers

Ken-Ichi Kusumoto

1 Introduction

RNA interference (RNAi) with siRNA has been revealed as a powerful technique that is capable of suppressing targeted genes with high specificity. A delivery system for siRNA into mammalian cells has broadened the scope of medical intervention since siRNA has recently emerged as potential therapeutic agents in the treatment of human genetic and nongenetic diseases. Several studies have reported various strategies for the siRNA delivery system. Viral vectors are accepted as the most effective tools for gene transfer into mammalian cells in vivo and in vitro. However, there are safety problems such as induction of immune reactions or tumorigenesis. Therefore, the use of nonpathogenic materials based on lipids or polymers has been attempted. Recently, a variety of studies have been exploring the novel nonpathogenic materials as potential siRNA carriers. Understanding of lipidic materials for small interfering RNA (siRNA) delivery system is essential for the effective design and selection of appropriate materials as potential applications in basic and therapeutic research.

Lipidic materials have been used as an easy-to-use system to transfer siRNA into mammalian cells. For example, commercial reagents such as Lipofectamine 2,000 (Invitrogen) are available for use in a variety of researches. The advantage of lipidic materials is the protection of RNA molecules by encirclement of their structures and low cytotoxicity and immunogenicity in in vivo transfection compared with the use of vectors such as calcium phosphate or viral vectors. However, how the chemical structure of lipidic materials functions as potential siRNA carrier has been controversial. Efforts toward a comprehensive knowledge of correlations between the structural features and biological functions of lipidic materials are crucial for controlling nonviral siRNA delivery system into mammalian cells. Here, we have focused on understanding how the structural features of glutamate-based lipidic materials that are designed by taking advantage of the chemical structure

K.-I. Kusumoto (✉)
Department of Biological Chemistry, Biotechnology and Food Research Institute, Fukuoka Industrial Technology Center, Kurume, Fukuoka 839-0861, Japan
e-mail: kkusumoto@fitc.pref.fukuoka.jp

M. Kamihira et al. (eds.), *Animal Cell Technology: Basic & Applied Aspects*, Animal Cell Technology: Basic & Applied Aspects 16, DOI 10.1007/978-90-481-3892-0_65,

having double-stranded hydrophobic chains in major cell membrane lipids such as phospholipids and sphingolipids can enhance its biological function to promote intracellular delivery of siRNA.

2 Materials and Methods

2.1 Materials

Glutamic acid, aspartic acid, 1-dodecanol, ρ-toluenesulfonic acid, chloroacetyl chloride, toluene, tetrahydrofuran, anti-EGFP siRNA duplex, were purchased from Wako Pure Chemical Industries (Japan). Trimethylamine, hypoxanthine, thymidine, and G418 were purchased from Sigma-Aldrich. Dulbecco's modified Eagle's medium (DMEM), trypsin, Lipofectamine 2,000, RNAiMax, and trypan blue dye solution were purchased from Invitrogen. Plasmid vector pCMV-IE EGFP was purchased from Takara Bio (Japan). Anti-β-galactosidase siRNA-1 duplex was purchased from GE Healthcare. Cy3-labeled anti-luciferase siRNA duplex was purchased from B-Bridge International.

2.2 Glutamate-Based Lipid TMA-C2-Glu-C12

Glutamate-based lipid TMA-C2-Glu-C12 was synthesized by refluxing with dean-stark-trap into dry toluene with glutamic acid, 1-dodecanol, and ρ-toluenesulfonic acid, by mixing into dry chloroform with chloroacetyl chloride, and then by mixing into dry tetrahydrofuran with trimethylamine. TMA-C2-Glu-C12 was derived from glutamic acid that was used as a connector to bind one head region consisting of trimethylamine (TMA) and hydrophobic chain comprising 2 carbon atoms (C2) and two tail regions, each consisting of hydrophobic chain comprising 12 carbon atoms (C12). Its analogs were synthesized by the same methods as those used for TMA-C2-Glu-C12. For preparation of lipidic solutions, each compound was dispersed into autoclaved deionized-distilled water at a final concentration of 1 mM by ultrasonication for 1 min.

2.3 CHO-EGFP Cell Line and Cell Culture

CHO-K1 cells were transfected with pCMV-IE EGFP vector by using transfection reagent DoFect-GT1 (Dojindo, Japan) and were cultured in DMEM containing HT (hypoxanthine and thymidine) and 10% FBS at 37°C in the humidified atmosphere of a 5% CO_2 incubator. The cells after 24 h transfection were cloned in 96-well plates containing DMEM with HT, 10% FBS, and 1 mg/mL antibiotic G418. The cells that constantly expressed EGFP gene, termed as a CHO-EGFP cell line, were maintained in DMEM containing HT, G418, and 10% FBS.

2.4 siRNA Transfer Assay

CHO-EGFP cells were precultured overnight in 24-well plates at a density of 1.0×10^5 cells per well in 1 mL DMEM containing HT and 10% FBS. Anti-EGFP siRNA duplex (50 pmol/well) and 1 mM TMA-C2-Glu-C12 solution (1, 2.5, 5, 7.5, or 10 μL/well) were gently mixed in tubes containing DMEM (25 μL/well) and then incubated for 5 min at room temperature. The cells were transferred into 0.5 mL DMEM with HT, and the transfer mixtures were gently added to the culture medium and incubated for 3 h at 37°C. Following transfection, the cells were cultured for 24 h with 1 mL fresh DMEM with HT and 10% FBS. For the quantitative estimation of transfer efficiency, the cells were harvested, washed once with DMEM, and analyzed on a flow cytometer. Lipidic analogs to TMA-C2-Glu-C12 were examined using the same methods as those used for TMA-C2-Glu-C12.

2.5 Flow Cytometry Analysis

The fluorescence intensity of EGFP silencing by siRNA uptake into CHO-EGFP cells was estimated under a flow cytometer. The cells were gently harvested using 0.2% trypsin-EDTA solution at 24 h post-transfection, washed once with 10 mL DMEM, and 5.0×10^4 events were analyzed on an EPICS flow cytometer equipped with a 488-nm excitation laser wavelength operated at 450 V. The untreated cells were gated as a population on a flow cytometry histogram, and the relative EGFP-reduced efficiencies were estimated as the percentage of decreased values in a gate of the untreated population. To estimate the fluorescence intensity of Cy3-labbeled anti-luciferase siRNA by the uptake into CHO cells, the cells were transfected for 3 h with the transfer mixtures and analyzed using a flow cytometer at 24 h post transfection (5.0×10^4 events, 525-nm excitation laser wavelength, 750 V). The transfer efficiencies of Cy3 siRNA-transferred cells were estimated as the percentage of a gate range of more than the untreated population.

3 Results

3.1 The Effects of Glutamate-Based Lipidic Materials with Different Head Region Structures on Sirna Delivery

Three glutamate-based materials having different head region structures were tested; TMA-C2-Glu-C12, TMA-C4-Glu-C12, and TMA-C6-Glu-C12 (Fig. 1). By gating of the flow cytometry histogram, the untreated cells were predominantly comprised of 98.3% ± 0.22% of the positive population. When associated with the complexes of TMA-C2-Glu-C12 and anti-EGFP siRNA, the relative EGFP-reduced efficiencies were 42.5% ± 9.86% at 5 μL (Fig. 2). In contrast, TMA-C4-Glu-C12 and TMA-C6-Glu-C12 resulted in the efficiencies of 84.5% ± 3.06% and 78.4% ± 3.06%

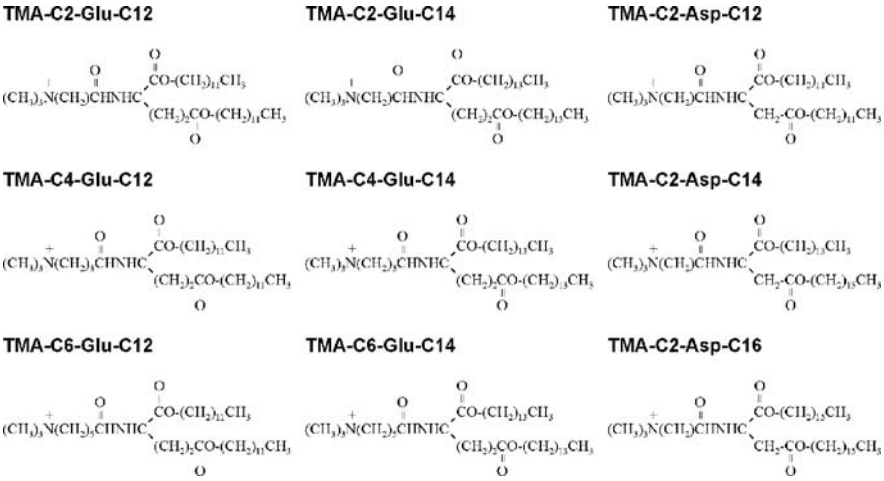

Fig. 1 Chemical structures of TMA-C2-Glu-C12 and its analogs

at 5 μL. These results showed the structural changing from C2 (-CH_2CO-) to C6 (-$(CH_2)_5CO$-) in the hea d region leads to the reduction of the ability of siRNA carrier. The chemical structure of -CH_2CO- in TMA-C2-Glu-C12 played an important role for the enhancement of biological functions as siRNA carrier.

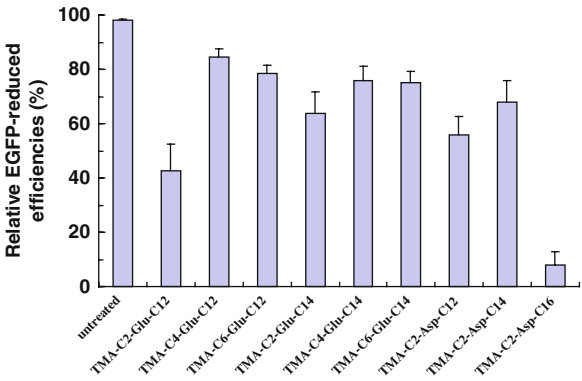

Fig. 2 The transfer effects of TMA-C2-Glu-C12 and its analogs

3.2 The Effects of Glutamate-Based Lipidic Materials with Different Tail Region Structures on siRNA Delivery

Three glutamate-based materials with different tail region structures were tested; TMA-C2-Glu-C14, TMA-C4-Glu-C14, and TMA-C6-Glu-C14. The relative EGFP-reduced efficiencies by TMA-C2-Glu-C14 were 63.7% ± 8.12% at

5 μL (Fig. 2). The ability of TMA-C2-Glu-C14 as siRNA carrier was approximately 1.5-fold less than that of TMA-C2-Glu-C12. Thus, the structural changing from C12 (-$(CH_2)_{11}CH_3$) to C14 (-$(CH_2)_{13}CH_3$) in tail regions diminished the ability of glutamate-based materials on siRNA delivery. In addition, the efficiencies by TMA-C4-Glu-C14 and TMA-C6-Glu-C14 at 5 μL were 75.9% ± 5.35% and 75.2% ± 4.01%, respectively. These results showed that TMA-C4-Glu-C14 or TMA-C6-Glu-C14 has the low ability in comparison with TMA-C2-Glu-C12, since their structures are different from the component of -CH_2CO- (C2) and -$(CH_2)_{11}CH_3$ (C12). Therefore, the chemical structure of -$(CH_2)_{11}CH_3$ in TMA-C2-Glu-C12 was crucial for the enhancement of biological functions as siRNA carrier.

3.3 The Effects of Aspartate-Based Lipidic Materials

Subsequently, the transfer abilities of aspartate-based materials having aspirate connector region were examined; TMA-C2-Asp-C12, TMA-C2-Asp-C14, and TMA-C2-Asp-C16. The silencing efficiencies by TMA-C2-Asp-C12 were 55.7% ± 7.08% at 5 μL (Fig. 2). The ability of TMA-C2-Asp-C12 was approximately 1.3-fold less than that of TMA-C2-Glu-C12. Thus, the structural changing from ethylene (-CH_2CH_2-) to methylene (-CH_2-) in connector region resulted in the reduction of its transfer ability. These results showed that the chemical structure of -CH_2CH_2- in TMA-C2-Glu-C12 is important for the enhancement of the ability as siRNA carriers. Additionally, TMA-C2-Asp-C14 and TMA-C2-Asp-C16 showed low efficiencies similar as TMA-C2-Glu-C14 or TMA-C6-Glu-C14. Among aspartate-based materials, TMA-C2-Asp-C12 had the highest potential as siRNA carrier; these observations were consistent with the results obtained on examination of glutamate-based materials.

4 Discussion

Attention has recently been focused on RNAi with siRNA as a powerful tool for gene silencing. Efforts toward the design and development of artificial materials on siRNA delivery system into mammalian cells are crucial for basic and therapeutic research. We are interested in studying the evolution of designed lipidic materials as potential siRNA carriers with high transfection efficiency and low cytotoxicity. In this study, we report for the first time that totally synthesized glutamate-based lipid TMA-C2-Glu-C12 is a more efficient material on siRNA delivery system.

Totally designed materials as potential siRNA carriers have been a major interest in an improvement of applications in the treatment of human genetic and non-genetic diseases. A number of studies have indicated that a variety of viral vectors, liposomes, and polycations can contribute to the development of siRNA delivery system. The question arises as to how the chemical structure of lipidic materials can perform to efficiently transfer siRNA into the cell cytoplasm. However, little

attempt has been made to investigate the structural and biofunctional features of lipidic materials as siRNA carriers. In this study, we demonstrate that the chemical structure of TMA-C2-Glu-C12 is essential for the enhancement of the transfer efficiencies on siRNA delivery system. Of particular interest is that, using analogs having different hydrocarbon chains and connector, a small structural alternation of TMA-C2-Glu-C12 leads to decreasing its ability as siRNA carriers. The structural features such as $-CH_2CO-$ and $-(CH_2)_{11}CH_3$ exhibited by TMA-C2-Glu-C12 may lead to a proper complex with siRNA to pass through the cell membrane barriers. Further, the ability of TMA-C2-Glu-C12 containing glutamate connector was superior to that of TMA-C2-Asp-C12 containing aspartate connector; the structural difference between TMA-C2-Glu-C12 and TMA-C2-Asp-C12 is only ethylene ($-CH_2CH_2-$) and methylene ($-CH_2-$). Although it is no obvious explanation for why the chemical structure of TMA-C2-Glu-C12 leads to biological function as potential siRNA carriers, ethylene group ($-CH_2CH_2-$) in TMA-C2-Glu-C12 structure may play an important role to facilitate intracellular delivery of siRNA. Taken together, these data provide a model of lipidic materials as potential carriers for siRNA delivery into cells. The chemical structure of TMA-C2-Glu-C12 having double-stranded dodecyl chains, modeled on cell membrane lipids, will be a good model of rational carrier design for a nonpathogenic delivery system.

Understanding of correlations between the chemical structure and biological function of lipidic materials may provide significant insights into the design and development of a new class of carrier agents. In future, the structural information of biological functions in our findings may be used for a rational design to regulate the transfer efficiency, the low cytotoxicity, and the tissue specificity on siRNA delivery system in vivo. Further investigations on glutamate-based lipidic materials are currently in progress. The development and optimization of lipidic materials for novel medical applications will be presented in the future.

Thin-Film Assembly of Totally Designed Lipidic Materials as Gene Carrier in Mouse Embryonic Neural Stem Cells: Thin-Film Assembly of Lipidic Material as Potential Gene Carrier

Ken-Ichi Kusumoto, Takahiro Nagata, and Itaru Hamachi

1 Introduction

Neural stem cells present in developing embryonic and adult nervous systems are immature and uncommitted cells that possess self-renewal potential and produce a vast array of highly specialized neural cells belonging to the central nervous system. Several studies have reported the development of gene delivery system for these neural cells as a potential application in gene therapy for neurodegenerative diseases and for understanding the genetic basis of brain development and function. Gene delivery system based on a variety of materials such as lipids, polypeptides, amino-dendrimers, and polyethylenimine have been used in mammalian cells, and currently, these systems are known to possess therapeutic applications. However, the transfer efficiencies of most lipidic materials with regard to neural cells, including neural stem cells, progenitor cells, neurons, and glia, are less than 5% compared to those of virus vectors.

Viral vectors are accepted as the most effective tools for gene delivery in neural cells in vivo and in vitro; however, there are problems such as immune reactions and tumorigenesis. Therefore, the use of nonpathogenic materials has attracted a considerable amount of interest. Efforts toward a comprehensive knowledge of the transfer activities of lipidic materials are crucial for developing a nonviral gene delivery system. The advantage of lipidic materials is the protection of DNA molecules by encirclement of their structures and low cytotoxicity and immunogenicity in in vivo transfection. Some of lipidic materials such as surfactants are known to form a variety of assembled structures such as spherical, rod-like, worm-like, and granular micelle. However, how lipidic assembly functions as potential gene carriers has remained controversial. Here, we have presented a detailed study on a novel model of gene delivery system mediated by thin-film assembly of diethanolamine-based lipid TMA-C2-DEA-C14 that is designed to take advantage of the chemical

K.-I. Kusumoto (✉)
Department of Biological Chemistry, Biotechnology and Food Research Institute, Fukuoka Industrial Technology Center, Kurume, Fukuoka 839-0861, Japan
e-mail: kkusumoto@fitc.pref.fukuoka.jp

M. Kamihira et al. (eds.), *Animal Cell Technology: Basic & Applied Aspects*, Animal Cell Technology: Basic & Applied Aspects 16, DOI 10.1007/978-90-481-3892-0_66,

structure of the presence of double-stranded hydrophobic chains in major cell membrane lipids such as phospholipids and sphingolipids.

2 Materials and Methods

2.1 Materials

The following chemicals, reagents, and equipment were obtained from the respective manufacturers: diethanolamine, myristic acid, ρ-toluenesulfonic acid, chloroacetyl chloride, toluene, tetrahydrofuran, chloroform, and pCMV-IE-hsGFP vector, Wako Pure Chemical Industries (Japan); trimethylamine, insulin, transferrin, selenium, human fibronectin, and poly-L-lysine, Sigma-Aldrich; Dulbecco's modified Eagle's medium/Ham's F12 medium (DMEM/F12), chemically defined lipid concentrate, and trypsin, Invitrogen; recombinant human EGF and FGF-basic, R&D Systems; micro slide glass, Matsunami Glass (Japan); carbon-coated grid, Okenshoji (Japan).

2.2 Diethanolamine-Based Lipid TMA-C2-DEA-C14

Diethanolamine-based lipid TMA-C2-DEA-C14 was modeled on the chemical structure having double-stranded hydrophobic chains in major cell membrane lipids such as phospholipids and sphingolipids. TMA-C2-DEA-C14 was synthesized by refluxing with dean-stark-trap in dry toluene with diethanolamine, myristic acid, and ρ-toluenesulfonic acid, by mixing in dry chloroform with chloroacetyl chloride, and then by mixing in dry tetrahydrofuran with trimethylamine. TMA-C2-DEA-C14 was purified on a silica gel column to more than 95% purity. TMA-C2-DEA-C14 with phase transition temperature of 33.7°C was derived from diethanolamine (DEA) that was used as a connector to bind 1 head region consisting of trimethylamine (TMA) and hydrophobic chain comprising 2 carbon atoms (C2) and 2 tail regions, each consisting of a hydrophobic chain comprising 14 carbon atoms (C14). For the preparation of lipidic assembly, TMA-C2-DEA-C14 was gradually self-organized by incubating in autoclaved deionized-distilled water for a month with a final concentration of 1.3 mM at 25°C (termed as TMA-C2-DEA-C14 assembly). For the preparation of dispersed solutions, TMA-C2-DEA-C14 was dissolved by ultrasonication for 1 min in autoclaved deionized-distilled water with a final concentration of 1.3 mM (termed as TMA-C2-DEA-C14-sonic) or by incubating for 15 min at each temperature above the phase transition temperature: 40, 50, 60, 70, 80, 90, and 100°C.

2.3 Mouse Embryonic Neural Stem Cells and Cell Culture

Neural stem cells were established from 14-day-old Balb/c mouse embryonic brains and were grown for a month in DMEM/F12 supplemented with 10 μg/mL insulin,

10 μg/mL transferrin, 1% chemically defined lipid concentrate, 10 μM selenium, 50 ng/mL EGF, and 25 ng/mL FGF-basic. Culture dishes and plates were coated and incubated for 16 h with 1 μg/mL fibronectin in DMEM/F12 at 37°C. Cells used in this study were subcultured until they had undergone 20–80 population doublings.

2.4 Transfection Assay by TMA-C2-DEA-C14

Neural stem cells were precultured overnight in poly-L-lysine-coated 24-well plates at a density of 1.0×10^5 cells/well in 1 mL DMEM/F12 with supplements. Tissue culture 24-well plates were coated with 20 μg/mL poly-L-lysine solution in H_2O for 16 h at 37°C. The pCMV-IE-hsGFP vector (1.5 μg/well) and 1.3 mM TMA-C2-DEA-C14 solution (5 μL/well) were mixed in 50 μL/well of DMEM/F12 without supplements and then incubated for 5 min at room temperature. The cells were transferred into 0.5 mL DMEM/F12 with supplements, and the transfection mixtures were added to the culture medium and incubated for 3 h at 37°C. Following transfection treatment, the cells were cultured in 1 mL fresh DMEM/F12 with supplements for 24 h. For quantitative estimation of the transfection efficiency, the GFP-expressed cells were counted under a fluorescence microscope in more than 3 different views (a minimum of 300 live cells/view) or analyzed on a flow cytometer.

2.5 Optical Microscopy Analysis

TMA-C2-DEA-C14 assembly or TMA-C2-DEA-C14-sonic was applied on a micro slide glass at a concentration of 1.3 mM and was observed under an Axiovert microscope (Carl Zeiss Ltd.). Subsequently, 5 μL of 1.3 mM TMA-C2-DEA-C14 assembly or TMA-C2-DEA-C14-sonic was mixed with the pCMV-IE-hsGFP vector (1.5 μg) in 50 μL of 150 mM sodium solution, incubated for 5 min, applied on a micro slide glass, and observed under an optical microscope (×1,000).

2.6 Transmission Electron Microscopy Analysis

TMA-C2-DEA-C14 assembly or TMA-C2-DEA-C14-sonic was applied on a carbon-coated grid at a concentration of 1.3 mM and incubated for 5 min. The grids were dried at room temperature and observed under a transmission electron microscope (TEM) H-7100 (Hitachi Ltd., Japan) at 75 kV. Subsequently, 5 μL of 1.3 mM TMA-C2-DEA-C14 assembly or TMA-C2-DEA-C14-sonic was incubated for 5 min with the pCMV-IE-hsGFP vector (1.5 μg) in 50 μL of 150 mM sodium solution, applied on a carbon-coated grid, and incubated for 5 min. The grids were individually washed with autoclaved deionized-distilled water and subjected to TEM analysis. The particle size of assembly was analyzed by counting at least 100 particles under TEM (×3,000) in different microscopic views.

3 Results and Discussion

3.1 Formation of TMA-C2-DEA-C14 Assembly

In order to determine an optimal formation of TMA-C2-DEA-C14 as potential gene carriers, the chemical structure of which is shown in Fig 1a, we investigated an appropriate method for preparing an aqueous solution of TMA-C2-DEA-C14. TMA-C2-DEA-C14 was found to generate lipidic assembly by incubation in water for a month at 25°C below the phase transition temperature. These particles were observed as opaque white (Fig. 1b). On the other hand, TMA-C2-DEA-C14 solutions prepared by ultrasonication or by incubation at more than 40°C in water were optically transparent (Fig. 1b).

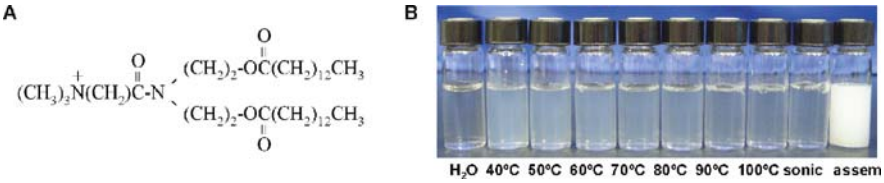

Fig. 1 (**a**) Chemical structure of TMA-C2-DEA-C14. (**b**) Photographs of TMA-C2-DEA-C14 assembly (assem) and dissolved solutions, TMA-C20DEA-C14-sonic, or 40–100°C

3.2 The Effects of TMA-C2-DEA-C14 Assembly on Gene Delivery in Neural Stem Cells

Neural stem cells were precultured in 24-well plates and incubated for 3 h with transfection mixtures containing pCMV-IE-hsGFP vector and TMA-C2-DEA-C14. On using TMA-C2-DEA-C14 assembly, fluorescence microscopy analysis at 24 h post-transfection showed that the transfection efficiency was 32.2% ± 6.93% of GFP-expressed cells. In contrast, the efficiency of TMA-C2-DEA-C14-sonic at 24 h post-transfection was 2.29% ± 2.02%, and those of the solutions prepared by incubation at 40 or 100°C were 5.00% ± 2.36% or 2.64% ± 3.62%, respectively. Thus, the transfer ability of TMA-C2-DEA-C14 assembly as gene carriers for neural stem cells was approximately 14-fold higher than that of TMA-C2-DEA-C14-sonic. These results showed that the biofunctional activity of TMA-C2-DEA-C14 is significantly enhanced by assembly.

3.3 Optical Microscopic Observation of TMA-C2-DEA-C14 Assembly

To investigate the structural characteristics of TMA-C2-DEA-C14 assembly, we first observed the assembly particles under an optical microscope (×1,000). Most of

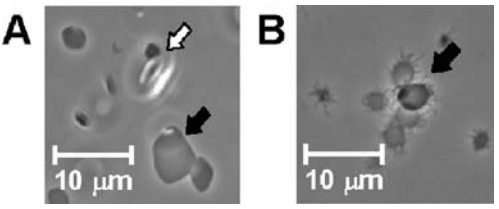

Fig. 2 Optical microscopy images (×1,000). (**a**) TMA-C2-DEA-C14 assembly (**b**) DNA/TMA-C2-DEA-C14.assembly complexes

the assembly particles were thin-film structures with polygonal shapes and rounded edges (Fig. 2a); however, the structural characteristics of TMA-C2-DEA-C14-sonic particles could not be observed since they were completely dispersed by ultrasonication. Subsequently, when TMA-C2-DEA-C14 assembly was associated with DNA, the shape of thin-film structures changed from polygonal to spherical, including ciliary morphogenesis (Fig. 2b). When TMA-C2-DEA-C14-sonic was associated with DNA, the complexes were observed as aggregate structures. Thus, the structural characteristic of TMA-C2-DEA-C14 assembly was completely different from that of TMA-C2-DEA-C14-sonic. These results showed that TMA-C2-DEA-C14 assembly was characterized by thin-film structures with polygonal shapes and rounded edges that can dramatically change to spherical structures, including ciliary morphogenesis, on association with DNA. This structural characteristic of TMA-C2-DEA-C14 assembly plays an important role in the enhancement of the biofunctional activity as gene carriers in neural stem cells.

3.4 Transmission Electron Microscopic Observation of TMA-C2-DEA-C14 Assembly

In order to further analyze the structural characteristic of TMA-C2-DEA-C14 assembly, we observed the thin-film structures under an electron microscope. TEM images revealed that TMA-C2-DEA-C14 assembly had thin-film microstructures with polygonal shapes and rounded edges with a particle size of 2.73 ± 1.48 μm. The structures of TMA-C2-DEA-C14-sonic were not observed. Subsequently, when associated with DNA, the thin-film microstructures with polygonal shapes were dramatically changed to spherical structures that contained a number of liposome complexes at a size of 50–300 nm (Fig. 3a). In contrast, DNA complexes formed with TMA-

C2-DEA-C14-sonic were aggregate structures containing a few liposomes (Fig. 3b). These results showed that TMA-C2-DEA-C14 assembly with a unique structural feature for generating a number of liposome complexes can deliver genes in neural stem cells. Therefore, we demonstrated that diethanolamine-based lipidic material TMA-C2-DEA-C14 is spontaneously self-organized by incubation at 25°C and that the biofunctional activity of TMA-C2-DEA-C14 assembly is to effectively deliver DNA into the cellular cytoplasm of neural stem cells by forming a number of liposome complexes.

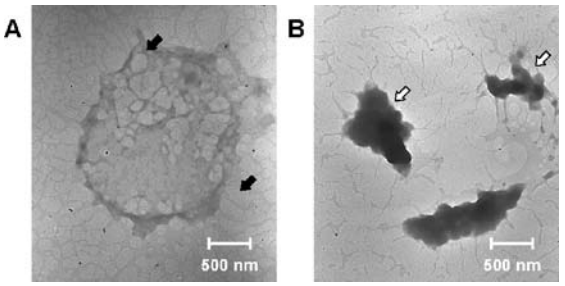

Fig. 3 TEM images (×15,000). (**a**) DNA/TMA-C2-DEA-C14 assembly complexes. (**b**) DNA/TMA-C2-DEA-C14-sonic complexes

In summary, this study demonstrated that lipidic assembly by TMA-C2-DEA-C14 has a promising potential to facilitate efficient gene delivery with low cytotoxicity into neural stem cells. We revealed that TMA-C2-DEA-C14 forms a thin-film structure of assembly (approximately 2.7 μm) after incubation at 25°C below the phase transition temperature; furthermore, TMA-C2-DEA-C14 assembly has the potential as gene carriers to deliver DNA into mouse embryonic neural stem cells with higher transfection efficiencies (up to approximately 40%) and low cytotoxicity. After association with DNA, TMA-C2-DEA-C14 assembly undergoes a conformational change from polygonal to spherical structures containing a number of liposomes. This structural feature of liposome complexes plays a key role in promoting successful gene delivery system for neural stem cells. Our findings are promising for future gene delivery research with regard to the design and development of lipidic materials for therapeutic applications.

Transfection System Using a Cocktail of Totally Designed Lipidic Materials in Chinese Hamster Ovary Cells: Lipidic Cocktail as Potential Gene Carrier for CHO Cells

Ken-Ichi Kusumoto, Takahiro Nagata, Eiichi Kanazawal, Takanori Sakai, Yoshihiko Yoshikawa, Takahiro Ogata, Naomi Nakatani, Tomoyuki Ishikawa, Shintaro Koga, Akio Shirasu, Shinji Morishita, Takayuki Emura, and Itaru Hamachi

1 Introduction

Chinese hamster ovary (CHO) cell line is known to be highly efficient for the production of therapeutic proteins, including cytokines and antibodies. Utilizing artificially constructed material as potential gene carrier is important for the bottom-up development of gene delivery system. However, few reports have focused on using totally designed lipidic compounds for gene transfer in mammalian cells. Several studies have reported various strategies for gene delivery system including viral vector-mediated introduction, liposome-mediated introduction, and polycation-mediated introduction. Viral vectors are accepted as the most effective tools for gene transfer into mammalian cells in vivo and in vitro. However, there are safety problems such as induction of immune reactions or tumorigenesis [1, 2]. Therefore, the use of nonpathogenic materials based on lipids or polymers has been attempted.

Lipidic materials have been used as an easy-to-use system to transfer DNA into mammalian cells. For example, commercial reagents such as Lipofectamine 2000 (Invitrogen) are available for use in a variety of researches. The advantage of lipidic materials is the protection of DNA molecules by encirclement of their structures and low cytotoxicity and immunogenicity in in vivo transfection compared with the use of vectors such as calcium phosphate or viral vectors. However, how the chemical structure and the structural feature of lipidic materials functions as potential gene carrier for CHO cells has been controversial. In previous studies, we demonstrated that totally designed lipidic materials provide a delivery system that is capable to improve the novel design and development of lipidic materials as

K.-I. Kusumoto (✉)
Department of Biological Chemistry, Biotechnology and Food Research Institute, Fukuoka Industrial Technology Center, Kurume, Fukuoka 839-0861, Japan
e-mail: kkusumoto@fitc.pref.fukuoka.jp

M. Kamihira et al. (eds.), *Animal Cell Technology: Basic & Applied Aspects*, Animal Cell Technology: Basic & Applied Aspects 16, DOI 10.1007/978-90-481-3892-0_67,

potential and nonpathogenic carriers in basic and therapeutic research [3–5]. Efforts toward a comprehensive knowledge of correlations between the structural features and biological functions of lipidic materials are crucial for controlling DNA/RNA delivery system into mammalian cells. Here, we have focused on understanding how lipidic materials that are designed by taking advantage of the chemical structure having double-stranded hydrophobic chains in major cell membrane lipids such as phospholipids and sphingolipids can enhance its biological function to promote intracellular delivery of DNA into CHO cells. Moreover, we have focused on whether lipidic materials can deliver DNA on three-dimensional large scale cultures of CHO cells.

2 Materials and Methods

2.1 Totally Designed Lipidic Materials

Totally designed lipidic materials were modeled on the chemical structure having double-stranded hydrophobic chains of phospholipids and sphingolipids in cell membranes [6–8]. A variety of lipidic materials (more than 150 of compounds), termed as a molecular repertoire, were synthesized. Each lipid had similar chemical structure (Fig. 1).

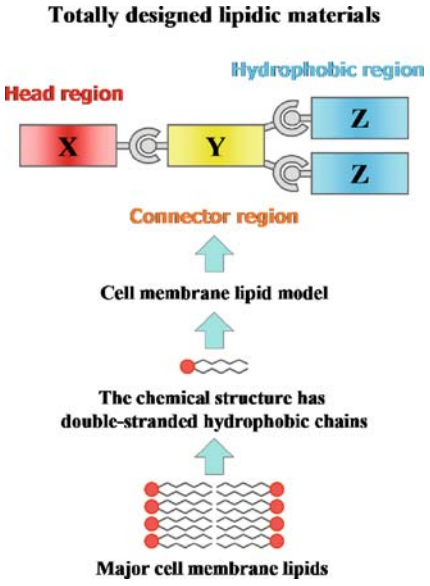

Fig. 1 Basic concept of totally designed lipidic materials

2.2 Combinatorial Analysis Using Lipidic Repertoire

CHO cells were precultured in 24-well plate in DMEM with 10% FBS. As shown in Fig. 2, each lipid, a repertoire of lipidic analog, was mixed to make the transfer complexes with DNA (pCMVIE-GFP). For the quantitative estimation of transfer efficiency, the cells were harvested and analyzed on an EPICS flow cytometer (Beckman Coulter Inc.).

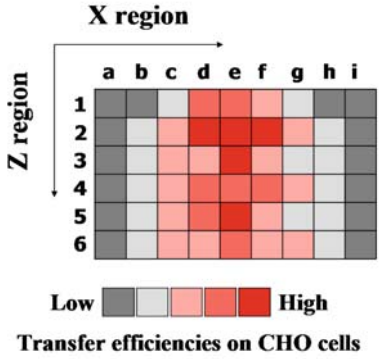

Fig. 2 Combinatorial analysis

2.3 Three-Dimensional Culture for CHO Cells

To develop three-dimensional culture system for CHO cells, we determined the optimal conditions for gas bag culture with ceramics scaffolds. CHO cells (1.0×10^7 cells/bag) were cultured for 3 days in 75–200 mL of DMEM with 10% FBS using gas bag (100 mL type) and 1.5 mg/bag of gold-loaded ceramics scaffolds (100–200 nm in diameter). After incubation, the cells were lysed with Triton X-100 and the cell numbers were estimated by measuring lactate dehydrogenase (LDH) activity (Promega). Subsequently, the cells were cultured for 3 days at different cell numbers (0.1–5.0×10^7 cells/bag), and the cells (1.0×10^7 cells/bag) were cultured for 5 days to identify growth curve.

2.4 Three-Dimensional Transfection Assay

CHO cells (1.0×10^7 cells/bag) were precultured overnight in 100 mL DMEM with 10% FBS in permeable gas bag (Nipro, Japan) including 1.5 mg gold-loaded ceramics scaffolds. The cells were transfected with 5 mL of the transfer mixtures including 100 mg pCMVIE-GFP and 140 μl of 5 mM CHO-cocktail. For the quantitative estimation of transfection efficiencies, the cells were harvested and analyzed on a fluorescent microscope, a flow cytometer, and Western immunoblot assay.

3 Results and Discussion

3.1 Optimization of Lipidic Materials for Transfection on CHO Cells

To identify lipid material as potential gene carrier for CHO cells, we examined first screening by using a lipidic repertoire. When 150 types of lipidic materials were tested for transfection on CHO cells, we could find out one of lipid (termed as CHO-specific lipid A) (Fig. 3a). Further, we tried to identify a quadratic lipid among a repertoire to be able to generate a synergic effect on transfection efficiencies. As a result, some lipid (termed as quadratic lipid B) could significantly enhance the transfer ability of CHO-specific lipid A (Fig. 3b). We further investigated the optimal ratio of CHO-specific lipid A versus quadratic lipid B to enhance the transfection efficiencies on CHO cells. The lipidic mixture (termed as CHO-cocktail) may be lead to a proper complex with DNA to pass through the cell membrane barriers. Further, the transfer ability of CHO-cocktail was a higher degree than superior commercial reagents Lipofectamine 2000 and FuGENE. The chemical structure of CHO-cocktail having double-stranded hydrophobic chains, modeled on cell membrane lipids, will be a good model of rational carrier design for a nonpathogenic delivery system.

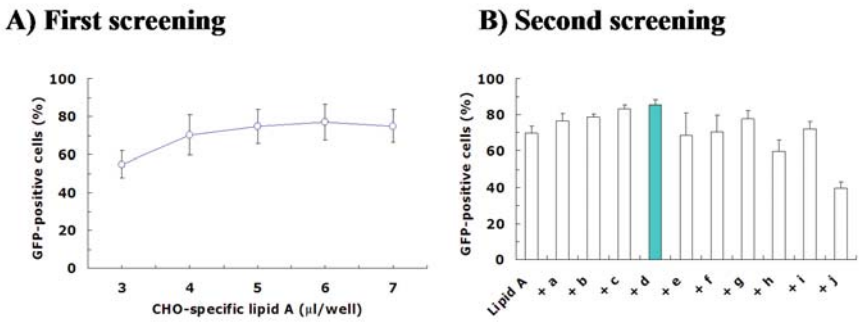

Fig. 3 (**a**) First screening of a lipidic repertoire for transfection on CHO cells; CHO-specific lipid A. (**b**) Second screening for enhancement of the ability of CHO-specific lipid A

3.2 Three-Dimensional Culture for CHO Cells

To develop the three-dimensional culture system for CHO cells, we examined the culture conditions of CHO cells using permeable gas bag and gold-loaded ceramics scaffolds (Figs. 4 and 5). We chose a condition; 1.0×10^7 cells/bag, 100 mL culture medium, and 1.5 g scaffolds/bag and observed the growth curve (Fig. 4c). These results showed that CHO cells can grow in gas bag system equipped with ceramics scaffolds.

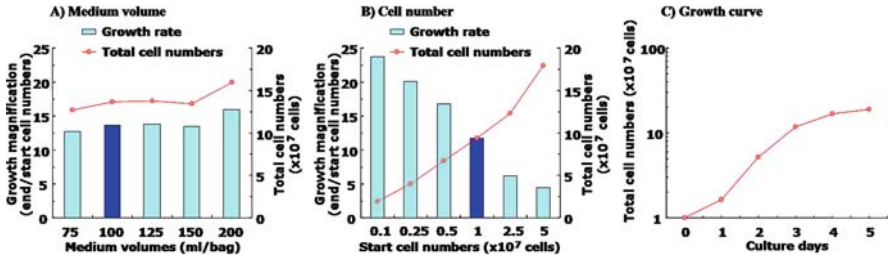

Fig. 4 Three-dimensional culture on CHO cells. (**a**) Medium volume dose response. (**b**) Different cell numbers. (**c**) Growth curve. The cells were cultured at each day in 100 mL DMEM with 10% FBS in gas bag including 1.5 g of scaffolds

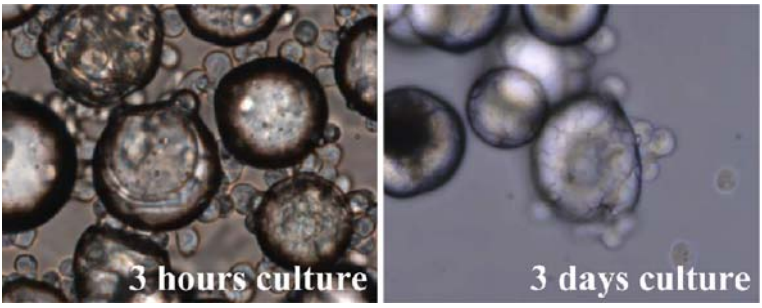

Fig. 5 Differential images (×400). The cells were cultured at 3 h (*left image*) or 3 days (*right image*) on gas bag culture conditions. A number of CHO cells were bound and adhered on gold-loaded ceramics scaffolds

3.3 Three-Dimensional Transfection for CHO Cells

CHO cells were precultured for 1 day in 100 mL DMEM with 10% FBS in gas bag including 1.5 g of scaffolds. Next day, the cells ($1.5–2.0 \times 10^7$ cells/bag) were transferred with 100 μg DNA/CHO-cocktail complexes. On 3 days culture, the cells were harvested and analyzed by a flow cytometer and Western immnoblot assay. As shown in Fig. 6, the transfection efficiencies on three-dimensional culture were 97.9%. Cell pellets were observed as yellow-green under a fluorescent lamp. Moreover, total amount of GFP in cell pellets was 2 mg at 10^8 cells/100 mL/2 days that is measured by Western immnoblot assay.

In summary, our findings may improve the development of gene delivery system through utilizing artificially lipidic compounds in a powerful research tool and in therapeutic research. Here, we have focused on understanding how the lipidic materials that are designed by taking advantage of the chemical structure having double-stranded hydrophobic chains in major cell membrane lipids such as phospholipids and sphingolipids can enhance its biological function to promote

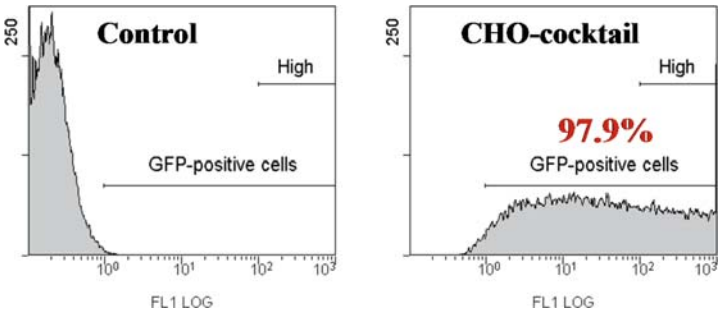

Fig. 6 The transfection efficiencies of lipidic material CHO-cocktail on three-dimensional culture of CHO cells. The cells were transfected on gas bag culture condition equipped with gild-loaded ceramics scaffolds. The cells were harvested at 48 h post-transfection and analyzed on a flow cytometer. Control; untreated cells. CHO-cocktail; transfected cells with CHO-cocktail

intracellular delivery of DNA. We demonstrate that a cocktail composed of 2 types of totally designed lipidic materials among a molecular repertoire is useful as a power tool to carry out three-dimensional transfection with high efficiency on CHO cells. Insight into this molecular repertoire may improve our understanding of how the chemical structure and the structural feature of artificial materials have a biological function as potential gene carrier target for various mammalian cells. This molecular repertoire may be able to lead to the rational design of artificially lipidic materials. In this study, our findings suggest that this approach can serve as a novel model for the development of the expression system for the large-scale production of recombinant proteins.

References

1. Check, E. (2005) Gene therapy put on hold as third child develops cancer. *Nature* **433**: 561.
2. Marshall, E. (1999) Gene therapy death prompts review of adenovirus vector. *Science* **286**: 2244–2245.
3. Kusumoto, K.I., Akao, T., Mizuki, E., Nakamura, O. (2006) Gene transfer effects on various cationic amphiphiles in CHO cells. *Cytotechnology* **51**: 57–66.
4. Kusumoto, K.I. (2009) Structural features of glutamate-based lipidic materials for small interfering RNA delivery system. *J. Biomed. Mater. Res. A*. **89**(3): 739–750.
5. Kusumoto, K.I., Yamashita, S., Nagata, T., Ido, T., Hamachi, I., and Akao, T. (2009) Thin-film assembly of diethanolamine-based lipidic material as potential gene carrier in mouse embryonic neural stem cells. *J. Biomed. Mater. Res. A*. **91**(1): 1–10.
6. Kunitake, T. and Okahata, Y. (1977) A totally synthetic bilayer membrane. *J. Am. Chem. Soc*. **99**: 3860–3871.
7. Kunitake, T., Nakanishi, N., Shimonura, M., Okahata, Y., Kano, K., and Ogawa T. (1980) Unique properties of chromophore-containing bilayer aggregates: enhanced chirality and photochemically induced morphological change. *J. Am. Chem. Soc*. **102**: 6642–6644.
8. Kunitake T. (1986) Organization and functions of synthetic bilayers. *Ann. NY Acad. Sci*. **471**: 70–82.

Size Dependent Heat Generation of Magnetic Nanoparticles Under AC Magnetic Field for Cancer Therapy

Jun Motoyama, Toshiyuki Hakata, Ryuji Kato, Noriyuki Yamashita, Tomio Morino, Takeshi Kobayashi, and Hiroyuki Honda

1 Introduction

Hyperthermic treatments have been used for many years, particularly in anticancer therapy. Magnetic nanoparticles, which is used as a heating mediator for a local hyperthermia, is easily focus on the heating region by injecting selectively. The use of such particles is based on the fact that multidomain ferro- or ferri-magnetic materials are heated by an alternating magnetic field due to hysteresis losses [1] Single domain particles of magnetite can also generate heat by relaxation loss. Ten nanometer of diameter is supposed to be a boundary size to allocate particles between single-domain and multi-domain. Optimal diameter of magnetic nanoparticle for magnetic nanoparticle-mediated hyperthermia should be investigated in detail. There, we drew attention to the specific-surface area (SSA) as a represented index for expressing particle size and microscopic structure. The SAR, which is defined as the energy amount converted into heat per unit time and unit mass of those magnetic particles were studied under several conditions of AC magnetic field.

Our group have introduced cationic liposome technology in order to enhance the surface interaction between cells and heating mediator, and thereby improve its localization. We called them the magnetic cationic liposome (MCL). In previous animal studies, we have demonstrated the efficacy of hyperthermia using them. In addition, we have described the capability of immunological reaction in cancer cells, which would occur by increased amount of the heat-shock protein 70 (HSP70), following hyperthermic treatment with MCL [2].

J. Motoyama (✉)
Graduate School of Engineering, Nagoya University, Nagoya, 464-8603 Japan;
Nanotherapy Co., Ltd, Nagoya, 451-0044 Japan
e-mail: jun.motoyama@nipponkayaku.co.jp

M. Kamihira et al. (eds.), *Animal Cell Technology: Basic & Applied Aspects*, Animal Cell Technology: Basic & Applied Aspects 16, DOI 10.1007/978-90-481-3892-0_68,

In this study, we applied our hyperthermic treatment system with the refined MCL to 7,12-Dimethylbenz(a)anthracene (DMBA)-induced rat mammary cancer model.

2 Heat Generation Capacity by SSA

2.1 Method

Magnetite nanopartiles were dispersed in distilled water with the same concentration of 20 mg/mL. Those magnetite dispersions were filled in the cylindrical polypropylene tubes and gelated with kappa-carrageenan. Temperature increase was caused by the upwardly generated AC magnetic field from the surface of the irradiation coil of the AMF radiator (Fig. 1). The samples contained 5 mg of magnetite nanoparticles in each. As a control, kappa-carrageenan gel was put into the sample tube without magnetite dispersions.

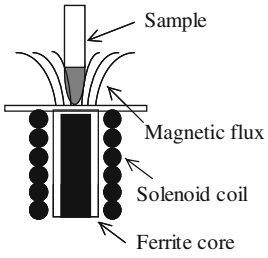

Fig. 1 Schematic apparatus of experiments

The alternating-magnetic-field (AMF) radiator was arranged to change its frequency and amplitude. A list of those arrangements of the experimental courses is shown in Table 1.

The magnetic properties of the magnetite nanoparticle are shown in Table 2.

The temperature of the samples were measured by using optical thermometer (FX-9020; Anritsu Meter Co., Tokyo). After the experiments, all samples were brought to measure the iron contents by the potassium thiocyanate method to determined the magnetite concentration in the sample precisely. The control was also exposed under the AMF, and confirmed that has no affection to heat generation.

The SAR values of the samples were determined from the time dependent calorimetric measurements.

Table 1 Applied AC magnetic energy for experiment

Applied Frequency (kHz)	Applied Power (kW)
360	1.6, 3.5, 5.2
200	2.5, 6.0, 13.0
110	2.5, 6.0, 13.1

Table 2 Physical properties of the magnetite particles for the experiment

Sample	Particle diameter			Saturated magnetization (Am^2/kg)	Coercivity (kA/m)	SSA (m^2/g)
	TEM method (nm)	DLS method (nm)	DLS method Polydispersity index			
A	120	1,986	0.57	82.5	7.2	12
B	40	1,657	0.45	75.0	10.4	30
C	14	539	0.28	67.7	6.4	57
D	11	109	0.15	63.2	3.0	74
E	10	109	0.21	64.1	2.3	84
F	10	109	0.25	57.9	1.2	92
G	10	146	0.23	57.5	6.0	107
H	10	93	0.30	51.6	3.0	121
I	10	84	0.18	52.9	0.32	125
J	10	94	0.29	49.7	1.4	131
K	10	107	0.19	48.9	3.5	145
L	10	130	0.25	47.4	2.6	159
M	10	105	0.22	38.1	0.9	190

3 Result

Figure 2 shows the typical profiles of the time-dependent temperature curve during the AC magnetic field irradiation. The SAR values (W/g) can be calculated by the following equation [3]:

$$\mathrm{SAR} = \mathrm{C}\frac{\Delta T}{\Delta t}\frac{1}{m_{\mathrm{mag}}} \tag{1}$$

where C is the sample-specific heat capacity which is calculated as a mass weighed mean value of magnetite and water. In this study, a heat capacity for water $\mathrm{C_{water}} = 4.18$ J/gK is used for the sample heat capacity. $\Delta T/\Delta t$ is the initial slope of the time-dependent temperature curve. As shown in Fig. 2, there are as good as the

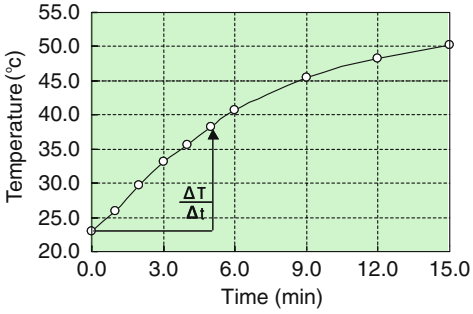

Fig. 2 Typical profile of heat generation under AC magnetic field

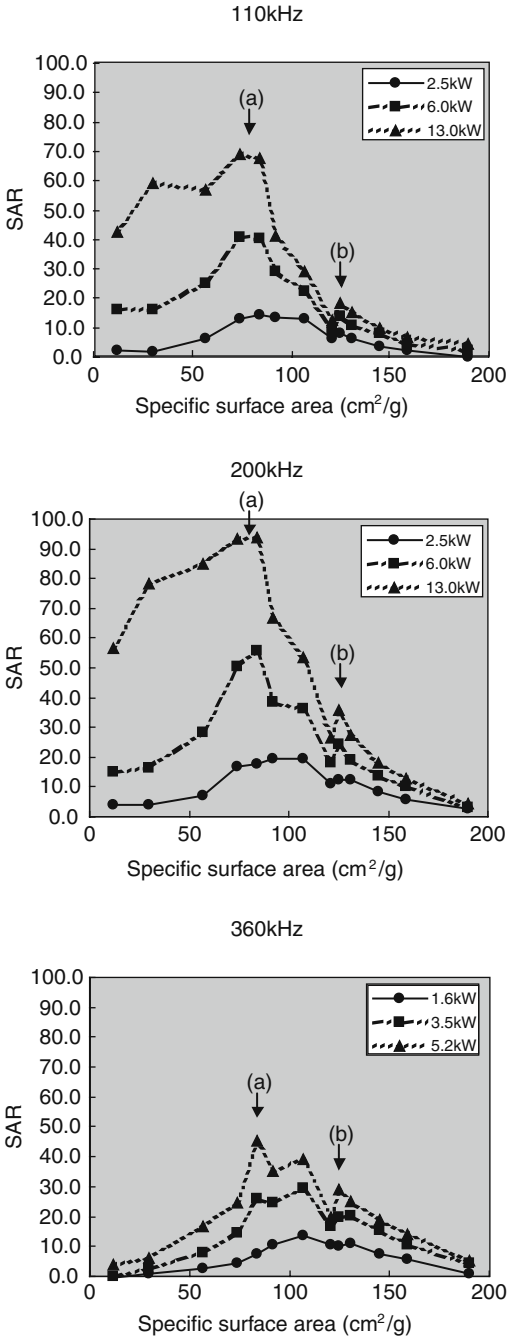

Fig. 3 SAR plots against SSA of the particles

linear relations in 0–5 min intervals for calculating $\Delta T/\Delta t$. m_{mag} is the magnetite content per gram of the sample tubes. The SAR values of the samples calculated by the equation (1) are plotted in Fig. 3.

The two local maximum values of the SAR were observed where SSA is approximately 90 m^2/g (a) and 120 m^2/g (b) separately in all the experimental intensities of AC magnetic field's frequency and power.

It has been reported that the SAR of magnetite particle in an external AC magnetic field can be attributed to two kinds of power loss mechanisms; one is hysteresis loss and others is relaxation loss [4]. Those two mechanisms are believed to be depended on particle sizes. The hysteresis losses are for larger particles and relaxation losses are for smaller particles. SSA value represent particle diameter, therefore, smaller SSA particles express larger diameter. Consequently, it is considered that the maximum value (a) in Fig. 3 correspond to hysteresis loss, and maximum value (b) attributes to relaxation loss.

The differential of magnitude of SAR by the AC power are also distinguishable by the particle sizes indicated by the SSA. Its boundary existed between two maximum values of the SAR in Fig. 3. As a result, two mechanisms of heating affects to the SAR value differently. The SAR values for the particles below the 110 m^2/g of SSA seemed more susceptible against to the power of AC magnetic field in all frequencies as well. Therefore, hysteresis loss induced heating is strongly affected by the strength of applied AMF.

4 Treatment of Spontaneous Cancer Model

4.1 Method

Eight-week-old Sprague-Dawley (SD) rats were purchased from the Charles River Laboratory Japan, Inc. (Kanagawa, Japan). A single dose of 20 mg DMBA dissolved in sesame oil were administered to 20 rats via esophageal intubation. After 10 weeks, 4 rats developed mammary tumors at more than 1 site in the body. In the each of these rats, we selected 1 tumor region that exceeded 10 mm in its long axis and used this for the experiments.

Magnetite nanoparticles (average diameter; 10 nm, SSA; approximately 90), N-(α-trimethyl-ammonioacetyl) didodecyl-D- glutamate chloride (TMAG), Dilauroyl- phosphatidylcholine (DLPC) and dioleoylphos- phatidylethanolamine (DOPE) were used to prepare the MCL.

The MCL were infused gradually into the tumor directly in approximately 30 min by using an infusion pump (SP100i; World Precision Instruments Inc., FL, USA). The applied dose of the MCL was approximately 2 mg MCL per mL tumor volume. After the injection, the rats were subjected to the first hyperthermia treatment for 30 min under anesthesia. The treatment were repeated on the following 2 days. The rats were bedded above an irradiation coil. The applied AC magnetic field

was 360 kHz. The temperatures at the surface of the tumor tissue and rectum were measured by optical fiber probe thermometers.

5 Result

Figure 4 shows tumor volume profiles after the treatment in each rat. In all 4 rats, we observed multiple growth of tumors at 1–3 sites in the body. Although those tumor areas were untreated, their growth volumes were also measured. In rat B, there were 3 sites of untreated sites of the tumor, 1 site of which grew rapidly. The others were, however, reduced in volume and had regressed completely after 31 days. In other rats, untreated sites of tumor were also reduced in volume, or well controlled.

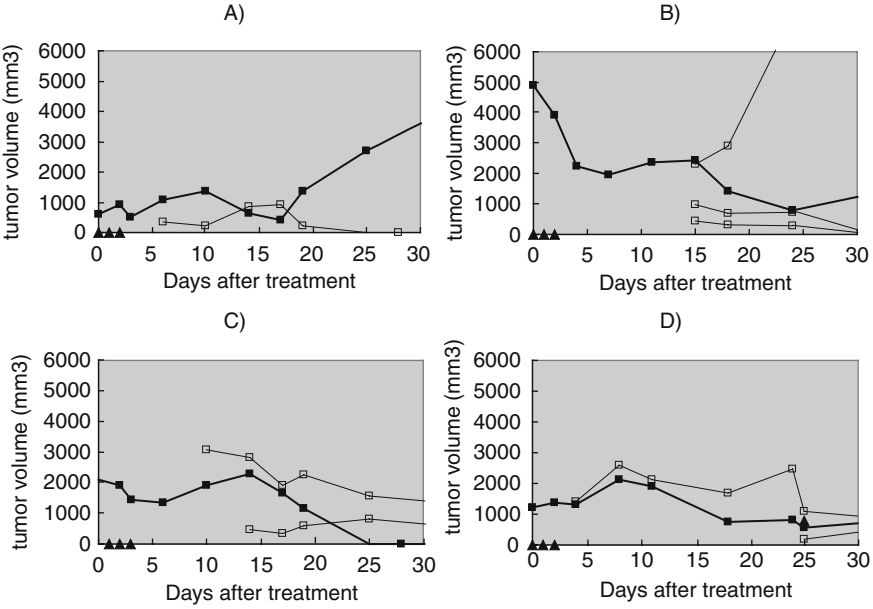

Fig. 4 Tumor growth profiles for each rat after 3 treatments. Closed square: treated tumor; Open square: untreated tumor

6 Conclusion

Magnetite nanoparticles that have approximately 10 nm diameter have different magnetic properties represented by SSA. By means of SSA, Mechanism of heat generation of magnetite nanoparitcles seems different in the vicinity of 110 m^2/g of SSA. Therefore, magnetite nanoparticles would be selective by its SSA and it will be reasonable to formulate MCL. By using those refined MCL, hyperthermia treatment is also effective in a spontaneous cancer model.

References

1. Andrä, W. and Nowak, H., (1998) *Magnetism in Medicine: A Handbook*. (p. 455) Wiley-VCH: New York.
2. Ito, A., Shinkai, M., Honda, H., Wakabayashi, T., Yoshida, J., and Kobayashi, T. (2001) Augmentation of MHC class I antigen presentation via heat shock protein expression by hyperthermia. *Cancer Immunol. Immunother*. **50:** 515–522
3. Babincova, M., Leszcznska, D., Sourivong, P., Čičmanec, P., Babinec, P. (2001) Superparamagnetic gel as a novel material for electromagnetically induced hyperthermia. *J. Magn. Magn. Mater*. **225:** 109–112
4. Mornet, S., Vasseur, S., Grasset, F., and Duguet, E. (2004) Magnetic nanoparticles design for medical diagnosis and therapy. *J. Mater. Chem*. **14**: 2161–2175

Functional Evaluation of Anticancer Drugs in Human Leukemia Cells Based on Metabolic Profiling Technique

Daisuke Miura, Yoshinori Fujimura, Hirofumi Tachibana, and Hiroyuki Wariishi

1 Introduction

To date, mass spectrometry (MS) coupled with pre-separation technique such as liquid chromatography (LC-MS) or gas chromatography (GC-MS) has been known to be a conventional strategy for metabolomics [1–3], but these methods have several disadvantages for pharmaceutical metabolomics. First, sample preparation of such methods includes complicated steps such as sample extraction, derivatization, desalting, and/or concentration before further MS analysis. Second, large sample volume is required because of lower sensitivity. Third, albeit with new LC developments such as ultra-performance liquid chromatography (UPLC), total LC analysis time is still on the order of several minutes. Although GC coupled with time-of-flight MS had been developed to take shorter time than conventional GC-quadrupole-MS because of the ability to deconvolute co-eluted peaks easily, analysis time of GC is almost the same as that of UPLC. There is another problem that thwarts the development of MS-based metabolomics techniques. The appearance of adduct ions containing sodium or potassium ion, especially in positive ion mode, makes metabolomic data more complicated [4]. Resolving of these issues is indispensable for highly sensitive and high-throughput analysis in pharmaceutical metabolomics research area because thousands of samples should be analyzed in the first large scale screening. Thus, 9-aminoacridine (9-AA) was utilized in the present study to develop MS mearsurement with negative ionization mode. In contrast to the methods mentioned above, direct MS analysis, especially, matrix-assisted laser desorption ionization (MALDI)-MS has advantages for metabolite analysis because it is a highly sensitive, high-throughput, and low sample-consuming (within 1 μL) technique compared to the other conventional analytical platforms based on LC-, GC- or CE-MS [5]. In addition, MALDI has recently been reported to be suitable not only for high-molecular-weight polymers or peptides but for low-molecular-weight

D. Miura (✉)
Innovation Center for Medical Redox Navigation, Kyushu University,
Higashi-ku, Fukuoka 812-8582, Japan
e-mail: daipon@agr.kyushu-u.ac.jp

M. Kamihira et al. (eds.), *Animal Cell Technology: Basic & Applied Aspects*, Animal Cell Technology: Basic & Applied Aspects 16, DOI 10.1007/978-90-481-3892-0_69,

metabolite analysis [6–8]. In the present study, we developed the methodology of the rapid and direct analysis of cellular metabolites by MALDI-MS for high-throughput and non-targeted metabolomic analysis, and applied this technique to multivariate analysis for recognizing the difference among cellular metabolite profiles.

2 Materials and Methods

2.1 Reagents

9-AA hydrochloride was obtained from Sigma-Aldrich (St. Louis, MO) and recrystallized prior to use 9 (–)-Epigallocatechin-3-O-gallate (EGCG), 5-fluorouracil (5-FU), superoxide dismutase (SOD), Trypan Blue, propidium iodide, and catalase were purchased from Sigma-Aldrich (St. Louis, MO). Methotrexate (MTX) and metabolite standards used in this study were bought from Wako Pure Chemical Industries, Ltd. (Osaka, Japan).

2.2 Cell Culture

Jurkat cells, human acute lymphoblastic leukemia, were obtained from the Japanese Cancer Research Resources Bank (Tokyo, Japan) and were maintained in RPMI-1640 (Nissui, Tokyo, Japan) supplemented with 5% fetal bovine serum (FBS: Biological Industries, Kibbutz Beit Kaemek, Israel), 100 U/mL penicillin G, 100 mg/mL streptomycin and 10 mM HEPES buffer in a humidified atmosphere with 5% CO_2 at 37°C. To assess cell proliferation, cells at a density of 2×10^5 cells/ml were treated with the indicated concentrations of either MTX, 5-FU, or EGCG for 72 h in RPMI supplemented with 2% FBS, 5 mg/mL BSA, 5 U/mL SOD and 200 U/mL catalase. After treatment, the trypan blue dye-exclusion test using 0.5% trypan blue dye was performed for counting viable cells.

2.3 Flow Cytometric Analysis

Jurkat cells treated with each anti-cancer drug with a IC50 concentration for 72 h were suspended in 70% ethanol and incubated at –20°C for more than 4 h. The cells were washed with phosphate-buffered saline (PBS) and resuspended in PBS together with 10 μg/mL RNaseA. Incubation was continued at 37°C for 20 min. The cellular DNA was then stained by applying propidium iodide (50 μg/mL) for 30 min at room temperature. The stained cells were analyzed by flow cytometry (FACS Calibur; Becton Dickinson, Sunnyvale, CA) for relative DNA content. ModFit LT software (Verity Software House, Inc., Topsham, ME) was used to assess cell cycle distribution and sub G1 region as the apoptotic cell population.

2.4 Samples Preparation for High-Throughput Metabolic Profiling

Jurkat cells incubated for 72 h were collected by centrifugation, 200*g*, for 5 min, followed by washing twice with ice-cold PBS. The cells that were resuspended in PBS at a density of 5×10^6 cells/mL were directly dropped onto a stainless MALDI sample plate, followed by mixing with 0.5 μL matrix solution (10 mg/mL 9-AA in methanol) on the sample plate. About 2,500 cells (0.5 μL) were applied onto the sample plate.

2.5 Mass Spectrometry and Multivariate Statistical Analysis

Mass spectrometric analysis was performed on an AXIMA-QIT-TOF mass spectrometer (Shimadzu, Japan). Metabolite peaks were assigned by searching accurate mass to KEGG or METLIN metabolite databases.

Multivariate data analyses, principal component analysis (PCA) and orthogonal partial least squares discriminant analysis (OPLS-DA) [9], were carried out using SIMCA-P+ version 11.5 (Umetrics, Sweden).

3 Results and Discussion

Inhibition of Jurkat cell growth by treatment with anticancer drugs.

It has been reported that MTX competitively and reversibly inhibits dihydrofolate reductase (DHFR), an enzyme that participates in the tetrahydrofolate synthesis. DHFR catalyses the conversion of dihydrofolate to the active tetrahydrofolate. Folate is compulsory for the de novo synthesis of the nucleoside thymidine, essential for DNA synthesis. In addition, folate was also known to be an indispensable molecule for purine base synthesis, and such purine synthesis may be inhibited upon treatment with antifolate [10]. Therefore, MTX is able to inhibit the synthesis of DNA, RNA, thymidylates, and proteins. On the other hands, 5-FU acts as a pyrimidine analogue and is transformed inside the cell into different cytotoxic metabolites that are then incorporated into DNA and RNA, finally inducing cell cycle arrest and apoptosis by inhibiting the cell′s ability to synthesize DNA [11]. Generally, EGCG has been known to be a naturally occurring anticancer drug, and has been shown to be an efficient inhibitor of DHFR, and be capable of disturbing folate metabolism in the cells, and causing the inhibition of DNA and RNA synthesis [12]. In the present study, we examined the antiproliferative effects of three anticancer drugs, MTX, 5-FU, and EGCG, on Jurkat cells. All three drugs inhibited the growth of Jurkat cells in a dose-dependent manner and the 50% inhibition concentration (IC50) of MTX, 5-FU, or EGCG was 2.5 nM, 0.5 μM, or 50 μM, respectively. In addition, flow cytometric analysis revealed that all three drug-treatments inhibited cell cycle progression based on the increase in the percentage of cells in the G2/M phase. Furthermore, the increase in subG1 population was also observed in both MTX- and

5-FU-treated cells, indicating that both drugs were able to induce apoptosis. Taken together, these results suggest that anticancer drug-induced reduction of the viable cell number may be due to the accumulation of the cells in G2/M phase and/or the induction of apoptosis.

High-through Metabolic Profiling of Anticancer Drug-treated Jurkat Cells.

There are little information about the metabolic response of cancer cells against MTX and 5-FU, although these drugs are well-known and well-established anticancer drugs that have been known to inhibit nucleotide biosynthesis. EGCG, a major component of green tea polyphenols, is also recognized to exhibit antiproliferative effects for cancer cells. High-throughput metabolite profiling method developed in this study is thought to be suitable for validating drug efficacy and investigating metabolic response of drug-treated cancer cells. Recently, multivariate statistical analysis, such as PCA or OPLS-DA, is thought to be a powerful tool for holistic evaluation of complex metabolic state by clustering each sample presuming acquired spectrum as multivariate data [9, 13]. Unsupervised multivariate analysis method, PCA model, provides a summary or overview of all observations or samples in the data table. In addition, groupings, trends, and outliers can also be found. First we applied MALDI-MS spectra to PCA for recognizing metabolic states of Jurkat cells treated with either MTX, 5-FU, or EGCG with an IC50 concentration. The cells suspended in PBS were applied onto the sample plate, and adjusted to the 2,500 cells/well. The result of PCA score plot clearly demonstrated that the independent cluster was formed among three kinds of anticancer drug-treated cells. The corresponding loadings plot showed the altered MS peaks in each samples. The peak intensities and corresponding positions on the loading plot of nucleotide derivatives were shown. In the loading plot, several nucleotide metabolites such as adenosines, guanosines, uridines, and these derivatives had a comparatively strong impact on the clear separation of each cluster along with component 1 and component 2. Especially, adenosines (ATP, ADP, cAMP) strongly contributed to the separation along with PC1, and UTP is responsible for separating the groups along with PC2. These data clearly showed that anticancer drugs used in this study strongly inhibited nucleotides biosynthesis of Jurkat cells. It was reported that MTX restricts purine nucleotide synthesis but to stimulate of pyrimidine biosynthesis [14], suggesting that high throughput metabolic profiling method developed in the present study can distinguish the difference of metabolic responses of the cells against each anticancer drug. Interestingly, the concentration of UDP-N-acetylglucosamine, which is one of the sources of building block of glycosaminoglycan, was dramatically decreased only in MTX-treated cell. Glucosaminoglycan has several number of physiological roles and biological functions such as anticoagulant activity, tissue hydration and several cellular functions, i.e., cell adhesion, motility, migration, proliferation and differentiation [15, 16]. This result indicates that down regulation of UDP-N-acetylglucosamine biosynthesis is one of the target of MXT for its anticancer efficacy. In summary, it can be concluded that metabolic profiling with MALDI-MS developed in this study is a useful tool for first screening in drug development since the method is not only very high throughput but also able to mine functional information from a multivariate analysis. A PCA model provided

an overview of all observations or samples in the data table by projecting and clustering each sample, and made us recognizing holistic difference of complex metabolic state in each sample. However, the details of the differences of each cluster are still unclear. Supervised method OPLS-DA was then used to facilitate the isolation of the variables responsible for the discrimination between MTX- and EGCG-treated cells. Figure 1a showed OPLS score plot, and the 2-component OPLS models were showed that R2Y and Q2 were 0.813 and 0.681, respectively. The OPLS S-plot, a plot of the covariance versus the correlation in conjunction with the variable trend plots allows easier visualization of the data. The variables that changed most will be plotted at the top or bottom of the 'S' shape plot, and that do not vary significantly be plotted in the middle9. OPLS S-plot against MTX- and EGCG-treated cells was also shown in Fig. 1b. Stearic acid and unknown compound (m/z 448.00) were found from the S-plot as variables that have strong contribution to separate MTX- and EGCG-treated cells, although the significance of accumulation of these compounds in each cells were still unclear. These peaks could not be found from PCA score plot, indicating that MALDI-MS metabolic profiling with OPLS-DA gave us enough information for data mining about the difference of cellular metabolic state, or validation of efficacy and safety of anticancer drugs.

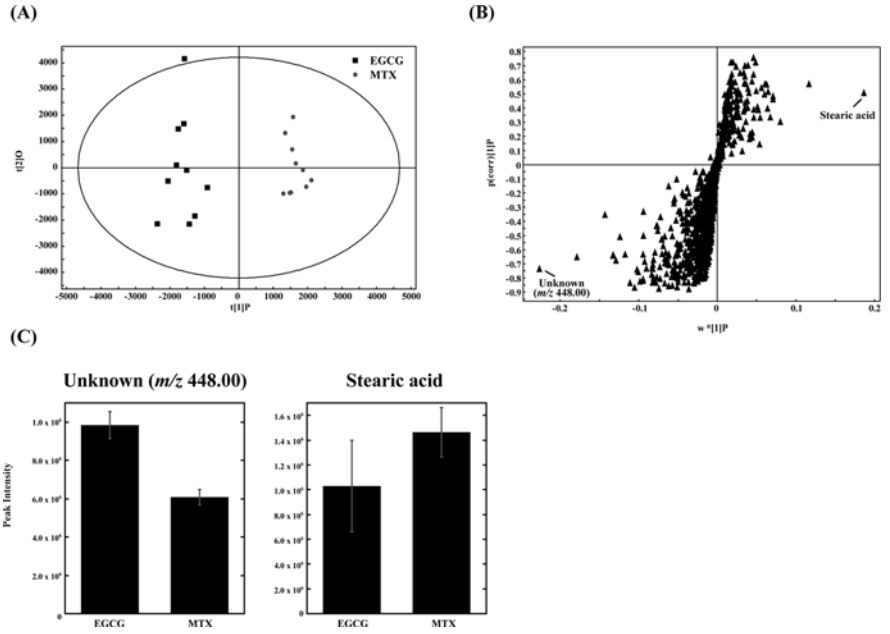

Fig. 1 OPLS-DA model based on metabolite profiles of direct MALDI-MS analysis of MTX- and EGCG-treated Jurkat cells. (a) OPLS-DA score plot of metabolite profiles from MTX- and EGCG-treated Jurkat cells. (**b**) OPLS-DA S-plot that is corresponding to score plot shown in (**a**). (**c**) Peak intensities of metabolites (unknown peak that showed *m/z* 448.00 and stearic acid) that showed strong discrimination power to separate each cluster of MTX- and EGCG-treated Jurkat cells metabolite profiles

References

1. Werner, E., Croixmarie, V., Umbdenstock, T., Ezan, E., Chaminade, P., Tabet, J.C., and Junot, C. (2008) Mass spectrometry-based metabolomics: accelerating the characterization of discriminating signals by combining statistical correlations and ultrahigh resolution. *Anal. Chem.* **80**(13): 4918–4932.
2. Major, H. J., Williams, R., Wilson, A.J., and Wilson, I.D. (2006) A metabonomic analysis of plasma from Zucker rat strains using gas chromatography/mass spectrometry and pattern recognition. *Rapid. Commun. Mass Spectrom.* **20**(22): 3295–3302.
3. Pohjanen, E., Thysell, E., Jonsson, P., Eklund, C., Silfver, A., Carlsson, I.B., Lundgren, K., Moritz, T., Svensson, M.B., and Antti, H. (2007) A multivariate screening strategy for investigating metabolic effects of strenuous physical exercise in human serum. *J. Proteome. Res*. **6**(6): 2113–2120.
4. Nordstrom, A., Want, E., Northen, T., Lehtio, J., and Siuzdak, G. (2008) Multiple ionization mass spectrometry strategy used to reveal the complexity of metabolomics. *Anal. Chem.* **80**(2): 421–429.
5. M'Koma, A.E., Blum, D.L.; Norris, J.L., Koyama, T., Billheimer, D., Motley, S., Ghiassi, M., Ferdowsi, N., Bhowmick, I., Chang, S.S., Fowke, J.H., Caprioli, R.M., and Bhowmick, N.A. (2007) Detection of pre-neoplastic and neoplastic prostate disease by MALDI profiling of urine. *Biochem. Biophys. Res. Commun*. **353**(3): 829–834.
6. Shroff, R., Muck, A., and Svatos, A. (2007) Analysis of low molecular weight acids by negative mode matrix-assisted laser desorption/ionization time-of-flight mass spectrometry. *Rapid. Commun. Mass Spectrom*. **21**(20): 3295–3300.
7. Edwards, J.L. and Kennedy, R.T. (2005) Metabolomic analysis of eukaryotic tissue and prokaryotes using negative mode MALDI time-of-flight mass spectrometry. *Anal. Chem*. **77**(7): 2201–2209.
8. Vaidyanathan, S., Gaskell, S., and Goodacre, R. (2006) Matrix-suppressed laser desorption/ionisation mass spectrometry and its suitability for metabolome analyses. *Rapid. Commun. Mass Spectrom*. **20**(8): 1192–1198.
9. Wiklund, S., Johansson, E., Sjostrom, L., Mellerowicz, E.J., Edlund, U., Shockcor, J.P., Gottfries, J., Moritz, T., and Trygg, J. (2008) Visualization of GC/TOF-MS-based metabolomics data for identification of biochemically interesting compounds using OPLS class models. *Anal. Chem*. **80**(1): 115–122.
10. McGuire, J.J. (2003) Anticancer antifolates: current status and future directions. *Curr. Pharm. Des*. **9**(31): 2593–2613.
11. Rich, T.A., Shepard, R.C., and Mosley, S.T. (2004) Four decades of continuing innovation with fluorouracil: current and future approaches to fluorouracil chemoradiation therapy. *J. Clin. Oncol*. **22**(11): 2214–2232.
12. Navarro-Peran, E.; Cabezas-Herrera, J.; Garcia-Canovas, F.; Durrant, M. C.; Thorneley, R. N.; Rodriguez-Lopez, J. N., The antifolate activity of tea catechins. *Cancer Res.* 2005, 65, (6), 2059–2064.
13. Trygg, J., Holmes, E., and Lundstedt, T. (2007) Chemometrics in metabonomics. *J. Proteome. Res*. **6**(2): 469–479.
14. Fairbanks, L.D., Ruckemann, K., Qiu, Y., Hawrylowicz, C.M., Richards, D.F., Swaminathan, R., Kirschbaum, B., and Simmonds, H. A. (1999) Methotrexate inhibits the first committed step of purine biosynthesis in mitogen-stimulated human T-lymphocytes: a metabolic basis for efficacy in rheumatoid arthritis? *Biochem. J*. **342**(Pt 1): 143–152.
15. Hardingham, T.E. and Fosang, A.J. (1992) Proteoglycans: many forms and many functions. *FASEB J.* **6**(3): 861–870.
16. Wight, T.N., Kinsella, M.G., and Qwarnstrom, E.E. (1992) The role of proteoglycans in cell adhesion, migration and proliferation. *Curr. Opin. Cell Biol*. **4**(5): 793–801.

Extracts from the Root of *Platycodon grandiflorum* Modulate Induction of Inflammatory Changes in Coculture of Adipocytes and Macrophages

Ju-Hye Lee, Koji Yamada, and Hirofumi Tachibana

1 Introduction

The root of *Platycodon grandiflorum* has been consumed as food stuff in East Asia as traditional oriental medicine for diseases such as bronchitis, asthma, pulmonary tuberculosis, hyperlipidemia, diabetes and inflammatory disease. Recently, extracts from the roots of *P. grandiflorum* (PGE) have been found to posses various biological properties, including anti-inflammatory, antiobesity, antiallergic and cholesterol-lowering activities [1–4]. However, the mechanisms of the beneficial effect of *P. grandiflorum* remain unclear.

Obesity is closely associated with a state of chronic, low-grade inflammation characterized by abnormal cytokine production and activation of inflammatory signaling pathways in adipose tissue [5, 6]. It is associated with the infiltration of macrophages into adipose tissue, which may contribute to an elevated inflammatory status by secreting a variety of proinflammatory mediators, including tumor necrosis factor alpha, TNF-α; monocyte chemoattractant protein-1, MCP-1; and reactive oxygen species.

Macrophages, producing the proinflammatory factors, are an important source of inflammation in adipose tissues in obesity [5]. Obesity-induced inflammation entails the enhancement of the recruitment of macrophages into adipose tissue and the release of various proinflammatory proteins from fat tissue. Macrophages are now recognized as an important non-adipocyte cell type in adipose tissue that contributes significantly to adipose tissue production of inflammatory factors [6]. Notably, the percentage of macrophage infiltration in adipose tissue correlates with obesity and insulin resistance [5, 7]. Suganami et al. reported that the paracrine loop involving adipocyte-derived free acid and macrophage-derived TNF-α establishes a vicious cycle that augments the inflammatory changes and insulin resistance in obese adipose tissue [8].

J.-H. Lee (✉)
Kyushu University, Higashi-ku, Fukuoka, Japan
e-mail: mousejerry@hotmail.co.jp

M. Kamihira et al. (eds.), *Animal Cell Technology: Basic & Applied Aspects*, Animal Cell Technology: Basic & Applied Aspects 16, DOI 10.1007/978-90-481-3892-0_70,

The aim of the present study is to obtain in vitro evidences that PGE can inhibit inflammatory responses in obesity. We investigated the effect of PGE on the production of proinflammatory mediators in lipopolysaccharide (LPS)-stimulated macrophages and in the interaction between adipocytes and macrophages using in vitro coculture system [8].

2 Materials and Methods

2.1 Reagents

Lipopolysaccharide (LPS), anti-β-actin polyclonal antibody and horseradish peroxidase (HRP)-conjugated anti-rabbit antibody were derived from Sigma (St. Louis, MO). Block Ace was purchased from Dainihon Pharmaceutical (Osaka, Japan). An anti-iNOS polyclonal antibody was purchased from Merck (Tokyo, Japan). An anti-mouse TNF-α antibody was obtained from Endogen (Woburn, MA). Biotinylated anti-mouse TNF-α antibody was obtained from Biosource (Camarillo, CA). HRP-conjugated anti-mouse antibody and HRP conjugated streptavidin were purchased from Zymed (San Francisco, CA).

2.2 Cell Preparation

The RAW 264.7 macrophage were cultured in Dulbecco's modified Eagle's medium (DMEM) (Sigma) with 10% fetal calf serum (FCS) and 100 U/ml penicillin/100 μg/ml streptomycin (Gibco BRL, NY, USA) at 37°C under a humidified 5% CO_2 atmosphere. The cells were seeded in 2 mL dish (1×10^6 cells/ml), and treated with 5 μg/ml LPS (Sigma) and various concentrations of PGE in serum-free medium for 24 h. 3T3-L1 preadipocytes were subcultured in DMEM with 10% FBS (Biological Industries, Kibbutz Beit Haemek, Israel), 100 U/ml penicillin/100 μg/ml streptomycin at 37°C in a humidified 5% CO_2 atmosphere. Differentiation of 3T3-L1 preadipocytes was induced by adipogenic agents (0.5 mM 3-isobutyl-1-methylxanthine (Nacalai Tesque, Kyoto, Japan), 0.25 μM dexamethasone (Sigma), and 10 μg/ml insulin (Sigma)) in DMEM containing 10% FBS for 2 days after the cells reached confluence (day 0). Then, the medium was replaced with DMEM containing 10% FBS and 5 μg/ml insulin, and was changed every two days. After induction of differentiation, the cells that accumulated lipid droplets were used as hypertrophied 3T3-L1 adipocytes.

2.3 Coculture of Adipocytes and Macrophages

Adipocytes and macrophages were cocultured in a contact system as previously described 7, RAW 264.7 cells (1×105 cells/ml) were plated onto dishes with serum-starved and hypertrophied 3T3-L1 cells, and the coculture was incubated in

serum-free DMEM for 24 h. As a control, adipocytes and macrophages, the numbers of which were equal to those in the contact system, were cultured separately and mixed after harvest. PGE was added to the coculture at various concentrations. After 24 h of treatment, culture supernatants were collected and stored at − 20°C until measurements.

2.4 Measurement of TNF-α Production

The amount of TNF-α in culture medium was measured by sandwich enzyme-linked immunosorbent assay (ELISA). An anti-mouse TNF-α antibody was used to fix TNF-α. Antibody solution diluted at 500 times by PBS was added to a 96-well plate, and incubated for 2 h at 37°C. After washing with 0.05% Tween20-PBS (T-PBS) three times, each well was blocked with 25% Block Ace solution for 2 h at 37°C. Following blocking reaction, each well was treated with 50 μl of culture supernatant for 1 h at 37°C. The well was then treated with biotinylated anti-mouse TNF-α antibody diluted at 1000 times by 10% Block Ace for 1 h at 37°C. HRP-conjugated streptavidin solution diluted at 1000 times by 10% Block Ace solution was added to each well at 100 μl. Then, 0.6 mg/ml of 2,2′-azino-bis(ethylbenzothazoline-6-sulfonic acid diammonium salt) (ABTS) dissolved in 0.03% H_2O_2–0.05 M citrate buffer (pH 4.0) was added to the well at 100 μl, and the absorbance at 405 nm was measured after the addition of 1.5% oxalic acid to terminate the coloring reaction at 100 μL. The well was rinsed three times with T-PBS between each step.

2.5 Reverse Transcription-Polymerase Chain Reaction (RT-PCR)

Cells were harvested by centrifugation and washed twice in PBS. Total cellular RNA was isolated using the Trizol reagent according to the manufacturer's instructions. Ten micrograms of total RNA was denatured at 70°C with 1 μl oligo-dT20 primer (0.5 mg/ml) in 13.8 μl final volume. Primers-RNA mixes were cooled on ice for 10 min, 2 μl dNTPs (10 mM), 0.1 μl M-MLV reverse transcriptase (20 units), 0.1 μl RNase inhibitor (10 units) and 4 μl 5 × buffer were added in 20 μl final volume. The resultant cDNA samples were subjected to 25 cycles of PCR amplification in the presence of specific sense and antisense primers. Mouse β-actin cDNA was amplified as an internal control. Each cycle consisted of denaturation at 94°C for 1 min, annealing at 60°C for 1 min (β-Actin and MCP-1), and DNA synthesis at 72°C for 1 min. Sequences for the PCR primers sizes and expected amplification product sizes are as follows: for the β-Actin: sense 5′-TGGAATCCTGTGGCATCCATGAAAC-3′, and antisense 5′-TAAAACGCAGCTCAGTAACAGTCCG-3′; for the MCP-1: sense 5′-TCCCCAAAGGG ATGAGAAGTTC-3′, and antisense 5′-TCATACCA GGGTTTGAGCTCAG-3′. The amplified PCR products were subjected to electrophoresis on a 1.5% agarose gel.

2.6 Measurement of Nitric Oxide Release

The amount of nitrite in cell-free culture supernatants was measured using Griess reagent [9]. Briefly, 100 μl of supernatant was mixed with an equivalent volume of Griess reagent [1:1 (v/v) of 0.1% N-1-naphthyl-ethylenediamine in distilled water and 1% sulfanilamide in 5% phosphoric acid] on a 96-well flat bottom plate. After 10 min, absorbance at 570 nm was measured, and the amount of nitrite was calculated from the $NaNO_2$ standard curve.

2.7 Western Blot Analysis

RAW 264 cells were carefully washed twice with ice-cold phosphate buffered saline (PBS) and placed immediately in lysis buffer containing 20 mM Tris HCl (pH 7.5), 15 mM NaCl, 1% Triton × 100 (Nacalai Tesque), and protease inhibitor cocktail (Nacalai Tesque). Lysate was centrifuged at 15,000 rpm for 5 min, and the supernatant was stored for subsequent analysis. Equal amount of protein (5 μg/lane) were resolved by 8% sodium dodecyl sulfate-polyacrylamide gel electrophoresis, and transferred onto a nitrocellulose membrane (Schleicher & Schuell BioScience, Dassel, Germany). The membrane was washed with Tris-buffered saline (TBS; 10 mM Tris, 150 mM NaCl), containing 0.1% Tween20 (TBST). The membrane was blocked with Blocking one solution at 37°C for 1 h. Following blocking, the membrane was incubated with antibodies against iNOS (1:2000) or β-Actin (1:10,000), and then continuously incubated with appropriate HRP-conjugated antibodies. The bands were developed by using of the ECL Western detection reagents.

2.8 Statistical Analyses

All data were expressed as the mean ± SD. Statistical significance was analyzed by Student's t-test. Each value of * $p < 0.05$, ** $p < 0.01$ or *** $p < 0.001$ was considered to be statistically significant.

3 Results and Discussion

To determine whether PGE suppresses proinflammatory mediators such as TNF-α, NO, and MCP-1, production in macrophages, RAW 264.7 macrophages were stimulated with LPS in the presence or absence of PGE. RAW 264.7 cells activated with LPS and secrete TNF-α [10]. LPS- induced TNF-α production by RAW 264.7 cells was significantly inhibited by PGE treatment in a dose-dependent manner. PGE also inhibited MCP-1 expression by LPS-stimulated RAW 264.7 cells (data not shown).

Next, to evaluate the effect of PGE on NO production in LPS-induced RAW264.7 cells, nitrite accumulation was examined by the Griess assay. LPS treatment for 24 h triggered significant nitrite accumulation, which was effectively inhibited by

10 μg/ml treatment with PGE (data not shown). Inducible NOS (iNOS) is stimulated by LPS or proinflammatory cytokines in murine macrophages [11, 12]. To elucidate the underlying mechanisms of the regulation of NO synthesis in the macrophages by PGE, we demonstrated whether PGE mediates the protein expression level of iNOS. As the result of that, the iNOS expression was markedly decreased in a PGE dose-dependent manner (data not shown).

We investigated the effect of PGE on the production of proinflammatory mediators in coculture of adipocytes and macrophages. Coculture of differentiated 3T3-L1 cells or RAW 264.7 cells in the contact system revealed a marked increase in TNF-α and MCP-1 level (Fig. 1a and b). PGE treatment in coculture significantly decreased TNF-α production level at 10 μg/ml MCP-1 mRNA expression in this coculture was significantly inhibited by PGE in a dose-dependent manner.

To examine the effect of PGE on NO production in coculture of adipocytes and macrophages, the cells were treated with PGE in the presence of LPS for 24 h. The coculture of differentiated 3T3-L1 adipocytes and RAW 264.7 cells showed an enhanced NO production compared with that of the control culture. PGE significantly decreased NO production at 10 μg/ml. Moreover, the expression of iNOS was also markedly inhibited in at 10 μg/ml, indicating inhibition of NO is an early event (data not shown).

In conclusion, our data demonstrated that PGE inhibited proinflammatory mediators production from LPS-induced macrophage and the inflammatory responses of macrophages such as activation induced by adipose tissue-conditioned medium, indicating that PGE may suppress the inflammatory responses of adipose tissue in obesity. Taken together, the present results suggest that PGE may be useful for suppressing the enhanced inflammatory responses of adipose tissue in obesity.

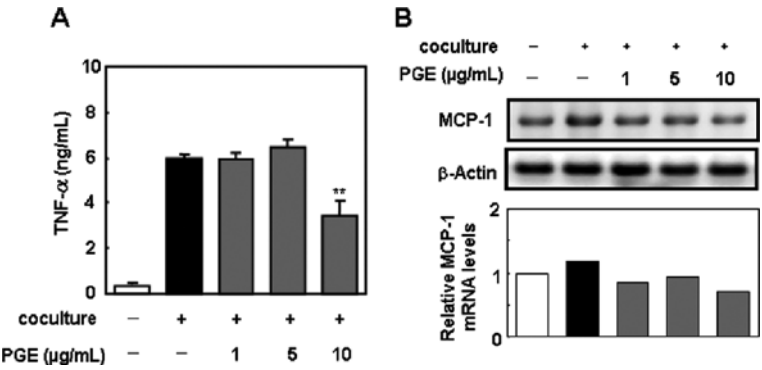

Fig. 1 Effect of PGE on proinflammatory mediator production by coculture of 3T3-L1 adipocytes and RAW 264.7 macrophages. Differentiated 3T3-L1 adipocytes were cocultured RAW 264.7 cells for 24 h. The cells were treated with PGE (1–10 μg/ml) for 24 h. (**a**) TNF-α level in the culture medium was measured ELISA. $^{**}p < 0.01$ compared with non-treated coculture. (**b**) MCP-1 mRNA expression in analyzed RT-PCR. The gene expression level was expressed relative to the control group (=1.0) after normalization using the β-actin gene expression level

However, a clearer understanding of the mechanism of PGE-regulating adipose tissue signaling in obesity will require further molecular studies.

References

1. Ahn, K.S., Noh, E.J., Zhao, H.L., Jung, S.H., Kang, S.S., and Kim Y.S. (2005) Inhibition of inducible nitric oxide synthase and cyclooxygenase II by *Platycodon grandiflorum* saponins via suppression of nuclear- B activation of activation in RAW 264.7 cells. *Life Sci*. **76**: 2315–2328.
2. Wang, C., Schuller Levis, G.B., Lee, E.B., Levis, W.R., Lee, D.W., Kim, B.S., Park, S.Y., and Park, E. (2004) Platycodin D and D3 isolated from the root of *Platycodon grandiflorum* modulate the production of nitric oxide and secretion of TNF-α in activated RAW 264.7 cells. *Int. Immunopharmacol*. **4**: 1039–1049.
3. Shin, C.Y., Lee, W.J., Lee, E.B., Choi, E.Y., and Ko, K.H. (2003) Platycodin D and D3 increase airway mucin release in vivo and in vitro in rats and hamsters. *Planta. Med*. **68**: 221–225.
4. Zhao, H.L., Cho, K.H., Ha, Y.W., Jeong, T.S., Lee, W.S., and Kim, Y.S. (2006) Cholesterol-lowering effect of platycodin D in hypercholesterolemic ICR mice. *Eur. J. Pharmacol*. **537**: 166–173.
5. Weisberg, S.P., McCann, D., Desai, M., Rosenbaum, M., Leibel, R.L., and Ferrante, A.W., Jr. (2003) Obesity is associated with macrophage accumulation in adipose tissue. *J. Clin. Invest*. **112**: 1785–1788.
6. Xu, H., Barnes, G.T., Yang, Q., Tan, G., Yang, D., Chou, C.J., Sole, J., Nichols, A., Ross, J.S., Tartaglia, L.A., and Chen, H. (2003) Chronic inflammation in fat plays a crucial role in the development of obesity-related insulin resistance. *J. Clin. Invest*. **112**: 1821–1830.
7 Di Gregorio, G.B., Yao-Borengasser, A., Rasouli, N., Varma, V., Lu, T., Miles, L.M., Ranganathan, G., Peterson, C.A., McGehee, R.E., and Kern, P.A. (2005) Expression of CD68 and macrophage chemoattractant protein-1 genes in human adipose and muscle tissues: Association with cytokine expression, insulin resistance, and reduction by pioglitazone. *Diabetes* **54**: 2305–2313.
8. Suganami, T., Nishida, J., and Ogawa, Y. (2005) A paracrine loop between adipocytes and macrophages aggravates inflammatory changes: Role of free fatty acids and tumor necrosis factor alpha. *Arterioscler. Thromb. Vasc. Biol*. **25**: 2062–2068.
9. Granger, D.L., Taintor, R.R., Boockvar, K.S., and Hibbs, J.B. Jr., (1996) Measurement of nitrate and nitrite in biological samples using nitrate reductase and Griess reaction. *Methods Enzymol*. **268**: 142–151.
10. Park, E., Quinn, M.R., Wright, C., and Schuller-Levis G.B. (1993) Taurine chloramine inhibits the synthesis of nitric oxide production and the release of tumor necrosis factor in activated RAW 264.7 cells. *J. Leukoc. Biol*. **54**: 119–124.
11. Ding, A., Nathan, C.F., and Stuehr, D.J. (1988) Release of reactive nitrogen intermediates and reactive oxygen intermediates from mouse peritoneal macrophages. *J. Immunol*. **141**: 2407–2412.
12. Higuchi, M., Higashi, N., Taki, H., and Osawa, T. (1990) Cytolytic mechanism of activated macrophages. Tumor necrosis factor and L-arginine-dependent mechanisms act synergistically as the major cytolytic mechanisms of activated macrophages. *J. Immunol*. **144**: 1425–1431

Position Specific Incorporation of Nonnatural Amino Acids into Proteins In Vivo

Satoshi Neki, Takashi Ohtsuki, and Masahiko Sisido

1 Introduction

The protein biosynthesis methods including nonnatural amino acids add new properties to proteins. And, the nonnatural proteins are valuable for analyzing their structure and function. The incorporation of nonnatural amino acids has accomplished by using an suppressor tRNA carrying the nonnatural amino acid to a ribosome associated with mRNA containing an expanded codon/anticodon pair (reviewed in [1–3]) However, the incorporation of nonnatural amino acids in cells is difficult.

In current, two methods are general to incorporate nonnatural amino acids into proteins in cells. (1) The method to use an artificial aminoacyl-tRNA synthetase (ARS) that charge a tRNA with a non-natural amino acid in cells, or (2) the method to internalize aa-tRNAs carrying nonnatural amino acids by cells. The former method needs a time-consuming step to create artificial ARS for each nonnatural amino acid, whereas the latter method can be used for all amino acids. In this study, we developed a method to internalize aa-tRNA by cells using Tat peptide fused EF-Tu mutant (TatEFTu). EF-Tu recognizes aminoacyl-tRNA, delivers them to the ribosome [4, 5]. EF-Tu part of TatEFTu was enlarged the amino acid binding pocket to improve binding ability to large nonnatural amino acids. In this study, *Escherichia coli* EF-Tu E215A/D216A mutant was used for the EF-Tu part of TatEFTu. The EF-Tu E215A/D216A mutant can bind tightly to aa-tRNAs with nonnatural amino acids [6]. Tat peptide part of TatEFTu is a cell-penetrating peptide (CPP), and it is expected to bring the EF-Tu/aa-tRNA complex across a cellular membrane.

For the position specific incorporation, an amber suppressor tRNAs, which were chemically aminoacylated with nonnatural amino acids, was used [7]. Firefly

S. Neki (✉)
Department of Bioscience and Biotechnology, Okayama University, Okayama, Japan
e-mail: gen20914@cc.okayama-u.ac.jp

M. Kamihira et al. (eds.), *Animal Cell Technology: Basic & Applied Aspects*, Animal Cell Technology: Basic & Applied Aspects 16, DOI 10.1007/978-90-481-3892-0_71,

luciferase (FLuc) was used as a target protein, and the FLuc expression vector with an amber mutation at FLuc 444th position was prepared.

In this study, we evaluated aa-tRNA binding efficiency and translation enhancing effect of TatEFTu. We also evaluated aa-tRNA delivery of TatEFTu into Chinese hamster ovary (CHO) cells.

2 Materials and Methods

2.1 Preparation of tRNA Transcripts

E.coli $tRNA^{Tyr}_{CUA}$ and *yeast* $tRNA^{Phe}_{CUA}$ transcripts were prepared as described [8]. Tyr- *E.coli* $tRNA^{Tyr}_{CUA}$ were synthesized by *E.coli* aminoacyl-tRNA synthetases mix (SIGMA-ALDRICH). *yeast* $tRNA^{Phe}_{CUA}$ transcripts were labeled TM-Rhodamine by following the Label IT® siRNA Tracker Intracellular Localization Kit protocol (Mirus). Nitrophenylalanine (ntrPhe)-tRNA were prepared by ligating transcribed tRNA without the 3′-CA sequence and the aminoacyl dinucleotide (pdCpA) with T4 RNA ligase as described [7, 9].

2.2 Preparation of Firefly Luciferase Vector

pGL3 luciferase plasmid was purchased from Promeg. Its 444th codon (TAC) which defined tyrosines ware mutated to amber codon (TAG) by QuikChange sitedirected mutagenesis (Stratagene). The sequences of the mutated plasmids were confirmed by using an ABI prism 310 Genetic Analyzer.

2.3 Preparation of EF-Tu Mutants

EF-Tu E215A/D216A mutant fused to HIV-1 TAT peptide (-YGRKKRRQRRR-), named as TatEFTu, were prepared as described above. Vectors expressing *E. coli* TatEFTu mutants were prepared using the pET-15b (Novagen)-derived expression vector encoding N-terminal His-tagged *E. coli* TatEFTu. The mutations were introduced by employing the Stratagene QuikChange site-directed mutagenesis protocol. The sequences of the mutated plasmids were confirmed by using an ABI prism 310 Genetic Analyzer. BL21 (DE3) *E. coli* cells were transformed with the plasmids and the expressed recombinant proteins were purified as described [10] with the following modifications. After first purification on Ni-NTA column, RNA contaminants which were included in purified EF-Tu mutants were separated from the EF-Tu by incubating with 1 mM EDTA at 37°C for 30 min. The mixture was then purified by anion exchange column chromatograph. The EF-Tu mutants were dissolved in the buffer containing 50 mM Hepes-KOH [pH 7.6], 50 mM KCl, 1 mM DTT, 2 μM GDP and 10% glycerol.

2.4 Gel Shift Assay

Binding of EF-Tu to tRNAs charged with Tyr or ntrPhe was investigated using a E.coli tRNATyrCUA mutant. The ternary complex of EF-Tu, GTP and aa-tRNA was prepared as follows. 10 μM EF-Tu was preincubated with 1 mM GTP at 37°C for 15 min in 5 μL total volume containing 70 mM HEPES-KOH (pH 7.6), 52 mM NH4OAc, 8 mM Mg(OAc)2, 30 mM KCl, 0.8 mM DTT, 1.6 μM GDP, 6% glycerol, 10 mM phosphoenolpyruvate and 0.04 U/μL pyruvate kinase. To the preincubated EF-Tu solution, 3 μL of 8.3 μM aa-tRNA (dissolved in 6 mM KOAc) and 2 μL of TC buffer, containing 50 mM HEPES-KOH (pH 7.6), 65 mM NH4OAc and 10 mM Mg(OAc)2,were added. The mixture, containing 50 pmol TatEFTu and 25 pmol of aa-tRNA, was incubated at 37°C for 15 min. Electrophoresis of samples was performed using 8% polyacrylamide gels at 4°C in a buffer containing 50 mM Tris-HCl (pH 6.8), 65 mM NH4OAc and 10 mM Mg(OAc)2. Gels were stained with SYPRO Red (Takara, Japan).

2.5 Cellular Internalization of aa-tRNA Using TatEFTu

Chinese hamster ovary (CHO) cells (Invitrogen Flp-In-CHO cell line) were cultured at 37°C under 5% CO_2 in Ham's F-12 medium supplemented with 10% fetal bovine serum (FBS). 20 μL of preincubation mixture containing 2 μL of TC buffer, 10 mM phosphoenolpyruvate, 0.04 U/μL pyruvate kinase, 1 mM GTP and 2.5 μM TatEFTu was incubated at 37°C for 15 min. 20 μL solution containing 2 μL of TC buffer and 250 nM Rhodamine-labeled RNA carrying Phe, was then added to this mixture, and incubated at 37°C for 10 min. Cells grown to 70% confluence in 96-well culture plates were overlaid with 80 μL of T buffer [20 mM HEPES-KOH (pH 7.4), 115 mM NaCl, 5.4 mM KCl, 1.8 mM $CaCl_2$, 0.8 mM $MgCl_2$ and 13.8 mM Glucose] and then 20 μL of the TatEFTu/aa-tRNA mixture was added to each well. After 3-h incubation at 37°C, cells were treated twice with culture medium containing 34 μg/ml RNase A for a total of 1 h at 37°C to remove RNAs adhering to the extracellular surface of the cells. Cells were then washed with T buffer, and fluorescence images were obtained using a fluorescence microscope (IX51/IX2-FL-1/MP5Mc/OL-2, Olympus, Japan).

3 Results and Discussion

3.1 Binding of TatEFTu to aa-tRNAs

Binding of TatEFTu (*E. coli* EF-Tu E215A/D216A mutant fused to Tat-peptide) to aa-tRNAs that carry tyrosine or nitrophenylalanine (ntrPhe) was analyzed by gel-shift assay. TatEFTu/aa-tRNA complex is separated from TatEFTu on the gel. The

result showed that TatEFTu has binding ability for Tyr-tRNA and ntrPhe-tRNA. Furthermore, protection of Tyr-tRNA by TatEFTu was observed when they were coincubated in 10 μL of T buffer at 37°C for 3 h. These results indicated that TatEFTu would be used for aa-tRNA delivery into cells.

3.2 Effects of TatEFTu Addition in the In Vitro Protein Synthesizing System

Translation activity with TatEFTu was analyzed using firefly luciferase (FLuc) mRNA containing an amber codon at 444th potion. The FLuc gene was translated in a cell-free translation system with rabbit reticulocyte lysate (Promega). As a positive control, wild-type Fluc mRNA was translated. When only ntrPhe-tRNA$_{CUA}$ was added to translation mixture containing amber muted firefly luciferase gene, very low translation activity was observed. Hydrolysis of ntrPhe-tRNA without TatEFTu seems to be one of the reasons for the low activity. Whereas, when ntrPhe-tRNA$_{CUA}$/TatEFTu was added to translation, higher activity of the luciferase was observed. This result indicated that TatEFTu raised ntrPhe-incorporation at the 444th amber position, probably due to ntrPhe-tRNA-protection efficiency of TatEFTu. Therefore, TatEFTu is valuable for mammalian translation.

3.3 Aminoacyl-tRNA Delivery into Mammalian Cells Using TatEFTu

TatEFTu was used to internalize aa-tRNA by cells. Tat-peptide has been known as a cell-penetrating peptide that can carry fused proteins. The internalization of aa-tRNA/TatEFTu was observed by using Rhodamine labeled tRNA carrying phenylalanine (Phe-Rho-tRNA).

CHO cells were incubated with TatEFTu/Phe-Rho-tRNA for 3 h. And, fluorescence of Rhodamine was observed in the cells. Figure 1 shows Phe-Rho-tRNA was delivered with TatEFTu into CHO cells. Whereas, in the absence of TatEFTu, Phe-Rho-tRNA was not delivered into the cells.

However, fluorescence of Rhodamine was granulated, indicating that TatEFTu/Phe-Rho-tRNA complexes were trapped in endsomes. Trapped aa-tRNA cannot be used for translation, which occurs in cytosol.

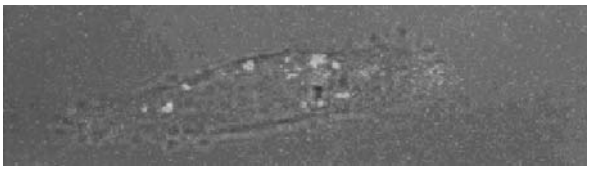

Fig. 1 Fluorescence of Rhodamine labeled Phe-tRNA internalization into CHO cells mediated by TatEFTu

4 Conclusions

TatEFTu slightly enhanced ntrPhe-incorporation into the protein in mammalian cell-free translation system. The aa-tRNA/TatEFTu complexes were internalized into CHO cells, but they were trapped in endosomes. We are now trying to use photochemical internalization (PCI) [11] for release of TatEFTu/aa-tRNA from endosomes to cytosol. If endosomal escape of aa-tRNAs can be done, TatEFTu enable position specific incorporation of nonnatural amino acids into proteins in mammalian cells.

References

1. Stromgaard, A., Jensen, A.A., and Stromgaard, K. (2004) Site-specific incorporation of unnatural amino acids into proteins. *Chembiochem*. **5**: 909.
2. Maskarinec, S.A. and Tirrell, D.A. (2005) Protein engineering approaches to biomaterials design. *Curr. Opin. Biotechnol*. **16**: 422.
3. Wang, L., Xie, J., and Schultz, P.G. (2006) Expanding the genetic code. *Annu. Rev. Biophys. Biomol. Struct*. **35**: 225.
4. Nissen, P., Kjeldgaard, M., Thirup, S., Polekhina, G., Reshetnikova, L., Clark, B.F., and Nyborg, J. (1995) Crystal structure of the ternary complex of Phe-tRNAPhe, EF-Tu, and a GTP analog. *Science* **270**: 1464.
5. LaRiviere, F.J., Wolfson, A.D., and Uhlenbeck, O.C. (2001) Uniform binding of aminoacyl-tRNAs to elongation factor Tu by thermodynamic compensation. *Science* **294**: 165.
6. Doi, Y., Ohtsuki, T., Shimizu, Y., Ueda, T., and Sisido, M. (2007) Elongation factor Tu mutants expand amino acid tolerance of protein biosynthesis system. *J. Am. Chem. Soc*. **129**: 14458.
7. Hohsaka, T., Ashizuka, Y., Murakami, H., and Sisido, M. (1996) Incorporation of nonnatural amino acids into streptavidin through in vitro frame-shift suppression. *J. Am. Chem. Soc*. **118**: 9778.
8. Sisido, M., Ninomiya, K., Ohtsuki, T., and Hohsaka, T. (2005) Four-base codon/anticodon strategy and non-enzymatic aminoacylation for protein engineering with non-natural amino acids. *Methods* **36**: 270.
9. Heckler, T.G., Chang, L.H., Zama, Y., Naka, T., Chorghade, M.S., and Hecht, S.M. (1984) T4 RNA ligase mediated preparation of novel "chemically misacylated" $tRNA^{Phe}$s. *Biochemistry* **23**: 1468.
10. Ohtsuki, T., Watanabe, Y., Takemoto, C., Kawai, G., Ueda, T., Kita, K., Kojima, S., Kaziro, Y., Nyborg, J., and Watanabe, K. (2001) An "elongated" translation elongation factor Tu for truncated tRNAs in nematode mitochondria. *J. Biol. Chem*. **276**: 21571.
11. Oliveira, S., Fretz, M.M., Hogset, A., Storm, G., and Schiffelers, R.M. (2007) Photochemical internalization enhances silencing of epidermal growth factor receptor through improved endosomal escape of siRNA. *Biochim. Biophys. Acta*. **1768**: 1211.

Novel Protease Inhibitor Inhibiting Proliferation of Influenza Virus: Purification and cDNA Cloning of a Novel Protease Inhibitor Secreted by MDCK Cells

Kiyoto Nishiyama, Keishin Sugawara, Kenji Soejima, Shin-ichi Abe, and Hiroshi Mizokami

1 Introduction

It is important for Influenza virus infection that the viral surface glycoprotein, hemagglutinin (HA) be cleaved by host cell derived protease. The HA molecule is activated by the host cell-derived protease at a specific cleavage site of non-activated HA (HA0) having a molecular weight of 75 kDa, and is divided into parts to the HA1 molecule of 55 kDa and the HA2 molecule of 25 kDa [1]. If the conformational change of the HA molecule under acidic pH occurs, the hydrophobic region in the HA2 molecule at the N terminal end is exposed, and the membrane fusion between the cell and the virus is promoted.

In the cell culture vaccine manufacturing of the influenza virus that uses the Madin Darby canine kidney (MDCK) cell derived from the dog kidneys, the trypsin is usually added to the medium for the above-mentioned purpose.

We sometimes observed the impairment of influenza virus proliferation in MDCK cells and we thought there were three possibilities to explain the impairment of multicycle influenza virus growth. The first possibility is the simple idea that exhausted nutrition in the medium results in impairment of virus growth. But this idea has specific properties: abrupt loss of virus growth occurs, and inhibition occurs with enough cell viability loss. The second possibility [2] is that interferon induced by persistent infection causes impairment of virus growth. There are some reports of persistent infection in MDCK cells where the cells secrete interferon which impairs the virus growth. The third possibility is that host cells secrete the trypsin-inactivating factors. This idea has the highest possibility of occurring in this situation. Dr. Webster et al. [3]. reported the phenomenon of impairment of influenza virus growth in Vero cells. They reported that this reason why the virus production in Vero cells is less than that of MDCK cells is because of the secretion of strong trypsin-inactivating factors into the medium of Vero cells. Using the UF membrane

K. Nishiyama (✉)
The Chemo-Sero-Therapeutic Research Institute, Kikuchi Research Center, Kikuchi, Kumamoto 869-1298, Japan
e-mail: nishiyama-ki@kaketsuken.or.jp

M. Kamihira et al. (eds.), *Animal Cell Technology: Basic & Applied Aspects*, Animal Cell Technology: Basic & Applied Aspects 16, DOI 10.1007/978-90-481-3892-0_72,

system, they roughly estimated that the molecular weight of this inactivating factor is more than 100 kDa.

As a result, two kinds of inhibitory factors in MDCK cells were purified and identified. One of them is a new protease inhibitor renamed as Canine Kidney Protease Inhibitor (CKPI).

2 Materials and Methods

2.1 Detection of Inhibiton of Influenza Virus Proliferation

When the cell density of MDCK cells reached over 4×10^6 cells/ml in four suspension culture flasks, the cells and the culture supernatant were harvested and the medium was exchanged at the following mixture ratios of the supernatant and fresh medium: 0%, 50%, 75%, and 100%. The inoculation of virus was done at an MOI of 0.001 with trypsin. After inoculation, each virus culture flask was cultured for 3 and 4 days and after culturing, the virus antigen in the supernatant was measured by HA-ELISA.

2.2 Detection and Purification for Trypsin -Inactivating Factors (TFs)

2.2.1 Detection

The trypsin activity and inhibitory activity were measured by skimmed milk Single Radial Diffusion Inhibition (SRDi) test [4] and synthetic substrate (Z-Arg-pNA.HCl; L-ZAPA) hydrolysis method. The reverse zymography [5] was used to estimate the molecular size of the inhibitors in the medium.

2.2.2 Purification

First of all the ultrafiltration was performed, in the next step heparin affinity chromatography was performed to purify the trypsin inhibitory activity from the ultrafiltrated supernatant. The fraction obtained by ultrafiltration was diluted with 20 mM phosphate buffer, pH 7.4 and the diluted sample was applied to a 5 mL heparin column (HiTrap Heparin HP) equilibrated with buffer A (10 mM phosphate, pH 7.5) attached to a low pressure chromatography system (BioLogic LP system). The chromatography was performed at 2–8°C, with a flow rate of 1.5 mL/min of buffer A. After loading the proteins, the column was washed with 25–50 mL of buffer A. Adsorbed proteins were eluted with a linear gradient of 0–0.6 M NaCl at a flow rate of 1.5 mL/min (Buffer B, 10 mM phosphate, 0.6 M NaCl). The pass-through fraction and eluted fractions were tested for trypsin inhibitory activity by SRDi and separated by reducing SDS-PAGE.

In order to obtain samples of greater purity for mass spectrometry, a 100–200 μg aliquot of pooled fractions of TF B by heparin affinity fractions was injected into a reversed-phase C8 column (UG120, 4.6 mm × 250 mm). Samples were prepared

by overnight dialysis against 50 mM Tris pH 7.0, 50 mM NaCl and the column was equilibrated with 0.1% (v/v) formic acid (buffer A). The sample was applied to the column and washed with buffer A before elution with a linear gradient (0–60% for 40 min) of buffer B (70% (v/v) acetonitrile). SDS-PAGE was performed on the pooled fractions of TF B before and after the C8 chromatography.

2.3 Peptide Mapping for TF B (CKPI)

In order to analyze the internal amino acid sequence of the TF B, the TF B sample is digested by trypsin. Aliquots of 100–200 mg of TF B protein from reverse-phase C8 chromatography were diluted in buffer to 100 ml at final concentrations of 6 M guanidine HCl, 0.5 M Tris HCl pH 8.0, 2 mM EDTA, 5 mM DTT. The sample was incubated for 75 min at 37°C. A further 75 min incubation period followed after the addition of 10 ml of 100 mM iodoacetamide. The reaction mixture was then applied onto a MicroSpin G-25 gel filtration column equilibrated in 10 mM phosphate buffer. The reduced and alkylated sample proteins were then digested with Trypsin Gold (MS analytical grade). An initial overnight digestion was performed by adding 10 ml of 1 mg/mL Trypsin Gold and incubated at 37°C. The following day, a further 10 ml of 1 mg/mL Trypsin Gold was added and the digestion continued for a further 7 h at 37°C. The reaction mixture was then applied to an ODS column (TSK-gel ODS-80Ts).

2.4 cDNA Cloning of TF B (CKPI)

Total RNA was extracted from 5.6×10^6 MDCK cells following manufacturer's instructions using ISOGEN. Amplification of the gene sequence was performed using the 5′ Full-RACE and 3′ Full-RACE kits from TaKaRa Shuzou Co. Ltd., with any further synthetic primers obtained from Operon Biotechnologies Inc. The following sets of primers were used, antisense 5′ AS1, atccagaaaggcaccgatca; 5′ AS2, agaagggcagagtccagctt; 5′ PAS1, aacgggatccaagca; and sense primers 5′ S1, aatttgagtgccggagtgac; 5′ S2, tgttgctctcatgcttgtgg; 3′ S1 cgagccacacgacgtctc. 5′ and 3′ RACE PCR reactions were performed according to manufacturer′s instructions. The RACE products were purified by agarose gel electrophoresis and subsequent TA cloning was done following manufacturer's instructions. The cloned DNA was sequenced using primers for the TA cloning vector (M13RV primer, caggaaacagctatgac; T7 primer, taatacgactcactataggg).

2.5 Virus Growth Inhibitory Activity of Purified TFs

We modified the neutralization assay [6] for antibody detection against the influenza virus by replacing the serum or antibody with the inhibitors. It was expected that the supernatant containing protease inhibitors will inhibit the infection of MDCK

cells with influenza virus. Serially diluted supernatants were pre-incubated with a standardized amount of virus prior to the addition of MDCK cells.

The neutralization assay of virus activity was based on directly observing the suppression of CPE by photometer detection of viable cells by Naphthol Blue Black (NBB) staining.

3 Results

3.1 Purification and Identification of TFs

As the ratio of fresh medium increased by 0%, 50%, 75%, and 100%, the amount of virus as HA antigen also increased. Therefore, it may be that the supernatant contained a virus growth inhibitor.

In order to measure the remaining of trypsin activity, the trypsin enzyme activity of the supernatant of the MDCK cell culture was measured.

Using synthetic substrate (Z-Arg-pNA.HCl; L-ZAPA), the TPCK treated trypsin activity was measured and the result shows that the medium (background) has a linear response. On the other hand the trypsin activity of the MDCK culture supernatant was decreased in comparison to the background.

Purification revealed that the inhibitory activity was divided into two peaks in the heparin affinity column chromatography results. One peak is named trypsin inactivating factor A (TF A, molecular weight: approximately 15 kDa), and the other is named trypsin inactivating factor B (TF B, molecular weight: approximately 11 kDa). Based on the results of the analysis of the N-terminal amino acid sequence of each molecule, TF A was identified to be a known protease inhibitor called the Submandibular Protease Inhibitor (SPI) which is secreted in dog saliva. On the other hand, TF B was found to be a novel polypeptide and was named as Canine Kidney Protease Inhibitor (CKPI). Results of peptide mapping revealed the internal amino acid sequence of CKPI.

Using primers, PCR cloning was performed. Isolation of CKPI genes showed that CKPI has two whey acidic protein (WAP) motif structures commonly found in acidic protease inhibitors.

Database searching with the predicted cDNA sequence derived from the amino-acid sequence of TF B revealed that this gene was coded as chromosome clone gi|54126067|ref|NW_139896.1|Cfa24_WGA61_1, *Canis familiaris* chromosome 24, with this gene sequence deposited as Genebank AAEX01031134.1. The gene sequence for TF B was found to be approximately 1.6 kb long and composed of 3 introns and 4 exons. This identity was confirmed by the full-length cDNA sequence we obtained for TF B and the sequence has been deposited in the Genebank (accession number; AB266058). CKPI was assumed to be a canine analogue of the human secretory leukocyte protease inhibitor (SLPI). Therefore, using porcine elastase [EC 3.4.21.36] instead of trypsin, the elastase inhibitory activity for CKPI was measured with SRDi. However the porcine elastase inhibitory activity was not detected.

3.2 Virus Growth Inhibitory Activity of Purified TFs

The minimum activity of 50% virus growth inhibition against 100 $CCID_{50}$ of virus was measured by a modified neutralization test. Using A/Wyoming (H3N2) the results show that the minimum activity of TF B was 0.35 U/mL and that of TF A was 3.09 U/mL. Therefore, the virus growth inhibitory activity of TF B is approximately eight times stronger than that of TF A with the same level of trypsin hydrolysis inhibition activity.

4 Discussion and Conclusions

The molecular structure of a novel protease inhibitor is predicted from the data of molecular structure of SLPI. CKPI has two whey acidic protein (WAP) motif structures commonly found in acidic protease inhibitors.

One unit of the WAP motifs has 4 disulfide-bounds, so this protein shows heat stability. The N terminal WAP motif has trypsin inhibitory activity, and the C terminal WAP motif has elastase inhibitory activity. CKPI has two WAP motif structures commonly found in acidic protease inhibitors.

These results suggest that MDCK cells secrete protease inhibitors that inhibit the activation of the influenza virus, which can be applied to protect host cells from viral infection.

Acknowledgements This research has been financed in part by Research on Health Science Focusing on Drug Innovation of the Japan Health Sciences Foundation. We are grateful to Dr. Noritaka Dr. Hashii, Dr. Nana Kawasaki, and Dr. Toru Kawanishi of the National Institute of Health Sciences. We also wish to thank colleagues of the Chemo-Sero-Therapeutic Research Institute (CSTRI) for N-terminal protein sequencing, in vitro virus infection tests, scientific advice, and Mr. Michael Leoncavallo for the polishing of this manuscript.

References

1. Skehel, J.J. and Waterfield, M.D. (1975) Studies on the primary structure of influenza virus hemagglutinin. *Proc. Natl. Acad. Sci. USA* **72**: 93–97.
2. Goshima, F.Y. and Maeno, K. (1989) Persistent infection of MDCK cells by influenza C virus: Initiation and characterization. *J. Gen. Virol.* **70**: 3481–3485.
3. Kaverin, N.V. and Webster, R.G. (1995) Impairment of multicycle influenza virus growth in Vero (WHO) cells by loss of trypsin activity. *J. Virol.* **69**: 2700–2703.
4. Nishiyama, K., Sugawara, K., Soejima, K., Abe, S., and Mizokami, H. (2008) Novel protease inhibitor inhibiting proliferation of influenza virus. *Biologicals* **36**: 122–133.
5. Katunuma, N. (2003) Reverse zymography. *Rinsyokensa* **47**: 871–874.
6. Webser, R., Cox, N., and Stohr, K. (2002)WHO manual on animal influenza diagnosis and surveillance. *WHO/CDS/CSR/NCS/2002.5 Rev.1*.